Characterization of the innate immunity elicited by vaccination and its interactions with adaptive immunity, depending on prime-boost delay

Jean-Louis Palgen

▶ **To cite this version:**

Jean-Louis Palgen. Characterization of the innate immunity elicited by vaccination and its interactions with adaptive immunity, depending on prime-boost delay. Innate immunity. Université Paris Saclay (COmUE), 2019. English. NNT : 2019SACLS146 . tel-02491320

HAL Id: tel-02491320
https://theses.hal.science/tel-02491320

Submitted on 26 Feb 2020

HAL is a multi-disciplinary open access archive for the deposit and dissemination of scientific research documents, whether they are published or not. The documents may come from teaching and research institutions in France or abroad, or from public or private research centers.

L'archive ouverte pluridisciplinaire **HAL**, est destinée au dépôt et à la diffusion de documents scientifiques de niveau recherche, publiés ou non, émanant des établissements d'enseignement et de recherche français ou étrangers, des laboratoires publics ou privés.

université PARIS-SACLAY

UNIVERSITÉ PARIS SUD
Comprendre le monde, construire l'avenir

NNT : 2019SACLS146

Characterization of the innate immunity elicited by vaccination and its interactions with adaptive immunity, depending on the delay between prime and boost

Thèse de doctorat de l'Université Paris-Saclay
préparée à l'Université Paris-Sud

Ecole doctorale n°569 Innovation thérapeutique, du fondamental à l'appliqué (ITFA)
Spécialité de doctorat : Immunologie

Thèse présentée et soutenue à Fontenay-aux-Roses, le 28 Juin 2019, par

JEAN-LOUIS PALGEN

Composition du Jury :

Isabelle Schwartz-Cornil Directrice de recherche, INRA / Université Paris-Saclay, Département de virologie et immunologie moléculaires	Présidente
Marc Dalod Directeur de recherche, CNRS / Université d'Aix-Marseille / Inserm, CIML	Rapporteur
Helder Nakaya Associate Professor, University of São Paulo, Department of Clinical Analyses and Toxicology Adjunct professor, Emory University, Department of Pathology	Rapporteur
Nathalie Mantel Responsable d'unité, Sanofi Pasteur, Virologie Recherche	Examinatrice
Jessica Quintin Chargée de recherche, Institut Pasteur, Département de mycologie	Examinatrice
Anne-Sophie Beignon Chargée de recherche, CEA / Inserm / Université Paris-Saclay, IDMIT / IMVA	Directrice de thèse

Thèse de doctorat

La vie est ton navire et non pas ta demeure.

Alphonse de Lamartine

A tous mes proches,

Acknowledgments/Remerciements

Je profite de ces quelques lignes (ou plutôt quelques pages) pour remercier l'ensemble des personnes, qui de près ou de loin, directement ou indirectement, ont participé à l'aboutissement de ce projet. Je pense à tous mes collègues, amis et famille qui par leur présence, leurs conseils et leur soutien m'ont permis de mener à bien cette thèse. Je tiens à tous vous dire merci du fond du cœur.

En premier lieu, j'aimerais adresser de profonds remerciements à tous mes collègues de travail avec qui j'ai eu le plaisir de partager ces trois dernières années.

J'aimerais particulièrement remercier ma directrice de thèse Anne-Sophie Beignon pour son encadrement et son soutien pendant mes stages de master et les trois années de thèse qui ont suivi. Un grand merci pour sa constante positivité, sa réflexion scientifique et son écoute des autres, qui m'ont permis de développer plus avant ma curiosité scientifique et me lancer dans ce projet. Merci également pour tous les congrès internationaux auquel j'ai eu la chance de pouvoir participer et qui ont contribué à forger ce projet.

Je voudrais remercier le directeur d'IDMIT, Roger Le Grand, qui a accepté ma candidature en stage dans la laboratoire et m'a fait rencontrer Anne-Sophie. Merci également pour tous les conseils scientifiques.

J'aimerais aussi adresser un mot de remerciement aux membres de mon jury qui ont accepté d'évaluer mes travaux de thèses et pour toutes les discussions constructives lors de la soutenance. Merci à Marc Dalod (également pour son évaluation de ma mi-thèse), Helder Nakaya, Isabelle Schwartz-Cornil, Nathalie Mantel et Jessica Quintin.

J'adresse également un immense remerciement à Nicolas Tchitchek qui m'a fait redécouvrir la bio-informatique, pour ses suggestions constructives face à tous les problèmes, que ce soit dans les conceptions algorithmiques, ou la génération au pied levé d'un site web interactif, sans oublier son moral d'acier à toute épreuve (on ne lâche rien !).

Je remercie aussi tous les membres, présents et passés, du groupe d'Anne-Sophie, qui ont participé à la réalisation du projet ImMemory de recherche sur l'immunité vaccinale dans lequel s'est inscrite ma thèse. Un grand merci à David, André, Simon, Inana, Malvina, Hadjer, Gaëlle et Yanis.

J'aimerais remercier mes co-bureaux depuis trois ans, Julien L., Sixtine et Laura L., les doctorants avec qui j'ai eu la chance de vivre cette expérience de thèse, Candie, Cindy, Karunasinee alias Mo, Pierre, Lamine, Samuel, Adrien L.-P., André, Mélis, Néla, Margaux, Matthieu et Thibaut, et tous ceux dont j'ai partagé le quotidien, Fanny, Marco, Laetitia B., Julie, Sophie B., Oscar, Ernesto (merci aussi pour le covoiturage !), Mario, Mylinda, Julien D., Rahima, Anna L., Quentin, Jamila, François, Brice, Salomé, Jean-Jacques, Nicolas G., Florian, Antoine, Diego, Mohammad, Sabine, Sophie L., Jérôme, Karine, Claude, Marie-Thérèse, Natalia, Stéphane, Louis, Yanis, Maxime E., Mathilde, Laetitia V. et Nastasia. Merci à tous pour votre présence, votre soutien, toutes les discussions et tous les moments passés ensemble. Sans vous cette thèse n'aurait pas été la même, vous avez permis de rendre ces années inoubliables.

Je voudrais aussi adresser mes remerciements à tous ceux qui m'ont aidé que ce soit par des discussions scientifiques, par la gestion de l'expérimentation animale, des systèmes informatiques (merci BatLab !) ou des formulations d'anglais. Merci à Oscar, Benoît F., Elisabeth, Frédéric M., Frédéric D., Brice, Jamila, Nadia, Antonio, Pauline, Romain, Vanessa, Delphine, Nathalie, Pascal, Christophe, Raphaël, Benoît D., Sébastien, Jean-Marie, Francis, Maxime P., Nina et Emma.

Enfin, je remercie tous les membres d'IDMIT, qu'ils soient doctorants, post-doctorants, directeurs d'étude, techniciens, ingénieurs, vétérinaires, commerciaux, stagiaires, maîtres de conférence, chargés de recherche, directeurs de recherche, ingénieurs-chercheurs..., qui font de ce laboratoire ce qu'il est aujourd'hui. Merci de créer ce cadre de travail et de vie unique qui a rendu cette thèse possible.

J'aimerais remercier aussi tous mes collègues enseignants de la faculté de Châtenay-Malabry, pour m'avoir fait découvrir le métier d'enseignant-chercheur. Merci en particulier à Audrey, Dorine, Marion, Eva, Damien G. et Clémence pour leur accueil au 5ème étage et pour tous les moments passés ensemble à côté des TP et ED. Et merci également à tous les étudiants que j'ai eu en cours sans qui cette expérience d'enseignement n'aurait pas eu lieu.

Parce qu'à côté du travail de thèse, l'environnement et la vie hors laboratoire sont aussi importants, j'aimerais adresser quelques mots à mes amis pour leur soutien, leurs attentions et tous les moments vécus au cours non seulement de ces trois années mais aussi de toutes celles qui ont précédé.

Je voulais remercier Flora, Sandrine, Damien H., Yoann, Nadège et Guillaume pour toutes les après-midi et soirées jeux de société et cartes, accompagnées de thé, crêpes, gaufres... sans oublier une dose incommensurable de bonne humeur. Merci pour tous ces moments précieux au cours de ces dernières années !

J'aimerais remercier Aaron, Laura V., Hadrien et Anna P. pour toutes les excursions à Bordeaux (et les soirées Frog and Rosbif !), sans oublier les délicieuses tortillas y paellas españolas.

Je voudrais aussi remercier Léane pour toutes les sorties en Bourgogne et dans la campagne lyonnaise.

J'aimerais également remercier Adrien S. pour son soutien pendant toutes ces années et tous les moments passés en Auvergne.

Enfin, je voudrais remercier toute ma famille, pour ces moments partagés, que ce soit au cours d'évènements particuliers (mariage, baptême, Noël, cousinades...), ou simplement du quotidien, pour toutes les bonnes ondes que vous n'hésitez pas à partager. Merci pour tout ce que vous apportez.

Plus particulièrement, j'aimerais remercier mes frères, belle-sœurs et nièces, Marc, Sienna, Vincent, Clara, Méryl et Nora, pour tous les moments conviviaux partagés ensemble, pour le soutien que vous m'avez toujours apporté malgré les kilomètres qui ont pu nous éloigner.

Merci à Ghislain pour la découverte des Monts d'Or, du Beaujolais et des Dombes. Merci pour toutes les sorties randonnées, barbecues et méchouis. Merci pour tous ces moments passés ensemble.

Je voudrais aussi remercier mes parents. La liste de tout ce que vous m'avez apporté est trop longue pour tenir en quelques mots. Merci pour toutes ces années où vous m'avez accompagné et soutenu, merci d'avoir toujours cru en moi, merci pour toutes les valeurs humaines que vous m'avez transmises, merci pour tous ces moments infiniment précieux. Merci pour tout.

Enfin, un infini merci à Lise, mon amour, pour tous les moments que nous partageons, des excursions à travers le monde jusqu'aux instants du quotidiens que je chéris tout autant. Merci pour toutes tes attentions, pour ton soutien constant, merci de ta présence qui m'incite à toujours donner le meilleur de moi. Sans toi, rien n'aurait la même saveur. Notre aventure continue bientôt de l'autre côté de la Terre !

Contents

Table of contents

Acknowledgments **vii**

Contents **xi**
Table of contents . . . xi
List of figures . . . xiv
List of tables . . . xv

List of abbreviations **xvii**

Introduction **1**
Vaccination: principle, successes and current limits . . . 3
Innate immunity and vaccination . . . 10
Innate immune cells, an overview . . . 10
Innate cells as effector cells . . . 12
Recognition of pathogens . . . 12
Clearance of pathogens . . . 17
Innate cells as modulator cells . . . 22
Activation and shaping of adaptive immunity . . . 22
Modulation of innate cell effector functions by adaptive and innate immunity . . . 27
Resolution of inflammation . . . 29
Memory within innate immunity . . . 32
Trained innate myeloid cells . . . 32
“Memory“ NK cells . . . 35
Hypotheses and aims of the project . . . 38

Part I.
Methodology **41**

Chapter 1. Experimental model and technologies used **43**
Animal model: cynomolgus macaque . . . 43
Animal models in immunology, towards the choice of non-human primate . 43
Mouse models . . . 43
Non human primate models . . . 46
Non human primate models and vaccination, an overview . . . 48
Cynomolgus macaques as a model among non human primates . . . 49
Vaccine model: modified vaccinia virus Ankara . . . 50
From vaccinia virus to a new smallpox vaccine . . . 50
Modified vaccinia virus Ankara: development and immunity . . . 52
Modified vaccinia virus Ankara as a vaccine vector . . . 54
Modified vaccinia virus Ankara as vaccine model in the project . . . 55
Main experimental technology: mass cytometry . . . 56
The requirement of single-cell measurement . . . 56
Proteomics *vs.* transcriptomics: pros and cons . . . 58
Mass cytometry as the main analysis technics . . . 59
Toward a systems immunology approach . . . 62
Bioinformatic tools are required for mass cytometry data exploration . . . 62
viSNE *vs.* SPADE algorithm, pros and cons . . . 63
viSNE: visualization of t-distributed stochastic neighbor embedding results . . . 63
SPADE: spanning-tree progression analysis of density normalized events . . . 66
Multi-dimensional analysis tools . . . 69
Experimental approach, summary . . . 71

Chapter 2. Validation of the experimental model: comparison of blood innate immune cells in human and cynomolgus macaques **75**
Overview . . . 75
"In Depth Comparative Phenotyping of Blood Innate Myeloid Leukocytes from Healthy Humans and Macaques Using Mass Cytometry" . . . 77

Part II.
Innate responses induced by a prime-boost vaccination following a classical vaccination schedule **93**

Chapter 3. Innate myeloid responses after a prime-boost vaccination following a classical schedule **95**
Overview . . . 95
"Prime and Boost Vaccination Elicit a Distinct Innate Myeloid Cell Immune Response" . . . 99

Chapter 4. NK cell responses after a prime-boost vaccination following a classical schedule 119
Overview . . . 119
"NK cell immune responses differ after prime and boost vaccination" . . . 122

Part III.
Impact of a shortened delay between prime and boost on vaccine-induced immune responses 143

Chapter 5. Innate myeloid cell responses during an early boost vaccination schedule and correlation with adaptive immune memory 145
Overview . . . 145
"The timing of vaccine boosting regulates the induction of memory innate myeloid cells and the quality of the secondary antibody response" . . . 149

Chapter 6. NK cell responses during an early boost vaccination schedule and correlation with adaptive immune memory 223
Overview . . . 223
"Boost vaccination timing impacts the quality of NK cell response, which correlates with a differential humoral response" . . . 225

Conclusions and perspectives 271
Results summary . . . 273
Opened questions . . . 277
Innate and cellular adaptive immunity interactions . . . 277
NK cell phenotyping . . . 278
Innate immune memory duration . . . 279
Enhanced functions of "likely trained" cells and adaptive immunity activation 281
"Likely trained" innate immune cell ontogeny . . . 282
Innate immune training related pathways . . . 285
Overtraining and innate immune exhaustion . . . 286
Impact of the immunization route . . . 287
Vaccine efficacy assessment . . . 288
Harnessing innate immune training to improve vaccine design . . . 289
Concluding remarks . . . 291

References 293

Appendix 349

French resume 351

List of figures

1 Principle of vaccination. . . . 4
2 Overview of vaccination impact on public health nowadays. . . . 7
3 Rationale for prime-boost strategy. . . . 9
4 Classical hematopoiesis overview. . . . 11
5 A wide range of receptors directly recognizing pathogen/vaccine. 13
6 Indirect recognition of pathogen through antibody or complement binding. . . . 15
7 Recognition of infected cell signature via MHC molecules. . . . 16
8 Signaling pathways activated upon PRR interaction with its ligands. . . . 18
9 Signaling pathways activated upon indirect pathogen recognition. 19
10 Signaling pathways activated upon NK receptor engagement. . . . 20
11 Consequences of innate immune cells activation by pathogens or vaccines. . . . 21
12 Activation of T cells by innate immune cells. . . . 25
13 Overview of direct anti-pathogen activity of adaptive response. . 26
14 Scheme of crosstalk between innate and adaptive immunity resulting in pathogen clearance. . . . 28
15 Integrated scheme of inflammation resolution. . . . 31
16 Current view of trained immunity in vaccination. . . . 34
17 Diverse populations within "memory" NK cells. . . . 37
18 Graphical abstract of the project aims. . . . 39

19 Phylogenetic tree of mammals. . . . 45
20 Non-human primates mirror human diseases. . . . 47
21 Poxvirus viral cycle. . . . 51
22 MVA sensing by the immune system. . . . 53
23 Principle of mass cytometry. . . . 59
24 Representation of the high dimensionality generated by mass cytometry. . . . 62
25 Examples of viSNE representation. . . . 64
26 The SPADE algorithm. . . . 68
27 Main data representations from the packages developed and used in this project. . . . 70
28 Experimental strategy. . . . 72

29 Characterization of innate responses after prime and boost with respect to vaccine schedule. . . . 275
30 Associations between innate responses and adaptive responses. . . 276
31 Potential impact of a late boost on the resulting immune response. 280
32 Generation of trained innate immune cells. . . . 283
33 Harnessing vaccine-induced training to optimize vaccines. . . . 290

List of tables

1 **Current vaccines.** 6

2 **Main technologies available to decipher vaccine-induced immune response.** 57

3 **High-dimensional technologies to study NK cell compartment.** . 278

List of abbreviations

ADCC: antibody dependent cell cytotoxicity
ADCP: antibody dependent cell phagocytosis
AIDS: acquired immune deficiency syndrome
ANRS: French agency for research on AIDS and viral hepatitis
APC: antigen-presenting cell
APRIL: A proliferation-inducing ligand
BCG: bacillus Calmette-Guérin
BCR: B cell receptor
CCL: chemokine (C-C motif) ligand
CCR: chemokine (C-C motif) receptor
CD: cluster of differentiation
cDC: classical DC
CEV: cell-associated enveloped virus
cGAS: cyclic guanosine monophosphate adenosine monophosphate synthase
CHIKV: chikungunya virus
CITE-seq: cellular indexing of transcriptomes and epitopes by sequencing
CLP: common lymphoid progenitor
CMP: common myeloid progenitor
CR: complement receptor
CXCL: chemokine (C-X-C motif) ligand
CXCR: chemokine (C-X-C motif) receptor
CyTOF: cytometry by time of flight
DAMP: damage/danger associated molecular pattern
DC: dendritic cell
DCIR: dendritic cell immunoreceptor
DC-SIGN: dendritic cell-specific intracellular adhesion molecule-3-grabbing non-integrin
DDA: dimethyldioctadecylammonium
DENV: dengue virus
DNA: desoxyribonucleic acid
ds: double-stranded
EBV: Epstein-Barr virus
EEV: extracellular enveloped virus
Fc: constant fraction

FoxP3: forkhead box 3
GAG: glycosaminoglycan
GBV-B: hepatitis G virus B /GB-virus B
GMP: granulocyte-monocyte progenitor
HCMV: human cytomegalovirus
HBV: hepatitis B virus
HCV: hepatitis C virus
HEV: hepatitis E virus
HIV: human immunodeficiency virus
HLA: human leukocyte antigen
HSC: hematopoietic stem cell
iC3b: inactive complement molecule C3b
iE-DAP: D-glutamyl-meso-diaminopimelic acid
IEV: intracellular enveloped virus
IFN: interferon
Ig: immunoglobulin
IL: interleukin
ILC: innate lymphoid cell
IMV: intracellular mature virus
IP-10: interferon gamma-induced protein 10 (alternative name: CXCL10)
ITAM: immunoreceptor tyrosine-based activating motif
ITIM: immunoreceptor tyrosine-based inhibitory motif
KLRG1: killer-cell lectin like receptor G1
KSHV: Kaposi's sarcoma associated herpes virus
LabEx: French laboratory of excellence
LAPV: live-attenuated pertussis vaccine
LASSO: least absolute shrinkage and selection operator
LDA: linear discriminant analysis
LGP2: laboratory of genetics and physiology 2
LPS: lipopolysaccharide
LRR: leucine rich repeat
MCMV: murine cytomegalovirus
MCP-1: monocyte chemoattractant protein 1 (alternative name: CCL2)
MDA5: melanoma differentiation-associated protein 5
MDSC: myeloid-drived suppressor cell
MDP: muramyldipeptide
MEP: megakariocyte-erythrocyte progenitor
MHC: major histocompatibility complex
Mincle: macrophage inducible Ca^{2+}-dependent lectin receptor
MIP: monocyte inflammatory protein
MPLA: monophosphoryl lipid A
mTOR: mechanistic target of rapamycin
MSI: mean signal intensity
MVA: modified vaccinia virus Ankara
NACHT: neuronal apoptosis inhibitor protein MHC class 2 transcription activator incompatibility locus protein from Podospora anserina telomerase-associated protein
NALP: NACHT, LRR and PYD containing domain

NET: neutrophil extra-cellular trap
NHP: non human primate
NK: natural killer
NKG2: Natural killer cell protein group
NLRP: NOD-like receptor family pyrin domain containing
NOD: nucleotide-binding oligomerization domain-containing protein
oxLDL: oxidized low-density lipoprotein
PAMP: pathogen associated molecular pattern
PBMC: peripheral blood mononuclear cell
pDC: plasmacytoid DC
PFU: plaque-forming unit
poly(I:C): polyinosinic-polycytidilic acid
PRR: pattern recognition receptor
PYD: pyrin domain
REAP-seq: RNA expression and protein sequencing assay
RhCMV: rhesus cytomegalovirus
RhLCV: rhesus lymphocryptovirus
RIG-I: retinoic acid-inducible gene I
RNA: ribonucleic acid
RNAseq: RNA sequencing
ROS: reactive oxygen species
RRV: rhesus macaque rhadinovirus
sCD40L: soluble CD40 ligand
SHIV: simian/human immunodeficiency virus
SIV: simian immunodeficiency virus
SPADE: spanning-tree progression analysis of density normalized events
ss: single-stranded
stHIV: simian tropic HIV
SVV: simian varicella virus
Tcm: central memory T cell
TCR: T cell receptor
Tem: effector T cell
Tfh: follicular helper T cell
TGF: transforming growth factor
Th: helper T cell
TLR: Toll-like receptor
TNF: tumor necrosis factor
Treg: regulatory T cell
TRIM: tripartite motif
VACV: vaccinia virus
VEGF: vascular endothelial growth factor
VIGIV: vaccinia immune globulin intravenous (human)
viSNE: visualization of t-distributed stochastic neighbor embedding algorithm
VZV: varicella-zoster virus
WHO: world health organization
YFV: yellow fever virus
ZIKV: zika virus

Introduction

Introduction

Vaccination: principle, successes and current limits

Vaccination, as defined by the World Health Organization, consists of the injection of any biological that enhances immunity toward a given disease. It relies on the ability of the immune system to remember previous encounters with a given pathogen, the so-called immune memory. As a consequence, the immune system can react more rapidly and efficiently at the next pathogen encounter, which usually prevents the disease to occur. This also impedes the transmission of the disease from person to person and thus also ensures group protection at the public health level (**Figure 1**). That is why vaccination was described as one of the main advances ever made along with access to clean water, sanitation and antibiotics discovery (Greenwood, 2014; Rappuoli et al., 2014).

Examples of vaccination can be found several centuries ago, with reports of inoculation of extract of smallpox sore into healthy people, a relatively unsafe process (potentially lethal) called variolation, which could reduce risks of infection but also propagate the disease. Such processes were still widely in use in the middle 18th century (Greenwood, 2014; Rappuoli et al., 2014). The field of vaccination knew a massive expansion with the work of Jenner in 1796 who immunized people with animal poxviruses that cause very mild symptoms in humans, but prevented them to develop the much more severe smallpox (Tognotti, 2010; Plotkin, 2014). A century after, in 1880, Louis Pasteur successfully inoculated dead/attenuated pathogens and prevented infection in the animals and humans inoculated. He notably developed the first vaccine against rabies. Afterwards, with the progresses made in molecular biology, recombinant vaccines were designed, consisting of purified proteins associated with adjuvants molecules designed to elicit a sufficiently intense inflammation. This technics notably led to the development of the first hepatitis B vaccine (Plotkin, 2014).

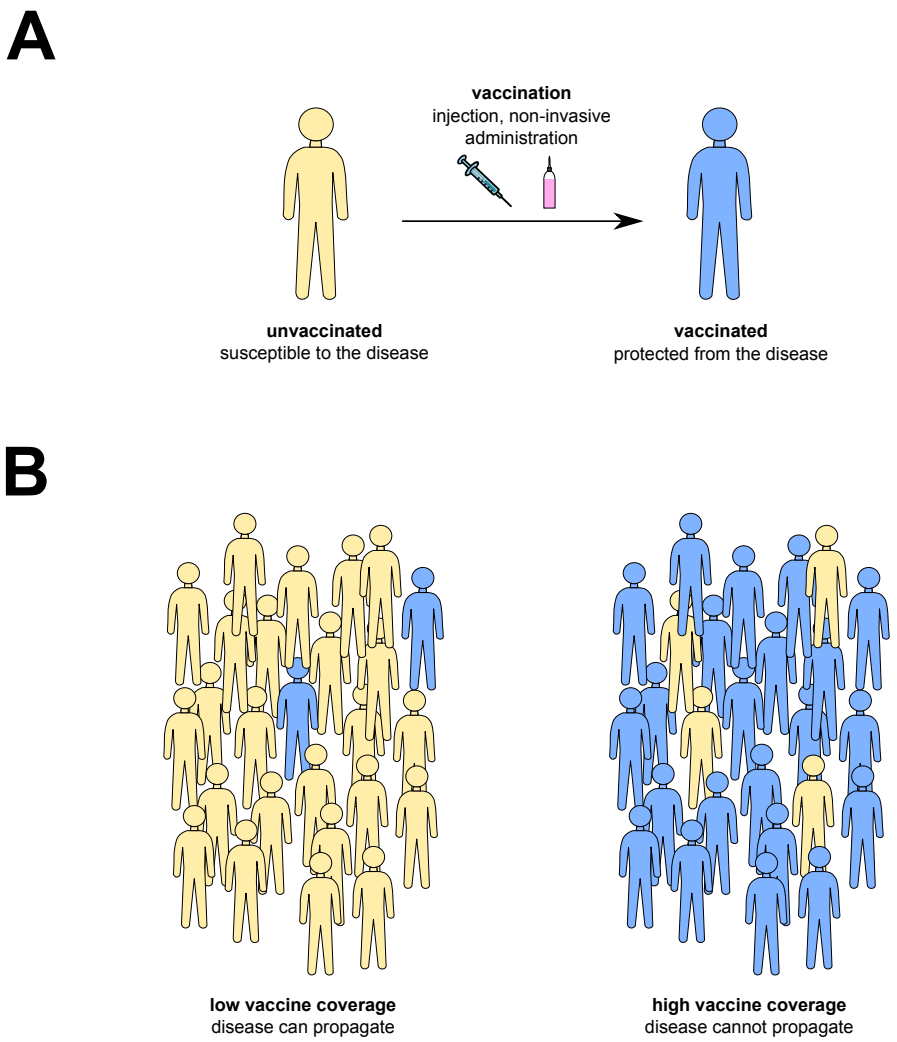

Figure 1. **Principle of vaccination.** Vaccination induces protection at **(A)** the individual level and **(B)** the population level, called herd immunity.

Nowadays, 26 vaccines are referenced by the WHO (including phase III vaccine trials) to prevent a wide variety of pathogens and diseases: cholera, dengue, diphteria, hepatitis A, B and E, *Haemophilus influenzae* B, human papillomavirus, influenza viruses, japanese encephalitis, malaria, measles, menincogoccal meningitis, mumps, pertussis, pneumococcal disease, poliomyelitis, rabies, rotavirus, rubella, tetanus, tick-borne encephalitis, tuberculosis, typhoid fever, chickenpox/shingles and yellow fever (**Table 1**). They consist either of live-attenuated micro-organisms (*e.g.* yellow fever virus vaccine), inactivated micro-organisms (*e.g.* inactivated poliovirus vaccine), recombinant microbe proteins with adjuvants (*e.g.*. hepatitis B virus vaccine), or toxoids –non toxic modified toxins– (*e.g.* diphteria vaccine).

Great successes were met in the past decades, with the eradication of smallpox in 1980 (WHO), the near-eradication of poliomyelitis (99% reduction of cases, with 29 cases reported to WHO in 2018), or the drastic reduction of cases of measles in the past decades (from around 4,000,000 deaths in 1980 *vs.* less than 100,000 deaths in the last few years) (**Figure 2A**). However, more than two centuries after the invention of the term vaccine, infectious diseases still remain one major threat to population with more than 10 million death every year (WHO). Vaccines are still lacking for many complex pathogens, including but not limited to, human immunodeficiency virus (HIV, causing the acquired immunodeficiency syndrome -AIDS), respiratory syncytial virus (RSV, causing neonatal bronchiolitis) or henipaviruses (causing lethal encephalitis). In addition, for some pathogens, existing vaccines are insufficiently efficient to allow for a good protection, such as influenza virus -seasonal flu (Wong & Webby, 2013; Sautto et al., 2018), mycobacterium tuberculosis –tuberculosis (Andersen & Doherty, 2005; Voss et al., 2018), dengue virus –dengue (McArthur et al., 2013; Bos et al., 2018), or Plasmodium –malaria (Snounou et al., 2005; Frimpong et al., 2018) (**Figure 2B**).

Difficulties to develop new vaccines can rely on the complexity of the pathogen itself, due to its ability to evade immune response (*e.g.* rapid genetic variation for HIV (Barouch, 2008), polymorphism of immunogenic antigen for Plasmodium (Hisaeda et al., 2005), genetic shift and drift for influenza viruses (van de Sandt et al., 2012)). But the main reason for this impediment in vaccine design is that despite decades of studies of the immune system and immune responses to pathogens, we are still nowadays far to completely understand all the aspects of the immune response.

For example, only few live vaccines (17D yellow fever virus vaccine and vaccinia virus smallpox vaccine) elicit a life-lasting immune protection (Amanna et al., 2007; Wrammert et al., 2009), while most vaccines, including live-attenuated (*e. g.* measles and mumps vaccine), inactivated (*e.g.* rabies virus vaccine) and recombinant (*e. g.* hepatitis B) vaccines require several injections to develop a long-lasting protection in most people –a first immunization called prime and latter ones called boost(s) (Ramshaw & Ramsay, 2000; Woodland, 2004). The sole prime can induce a short-lasting and/or only partial protection from the disease (**Figure 3A**). In addition, since responses to vaccines differ between individuals, prime may only induce a protective immunity in a fraction of the population (**Figure 3B**). Overall prime-boost strategies aim to enhance individual response by recalling a primary immune memory, and enhance the frequency of vaccine responders among the population, to ensure protection from the disease at both level.

Determination of the best vaccination schedule is still empirically defined, based on clinical trials that may miss the optimal settings. For example the schedule reported by WHO for diphteria, tetanus, poliomyelitis and pertussis combination vaccine is 2, 4, and 11 months old in France, 2, 3, 4 and 15 months in Belgium, and 2, 4, 6, 15-24 months old in Switzerland, but we miss an objective argumentation to rationally choose any of these schedules.

Table 1. Current vaccines.

Disease and main pathogen targeted	Type of vaccine	Limitations
Cholera *Vibrio cholerae*	inactivated bacterium	-
Dengue Dengue virus	live-attenuated viral vector YFV-based	recommended only for individuals with pre-existing immunity against DENV
Diphteria *Corynebacterium diphtheriae*	toxoid	-
Viral hepatitis Hepatitis A virus	inactivated or live-attenuated virus	-
Viral hepatitis Hepatitis B virus	recombinant protein	-
Viral hepatitis Hepatitis E virus	recombinant protein	-
Bacterial pneumonia/meningitis *Haemophilus influenzae B*	recombinant saccharide	-
Viral genital cancers Human papillomavirus	recombinant protein	-
Flu Influenza virus	inactivated virus	low efficiency (around 50% each year)
Japanese encephalitis Japanese encephalitis virus	inactivated or live-attenuated virus	-
Malaria *Plasmodium falciparum*	recombinant protein	short-term and partial protection
Measles Measles virus	live-attenuated virus	-
Bacterial meningitis *Neisseria meningitidis*	recombinant saccharide	-
Mumps Mumps virus	live-attenuated virus	-
Whooping cough *Bordetella pertussis*	inactivated bacterium or recombinant protein	prevention of the symptoms but not infection (recombinant vaccine)
Pneumococcal diseases *Streptococcus pneumoniae*	recombinant protein	-
Poliomyelitis Poliomyelitis virus	inactivated or live-attenuated virus	rare paralysis with the live-attenuated vaccine
Rabies Rabies virus	inactivated virus	-
Viral diarrhea Rotavirus	live-attenuated virus	-
Rubella Rubella virus	live-attenuated virus	-
Tetanus *Clostridium tetani*	toxoid	-
Tick-borne encephalitis Tick-borne encephalitis virus	inactivated virus	-
Tuberculosis *Mycobacterium tuberculosis*	live-attenuated bacterium	poor protection against adult pulmonary disease
Typhoid fever *Salmonella typhi*	live-attenuated bacterium or recombinant saccharides	-
Yellow fever Yellow fever virus	live-attenuated virus	-

Currently available vaccines, as reported by the WHO, are provided. The type of the vaccine (live-attenuated, inactivated, recombinant or toxoid) is also indicated. DENV: dengue virus. MPLA: monophosphoryl lipid A. YFV: yellow fever virus.

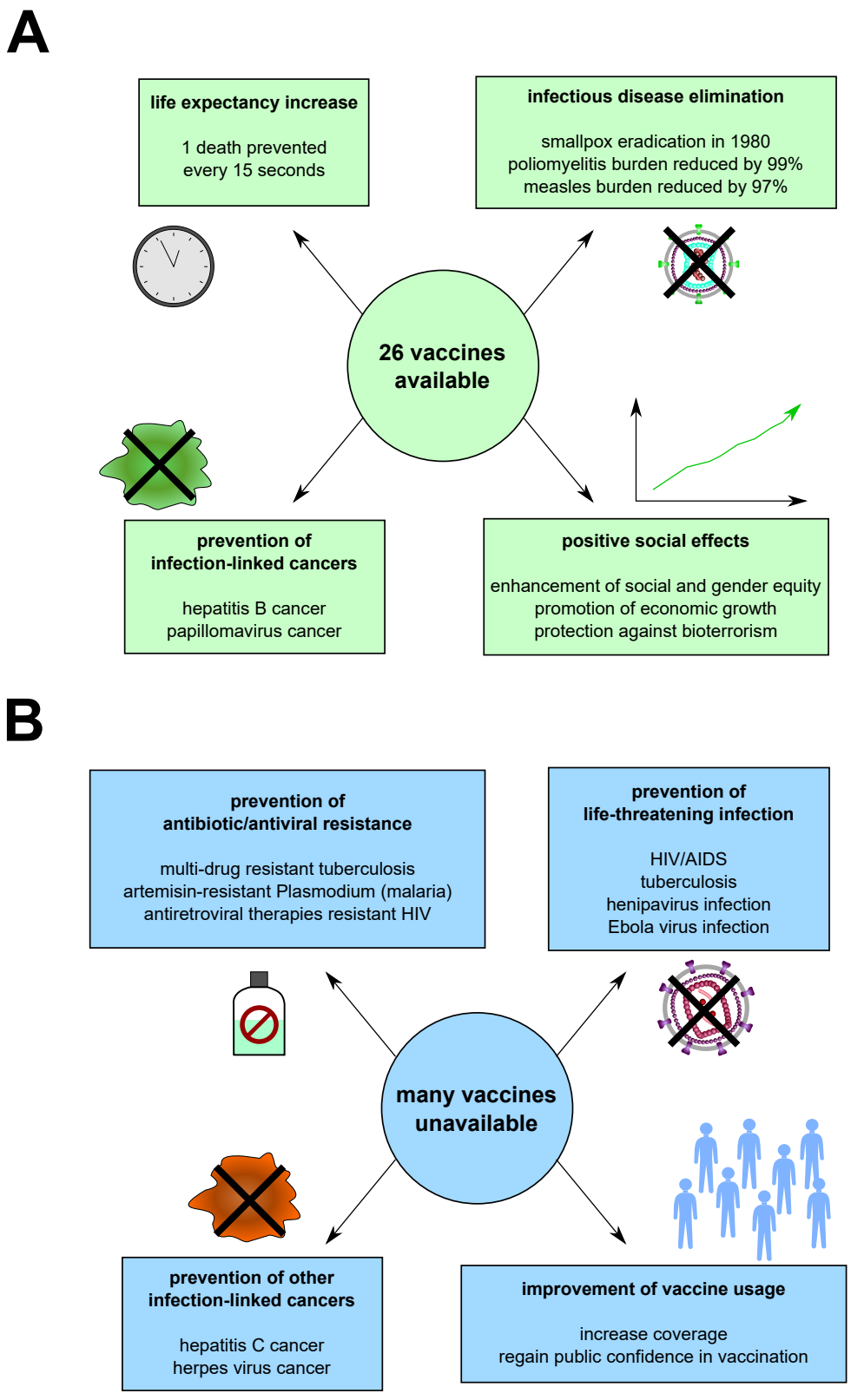

Figure 2. Overview of vaccination impact on public health nowadays. Current successes **(A)** and unmet challenges **(B)** of vaccination, based on WHO estimations, are represented.

This sheds light on the fact that despite decades of studies on vaccine-induced response, we still miss the complete picture and are unable to capitalize our current knowledge in simple parameters that vaccinologists could use to modulate immunity (*e.g.* route of immunization, type of antigens, number of injections, delay between each injection...). Going further into the rational design of vaccine requires a better characterization of the initial trigger of vaccine-induced immune response, the innate immunity, and how this impacts the adaptive immune response that is known to mediate memory.

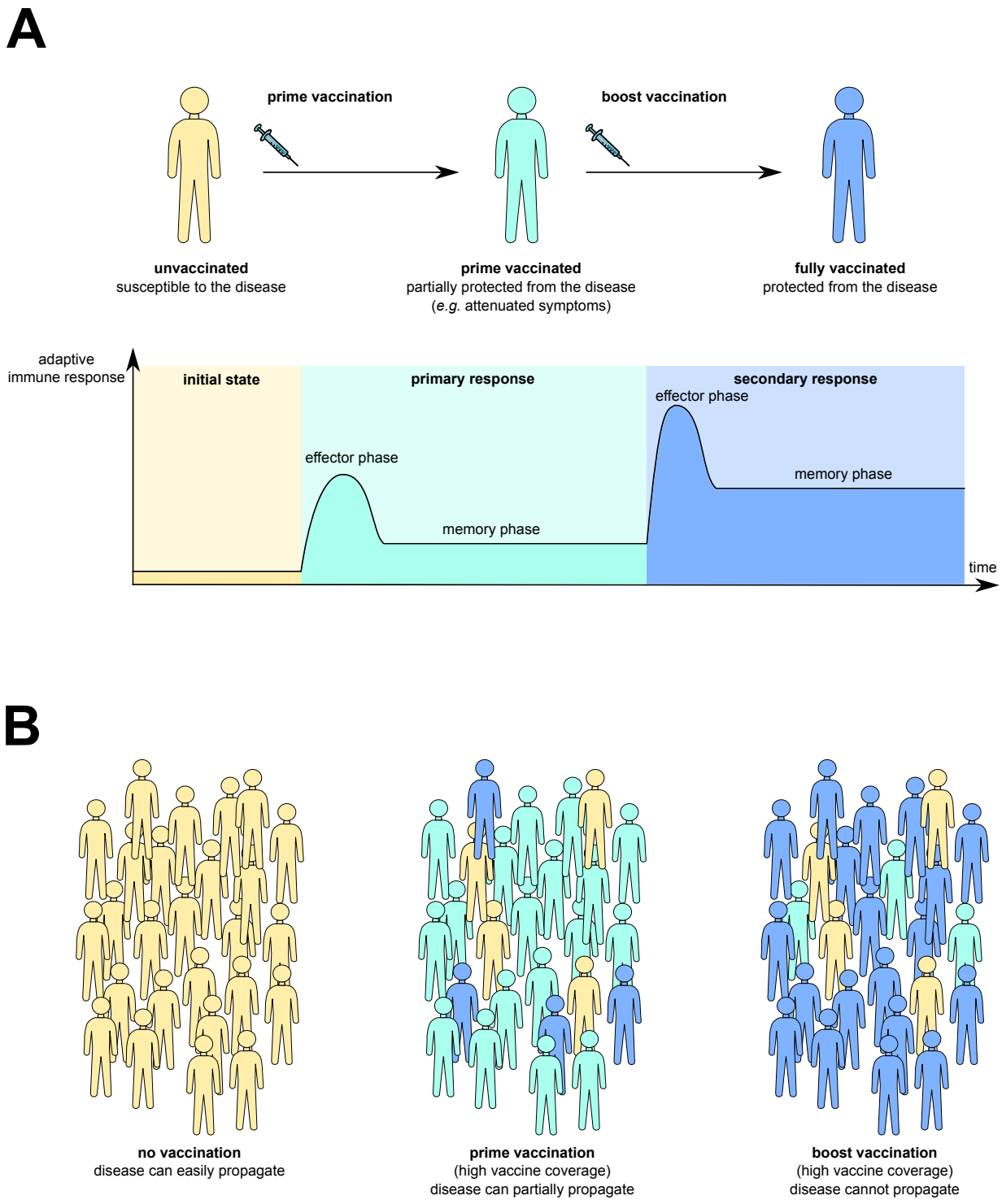

Figure 3. Rationale for prime-boost strategy. **(A)** Impact of prime-boost at individual level. Prime vaccination induces a primary memory, which can be only partially protective, whereas boost vaccination recalls the primary memory, giving rise to a secondary immune memory that is likely more protective. **(B)** Impact of prime-boost strategy at the population level. Prime vaccination results in only a fraction of the population that is fully protected from the disease, whereas after boosting, individuals whose primary immune memory was not fully protective developed a protective secondary immune memory.

Innate immunity and vaccination

Innate immune cells, an overview

Vaccines are designed to mimic at most the infection of pathogen, including the triggering of a strong and robust immune response, but obviously without the pathogenicity associated with the pathogen. As a consequence, the detection of a vaccine follows similar pathways as a pathogen, including the recognition by innate immune cells.

Innate immunity is composed of a wide range of cells, including both myeloid and lymphoid ones. They essentially arise from bone marrow hematopoiesis (Orkin & Zon, 2008; Laurenti & Göttgens, 2018), although some new cell generation can also occur in other organs, including yolk sac during development and adult liver (Taniguchi et al., 1996; Palis & Yoder, 2001; Yamamoto et al., 2016) (**Figure 4**). Note that beyond the simplified overview represented here, several intermediate cells are involved in the generation of a wide range of fully differentiated immune cells, including a high plasticity potential of cell progenitors (Manz et al., 2001). In addition, the development of new recent technologies allowed to unveil an unprecedented heterogeneity among immune cell precursors, suggesting that immune cell development is likely more complex than what was initially thought (Perié & Duffy, 2016).

Innate immune cells share the ability to react rapidly upon pathogen infection or vaccine injection. They are often described as the first line of defense of the immune system, although non-immune cells (*e.g.* epithelial cells, fibroblasts) are actually the first to encounter pathogen in most cases. Overall, innate immune cells accomplished numerous functions.

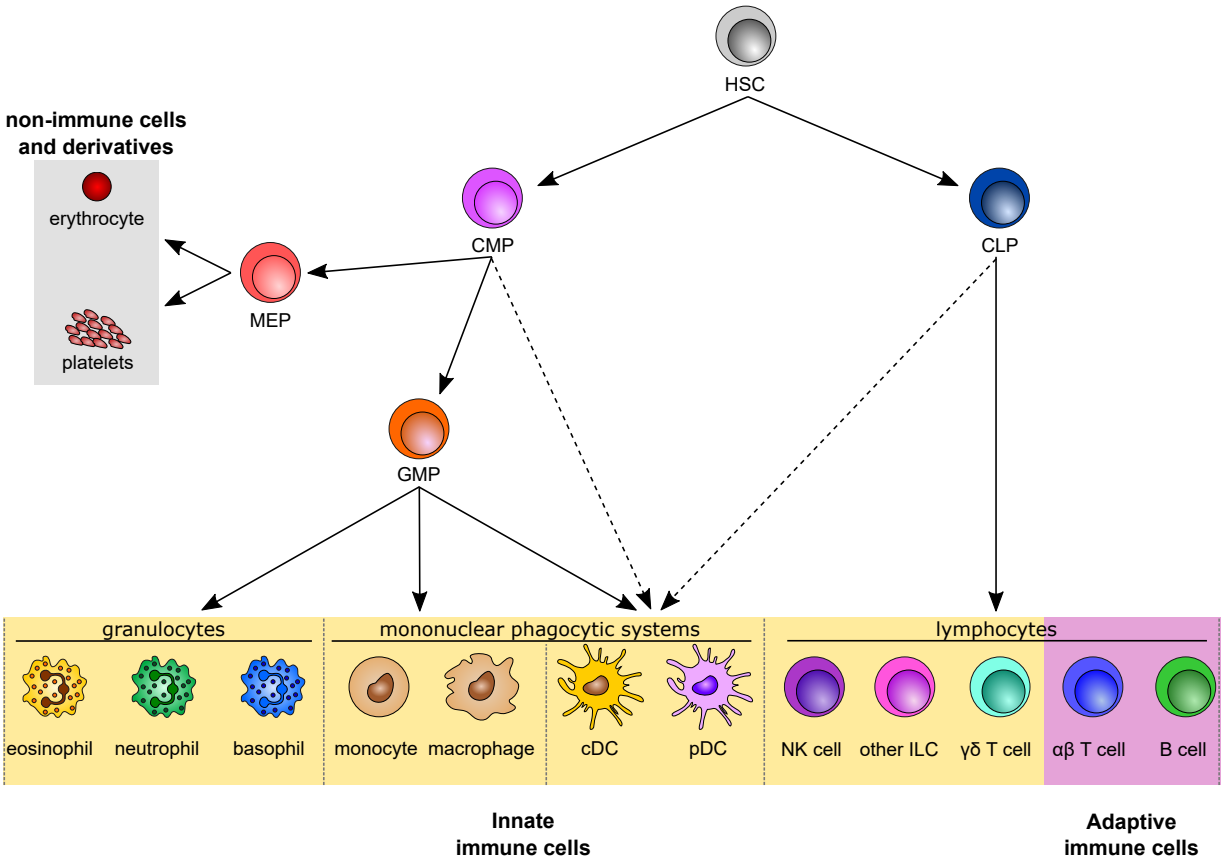

Figure 4. Classical hematopoiesis overview. A simplified overview of the generation of the major immune cell populations is displayed. Intermediate populations between the different progenitors and precursors are not represented, neither the heterogeneity within each progenitor population. Dotted arrows indicate suggested alternative differentiation pathways of DCs. Dotted lines separate each compartment (granulocytes, monocytes, DCs and lymphocytes). Innate and adaptive immune cells are highlighted in yellow and purple frames respectively. Non-immune cells and derivatives arising from hematopoiesis are highlighted in a gray frame. HSC: hematopoietic stem cell. CMP common myeloid progenitor. CLP: common lymphoid progenitor. MEP: megakaryocyte-erythrocyte progenitor. GMP: granulocyte-monocyte progenitor. DC: dendritic cell. cDC: classical DC. pDC: plasmacytoid DC. NK: natural killer. ILC: innate lymphoid cell.

Innate cells as effector cells

Recognition of pathogens

Once a pathogen or a vaccine enters the body, it can be directly recognized by receptors expressed by innate immune cells, but also non-immune cells, called pattern recognition receptors (PRR) (Takeuchi & Akira, 2010). These receptors can specifically recognize patterns associated with danger, damage or pathogen (Damage/Danger/Pathogen associated molecular pattern DAMP or PAMP). The list of PRR and associated DAMP/PAMP is wide and still growing (Akira et al., 2006; Takeuchi & Akira, 2010; Cai et al., 2014). We will here just give an overview of the main PRR triggering direct pathogen recognition (**Figure 5**).

Toll-like receptors (TLR) are transmembrane proteins recognizing several patterns associated with micro-organisms, including proteins (*e.g.* TLR2), saccharides (*e.g.* TLR4), or nucleic acids (*e.g.* single-stranded RNA and derived products -TLR7 and TLR8- or extra-nuclear DNA -TLR9) (Medzhitov, 2001; O'Neill et al., 2013; Tanji et al., 2015; Zhang et al., 2016; Ohto et al., 2018). RIG-like receptors (RLR) especially recognize double-stranded RNA (Reikine et al., 2014; Yoneyama et al., 2015; Hur, 2019). NOD-like receptors (NLR) are cytosolic receptors that can recognize peptidoglycans (*e.g.* NOD1), proteins (*e.g.* NLRP1), or nucleic acids (*e.g.* NLRP3) (Kanneganti et al., 2007; Franchi et al., 2009); mutations in NLR genes were recently linked with cancer progression (Saxena & Yeretssian, 2014). C-type lectin like receptors (CLR) mainly recognized sugars (*e.g.* mannose, β glucan) present in fungi, viruses, but also in auto-immune diseases, allergy or cancer (Dambuza & Brown, 2015; Saijo & Iwakura, 2011; Shrimpton et al., 2009; Lu et al., 2018). Finally the recently discovered cGAS protein can recognize cytosolic DNA dimers through a complex pathway (Sun et al., 2013; Wu et al., 2013; Li et al., 2013; Cai et al., 2014). It was also recently shown that it could detect HIV nuclear DNA, in cooperation with the NONO protein that targets a conserved region of the HIV capsid (Lahaye et al., 2018).

Since recognition by PRR is one the most initial events in immune response, it is a crucial event in vaccine-induced immune response. Actually, PRR can be targeted by vaccine adjuvants used with recombinant vaccines (which are not immunogenic enough by themselves, in contrast to live-attenuated vaccines), to elicit a strong immune response. For example, among adjuvants widely used in clinical development, poly(I:C) (polyinosinic-polycytidilic acid) and its derivatives activate TLR3 and RLRs, MPLA (monophosphoryl lipid A) activates TLR4, flagellin activates TLR5, imiquimol activates TLR7 and CpG containing oligonucleotides activate TLR9 (Coffman et al., 2010; Vasou et al., 2017). Note that the activation of distinct PRR trigger qualitatively different innate responses, as shown for TLR stimulation (Kwissa et al., 2012). Surprisingly, for alum, the most widely used adjuvant, it is not fully clear which receptor is at play, though NLRP3 inflammasome seems important (Coffman et al., 2010).

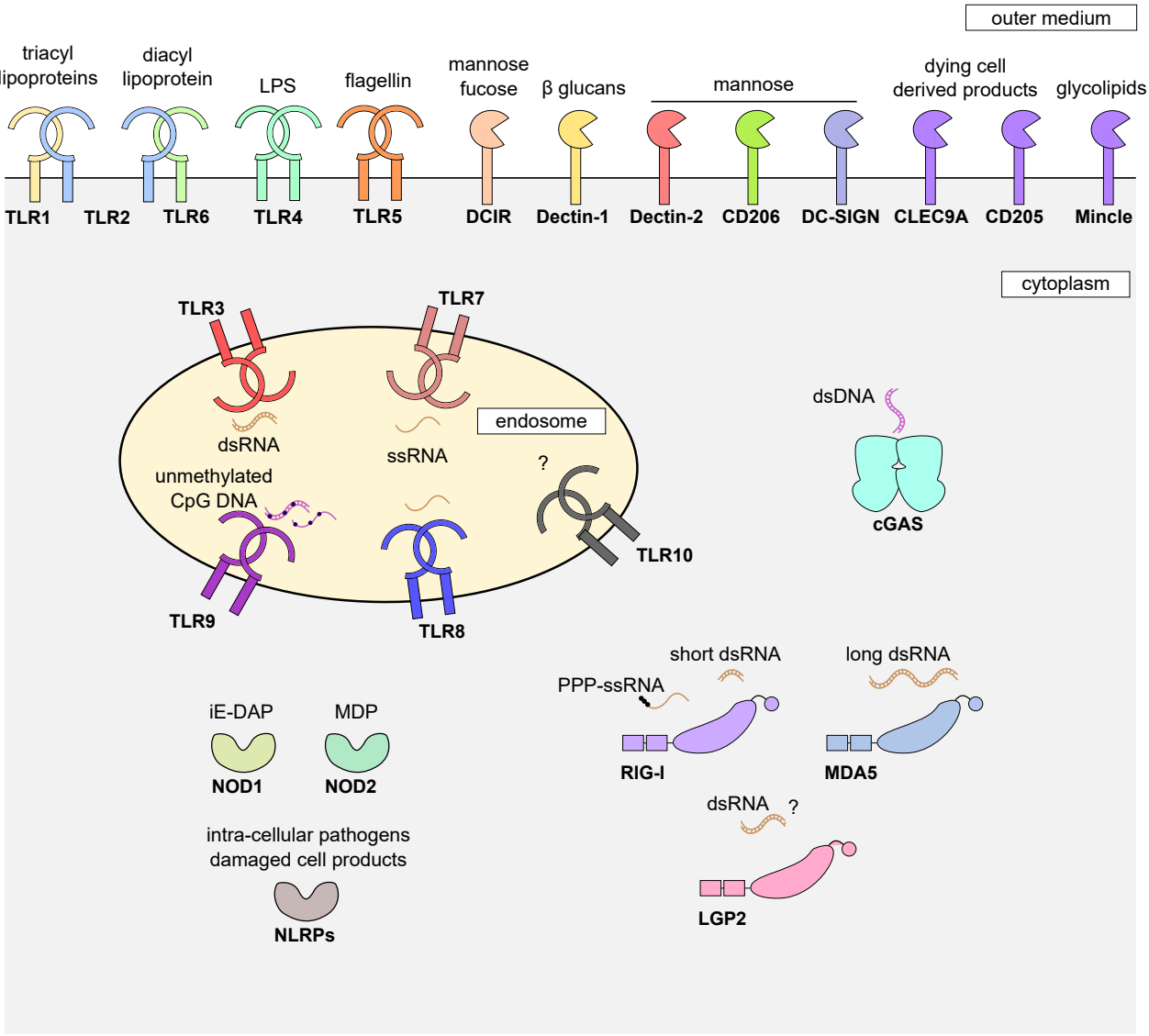

Figure 5. A wide range of receptors directly recognizing pathogen/vaccine. The main human pattern recognition receptors are represented with their cognate ligands, when known. TLR: Toll-like receptor. CD: cluster of differentiation. DCIR: dendritic cell immunoreceptor. DC-SIGN: dendritic cell-specific intracellular adhesion molecule-3-grabbing non-integrin. Mincle: macrophage inducible Ca^{2+}-dependent lectin receptor. cGAS: cyclic guanosine monophosphate adenosine monophosphate synthase. NOD: nucleotide-binding oligomerization domain-containing protein. NLRP: NOD-like receptor family pyrin domain containing. RIG-I: retinoic acid-inducible gene I. MDA5: melanoma differentiation-associated protein 5. LGP2: laboratory of genetics and physiology 2. LPS: lipopolysaccharide. ss: single-stranded. ds: double-stranded. iE-DAP: D-glutamyl-meso-diaminopimelic acid. MDP: muramyldipeptide.

In parallel, live-attenuated or dead pathogens used for vaccines are self-adjuvanted since they are strongly recognized by multiple PRRs. For example, yellow fever vaccine is recognized by TLR2, 7, 8 and 9 to trigger a robust immune response (Querec et al., 2006). Measles vaccine activate TLR2, 4, 5, 7 and 8, as well as RIG-I (Kennedy et al., 2012). Influenza vaccine is recognized by several PRRs including TLR3,7 and 8, RIG-I, NLRP3 inflammasome, as well as NLRs (Iwasaki & Pillai, 2014).

In addition to this direct PRR-mediated recognition, pathogens/vaccines can be detected through antibody-binding. Antibodies are immunoglobulin molecules synthesized by plasmablasts and plasma cells, which are specific to antigens. Following a previous encounter with the same pathogen/vaccine by the immune system, antibodies against the same pathogen/vaccine can be constitutively secreted in the body. They will thus bind to their target and stain the pathogen/vaccine for the innate immune cells. The recognition of these antibody-coated pathogen/vaccine is driven by so called Fc receptors (FcRs) that can recognize the constant fraction of antibodies, each receptors displaying its own specificity (in term of antibody classes) and affinity (Bruhns & Jönsson, 2015; Cho et al., 2006) (**Figure 6A**). An intra-cellular FcR, named TRIM21, which can recognize IgM and IgG was also identified (McEwan et al., 2013).

Besides, complement molecules, consist of proteins (constitutively present in the body, but inducible upon infection/vaccination) that activate themselves when bound to a pathogen or a vaccine, or an antibody-bound pathogen/vaccine, eventually leading to membrane disruption of the pathogen/vaccine (Merle et al., 2015a;b). Complement-bound pathogens can be recognized by so-called complement receptors (CR) expressed on immune and non-immune cells –*e.g.* erythrocytes expressing CR1 (Merle et al., 2015a; Dustin, 2016) (**Figure 6B**).

Note that infected cells can also be labelled by both antibodies and complement molecules, and produce DAMPs.

Eventually, the abnormal immune signature of infected cell can be detected (**Figure 7**). Indeed, all cells express molecules called major histocompatibility complex (MHC) of class I that carries peptides deriving from the degradation of the proteins expressed within the cells (Neefjes et al., 2011; Rock et al., 2016). Should the cell be infected then pathogen/vaccine protein derived peptides will be presented by MHC I molecules on cell surface. In addition non-classical MHC molecules induced by cellular stress (*e.g.* MICA, MICB) will be expressed on cell surface. The MHC signature can be detected by the CD8 T cells in the adaptive part of the immune system and the natural killer (NK) cells on the innate side of the immune system (Vivier et al., 2008; Neefjes et al., 2011; Campbell & Hasegawa, 2013; Rock et al., 2016). CD8 T cells are specific of a given MHC I bound antigen, which they recognize through their T cell receptor (TCR). By contrast, NK cells have a broader repertoire of ligands, MHC class I molecules as well as non-classical MHC molecules, that are recognized by several NK receptors, whose expression is highly stochastic among NK cells (Wilk & Blish, 2018). NK cells can also be activated by a downregulation of MHC molecules, which can be induced by infection.

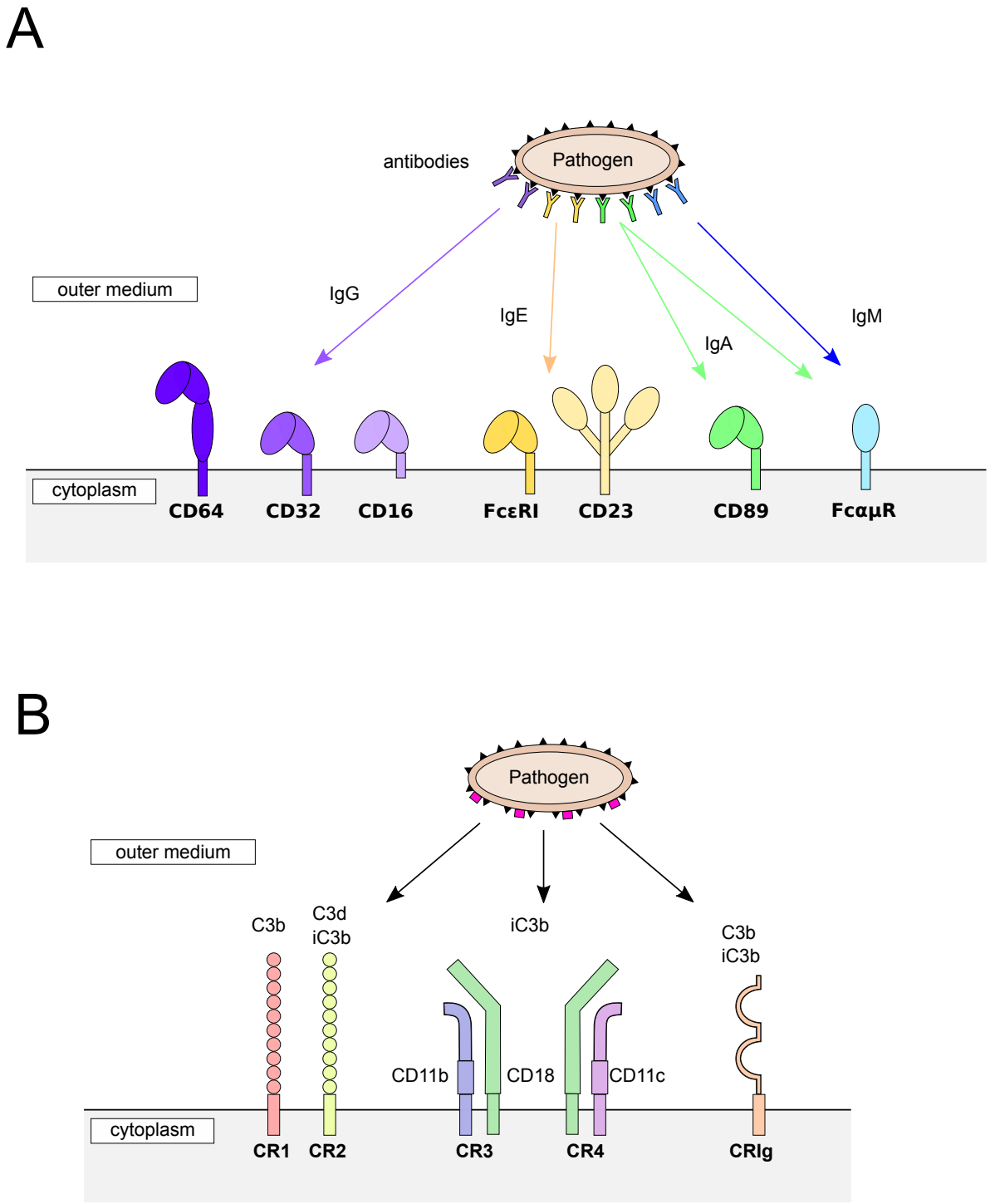

Figure 6. Indirect recognition of pathogen through antibody or complement binding. Mechanisms of indirect detection of pathogen via bound antibodies **(A)** or bound complement **(B)** is displayed. The main receptors are displayed in each panel. Fc: constant fraction. CD: cluster of differentiation. CR: complement receptor. iC3b: inactive C3b.

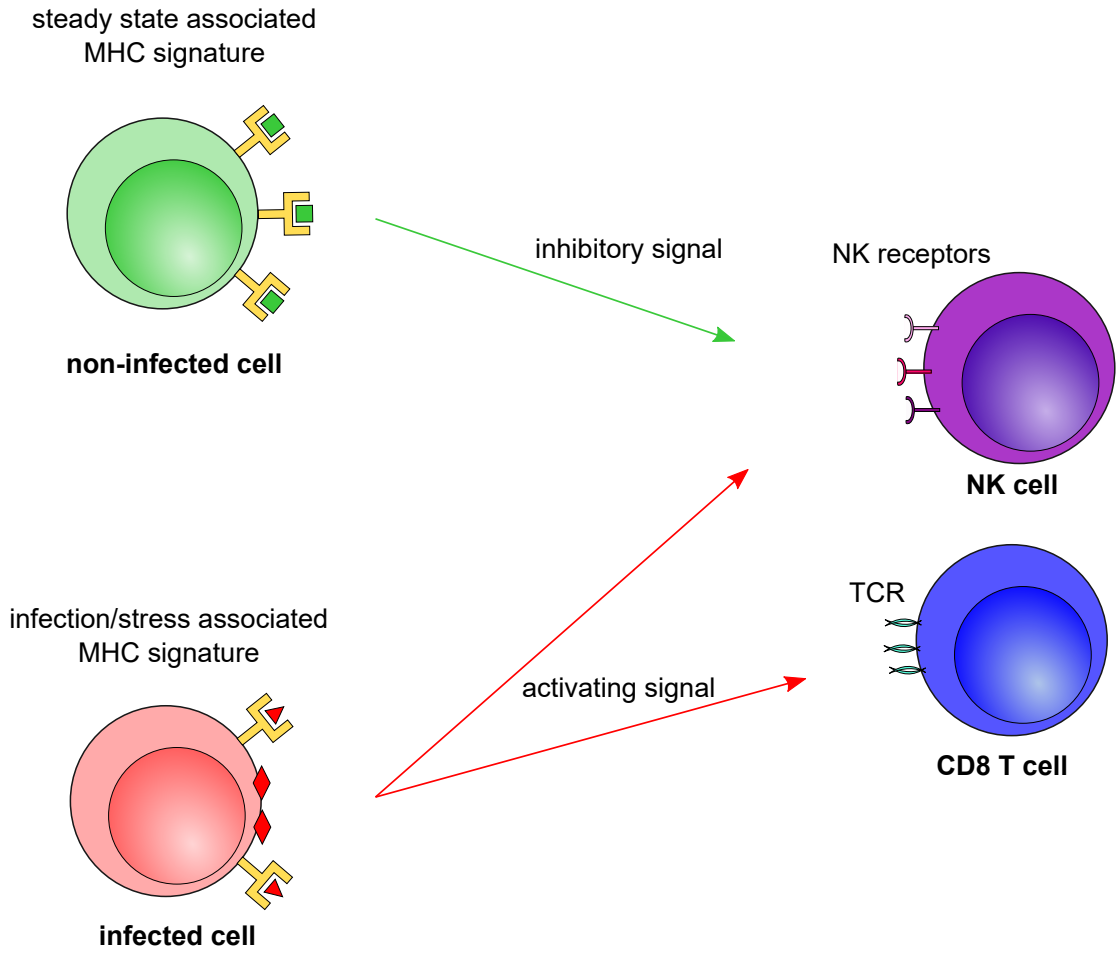

Figure 7. Recognition of infected cell signature via MHC molecules. Cells infected by a pathogen present peptides on MHC I that differ from non-infected cells. The infected cells also present stress-induced non-classical MHC molecules. Eventually MHC class I molecule expression can be downregulated upon infection. NK cells detect this overall abnormal MHC signature through several NK receptors. CD8 T cells detect a sole MHC I carrying a given antigen, through their T cell receptor (TCR).

Clearance of pathogens

The recognition of a pathogen will trigger a cascade of activation involving several pathways (*e.g.* MyD88/TRAF, TRIF, ZAP kinases), depending on the receptor involved, such as PRR (Takeuchi & Akira, 2010; Shaw et al., 2010; Loo & Gale, 2011; Wen et al., 2013; Reikine et al., 2014; Cai et al., 2014; Hoving et al., 2014; Sellge & Kufer, 2015; Balka & De Nardo, 2018) (**Figure 8**), FcR (Sánchez-Mejorada & Rosales, 1998; Getahun & Cambier, 2015) (**Figure 9A**) and complement receptors (Bohana-Kashtan et al., 2004; Dustin, 2016) (**Figure 9B**). Regarding the particular case of NK cells, the balance between inhibitory signals (steady-state associated MHC signature) and activating signals (for example infection associated MHC signature) provided by a target cell determines whether an NK cell will be activated or not (Vivier et al., 2008; Chan et al., 2014) (**Figure 10**).

Note that despite the precise molecular characterization of the pathways involved, this knowledge at cell level does not allow to draw a comprehensive picture of the impact of each receptor activation at the immune system level.

Overall, these cascades will activate innate immune cells triggering several functions (**Figure 11**). Upon activation, some cells such as neutrophils, eosinophils, monocytes, macrophages and DCs can phagocyte the whole pathogens/vaccines they recognized (Gordon, 2016; Rosales & Uribe-Querol, 2017). This can be done following PRR-mediated recognition, complement-based recognition or antibody-mediated recognition (in this case, it is called antibody dependent cell phagocytosis ADCP). The process to facilitate pathogen uptake by phagocytic cells is called opsonization. Besides, some cells, mainly NK cells, NKT cells and $\gamma\delta$ T cells in the innate immunity can secrete cytotoxic molecules that can disrupt pathogen/vaccine or infected cell membranes (*e.g.* perforin) and proteases that can trigger an apoptosis cascade in infected cells (*e.g.* granzyme) (Trapani, 2001; Trapani & Smyth, 2002; Caligiuri, 2008; Osińska et al., 2014). NK cell cytotoxicity can be triggered by an aberrant MHC I signature as well as by antibody-bound pathogen, the latter process being called antibody dependent cell cytotoxicity (ADCC). Besides, a specificity of neutrophils is their ability to expulse DNA out of their nucleus to capture microbes into DNA fibers, a process called neutrophil extra-cellular trap (NET) (Kaplan & Radic, 2012; Yang et al., 2016; Delgado-Rizo et al., 2017; Boeltz et al., 2019).

Eventually, upon activation every innate immune cells, as well as non-immune cells, can produce a wide range of cytokines (small proteins modulating cell behavior). In particular, they produce so-called inflammatory cytokines (such as IL-1α, MIP-1α, MIP-1β, CCL5, IL-12...). In addition to cytokines, some complement proteins, the so-called anaphylotoxins (C3a, C4a and C5a), also share these pro-inflammatory properties (Klos et al., 2009). These molecules will be recognized by immune and non-immune cells and initiate a process called inflammation.

Inflammation notably includes the recruitment of effector cells through the binding of chemokines (cytokines driving effector cell chemotaxis) on their cognate receptor on innate cells, the enhanced phagocytosis on phagocytes (*e.g.* macrophages, DCs, neutrophils), the increased permeability of vascular vessel to allow for recruitment of effector cells, and the generation and release of effector cells from bone marrow (Akdis et al., 2016; Pietras, 2017). Also, some cytokines produced have direct anti-pathogen effects and stimulate intrinsic immunity -a constitutive immunity of individual cells, mediated by endogenously expressed proteins inhibiting pathogen replication. For example type I interferon (*e.g.* IFNα and IFNβ) induces the production of anti-viral genes in all cells, the so-called interferon stimulated genes (ISG), in addition to its immunomodulatory effect on immune cells (Yan & Chen, 2012; Schneider et al., 2014; McNab et al., 2015). All cells cannot produce all cytokines (*e.g.* pDCs are specialized in IFN I production, NK cells are main producers of IFN II (IFNγ) (Akdis et al., 2016)), but all will contribute to the overall inflammatory state. Inflammation is a positively self-regulated process, since a consequence of cell activation by pro-inflammatory molecules is the release of more pro-inflammatory molecules.

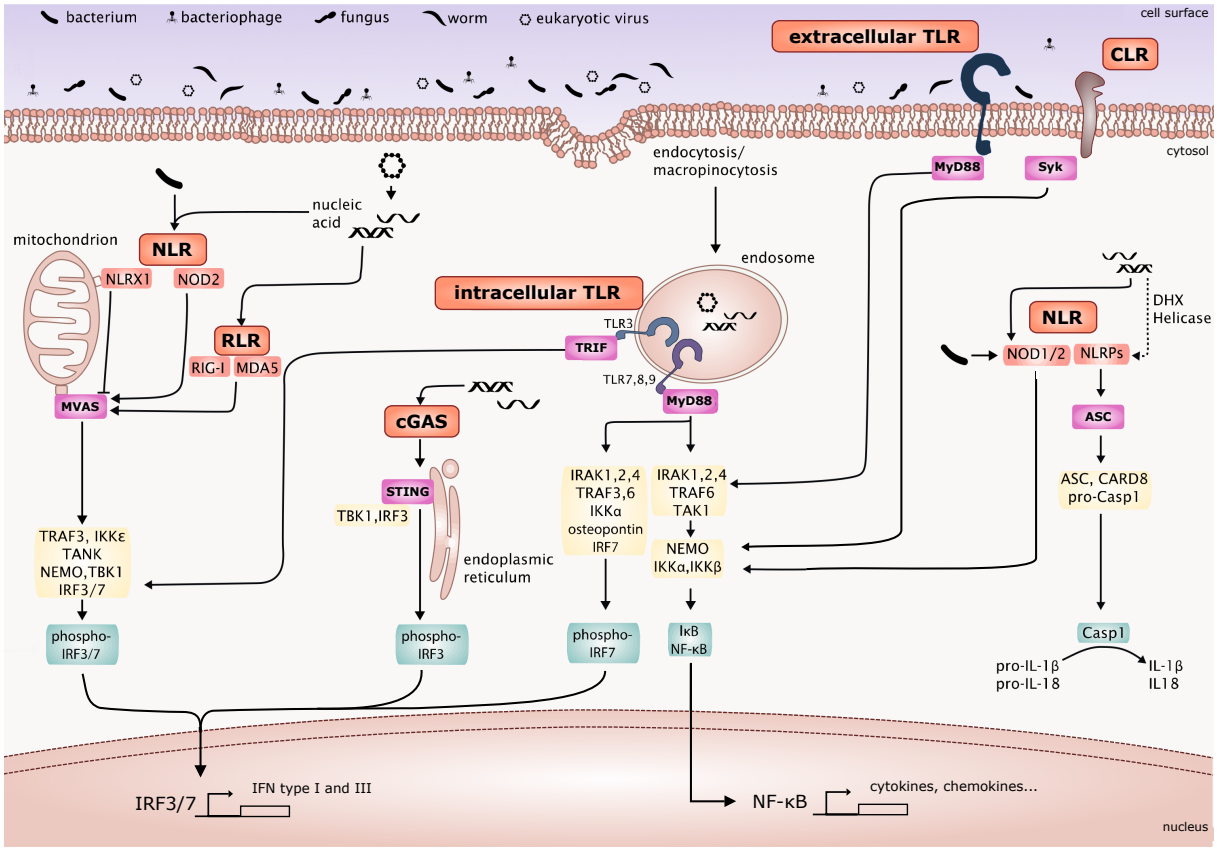

Figure 8. Signaling pathways activated upon PRR interaction with its ligands. The signaling cascade is indicated for each of the aforementioned PRR. Red/orange: PRRs. Magenta: adapter protein. Yellow: downstream components. Green: transcription factor. Modified from Metzger et al. (2018).

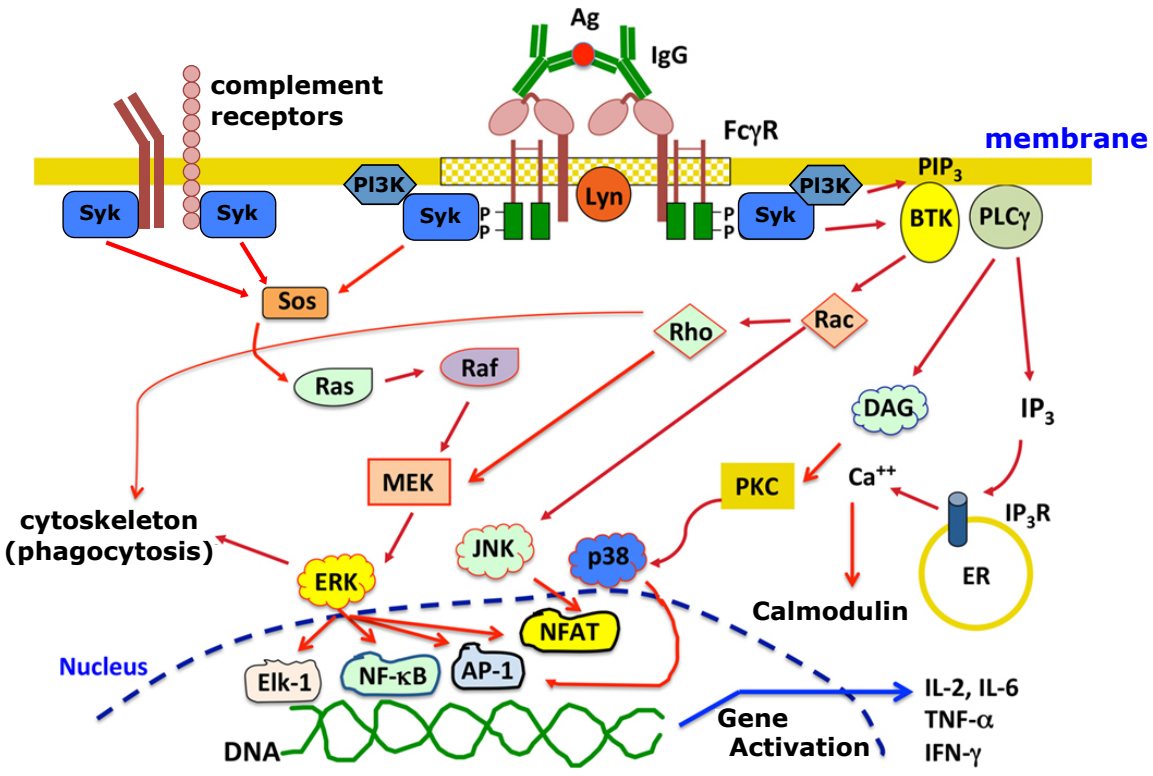

Figure 9. Signaling pathways activated upon indirect pathogen recognition. Exemplified signaling pathways induced by indirect pathogen recognition via IgG receptors (FcγR) and complement receptors. Only activating receptor signaling pathway is displayed here, and not inhibiting receptor signaling pathway (*e.g.* CD32b signaling pathway). Modified from Rosales (2017).

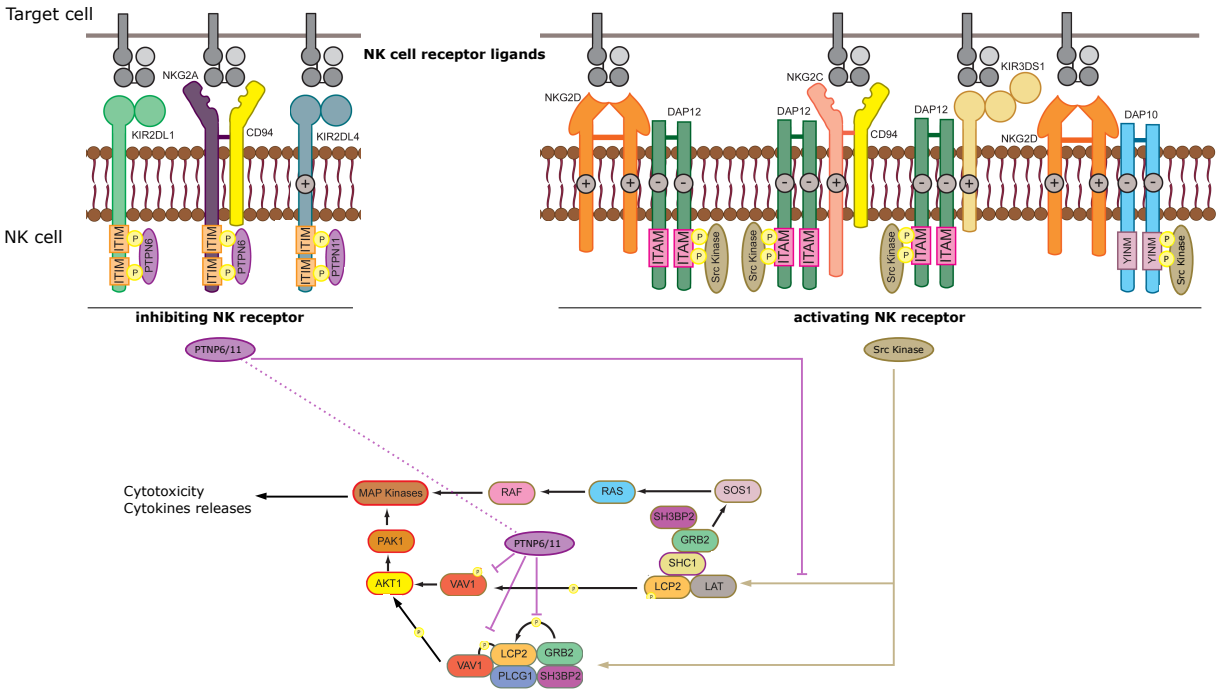

Figure 10. **Signaling pathways activated upon NK receptor engagement.** Exemplified signaling pathways induced by the engagement of some of the main NK receptors. ITIM: immunoreceptor tyrosine-based inhibitory motif. ITAM: immunoreceptor tyrosine-based activating motif. Modified from Kelley et al. (2005).

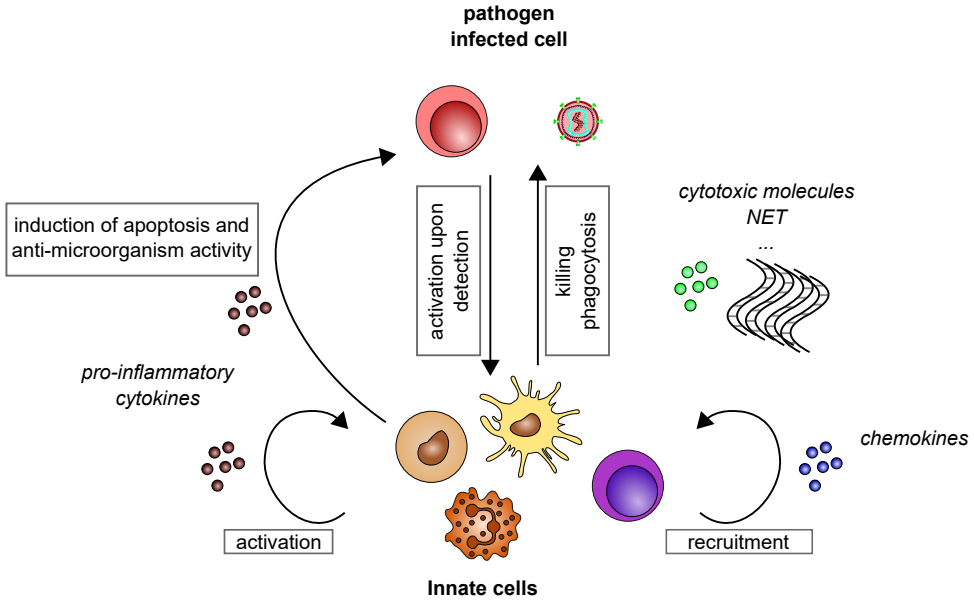

Figure 11. Consequences of innate immune cells activation by pathogens or vaccines. Upon activation, innate cells will produce inflammatory cytokines (activating themselves and promoting apoptosis of infected cells), produce chemokines (attracting more effector cells) and kill pathogen and infected cells (*e.g.* through phagocytosis, cytotoxic activity, NET (neutrophil extra-cellular trap)).

In term of spatio-temporal dynamics, the resident cells at the site of infection or immunization (such as macrophages, dendritic cells, ILCs, $\gamma\delta$ T cells on the immune part, but also non-immune cells, such as epithelial cells) will trigger the initial inflammatory response recruiting more effector cells, essentially neutrophils, the most abundant and short-lived cell population in blood (Pillay et al., 2010), but also monocytes, which could notably differentiate in macrophages and potentially cDCs (Gonzalez-Mejia & Doseff, 2009). This initial response can clear the pathogen/vaccine from the body, especially if few infectious agents or vaccine particles were present. But in addition to this effector function, a second function of the innate immune system is to activate, modulate and shape not only itself but also the second arm of the immune system, the adaptive one, constituted by T and B cells.

Innate cells as modulator cells

Activation and shaping of adaptive immunity

T cell activation and polarization

Each T cell is able to recognize one sole antigen, encoded by non-self cells or micro-organisms, that is presented on an MHC molecule after processing. This recognition is mediated through its TCR arising from somatic rearrangements, during T cell maturation. (Zúñiga-Pflücker, 2004; Koch & Radtke, 2011).

Cells such as dendritic cells, monocytes/macrophages and B cells, carry MHC class II molecules (in addition to class I), which can present antigen, not expressed within the cell (conversely to class I) but from pathogens/vaccines or infected cells they internalized (Neefjes et al., 2011; Rock et al., 2016). They are thus called professional antigen-presenting cells. Among them, cDCs are almost the only ones that can activate previously naive T cells (priming), while the other APCs can restimulate primed T cells. cDCs can migrate from the site of infection/immunization to secondary lymphoid organs (lymph nodes, spleen, gut associated lymphoid tissue, nasal associated lymphoid tissue) through lymphatic vessels. Note that some cDCs also reside within lymphoid organs. In these tissues, cDCs can present MHC II carrying antigen to so-called CD4 T lymphocytes, and MHC I carrying antigen to so-called CD8 T lymphocytes, to activate them (**Figure 12A**). T cell priming was also shown to occur in bone marrow in several contexts, including cancer and infections (Schirrmacher et al., 2003). Strikingly, following vaccination with a smallpox vaccine, transport of antigen to the bone marrow was made by neutrophils and not cDCs in mice (Duffy et al., 2012). Still, in mice also, blood circulating antigens are eventually presented to T cells by cDCs (Feuerer et al., 2003).

All cDCs can do both presentations (to CD4 and CD8 T cells) but not with the same efficacy; actually two main subclasses of cDCs are defined: cDC1s and cDC2s (Schlitzer et al., 2015; Vu Manh et al., 2015; Collin & Bigley, 2018). cDC1s essentially present antigen captured during phagocytosis on MHC class I molecules (a process called cross-presentation) and are more efficient in antigen presentation to CD8 T cells (**Figure 12B**), though they also activate CD4 T cells via MHC II (Bedoui et al., 2009; Eickhoff et al., 2015). cDC2s essentially present antigen on MHC II molecules and are major activator of CD4 T cells (**Figure 12C**), though they can also perform cross-presentation (Segura et al., 2013; Sheng et al., 2017). Note also that other cDC population exist, such as tissue resident Langherans cells or monocyte-derived DCs (Vu Manh et al., 2015).

Three signals are required to activate T cells, the first is the interaction between MHC (MCH I for CD8 T cells and MHC II for CD4 T cells) and the TCR, the second is the interaction between co-stimulation molecules expressed on both cells (*e.g.* CD80/86-CD28, CD40-CD40L), the last and third signal is the cytokine micro-environment that is essential to polarize T cell differentiation.

Several subpopulations of CD4 T cells were identified based on their cytokine production, transcription factors expression, immune functions, and protective capacity (O'Garra, 2000; Zhu & Paul, 2008; Zhu et al., 2010; Geginat et al., 2014; Crotty, 2015; Raphael et al., 2015; DuPage & Bluestone, 2016). For example, among CD4 helper T cells (Th), Th1 cells are described as potentiators of macrophage activation and NK cell activation through IFNγ production, whereas Th2 cells as activator of eosinophils, basophils and mast cells via IL-4, IL-5 and IL-13 production (Raphael et al., 2015; DuPage & Bluestone, 2016). Follicular helper T cells (Tfh) were shown to be crucial in B cell activation and antibody production and maintenance, notably via IL-21 production (Tangye et al., 2013). By contrast, CD8 T cells are usually more homogeneously described as producer of cytotoxic molecules and proteases, allowing them to kill infected cells they recognized via MHC I mediated antigen presentation (Zhang & Bevan, 2011; Halle et al., 2017).

The differentiation in one or the other T cell subset is dependent of multiple factors, including the tissue of T cell activation and the quality of the initial innate immune response (relying notably on the site of injection, the PRR targeted, the cDC subpopulation activated and the inflammation induced). Accordingly, vaccine response can be shifted towards one of the other T cell response, based on the adjuvant used. For example, MPLA formulated with cationic DDA (dimethyldioctadecylammonium) liposome (DDA/MPL) was described as inducing a Th1 response, including a potent IFNγ production (Rosenkrands et al., 2005), whereas alum was described as an inducer of a Th2 with poor CD8 T cell mediated immunity (HogenEsch, 2002). As adjuvant in mice vaccination, lipopolysaccharide (LPS) stimulates TLR4 and lead to generation of T helper 1 (Th1) cells in the lymphoid tissue, but Th17 cells in the gut (McAleer & Vella, 2010). In combination with a tuberculosis candidate vaccine in mice also, the liposome system CAF01 induced Th1/Th17 cells, while squalene-based oil-in-water emulsion triggered Th1/Th2 responses (Ciabattini et al., 2016). Also, cyclic dinucleotides targeting the cGAS pathways induced preferentially Th1/Th17 cells during tuberculosis vaccination of mice (Van Dis et al., 2018). Note that adjuvants inducing distinct T cell response, also induced distinct early innate response, both qualitatively and quantitatively, further supporting the deep interconnection between innate and adaptive immunity (Korsholm et al., 2010).

Overall, given the key role of dendritic cells at the interface between innate and adaptive immunity, better targeting them to trigger a more efficient antigen presentation is a promising filed of research in vaccinology (Dubsky et al., 2005; Palucka & Banchereau, 2013). For instance, targeting some DC-expressed PRRs (such as DCIR and CD205), was shown to potentiate and orientate the subsequent T cell response (Dudziak et al., 2007; Soares et al., 2007).

Interestingly, other innate immune cells, not classified as professional APCs, were shown to participate directly or indirectly to T cell activation and shaping. Indeed, neutrophils and in a lesser extent eosinophils and basophils, which are usually not classified as APCs were shown to express MHC class II molecules and acquire a functional ability to present antigen *in vitro* and *ex vivo* in both mice and humans (Abi Abdallah et al., 2011; Vono et al., 2017; Lin & Loré, 2017; Costa et al., 2019). NK cells and cDCs interaction

was proved crucial in CD8 T cells activation, allowing for CD4 T helper cells independent activation (Mocikat et al., 2003; Adam et al., 2005; Ge et al., 2012). NK cells were also shown to regulate the differentiation of T helper cells induced by cDCs (Martín-Fontecha et al., 2004), to initiate IFN I production required for CD8 T cell response induction (Cocita et al., 2015), to kill infected cDCs -dampening T cell activation (Andrews et al., 2010)-, and kill CD4 T cells -dampening CD8 T cells activation (Welsh & Waggoner, 2013).

B cell activation and polarization

B lymphocytes can recognize one sole native antigen (unprocessed), on the variable part of their B cell receptor (BCR), deriving from genetic recombinations (Batista & Harwood, 2009; Pieper et al., 2013). The antigens recognized by B cells can be captured as they circulate through lymphoid organs and/or be presented unprocessed by macrophages and DCs in these organs (Heesters et al., 2016).

The mature B cells are activated only when co-activated by both the circulating antigen (either released from the pathogen/infected cell directly in the lymph or carried by immune cells toward the lymph nodes) and by CD4 T cells. Few exceptions exist, with some extremely potent antigens able to induce a B cell response in the absence of CD4 T cell co-stimulating signal (Levinson et al., 1995; Goodyear & Silverman, 2005). Upon activation, B cell will undergo a complex maturation process, including several cycle of mutations of the BCR sequence, the so-called somatic hyperrmutation (Dörner & Radbruch, 2005; Pieper et al., 2013; Suan et al., 2017). This maturation process, tightly regulated by Tfh, will allow for the generation of new B cell clone carrying high affinity BCR. From these B cells, antibody secreting cells will be induced, that can secrete the soluble form of the BCR, the antibody (**Figure 13**). NK cells were shown to be involved in B cell differentiation and maturation (Gao et al., 2001; 2008), as well as modulation of antibody generation, especially via Tfh regulation (Cook et al., 2015; Rydyznski et al., 2018). Inflammatory monocytes also take part in this modulation (Sammicheli et al., 2016), as well as neutrophils (Costa et al., 2019). Antibody secreting cells will produce antibody that will bind pathogen and/or the infected cell. This can impair pathogen ability to move and/or enter target cell (neutralizing effect), but also activate FcR expressed by innate cells as previously described. Note that some FcR are also expressed by adaptive cells.

Adaptive immune response: effector and memory phase

T and B cells, activated in the lymph node, will be recruited into the inflamed tissue via interaction between chemokines receptor and chemokines produced at the site of infection/injection. They will also participate in the elimination of the pathogens/vaccines, via the previously mentioned functions (*e.g.* cytotoxicity, pathogen neutralization). This corresponds to the effector phase of the adaptive immunity (**Figure 13**).

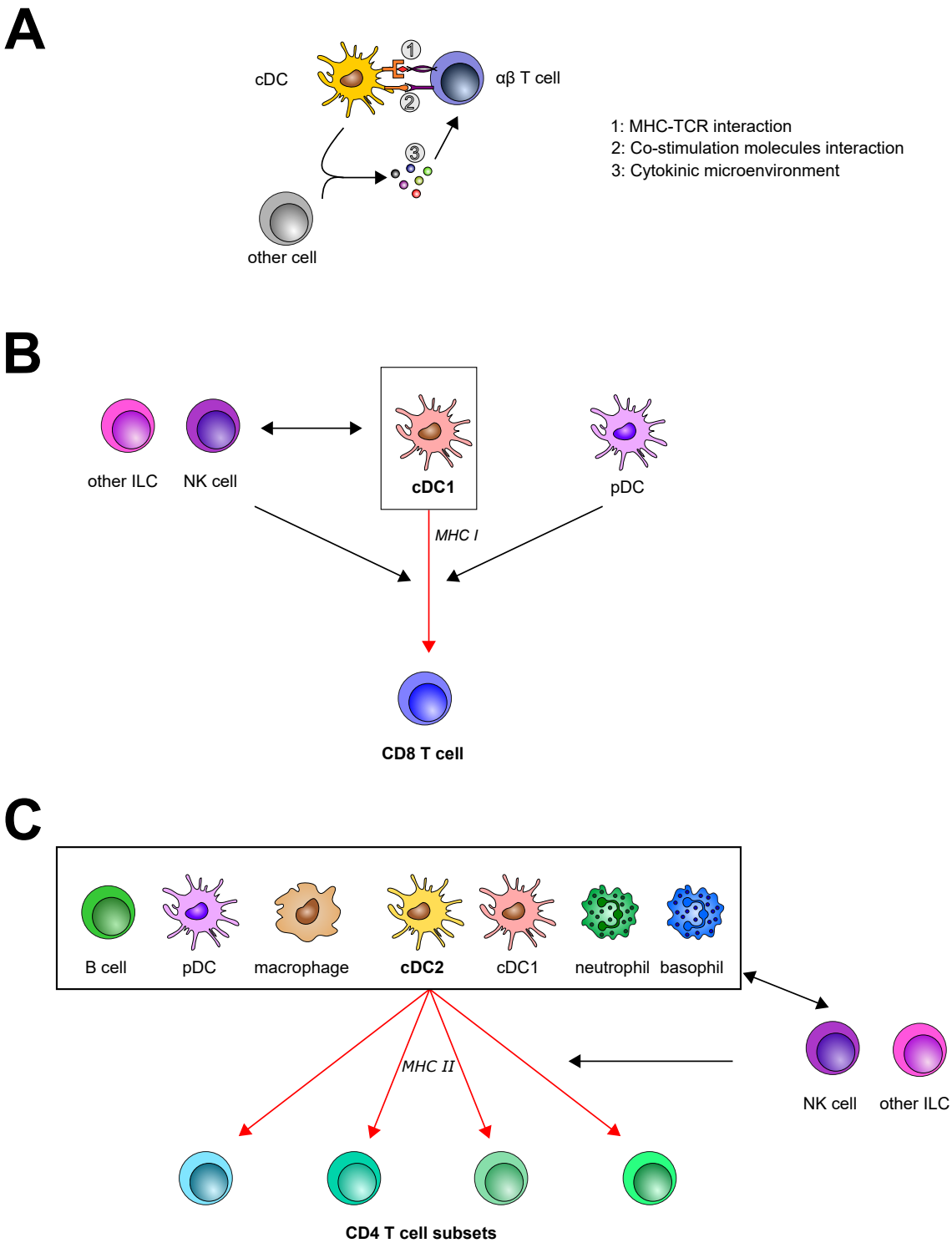

Figure 12. Activation of T cells by innate immune cells. (A) General mechanism of T cell priming by a dendritic cell in the lymph node. The three signals received by T cells are indicated. For cytokine-mediated signal 3, cDC can be assisted by another cell. **(B-C)** Overview of cells involved in MHC I-dependent CD8 T cell (re-)activation **(B)**, and MHC II-dependent CD4 T cell (re-)activation **(C)**. Antigen-presenting cells (APCs) are indicated in the frame, the main APC able to prime the T cell is indicated in bold. Cells that do not directly present antigen but modulate antigen presentation or orientate differentiation are also indicated.

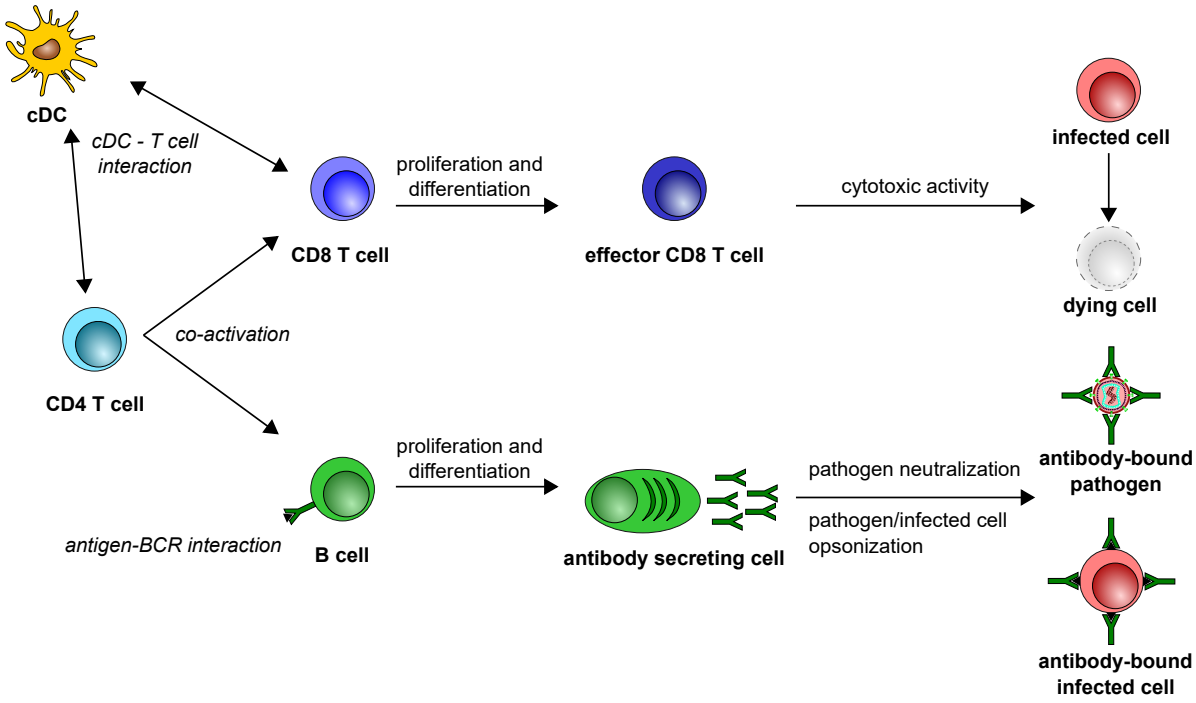

Figure 13. Overview of direct anti-pathogen activity of adaptive response. The different adaptive cells are represented, with their main direct impacts on pathogen clearance after activation. Note that the different subsets within each population are not represented, neither are the different steps of differentiation process.

While the pathogen/vaccine is being cleared, some long-lived (years) subsets will arise among these adaptive cells. These subsets can react more rapidly at any subsequent infection with the same pathogen, the previously mentioned immune memory (Dörner & Radbruch, 2005; Farber et al., 2014; Omilusik & Goldrath, 2017; Phan & Tangye, 2017). Some of these subsets will be maintained in the periphery (*e.g.* Tcm cells), whereas other will patrol in the tissues (*e.g.* Trm cells). Antibodies will be produced in the long term by long-lived antibody producing cells and will result in the constitutive presence of pathogen-specific antibodies in the serum (Yoshida et al., 2010; Brynjolfsson et al., 2018).

The maintenance of these long-lived cells requires notably cytokine signals (*e.g.* IL-7 and IL-15 for T cells, IL-6 and APRIL for plasma cells) (Sallusto et al., 2010). Besides, restimulation of primary memory cells at recalls will give rise to qualitatively distinct secondary memory responses (*e.g* increased cytokine production, increased antibody affinity) (Masopust et al., 2006; Peixoto et al., 2007; Blanchard-Rohner et al., 2009; MacLeod et al., 2010; Wirth et al., 2010; Zabel et al., 2014).

These memory populations as well as resulting antibodies are the ones vaccines aim to induce. Indeed, these T and B cell populations (and antibodies) will mediate a more efficient response towards subsequent pathogen encounter, thus potentially protecting the body from the corresponding infectious agents. Since T cells and B cells recognize specific antigens, this highlights the crucial role the choice of the antigen(s) vaccines should contain to be efficient (Flower et al., 2010; Rueckert & Guzmán, 2012).

Modulation of innate cell effector functions by adaptive and innate immunity

Adaptive cells produce cytokines that modulate innate cells functions. For example, CD8 T cells produce IFNγ, notably enhancing phagocytosis by macrophages/monocytes and DCs (Zhang & Bevan, 2011). CD4 T cells, including memory cells, produce cytokines that will alter innate cell behavior, notably cytokine production, and allow for a more efficient innate response at recall (Strutt et al., 2010; 2011). Memory CD8 T cells increase innate effector functions (Narni-Mancinelli et al., 2007; Soudja et al., 2014; Schenkel et al., 2014; Ariotti et al., 2014). T cells modulate NK cells mediated IFNγ production and cytotoxic activity in infectious contexts (He et al., 2004) and following vaccination (Horowitz et al., 2010). B cells are known to produce cytokines, including IFNγ and IL-12, that will regulate innate cells in addition to T cells (Lund, 2008). They can also participate to inflammation through production of TNFα, lymphotoxin and IL-6 (Vazquez et al., 2015). Eventually, antibodies will form immune complexes labelling pathogens and infected cells for phagocytosis or cell killing by innate cells.

Besides, innate cells mutually interact with one another, modulating their functions. For example, NK cells are potent producers of IFNγ and TNFα, which will activate DC and macrophages for phagocytosis. Upon activation, DCs and macrophages produce type I IFN, as well IL-12, IL-15 and IL-18 that will activate NK cells (Vivier et al., 2008). Modulation of DC activation and maturation was proved crucial for the efficient removal of infectious agents (Alter & Altfeld, 2011). In addition, direct cell-cell contact between monocytes and NK cells was shown to regulate NK cell activity (Michel et al., 2012).

Overall, all innate lymphoid cells (ILCs) are potent modulators of adaptive immunity activation (Withers, 2016; Vivier et al., 2018). Since modalities of vaccination strongly impact ILC response (*e.g.* route of immunization (Li et al., 2018)), ILCs stand as a promising target for vaccine optimization. Few adjuvants/self-adjuvanted vaccines are known or designed to directly target NK cells. Though, since NK cells can express PRRs (notably TLRs and NLRs), many adjuvants likely activate NK cells as a *bona fide* mechanism (Martinez et al., 2010; Souza-Fonseca-Guimaraes et al., 2012; Adib-Conquy et al., 2014). In addition, NK cell activity can be enhanced via the induction of Th1 response (Jost et al., 2014; Martins et al., 2014; Van den Bergh et al., 2014). Also, for therapeutic vaccines, injection of NK cell–susceptible targets (*e.g.* MHC deficient cells) enhanced NK-cell mediated potentiation of adaptive responses (Kelly et al., 2002; Krebs et al., 2009).

Besides, neutrophils and monocytes/macrophages can mutually potentiate their activity during inflammation (Prame Kumar et al., 2018). Moreover, neutrophils can take part in cDCs activation and function (van Gisbergen et al., 2005). Eventually, neutrophils and NK cells deeply modulate their mutual activity via cytokine production (Costantini & Cassatella, 2011), including for example potentiation of NK cells functions (Amano et al., 2015). Overall, several studies highlighted the important role of neutrophils in vaccination (Di Pilato et al., 2015; Trentini et al., 2016; Musich et al., 2018).

These cross-interactions of both innate and adaptive cells usually end up with the clearance of the pathogen/vaccine (**Figure 14**).

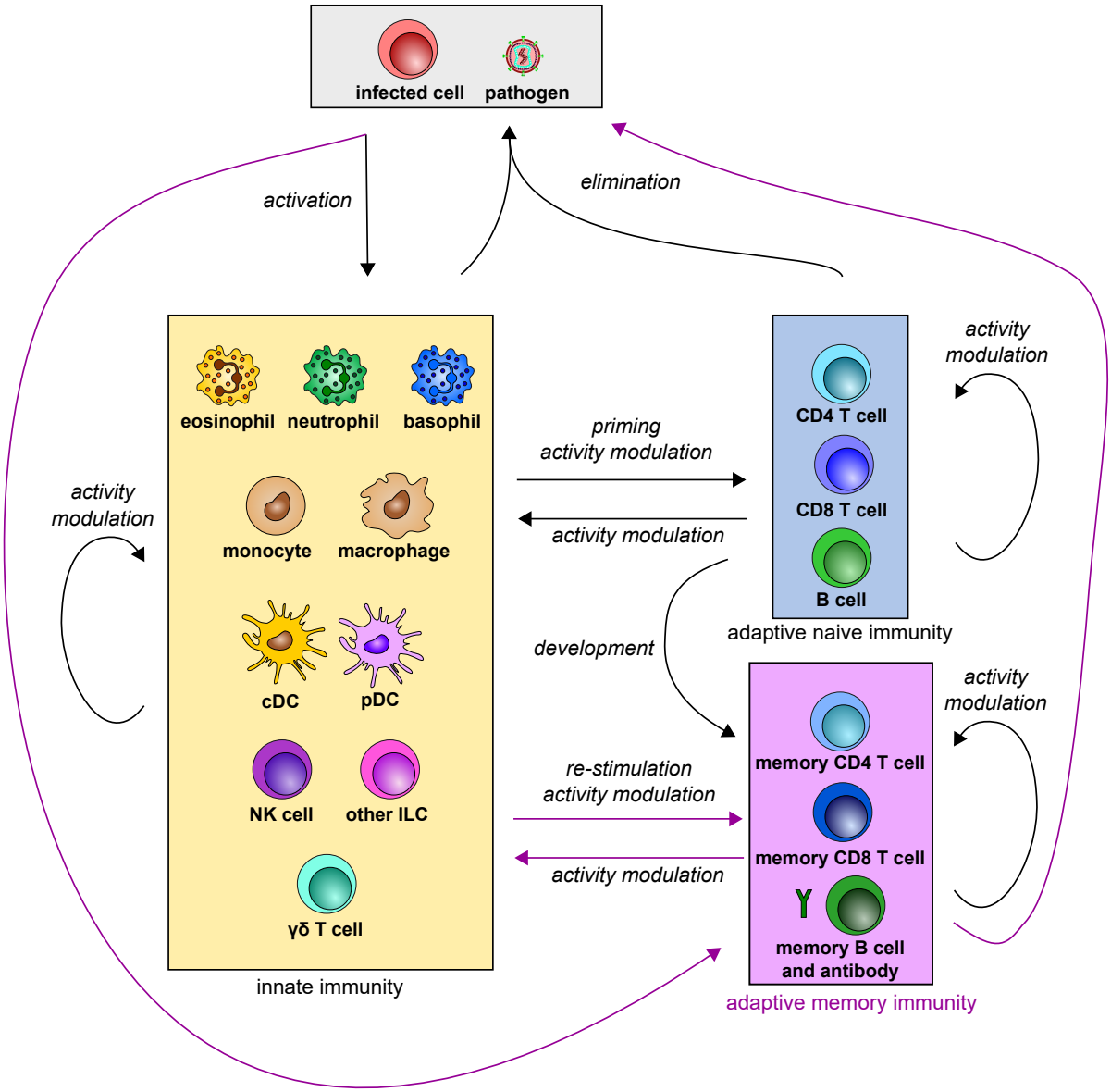

Figure 14. Scheme of crosstalk between innate and adaptive immunity resulting in pathogen clearance. Black arrows indicate interactions occurring at every pathogen encounters. Purple arrows indicate interactions at recall responses only. Pathogen/infected cells activate innate immunity, triggering a crosstalk between innate and adaptive immunity, resulting in pathogen clearance. At a second encounter, pathogens and infected cells activate innate cells and restimulate memory responses, resulting in a faster pathogen clearance.

Resolution of inflammation

Eventually, after the clearance of pathogen/vaccine, in the absence of danger signals, inflammation resolves (Ortega-Gómez et al., 2013; Headland & Norling, 2015; Sugimoto et al., 2016) (**Figure 15**).

Inflammation resolution is mediated by several molecular and cellular interactors. Indeed, IL-10, TGFβ and other anti-inflammatory signals, promoting resolution of inflammation, can be produced by numerous cells upon pathogen detection (Saraiva & O'Garra, 2010; Johnston et al., 2016), likely simultaneously with pro-inflammatory signals (Serhan & Savill, 2005). They will avoid excess of inflammation that could be detrimental to the body, notably by dampening immune cell activation (Headland & Norling, 2015).

Besides, neutrophil apoptosis is a crucial trigger of inflammation resolution (El Kebir & Filep, 2010; Sugimoto et al., 2016). Indeed, neutrophils half-life is less than a week (Pillay et al., 2010), and will then likely die at their site of recruitment (Wang, 2018). Some reports indicate that in addition neutrophils could also leave the site of recruitment and migrate to bone marrow to die, a process called reverse migration (Robertson et al., 2014; Powell et al., 2017; Wang et al., 2017). At their death site, they will undergo apoptosis, a process that is amplified by the anti-inflammatory signals released by effector cells. This apoptosis will trigger the release of several anti-inflammatory signals (Ortega-Gómez et al., 2013), including "eat-me signals".

These "eat-me" signals trigger the phagocytosis of dying neutrophils by monocytes (Fox et al., 2010), a process called efferocytosis, which is highly regulated by the production of the anti-inflammatory cytokine IL-10 (Saraiva & O'Garra, 2010; Gabryšová et al., 2014). The efferocytosis will promote the conversion of monocytes from an inflammatory M1 phenotype to an anti-inflammatory tissue repairing M2 phenotype (Martinez & Gordon, 2014). They will notably cleave chemokines, stopping the influx of incoming neutrophils and classical monocytes (Ortega-Gómez et al., 2013). In addition they will produce high levels of inflammatory cytokines such as IL-10 and TGFβ that will promote an amplifying loop of immune response dampening. They will also promote tissue repair and especially vascularization through production of VEGF (Wu et al., 2010; Johnson & Wilgus, 2014).

The so-called myeloid derived suppressor cells (MDSCs) could also play a concomitant role in inflammation resolution (Gabrilovich & Nagaraj, 2009; Budhwar et al., 2018; Veglia et al., 2018). These cells, including monocyte and neutrophil subpopulations, were firstly described in cancer patients as cells promoting tumor growth and preventing immune response, but were later shown to have a beneficial role in inflammatory disorders including auto-immune diseases and sepsis (Ortega-Gómez et al., 2013; Budhwar et al., 2018). These cells notably produce arginase which degrades arginine an amino-acid required for T cell survival, as well reactive oxygen species (ROS) triggering neutrophil apoptosis (Gabrilovich & Nagaraj, 2009). They are known to produce the anti-inflammatory cytokines IL-10 and TGFβ.

MDSCs were shown to be major player in several contexts including cancer, infectious diseases, auto-immune diseases; obesity and pregnancy (Ortega-Gómez et al., 2013; Veglia et al., 2018). In particular, high MDSC levels were associated with therapeutic vaccine failure in melanoma, non small cell lung carcinoma and colon adenocarcinoma (Kimura et al., 2013; Butterfield et al., 2017). MDSCs were shown detrimental in both acute and chronic infectious diseases, including Staphylococcus aureus, hepatitis B and HIV infection (Veglia et al., 2018). It is not clear however what their role is during preventive vaccination, and few studies actually focused on that question. Though, MDSCs were induced following immunization of rhesus macaques with influenza vaccine (Lin et al., 2018) and are thought to play a role in the reduced vaccine responsiveness of infants (Gervassi et al., 2014).

Besides, upon activation, NK cells can also differentiate into so-called regulatory NK cells, which dampens T cells activation and amplify IL-10 production (Lee et al., 2009; Perona-Wright et al., 2009). Also, anti-inflammatory N2 neutrophils could be induced, though they were mostly described in cancer context and their potential role in vaccination and acute infection is not established yet (Shaul & Fridlender, 2017). Note that they differ from MDSCs in term of transcriptomic profile and cytokine production (Fridlender et al., 2012).

Eventually, on the adaptive part of the immune system, a subset of $CD4^+$ T cells notably expressing high level of CD25 and FoxP3 called $CD4^+$ regulatory T cells (Treg) are T cells can promote an anti-inflammatory response by producing high levels of both IL-10 and TGFβ (Corthay, 2009; Kondělková et al., 2010; Josefowicz et al., 2012). They were first described to inhibit effector T cells functions, but the cytokines they produce obviously impact also innate cells effector functions (Taams et al., 2005; Pedroza-Pacheco et al., 2013; Romano et al., 2018). For example they are known to be one the main regulator of NK cell activity through IL-2 production (Sitrin et al., 2013; Gasteiger et al., 2013a;b). As for regular T cells, the development of Treg is tightly regulated by innate immunity and especially by cDCs (Kabelitz et al., 2006), but they can also be induced by MDSCs, at least in cancer context (Huang et al., 2006; Serafini et al., 2008). The role of Treg in vaccination is important though not fully clear, since on one side they prevent over-inflammation, but on the other side they also dampen overall immune response (Brezar et al., 2016).

Similarly, B regulatory cells were also described (Lund, 2008; Mauri & Menon, 2015; Rosser & Mauri, 2015). They also modulate and dampen immune responses through the production of anti-inflammatory cytokines (IL-10, TGFβ, IL-35).

Overall, the anti-inflammatory crosstalk between innate and adaptive immunity will result in inflammation resolution after pathogen/vaccine clearance (**Figure 15**). This notably includes the reduction of immune cell number in the site of inflammation via different cell death pathways including autophagy, notably based on the end of antigen/pathogen/vaccine stimulation of the immune system (Marrack et al., 2010; Freire & Van Dyke, 2013).

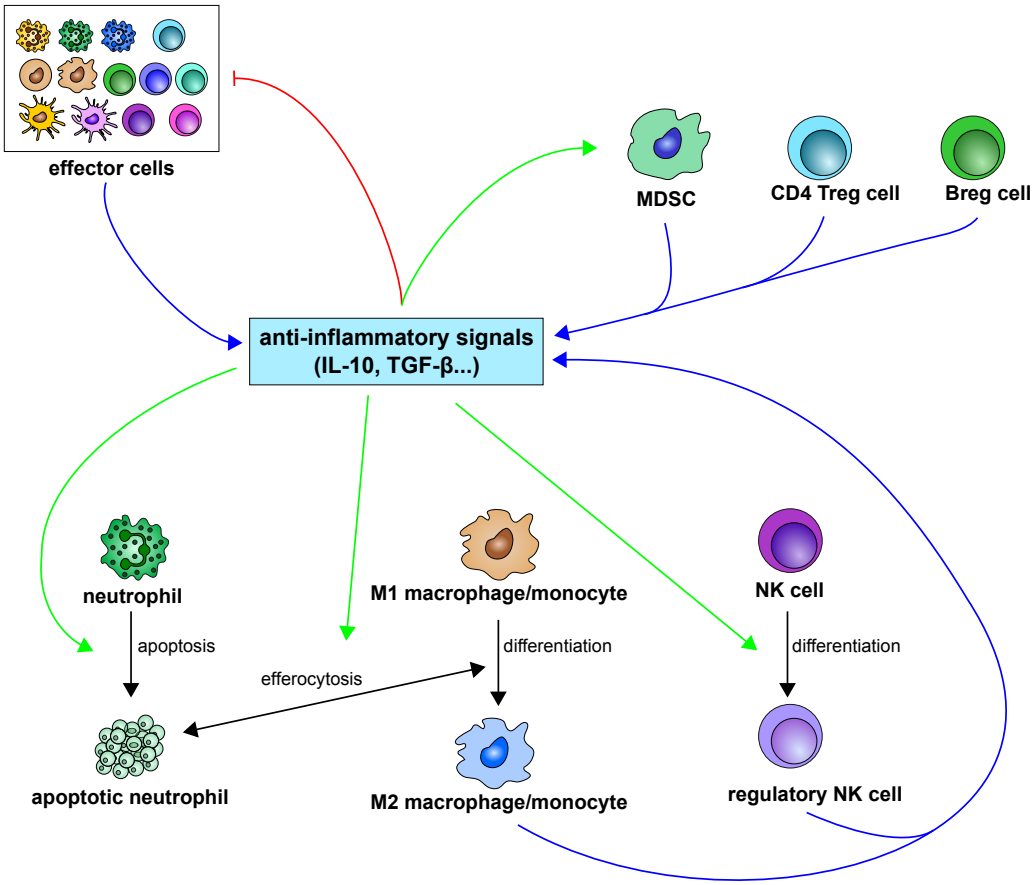

Figure 15. Integrated scheme of inflammation resolution. The main cell types involved in the resolution of inflammation are represented and their interactions depicted. The group of effector cells include most innate and adaptive immune cells. Blue arrows indicate production. Red arrow indicate inhibition of functions and recruitment. Green arrow indicate activation. Black arrow correspond to the indicated cellular processes, likely the initial trigger of the resolution of inflammation. MDSC: myeloid-derived suppressor cells.

Memory within innate immunity

Trained innate myeloid cells

The concept of immune memory was discovered on the study of B and T cell response and thought to be specific of adaptive immune cells. Innate immunity was then assumed to lack memory and react the same at each encounter with a pathogen. This concept was put in question by several findings showing that innate myeloid cells could have memory features, a concept called trained innate immunity (Song & Colonna, 2018; Mourits et al., 2018; Gourbal et al., 2018; Boraschi & Italiani, 2018).

Historically, epidemiological data on children receiving BCG vaccine (Bacillus Calmette-Guérin, the first tuberculosis vaccine strain) in Sweden between 1927 and 1932 suggested that BCG vaccination protected against other diseases than tuberculosis. Similar findings were obtained in the following decades (Benn et al., 2013; Goodridge et al., 2016; Netea & van der Meer, 2017). Also, in mouse model, BCG vaccination, fungi infection with *Candida albicans*, and viral infection with murine cytomegalovirus (MCMV) induced non-specific protection against unrelated infections (Bistoni et al., 1988; van't Wout et al., 1992; Barton et al., 2007).

At cell level, this protection seemed not mediated by lymphocytes but rather by monocytes/macrophages that react more strongly to stimuli compared to untrained innate cells. Later, it was shown that injection of β glucan (a component of fungi such as *Candida albicans* and *Saccharomyces cerevisiae*) and BCG vaccination of mice and healthy volunteers resulted in epigenetic modifications of monocytes and non-specific protection against re-infection in mice (Quintin et al., 2012; Kleinnijenhuis et al., 2012). NOD2 signaling was shown crucial in this last study. Innate training was also shown by *in vitro* stimulation of monocytes with β glucan or BCG (Quintin et al., 2012; Bekkering et al., 2016; Garcia-Valtanen et al., 2017). Cell wall chitin from *Saccharomyces cerevisae* also induced training in monocytes with increase IL-6 and TNFα production, though the intensity differed qualitatively across the different strains (Rizzetto et al., 2016).

More recently, trained monocytes induced by BCG vaccination in human volunteers were able to protect individuals from unrelated yellow fever vaccine infection (Arts et al., 2018b). In addition, in mouse model, BCG vaccination and β glucan injection resulted in transcriptional modifications of short-term hematopoietic stem cells (in addition to circulating monocytes and bone-marrow derived monocytes). These cells were altered towards myelopoiesis and gave rise to new trained progeny that were notably able to protect against a subsequent infection (Kaufmann et al., 2018; Mitroulis et al., 2018).

In immune cells, cross-protective training was reported in monocytes/macrophages and their progenitor (essentially short-term stem cell), but not in DC and neutrophils, though all these cells share the same myeloid origin. A recent study reported the induction of functionally enhanced neutrophils after adenovirus vaccination in rhesus macaques, but these cells were not formally called trained (Musich et al., 2018). Interestingly, some non-immune cells, including epithelial stem cells, interstitial stromal cells and fibroblasts

were also shown to carry epigenetics features linked to memory, suggesting that memory is not the attribute of the sole immune system (Hamada et al., 2018).

The pathways involved in innate cells training is not well understood although some metabolites were reported to be of major importance in the process, such as mevalonate, in addition to cytokines such as IL-1 and IFNγ (Bekkering et al., 2018; Moorlag et al., 2018; Domínguez-Andrés et al., 2018). Also, activation of the NALP3/NLRP3 inflammation may also participate in the training process, as shown in mice under western-diet (Christ et al., 2018). Note that adaptive immunity could play a role in trained immune cell induction, since CD8 T cell were proved crucial for the priming of alveolar macrophages following adenovirus infection in mice (Yao et al., 2018). Also, trained innate myeloid cells potentiate NK cell and adaptive CD8 T cell response, as shown during controlled malaria infection in human after BCG-vaccination induced training (Walk et al., 2019).

Also the duration of this training is not clear. A duration of weeks to months was suggested (Cassone, 2018), but epidemiological studies that unveiled cross-protection of vaccinated people against unrelated infections pledge for years instead (Benn et al., 2013). Interestingly, in addition to BCG, several live-attenuated vaccines, including smallpox, measles, poliomyelitis and yellow fever vaccines, as well as the live-attenuated pertussis vaccine candidate BPZE1, were shown epidemiologically and/or in animal studies to confer cross-protection against unrelated infections, suggesting that trained immunity could be at play (Benn et al., 2013; Saadatian-Elahi et al., 2016; Cauchi & Locht, 2018).

Eventually, which pathogen(s) and vaccine(s) are able to induce trained immunity, and how, is still unknown yet (**Figure 16**). Also, the exact link between the early innate effector response and the generation of trained innate immunity remains to be addressed. But trained immunity stands now as a promising targets for vaccination, for instance to induce both specific and non-specific protection (Töpfer et al., 2015; Sánchez-Ramón et al., 2018).

Note that training of innate cells can be detrimental in certain conditions. For example, patients recovering from sepsis were shown to exhibit epigenetically modified tolerant monocytes that were less protective against secondary infections (Bomans et al., 2018; Bouras et al., 2018). It was suggested to be mediated by LPS, since LPS stimulation induced tolerance in monocytes (Foster et al., 2007; Ifrim et al., 2014). Also, in mice, systemic inoculation of TLR ligands, malaria parasite infection and respiratory infections in mice were shown to impair DC functions at least for weeks, notably cross-presentation (Wilson et al., 2006; Roquilly et al., 2017). Similarly, vaccination with the recombinant diphteria-tetanus-pertussis vaccine was suggested to reduce innate immune responsiveness in children, especially in girls, though the involved mechanism remains elusive (Aaby et al., 2012; Saadatian-Elahi et al., 2016). Quite interestingly, in both cases, these effects could be reverse by BCG or β glucan stimulation, which revealed the plasticity of training/tolerance of innate immunity (Novakovic et al., 2016; Blok et al., 2019a).

Furthermore, following graft, trained infiltrating macrophages were shown as potent activators of alloreactive CD8 T cells, promoting graft rejection (Braza et al., 2018). In-

terestingly, targeting of lipoprotein pathway prevented the generation of those trained macrophages, supporting the involvement of metabolism in the training of innate cells (Braza et al., 2018). Also, several studies reported the role that trained immunity could play in the development and maintenance of auto-immune and inflammatory disorders, such as rheumatoid arthritis, systemic lupus erythematosus, Sjögren's syndrome, Behçet's disease, systemic sclerosis, Wegener's granulomatosis, sarcoidosis, type 1 diabete mellitus (Arts et al., 2018a), and especially in atherosclerosis (Bekkering et al., 2013; Leentjens et al., 2018). Indeed, in those contexts, several innate immune functions are altered. The same was true for monocytes from hyper-IgD syndrome patients (Bekkering et al., 2018). This goes with epigenetic modifications, as well changes in metabolism, which resembles innate immune training (Dowson et al., 2017; Weidenbusch et al., 2017; Kiripolsky et al., 2017; Arts et al., 2018a). Eventually, BCG-induced innate immune training, including enhanced innate functions, was shown potentially detrimental to simian/human immunodeficiency virus (SIV/HIV) infection. Indeed, the increased activation of the immune system by innate cells, trained with BCG vaccination, goes with an increased recruitment of CD4 T cells that could be infected by SIV (Jensen et al., 2017).

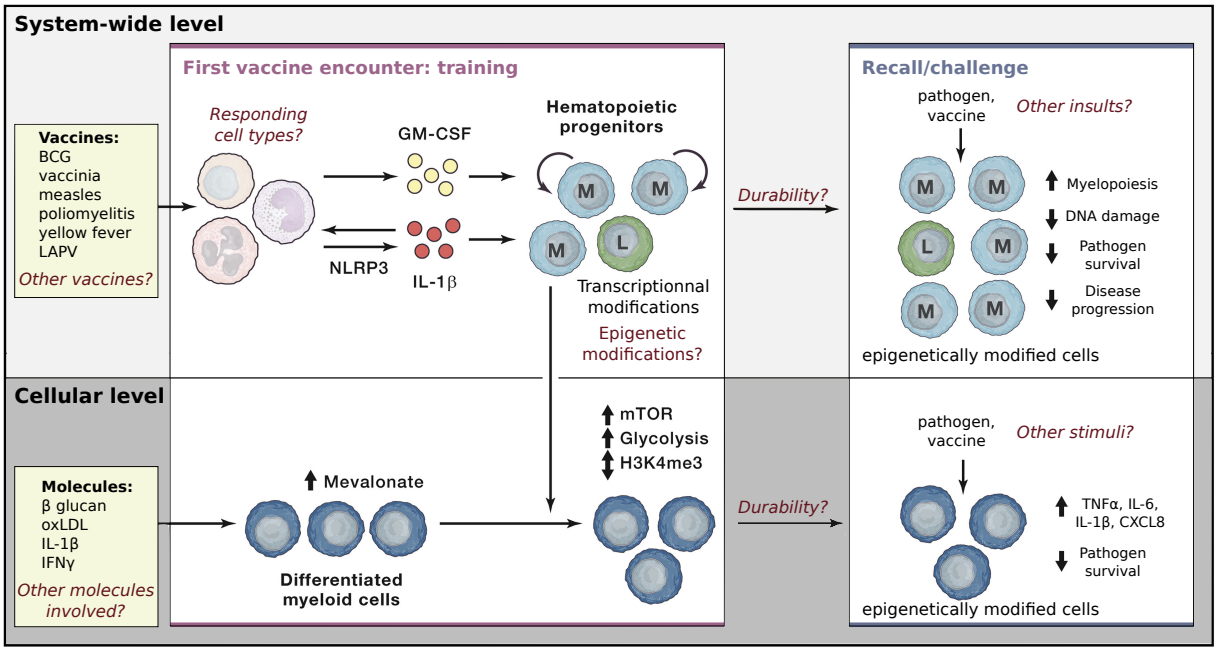

Figure 16. Current view of trained immunity in vaccination. The current cellular and molecular knowledge of trained immunity are exemplified here, as well as remaining unknown features. Innate immune training can occur at system-wide level, with pathogen encounter triggering modifications of hematopoietic progenitors that will give rise to a trained progeny, more potent to clear subsequent pathogen encountered. Simultaneously, innate immune training can occur at the cellular level, inducing epigenetic modifications of the fully differentiated cells. Vaccines proved or suspected to trigger training are indicated. LAPV: live-attenuated pertussis vaccine. mTOR: mechanistic target of rapamycin. oxLDL: oxidized low-density lipoprotein. Modified from Song & Colonna (2018).

"Memory" NK cells

Memory-like features were also reported amongst NK cells, although the mechanisms could be distinct from the myeloid training (Min-Oo et al., 2013; Geiger & Sun, 2016; Paust et al., 2017). Still, the terms trained NK cell immunity can be found in the literature (Kleinnijenhuis et al., 2014b; Schlums et al., 2015; Mourits et al., 2018; Gamliel et al., 2018).

In mice, NK cells displaying antigen-specificity, a feature thought to be the sole attribute of adaptive immunity, were generated after vaccination (Ly49C-I$^+$ NK cells) (O'Leary et al., 2006) or MCMV infection (Ly49H$^+$ NK cells) (Smith et al., 2002; Arase et al., 2002). Interestingly these NK cells were able to induce protection against the same pathogen after adoptive transfer into naive animals (Sun et al., 2009; van Helden et al., 2012). Such antigen-specific NK cells were also observed in primates (Reeves et al., 2015), as well as in humans in which human cytomegalovirus (HMCV) infection was reported to induce such NK cells, which expressed high levels of NKG2C and CD57 (Lopez-Vergès et al., 2011; Foley et al., 2012). Actually, NKG2C was reported as the receptor for the viral UL40 encoded by HCMV (Hammer et al., 2018); interestingly CD8 T cell clones were also found specific to HLA-E bound UL40.

Also, *in vitro* stimulation of NK cells with cytokines (essentially IL-12, IL15 and IL-18) was sufficient to induce so-called cytokine-induced NK cells (Min-Oo et al., 2013). These cells were phenotypically similar to naive NK cells in mice and expressed high levels of CD94, NKG2A, CD69 and NKp46 in humans, but had stronger ability to secrete cytokines, in particular IFNγ (Cooper et al., 2009; Romee et al., 2012; 2016). In addition to antigen-specific NK cells, MCMV infection in mice also induced so-called cytokine-activated NK cells, which were long-lasting and secreted more IFNγ upon pathogen encounter but not after cytokines restimulation and might thus not be perfectly similar to cytokines-induced memory-like NK cells (Nabekura & Lanier, 2016). Similarly, BCG vaccination in both humans and mice was shown to give rise to trained NK cells with enhanced cytotoxicity and cytokines production ability (Kleinnijenhuis et al., 2014b). These trained NK cells protected mice against unrelated infections.

In addition, liver-restricted pathogen-specific memory NK cells could be generated in a contact hypersensitivity model in mice (O'Leary et al., 2006). These NK cells are crucially dependent on CXCR6 for their functions and were able to induce protection against lethal infection with the same pathogen (Paust et al., 2010).

Besides, in mice, the adoptive transfer of resting NK cells into NK cell deficient host was shown to induce the proliferation of the transferred NK cells. They infiltrated both lymphoid and non-lymphoid tissues and were maintained for several months. These so-called homeostatic proliferation-induced memory NK cells displayed enhanced cytotoxic activity and ability to secrete cytokines (Sun et al., 2011).

Overall, a quite large nomenclature co-exist in literature, notably including memory NK cells, memory-like NK cells, adaptive NK cells, cytokines induced NK cells, cytokines activated NK cells, antigen-specific NK cells, each referring to a given subset in given condition, and the phenotype and transcriptional profile of each is not always well defined (**Figure 17**). The pathways involved in their differentiation is not yet solved, though the inflammasome was proved important, as for innate myeloid cell training (van den Boorn et al., 2016).

In addition to their previously mentioned role as modulator of immune cell functions, this memory-like feature made NK cells a key player in vaccine design optimization (Rydyznski & Waggoner, 2015). Inducing potent long-lasting NK cells with enhanced functions is indeed a promising target in vaccine design, since such NK cells were reported after vaccination against influenza, yellow fever and tuberculosis (BCG) in human, as well as SIV vaccination in macaques (Wagstaffe et al., 2018). The lifespan of these memory NK cells is still under debate. In mice, MCMV-induced memory NK cells were shown to wane after 4-5 months (Sun et al., 2009; 2010), though the extrapolation to human lifespan with respect to mice suggest a longer duration. Consistently some results pledged for a memory NK cell lifespan of more than a year in humans (Suliman et al., 2016). NK cell repertoire was also shown to shift durably along lifetime according to previous infections (Strauss-Albee et al., 2015). Moreover, NK cell count is similar in elderly *vs.* young people, despite a reduced generation of *de novo* NK cells in elderly people (Zhang et al., 2007). Overall, these results suggested an even longer lifespan for memory NK cells.

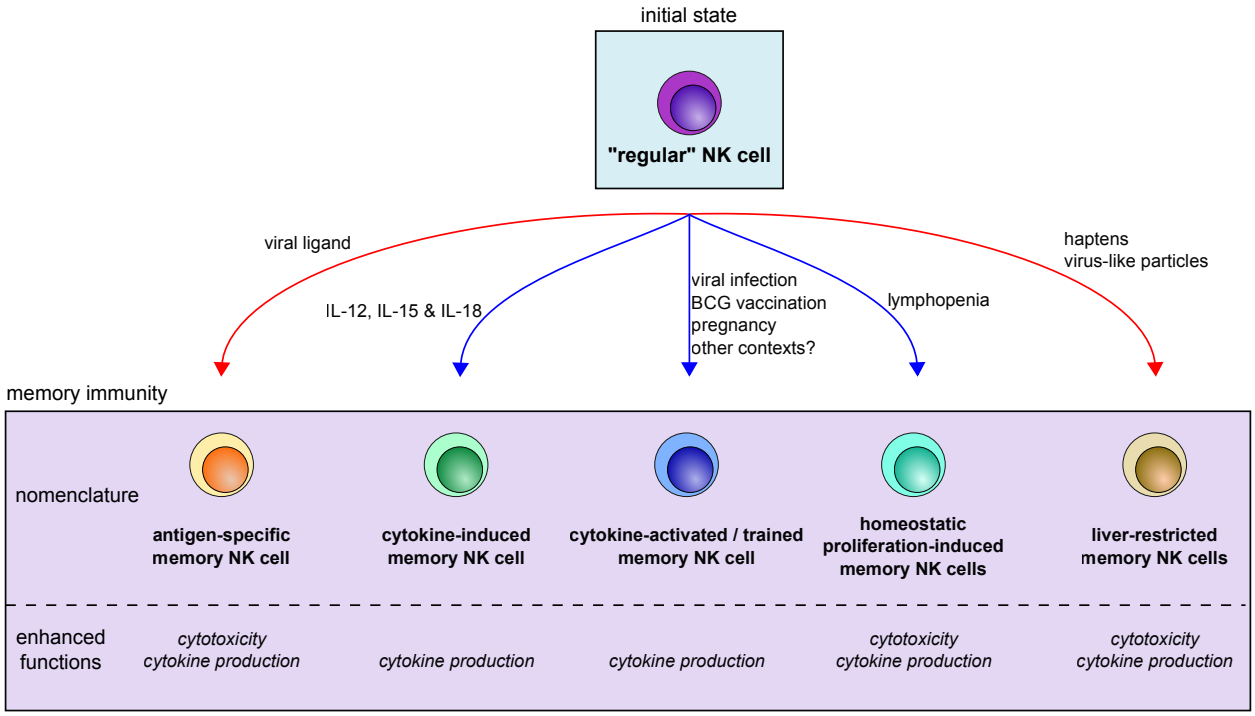

Figure 17. **Diverse populations within "memory" NK cells.** The main contexts giving rise to memory NK cells and the resulting functions of those cells are presented. Some of these NK cells (*e.g.*, cytokine-activated and cytokine-induced NK cell) show similar enhanced functions, but not following the same stimuli. Red arrows indicate that the resulting NK cell is pathogen-specific. Blue arrows indicated that the resulting NK cell is non-pathogen specific.

Hypotheses and aims of the project

Overall, massive data were generated in the past decades on immune cell biology and functions in several contexts (*e.g.* steady-state, infection, cancer), which helped us to better understand the immune response induced by pathogen or vaccine. In particular, tremendous findings have been made in fundamental immunology, including cDC development and functions, NK cell and ILC subpopulations characterization and their interactions with other cell types, unveiling of neutrophil plasticity, maturation and development of T and B cells, humoral response establishment and maintenance. These findings as well as the wide literature of immunology opened numerous perspectives of research in several fields, including of host-pathogen interaction and co-evolution, cancer control and treatment, allergy or auto-immune disorders, as well as vaccinology.

Still, our current knowledge is unsufficient to answer basic and pragmatic questions to optimize current and future vaccines, such as choice of the route of immunization, vaccine type, dose, number of immunizations and delay between each immunization. Such knowledges are required to come closer to personalized vaccines for all populations (*e.g.* the general population, young children, elderly people, immunocompromised people).

Besides, the scheme of vaccine-induced immunity was complexified by the description of several cell subsets especially in innate immunity, but their exact dynamics upon infection/vaccination are not well known, neither are the exact interactions existing between theses cell types. In addition, the recently described innate immune memory opens new possibilities on the potential modulation of vaccine design.

Also, there is a complex interplay between innate and adaptive immunity with all cells modulating the behavior of each other. Furthermore, adaptive memory B and T cells respond differently at each pathogen encounter and produce different cytokines with different kinetics compared to naïve cells. Though the literature is more abundant on the ability of innate cells to activate adaptive immunity rather than the impact of adaptive immunity on innate cells at prime and recall, we assume that innate immune cells can receive different activation signals at each pathogen encounter (*e.g.* different cytokines, antibody-bound pathogen rather than raw one), and thus differently respond at each immunization. Finally, given the memory-like potential of innate immunity via epigenetically modified cells following several stimuli, we suspect that such trained innate cells can be induced during vaccine encounters.

In addition, since most vaccines require several injections to induce a potent memory response, given the time-lapse that is required for memory to be set and that both innate and adaptive responses are continuous dynamic phenomena, we assume that the delay between each immunization will impact the immune response at each immunization. Consequently, we hypothesize that the delay between prime and boost is of high importance for optimizing vaccines. Indeed, should the boost occur too early, it will re-activate a memory that is not yet fully established, thus disrupting the maturation process; conversely, should the boost be given too late, the primary immune memory could have started to wane.

Eventually, since innate immunity mediates effector functions, activates and shapes adaptive immunity, modulates its own effector functions, and includes potential memory cells, understanding vaccine-induced innate immune response appear crucial to optimize vaccine design.

In my PhD project, I thus address the following questions (**Figure 18**):
- which precise innate subsets are impacted by vaccination and with which kinetics?
- are the innate responses similar between the prime and the following boost(s)?
- what is the impact of the delay between prime and boost on innate immune responses?
- what are the link between the kinetics and quality of the innate responses and the adaptive immune memory resulting from immunizations?

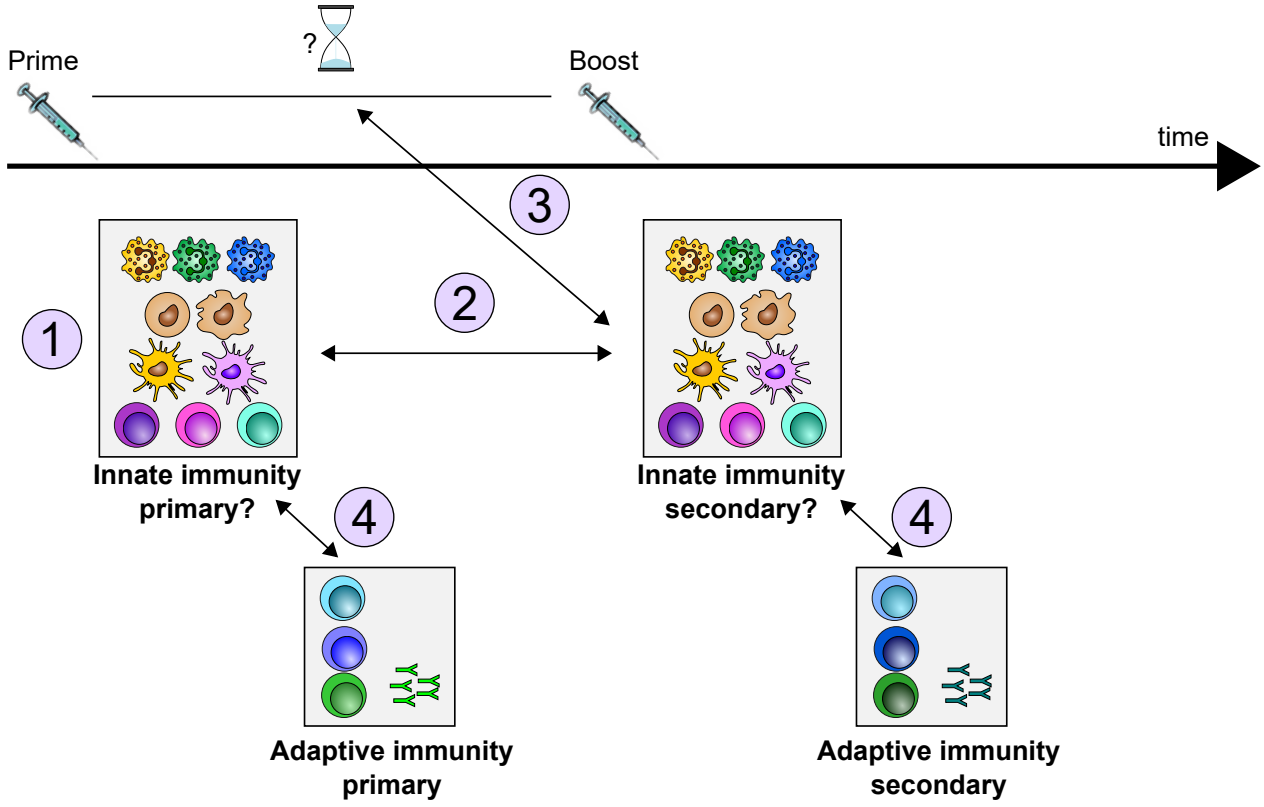

Figure 18. Graphical abstract of the project aims. The main objectives of the project are depicted, along the timeline of the prime-boost vaccination schedule. 1: determining the innate subsets impacted by vaccination with their dynamics. 2: comparing innate responses to prime and boost. 3: determining the impact of prime-boost delay on the innate response. 4: assessing the correlations between innate and adaptive responses.

Part I.
Methodology

Chapter 1. Experimental model and technologies used

Animal model: cynomolgus macaque

The overall aim of the research group is to have an integrated vision of all immune compartments, including not only blood but also other tissues, with very close sampling dates, to have a longitudinal follow-up. This was the main criterion to choose an animal model. Humans were indeed excluded, since one part of the project, beyond the scope of this thesis, was to assess the cells that remained in different tissues, long-time after vaccination, which required euthanasia.

Animal models in immunology, towards the choice of non-human primate

Mouse models

A common animal model in immunology is rodents (mice essentially), for which many interesting tools exist. For examples, genome of mice is well-characterized, which allow for the use of genetic engineering (*e.g.* knock-out/knock-in to study the impact of a peculiar set of genes and to perform mechanistic studies) (Bouabe & Okkenhaug, 2013). The existence of two isoform of the CD45 molecules (expressed by all immune cells) across mice strains is an efficient tool to track down the origin and fate of immune cells during adoptive transfer. Also, humanized mice carrying parts of the human immune system allow to mimic human diseases (Shultz et al., 2012; Walsh et al., 2017).

These models were shown to be highly valuable in various contexts, including cancer, infectious diseases, aging, neurosciences and neurodegenerative diseases (Wong et al., 2002; Shultz et al., 2012; Vandamme, 2015; Zitvogel et al., 2016; Drechsler et al., 2016; Ellenbroek & Youn, 2016; Walsh et al., 2017; Kipp et al., 2017; Evering & Tsuji, 2018). Indeed, the relatively low cost and constraints of housing make it a very powerful tool to study several aspects of the immune system with a strong statistical power given by a high number of animals. Overall, mouse models led and continue to lead to several major discoveries in immunology.

Still, mice are far from humans in term of phylogenetics (**Figure 19**). Accordingly, they display strong differences in term of immune system composition, response to treatment or infectious agents (Mestas & Hughes, 2004; de Jong & Maina, 2010). For example, mice and humans differ in immune cell composition in blood: in humans 50-70% of leukocytes cell are neutrophils and lymphocytes represent around 30-40%, whereas in mice, 75-90% of leukocytes are lymphocytes and neutrophils represent less than 25% of all leukocytes (Mestas & Hughes, 2004; Bjornson-Hooper et al., 2019). B cells are far more abundant in mice (more than 10%) than in humans and NHPs (around 1-10%) (Bjornson-Hooper et al., 2019). Hematopoietic stem cell differ by the expression the tyrosine kinase FLT3 between mice and humans (Mestas & Hughes, 2004). Mice macrophages produce nitric oxide upon IFNγ and LPS stimulation (Bogdan, 2001), but not their human counterpart, in which IFN I, IL-4 and CD23 signaling seemed more important (Weinberg, 1998). Actually mice and human macrophages were reported to use different pathways to synthesize nitric oxide (Schneemann & Schoedon, 2002). Besides, the receptors activating NK cells in mice and humans are highly distinct, suggesting differential abilities to respond to stimuli beyond an overall conserved function (Lanier, 1998; Colucci et al., 2002).

These interspecies differences can make the translation to humans difficult. For example, rodents do not have the same susceptibility and pathology to tuberculosis than humans (Dharmadhikari & Nardell, 2008). In pertussis infection, mice do not cough (Elahi et al., 2007), which impairs the assessment of vaccine or treatment efficacy on symptoms and disease transmission. In multiple sclerosis, IFNγ treatment was protective in a mouse model (Lublin et al., 1993; Heremans et al., 1996) but not in human patients (Panitch et al., 1987). In humanized mouse model limits exist, since humanization is not complete (*e.g.* stromal cells are murine), impeding the full mimicry human immunity (*e.g.* mucosal immunity) (Brehm et al., 2013; Akkina et al., 2016; Laudanski et al., 2018).

The small size and weight of the animal also matters. Indeed, the size limits the volume of vaccine/treatment that one could inject in the mice, and it is not easy to determine which dose in mice will accurately reproduce what happens in humans, especially when it comes to pharmacodynamics/pharmacokinetics (de Jong & Maina, 2010). The heart bite of mice is around 600 per minute (compared to around 80 for human). As a consequence, mice tolerate higher dose of drugs than human (the half-life of many compounds is shorter in mice than in humans), which can impair their use in dosage safety studies, although allometric scaling across species reduced this bias (de Jong & Maina, 2010).

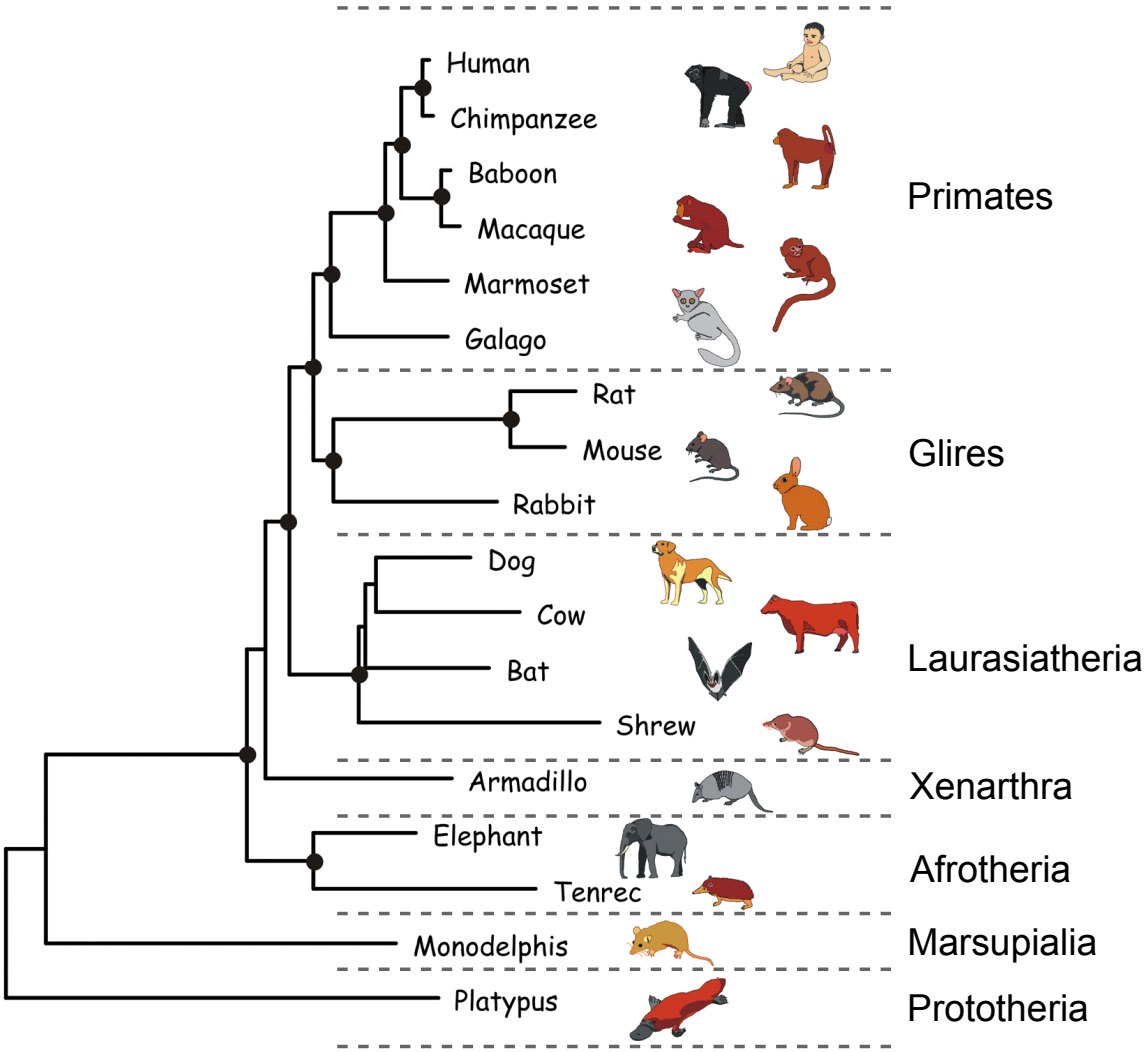

Figure 19. **Phylogenetic tree of mammals.** The phylogenetic distance between each mammal taxon is represented. The tree was built based on the alignment of 68,262 codons. Branch length is proportional to the number of substitutions per site. Modified from Nikolaev et al. (2007).

Eventually, the amount of blood that could be collected is reduced in mice, making longitudinal analyses with very narrow sampling dates (required to study innate immunity kinetics) tricky (de Jong & Maina, 2010), although it was proved feasible (Kadoki et al., 2017).

Given the narrow sampling schedule we need to put in place, the amount of blood required to investigate in deep the innate immunity of each immunization, and since we wanted to be as close to human as possible, we chose not to use mouse models.

Non human primate models

Among other mammals available for animal experimentation, non-human primates (NHPs) are the closest to humans (**Figure 19**), since the NHP branch diverged from the human very lately in evolution, around 5 million years ago (Perelman et al., 2011). Indeed, NHPs are usually susceptible to human pathogens (and thus to vaccines derived from them) with similar clinical outcomes (Estes et al., 2018) (**Figure 20**), though not all NHPs are susceptible to all human pathogens. For example HCV infection is restricted to humans and chimpanzee (Sandmann & Ploss, 2013). Also NHPs are usually not susceptible directly to HIV but rather to SIV, although simian tropic HIV have now been developed to overcome species specific restrictions (Hatziioannou & Evans, 2012; Fennessey & Keele, 2013; Misra et al., 2013).

Inconvenients for this model exist. Indeed, their price is higher than for mice. Also they require specific and more complex installations, both due to their size and ethical considerations. This notably limits the number of animals one can use. As a consequence, this can limit the statistical power of the study. Besides, although closer to humans than mice, NHPs are still not humans with respect to their immune system composition (*e.g.* NHP leukocytes comprised around 6% of NK cells whereas human ones contained around 2% of NK cells) (Bjornson-Hooper et al., 2019). NK cells that are defined via the expression of CD56 in humans, are $CD56^{-}$ $CD8^{+}$ in NHPs (Hong et al., 2013), whereas human monocytes are $CD56^{-}$ and NHP monocytes are $CD56^{+}$. Similarly, NKp46 which is widely express in all human NK cells, is only express in some NK cell subpopulations in NHPs (Hong et al., 2013). Also NHP carry more alleles of HLA genes, which makes antigen recognition trickier than in humans (de Groot et al., 2012).

Despite these caveats, NHP immune system is very close to human in term of cell composition (Messaoudi et al., 2011). As a consequence, NHP was proven valuable in the understanding of the human immune system in various context, including infectious diseases such as tuberculosis or HIV/AIDS and auto-immune diseases, such as multiple sclerosis (Brok et al., 2001; Hatziioannou & Evans, 2012; Phillips et al., 2014; Peña & Ho, 2015), and their high size and weight allowed narrow longitudinal sampling.

For these reasons we chose to use NHP for this project.

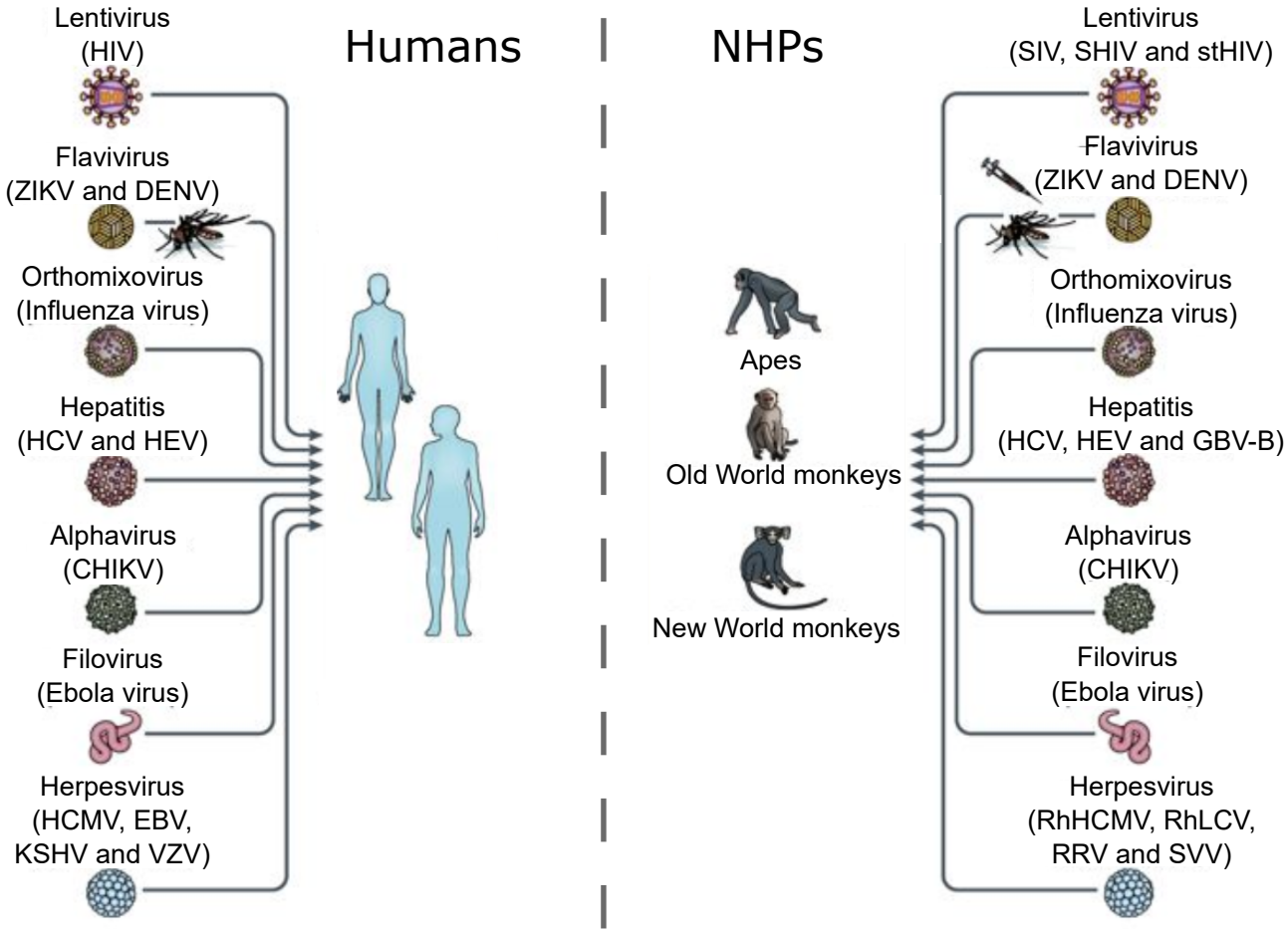

Figure 20. **Non-human primates mirror human diseases.** Pathogens infecting humans and non-human primates are presented on each side of the doted line. Note that apes represented here cannot be used as animal model for ethical reasons. HIV: Human immunodeficiency virus. SIV: simian immunodeficiency virus. SHIV: simian/human immunodeficiency virus. stHIV: simian tropic HIV. ZIKV: Zika virus. DENV: dengue virus. HCV: hepatitis C virus. HEV: hepatitis E virus. GBV-B: hepatitis G virus B /GB-virus B. CHIKV: Chikungunya virus. HCMV: human cytomegalovirus. EBV: Epstein-Barr virus. KSHV: Kaposi's sarcoma associated herpes virus. VZV: varicella-zoster virus. RhCMV: rhesus cytomegalovirus. RhLCV: rhesus lymphocryptovirus. RRV: rhesus macaque rhadinovirus. SVV: simian varicella virus. Modified from Estes et al. (2018).

Non human primate models and vaccination, an overview

NHPs have been used to develop vaccine for a long time period and for several vaccines (Rivera-Hernandez et al., 2014). We will here mention some of these fields of research.

In tuberculosis research, NHPs displayed a similar susceptibility and pathology compared to humans, which allows for a good assessment of candidate-vaccine protection (Dharmadhikari & Nardell, 2008). Cynomolgus macaques were especially reported as the best model in this context (Lin et al., 2009). Furthermore NHP allowed for the assessment of vaccine efficacy in co-infection settings, such as co-infection with HIV/SIV, a major threat to public health nowadays (Shen et al., 2002).

In pertussis vaccine development, NHPs (more particularly baboons) were shown to reproduce human pathology including cough and were proven valuable in the assessment of vaccine efficacy (Elahi et al., 2007; Warfel et al., 2012). In particular, NHP model allowed to establish that the acellular recombinant vaccine, in contrast to whole cell vaccine, prevented only the symptoms of whooping cough, but not the propagation of the bacteria (Warfel et al., 2014).

In dengue vaccines, current vaccine development pipelines widely use NHPs to assess safety, immunogenicity and efficacy of vaccine candidates (Guirakhoo et al., 2000; 2004; Guy et al., 2009; Halstead, 2013), generating valuable data for human clinical trial design. Eventually, neutralizing antibody titer in NHP serum was identified as a relevant correlate of protection for vaccine efficacy (Barban et al., 2012).

In HIV vaccine research, NHP model has already been proven valuable since it reproduces the human pathology (Geretti, 1999; Misra et al., 2013). Still, some criticisms emerged, since a trial using adenovirus 5 vector encoding for HIV proteins, a construct suggested strongly potent in non-human primates (Shiver et al., 2002; Casimiro et al., 2005) failed in humans (Buchbinder et al., 2008). This called for the improvement of NHP models and better understand the extent of the findings (Shedlock et al., 2009; Robb, 2011). Still, given its ability to reproduce pathogenicity, NHPs remain nowadays the most promising model to assess HIV pathology in acute and persistent phase and design future anti-HIV vaccines (Lynch et al., 2013; Kumar et al., 2016).

Cynomolgus macaques as a model among non human primates

For all the previously mentioned reasons, we chose to use NHPs as animal model. Among NHPs, a wide number of model were developed to mimic human infectious diseases and thus serve as a good basis for vaccine efficacy evaluation (Gardner & Luciw, 2008).

For example, both cynomolgus and rhesus macaques were shown to mimic *Streptococcus pyogenes* infection, and were thus considered as promising model for vaccine design (Skinner et al., 2011). Regarding measles infection, both models were shown valuable, although cynomolgus tend to reproduce more accurately human infection (El Mubarak et al., 2007). In tuberculosis infection, rhesus and Mauritian cynomolgus macaques were closer to humans in term of pathology, compared to Chinese cynomolgus macaques (Maiello et al., 2018). Besides, cynomolgus macaques were more homogeneously permissive to SIV and simian/human immunodeficiency virus (SHIV) infection than rhesus macaques and are thus an important model in HIV vaccine design (Antony & MacDonald, 2015).

We then eventually chose the cynomolgus macaques (*macaca fascicularis*) as our animal model, a widely used model in biomedical research, including vaccination (Carlsson et al., 2004; Ebeling et al., 2011). These cynomolgus macaques originated from Mauritius and arose from a restricted number of animals, which implies a reduced genetic variability (Kawamoto et al., 2008; Ogawa & Vallender, 2014). This relatively low genetic heterogeneity also reduced inter-individual heterogeneity and may mitigate the low statistical power inherent to NHP studies.

Vaccine model: modified vaccinia virus Ankara

Among the existing vaccines, poxviruses were used as anti-variola vaccines, which led to the first, and currently sole, eradication of a human pathogen, the smallpox virus. These viruses indeed induce a robust and protective immunity. Among them, our interest came on the modified vaccinia virus Ankara (MVA).

From vaccinia virus to a new smallpox vaccine

MVA derives from vaccinia virus (VACV), the virus efficiently used as smallpox vaccines, which allowed for smallpox eradication. VACV is a poxvirus, from the orthopoxivrus genus (as variola virus causing smallpox). VACV is a complex DNA virus of around 200kb encoding for approximately 200 genes (Condit et al., 2006). As most poxviruses, it is not clear which receptors VACV actually uses to enter cells (Moss, 2006; Schmidt et al., 2012). VACV can infect a wide range of cells, including immune and non-immune ones, from several animal species (McFadden, 2005; Jacobs et al., 2009). Though, intra-cellular factors can restrict cell infection. Actually, the infection cycle of poxvirus is quite complex and includes several steps of maturation, and two potentially infectious particles (McFadden, 2005). Details on this infectious cycle are given in **Figure 21**.

VACV was able to induce a strong and long-lasting anti-smallpox immunity, mediated by both T and B cells, although the exact contribution of each is not well defined (Fulginiti et al., 2003a). VACV was the trigger to smallpox eradication (Jacobs et al., 2009). Still, some concerns emerged about its safety, since documented side-effects, ranging from mild to life-threatening were reported during the vaccination campaign (Fulginiti et al., 2003b; Belongia & Naleway, 2003). These effects notably included generalized vaccinia (241 cases per million), eczema (39 cases per million), post-vaccinal encephalitis (12 cases per million) and death (1 case per million). This called for a safer smallpox vaccine.

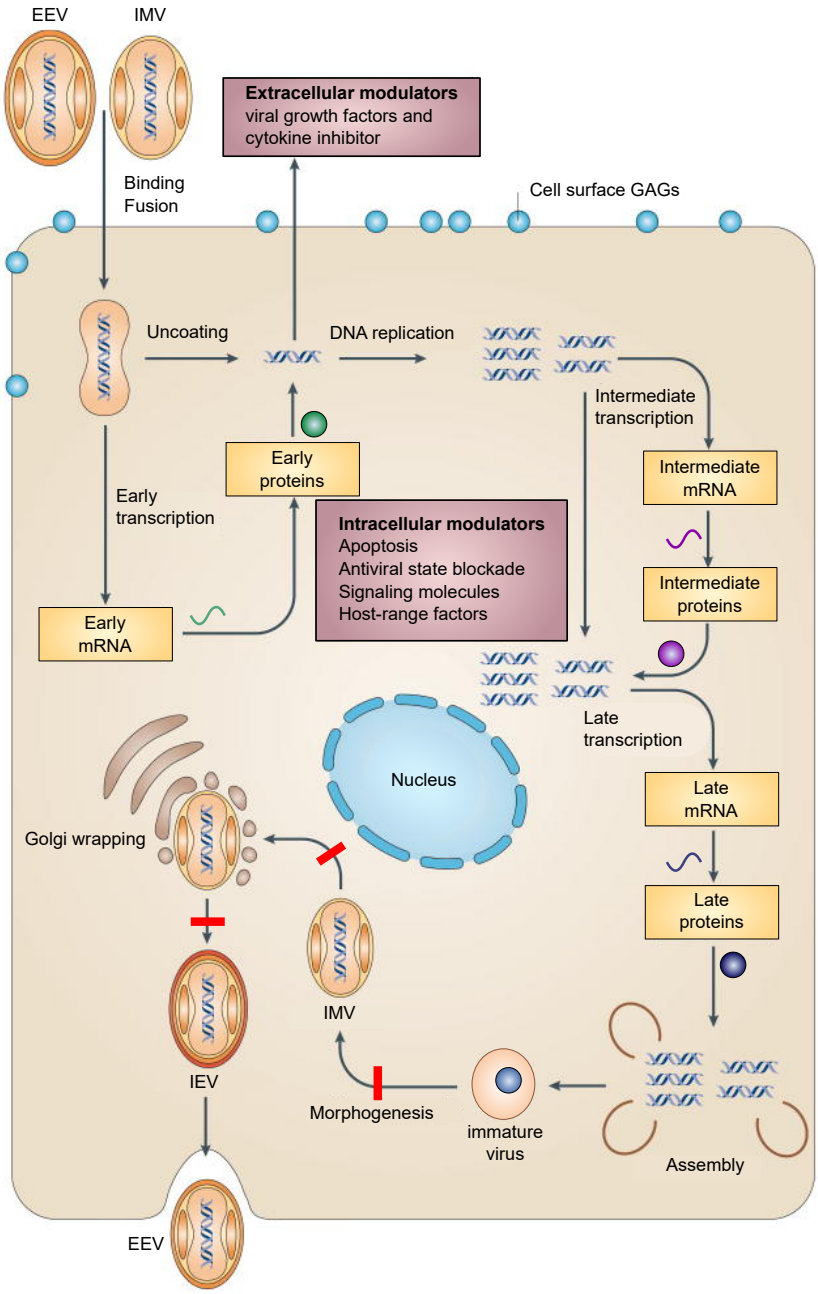

Figure 21. **Poxvirus viral cycle.** The complex infectious cycle of poxviruses is presented here. Briefly, infection can be initiated by two virions, IMV and EEV (both differ in the glycoproteins they contain and the number of membranes that surround them). Several proteins are at play for viral binding and entry (both on virus and cell surface). Full replication goes with three consecutive steps of protein expression (early, intermediate and late). The resulting IMV traffics to Golgi network where it is wrapped to form IEV. The IEV fuses with plasma membrane, forming cell-associated enveloped virus (CEV not represented here). CEV can be released as EEV. Note also that IMV can directly bud through the cell membrane, without going through the IEV form. Red bars indicate the steps that are defective in the replication incompetent MVA cycle. GAG: glycosaminoglycans. EEV: extracellular enveloped virus. IMV: intracellular mature virus. IEV: intracellular enveloped virus. Modified from McFadden (2005).

Modified vaccinia virus Ankara: development and immunity

The attenuated MVA was randomly obtained after more than 500 passages on embryonated chicken egg (Volz & Sutter, 2017). It resulted in a loss of around 15% of its genome and many virulence factors (Meyer et al., 1991). As a consequence, MVA was unable to replicate in mammalian cells, since it cannot form mature particle due to defect in morphogenesis steps (**Figure 21**) although it could infect them (Drexler et al., 1998). Still, MVA induced a protective immunity against other poxviruses in several animal models including NHPs (Wyatt et al., 2004; Earl et al., 2004; Stittelaar et al., 2005; Knitlova et al., 2014; Jones et al., 2016). It was successfully inoculated to individuals considered at high risk with regard to VACV vaccination, without triggering any adverse effect (Blanchard et al., 1998).

MVA induced a very mild local reaction, by contrast to VACV, in cynomolgus macaque model (Volz & Sutter, 2017). Though, it is a very efficient inducer of innate immunity. MVA is thought to be recognized via TLR2-TLR6, MDA-5 and activation of NLRP3/NALP3 inflammasome, which trigger the production of several pro-inflammatory cytokines (*e.g.* TNF, IL-6, MIP-1α, IL-1β and IL-8) (Delaloye et al., 2009) (**Figure 22**). In addition, MVA induces a strong interferon response (both type I and II), by contrast to VACV that possesses virulence factors inhibiting interferon responses, notably soluble interferon receptors (Waibler et al., 2009; Price et al., 2013). Type I response seemed to be independent of TLR9 signaling (Waibler et al., 2007; Delaloye et al., 2009) and rather dependent on cGAS/STING pathway activation (Dai et al., 2014) (**Figure 22**). Also, chemokines, such as CCL2, CCL3, CCL4, CXCL8 and CXCL10 (IP-10), are produced. They allow for the efficient recruitment of monocytes, NK cells and T cells. Among them, CCL2 was proven the key chemokine (Lehmann et al., 2009).

Similarly to VACV, MVA was reported to induce a strong adaptive immunity, including both cellular (T cell mediated) and humoral (antibody mediated) responses (Amanna et al., 2006; Panchanathan et al., 2008; Kennedy et al., 2009). However, MVA required two doses (prime and boost) to induce an efficient seroconversion in all participants (Vollmar et al., 2006). To date, the delay between prime and boost seemed important, since reducing the delay below three weeks (by contrast to one month) impairs neutralizing antibodies generation in healthy volunteer (Jackson et al., 2017). Note also that the route of immunization was shown to impact the quality of the humoral response induced, and the subcutaneous route seemed to be more efficient in neutralizing antibodies induction (Damon et al., 2009).

MVA was licensed as a third generation vaccine against smallpox in Europe and Canada, in accordance with the European medical agency and Health Canada respectively (Volz & Sutter, 2017).

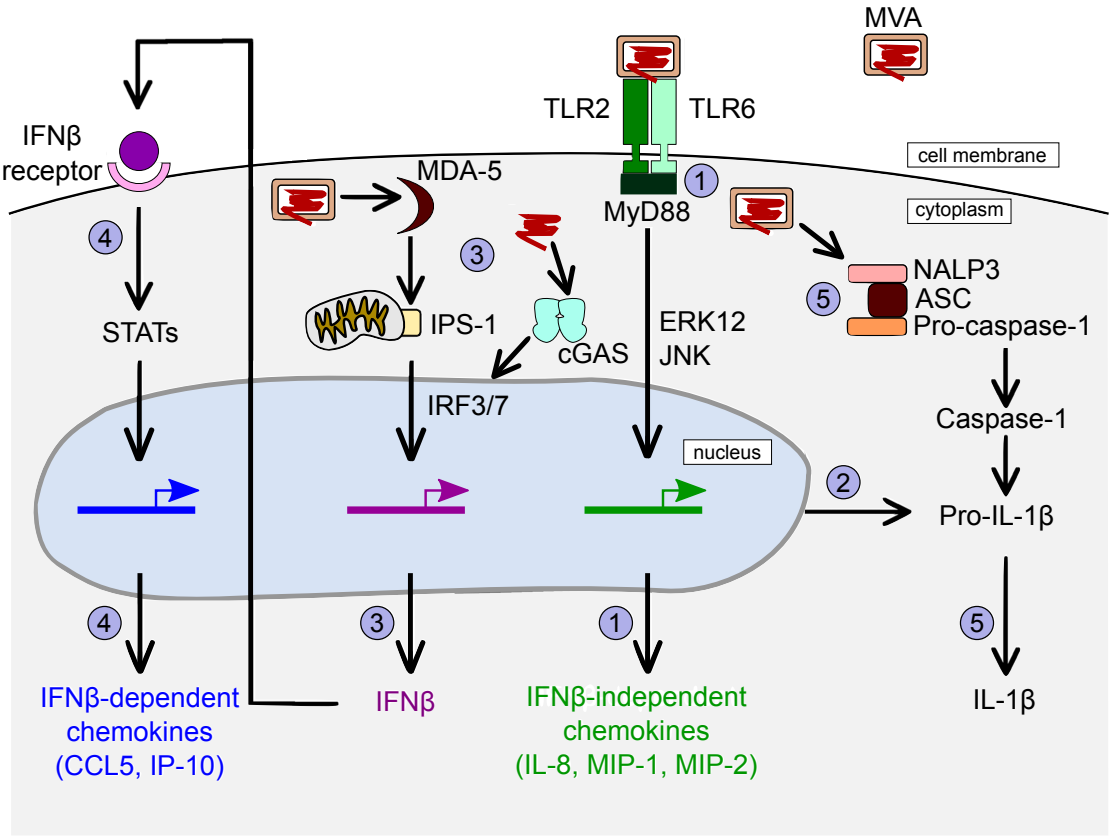

Figure 22. MVA sensing by the immune system. The PRR involved in MVA recognition (TLR2/6, MDA-5, NALP3/NLRP3 inflammasome and cGAS) and the resulting pathways activated, notably including IFNβ production, are represented. Numbers indicate the chronology of events. Modified from Delaloye et al. (2009).

Modified vaccinia virus Ankara as a vaccine vector

Given their large genome, poxviruses including MVA allow for insertion of foreign genes. This permits to use MVA as a vector to build vaccines (mostly preventive but also therapeutic) against a wide variety of pathogens and diseases, including respiratory diseases, yellow fever, Ebola virus, papillomavirus, malaria, tuberculosis and HIV (Martinon et al., 2008; Altenburg et al., 2014; Iyer & Amara, 2014; Borducchi et al., 2016; Sebastian & Gilbert, 2016; Schweneker et al., 2017; Julander et al., 2018; Leung-Theung-Long et al., 2018; Cabo Beltran & Rosales Ledezma, 2019).

Note that many viral vectors exist, such as lentivirus, adenovirus, alphavirus or cytomegalovirus based vaccines (Choi & Chang, 2013; Ura et al., 2014). Each presents several advantages and disadvantages. For example, retrovirus-based vaccine, allow for long-term gene expression, but can give rise to replication-competent virus. By contrast, adenovirus-based vaccines are highly immunogenic but efficiency can be reduced by pre-existing immunity against the vector (Ura et al., 2014).

Overall, MVA was shown to induce a strong immune response against the transgene during a prime-boost vaccination schedule (Cottingham & Carroll, 2013). Still note that as for other vectors, heterologous prime-boost (with a distinct vector, such as an adenovirus for instance) are widely used to reduce the impact of anti-vector immunity at the boost (Cottingham & Carroll, 2013; Ura et al., 2014). MVA exhibits a remarkable genetic stability, even with foreign genes inserts. Thus, altogether with the other viral vectors, MVA is a potent vaccine vector candidate against diseases for which an efficient vaccine is not yet available (Cottingham & Carroll, 2013; Choi & Chang, 2013; Ura et al., 2014; Ramezanpour et al., 2016).

Modified vaccinia virus Ankara as vaccine model in the project

MVA is a potent inducer of innate responses (Delaloye et al., 2009; Teigler et al., 2014; Dai et al., 2014). This allows to easily study vaccine-induced innate immunity. Also, MVA requires a prime-boost regiment to fully induce a long-lasting immune memory, which is crucial in order to study the impact of the prime-boost delay on the resulting immunity. Strikingly the delay between prime and boost seemed to have a strong effect an antibody generation (Jackson et al., 2017). Accordingly, the recommendation for MVA vaccination is a prime-boost delay of more than 28 days.

Besides, given that MVA can induce both humoral and cellular responses, including in macaques (Earl et al., 2004; Grandpre et al., 2009), one can hypothesize that vaccination strategy (in particular vaccine schedule), and the resulting innate immunity induced can have a differential impact on the quality of both arms (B and T cells) of immune memory developed. For all these reasons, we chose to use MVA as our vaccine model in this project.

Note that for practical reasons, we used the recombinant MVA HIV B vaccine developed by the French ANRS (MVATG17401; Transgene, Illkirch-Graffenstaden, France) (Brandler et al., 2010), encoding several HIV proteins fragments (Gag, amino-acids 1-519; Pol, amino-acids 172-219, 325-383 and 461-519; Nef, amino-acids 66-147 and 182-206), to which we had access via our LabEx "Vaccine Research Institute". Since we were interested in the response to the vaccine itself, and not the HIV insert at first intention, we used a homologous prime-boost strategy (as for vaccination against smallpox), rather than an heterologous prime-boost strategy (as for current candidate vaccines focusing on anti-insert immunity).

The European medical agency recommend to use subcutaneous injection for human MVA vaccination. Besides, preliminary pilot studies from the laboratory indicated that subcutaneous injections induced a stronger neutralizing antibody response than other routes of immunization, consistently with literature (Damon et al., 2009). Neutralizing antibody response, in addition to T cell response, was proved a good correlate of protection for several vaccines including smallpox (Sarkar et al., 1975; Plotkin, 2008; Kennedy et al., 2009; Moss, 2011). For these reasons, the subcutaneous immunization route was used for this project.

Also, the dose recommended for MVA vaccination is more than 5.10^7 infective units. A pilot study in the laboratory led us to choose an injection dose of 4.10^8 plaque-forming units (PFU), since it induced a more homogeneous response across tested animals compared to lower doses. This dose is consistent with the dosage usually used in humans (1-5.10^8 PFU).

Main experimental technology: mass cytometry

The requirement of single-cell measurement

Defining a precise picture of the immune system require a multi-dimensional measurement given the complexity of the immune system. In addition, since we aimed to investigate immune cell response, we needed a technology that allows for measurements of cell phenotypes, rather than genomic analyses (Brodin et al., 2015). Eventually, to precisely decipher the exact subphenotypes that are impacted by vaccination, we needed to assess it at a single-cell level.

Indeed, beyond the classical populations of innate cells (*e.g.* neutrophils, monocytes, NK cells, cDC1, cDC2), innate immunity is composed of heterogeneous cell populations comprising several subphenotypes (Taylor & Gordon, 2003; Freud et al., 2017; Collin & Bigley, 2018; Ng et al., 2019; Olingy et al., 2019). Whether distinct subphenotypes define distinct subpopulations, or solely reflect distinct activation or maturation status within the same population adds alayer in immune system complexity.

Within neutrophil population, although the nomenclature and associated phenotype is not completely established nowadays, it is acknowledged that intermediate subpopulations exist between granulocyte-monocyte progenitor and mature neutrophils (proposed names, pro-neutrophils, pre-neutrophils and immature neutrophils) (Marini et al., 2017; Evrard et al., 2018; Ng et al., 2019). Also, in blood, "aged" neutrophils differ in phenotype (*e.g.* CD62L^{low} CXCR4^{high}) and function (*e.g.* increased phagocytic potential) from "young" neutrophils (Martin et al., 2003; Adrover et al., 2016; Uhl et al., 2016).

Among cDC2 populations, CD5^{low} and CD5^{high} cDC2 induced differential differentiation of CD4 T cells (Collin & Bigley, 2018). Besides, precursor of DC, the so-called pre-DC were identified, and actually several cDC subpopulations were proposed (Villani et al., 2017). Also according to tissues, different phenotypes can be found, for example CD1a^{+} DC in the skin (Ochoa et al., 2008). Langerhans cells or dermal DC also exhibited distinct functions including the differential activation adaptive immunity (Klechevsky et al., 2008). Similarly, several subpopulations of DC deriving either from CD34^{+} precursors or from monocytes were proposed (Kohl et al., 2007). In monocytes-macrophages derived populations, phenotypes and function highly differ according to the tissue (*e.g.* brain, skin, gut, lung) (Ginhoux & Guilliams, 2016; Gordon & Plüddemann, 2017), giving rise to self-maintaining distinct subpopulations (Perdiguero & Geissmann, 2016).

Regarding NK cells, the distinction between CD56^{dim} and CD56^{bright} subpopulations dominated the field in humans for a long time (Cooper et al., 2001; Poli et al., 2009), but new subpopulations were identified, for example based on CD27 and CD11b in humans (Hayakawa et al., 2010), or CD2, CD7, CD16, CD161 and NKG2A in rhesus macaques (Webster & Johnson, 2005). In addition, NK cell subpopulations strongly differ in phenotype according to the tissue they reside in (Freud et al., 2017). Also, the increasing diversity of NK receptors strongly suggests a wide heterogeneity within each NK cell subpopulation (Wilk & Blish, 2018).

To assess and understand in depth this wide diversity of innate immune cells that can be impacted by vaccination, we thus needed an analysis strategy working at single-cell level. Overall, two class of approaches fitted these criteria, each with it own advantages and drawbacks: transcriptomics (targeting RNAs), and proteomics (targeting proteins) (Chattopadhyay & Roederer, 2015; Furman & Davis, 2015; Reeves et al., 2018) (**Table 2**).

Table 2. Main technologies available to decipher vaccine-induced immune response.

Technology	Advantages	Challenges
microarray, RNAseq	Unbiased transcriptional profile of cell populations or tissue	Loss of single-cell information
single-cell RNAseq	Unbiased transcriptional profile of individual cells	Reduction in throughput
mass spectrometry	Unbiased proteomic profiling of cell populations or tissue	Loss of single-cell information
flow cytometry	Cost effective, low acquisition time, cell size discrimination, live-cell sorting , tracking of cell division with CFSE	Reduced number of parameters resulting from spectral overlap and background
mass cytometry	High parameter analysis of single cells using metal tags conjugated to standard antibodies, significant reduction in background and channel spil, data maximization from small volume serial study samples	Per sample cost is higher than standard flow, reduced acquisition rates and sampling efficiency

The main advantages and drawbacks of each technology is indicated. Transcriptomic approaches are described on top. Proteomic approaches are described at bottom. Modified from Reeves et al. (2018).

Proteomics *vs.* transcriptomics: pros and cons

On the one hand, transcriptomics allows for the simultaneous measurement of virtually all genes expressed by a given cell (RNAseq), or at least a high number of them (microarrays) (Furman & Davis, 2015). Still, these measurements are usually done on bulk of cells, which allow to extract an overall signature but not to define precise cell populations. Newly developed technologies, such as single-cell RNAseq, combine single-cell isolation and RT-qPCR sequencing to perform such analyses at a single-cell level (Kolodziejczyk et al., 2015). Though powerful, this can only be done on a relatively low number of cells (from hundreds to few thousands), and thus requires to determine *a priori* the cell population one would like to investigate. In addition the sensitivity is not high, thus rare transcripts may not be detected.

Since my project was more exploratory and not limited to precise cell subsets within the innate immune system, we did not use these technologies in first intention (**Table 2**).

On the other hand, proteomics allows for the direct measurement of several markers. Technics working on bulk cells (*e.g.* mass spectrometry) allow for the definition of signature but not yet for individual cell response (Glish & Vachet, 2003), although new single-cell measurement methods are currently being developed in the community (Budnik et al., 2018). Still, multiplex fluorescence-based luminex technics that allows to measure soluble factors (including cytokines) secreted by cells can be valuable in our context to understand immune cell functions (Furman & Davis, 2015).

Single-cell proteomics analysis technics allow for the simultaneous measurement of several (dozens) markers. One historical and widely used technology is flow cytometry that used antibodies combined with fluorochromes to stain cells, allowing to assess up to 18 markers at a single-cell level (O'Donnell et al., 2013; Furman & Davis, 2015). Among the main advantages of flow cytometry is the high-throughput (millions of cells can be analyzed in minutes), and ability to sort cells to perform further analyses, such as transcriptional profiling or functional tests, on purified cells. Still, the main limitation is the number of markers, since adding new markers require to carefully redesign each antibody panel due to overlapping emission spectra of the fluorochromes used. In practical, 12-colors panel are widely used, panels with higher number of markers are scarcer, even with newly developed spectral flow cytometry, which relies on the deconvolution of emitted signal rather than on signal compensation (Nolan & Condello, 2013; Schmutz et al., 2016). In any case, even 20 markers would be somewhat limitating to assess a wide range of immune cells (**Table 2**). This drove us to use rather mass cytometry.

Mass cytometry as the main analysis technics

Mass cytometry is a technology that was developed around 10 years ago (Bandura et al., 2009; Ornatsky et al., 2010; Bendall et al., 2012; Atkuri et al., 2015; Spitzer & Nolan, 2016), which combines flow cytometry (cells are stained with antibodies and signal is measured at a single-cell level) and mass spectrometry (antibodies are labelled with heavy metals, essentially lanthanides, which are not naturally found in cells). Since each metal label can be uniquely identified without interference with its neighbors, this technology allows for the simultaneous measurement of up to 40 markers at a single-cell level (**Figure 23**).

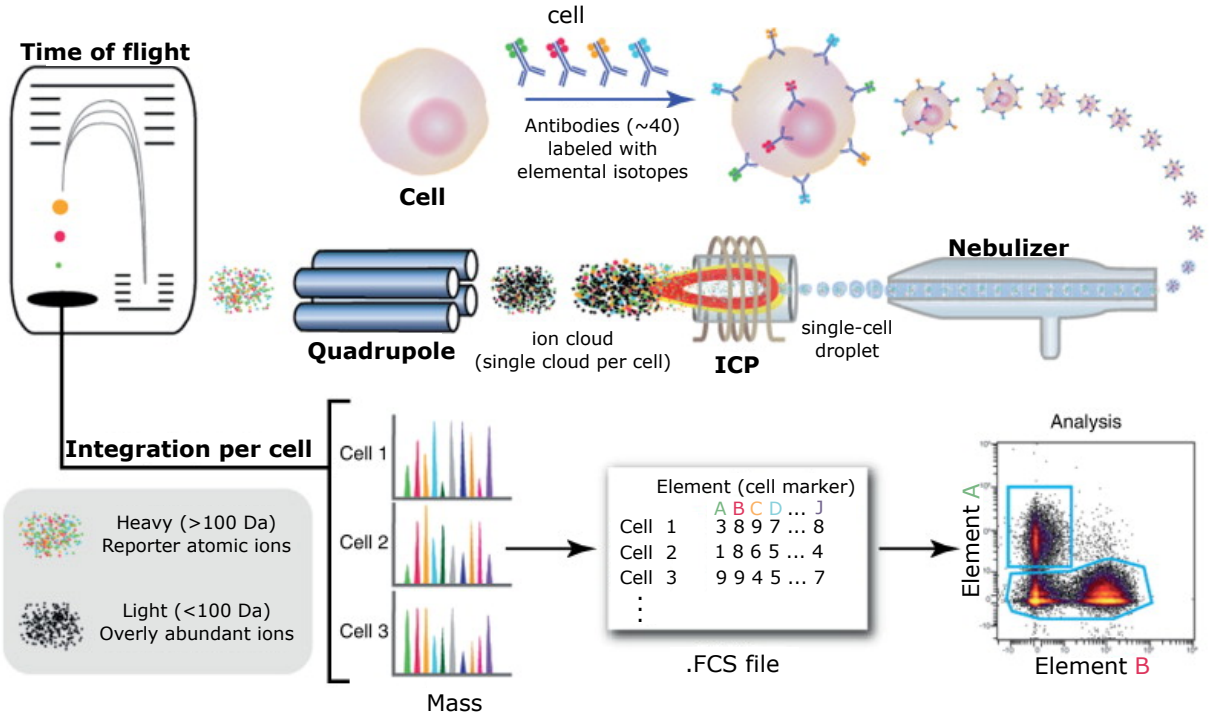

Figure 23. Principle of mass cytometry. The different steps of mass cytometry analysis of single-cells are described. Briefly, cells are labelled using heavy metal-bound antibodies. Then cell are nebulized and ionized so that each single cell forms a unique ion-cloud that can be analyzed with mass spectrometer. Each heavy metal contained in the ion cloud is then detected, so that the expression of the marker (targeted by the antibody) expressed by the cell can be quantified and analyzed by the user. Modified from Bendall et al. (2012).

The main caveat is the low throughput (around 1 million cells are analyzed in 1h) and the inability to sort cells (since cells are vaporized during analysis process) (**Table 2**).

Processing of mass cytometry data requires data normalization (to compensate for the loss of signal overtime during acquisition (Finck et al., 2013)). Also, barcoding technics allow to pool all samples during the procedure, before deconvolution afterwards during FCS files processing. This ensures that all samples are treated equally during the whole staining/acquisition procedure, reducing intra-staining variability. The most widely used barcoding technics in mass cytometry is based on the individual staining of each sample by a unique trio of three palladium isotopes (Zunder et al., 2015).

In addition, to reduce discrepancies in intensity across different stainings, one needs to use the same batch of antibodies for a full experiment. Besides, the use of control samples included in all stainings allow to measure technical inter-staining variability and ensure a good quality of the data generated, a procedure reported for both flow and mass cytometry (Lillacci & Khammash, 2013; Kleinsteuber et al., 2016). Eventually, recent findings suggest that even though signal should not overlap from one metal to the other in theory, background spillover can still be observed due to metal impurity or oxidation for example. As a consequence, the signal can be compensated as for flow cytometry (Chevrier et al., 2018). Still this multidimensional analysis potential makes of mass cytometry an excellent candidate to explore immune system characteristics on several cell populations.

Indeed, mass cytometry was successfully applied to characterize in depth numerous cell populations including notably T cells (Newell et al., 2012; Mason et al., 2015; Sen et al., 2015; Wong et al., 2015; 2016; Corneau et al., 2017; Kunicki et al., 2018; Norton et al., 2019), including $\gamma\delta$ T cells (Wanke-Jellinek et al., 2016), B cells (Bendall et al., 2014; Hansmann et al., 2015; Nair et al., 2016; Good et al., 2018), DC (Guilliams et al., 2016; Alcántara-Hernández et al., 2017; See et al., 2017), monocytes (Roussel et al., 2017), neutrophils (Blazkova et al., 2017; Evrard et al., 2018), basophils (Tordesillas et al., 2016), brain-resident myeloid cells (Mrdjen et al., 2018), and ILCs including NK cells (Horowitz et al., 2013; Strauss-Albee et al., 2014; 2015; Simoni et al., 2018). This includes longitudinal follow-up studies, for example after *Mycobacterium tuberculosis* infection (Roy Chowdhury et al., 2018), HBV infection (Cheng et al., 2019) or *Plasmodium falciparum* infection (Sundling et al., 2019).

On the innate side, those studies, conducted in various contexts including steady states, infection and cancer, contributed to unveil a high phenotypic diversity within the innate myeloid and lymphoid compartment. This further complexified the picture of innate immunity composition, notably in term of tissue, development and immune experience based variations, strengthening the requirement to use single-cell analysis in our setting. Note that non-immune cells were also recently studied with mass cytometry, for example epithelial cells (Pelissier Vatter et al., 2018; Scurrah et al., 2019), basal cell from mammary glands (Knapp et al., 2017), myogenic cells (Porpiglia et al., 2017) or pancreatic cells (Wang et al., 2016).

Still, despite these numerous results obtained so far, the use of mass cytometry in vaccination is quite scarce. For flu vaccine, PBMCs from vaccinated participants were re-stimulated either with split influenza virus or TLR7/8 agonists *in vitro* to assess similarities and noteworthy discrepancies in immune cell activation profiles. The authors looked at multiple immune cells including T cells, B cells, $CD14^{high}$ and $CD16^{high}$ monocytes, $CD66^{+}$ granulocytes, pDCs, cDCs and NK cells (O'Gorman et al., 2014). After adenovirus-MVA based HCV vaccination of human volunteers, hepatitis C virus (HCV) specific T cells were longitudinally tracked in two members of the cohort, and the functionality of those cells in term of cytokine production was assessed (Swadling et al., 2014). In RSV vaccination, pre- and post-vaccination samples from elderly participants helped defining a predictive vaccine responsiveness immune signature, based antigen-specific on T cell subpopulations, in this elderly populations (Lingblom et al., 2018). They notably identified HLA-DR^{+} T cells as a good predictor. Also, after typhoid vaccination, CD4 and CD8 T cell responses were compared in adult and children, evidencing a stronger multifunctionality of adult T cells (Rudolph et al., 2019).

Given the successes met by mass cytometry in several contexts, it stands as a promising tool to assess vaccine-induced innate immunity.

Toward a systems immunology approach

Bioinformatic tools are required for mass cytometry data exploration

Classical methods in flow cytometry are based on 2 dimension representations, called bi-plots, which allow for the visualization of the expression pattern of two markers at a time. Doing so, one can isolate cell subpopulations or subphenotypes, based on the expression each marker (usually defining positive and negative expression, rather than the staining intensity itself).

Given the number of parameters measured at a single-cell level for a high number of cells, classical ways of analysis (*e.g.* manual gating on bi-plots) cannot be applied for mass cytometry dataset analysis. Indeed, should one analyze manually the expression pattern of 32 markers by manual gating, one should go through 496 plots for each cell population studied, which is strongly time-consuming, error prone and at high risk to neglect large parts of the dataset (Bendall et al., 2012) (**Figure 24**).

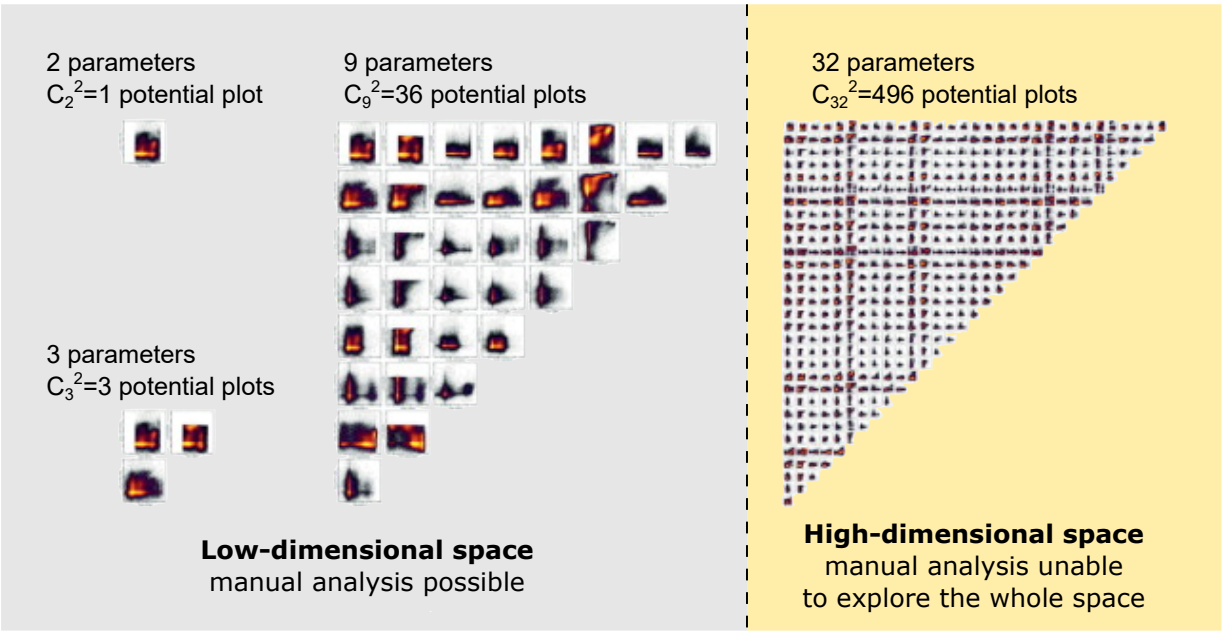

Figure 24. Representation of the high dimensionality generated by mass cytometry. While it is possible to manually explore a space defined by less than 10 dimensions, spaces with more than 30 dimensions generated by mass cytometry makes manual analysis time-consuming and error prone. $C_n{}^k$ indicates mathematical combination (k among n). Modified from Bendall et al. (2012).

New analysis tools dedicated to explore and analyze such multi-dimensional datasets are required to go further. Several analysis tools and algorithms were developed for mass cytometry dataset (Reeves et al., 2018), but two main approaches are widely used in the field, viSNE (based on dimension reduction) and SPADE (based on cell clustering).

viSNE *vs.* SPADE algorithm, pros and cons

viSNE: visualization of t-distributed stochastic neighbor embedding results

viSNE (Amir et al., 2013) is an adaptation of a non-linear dimensionality reduction method, performed through t-distributed stochastic neighbor embedding algorithm (t-SNE) (Maaten & Hinton, 2008) to single-cell analysis. It is notably widely used in the single-cell RNAseq community.

Computationally, a similarity matrix is computed to assess the distance between every points (cells) in the high-dimensional space. Briefly, similarity between cells is defined as the conditional probability than one cell would "choose" the other one as its neighbor, assuming that neighbor cells are chosen based on a Gaussian distribution of cell density, centered on the first cell (Maaten & Hinton, 2008; Amir et al., 2013). Note that the standard deviation of the distribution is indirectly set through the definition of perplexity, which consists roughly in the measure of the number of neighbors of each cell. This parameter has to be manually defined for each dataset, and should be all the smaller since the dataset is denser (Maaten & Hinton, 2008).

A random mapping in a low dimensional space (typically 2D or 3D) is then performed and a new similarity matrix is computed, based on Student t-distribution. Quality of the resulting space is assessed with the Kullback-Leibler divergence (which is proportional to the distance between the similarity between two cells in the high-dimensional space, and the same similarity in the low dimensional space) (Maaten & Hinton, 2008). An optimization of this low dimensional mapping is applied, based on gradient descent, in which the gradient is proportional to sum of dissimilarities between cells, and the actual difference observed between two cells, for all the pairs of cells in the dataset (Maaten & Hinton, 2008). Note that a user-defined epsilon factor (learning rate) is also applied to define the amplitude of the strength of each iteration.

As a result, each iteration moves further apart cells that are closer in the low-dimensional space than in the original space, and attracts to each other cells that are more distant in the low-dimensional space than in the high-dimensional space (Maaten & Hinton, 2008). The use of Student distribution to measure neighborhood in the low-dimensional space aims to avoid the so-called crowd problem, resulting from the loss of information during dimensionality reduction, which can lead to an artificially cell crowded area in the center of the representation. Indeed, the tailed t-distribution allow for expulsing force to prevent two cells to become too close to each other in the final representation (Maaten & Hinton, 2008).

The final low-dimensional mapping can be visualized using the *cyt* tool implemented in viSNE, that can help visualizing marker expression in each cell plotted on the final mapping (Amir et al., 2013) (**Figure 25**).

The heaviness of the overall approach precludes the use of too many cells, and no more than 2-3 million cells are usually used in a single analysis. It means that a random pre-downsampling of the data is required prior to the viSNE analyis itself (resulting in the loss of the non-sampled data), though new methods were developed to circumvent this issue, notably using hierarchical t-SNE analyses (Pezzotti et al., 2016; Höllt et al., 2016; van Unen et al., 2017).

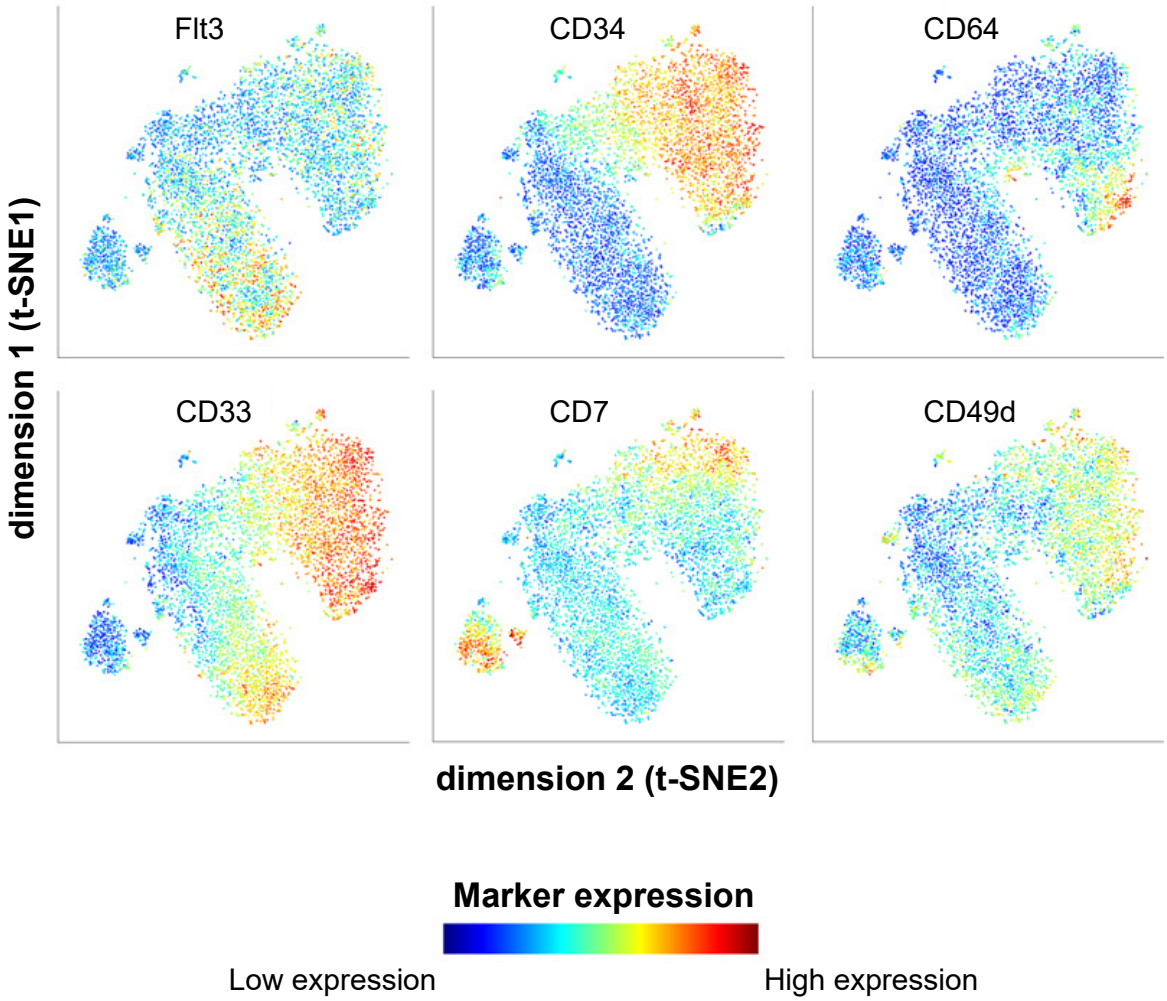

Figure 25. Examples of viSNE representation. Cells were mapped into a low-dimensional space (2D). The corresponding projection is colored on each panel with the expression of the indicated marker. Modified from Amir et al. (2013).

This algorithm is very powerful to visualize at a glance cell heterogeneity across samples, and has the advantage to plot individual cells, as done by most manual technics used so far. Thus all the information obtained at a single-cell level are conserved and visualized.

Still, one has to be careful when interpreting the resulting viSNE plots (Wattenberg et al., 2016). Indeed, several parameters, such as number of iterations and perplexity, have a tremendous impact on cell segregation or splitting. But quite worryingly, it is not clear neither *a priori* nor *a posteriori* which parameters give the best representation of the data. Indeed, according to the parameters used, even random noise could display potential cluster based organization (Wattenberg et al., 2016). Also, based on the parameters used, a great distance between two cells, may or may not mean anything.

Given these drawbacks, we chose not to use this method as first approach for our analyses, although it was successfully applied in the past in the laboratory to confirm results obtained from SPADE analysis (Pejoski et al., 2016).

SPADE: spanning-tree progression analysis of density normalized events

On the other side, the clustering approaches proposed by SPADE is based on the clustering of cells that share similar staining profiles in all markers, so that one only needs to look at hundreds of clusters instead of millions of cells (Qiu et al., 2011).

Briefly, it relies on a first downsampling of events acquired in each sample. Conversely to viSNE though, this downsampling is not random but density-based, (*e.g.* a downsampling of 10% will remove cells in part of the multidimensional space where density is above 10%). Density corresponds to number of cells in the neighborhood of a given cell. Neighborhood is defined with L1 norm with a threshold so that each cell possesses at least one neighbor (Qiu et al., 2011). Note that a threshold is also applied to remove all cells within too low density part of the multidimensional space (usually a cut-off of 0.01% is used).

This density-based downsampling allows to enrich the downsampled pool with rare events (**Figure 26**). Afterwards, the algorithm combined all downsampled cells from the different files and performs a randomly initiated agglomerative clustering. Briefly, one cell is randomly chosen and clustered with its nearest neighbor. Then at each step of this iterative process, another cell (out of the cells already clustered) is chosen and clustered with its nearest neighbor that was not previously clustered. Thus, at the end of the first round, the number of clusters is reduced to half the number of cells. Each cluster characteristics are defined as the median marker expression of the cells that compose the cluster.

At the next round, a random cluster is chosen and clustered with its nearest cluster neighbor, as for the cells of the first round. The process continues so on and so forth until the number of clusters reaches a number defined manually by the user.

A minimum spanning tree is then constructed to link the resulted nodes (clusters), based on Boruvka's algorithm and L1 metric (Pettie & Ramachandran, 2002). Briefly, each edge is added iteratively. At first iteration, the two nodes with the shortest in-between distance are connected together. At each iteration then, all the distances between each node within the tree and the unconnected nodes are computed. The two nodes (one within the tree, one outside) with the shortest in-between distance are then connected. The process continues until all nodes are at least connected to another one (Qiu et al., 2011).

Finally, the clusters are upsampled with the cells that were discarded during the density-based downsampling. This is done by associating each non-donwsampled cell to the same cluster as its closest neighbor among downsampled cells (Qiu et al., 2011).

Overall, this is a very powerful algorithm, designed to extract rare cell populations, which also allows for an easy quantification of cell populations in different conditions, compared to viSNE. Still two main drawbacks remained.

Firstly, should two samples contain highly distinct number of cells (*e.g.* one with 1 million cells, and one with 10,000 cells), the number of downsampled cells will differ across samples. The initial pre-downsampling is indeed density-based, thus proportional to the initial number of cells in the sample. As a result, the generation of the clusters will be biased by the samples containing many cells. To avoid this issue, we designed an analysis pipeline that equally and randomly pre-downsamples each sample before applying the SPADE algorithm and the density-based downsampling, and re-upsamples all cells afterwards, not to lose any information in the process (**Figure 26**).

Secondly, the user still needs to indicate two parameters: downsampling thresholds and number of cluster targeted. This choice can be user biased, and in addition, one does not have an *a priori* idea of the best parameters to choose. We thus developed an R-package, called SPADEVizR (Gautreau et al., 2017), which is notably able to assess the quality of the SPADE clustering. Briefly, to be defined as good quality, a clustering should contain mostly clusters with a unimodal and narrow distribution for all markers. With this criterion, we can assess the quality of the clustering with each set of parameters. Thus, after parameter benchmarking one can choose the combination of parameters that allows for the normatively best classification. In addition, one knows exactly which marker is not unimodally and narrowly expressed in which cluster.

Admittedly, the main reproach done for SPADE is that, conversely to viSNE, one does not look at individual cells directly but rather on cluster of cells. Still, given the possibility to ensure a good clustering quality, the ability to find rare populations, and since the interpretation is less subject to biased representation (compared to viSNE), we preferably chose SPADE as a strategy to analyze our mass cytometry data.

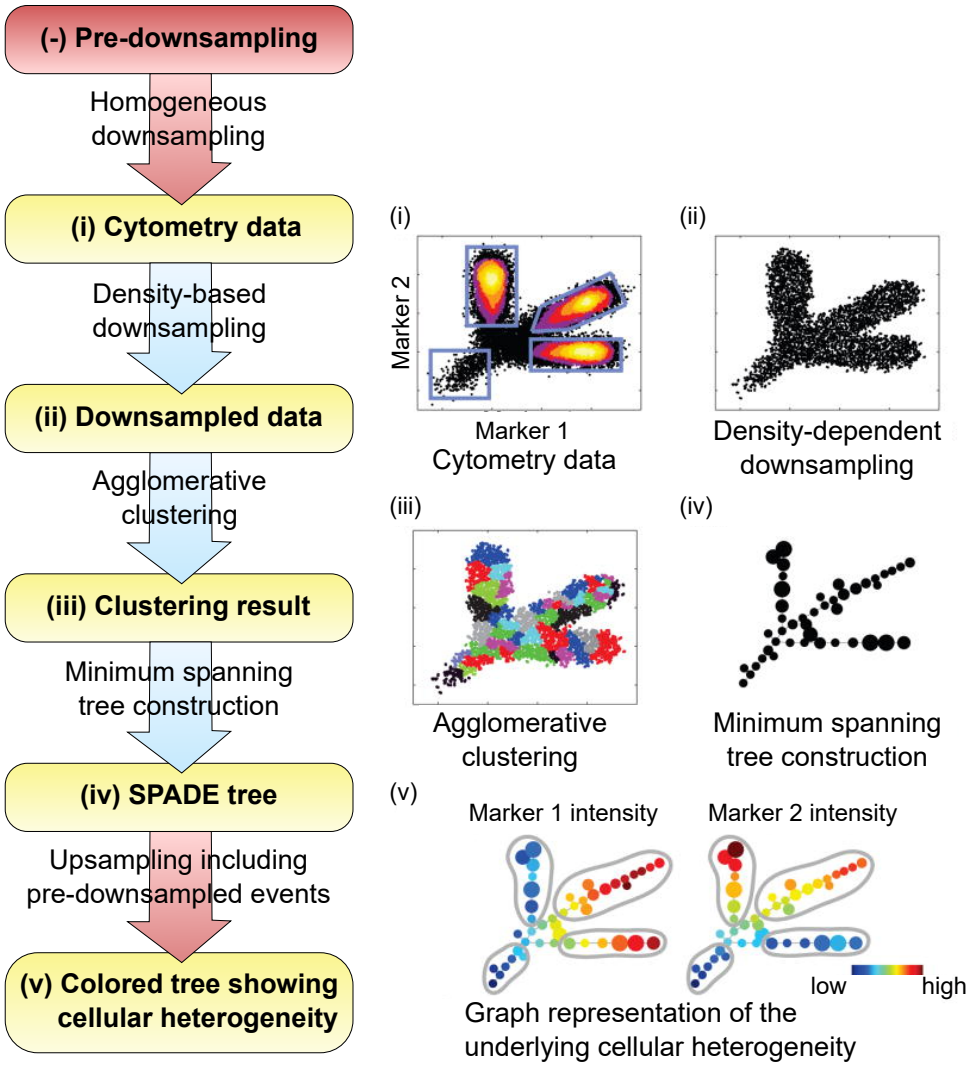

Figure 26. The SPADE algorithm. The different steps of the modified SPADE algorithm are indicated, as detailed in the text. Changes made in the original algorithm are displayed in red. Modified from Qiu et al. (2011).

Multi-dimensional analysis tools

To analyze the results from SPADE clustering, several bioinformatic tools were needed. Some were embedded in the SPADEVizR package (Gautreau et al., 2017). We refined the existing package during the thesis project, by adding new functionalities (cell cluster fusion, histogram representation...). An overview of the main tools is given hereafter.

A first tool is the possibility to visualize the SPADE tree, consisting of all the clusters with their connection. It notably allows, when coloring the tree with each marker, to annotate each cluster (*e.g.* $CD3^+$ T cells, HLA-DR^+ $CD20^+$ B cells, HLA-DR^+ $CD14^+$ monocytes...), and thus extract each cell compartment (granulocytes, monocytes-DCs, NK cells...) for the rest of the analysis (**Figure 27A**).

In addition, to visualize at a glance the phenotypic diversity of the dataset, phenotypic heatmaps were used. Briefly, for each marker, the range of expression was divided into five categories between the 5^{th} and 95^{th} percentiles, and each cluster was then given a category for each marker (1 to 5). Based on these categories, a hierarchical clustering of markers and clusters was performed (**Figure 27B**).

Kinetics of individual clusters or of cell populations (groups of clusters) can be visualized overtime. Similarly, individual cluster / cell population phenotype can be visualized through classical dotplots/bi-plots or histogram displaying mean signal intensity (MSI) for each marker.

Also, to compare datasets arising from different stainings, we developed and refined another package called CytoCompare that notably allows to assess similarities and dissimilarities between two SPADE clusterings (Platon et al., 2018). It basically uses the mean signal intensity (MSI) of every marker for each cluster, and addresses the correlation between every cluster from one dataset and all the clusters from the other, as a surrogate of cluster proximity. One can then easily appreciate similarity and dissimilarity of the two datasets (**Figure 27C**). This package was also refined during this thesis project, notably to allow to compare not only MSI but also categories of expression, as well as using different metrics of comparisons.

Other data analysis approaches were also used. In particular, our aim is to distinguish features similar and dissimilar between responses to prime and boost. To do so, discriminant analyses, such as linear discriminant analyses (LDA), can be used to segregate features (cell populations) distinguishing each class (prime response or boost response). It relies on the optimal orthogonal projection of each sample on an n-1 dimension space (where n is the number of classes targeted), so that the distance between classes is maximized. Since a selection of the informative features among non-informative ones is needed, selection approaches, such as least absolute shrinkage and selection operator (LASSO) can be used. It is based on the iterative construction of linear models with an increasing penalization of feature numbers and weight. Quality of the model built at each iteration is assessed using leave-one-out crossvalidation.

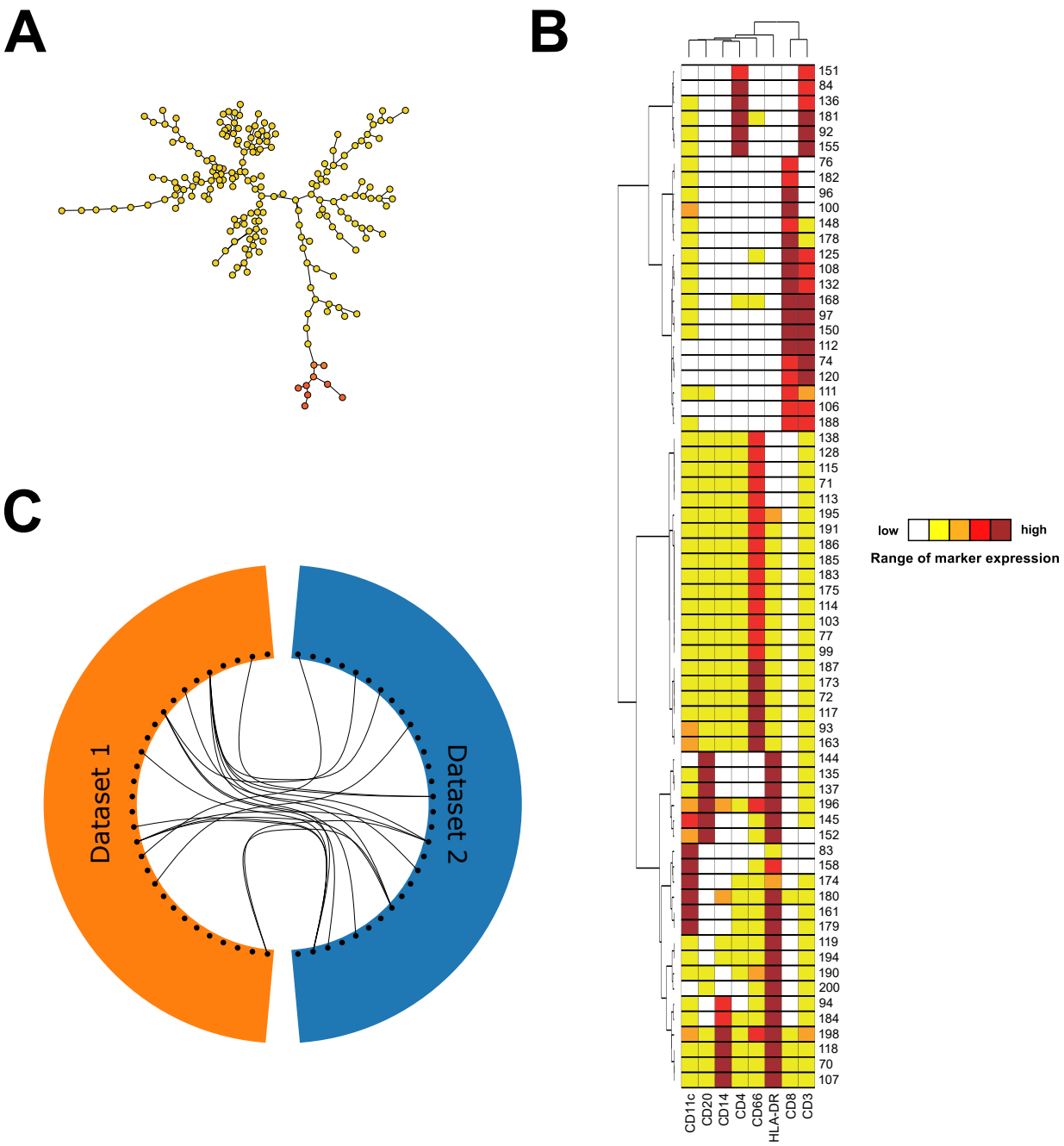

Figure 27. **Main data representations from the packages developed and used in this project.** **(A)** Visualization of a SPADE tree, colored by CD20 expression. **(B)** Heatmap representation of the phenotype of a given set of clusters on a given set of markers. Each column correspond to a marker, each line to a cluster. Marker expression was divided into five bins between the 5^{th} and 95^{th} percentiles of expression among all clusters, each bin was associated with the indicated color. **(C)** Circos representation of correlations existing between clusters from two datasets (in orange and blue). Links correspond to phenotypic correlation between clusters with $R > 0.65$ and $p < 0.05$.

Experimental approach, summary

Eventually, we used cynomolgus macaques, MVA and mass cytometry to assess the innate responses induced by vaccination, its interactions with adaptive immunity, with respect to vaccine schedule (**Figure 28**).

Since a longitudinal follow-up is required, we essentially used blood samples, and although it is obviously relevant, we could not assess in parallel the local immunity (at the site of injection or draining lymph nodes for example), nor bone marrow, since this could alter the normal development of immune responses. Dedicated animals should be used to do so.

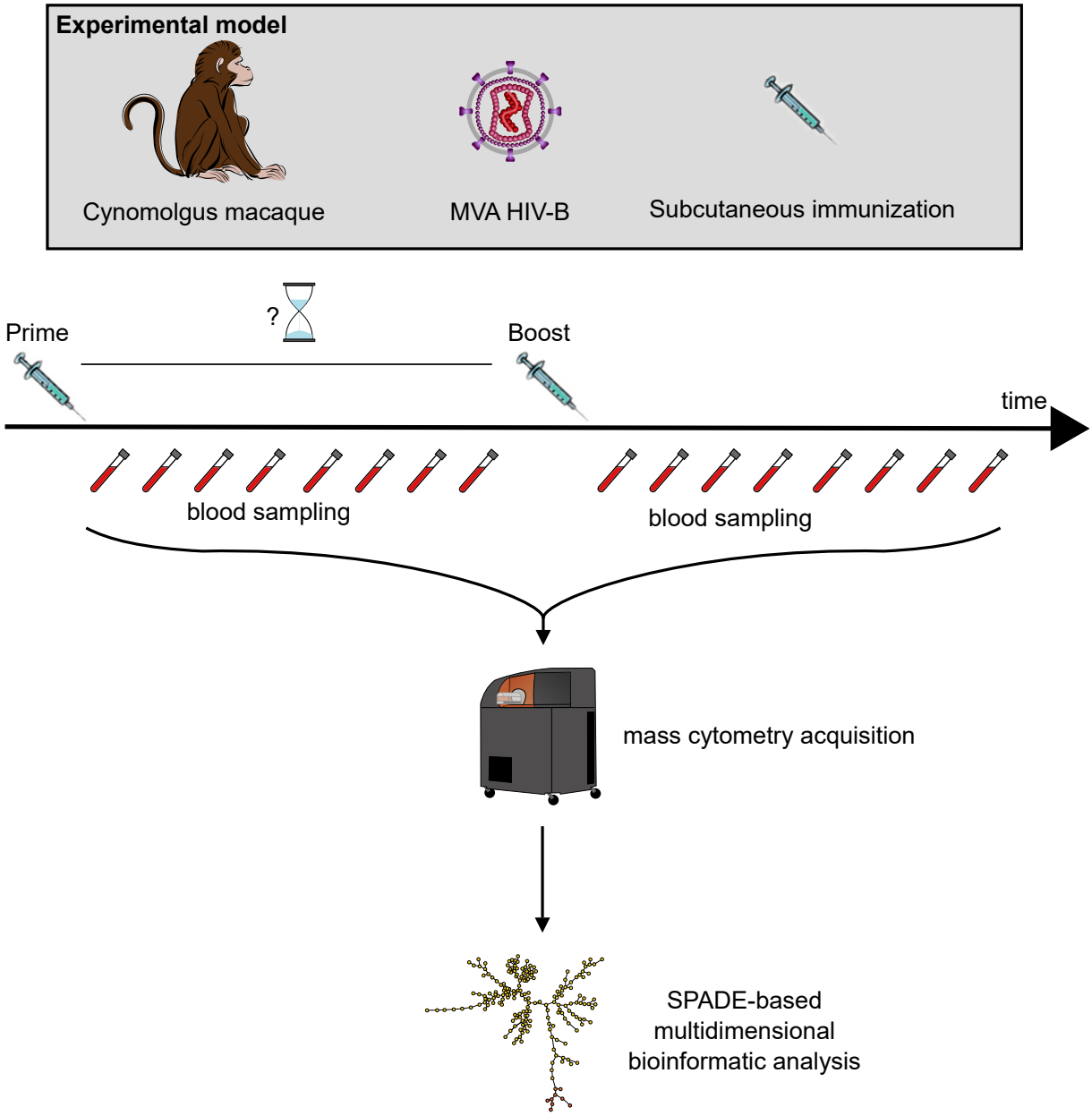

Figure 28. **Experimental strategy.** As a vaccination model, we used cynomolgus macaques immunized subcutaneously with MVA-HIV B vaccine, following a prime-boost vaccination schedule. Different delays between prime and boost were used to assess the impact of this time-lapse on the resulting immunity. Both innate and adaptive immunity were studied among the research group. Blood samples were collected after prime and boost for each schedule, including samples taken in the first few hours following immunization, to reconstruct the kinetics of innate immunity more accurately. These samples were analyzed with mass cytometry. A dedicated bioinformatic pipeline, based on SPADE clustering, was developed to explore, efficiently use and compare the resulting high-dimensional datasets.

Chapter 2. Validation of the experimental model: comparison of blood innate immune cells in human and cynomolgus macaques

Overview

Before the direct evaluation of vaccine-induced immune response to vaccine, we wanted to validate our experimental strategies. To do so, we used blood samples at steady state from macaques and humans, and performed mass cytometry analyses on them. Human blood samples were analyzed by Jamila Elhmouzi-Younes, a former post-doctoral fellow from the laboratory.

On an immunological point of view, we wanted to assess the immunological proximity between cynomolgus macaques and humans at a high-resolution. On an analytical point of view, we wanted to refine and validate our tools to explore and analyze high-dimensional datasets generated with mass cytometry.

We wanted to study not only monocytes and DCs, which are usually targeted by vaccinologists as APCs, but also granulocytes, which are very labile and difficult to preserve due to cryosensitivity. For this reason, their role in vaccine-induced immunity has been overlooked and is thus potentially undersestimated. We thus developed a strategy to store samples, preserving granulocytes. Based on a methodology previously described (Egger et al., 2001), we adapted a fixation mixture, containing formaldehyde and glycerol, which extemporaneously fixes whole blood leukocytes without activating them, also allowing to lyze red blood cells before freezing. This protocol was latter used for all our analyses.

Note that eosinophils were excluded from the analysis, since they capture heavy metals through interaction with their positively charged granules, and are thus artefactually positive for all markers used in the panel. A procedure based on the use of heparin during the staining allows to prevent this binding. This method was unfortunately not available at that time our first studies were performed (Rahman et al., 2016).

We then designed antibody panels dedicated to the biology of innate myeloid cells, one reacting with human cells (19 markers), one reacting on macaque cells (20 markers). These panels notably include markers targeting activation markers, chemokine receptors and FcR. For each antibody clone, we validated their reactivity not only with macaque cells, but also with fixed cells, a caveat inherent to our settings. Some markers were excluded during the process of antibody panel design, due to lack of reactivity (*e.g.* CD33).

Consistently with the close phylogenetic proximity between humans and NHPs, strong similarities were found between human and macaque innate myeloid compartments, in term of cell number and composition.

Some discrepancies were found though, such as a wider expression of CD23 in human neutrophils, compared to macaque neutrophils that expressed a wider range of expression of CD32. Also, the activation status of innate myeloid cells seemed higher in macaques compared to humans, with an increased expression of CD11b and CD32 in neutrophils, CD11b, CD32 and CD86 in monocytes and CD16 in cDCs. Interestingly, while CD16 expression clearly distinguished cDCs subphenotypes in humans, CD16 was highly and homogeneously expressed in all cDCs in macaques. Note that our cDCs were defined as (HLA-DR$^+$ CD11c$^+$ CD14$^-$) and the use of CD11c to define cDCs is quite controversial in NHPs since some monocytes were shown to express CD11c in rhesus macaques (Dutertre et al., 2012; Sugimoto et al., 2015), but not in cynomolgus (Guilliams et al., 2016). CD16 expression by cDCs was previously reported in literature for rhesus macaques (Brown & Barratt-Boyes, 2009; Autissier et al., 2010; Soulas et al., 2015).

Eventually, we detected the expression of the Fc receptor CD64 on a wide range of cells (neutrophils and monocytes as expected, but more surprisingly on lymphocytes and cDCs).

Interestingly, we identified a population of CD14$^+$ CD11c$^+$ CD16$^+$ cells that were phenotypically close to both monocytes and cDCs. We annotated them as inflammatory cDCs / non-classical monocytes, for consistency purpose with the literature. The exact frontier between CD16$^+$ cDCs and CD14$^{low/dim}$ CD16$^+$ non-classical monocytes is indeed not fully clear in literature (Collin & Bigley, 2018).

Overall, we used the Cytocompare R-package, our comparison tool dedicated to cytometry profiles (Platon et al., 2018), to assess the similarities and discrepancies between both species. We unveiled very close associations between each compartment in both species, strengthening the value of the cynomolgus model for the study of human immunology.

"In Depth Comparative Phenotyping of Blood Innate Myeloid Leukocytes from Healthy Humans and Macaques Using Mass Cytometry"

All these results were published in a co-first authorship paper in *Cytometry part A* in 2017 (Elhmouzi-Younes et al., 2017), provided hereafter.

Cytometry PART A
Journal of the International Society for Advancement of Cytometry

MIFlowCyt

In Depth Comparative Phenotyping of Blood Innate Myeloid Leukocytes from Healthy Humans and Macaques Using Mass Cytometry

Jamila Elhmouzi-Younes,[1†] Jean-Louis Palgen,[1†] Nicolas Tchitchek,[1] Simon Delandre,[1] Inana Namet,[1] Caroline L. Bodinham,[2] Kathleen Pizzoferro,[2] David J.M. Lewis,[2] Roger Le Grand,[1] Antonio Cosma,[1] Anne-Sophie Beignon[1*]

[1]Immunology of viral infections and autoimmune diseases, CEA – Université Paris Sud 11 – INSERM U1184, 92265 Fontenay-aux-Roses, France

[2]Surrey Clinical Research Centre, University of Surrey, Guildford, GU2 7XP, UK

Received 1 December 2016; Revised 4 February 2017; Accepted 15 March 2017

Grant sponsor: Innovative Medicines Initiative Joint Undertaking "BIOVACSAFE", from the European Union's Seventh Framework Programme (FP7/2007-2013) and EFPIA companies, Grant number: 115308

Grant sponsor: French government program: "Investissement d'avenir: Equipements d'Excellence" (EQUIPEX)-2010 FlowCyTech, Grant number: ANR-10-EQPX-02-01

Grant sponsor: Laboratoire d'Excellence (LABEX)-2011 Vaccine Research Institute (VRI), Créteil, Grant number: ANR-10-LABX-77

Grant sponsor: Infrastructures Nationales en Biologie et Santé (INBS)-2011 Infectious Disease Models and Innovative Therapies (IDMIT), Grant number: ANR-11-INBS-0008

Additional Supporting Information may be found in the online version of this article.

[†]These authors contributed equally to this work.

ISAC
International Society for Advancement of Cytometry

Abstract

Comparative immune-profiling of innate responses in humans and non-human primates is important to understand the pathogenesis of infectious and chronic inflammatory diseases as well as for the preclinical development of vaccines and immune therapies. However, direct comparisons of the two species are rare and were never performed using mass cytometry. Here, whole-blood-derived leukocytes from healthy humans and cynomolgus macaques were analyzed with mass cytometry. Two similar panels of around 30 monoclonal antibodies targeting human markers associated with innate myeloid cells to stain fixed human and macaque leukocytes were constructed. To compare the circulating innate cells from the two primate species, an analysis pipeline combining a clustering analysis by the Spanning-tree Progression Analysis of Density-normalized Events (SPADE) algorithm with a two-step hierarchical clustering of cells nodes and markers was used. Identical SPADE settings were applied to both datasets, except for the 20 clustering markers which slightly differed. A correlation analysis designed to compare the phenotypes of human and macaque cell nodes and based on 16 markers, including 15 shared clustering markers and CD19 for humans or CD20 for macaques, revealed similarities and differences between staining patterns. This study unique by the number of individuals (26 humans and 5 macaques) and the use of mass cytometry certainly contributes to better assess the advantages and limits of the use of non-human primates in preclinical research. © 2017 International Society for Advancement of Cytometry

Key terms

CyTOF; mass cytometry; whole blood; leukocytes; innate myeloid immunity; macaque; human

THE contribution of non-human primates (NHP) to the development of modern medicine is historically proven. Yellow fever virus was isolated in rhesus macaques and the subsequent development of an effective vaccine heavily relied on the use of the same experimental model (1). The similar manifestations of tuberculosis disease in humans and monkeys were the ground for the use of this model for vaccine and drug regimens development (2). The immunological similarity between humans and NHP is also the basis for their use as models for infectious and autoimmune diseases (3–5). More recently, a clear description of HIV-1 pathogenesis was obtained by the use of NHP models (6). Nevertheless, experimental data generated in NHP models need the continuous cross-validation with human data (7).

*Correspondence to: Anne-Sophie Beignon, 18, route du panorama; 92265 Fontenay-aux-Roses; France. E-mail: anne-sophie.beignon@cea.fr

Published online 00 Month 2017 in Wiley Online Library (wileyonlinelibrary.com)

DOI: 10.1002/cyto.a.23107

© 2017 International Society for Advancement of Cytometry

In the field of flow cytometry based immune-monitoring, efforts have been already initiated to build experimental tools, such as shared flow cytometry multicolor antibody (Ab) panels, to investigate human and monkey immune system in a parallel fashion (8–10).

Here, we show two multi-parameter mass cytometry Ab panels and their application in healthy humans and cynomolgus macaques. Samples were collected using a protocol able to recover the whole leukocytes, including granulocytic populations. Human and macaque fixed leukocytes were stained with similar panels of 32 and 33 Abs respectively and targeting markers associated with innate myeloid cells. Twenty-five markers were included in both Ab panels, including 13 shared Abs clones. We used an analysis pipeline combining a clustering analysis by the Spanning-tree Progression Analysis of Density-normalized Events (SPADE) algorithm with a two-step hierarchical clustering to identify cell population, also called cell nodes, in both datasets and to classify them. Identical SPADE settings were applied to both datasets, except for the clustering markers which slightly differed. In order to compare the phenotypes between human and macaque cell nodes, we performed a correlation analysis based on 16 markers, 15 shared clustering markers plus CD19 for humans, allowing to target B-cell subsets at various developmental stages (such as plasmablasts and plasma cells) or CD20 for macaques. We were then able to highlight significant similarities and differences of staining profile and intensity between immune cells derived from the two species. Macaque cells showed a generalized stronger staining for markers associated with activation and inflammation, such as CD32, CD11b on neutrophils and monocytes, and a homogeneously high expression of CD16 on myeloid dendritic cells (mDC). In contrast, macaque mDC showed a lower staining of HLA-DR and CD86 compared with macaque monocytes and human monocytes and mDC. Discrepancies between species can be explained by the relative cross-reactivities of human Abs with macaque determinants inherent to any cross-species comparison, or by true biological differences between humans and macaques. This comprehensive map of healthy human immune cells in comparison to macaque cells admittedly calls for gene expression and functional analyses to further define similarities and differences between innate myeloid cells in humans and macaques. Nevertheless, our work already constitutes a strong basis for comparative and translational studies in the field of immunology.

Materials and Methods

Volunteers and Whole Blood Collection

Human whole blood was collected from informed and consenting volunteers enrolled into a clinical study conducted at the Surrey Clinical Research Centre, University of Surrey (UK), as part of the BioVacSafe consortium-funded clinical study protocol CRC305A (11). Inclusion criteria are described in Supporting Information Table 1. The aim of the study is to generate an exploratory training dataset to characterize clinical events, physiological and metabolic responses, and innate and adaptive immune responses following immunization with commercial vaccines or saline placebo in healthy adults with no previous immunity. Whole blood was collected into lithium heparin vacutainer tubes (BD Biosciences, San Jose, CA) and cells were fixed within 3 hours of blood draw. In the present manuscript, 26 subjects were analyzed before any vaccine or saline injection to study blood innate myeloid cells at steady-state. This cohort is aged of 29.3 years ($\pm$7.23) with a mean body mass index (BMI) of 23.95 ($\pm$3.17). It contains 16 males and 10 females, split on race in 18 White, 5 Asian, and 3 other persons and on ethnicity in 1 Hispanic or Latino, 24 non-Hispanic nor Latino, and 1 not reported.

Non-Human Primates and Whole Blood Collection

Five healthy adult male cynomolgus macaques (*Macaca fascicularis*) were imported from Mauritius and housed in the animal facility of IDMIT infrastructure at CEA, Fontenay-aux-Roses, France. Blood was collected using lithium-heparin tubes (Vacutainer BD, USA) under anesthesia using an intramuscular injection of 10 mg/kg of ketamine (Rhone-Mérieux, Lyon, France) and processed with the same protocol as used in the human trial.

Ethics Statements for the Human Study

The human study was approved by London - Surrey Borders Research Ethics Committee (REC Ref: 12/LO/1871) and the study was registered on http://clinicalltrials.gov (NCT01765413) before participant enrollment. All participants provided written informed consent after adequate explanation of the aims, methods, anticipated benefits, and potential hazards of the study.

Ethics Statements for the Non-Human Primate Study

The macaque study was approved by the "Ministère de l'éducation nationale, de l'enseignement supérieur et de la recherche" (France) and the ethics committee "Comité d'éthique en expérimentation animale n°44" under the reference 2015031314518254.02 (APAFIS#319). Animals were handled by veterinarians in accordance with national regulations (CEA Permit Number A 92-32-02) and the European Directive (2010/63, recommendation N°9) and in compliance with Standards for Human Care and of the Office for Laboratory Animal Welfare (OLAW, USA) under OLAW Assurance number #A5826-01.

Table 1. Restricted set of markers used to manually annotated nodes in SPADE tree and for manual bi-variate gating

	MARKERS USED TO ANNOTATE NODES (NUMBER OF NODES)	
CELL POPULATION	HUMAN	MACAQUE
Neutrophils	CD66+(27)	CD66+(26)
Basophils	CD66- CD123+ HLA-DR-(2)	CD66- CD123+ HLA-DR-(1)
Monocytes	CD14+ HLA-DR+(18)	CD14+ HLA-DR+(12)
pDC	CD19- CD14- HLA-DR+ CD123+(1)	CD20- CD14- HLA-DR+ CD123+(1)
mDC	CD19- CD14- HLA-DR+ CD11c+(5)	CD20- CD14- HLA-DR+ CD11c+(8)
NK cells	CD66- CD3- Granzyme B+(5)	CD66- CD3- CD8+(9)
T-cells	CD3+(27)	CD3+(22)
B-cells	CD19+ HLA-DR+(8)	CD20+ HLA-DR+(17)

Reagents and Solutions

Fixation Mixture (FM) used to store cells was prepared extemporaneously as previously described (12). Briefly, two parts of double concentrated Dulbecco's phosphate buffer (DPBS) was prepared from a solution of DPBS modified 10× without $CaCl_2$ and without $MgCl_2$, pH 7.4 (Gibco by Life Technologies, Villebon-Sur-Yvette, France). One part of 20% formaldehyde was prepared from 36% paraformaldehyde (VWR BDH Prolabo, Fontenay-sous-Bois, France) and mixed all together with one part of 75% glycerol (Sigma-Aldrich, Lyon, France). The resulting solution was stored at +4°C and used within three days. Fixation solution (PBS/PFA 1.6%) used for the staining, was prepared by diluting 16% paraformaldehyde (PFA; Electron Microscopy Sciences, Hatfield, USA) in DPBS modified 10× and Milli-Q water. Staining buffer (PBS/BSA 0.5%) was prepared by mixing DPBS modified 1× (Gibco by Life Technologies) with 0.5% BSA (Sigma-Aldrich, Lyon, France).

Cell Preparation and Storage

Blood samples were processed accordingly to a freezing procedure allowing the recovery of all blood leukocytes, especially polymorphonuclear cells, which are highly labile and cryosensitive cells. We adapted a previously described cell preparation procedure consisting of fixation, red cell lysis, and freezing (12). One ml of whole blood was mixed with 10 mL FM and incubated on ice for 10 min. After centrifugation, red cells were lysed by adding 10 mL of Milli-Q water at room temperature (RT) for 20 min. After two washes with DPBS modified 1×, cells were counted and stored at −80°C in FM at a final concentration of 15×10^6 fixed leukocytes/mL and distributed in aliquots containing 3×10^6 cells.

Staining and CyTOF Acquisition

Three millions of cryopreserved fixed cells were thawed at 37°C, washed twice with PBS/BSA 0.5% and incubated on ice for 30 min with the metal-labeled surface antibodies listed in Supporting Information Table 2. After two washes with DPBS modified 1×, cells were fixed with PBS/PFA 1.6% at RT for 20 min and permeabilized with 1× Perm/Wash Buffer (BD Biosciences) at RT for 10 min. Intracellular Abs and iridium nucleic acid intercalator were incubated on ice for 30 min. After two washes with DPBS modified 1×, cells were fixed with PBS/PFA 1.6% at RT for 20 min, centrifuged and stored overnight with 0.1 μM iridium nucleic acid intercalator in PBS/PFA 1.6%. The following day, cells were washed with Milli-Q water, resuspended in 1 mL of Milli-Q water and filtered by using a 35 μm nylon mesh cell strainer (BD Biosciences), before the addition of EQ^{TM} Four-Element Calibration Beads (Fluidigm, San Francisco, USA) according to the manufacturer's instructions. Each sample was split into two and distributed in a 96-well microplate (Sigma-Aldrich, St Louis, MO). The acquisition was done using the autosampler device to automatically deliver samples into the CyTOF instrument (Fluidigm). The number of acquired cells is given in Supporting Information Table 3 for each sample.

Data Processing and Analysis

Cytometry data were normalized using Rachel Finck's MATLAB normalizer (13). Replicates were concatenated using the FCS file concatenation tool (Cytobank, Mountain View, CA). Four-Element Calibration Beads were excluded by manual gating on the Ce140 channel. Singlets were selected on an Ir191 (DNA intercalator)/cell_length bivariate plot. Of note, a clear population of cells showing a strong background in all channels was consistently observed in all samples and excluded on a CD66abce/CD3 bivariate plot. The number of cells non-double positive ($CD66abce^+/CD3^+$) is given in Supporting Information Table 3 for each sample. Recently, Rahman et al. (14) showed a generalized nonspecific metal conjugated antibody binding by eosinophils during staining of fixed whole blood resembling to the pattern observed in our fixed whole blood samples, suggesting these double-positive cells could be eosinophils.

Two Spanning-tree progression analyses of density-normalized events (SPADE) (15) were independently performed on the human and macaque datasets using 19 and 20 clustering channels respectively (Supporting Information Table 2). Cell nodes generated by SPADE were manually annotated according to the rules shown in Table 1.

For a deeper analysis of these nodes, we used the recently released SPADEVizR R-package (16), dedicated to cytometry data analysis with a main emphasis on SPADE-derived data. To categorize these SPADE-nodes, we calculated the 1st and 99th percentiles of the expression distribution of the total cells for each marker and divided this range into five categories. The mean of the median marker expression of cells contained in each node was then used to assign each marker expression to one of the five categories. Individuals with less than 50

events in a given node were excluded from this calculation since we considered that medians calculated on less than 50 events might bias the phenotypical characterization of these cell nodes. Hierarchical clusterings were performed using the Euclidean metric and the complete linkage method. Correlation analysis between humans and macaque nodes was generated based on their categories using the Spearman coefficient of correlation, based on the relative expression of CD66abce, HLA-DR, CD3, CD64, CD123, CD11a, CD11b, CD23, CD86, CD32, CXCR4, CCR5, CD16, CD11c, CD14, and CD19 for humans and CD20 for macaques. Raw FCS files have been uploaded on FlowRepository and are available through accession ID: FR-FCM-ZZSR (for the macaque dataset) and FR-FCM-ZZSQ (for the human dataset). All Supporting Information materials were also uploaded at the same IDs.

Results

Definition of the Main Leukocyte Populations in Humans and Non-Human Primates

Leukocytes derived from 26 healthy humans and 5 healthy cynomolgus macaques were characterized using similar Ab panels shown in Supporting Information Table 2, and staining was compared within and between the two species by the use of a common analytical pipeline.

The panel dedicated to define human samples was firstly established to analyze cells mediating innate responses at steady state or following in vitro stimulation with TLR ligands. This panel comprised 33 human monoclonal Abs. On the basis of this first human Ab panel, Ab clones were tested for cross-reactivity with cynomolgus macaque cells. In the case of lack of cross-reactivity, Abs were replaced by other clones or even with Abs having other specificities. Additionally, studies conducted in human subjects showed that despite the innate cell orientation, the inclusion of markers such as CD4 and CD8, might uncover unforeseen patterns during data analysis. As a consequence, the Ab panel designed to define macaque cells targeted 32 markers, 25 of which were shared with the human analysis, including 13 identical Ab clones. The differences in the two Ab panels account for the above considerations.

Doublets and background events were removed from data files. In particular, $CD66abce^{+}CD3^{+}$ aberrant leukocytes (likely due to the non-specific binding resulting from the recently reported interactions between metals from the conjugated Abs and charged proteins present in eosinophilic granules) were discarded (14).

To assess the validity of our interspecies comparison, we first confirmed that the markers in common between the two Ab panels had a comparable dynamic range of expression using histograms, excepted for CCR5, CD11c, CD32, CD64, and CXCR4 (Supporting Information Fig. 1). The relative ranges of expression were also computed and summarized by displaying the 1st and 99th percentiles of the expression distribution on total leukocytes (Supporting Information Fig. 2). We observed some heterogeneity of staining intensity and of marker expression density between individuals within the same species for some markers, such as CD11b in humans or CD32 both in humans and macaques (Supporting Information Fig. 1).

We then performed two SPADE analyses (15) on the human and macaque datasets using similar settings. Specifically, we targeted a total of 100 nodes and we applied a 5% of downsampling. To perform clustering, we used 15 surface markers shared between the human and macaque Ab panels, to which we added CD19, CD28, Perforin and Granzyme B for humans, and CD20, CD4, CD8, CCR7, and CD45 for macaques (Supporting Information Table 2) with the goal to cluster cells as much as possible and to capture the largest phenotypic diversity and complexity for each species. It is of note that intracellular cytokines, TLRs and NF-kB-pS529 were not used as clustering markers. Actually, neither cytokine secretion, TLR expression modulation, nor NF-kB activation were detected as steady-state without ex vivo restimulation with stimuli and addition of brefeldin A (data not shown).

The SPADE algorithm does not have the possibility to simultaneously visualize multiple trees, to perform aggregations, or to specifically filter nodes. Therefore, median staining intensities (MSI) associated to each node were extracted, formatted using the Google Refine application and visualized using the Tableau Desktop software (Fig. 1). In human samples, CD66abce, CD3, CD19, CD14, HLA-DR, CD11c, CD123, and Granzyme B were used to manually categorize SPADE nodes into eight distinct main cell populations; namely neutrophils, basophils, monocytes, mDC, plasmacytoid DC (pDC), NK cells, T cells, and B cells (Table 1). The same populations were identified in the macaque dataset but CD19 and Granzyme B were substituted by CD20 and CD8, respectively, to identify B, T, and NK cells. Following these rules, we were able to assign to these 8 main cell populations 93 and 96 nodes out of 100 nodes for the human and the macaque dataset, respectively (Fig. 1 and Supporting Information Fig. 3). Note that for both species, since CD16 was not included as annotation marker, $HLA\text{-}DR^{+}\ CD14^{-/low}\ CD16^{+}$, described in the literature either as inflammatory mDC (8,17,18) or non-classical monocytes (19,20) were considered here as inflammatory mDC, solely to account for this initial annotation choice. Seven human nodes and four macaque nodes remained undefined. Some nodes corresponded to abundant cell subphenotypes (e.g., human node 21 with up to 20% of parents), while others contained very few cells (e.g., human node 97 with $<0.06\%$ of parents), but they still displayed a singular markers co-expression profile (Supporting Information Figs. 4 and 5). This demonstrates the power of the SPADE algorithm to reach equal representation of rare and abundant cell types thanks to its density-based downsampling procedure. Using these restricted sets of eight markers, some similarities and differences could already be documented between the two species for the intensity and profile of markers expression, with different patterns for CD3, CD11c, and CD123, visualized on the colored SPADE trees (Fig. 1).

To further control our interspecies comparison, we analyzed the relative marker expression using bivariate plots over

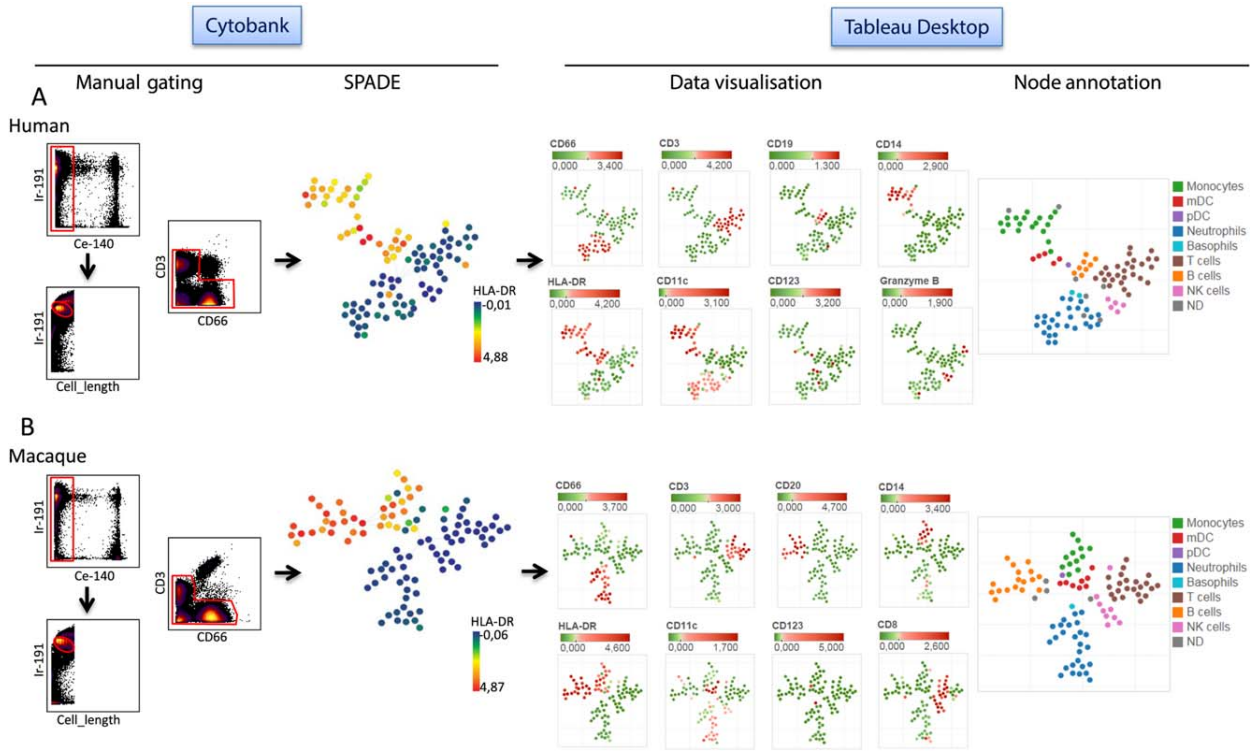

Figure 1. Data analysis workflow. Events generated from human **(A)** and macaque **(B)** samples were manually gated to exclude the EQ™ Four-Element Calibration Beads, select singlets and gate out nonspecific background likely generated by metal conjugated Ab binding eosinophils (see Materials and Methods). The SPADE algorithm was performed independently on the human and macaque samples. Mean staining intensities and number of event per node were extracted from Cytobank and exported to Tableau Desktop for optimal visualization and annotation purpose. The Tableau Desktop rendered SPADE trees are shown for humans and macaques. Eight trees are shown for each species according to the markers used to discriminate the eight distinct leukocyte populations as described in Table 1. Each circle represents a node colored according to the median expression of all the 26 humans or 5 macaques. Node dimension size does not relate to the number of events. The color gradient is proportional to the expression of each marker and is shown on the top of each tree. The tree manually annotated for the eight leukocyte populations is shown on the left with the relative color legend. The gray node, labeled ND, remained undefined according to the rules of Table 1. A magnified version of the annotated trees with node ID is available as Supporting Information Fig. 3.

the main eight blood cell populations identified by SPADE analyses followed by manual nodes annotation in representative individuals (Fig. 2 and Supporting Information Fig. 6), as well as parallel coordinate representations showing the marker expression ranges for each SPADE nodes (Supporting Information Figs. 4 and 5). The 15 surface markers shared between the human and macaque Ab panels as well as CD19 for humans and CD20 for macaques showed a quite similar dynamic range over the eight main cell populations. CD86 range of expression is difficult to assess on the whole leukocytes population. Nevertheless, while clearly showing a positive signal in a subpopulation of human HLA-DR^{mid} mDCs, CD86 appeared to have a negative profile on the macaque main cell populations, except in HLA-DR^{mid} monocytes. Note that HLA-DR shows a similar range of expression in both species. In contrast to human cells, CD32 was strongly expressed by macaque cells, in particular by neutrophils, basophils, monocytes, pDCs and B cells (Supporting Information Fig. 6). Similarly, CD64 expression differed between humans and macaque, with a higher expression by macaque neutrophils, basophils and pDCs. CD16 and in a lesser extent CD11a expression was differentially expressed by human HLA-DR^{high}CD86^{mid} and HLA-DR^{mid}CD86^{low} mDCs contrary to macaque mDCs which express more homogeneously a high-level of CD16 and CD11a. CD11b was expressed by macaque monocytes in contrast to human monocytes, while human monocytes expressed CD11c in contrast to macaque monocytes (Supporting Information Fig. 6). The clone 3.9 we used for macaque staining was described to preferentially bind the activated form of CD11c (21) while this is unclear for the clone B-ly6 (22) we used in the human dataset. It is thus possible that macaque monocytes carry inactivated CD11c molecules. Besides, as the CD11c expression was high on macaque mDC, it would also suggest that macaque mDC express constitutively active CD11c molecules. In addition, in humans only, one subpopulation of mDC (mainly node 78, but also node 27 and 38) express CD123 in addition to CD86 and CD16 (as well as CCR5^{mid}, CXCR4^{mid}, HLA-DR^{mid}, CD11a-^{mid}, and CD11c^{mid} as all mDC nodes). This population is described in the literature to be a potential immature mDC population with high pro-inflammatory potential (23–25), suggesting that mDC in macaque could be more mature than in humans. The staining profiles of the anti-CXCR4 and anti-CCR5 Abs did not match between species with an overall

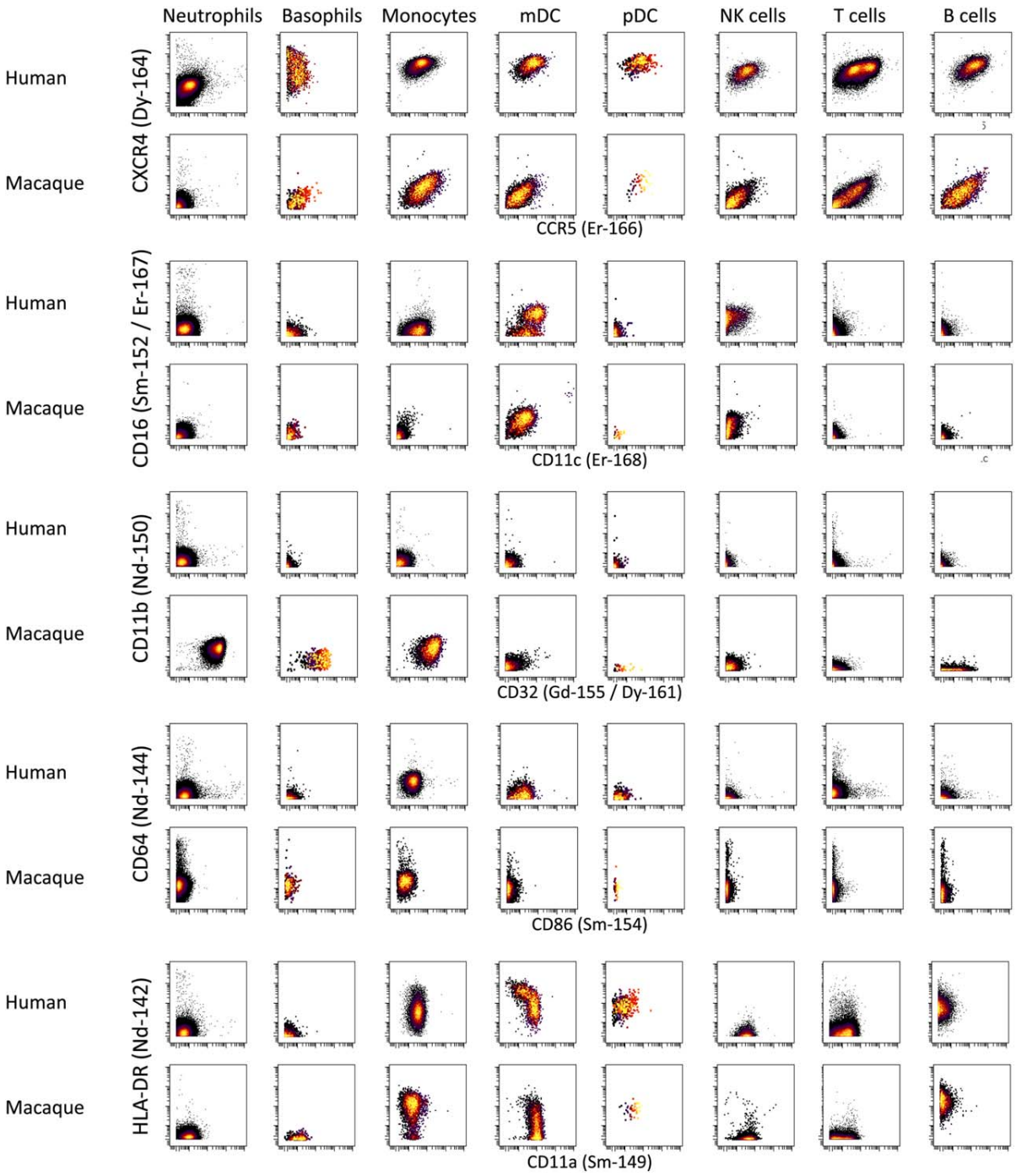

Figure 2. Bi-dimensional dot plot representations of selected markers on human and macaque leukocyte populations. Representations were performed on the leukocyte populations identified in the spade trees. Human cell populations were compared with their macaque cell counterparts for the expression of the following marker pairs: CXCR4 (Dy-164)/CCR5 (Er-166), CD16 (Sm-152/Er-167) [for human/macaque respectively]/CD11c (Er-168), CD11b (Nd-150)/CD32 (Gd-155/Dy-161), CD64 (Nd-144)/CD86 (Sm-154), HLA-DR (Nd-142)/CD11a (Sm-149). For each species one representative subject is shown (human #7017 and macaque #BB078).

higher detection in human cells. However, CXCR4 staining was detected on macaque monocytes and pDCs. Finally, the intensity of HLA-DR expression was higher in human than in macaque monocytes and mDCs (Supporting Information Fig. 6). Further experiments are obviously required to understand better the impact of these discrepancies of pattern of expression between the two species, mostly between monocytes and mDCs.

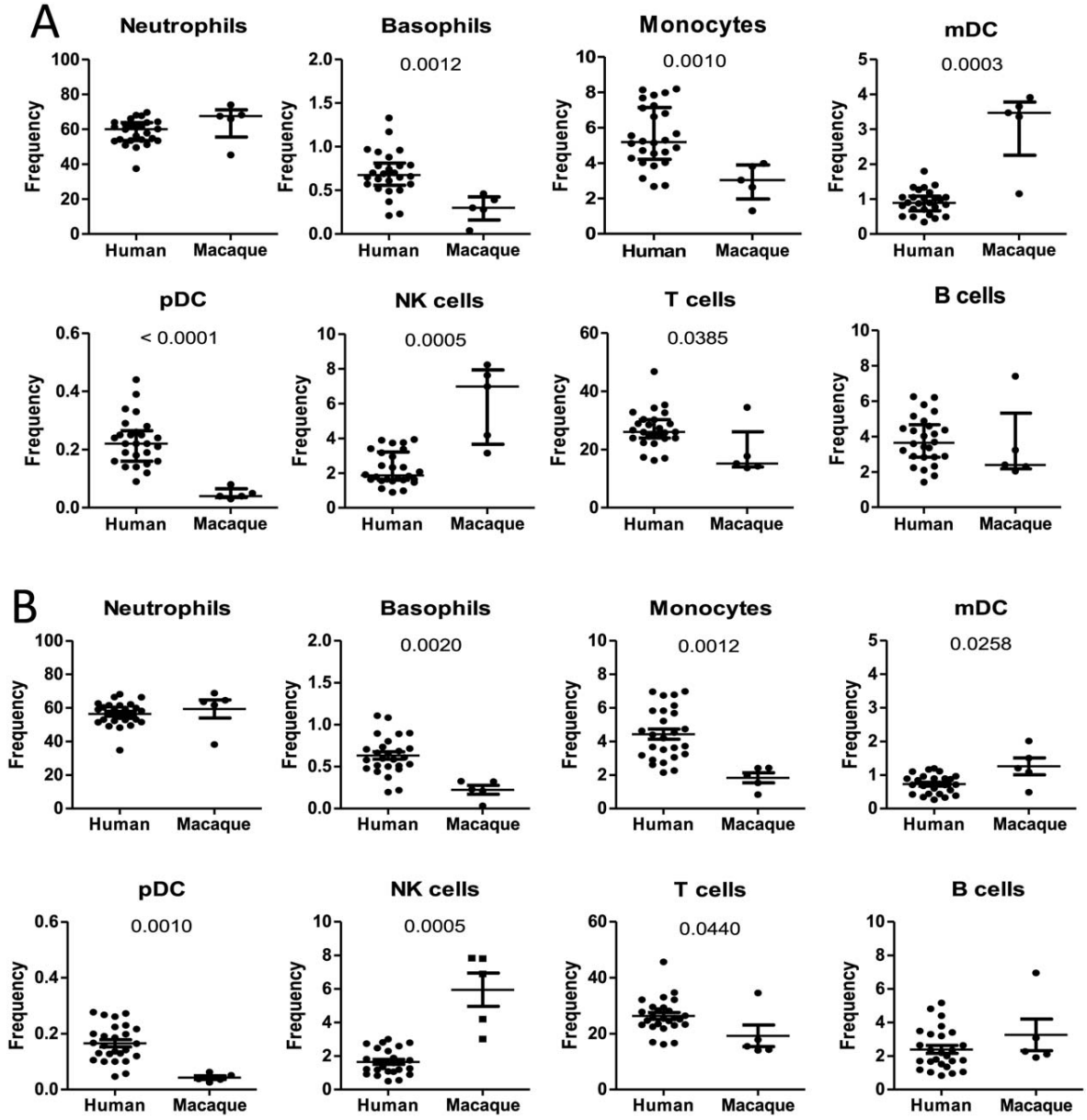

Figure 3. Comparison in the proportion of leukocyte populations between human and macaque. Frequencies of leukocytes populations were calculated over the total amount of leukocytes. Data from 26 humans and 5 macaques are shown; each point represents one individual. Percentages of neutrophils, basophils, monocytes, mDC, pDC, NK cells, T cells, and B cells were defined either after SPADE analysis followed by manual annotation of the SPADE tree (Fig. 1 and Table 1) (**A**) or after "classical" manual bi-variate gating (**B**); the gating strategy used is described in Supporting Information Figure 7. They were compared between humans and macaques using a Mann–Whitney test implemented in GraphPad Prism version 6 and $P < 0.05$ are shown. Medians with interquartile ranges are shown.

We then compared the frequencies of the manually annotated main cell populations in humans and macaques (Fig. 3A). Considering the limitations cited above as well as the restricted number of individuals, our approach showed that similar frequencies of neutrophils were found in the two species whereas significantly lower frequencies of basophils were observed in macaques (P values = 0.0012). Lower monocytes frequencies were detected in macaque in comparison to human (P values = 0.0010) while mDC showed an inverse pattern (P values = 0.0003). Of note, pDC already considered a rare population in humans (median 0.22%: range 0.09–0.44) showed frequencies ranging between 0.03% and 0.08% in macaques (P values < 0.0001). These results may partially contradict our previous reported observations (22) and may argue for technical limitations in accurately identifying these populations with the defined panels. The frequency of NK cells was significantly higher in macaque when compared with human (P values = 0.0005). T cells showed significant lower

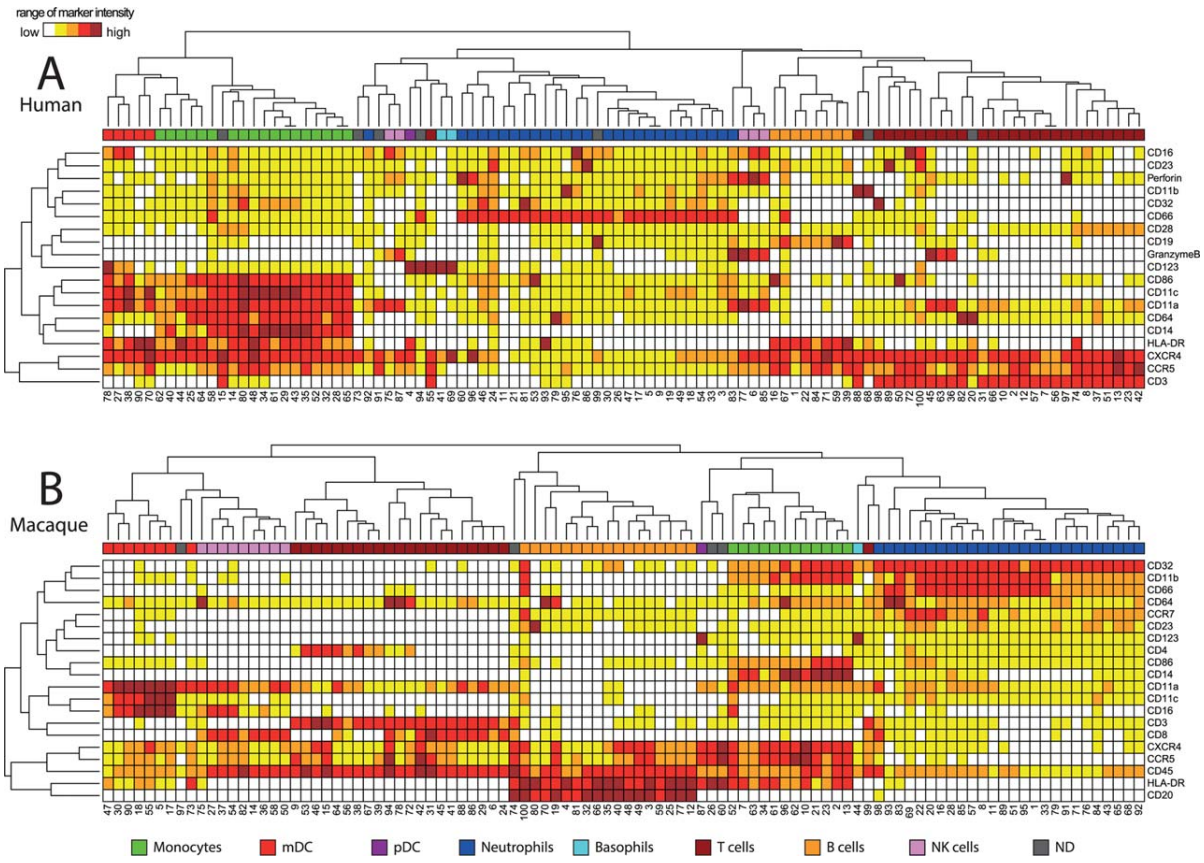

Figure 4. Heatmaps showing the phenotypes of identified SPADE nodes for both species. The five-tiered color scale, from white to deep red, represents marker expression within the range from the 1st and 99th percentile of the distribution of the totality of cells for each marker of each cluster for the human (**A**) and macaque (**B**) datasets. Hierarchical clusterings were performed on SPADE nodes and SPADE clustering markers to identify groups of nodes or markers having similar expression patterns. ND: not defined.

frequencies in macaque, whereas no significant difference was observed in B cells. To validate our comparison, we confirmed these frequencies after SPADE analysis followed with manual annotation of cell nodes with bivariate plots (Fig. 3B, Supporting Information Figs. 7 and 8).

In Deep Phenotypic Characterization of Human and Non-Human Primate Cell Populations

To visualize at a glance the expression profiles of the 100 SPADE nodes for the totality of their respective clustering markers, we charted the relative mean of marker median intensities using heatmap representations with hierarchical clustering at both the cell nodes and marker levels (Fig. 4).

Marker intensities were classified in five bins calculated based on the 1st and 99th percentile range expression divided into uniform categories (shown in Supporting Information Fig. 2). This approach allowed to compare and contrast more easily the sub-phenotypes from the same or between the two species and also to uncover patterns of marker co-expressions.

Nodes manually classified on the SPADE trees using a limited set of eight canonical markers (Fig. 1) clustered together in the heatmaps demonstrating the validity of the hierarchical clustering approach. In addition, to quantify the number of phenotypically similar human and macaque nodes and their degree of similarity, we performed a Spearman's rank correlation analysis based on the 15 markers shared between the human and macaque Ab panels in addition to CD19 for humans and CD20 for macaques (Fig. 5 and Supporting Information Table 2). Although these two markers do not exactly define the same populations, the circular graph representation (Fig. 5A) show that a large panel of human and macaque nodes correlated with each other.

Neutrophils were the most represented population in frequency and number of nodes in both species (Fig. 3). In macaque, neutrophils were clearly divided into two subsets characterized by the simultaneous differential detection of CD11b and CD66 ($CD11b^{high}/CD66^{high}$ or $CD11b^{mid}/CD66^{mid}$). Within these two subsets, CCR7 showed a wide range of expression from high to low range and CD45 expression varied from mid to low range. Strikingly, the overall level of expression of CXCR4 and CCR5 in neutrophils was lower in macaques as compared with humans. In humans, neutrophils stained by our Ab panel were more homogeneous with some scattered single nodes expressing high levels of CD16, CD23, Perforin, CD11b, CD32, Granzyme B, CD86, CD64,

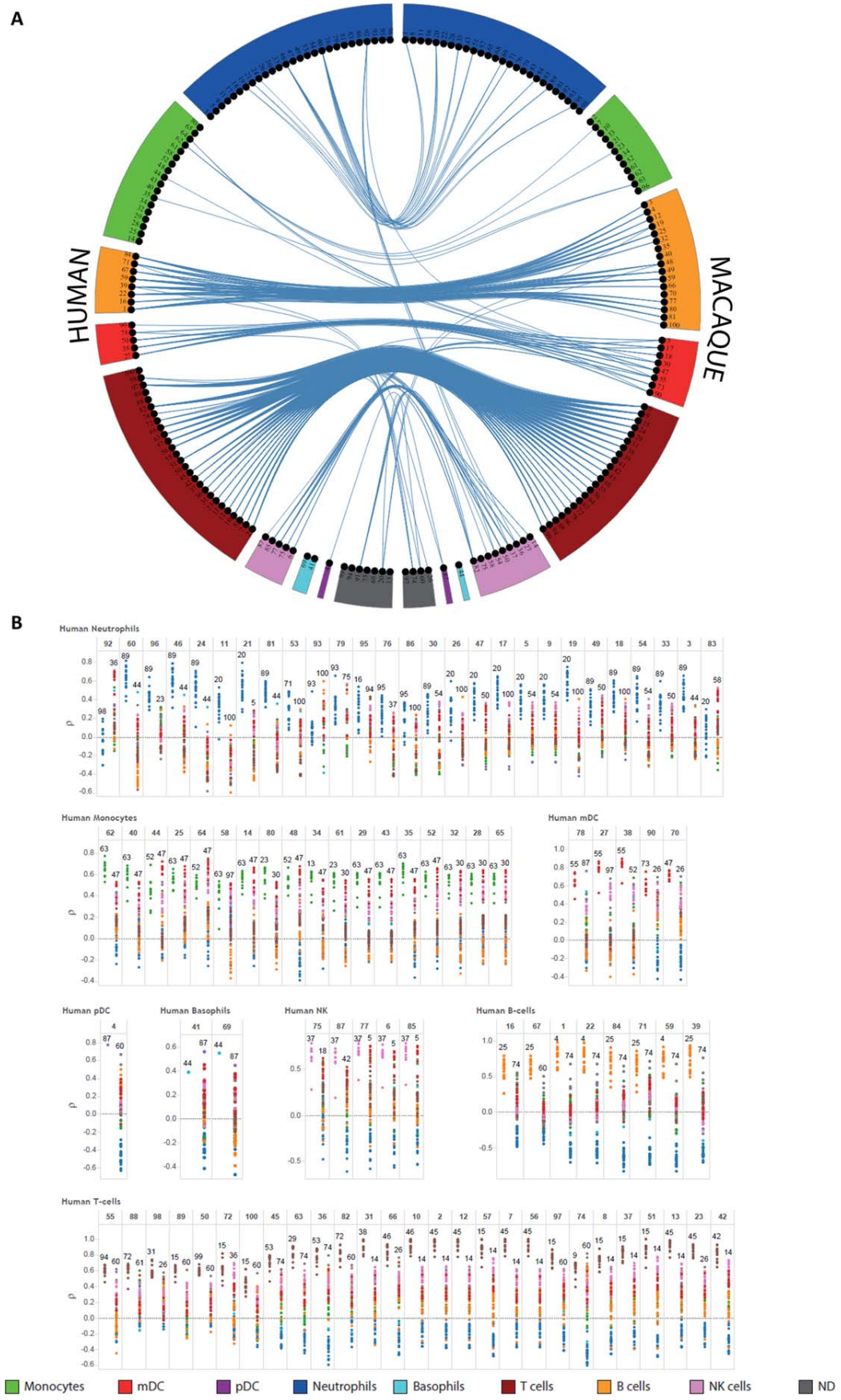
A
HUMAN
MACAQUE
B
Human Neutrophils
Human Monocytes
Human mDC
Human pDC
Human Basophils
Human NK
Human B-cells
Human T-cells
ρ
Monocytes
mDC
pDC
Neutrophils
Basophils
T cells
B cells
NK cells
ND

Figure 5.

HLA-DR, and CXCR4. Of note, human nodes 46 and 24 (2.93% ± 6.49 of all leukocytes, reaching >10% for 3 out of 26 individuals) co-expressing higher levels of CD11b, CD32, CD86 and CD11c as compared with other neutrophil nodes might represent granulocytic myeloid-derived suppressor cells (G-MDSC) (26). A similar population was not clearly distinguishable in macaque since CD32 and CD11b markers were widely expressed in all the neutrophils nodes. Nevertheless, macaque nodes 69, 22, and 20 (10.20% ± 4.86 of all leukocytes) might represent G-MDSC characterized by a higher expression of CD86 as the human counterpart and the novel expression of CD23. If so, this would imply that macaques carry in average more G-MDSC than their human counterpart. Interestingly, both in humans (node 79) and macaques (node 83 and 93), some neutrophil nodes displayed a high expression of CD64, previously reported as a marker of bacterial infection (27). Correlation coefficients relative to all macaque nodes were plotted for each human neutrophils node (Fig. 5B). Overall, human neutrophil nodes showed the highest correlation with macaque neutrophil nodes in 24 out of 27 instances (58.09% ± 7.09 of all leukocytes), except for human neutrophils nodes 92, 93, and 83, (which are $CD66^{low}$ $HLA\text{-}DR^{high}$ and $CD11a^{high}$ $Granzyme\ B^{high}$ $Perforin^{high}$, respectively) and many of them with macaque neutrophil nodes 89 and 20 (6.12% ± 3.96 of all leukocytes, both nodes being $CD66^{high}$ $CD11b^{high}$ $CD32^{high}$ and node 20 being in addition $CCR7^{high}$), confirming our previous visual approach with the circular graph.

Two basophil nodes ($HLA\text{-}DR^{-}$ $CD123^{+}$) were observed in humans (node 41 and 69), whereas a unique node was observed in macaque (node 44). Correlation analysis associated the human basophil nodes 41 and 69 to the macaque pDC node 87 ($HLA\text{-}DR^{+}$ $CD123^{+}$) and the macaque basophil node 44, respectively (Fig. 5B).

Mononuclear phagocytes are a heterogeneous cell population with antigen presenting functions including monocytes, DC and macrophages; these latter predominantly found in tissues (28). In the present study, performed on circulating leukocytes, monocytes, mDC and pDC were classified on the SPADE tree (Fig. 1) and distinctly represented on the heatmaps (Fig. 4). In macaque, the dendrogram clearly divided the 12 monocyte nodes into two distinct subpopulations according to the simultaneous higher expression of CD32, CD11b, CD64, CD86, and CD14. In humans, the 18 monocyte nodes are patchier. Nevertheless, we could identify a group of nodes expressing higher levels of CD32 localized in a region of the heatmap where the expression of CD11c and CD14 was more elevated. CD64 expression in human monocytes was expressed in all nodes and reached the top 2 expression bins in 13 out of 18 nodes (3.59% ± 2.25 of all leukocytes), while in macaque, CD64 expression reached the top 2 expression bins in only 1 out of 12 nodes (node 96 expressing in addition CD32, CD11b, CD86, CD14, CXCR4, CCR5, CD45, and HLA-DR, 0.06% ± 0.06 of all leukocytes), which represents a very low amount of cells compared with their human counterparts. CD11a and CD11c displayed a similar pattern as shown with the marker dendrograms with 16 and 13 human nodes in the top 2 expression bins respectively (4.19% ± 2.36 and 3.26% ± 2.06 of all leukocytes, respectively). Remarkably, the staining of CD11c was very low or absent in all macaque monocytes nodes, which may reflect the difficulty in identifying anti-human antibody clones with good cross-reactivity with the macaque determinant, as previously reported by others (29). As expected, all human monocytes nodes are characterized by a clear expression of this marker. Diversity between human and macaque monocytes was evident also by correlation analysis (Fig. 5B). Human monocyte nodes showed the highest correlation value with a corresponding macaque monocyte node in only 9 out of 18 instances (human monocytes nodes 62, 40, 58, 80, 34, 61, 29, 43, and 35; 2.76% ± 1.08 of all leukocytes), and most of them correlated with macaque monocyte node 63 (which is $CD32^{mid}$ $CD11b^{mid}$ $CD64^{mid}$, $CD86^{mid}$ $CD14^{high}$ $CD11a^{mid}$ $CXCR4^{mid}$ $CCR5^{mid}$ $CD45^{mid}$ $HLA\text{-}DR^{mid}$). In all the other cases, the human monocyte nodes were more similar to the macaque mDC nodes 47 or 30 (which are $CD11a^{high}$ $CD11c^{mid}$ $CD16^{mid}$ $HLA\text{-}DR^{mid}$ and $CD11a^{high}$ $CD11c^{high}$ $CD16^{high}$ $HLA\text{-}DR^{low}$, respectively).

Myeloid DC nodes were more abundant in macaque and, except for node 73 ($HLA\text{-}DR^{high}$, $CD11a^{high}$ $CD11c^{low}$ $CD16^{low}$), showed a high expression of CD16. In humans, we identified 5 mDC nodes with CD16 expression varying from negative to positive. CD123, a marker of pDC and basophils, was expressed at low levels in three macaque mDC nodes (18, 55, and 17; $HLA\text{-}DR^{mid}$, $CD11a^{high}$ $CD11c^{high}$ $CD16^{high}$ $CXCR4^{mid/high}$ 0.94% ± 0.53 of all leukocytes) whereas we found a full expression range in the 5 human mDC nodes (0.92% ± 0.35 of all leukocytes). Of note, CD16 negative mDC were also CD123 negative (node 90). In macaque mDC, staining of CD86, CXCR4, CCR5, and HLA-DR was weaker

Figure 5. Correlation analysis of the node expression vectors of humans and macaques. (**A**) Circular graph representation showing the significant correlations between the SPADE nodes of the human and macaque analyses. Each node of the graph corresponds to a SPADE node and each line corresponds to a significant phenotype correlation between two human and macaque cell nodes ($P > 0.7$). (**B**) The expression vector of each human node from the eight main subpopulations annotated manually on the spade tree, neutrophils, monocytes, mDC, pDC, basophils, NK cells, B cells, and T cells, was compared with all the macaque node expression vectors. In each panel representing one human node, the *P* values are shown for all the macaque nodes. Macaque nodes values shown on the first column share the same annotation with the human node, in contrast to macaque nodes shown in the second column. The ID of the macaque node with the highest *P* value is indicated. Macaque nodes are color coded as in Figure 1. For example, if we consider the human neutrophil node 92 (first panel at the top of the figure), it shows a higher correlation with macaque nodes in the second column (i.e., not belonging to the neutrophil population) and especially to the monocyte node 32, than with nodes in the first column belonging to the macaque neutrophil population. On the contrary, the human neutrophil node 60 clearly correlates with macaque neutrophil nodes shown in the first column and in particular it shows the highest correlation with node 89. ND: not defined.

than in macaque monocytes and indeed they were not partitioned next to each other on the heatmap (Fig. 4B), whereas in humans these same markers were equally expressed in the two cell populations. Despite these disparities between the two species, the correlation analysis showed that 4 out of the 5 human mDCs nodes (0.83% ± 0.27 of all leukocytes) showed the highest correlation value with a corresponding macaque mDC node, except human mDC node 78 (0.09% ± 0.21 of all leukocytes, reaching 1% in one individual) a rare population which expresses the highest level of CD123 (a feature not found in macaque mDC) (Fig. 5B).

The exploration of the innate myeloid leukocytes was the main aim of our comparative study. Nevertheless, the inclusion of lineage markers in separate channels for the definition of monocytes and DC and the unsupervised and global nature of the analysis opened the way to a non-conventional vision of NK cells, T, and B lymphocytes with the potentials to uncover new patterns of expression of unusual markers. Five and nine nodes were observed for human and macaque NK cells, respectively. In humans, the five nodes were quite homogeneous although separated into two clusters by the neutrophil nodes. Perforin expression was the only evident difference between the two groups of nodes, although Granzyme B expression tends to follow the same pattern. Correlation analysis showed that the totality of human NK nodes correlated with the macaque NK cell node 37 (Fig. 5B). In macaque, the dendrogram divided NK cells into three groups. Node 37, together with nodes 27 and 54 (2.53% ± 1.09 of all leukocytes) formed a group of NK cells expressing high levels of CD16 and CD11a as opposed to a group expressing these two molecules at a lower level (node 82, 14, 36, 58, and 50; 3.44% ± 1.25 of all leukocytes). Node 75 (0.07% ± 0.03 of all leukocytes) set apart with a characteristic high expression of CD64, a marker not previously reported to be expressed in NK cells, to our knowledge.

Similarly to NK cells, B cells were quite homogeneous in humans (8 nodes) whereas in macaque, we observed 16 distinct nodes divided into two distinct populations by the expression of CXCR4 and CCR5. In addition, some nodes were characterized by the punctual high expression of CD32, CD11b, CD66, CD64, CCR7, and CD23.

Surprisingly for an Ab panel combination dedicated to the innate response (Table 1), T cells comprised 27 and 22 nodes (out of 100 nodes) in humans and macaques, respectively (Fig. 1). In humans, the absence of anti-CD4 and anti-CD8 Abs in the panel prevented a straightforward data analysis. Nevertheless, we were able to observe some peculiar nodes expressing the Fc receptors CD16, CD23, CD32, or CD64. $CD16^{Pos}$ $CD3^{Pos}$ might represent NKT cells whereas the expression of Fc receptors on T cells have been previously observed only on T cell lines (30). In macaque, where Abs directed to CD4 and CD8 were included in the panel, the dendrogram clearly divided the T cells into two groups: $CD4^{Pos}$ T cells (node 9 to 39; 8.01% ± 2.67 of all leukocytes) and $CD8^{Pos}$ T cells (node 94 to 24; 11.01% ± 6.44 of all leukocytes). As previously described (10,31), double positive $CD4^{Pos}$ and $CD8^{Pos}$ T cells were observed and some of them were highly positive for the Fc gamma RI CD64.

Discussion

Simultaneous analysis of frequency and quality of immune cell populations is key for understanding immunopathogenesis of infectious diseases, cancer and autoimmune syndromes. Flow cytometry was the technology of choice to look at immune cells at the single cell level until the recent advent of mass cytometry expanded the number of analyzable marker to greater than 40 and, hence, amplified the number of discernable cell populations (32). The present study takes advantage of the multiparameter capacities of mass cytometry to simultaneously analyze innate myeloid leukocytes in both humans and macaques with the aim of obtaining a global vision of the different cellular populations and setting the ground for future translational studies across human and NHP models in healthy and pathological situations.

Our Ab panels used to stain fixed human and macaque leukocytes were similar, but not absolutely identical. This limit is intrinsic to studies using Ab-based tools for interspecies comparisons though. Abs clones generated against human targets were compared and selected for their reported or tested reactivity with macaque cells, but attesting for a full cross-reactivity with comparable affinity is tricky. This led us to use different clones, antibodies concentration and sometimes different metals for the same marker in the two panels, which may increase inter-species staining profiles differences. To circumvent these technical issues, we chose to reason on categories of expression for our analysis (Fig. 4). We compared markers expression with respect to other cells from the same species, so that we consider that a "high" or "low" expression has the same "meaning" for human and macaque cells, although absolute MSI can differ between the two species. This constitutes a first limit of our approach. To ultimately validate inter-species comparison, a negative cell line should be transfected with human versus macaque cDNA and stained with the suspect Ab clones and functional studies should be performed by stimulating cells with ligands of the "suspect" receptors and by assessing their response. Throughout the manuscript, we also considered that a given marker ensures the same function or has the same "meaning" on human or macaque leukocytes, nevertheless this hypothesis might not be always true as previously observed by Autissier et al. (8) for the CD141 antigen in human and rhesus macaque mDC. This constitutes a second limit of our approach. In overall, this analysis remains explorative and oriented to build the basis for future translational studies aiming to refine our knowledge on inter-species similarities and differences. Finally, key markers, such as CD1c or CD33 to identify mDC subsets and MDSCs, were lacking. Actually, at the time when the experiments were done we were not able to find Ab clones reactive with fixed samples and it was mandatory to fix samples to include granulocytes in our analysis since these cells are very labile and cryosensitive.

SPADE was used to mine our high-dimensional data as it can handle large datasets and overall because its density-based downsampling step avoids that abundant cells outnumber rare cells which can then form their own cell nodes. SPADE analyses were computed separately for the human and macaque datasets. The main reasons for this parallel analysis were that our sample sizes were not equal ($n = 26$ humans and $n = 5$ macaques) and the ranges of expression of some markers were different between species, even for markers with the same cellular tropism of expression. This made difficult to segregate meaningful cell populations based on the mean signal intensity using a single clustering analysis for both human and macaque samples, without normalizing or transforming data. In addition, similar but not identical markers were used to cluster humans and macaque cells, with 15 markers shared between the two species though. By increasing the number of clustering markers rather than restrict ourselves to the shared markers, we aimed to capture, for each species, cells clusters defined with the deepest phenotype and more branch points between them (15). In any cases, the subsequent correlation analysis was computed only on the 15 shared markers, plus CD19 for humans and CD20 for macaques.

It is also important to point out that five animals from one facility and one gender are not a representative population of the species. A representative population would require hundreds of animals from different primate centers. This small sample size for the macaque dataset size might explain why we observed a lower pDC frequency in macaques than in humans, in contrast to previous reports, including ours (33). This statement is also true for the 26 human volunteers (34). However, it should also be emphasized that the BIOVACSAFE clinical training trials are conducted in an inpatient setting with the confinement of the volunteers and the control of many parameters such as diet and sleep, to ensure minimal background variability and noise.

Despite efforts to control many parameters, sample collection and processing likely differ between macaques co-housed in an animal-care facility and human volunteers in a hospital, which can also impact the variations we observed.

Variations can indeed be observed among individuals from the same species, especially in humans (Supporting Information Figs. 4 and 5), consistently with human variability described in literature (34,35). These differences can also be visualized in term of variations of the relative abundance of each cell population (Fig. 2). Obviously 5 or even 26 individuals do not allow to fully assess intra-species variations. Further functional and larger analyses will be required in order to assess more deeply these variations as well as changes among individuals after infection or vaccination. In particular, the differences observed in term of maturation markers and cell abundance in different cell types including NK cells and T cells, may also be linked to different infection history between wild animals and city-living humans, in addition to species differences and genetics.

Finally, to our knowledge, only two studies reported a high-dimensional phenotypic comparison between immune cells from two different species (36,37). Using a new algorithm, named Scaffold, (which stands for Single-Cell Analysis by Fixed Force- and Landmark-Directed) map designed to visualize and compare complex cellular systems, Spitzer and colleagues compared human and murine blood cells on the basis of the staining profiles for 15 shared markers displaying similar cell subset expression patterns between humans and mice (36). After independent clustering of each sample using a clustering algorithm called CLARA (Clustering for large applications), cell nodes with similar phenotypes were linked by edges whose lengths were proportional to their similarity measured using cosine as a distance metric. Human samples were overlaid over the murine reference map. This approach revealed previously known differences between mice and humans as well as a similar overall immune compartment organization. In the second study (37), Guilliams et al. developed a toolbox using unsupervised approaches (FlowSOM, One-SENSE, and tSNE algorithms) to identify and align DC subtypes (cDC1, cDC2, and pDC) in different tissues (blood, skin, lung, spleen, lymph node) and species (mouse, macaque, and human). They also confirmed these methods by manual gating. Using flow cytometry data for the three species, as well as mass cytometry data for mice and humans only, they built a reference framework which we believe will be highly valuable for future studies focusing on DC response in different species and/or tissues.

Our approach aims to give both a global (different cell types are studied) and a precise (several markers are analyzed) insight of the immune structure of two species, human and macaques, using mass cytometry approach. We believe these kind of studies will be important to improve the transfer of knowledge from animal models to humans and vice versa.

Despite the aforementioned caveats in our study to keep in mind, our side by side analysis suggests a generalized higher staining of markers associated with activation and inflammation in macaque neutrophils, and a lower expression of markers associated with maturation in mDC. Indeed, CD11b and CD32 were widely expressed in macaque neutrophils. CD32, CD11b, and CD86 expression was observed in the totality of macaque monocytes and defined two clear subsets with high and mid expression. In addition, CD11b showed a similar range of expression in both species, strengthening this claim. Note that the range of expression of CD32 in macaques was wider than in humans which can partially be due to different clones and metal used. In any case, relatively to other cell types from the same species, macaque monocytes and neutrophils expressed a higher level of CD32 compared with human monocytes and neutrophils. CD16 absolute MSI differed between humans and macaques, which may be due to cross-reactivity differences. CD16 was expressed at a high level in almost all macaques mDC nodes while it was bimodal in humans. Also, the distribution of chemokine receptors on neutrophil nodes suggested a phenotype orienting their localization in the circulation. Similarly, the lower expression of CD64 in macaque monocytes suggested a more mature phenotype. Indeed CD64 was detected at high MSI in different cell types (including neutrophils and T cells), thus this low expression in monocytes is unlikely to be solely caused by

previously reported CD64 polymorphism (38), although it can participate to it. Taken together, these observations suggest a macaque innate immune system tuned to a high activation threshold compared with the Caucasian human counterpart and a pool of circulating neutrophils ready to be directed but not yet committed toward an eventual site of inflammation. Alternatively, we could imagine innate immune leukocytes of macaque, although from a breeding facility, as exposed to a more intense antigenic challenge in comparison to humans. Indeed, differences in inflammatory and homing markers might be genetically determined or controlled by the environment (39–41). The potential increased immune activation observed in macaque might help to explain differences in the host-pathogen interaction between humans and NHP. For instance, increased SIV replication kinetics in NHP models of infection might be influenced by the global activation status of the innate immune system and the best NHP model might be the one with the lower activation threshold (42). To support such hypothesis, studies correlating the kinetic of infection in macaque and the expression of innate leukocytes markers need to be performed. Such studies may also uncover possible therapeutic targets aiming to modulate the control of viral replication by the immune system.

Monocytes, together with CD4 T cells and macrophages, can be infected by HIV and SIV, and are considered as a latent proviral reservoir (43). Our analysis revealed a complexity in human and macaque monocytes beyond the classical and non-classical subsets, shaped by Fc receptors, adhesion molecules and activation markers. Indeed, in macaque, within classic monocytes, we were able to identify two clear subsets characterized by a differential expression of CD32, CD11b, CD64, CD86, and CD14. Human nodes with a moderate expression of CD32 were also observed in few instances without shaping clear bimodal subsets. It will be of interest to study which role these subsets play as virus reservoirs or during the inflammation induced by HIV/SIV infection.

Neutrophils, previously considered as a homogeneous cell population with simple functions were recently recognized as a complex population able to shape the adaptive response and exert multiple specific functions (44,45). In the present work, we confirm this intraspecies heterogeneity and we extend this knowledge to NHP. Neutrophils and basophils were clearly identified by our analysis strategy but since CD16 expression on $CD66^{pos}$ cells was relatively low, it was difficult to differentiate eosinophils, usually identified as $CD66^{pos}$ $CD16^{neg}$ events in human (46). Moreover, the recent description of nonspecific binding by eosinophils of the metal conjugated antibodies (14) and our gating strategy excluding background producing events might also account for the absence of eosinophils. CD16 expression was clearly observed on mDC and NK cells demonstrating the recognition of the CD16 molecules by the clones B73.1 and 3G8 in humans and macaque, respectively. It has been previously reported that CD16 expression on neutrophils is down-modulated upon apoptosis and that macaque neutrophils would lack CD16 (47–49). Therefore, it is conceivable that, despite our cell preparation procedure was able to preserve polymorphonuclear cells, neutrophils might have engaged an apoptotic phase losing CD16 on their surface and hence decreasing our capacity to discriminate neutrophils from eosinophils in humans. Using another eosinophils-specific marker should allow us to circumvent this issue in the next studies.

Antibody panels were not specially dedicated to analyze T cells and the capacity of the selected markers to unravel such diversity was unexpected. T cells do not normally express Fc receptors even though their expression was observed in T cell-derived cell lines (30). Expression of Fc receptor by T cells merits further investigation from a phenotypical and functional point of view.

This comparison of human and macaque innate myeloid cells revealed some differences between species, such as a distinct intensity of expression of some markers (and one of the trick was to compare species specific relative marker expression) or co-expression of some markers. In particular, neutrophils and monocytes appeared more activated in macaques than in humans, with a higher expression of CD11b and CD32. In addition macaques mDC displayed a higher homogenous CD16 expression than their human counterparts. However, these differences were subtle and overall humans and macaques share a common global innate myeloid compartment both in terms of number (Fig. 2) and phenotype (Figs. 4 and 5A), supporting the use of NHP as preclinical models for human infections and diseases.

Acknowledgments

The authors thank Marie-Laurence Baron (Institut Pasteur, Paris, France) and Malvina Schatz (Centre d'études d'agents Pathogènes et Biotechnologies pour la Santé, Montpellier (CPBS), France) for their help in building the antibody panels. They thank the staff of the IDMIT infrastructure and especially the Animal Science and Welfare, L2I, and FlowCyTech core laboratories.

Conflict of Interest

The authors declare that they have no conflicts of interest.

Literature Cited

1. Theiler M, Smith HH. The use of yellow fever virus modified by in vitro cultivation for human immunization. J Exp Med 1937;65:787–800.
2. Peña JC, Ho W-Z. Monkey models of tuberculosis: Lessons learned. Infect Immun 2015;83:852–862.
3. Brok HP, Bauer J, Jonker M, Blezer E, Amor S, Bontrop RE, Laman JD, 't Hart BA. Non-human primate models of multiple sclerosis. Immunol Rev 2001;183:173–185.
4. Blair TC, Manoharan M, Rawlings-Rhea SD, Tagge I, Kohama SG, Hollister-Smith J, Ferguson B, Woltjer RL, Frederick MC, Pollaro J, et al. Immunopathology of Japanese macaque encephalomyelitis is similar to multiple sclerosis. J Neuroimmunol 2016;291:1–10.
5. T Hart BA, Bogers WM, Haanstra KG, Verreck FA, Kocken CH. The translational value of non-human primates in preclinical research on infection and immunopathology. Eur J Pharmacol 2015;759:69–83.
6. Hatziioannou T, Evans DT. Animal models for HIV/AIDS research. Nat Rev Microbiol 2012;10:852–867.
7. Shedlock DJ, Silvestri G, Weiner DB. Monkeying around with HIV vaccines: Using rhesus macaques to define "gatekeepers" for clinical trials. Nat Rev Immunol 2009;9:717–728.
8. Autissier P, Soulas C, Burdo TH, Williams KC. Immunophenotyping of lymphocyte, monocyte and dendritic cell subsets in normal rhesus macaques by 12-color flow cytometry: Clarification on DC heterogeneity. J Immunol Methods 2010;360:119–128.

9. Autissier P, Soulas C, Burdo TH, Williams KC. Evaluation of a 12-color flow cytometry panel to study lymphocyte, monocyte, and dendritic cell subsets in humans. Cytometry Part A 2010;77A:410–419.
10. Guenounou S, Bosquet N, Dembek CJ, Le Grand R, Cosma A. OMIP-016: Characterization of antigen-responsive macaque and human T-cells. Cytometry Part A 2013;83A:182–184.
11. Lewis DJM, Lythgoe MP. Application of "systems vaccinology" to evaluate inflammation and reactogenicity of adjuvanted preventative vaccines. J Immunol Res 2015; 2015:909406.
12. Egger G, Burda A, Glasner A. A simple method for measuring the F-actin content of human polymorphonuclear leukocytes in whole blood. Virchows Arch 2001;438: 394–397.
13. Finck R, Simonds EF, Jager A, Krishnaswamy S, Sachs K, Fantl W, Pe'er D, Nolan GP, Bendall SC. Normalization of mass cytometry data with bead standards. Cytometry Part A 2013;83A:483–494.
14. Rahman AH, Tordesillas L, Berin MC. Heparin reduces nonspecific eosinophil staining artifacts in mass cytometry experiments. Cytometry Part A 2016;89A:601–607.
15. Qiu P, Simonds EF, Bendall SC, Gibbs KD, Bruggner RV, Linderman MD, Sachs K, Nolan GP, Plevritis SK. Extracting a cellular hierarchy from high-dimensional cytometry data with SPADE. Nat Biotechnol 2011;29:886–891.
16. Gautreau G, Pejoski D, Cosma A, Le Grand R, Beignon A, Tchitchek N. SPADEVizR: An R package for Visualization, Analysis and Integration of SPADE results. Bioinformatics 2016;2:2567–2576.
17. Piccioli D, Tavarini S, Borgogni E, Steri V, Nuti S, Sammicheli C, Bardelli M, Montagna D, Locatelli F, Wack A. Functional specialization of human circulating CD16 and CD1c myeloid dendritic-cell subsets. Blood 2007;109:5371–5379.
18. Macdonald KP, Munster DJ, Clark GJ, Dzionek A, Schmitz J, Hart DNJ. Characterization of human blood dendritic cell subsets. Cell 2002;100:4512–4520.
19. Dutertre CA, Amraoui S, DeRosa A, Jourdain JP, Vimeux L, Goguet M, Degrelle S, Feuillet V, Liovat AS, Muller-Trutwin M, et al. Pivotal role of M-DC8(+) monocytes from viremic HIV-infected patients in TNFalpha overproduction in response to microbial products. Blood 2012;120:2259–2268.
20. Ziegler-Heitbrock HWLW. Heterogeneity of human blood monocytes: The CD14+ CD16+ subpopulation. Immunol Today 1996;17:424–428.
21. Sadhu C, Hendrickson L, Dick KO, Potter TG, Staunton DE. Novel tools for functional analysis of cd11c: Activation-specific, activation-independent, and activating antibodies. J Immunoass Immunochem 2007;29:42–57.
22. Ihanus E, Uotila LM, Toivanen A, Varis M, Gahmberg CG. Red-cell ICAM-4 is a ligand for the monocyte/macrophage integrin CD11c/CD18: Characterization of the binding sites on ICAM-4. Blood 2007;109:802–810.
23. Ho CSK, Munster D, Pyke CM, Hart DNJ, López JA, Lo JA. Spontaneous generation and survival of blood dendritic cells in mononuclear cell culture without exogenous cytokines Spontaneous generation and survival of blood dendritic cells in mononuclear cell culture without exogenous cytokines. Immunobiology 2008;99:2897–2904.
24. Shi J, Ikeda K, Maeda Y, Shinagawa K, Ohtsuka A, Yamamura H, Tanimoto M. Identification of CD123+ myeloid dendritic cells as an early-stage immature subset with strong tumoristatic potential. Cancer Lett 2008;270:19–29.
25. Comeau MR, Van der Vuurst de Vries A-R, Maliszewski CR, Galibert L. CD123bright plasmacytoid predendritic cells: Progenitors undergoing cell fate conversion? J Immunol 2002;169:75–83.
26. Pillay J, Kamp VM, van Hoffen E, Visser T, Tak T, Lammers J-W, Ulfman LH, Leenen LP, Pickkers P, Koenderman L. A subset of neutrophils in human systemic inflammation inhibits T cell responses through Mac-1. J Clin Invest 2012;122: 327–336.
27. Cid J, Aguinaco R, Sanchez R, Garcia-Pardo G, Llorente A. Neutrophil CD64 expression as marker of bacterial infection: A systematic review and meta-analysis. J Infect 2010;60:313–319.
28. Haniffa M, Bigley V, Collin M. Human mononuclear phagocyte system reunited. Semin Cell Dev Biol 2015;41:59–69.
29. Sugimoto C, Hasegawa A, Saito Y, Fukuyo Y, Chiu KB, Cai Y, Breed MW, Mori K, Roy CJ, Lackner AA, et al. Differentiation kinetics of blood monocytes and dendritic cells in macaques: Insights to understanding human myeloid cell development. J Immunol 2015;195:1774–1781.
30. McLain L, Dimmock NJ. A human CD4+ T-cell line expresses functional CD64 (Fc gamma RI), CD32 (Fc gamma RII), and CD16 (Fc gamma RIII) receptors but these do not enhance the infectivity of HIV-1-IgG complexes. Immunology 1997;90: 109–114.
31. Wang X, Das A, Lackner AA, Veazey RS, Pahar B. Intestinal double-positive CD4+CD8+ T cells of neonatal rhesus macaques are proliferating, activated memory cells and primary targets for SIVMAC251 infection. Blood 2008;112:4981–4990.
32. Bendall SC, Nolan GP, Roederer M, Chattopadhyay PK. A deep profiler's guide to cytometry. Trends Immunol 2012;33:323–332.
33. Malleret B, Karlsson I, Manéglier B, Brochard P, Delache B, Andrieu T, Muller-Trutwin M, Beaumont T, McCune JM, Banchereau J, et al. Effect of SIVmac infection on plasmacytoid and CD1c+ myeloid dendritic cells in cynomolgus macaques. Immunology 2008;124:223–233.
34. Duffy D, Rouilly V, Libri V, Hasan M, Beitz B, David M, Urrutia A, Bisiaux A, Labrie ST, Dubois A, et al. Functional analysis via standardized whole-blood stimulation systems defines the boundaries of a healthy immune response to complex stimuli. Immunity 2014;40:436–450.
35. Sekiguchi DR, Smith SB, Sutter JA, Goodman NG, Propert K, Louzoun Y, Rogers W, Luning Prak ET. Circulating lymphocyte subsets in normal adults are variable and can be clustered into subgroups. Cytometry Part B Clin Cytom 2011;80B:291–299.
36. Spitzer MH, Gherardini PF, Fragiadakis GK, Bhattacharya N, Yuan RT, Hotson AN, Finck R, Carmi Y, Zunder ER, Fantl WJ, et al. IMMUNOLOGY. An interactive reference framework for modeling a dynamic immune system. Science 2015;349:1259425.
37. Guilliams M, Dutertre C-A, Scott CL, McGovern N, Sichien D, Chakarov S, Van Gassen S, Chen J, Poidinger M, De Prijck S, et al. Unsupervised high-dimensional analysis aligns dendritic cells across tissues and species. Immunity 2016;45:669–684.
38. Nguyen DC, Scinicariello F, Attanasio R. Characterization and allelic polymorphisms of rhesus macaque (Macaca mulatta) IgG Fc receptor genes. Immunogenetics 2011; 63:351–362.
39. Beura LK, Hamilton SE, Bi K, Schenkel JM, Odumade OA, Casey KA, Thompson EA, Fraser KA, Rosato PC, Filali-Mouhim A, et al. Normalizing the environment recapitulates adult human immune traits in laboratory mice. Nature 2016;532: 512–516.
40. Muyanja E, Ssemaganda A, Ngauv P, Cubas R, Perrin H, Srinivasan D, Canderan G, Lawson B, Kopycinski J, Graham AS, et al. Immune activation alters cellular and humoral responses to yellow fever 17D vaccine. J Clin Invest 2014;124:3147–3158.
41. Reese TA, Bi K, Kambal A, Filali-Mouhim A, Beura LK, Burger MC, Pulendran B, Sekaly R-P, Jameson SC, Masopust D, et al. Sequential infection with common pathogens promotes human-like immune gene expression and altered vaccine response. Cell Host Microbe 2016;19:713–719.
42. Sui Y, Gordon S, Franchini G, Berzofsky JA. Nonhuman primate models for HIV/AIDS vaccine development. Curr Protoc Immunol 2013;102:Unit 12.14.
43. Coleman CM, Wu L. HIV interactions with monocytes and dendritic cells: Viral latency and reservoirs. Retrovirology 2009;6:51.
44. Saitoh T, Komano J, Saitoh Y, Misawa T, Takahama M, Kozaki T, Uehata T, Iwasaki H, Omori H, Yamaoka S, et al. Neutrophil extracellular traps mediate a host defense response to human immunodeficiency virus-1. Cell Host Microbe 2012;12:109–116.
45. Thomas CJ, Schroder K. Pattern recognition receptor function in neutrophils. Trends Immunol 2013;34:317–328.
46. Hansel TT, De Vries IJ, Iff T, Rihs S, Wandzilak M, Betz S, Blaser K, Walker C. An improved immunomagnetic procedure for the isolation of highly purified human blood eosinophils. J Immunol Methods 1991;145:105–110.
47. Moulding DA, Hart CA, Edwards SW. Regulation of neutrophil FcgammaRIIIb (CD16) surface expression following delayed apoptosis in response to GM-CSF and sodium butyrate. J Leukoc Biol 1999;65:875–882.
48. Nusbaum P, Lainé C, Seveau S, Lesavre P, Halbwachs-Mecarelli L. Early membrane events in polymorphonuclear cell (PMN) apoptosis: Membrane blebbing and vesicle release, CD43 and CD16 down-regulation and phosphatidylserine externalization. Biochem Soc Trans 2004;32:477–479.
49. Rogers KA, Scinicariello F, Attanasio R. IgG Fc receptor III homologues in nonhuman primate species: Genetic characterization and ligand interactions. J Immunol 2006;177:3848–3856.

Part II.
Innate responses induced by a prime-boost vaccination following a classical vaccination schedule

Rationale

First, we wanted to determine the innate responses induced by vaccination following a "classical" prime-boost schedule. Since the European medicines agency recommends a delay of at least one month between each MVA immunization, a delay of two months was chosen between prime and boost and considered as classical. At each immunization, a dose of 4.10^8 PFU of MVA HIV B was injected subcutaneously to each of the five animals of the cohort. This cohort will be latter referred as the classical boost group.

Preliminary analyses from the lab indicated that this schedule was able to induce a long-lasting humoral response, including neutralizing antibodies (Pejoski et al., 2016). In the very same animals, in addition to the measurement of the local and systemic inflammation induced by each immunization and the level of cytokines present in plasma, we used mass cytometry to decipher the phenotype of blood innate immune cells responding to vaccination. We developed two antibody panels to decipher the phenotype of innate immune cells following vaccination. The first panel targeted innate myeloid cells. The second panel targeted NK cells. Giving the complexity of the analyses of each of these cell populations, two distinct analyses were done and gave rise to two published papers.

Chapter 3. Innate myeloid responses after a prime-boost vaccination following a classical schedule

Overview

In this classical boost group, we noticed that a local and systemic inflammation (assessed via skin reaction scoring and C-reactive protein level respectively) was induced by each immunization, but they were reduced in amplitude after boost compared to after prime. Accordingly, the level of pro-inflammatory cytokines (IP-10, IL-6, MCP-1) induced by both immunizations differed between the response to prime and to boost. Still, at the scale of leukocytes, granulocytes and monocytes-DCs, the same early and transient enrichment in cell number was observed after prime and after boost.

To challenge in more details these apparent discrepancies, we developed *de novo* a computational pipeline of analysis to decipher the phenotype of these innate myeloid cells. Briefly, as previously stated, we used SPADE to define cell clusters regrouping cell sharing similar phenotypes. We notably used SPADEVizR R-package (Gautreau et al., 2017) to deeply optimize the user-defined settings of our SPADE analysis. Based on the resulting SPADE tree, each cluster was manually annotated (neutrophils, basophils, monocytes, DCs, T cells, B cells, NK cells...) and we extracted granulocytes (neutrophils and basophils) on one hand and monocytes-DCs (monocytes, cDCs, pDCs and the previously mentioned uncharacterized APCs) on the other hand. Note that similarly to our previous study (Elhmouzi-Younes et al., 2017), eosinophils had to be excluded from this analysis.

We used heatmap representations to visualize the phenotype of each subcompartment. Given the stringency of our clustering, we likely overclustered the data so that marker expression in every clusters was homogeneous (uniform and narrow). As a result, a given cell subpopulation is likely subdivided in several clusters. To mitigate this effect, we used cell cluster hierarchical clustering to pool together clusters that shared a similar phenotype into so-called phenotypic families, which more likely represent cell subpopulations.

Note that the phenotypic characterization we performed was not perfect, in particular regarding cDCs, since key markers discriminating known subsets (*e.g.* CADM1, CD1c and CD172a distinguishing cDC1 and cDC2 populations (Guilliams et al., 2016)) could not be included. Indeed, one of the limitation of our study is the use of fixed samples. As fixation can alter some epitopes recognized by commercial antibodies, some markers could not be targeted, since no antibody clone cross-reacting with macaque fixed cells could be found. Some new clones were latter described, after the results of this first cohort were acquired (Guilliams et al., 2016). In addition, at the time of these analyses, and still nowadays, the nomenclature of neutrophil subpopulations is still being established, and some markers that are now used to characterize them, such as CD10, CD101 or CD49d (Ng et al., 2019), could not be included.

Despite these caveats inherent to our dataset, we documented a large phenotypic diversity of blood innate myeloid cells. We notably identified striking features, in addition to the ones previously reported in Chapter 2 (Elhmouzi-Younes et al., 2017). For example, within the granulocytes compartment, three differentially activated (highly, intermediately and poorly activated) subphenotypes of neutrophils, differing in the expression of CD66, CD32, CD11b, CCR7 and CD45 were observed. Also, a population of $CD4^+$ neutrophils was found, which displayed a highly activated phenotype, including the high expression of CD66, CD11b, CD23, CD32abc and CD11c. Such a $CD4^+$ neutrophil subphenotype was previously but scarcely reported in literature (Biswas et al., 2003), but its exact role remained unknown. Based on the phenotype observed in our study, they are very likely linked to a strong inflammation induction (Vella et al., 1999; Benoni et al., 2001; Lewis et al., 2015). Also, note that within the monocyte-DC compartment we identified $CD3^-$ $CD8^-$ $CD14^-$ $CD20^-$ $CD11c^-$ $CD16^-$ $CD123^-$ HLA-DR^+ cells that we classified as uncharacterized APCs. Since they produce IP-10 and were clustered closely to monocytes, they might correspond to activated monocytes, which have downregulated the expression of CD14.

To further assess the kinetics of the cell populations we identified, we then clustered together the phenotypic families that share a similar kinetic into so-called kinetic families. While some of these kinetic families were poorly or similarly impacted by vaccination, others only expanded after one but not the other immunization. Actually, some cell subphenotypes were present at baseline, increased in number after prime, but disappeared in late time post-prime and were missing at the time of the boost. A tremendous shift in cell subphenotype composition was indeed observed between 14 and 58 days post-prime. Thus some subphenotypes that were missing in the early response to the prime appeared at the time of the boost. Consequently, the subphenotypes responding to the boost strongly differ from those responding to the prime. This is in better accordance to the measurement of overall inflammation mentioned above.

To characterize the phenotypic differences existing between prime and boost, we used linear discriminant analyses combined with LASSO approaches, to define which of the kinetic families were characteristic of the prime and which were characteristic of the boost.

On the resulting segregation, we identified the most differentially expressed markers between subphenotypes discriminating each response, using Kolmogorov-Smirnov distances, computed with the CytoCompare R-package (Platon et al., 2018). Interestingly, in all innate myeloid cell populations, markers of activation/maturation (including CD11b and CD11c -the α-chains of CR3 and CR4-, chemokine receptors CCR5 and CXCR4, FcRs CD16 (FcγRIII) and CD32 (FcγRII), antigen-presentation molecule HLA-DR, pro- and anti-inflammatory cytokines IL-8, IL-12 and IL-10), were upregulated in cells responding to the boost. Note that both $CD4^+$ neutrophils and inflammatory cDCs/non-classical monocytes were more numerous after the boost than after the prime.

This suggests that cells responding to the boost were more mature/active, better equipped to respond to the immunization and likely to get activated further upon pathogen encounter. The upregulation of CD14 and CD11b by monocytes induced by MVA prime and responding to MVA boost in our study is consistent with the phenotype of modified phenotype of trained monocytes reported after BCG vaccination in humans without *ex vivo* restimulation (Kleinnijenhuis et al., 2012; 2014a), supporting the hypothesis that the monocytes responding to MVA boost were trained by MVA prime. In addition, it was similarly shown that neutrophils isolated from rhesus macaques vaccinated against SIV (adenovirus vector at prime, canary poxvirus –ALVAC at boost) displayed stronger ability to phagocyte pathogens, produce reactive oxygen species and activate B cells than their baseline counterparts (Musich et al., 2018). Consistently with our results, these neutrophils had a higher expression of CD11b. The proportion of $CD11b^+$ neutrophils two weeks post-boost seemed lower than at baseline in their setting though. This may be a result from a stronger neutrophil turnover (including neutrophil death) two weeks after the boost compared to baseline. The overall phenotype of trained cells is largely elusive, and may have been overlooked, within the literature. This may be attributed to the limited number of markers that can be simultaneously assessed with flow cytometry, the most widely used technique in the community. Consequently, the term trained is admittedly restricted to cells with enhanced functions. Since no functional tests were performed in our setting, we will cautiously call "likely trained" cells the aforementioned cells that respond to the boost.

Note that the primary memory adaptive responses existing at the boost (anti-MVA antibodies, as well as memory B and T cells) may also contribute to give a distinct signal to innate cells. In addition, it is not clear which innate myeloid cells are modified exactly. Indeed, monocyte-derived macrophages can survive for years (Gonzalez-Mejia & Doseff, 2009) but neutrophils are expected to die in a week (Pillay et al., 2010), a duration not compatible with the persistence of the late phenotypic changes we observed here. This suggests that these phenotypic modifications occur not on the terminally differentiated cells but rather on the progenitors (likely in the bone marrow), as it was strongly suggested in BCG- and β glucan-induced training in mice (Kaufmann et al., 2018; Mitroulis et al., 2018). This would be consistent with the delay of apparition of these "likely trained" cells in blood (between two weeks and two months after the first immunization).

In any case, as a final take-home message, this study indicated that in classical prime-boost schedule, prime induced a late modification of the innate myeloid compartment, compatible with innate immune training, not only in monocytes, but strikingly in cDCs and neutrophils also. This results in a distinct innate myeloid cell response to the boost two months after prime.

"Prime and Boost Vaccination Elicit a Distinct Innate Myeloid Cell Immune Response"

These results were published in *Scientific Reports* (Palgen et al., 2018). The corresponding paper is provided hereafter. The data are also available in an interactive fashion on the IDMIT dissemination platform (http://data.idmitcenter.fr/). This publicly available dataset was used by an independent team to develop a computational analysis tool called CytoFast, with which they also found a distinct innate myeloid response between prime and boost (Beyrend et al., 2018).

SCIENTIFIC REPORTS

OPEN

Prime and Boost Vaccination Elicit a Distinct Innate Myeloid Cell Immune Response

Received: 12 September 2017
Accepted: 31 January 2018
Published online: 15 February 2018

Jean-Louis Palgen[1,2], Nicolas Tchitchek[1,2], Jamila Elhmouzi-Younes[1,2], Simon Delandre[1,2], Inana Namet[1,2], Pierre Rosenbaum[1,2], Nathalie Dereuddre-Bosquet[1,2], Frédéric Martinon[1,2], Antonio Cosma[1,2], Yves Lévy[2,3], Roger Le Grand[1,2] & Anne-Sophie Beignon[1,2]

Understanding the innate immune response to vaccination is critical in vaccine design. Here, we studied blood innate myeloid cells after first and second immunization of cynomolgus macaques with the modified vaccinia virus Ankara. The inflammation at the injection site was moderate and resolved faster after the boost. The blood concentration of inflammation markers increased after both injections but was lower after the boost. The numbers of neutrophils, monocytes, and dendritic cells were transiently affected by vaccination, but without any major difference between prime and boost. However, phenotyping deeper those cells with mass cytometry unveiled their high phenotypic diversity with subsets responding differently after each injection, some enriched only after the primary injection and others only after the boost. Actually, the composition in subphenotype already differed just before the boost as compared to just before the prime. Multivariate analysis identified the key features that contributed to these differences. Cell subpopulations best characterizing the post-boost response were more activated, with a stronger expression of markers involved in phagocytosis, antigen presentation, costimulation, chemotaxis, and inflammation. This study revisits innate immunity by demonstrating that, like adaptive immunity, innate myeloid responses differ after one or two immunizations.

Many biological mechanisms involved with vaccination are still unclear and require further characterization. Several studies have highlighted the modulation of adaptive immunity by early innate immunity[1], which may provide biomarkers to predict immune memory. Deciphering the mechanisms of the early innate immune response to vaccines will be valuable for optimizing them for protective immunity.

Innate myeloid cells are composed of mononuclear phagocytes, monocytes and dendritic cells (DCs), and granulocytes. They are involved in pathogen clearance, induction and resolution of inflammation, and antigen presentation[2,3]. They are often believed to react similarly to the first and subsequent pathogen encounters. Indeed, these cells are activated by germline-encoded pattern recognition receptors (PRR), are short-lived, except macrophages, and unlikely to show memory features[4]. However, enhanced responsiveness to pathogen re-encounter, called trained immunity and related to epigenetic modifications, was reported for monocytes and macrophages[5]. The overall immune status also differs between the first and second pathogen encounters due to the presence of memory B and T cells and antibodies at the second encounter. In particular, antigen-antibody complexes are known to affect innate responses through the interaction of antibodies with Fc receptors found in most innate cells including granulocytes, monocytes/macrophages, and DCs[6,7]. This likely affects the behaviour of innate immune cells. However, this crosstalk between innate and adaptive immunity in the context of repeated vaccine injections, called prime-boost vaccine strategies, is still poorly understood, although they are widely used to increase the frequency of responders and enhance the immunogenicity and protective efficacy of vaccines[8].

We studied the impact of vaccination on innate myeloid cells by immunizing cynomolgus macaques, which represent a relevant species for human vaccine research[9,10]. We used the modified Vaccinia virus Ankara (MVA), a smallpox vaccine, as a vaccine model to induce robust cellular and humoral immunity[11]. Unlike the vaccinia virus (VACV) from which it was derived, MVA requires a two-dose regimen to induce a strong antibody response

[1]CEA – Université Paris Sud 11 – INSERM U1184, Immunology of Viral Infections and Autoimmune Diseases, IDMIT department, IBFJ, 92265, Fontenay-aux-Roses, France. [2]Vaccine Research Institute, Henri Mondor Hospital, 94010, Créteil, France. [3]Institut Mondor de Recherche Biomédicale – INSERM U955, équipe 16 physiopathologie et immunothérapies dans l'infection VIH, 94010, Créteil, France. Correspondence and requests for materials should be addressed to A.-S.B. (email: anne-sophie.beignon@cea.fr)

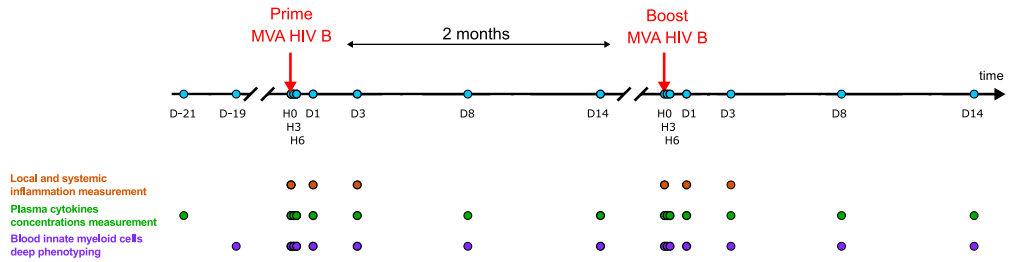

Figure 1. Experimental design and analysis pipeline. Five adult cynomolgus macaques were immunized, two months apart with MVA HIV-B at a dose of 4×10^8 PFU injected subcutaneously. Blood was collected longitudinally at the indicated timepoints, hours (H) or days (D), post-prime (PP) and post-boost (PB), for Luminex, ELISA, and mass cytometry analyses to evaluate the plasma concentrations of cytokines and CRP and to phenotype in deep innate myeloid cells. Local inflammation was also scored at the indicated timepoints. Baseline samples were collected 21 and 19 days before the first vaccine injection for plasma soluble factors and single cell mass cytometry analysis, respectively, as well as just before the first immunization at H0PP. A blood draw was also collected just before the boost at D58PP/H0PB.

and provide full protection against VACV challenge in humans[12,13] or monkeypox challenge in non-human primates[14]. MVA is also a potent vaccine vector currently being developed against several infectious diseases and cancers[15]. Many studies on cell tropism, innate immune activation and immune evasion used *in vitro* models[16]. However, a comprehensive overview of the mechanisms of MVA-induced immunity *in vivo* is still lacking.

Here, we developed a mass cytometry panel, focusing on innate myeloid cells, with the aim of identifying cell subphenotypes altered by vaccination. Mass cytometry is a promising technology for discovering cell subsets. It can unravel new mechanisms of the immunization process and help to design new vaccines. Currently, longitudinal mass cytometry data analyses following immunization are scarce[17,18]. One of the main analysis challenge is the lack of appropriate pipelines. Here, we used the SPADE algorithm[19] together with SPADEVizR[20] to analyze our high-dimensional cytometry data. This analysis pipeline can be used for any kind of multidimensional cytometry data analysis, beyond the study of the dynamic of vaccine-induced immune responses or the study of vaccines modes of action. To make these complex data fully accessible to the scientific community, we publicly released them on the FlowRepository database and the Cytobank platform. We also created a website with interactive representations. We provide evidence of the phenotypic diversity of innate myeloid cells and of the qualitative and quantitative differences in their recruitment following MVA prime-boost immunization. This work constitutes the basis for future studies aiming to decipher how the differences in innate responses after one or two vaccine encounters depend on primary memory responses, and conversely how they affect the development of secondary memory responses.

Results

Changes in local and systemic inflammation following MVA prime and boost. Macaques were subcutaneously injected twice with MVA two months apart (Fig. 1). The specific antibody response developed by each animal was reported in a previous publication, and showed higher serum anti-MVA antibody titers after the boost than the prime[18]. We investigated in the very same animals the early responses to MVA injections. We tested if innate responses differed after prime and boost, as did adaptive immune responses. MVA injections induced low-grade, transient local inflammation at the injection site at early timepoints (Fig. 2a). Inflammation following prime was graded as 1.10 ± 0.22 and resolved by day 3 post-prime (D3PP), whereas it was milder (0.40 ± 0.55) and shorter after the boost.

The blood concentration of C-reactive protein (CRP) showed a transient peak at D1 post-injections (Fig. 2b). This peak was smaller after the boost than the prime (Supplementary Table S1). Among 24 tested soluble factors, only MCP-1, IL-6, and IP-10, were affected by vaccination, with concentrations differing significantly from pre-vaccination levels at two timepoints at least (Fig. 2c, Supplementary Figure S1 and Table S1). MCP-1 and IL-6 were significantly induced after each MVA injection, with an earlier peak post-boost. We also detected high levels of IP-10 early after both the prime and boost. The area under the curve (AUC), as an approximation of exposure over time, showed that the cumulated concentration of IP-10 differed more between each immunization, than those of MCP-1 and IL-6. In addition, although non-significantly impacted, IFNγ, IL-10, IL-13, IL-15, IL-1Rα, IL-5, TGFα and TNFα concentrations tended to follow similar dynamics as MCP-1 and IP-10, whereas IL-1β tended to be closer to IL-6 (Figure S1).

Blood leukocytes following MVA injection. Changes in local and systemic inflammation after MVA prime-boost immunization were also accompanied by changes in blood cell concentration and composition. The absolute number of leukocytes increased significantly, as early as H3PP and H3PB, and rapidly returned to baseline levels (Fig. 2d and Supplementary Table S2). However, in contrast to the macroscopic local reaction (Fig. 2a), leukocytes AUC were similar after each vaccine injection. Note that these transient post-injections increases of blood cell counts were specific to vaccine injections. Indeed, buffer injection only moderately impacted leukocytes counts, and at a statistically significant lower level at H6 and D1 as compared to MVA (Supplementary Figure S2).

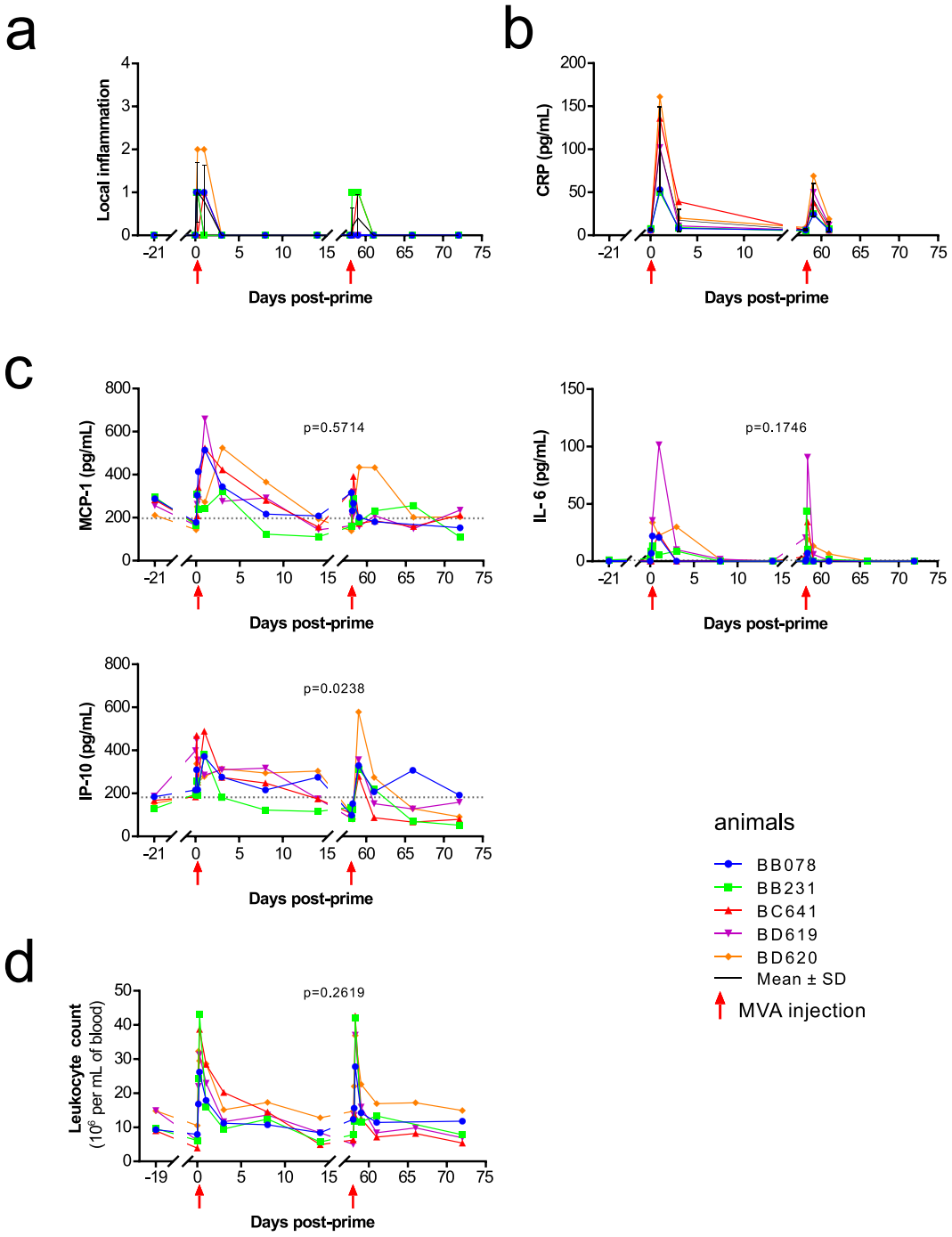

Figure 2. Local inflammation, systemic inflammation and complete blood count. (**a**) Individual local inflammation scores, as well as mean ± standard deviation, are represented over time. Local skin reactions at the site of the subcutaneous MVA injection were scored from 0 to 4, based on the evaluation of edema and erythema. 0: no swelling and normal color; 1: slight swelling with indistinct border and light pink erythema; 2: defined swelling and bright pink erythema, both with distinct borders; 3: defined swelling with a raised border (<1 mm) and bright red erythema with a distinct border; 4: pronounced swelling with a raised border (>1 mm) and dark red erythema. (**b**) The concentration of C-reactive protein (CRP), as well as mean ± standard deviation, was assessed in plasma before and after MVA immunization. Individual levels are shown. (**c**) The concentrations of MCP-1, IL-6, and IP-10 were measured in plasma after the first and second MVA injection. Individual concentrations are shown. The individual AUC after the prime (H3-D14PP) and boost (H3-D14PB) were computed and compared using a permutation test. The mean PP and PB AUC, and the p-values after the permutation test to compare them are indicated. The red arrows indicate prime and boost injections. The dotted line indicates the median concentrations for each cytokine at baseline (D-21PP and H0PP). (**d**) Blood leukocyte counts were followed over time. Individual absolute numbers are shown. Leukocyte counts were missing for macaques BB078 and BB231 at D8PB.

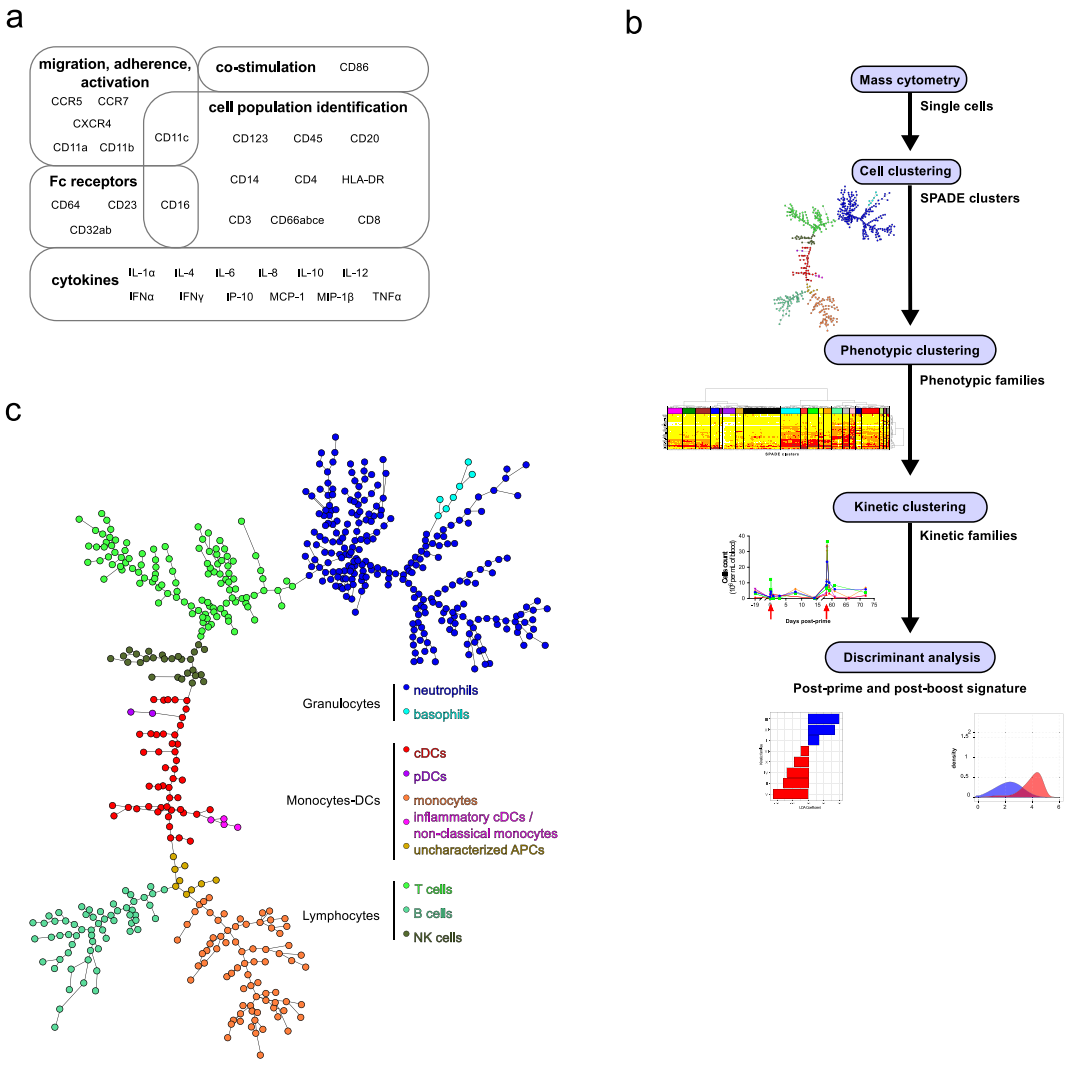

Figure 3. Mass cytometry. (**a**) Fixed leukocytes were stained with a panel of Abs designed to analyze innate myeloid cells by mass cytometry. Thirty-two targeted markers and their associated biological functions are indicated. (**b**) The steps of the mass cytometry data analysis are displayed. As the first analysis step, single cells from FCS files were grouped into clusters sharing similar phenotype using the SPADE algorithm. Clusters were annotated on the resulting SPADE tree based on the expression of a set of 10 markers, and granulocytes and monocytes-DCs were identified. As the second analysis step, clusters of granulocytes and monocytes-DCs sharing the same categories of marker expression were regrouped into phenotypic families. As the third analysis step, phenotypic families sharing the same abundance profiles were clustered into kinetic families. Finally, after these three successive clusterings, and as the last analysis step, discriminant analyses were used to determine which kinetic families best distinguished between post-prime and post-boost immune response, and to define the phenotypic signature of each response. (**c**) Mass cytometry data were analyzed using SPADE. The topology of the SPADE tree is shown. This tree was built using all samples (all macaques and all timepoints). Only the topology of the tree is displayed where each node corresponds to a cell cluster. It does not correspond to a particular sample and size of node is not related to their cell content. Clusters with similar phenotypes are linked using a minimal spanning tree approach. SPADE clusters were annotated and colored with respect to the expression of markers indicated in Supplementary Figure S3 and as follows: neutrophils ($CD66^+$), basophils ($CD66^-CD123^+HLA\text{-}DR^-$), monocytes ($CD14^+HLA\text{-}DR^+$), cDCs ($CD14^-HLA\text{-}DR^+CD11c^+CD16^+$), inflammatory cDCs/non-classical monocytes ($CD14^+HLA\text{-}DR^+CD11c^+CD16^+$), pDCs ($CD123^+HLA\text{-}DR^+$), uncharacterized APCs ($CD3^-CD8^-CD14^-CD20^-CD11c^-CD16^-CD123^-HLA\text{-}DR^+$), B cells ($CD20^+HLA\text{-}DR^+$), T cells ($CD3^+$), and NK cells ($CD3^-CD8^+$). Granulocytes were defined as neutrophils and basophils, and monocytes-DCs as monocytes, cDCs, pDCs, inflammatory cDCs/non-classical monocytes and uncharacterized APCs.

Leukocytes correspond to the sum of several immune cell types with heterogeneous phenotypes and functions. Thus, we used mass cytometry to more deeply phenotype blood immune cells over time after immunization, focusing on innate myeloid cells (Fig. 3a and Supplementary Table S3). We developped an analysis pipeline adapt to longitudinal mass cytometry data. We used three successive complementary clusterings, which led to

the identification of cell clusters, phenotypic families and kinetic families respectively. They were followed by the automated identification and ranking of the cell populations and markers that best discriminate the responses after the first and the second immunizations (Fig. 3b).

Mapping the phenotypic diversity of blood granulocytes, monocytes, and DCs. We first used the SPADE algorithm[19] to identify clusters of leukocytes with similar phenotypes within the whole dataset (all animals and all timepoints). SPADE was optimally parameterized and resulted in the partition of leukocytes into 600 clusters (Supplementary Figure S3 and Tables S5-S6). The stringency of our analysis likely resulted in 'over-clustering', generating many artificial cell subpopulations. However, we and others consider 'over-clustering' to be less misleading than 'under-clustering', particularly as an initial step[21].

We annotated each cluster based on the SPADE tree and the expression of a restricted set of markers (Fig. 3c and Supplementary Figure S4). We identified 252 clusters of neutrophils ($CD66^+$), seven of basophils ($CD66^-HLA\text{-}DR^-CD123^+$), 76 of monocytes ($HLA\text{-}DR^+CD14^+$), 47 of $CD11c^+$ cDCs latter referred as cDCs ($HLA\text{-}DR^+CD14^-CD11c^+$), four of inflammatory cDCs/non-classical monocytes ($HLA\text{-}DR^+CD14^+CD11c^+CD16^+$), two of plasmacytoid dendritic cells (pDCs, $HLA\text{-}DR^+CD123^+$), and nine of uncharacterized antigen-presenting cells (APCs, $HLA\text{-}DR^+CD123^-CD14^-CD11c^-CD16^-$). We focused our analysis on these innate myeloid cells. We also identified 61 clusters of B cells ($HLA\text{-}DR^+CD20^+$), 115 of T cells ($CD3^+$), and 27 of NK cells ($CD3^-CD8^+$), which were not further studied.

Note that we previously reported that cynomolgus macaque cDCs expressed CD16 at a high and homogeneous level in cynomolgus macaques[10]. The use of CD11c to define cDCs in macaque is controversial. In rhesus and cynomolgus macaques, it has been shown that $CD14^{high}CD16^{high}$ and $CD14^{low/mid}CD16^{high}$ monocytes expressed higher levels of CD11c than cDCs[22,23]. In contrast, cynomolgus macaques cDCs were recently defined based on their CD11c expression, although it did not allow to fully segregate cDCc into cDC1s and cDC2s by itself and other markers were required[24]. We annotated clusters that shared common features with monocytes and cDCs ($HLA\text{-}DR^+CD14^+CD11c^+CD16^+$) as inflammatory cDCs/non-classical monocytes, given that there is no consensus yet for cynomolgus macaques DCs/monocytes subsets and that we lacked the critical markers to fully discriminate cDC1s and cDC2s.

We analyzed the dynamics of granulocytes (comprising neutrophils and basophils) (Supplementary Figure S5a and Supplementary Table S2) and monocytes-DCs (comprising monocytes, cDCs, pDCs, inflammatory cDCs/non-classical monocytes and uncharacterized APCs) (Supplementary Figure S5b and Supplementary Table S2) in response to each vaccine injection. We calculated the absolute number of each cell population instead of using the percentage of parent cells because leukocyte counts highly varied during vaccination. Granulocytes represented the most abundant population among leukocytes at all timepoints and showed two significant rapid, transient increases, peaking at H6PP and H6PB. Granulocyte counts returned to baseline levels faster after the boost than the prime. However, their AUC were similar after each vaccine injection. The absolute number of monocytes-DCs also showed a first peak at H6-D1PP and a second, smaller one at H6PB, but without significant differences between the two immunizations.

The local macroscopic reaction likely reflected the recruitment of cells from the circulation and bone marrow to the vaccine injection site[25]. We next deeply characterized the phenotype of granulocytes and monocytes-DCs to reconcile the difference in local and systemic inflammation between prime and boost with the absence of major differences in blood cell counts on the scale of leukocytes, granulocytes, and monocytes-DCs.

SPADE clustering was followed by a second clustering (Fig. 3b). Hierarchical clustering was performed at both cell cluster and marker levels to better visualize the similarities between cell cluster phenotypes and marker co-expression patterns. We generated two categorical heatmaps to visualize phenotype of each cell cluster at a glance, as oppposed to SPADE trees: one heatmap for the granulocytes compartment and one for the monocytes-DCs compartment (Fig. 4). Heatmaps represent the phenotypic diversity within the dataset, but not a particular sample and, in no case, a particular timepoint. They are not snapshots.

Clusters sharing similar phenotypes as measured by a close proximity on the heatmap cluster dendrogram, were gathered into phenotypic families. This analytical strategy prevents inaccurate interpretations due to potential 'over-clustering'. Indeed, clusters may actually account for different stages of activation or maturation within a cell subpopulation, whereas phenotypic families may represent actual subpopulations.

For the granulocytes compartment (Fig. 4a and http://data.idmitcenter.fr/MVA-innate-myeloid/ for interactive heatmaps), 21 phenotypic families were distributed across five superfamilies, highlighting the richness of their phenotypes. The first superfamily A represented highly activated neutrophils ($CD66^{mid/high}CCR7^{high}CD32^{high}CD45^{high}CD11b^{high}$) and comprised phenotypic families 9, 16, 6, 15, and 2. The second superfamily B represented intermediately activated neutrophils ($CD66^{mid/high}CCR7^{mid}CD32^{mid}CD45^{mid}CD11b^{mid}$) and contained phenotypic families 3, 7, and 5. The third superfamily C represented poorly activated neutrophils ($CD66^{low/mid}CCR7^{low}CD32^{low}CD45^{low}CD11b^{low}$) and comprised phenotypic families 4, 13, 11, 19, and 1. Strikingly, phenotypic family 13 and a subpart of family 2 showed high expression of CD14. $CD14^{high}$ neutrophils were described in the literature[26] but their functional importance remains to be characterized.

The fourth superfamily D corresponded to $CD4^{mid/high}CD23^{high}CD11c^{high}$ neutrophils and comprised phenotypic families 17, 12, and 10. The expression of CD4 and CD23 correlated among granulocytes ($R = 0.78$) (Supplementary Figure S6a). CD4 expression was previously reported in neutrophils[27] but was not functionally characterized. In addition, the expression of CD23 and CD11c by neutrophils was shown to be linked to inflammation[28–30]. Family 17 showed a high level of several markers, including CD123, CD14, CD86, CD16, IP-10, MCP-1, CD4, CD3, CD8, IL-4, and IL-6. This phenotypic signature may be due to nonspecific staining or to the presence of contaminating cell doublets. It may account for the unexpected strong correlation between the expression of CD3 and CD8 ($R > 0.75$). One cluster (cluster 416) was annotated as basophils, based on the SPADE

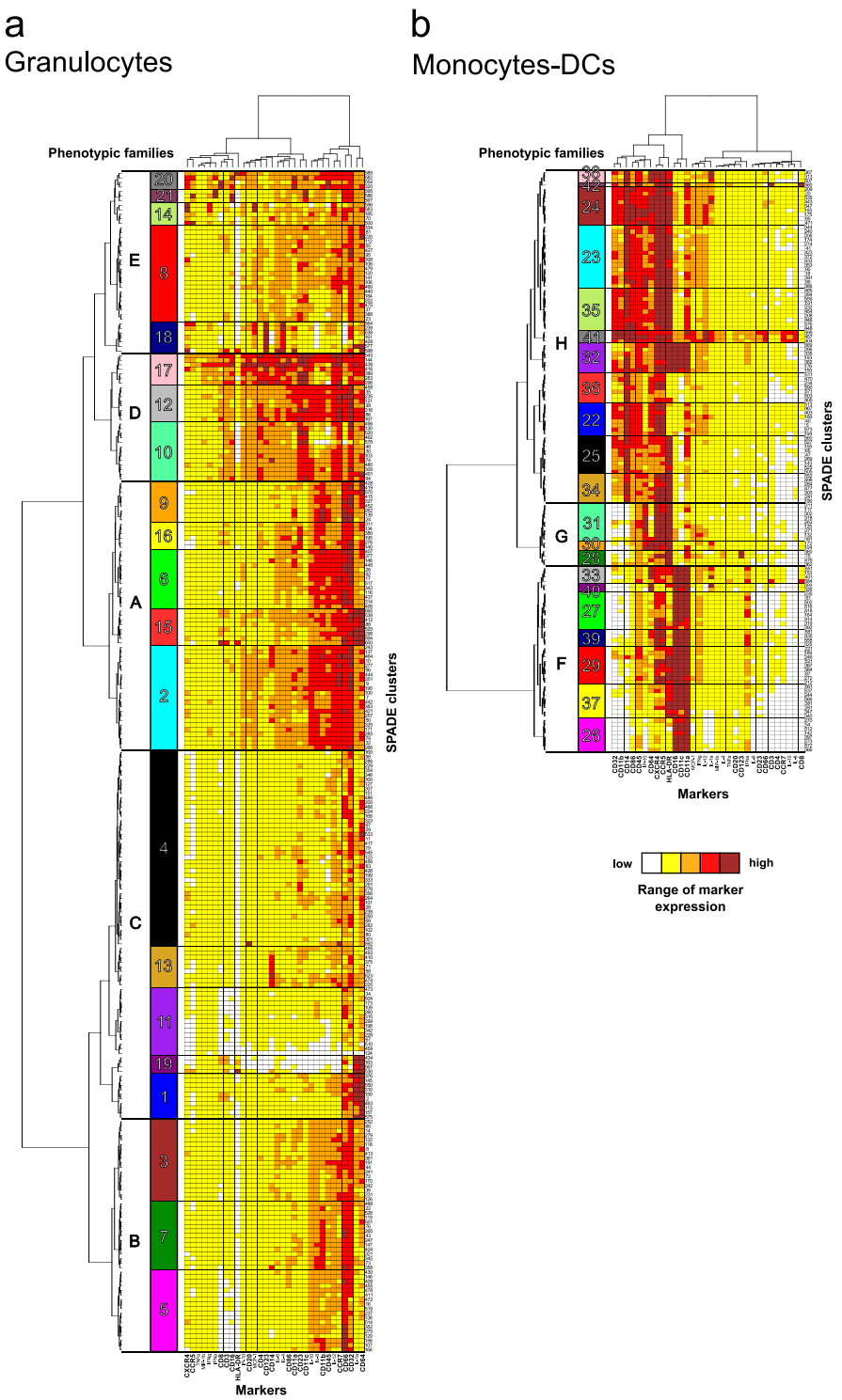

Figure 4. High phenotypic diversity of granulocytes and monocytes-DCs. Hierarchical clustering of markers and (**a**) granulocytes or (**b**) monocytes-DCs clusters were computed and represented as heatmaps. Each line of the heatmaps corresponds to one cell cluster and each column to one marker. Marker and cluster dendrograms were generated to bundle clusters with similar phenotypes and markers with similar expression patterns. Based on the cluster dendrograms, 21 groups of clusters, called phenotypic families, which are arbitrarily colored and numbered using Arabic numerals, were identified for both granulocytes and monocytes-DCs. Groups of phenotypic families defining superfamilies were framed with bold lines, and labeled with capital letters. When describing the heatmaps, phenotypic families are always listed from top to bottom, with ';' to separate them according to their superfamily origin. SPADE clustering markers are written in bold. Interactive heatmaps are available at http://data.idmitcenter.fr/MVA-innate-myeloid/.

tree. Indeed, it showed far higher CD123 expression than its neutrophil counterparts (Supplementary Figure S3), confirming the relevance of our SPADE tree annotation.

The fifth superfamily E included basophils and neutrophils and comprised phenotypic families 20, 21, 14, 8, and 18. Family 18 contained six clusters of CD66^{low}CD123^{high}IL-4^{high} basophils and one cluster (cluster 598) annotated as neutrophils, based on the SPADE tree. Although high, its CD123 expression was lower than in basophils clusters (Supplementary Figure S3), confirming the relevance of our SPADE tree annotation. Families 20, 21, and 14 corresponded to neutrophils, displaying a unique phenotype characterized by varying expression of CD16, CD11c, CD45, CCR5, CXCR4, MCP1, IFNα, and IFNγ. CD16 and CD11c expression correlated with each other in granulocytes (R = 0.77) (Supplementary Figure S6a), suggesting that phenotypic families 20 and 21 could be highly activated neutrophils and linked to inflammation or modulation of the immune response, with potential IFNα production[31,32].

We identified four phenotypic families (17, 15, 19, and 1) scattered throughout distinct superfamilies, as well as two clusters of basophils (cluster 577 and 598), expressing a high level of CD64 and IL-1α. The presence of these two markers highly correlated (R = 0.82) with each other (Supplementary Figure S6a). The expression of CD64 in neutrophils was described as a biomarker of infection[33,34], whereas IL-1α was shown to be important for the recruitment of neutrophils and other myeloid cells[35,36]. In addition, there was a high correlation between IL-12 and CCR7 expression among granulocytes (R = 0.75) (Supplementary Figure S6a). This association suggests a more mature and activated phenotype, since CCR7 was shown to be involved in granulocyte activation[37] and IL-12 is also key to neutrophil activation[38].

In the monocytes-DCs compartment, 21 phenotypic families were also identified (Fig. 4b and http://data.idmitcenter.fr/MVA-innate-myeloid/ for interactive heatmaps). These phenotypic families segregated into three superfamilies. The first superfamily F corresponded to cDCs (phenotypic families 33, 40, 27, 39, 29, 37 and 26). The second superfamily G comprised pDCs, CD14^{low}monocytes, and uncharacterized APCs (phenotypic families 31, 30 and 28). Finally, the third superfamily H was composed of monocytes and inflammatory cDCs/non-classical monocytes (phenotypic families 38, 42, 24, 23, 35, 41, 32, 36, 22, 25 and 34).

As expected, cDCs and monocytes clearly segregated apart from each other within distinct superfamilies, the former expressing a high level of CD16, CD11c and CD11a, whereas the latter expressed a high level of CD14. CD14^{+}CD16^{+}HLA-DR^{+} inflammatory cDCs/non-classical monocytes (phenotypic family 32) segregated with monocytes.

CD11a, CD11c, and CD16 expression highly correlated with each other (R > 0.75 for each correlation) (Supplementary Figure S6b), confirming this characteristic of macaque cDCs. cDCs showed varying expression patterns for CCR5, CXCR4, CD64 and HLA-DR. Phenotypic families 29 and 37 consisted of highly activated HLA-DR^{high}CCR5$^{mid/high}$CXCR4$^{mid/high}$ cDCs. Phenotypic families 33, 40, 27, 39 and 26 regrouped less activated (potentially immunosuppressive) HLA-DR$^{low/mid}$ cDCs. Phenotypic families 33, 40, 27 and 39 were CCR5^{high}CXCR4^{high}, whereas family 26 was CCR5^{low}CXCR4^{low} suggesting different recruitment abilities to the site of inflammation. In addition, phenotypic families 27 and 39 were CD64^{low} whereas phenotypic families 33 and 40 were CD64^{high} indicating different antibodies binding capacities and suggesting they could be monocytes-derived cDCs[39].

Besides, CD14, CD11b, and CD32 expression correlated with each other (R > 0.75 for each correlation) (Supplementary Figure S6b), confirming these monocyte-specific features. Surprisingly, CD86 also correlated with CD14 (R = 0.81) and CD32 (R = 0.82) (Supplementary Figure S6b), suggesting that this costimulatory molecule is poorly expressed on macaque blood cDCs, in contrast to monocytes. Overall, monocytes displayed varying expression of CD32, CD11b, and CD45. Phenotypic families 36 and 22 regrouped likely immature and potentially immunosuppressive HLA-DR^{low} monocytes. Phenotypic families 25 and 34 regrouped poorly activated CD32^{low}CD11b^{low}HLA-DR^{high} monocytes. Phenotypic family 32 consisted solely of inflammatory cDCs/non-classical monocytes. Phenotypic families 23 and 35 consisted of moderately to highly activated CD32$^{mid/high}$CD11b$^{mid/high}$CD11a^{mid}HLA-DR^{high} monocytes. Finally, phenotypic families 38, 42 and 24 consisted of highly activated CD32^{high}CD11b^{high}CD11a^{high}HLA-DR^{high} monocytes. Phenotypic family 41 consisted of IL-12 producing CD66^{high}CCR7^{high}HLA-DR^{high} monocytes.

In the second superfamily G, clusters expressed a high level of HLA-DR and segregated closer to monocytes than cDCs. Phenotypic families 31 and 30, labeled as uncharacterized APCs, contained CCR5^{high}CXCR4^{high}IP-10^{high} cells. These cells could correspond to activated monocytes which have downregulated CD14 and CD11b, a feature linked to activation and macrophage differentiation[40,41]. Family 28 contained two CD123^{high}IL-4^{mid} clusters, labeled as pDCs (clusters 360 and 75), and two clusters labeled as monocytes, that were solely HLA-DR^{high}CD14^{low} (clusters 476 and 362). Interestingly, the two clusters of pDCs differed by the expression of CCR5 and CXCR4, suggesting different recruitment and/or maturation abilities. Most pDCs were CCR5^{high}CXCR4^{high} but surprisingly IFNα^{low} (Supplementary Figure S3). This may be explained by the *ex vivo* staining without cytokine secretion inhibitors. Indeed, whole blood was extemporaneously fixed after sampling and without blocking cytokine secretion to avoid granulocytes alteration. Using these settings, we may not capture the production of cytokines whose concentrations did not reach a certain threshold or that were secreted very fastly. Alternatively, blood pDCs may be non-activated and thus would not produce IFNα[42]. In addition, we may not capture all the pDC diversity due to the low amount retrieved from macaque blood (Supplementary Figure S7).

Our data show a high degree of phenotypic diversity among blood granulocytes and monocytes-DCs with several degrees of activation/maturation. We uncovered potential novel subsets with newly described marker co-expression. Such diversity was captured because of the high number of markers specifically targeting innate myeloid cells and the high number of clusters defined. However, this diversity was also captured because our original longitudinal dataset was composed of samples collected at steady state, before or long after immunization, outnumbered by samples collected early after immunization, during acute inflammation.

Distinct subphenotypes respond to first and second immunizations. The categorical heatmaps that we generated provided good information on cell subsets phenotypic diversity within the dataset. But these still pictures did not provide information on cell subset frequencies, or their continuous or transient presence. To go beyond these pictures, we studied the impact of MVA injections on the abundance of cells from the different phenotypic families with respect to animals and time. Various abundance profiles depending on the phenotypic families were found and the post-prime and post-boost transient expansions were not always equal (Supplementary Figures S8 and S9). Using a third clustering step (Fig. 3b), the 21 phenotypic families of granulocytes and 21 phenotypic families of monocytes-DCs were gathered together into 12 kinetic families sharing similar abundance profiles (Fig. 5, Supplementary Figures S9, S10 and Supplementary Table S4). The correspondence between kinetic families and phenotypic families is given in Table 1 and in Supplementary Figures S9 and S10, but more simply thanks to interactive heatmaps on http://data.idmitcenter.fr/MVA-innate-myeloid/.

Strikingly, although there was no significant difference between prime and boost leukocytes AUC (Fig. 2d), nor granulocyte AUC or monocytes-DCs AUC (Supplementary Figure S5), the dynamics of five of the 12 kinetic families displayed significant differences (measured with AUC) after the prime and boost. Poorly to moderately activated neutrophils (granulocytes phenotypic families 14, 8, 4, 13, 11, 19, 1, 3), as well as uncharacterized APCs (monocytes-DCs phenotypic family 30) belonged to kinetic families I and III, and were mostly present in the blood after the prime (Fig. 5a and Supplementary Figure S10). The enrichment of cells from kinetic family III was not as transient as those of cells from kinetic family I.

Conversely, moderately to highly activated neutrophils (granulocytes phenotypic families 12, 9, 16, 6, 15, 2, 7, and 5), activated monocytes (monocytes-DCs phenotypic family 24, 35, and 41), inflammatory cDCs/non-classical monocytes (monocytes-DCs phenotypic family 32), and $CCR5^{high}CXCR4^{high}$cDCs (monocytes-DCs phenotypic family 39 and 29) composed kinetic families II, IV, VI and X, and were mostly present after the boost (Fig. 5a and Supplementary Figure S10). We observed two successive waves of enrichment for kinetic families IV, VI, and X. The second wave was especially late for family IV.

Neutrophils (granulocytes phenotypic families 20, 21, 17, and 10), monocytes (monocytes-DCs phenotypic families 38, 42, 23, 36, 22, 25, and 34), uncharacterized APCs (monocytes-DCs phenotypic family 31), and $HLA\text{-}DR^{low}$cDC (monocytes-DCs phenotypic family 27) were part of kinetic families V, VIII, and IX, and were both affected after the prime and boost, albeit differently (Fig. 5a and Supplementary Figure S10). For kinetic family V, there was only one rapid and transient increase at D1PP, whereas there were two rapid and transient increases at D1 and D8PB, the second being stronger. Kinetic family VIII showed an increase at H6-D1 post-injections with a stronger and faster increase after the prime. Kinetic family IX displayed a rapid and transient increase at H6 post-injections, the PP peak being larger.

There was no significant impact of MVA immunizations on cell abundance for the basophils (granulocyte phenotypic family 18), pDCs, $CD14^{low}$ monocytes (monocytes-DCs phenotypic family 28), as well as $HLA\text{-}DR^{low}$ and $CD64^{high}$ cDCs (monocytes-DCs phenotypic family 33, 40, 37 and 26) belonging to the three remaining kinetic families VII, XI, and XII (Fig. 5a and Supplementary Figure S10). Cells from these kinetic families were scarce.

To provide a more general picture of the distribution of the different phenotypic families and its evolution, pie charts were displayed at key timepoints: just before the prime (H0PP), just before the boost (H0PB), at the acute peak of the innate immune response (H6PP and H6PB), and at later timepoints (D14PP and D14PB) (Fig. 5b,c). This representation highlighted that, strikingly, the composition in phenotypic families already differed just before the boost as compared to just before the prime. Also, at D14PP, granulocyte counts were back to baseline, but the repartition in phenotypic families was still closer to H0PP than H0PB, suggesting that innate myeloid responses were not over at D14 post-injection and that a switch in phenotype occurred later, between D14PP and D58PP/H0PB. Differences between prime and boost were not as pronounced within the monocytes-DCs compartment.

Biological relevance of kinetic families. Before going further, we addressed the relevance of the kinetic families identified through three successive clustering steps (Fig. 3b). We assessed whether there were any associations between a direct measurement of inflammation and the enrichment of these kinetic families.

We used a linear regression analysis to predict IP-10 concentration based on kinetic family abundances. We chose IP-10 because it differed the most in AUC between prime and boost. IP-10 was also proposed as a candidate biomarker for diagnosis, prognosis, or responsiveness to therapy for several inflammatory and infectious diseases[43]. The prediction highly fit our observations (Fig. 6a,b), validating the computational analysis designed to define kinetic families. Linear regression showed that IP-10 concentrations positively correlated with the abundance of two kinetic families, III and VI (Fig. 6c), corresponding to neutrophils enriched only after the prime (granulocyte phenotypic families 8; 4 and 13; and 3) and only after the boost (granulocyte phenotypic families 16 and 2) (Table 1). These neutrophils surprisingly did not produce IP-10, in contrast to granulocyte phenotypic family 17. It is possible that plasma IP-10 was mainly released by cells present at the MVA injection site rather than in blood.

Key phenotypic features that discriminate between post-prime and post-boost immune responses. Our findings show that innate myeloid immune responses strongly differed between prime and boost, but it did not take into account the absolute number of cells in each kinetic family. Thus, we performed a Multidimensional Scaling (MDS) analysis to represent the similarities between all samples, based on cell abundances of each kinetic family.

H3PP, H6PP, D1PP, and H6PB clearly segregated apart from most timepoints, which were close to one another in the MDS representation (Fig. 7a). H3PP, H6PP and D1PP were also distant from H6PB. This segregation confirmed that innate myeloid responses differed between prime and boost. It also showed that the innate immune response was strongly affected during three timepoints post-prime and only a single timepoint post-boost.

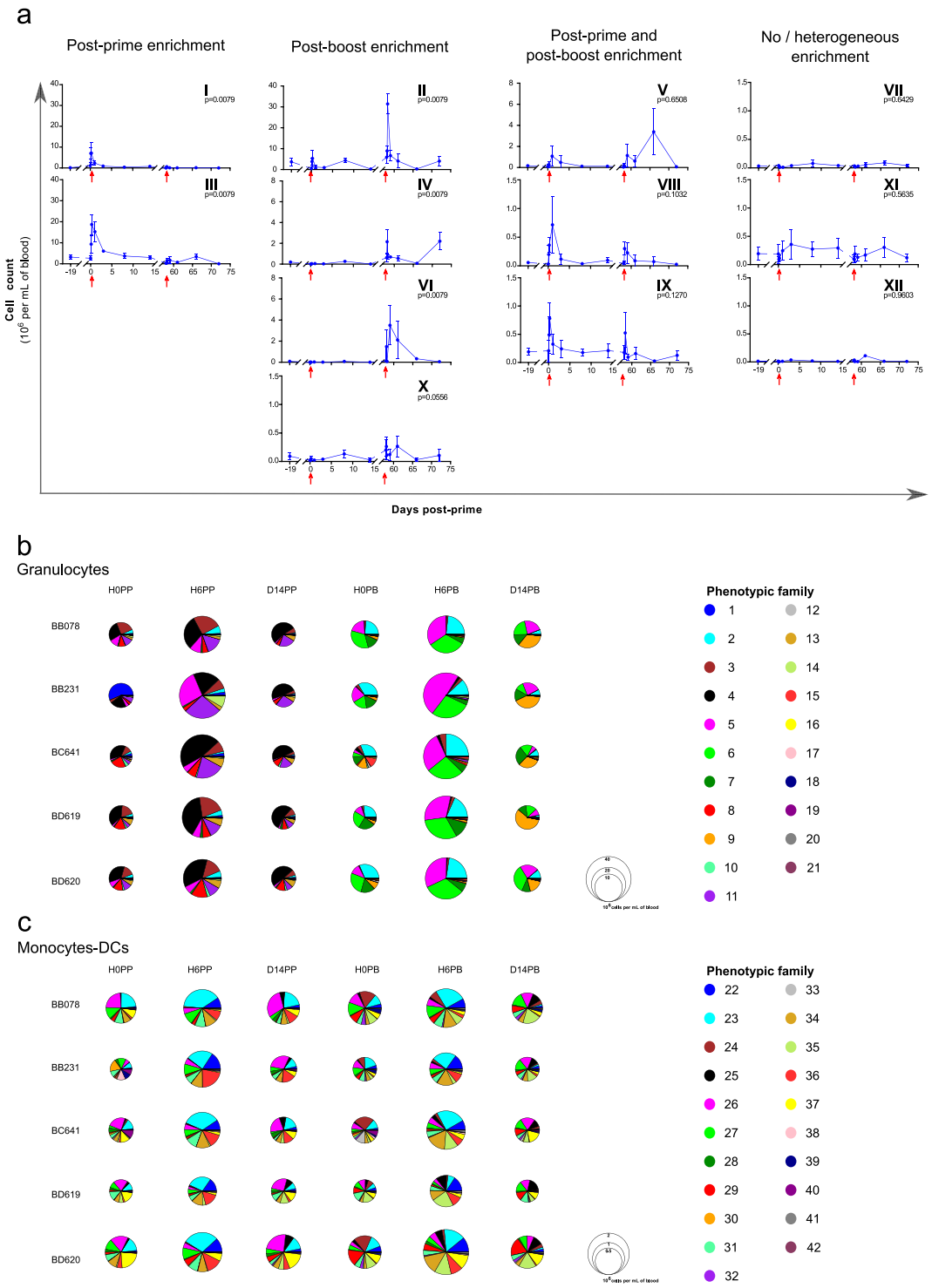

Figure 5. Different enrichment of innate myeloid cells after first and second immunizations. (**a**) Phenotypic families sharing similar abundance profiles were gathered into kinetic families after hierarchical clustering based on abundance profiles with the Pearson correlation. Twelve kinetic families were defined and arbitrarily numbered from I to XII. They were further regrouped based on their kinetic pattern with an enrichment essentially post-prime, essentially post-boost, both after the prime and boost, or no or heterogeneous enrichment after each immunization. The mean abundance among the five animals is displayed ± standard deviation. The individual AUC after the prime (H3-D14PP) and boost (H3-D14PB) were calculated for each kinetic family and compared using a permutation test. The p-values are indicated and considered to be significant when $p \leq 0.01$. Note that the scale of the Y-axis is specific to each kinetic family. The red arrows indicate the prime and boost injections. (**b**,**c**) Composition in phenotypic families of the granulocytes (**b**) and monocytes-DCs (**c**) compartment at H0PP, H6PP, D14PP, H0PB, H6PB and D14PB for each macaque. The size of the pie chart is proportional to the cell concentration. The color-code for each phenotypic families is identical for the pie-charts and the heatmaps.

Kinetic family	Composition		Kinetic pattern
	Phenotypic family	Cell population	
I	Granulocytes 14; 11, 19, and 1 Monocytes-DCs 30	Neutrophils, including poorly to moderately activated neutrophils and uncharacterized APCs	Post-prime enrichment
III	Granulocytes 8; 4 and 13; 3		
II	Granulocytes 6 and 2; 7 and 5 Monocytes-DCs 35 and 41	Neutrophils, including moderately to highly activated neutrophils, highly activated monocytes, $CCR5^{high}CXCR4^{high}$cDCs, and inflammatory cDCs/non-classical monocytes	Post-boost enrichment
IV	Granulocytes 9 and 15		
VI	Granulocytes 12 and 16		
X	Monocytes-DCs 24 and 32; 39 and 29		
V	Granulocytes 20; 17 and 10 Monocytes-DC 42 and 25	Neutrophils, poorly to highly activated monocytes, $HLA\text{-}DR^{low}$cDCs, and uncharacterized APCs	Post-prime and post-boost enrichment
VIII	Granulocytes 21 Monocytes-DCs 38, 36 and 22		
IX	Monocytes-DCs 23 and 34; 31; 27		
VII	Granulocytes 18	Basophils, pDCs, $CD14^{low}$monocytes, and cDCs including $HLA\text{-}DR^{low}$and $CD64^{high}$cDCs	No/heterogeneous enrichment
XI	Monocytes-DCs 28; 37 and 26		
XII	Monocytes-DCs 33 and 40		

Table 1. Correspondence between kinetic and phenotypic families. For each kinetic family, its composition in terms of phenotypic families (listed from top to bottom from the corresponding heatmaps (Fig. 4) and separated by ";" to designate their being from different superfamilies) and its main cell populations and phenotypes, as well as its kinetic pattern, as classified in Fig. 5a, are indicated.

We further identified the main features that differed between the post-prime and post-boost immune response by using a Least Absolute Shrinkage and Selection Operator (LASSO) approach (Supplementary Figure S11). This approach allowed to statistically select the kinetic families that best characterized the post-prime or post-boost immune response. In particular, it permitted to exclude, in a statistical manner, kinetic families that were not impacted by vaccination or were impacted similarly at both immunizations. Among the twelve kinetic families, eight (I, II, III, IV, V, VI, X and XI) were sufficient to fully discriminate between the two responses (Fig. 7b). Linear discriminant analysis (LDA) allowed us to score their contribution to post-prime and post-boost category and gave a statistical criterion to classify the selected kinetic families in post-prime or post-boost signature (Fig. 7c). This analysis revealed that the main components of the post-prime immune response were kinetic families III, XI, and, to a lesser extent, I. They were composed of granulocyte phenotypic families 14 and 8; 4 and 13; 11, 19, and 1; and 3 (poorly to moderately activated neutrophils) and monocytes-DCs phenotypic families 30 and 28; and 37 and 26 (pDCs, $CD14^{low}$ monocytes, uncharacterized APCs, and cDCs). Conversely, the main components of the post-boost immune response were kinetic families V, II, IV, X, and, to a lesser extent, VI. They were composed of granulocyte phenotypic families 20; 17, 12, and 10; 9, 16, 6, 15, and 2; and 7 and 5 (moderately to highly activated neutrophils) and monocytes-DCs phenotypic families 42, 24, 35, 41, 32 and 25; and 39 and 29 (monocytes, including inflammatory cDCs/non-classical monocytes, and cDCs) (Table 1).

We identified markers differentially expressed by cell populations that best discriminated the post-prime from the post-boost response, based on a Kolmogorov-Smirnov distance criterion (Supplementary Figure S12). The expression of CD11b, CD66, CD45, IL-8, CD32, CD11a, HLA-DR and IL-10, and to a lesser extent CCR7, was higher in neutrophils found in abundance in blood after boost than after prime (Fig. 7d and Supplementary Figure S12a). CCR5, CXCR4, CD11c, CD16, CD45, IL-12, HLA-DR, and CD11b were more highly expressed by cDCs enriched after the boost than those enriched after the prime (Fig. 7e and Supplementary Figure S12b). To a lesser extent, CD11a expression was also associated with cDCs enriched after the boost. Finally, CD32, CD11b, HLA-DR, CD11a, CD14, CD45, IP-10, and IL-12 expression was higher in monocytes involved in the post-boost response than those participating in the post-prime response (Fig. 7f and Supplementary Figure S12c).

In conclusion, innate myeloid subpopulations that distinguished the post-boost from the post-prime response, and that were actually already present at the time of the boost, showed higher expression of several activation/maturation markers. Among them, three markers were shared by neutrophils, cDCs, and monocytes: CD45, CD11b and HLA-DR.

Discussion

We report a mild local reactogenicity to subcutaneous MVA injection in macaques, which was weaker and more rapid after the second injection. Plasma CRP and IP-10 concentrations, used as systemic inflammation readouts, were also more attenuated after the boost. We observed an early and transient enrichment of innate myeloid cells in the circulation both after the prime and the boost. Strikingly, at the level of each compartment (granulocytes and monocytes-DC), no major differences in cell abundance intensity or kinetics were observed between the two injections. Qualitative differences between the blood innate myeloid cell responses after one or two immunizations were only observable after deep phenotyping using mass cytometry combined with an analysis pipeline consisting of three successive clusterings specifically developed for longitudinal multidimensional data, and a final discriminant analysis. Neutrophils, monocytes and DCs, which expanded transiently at each immunization, were not composed of the same cell subpopulations. While circulating innate myeloid cells rapidly returned to baseline level in terms of their number after prime, their sub-phenotype composition was modified over time,

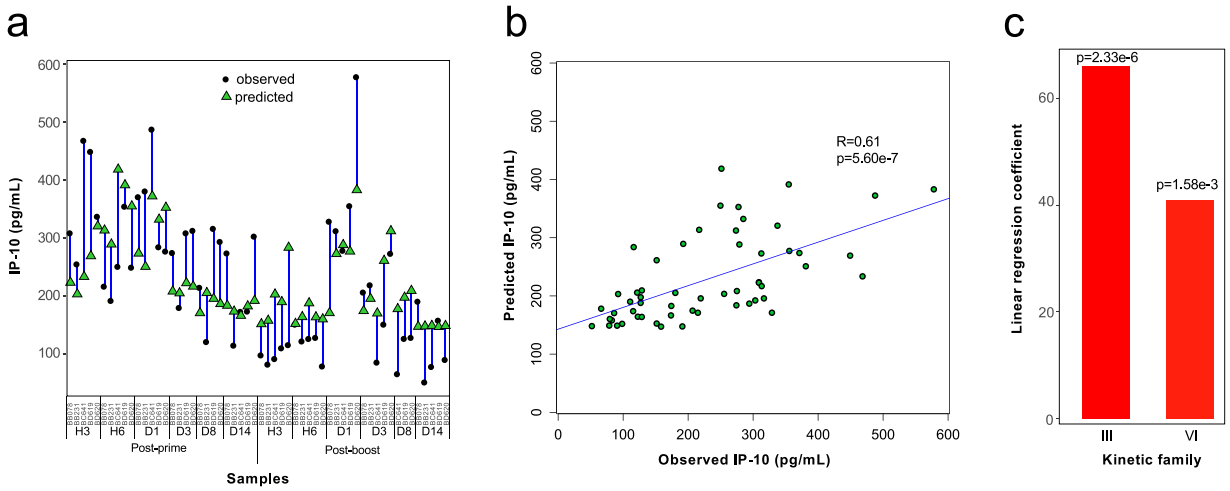

Figure 6. Association of kinetic families with a direct biological measurement. (**a**) The relationship between kinetic family abundances and IP-10 plasma concentration was analyzed using linear regression. Iterative linear regressions were generated until all coefficients had a p-value ≤ 0.05. At each iteration, the coefficient having the highest p-value higher than 0.05 was removed. The differences between predicted *vs*. observed concentrations of IP-10 are shown. (**b**) The ELISA measured and linear regression predicted IP-10 concentrations are shown in a bi-plot representation. The Pearson correlation coefficient and p-value are indicated. (**c**) The linear regression coefficients of kinetic families III and VI, which are necessary and sufficient to predict IP-10 concentrations, are displayed along with their p-values.

and finally different at the time of the boost. Some subsets expanded after each immunization, whereas others were enriched primarily after the prime or the boost. Neutrophils, monocytes, and DCs responding to the second injection expressed higher levels of CD45, HLA-DR, Fc receptors CD16 and CD32, integrins CD11a, CD11b, and CD11c, some of which form complement receptors CR3 (CD11b/CD18) and CR4 (CD11c/CD18), chemokine receptors CCR5 and CXCR4, pro-inflammatory cytokines IL-8, IL-12, and IP-10, and anti-inflammatory cytokine IL-10. Thus, local and systemic inflammation after the boost was attenuated with respect to after the prime, whereas as many innate myeloid cells were recruited after the boost as after the prime. However cells mobilized after the boost were more activated and mature. We also highlight the importance of neutrophils, in addition to professional APCs monocytes and DCs, in the early response to MVA, unveil their high degree of phenotypic heterogeneity, and discover new subsets.

The transient mobilization of leukocytes was specific to the vaccine, since buffer injection did not result in such a dramatic effect. However, we cannot formally rule out a role played by the recombinant fusion protein HIV gag-pol-nef encoded in our vaccine.

The mild local adverse reaction is typical of subcutaneously administered vaccines and was expected for a non-replicating vaccine such as MVA. The subcutaneous injections of IMVAMUNE® or ACAM3000, which are third generation MVA vaccines against smallpox, have been described as safe, in contrast to replicating VACV which is more reactogenic[44,45]. The local reaction to VACV and MVA was reported to be stronger and longer-lasting for primary vaccinees than for non-naive participants, and after the first injection than after the second one[44,46,47]. This was also supported by our data on MVA vaccination in macaques.

We found that IL-6, MCP-1, and IP-10 plasma concentrations were altered after subcutaneous injections of cynomolgus macaques with MVA. The differences between post-prime and post-boost AUC were higher for IP-10. There are only limited *in vivo* studies on the early plasma cytokine response to MVA, contrary to *in vitro* data after restimulation of PBMCs or *in vivo* studies on earlier generation smallpox vaccines, for which correlations between cytokine expression patterns and adverse events or vaccine take were identified. A study in rhesus macaques showed that IL-6 and IP-10 were the only cytokines for which levels increased in plasma one day after a single MVA intramuscular injection[48]. Comparison of serum cytokines after primary vaccination or re-vaccination with VACV in human volunteers showed that the peak levels were also statistically different for IP-10, in addition to IFNγ and MIG (CXCL9)[49], which are induced by IFNγ and/or IFN type I and interact with the same receptor, CXCR3[43]. Among many other soluble factors, IL-6, MCP-1, and IP-10 are produced *in vitro* in response to MVA by whole blood, PBMC, primary human monocytes and macrophages[50,51], and the pathways involved have been elucidated[51,52]. The capacity of MVA to induce MCP-1 production distinguished it from other VACV strains[50]. Whether they are produced by infected cells and/or bystander cells[53] is yet to be fully determined. Whether their presence in plasma originates from their release by cells from the injection site and/or from blood cells requires further investigation.

Beyond reactogenicity and plasma cytokine responses, the novelty of our study is the analysis of early innate cellular events after vaccination. Innate responses in blood or locally after injection of adjuvants or vaccines, including MVA, have been characterized in mice or macaques to better understand the mode of action of vaccines[54–59]. However, none of these studies analyzed the early cellular response to vaccines in the context of prime/boost strategies. One seminal study[54] compared distinct TLR adjuvants in rhesus macaques and demonstrated that

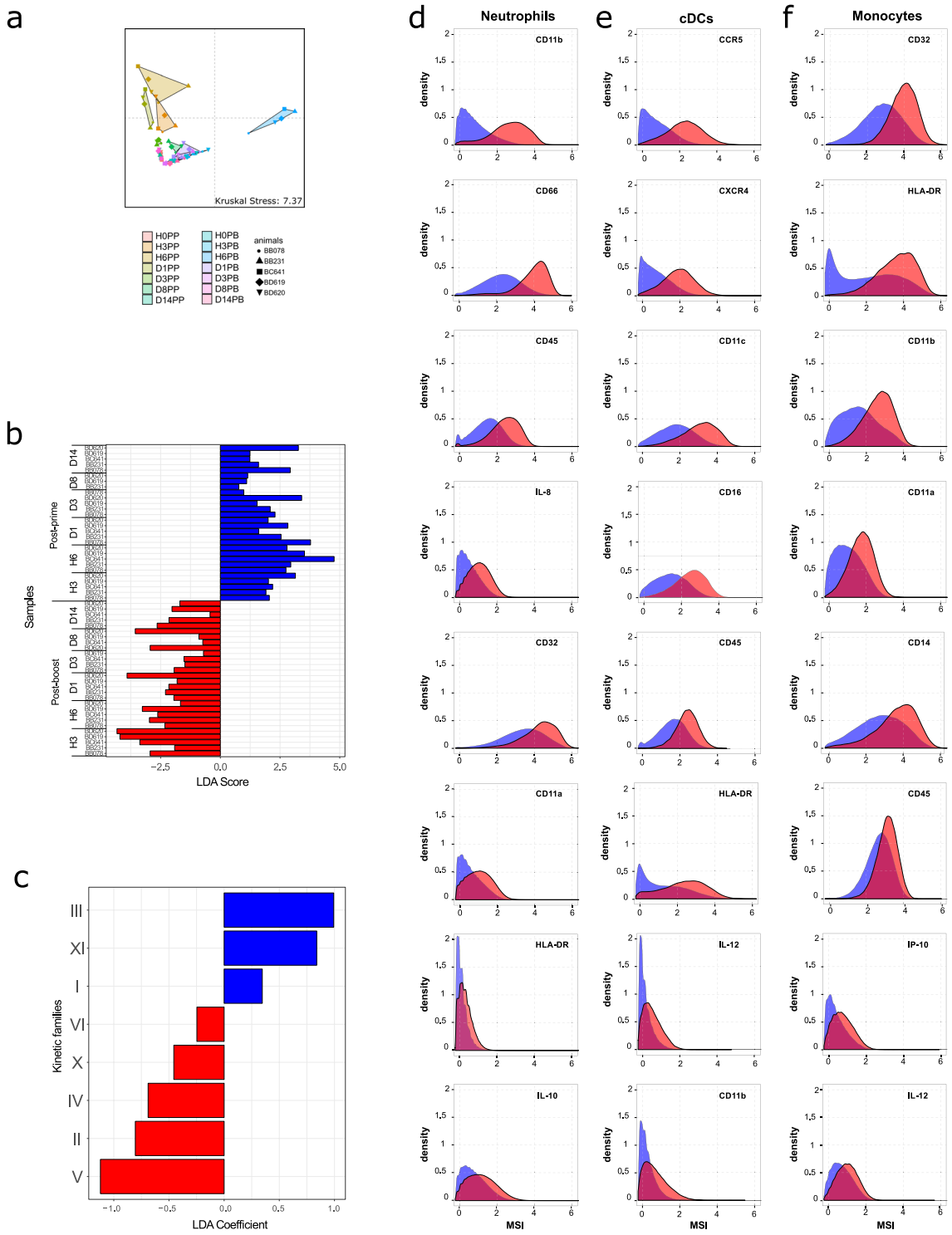

Figure 7. Visualization of and discrimination between post-prime and post-boost innate myeloid cell responses. (**a**) The Multidimensional Scaling (MDS) representation was calculated based on the abundance of each kinetic family. The Kruskal Stress is indicated and corresponds to the percentage of information lost during the dimensionality reduction process. Samples collected long before the prime injection (D-19PP) were not included. (**b**) Linear Discriminant Analysis (LDA) was performed after Least Absolute Shrinkage and Selection Operator (LASSO) (Supplementary Figure S11). Samples from the timepoints D-19PP, H0PP, and H0PB were not used for this analysis. The LDA scores of each sample are shown. The LDA score indicated whether a given sample was classified as post-prime (positive score) or post-boost (negative score). The samples colored in blue correspond to post-prime samples and the samples colored in red correspond to post-boost samples. (**c**) The LDA coefficients for each kinetic family are shown. (**d–f**) Kolmogorov-Smirnov (KS) distances of expression distribution densities were computed for each marker for neutrophils, cDCs, and monocytes (Supplementary Figure S12). This distance corresponds to the maximal difference between the distributions of marker

expression in the two compared cell populations. KS distance is commonly used in flow cytometry analyses[93]. MSI histograms for the top 8 markers with the highest KS distance are displayed for (**d**) neutrophils, (**e**) cDCs, and (**f**) monocytes from kinetic families that discriminate between the post-prime (blue) and the post-boost responses (red) as defined in Fig. 7c. Histograms were built on the whole dataset and did not represent a particular sample (animal or timepoint).

they differentially stimulated systemic immune responses. The intensity quality and kinetics of blood cells enrichment were specific of each adjuvant. MPL, R848, and CpG ODN induced a rapid increase of blood neutrophils and $CD14^+$ monocytes. However, neutrophil counts reached a higher level with R848 and two successive neutrophil expansions were observed with CpG ODN. In addition, only R848 and CpG ODN mobilized the intermediate $CD14^+CD16^+$ followed by non-classical $CD14^{dim}CD16^{high}$ monocytes and mediated pDCs and cDCs activation.

We identified potential new subsets of innate myeloid cells. There were more $CD4^{high}CD23^{high}CD11c^{high}$ neutrophils after the boost than the prime. They are likely linked to inflammation[27–29], and may exert regulatory/suppressive effects. $CD66^{high}CD32^{high}CD11b^{high}CD45^{high}CCR7^{high}IL\text{-}10^{high}$ neutrophils were also more highly enriched after the boost than the prime[37]. They may have a critical role in the resolution of infection upon the second encounter with pathogens. As previously described[10,60–63], we observed a population of cells sharing cDC and monocyte phenotypic patterns ($CD11c^{high}CD16^{high}CD11a^{high}CD14^{high}CD45^{high}IP\text{-}10^{mid/high}$), which we designated inflammatory cDCs/non-classical monocytes. This pro-inflammatory cell type expanded more after the boost than the prime. We also identified HLA-DR^{low} monocytes and cDCs, which are likely immature or immunosuppressive. Comparative functional analyses are required for their definitive classification as new subsets. In future studies, a refined panel should also include antibodies targeting additional markers, such as CD1c, CD141, CD172a, CD33, CD45RA and SIGLEC6, to clearly distinguish DC precursors from pDCs, separate the various cDC and monocyte subtypes, and identify myeloid-derived suppressive cells (MDSCs)[24,64–66].

Innate immune responses differ after one and two immunizations, as adaptive immune responses do. There are many possible reasons for this difference which are yet to be tested. At the boost, there were antibodies directed against MVA, contrary to the prime[18]. The vaccine was probably rapidly cleared and sensed differently, not as free viral particles, but as immune complexes. A different sensing could translate into a different alarm. It was recently shown, using mass cytometry, that the activation of signaling pathways and cytokine production by blood innate myeloid cells in response to the split influenza vaccine was dependent on immune complex formation and CD16 and CD32 FcγR activation[67]. Several studies, based on monoclonal antibody therapies, have also reported the importance of immune complexes and Fc receptor engagement in enhanced protective immune responses and vaccine-like effect[7]. This would be consistent with the higher expression of the FcR (CD16 and CD32) we observed among blood neutrophils, monocytes, and cDCs responding to the boost. Local memory cells established after the first immunization could also have played a role in the different innate myeloid responses after one and two immunizations. It has been shown in mice that IFNγ and MIP-1α produced by memory T cells after antigen recognition resulted in faster activation and recruitment of innate cells as well as better killing capacities by phagocytes[68,69]. In addition, TNFα produced by resident memory $CD8^+$ T cells was reported to induce local DC maturation[70]. The induction of resident $CD8^+$ T cells in the skin has been demonstrated in mice after MVA[71] and VACV skin infection[72,73]. Finally, trained innate immunity[5] could participate in the different innate immune responses during prime/boost immunizations, assuming that trained cells survive long enough between the two immunizations. Tissue-resident macrophages and/or cells recruited from blood or their progenitors after the prime could be involved.

Conversely, the different innate responses after the prime and boost may affect the restimulation of primary memory B and T cells and their differentiation into secondary memory cells. Neutrophils the most specific for the post-boost response expressed higher levels of CD66, which plays a role in adhesion and interactions with DCs[74], and of IL-8, a key chemoattractant of neutrophils to the site of inflammation and inducer of phagocytosis[75]. Neutrophils expanding after the boost also produced more IL-10. Immunosuppressive IL-10 producing neutrophils have been reported in mice[76,77], whereas their presence in humans is more controversial[78]. Finally, neutrophils recruited after the boost expressed a higher level of CCR7, suggesting their capacity to migrate directly to lymph node[37,79]. cDCs and monocytes, and to a lesser extent neutrophils, participating in the early response after the boost expressed higher levels of HLA-DR, involved in antigen presentation to $CD4^+$ T cells, and IL-12, promoting Th1 development and controlling the $CD8^+$ T cell response[80]. Neutrophils, cDCs, and monocytes mobilized after the boost were more prone to phagocytosis with higher expression of FcR (CD32 and CD16) and integrins CD11a, CD11b and CD11c, which are also involved in tissue-specific homing of leukocytes during inflammation and leukocyte activation[81,82]. Monocytes were more activated, as they expressed a higher level of CD14, which acts as PRR[83], and IP-10. cDCs were also more mature, with a higher expression of CXCR4 and CCR5, which allow their trafficking to the vaccine injection site and its draining lymph node[84,85]. Finally, innate myeloid cells elicited after the boost were more responsive with higher expression of CD45. CD45 is well known to lower the threshold of BCR and TCR signaling on B and T cells. It was also shown to regulate FcR, TLR, and cytokine signaling in phagocytes and DCs, as well as neutrophils migration[86]. Overall, better antigen uptake and presentation is more likely after the boost than after prime, contributing to enhanced T cells restimulation, although the requirements of signal 1 (TCR stimulation), 2 (co-stimulation), and 3 (inflammatory cytokines) differ between naive and memory T cells activation[87].

Whether the observed differences between the early response to the first and second vaccine injections also hold true for innate lymphoid cells needs to be tested. Additionally, it is important to define what is MVA-specific from what is shared with other vaccines. Another challenge will be to determine predictive correlations between innate and adaptive responses in the context of prime/boost immunizations, as previously done for one-dose vaccines[88], or yearly influenza vaccine[89]. Nonetheless, the differential innate responses described here can be valuable to tailor vaccine-induced immunity.

Methods

Ethics statement. This experiment was approved by the «Ministère de l'Éducation Nationale, de l'Enseignement Supérieur et de la Recherche» (France) and the ethical committee «Comité d'éthique en expérimentation animale n°44» (France) under the reference 201503131451825402 (APAFIS#319) and 2015062215324227v1(APAFIS#891) for Figure S2. Animals were handled by veterinarians in accordance with national regulations (CEA Permit Number A 92–32–02) and the European Directive (2010/63, recommendation N°9) and in compliance with Standards for Human Care and Use of Laboratory of the Office for Laboratory Animal Welfare (OLAW, USA) under OLAW Assurance number #A5826-01.

Vaccine, animals, and blood samples. The ANRS recombinant MVA HIV B vaccine (MVATG17401; Transgene, Illkirch-Graffenstaden, France) was injected subcutaneously into five cynomolgus macaques, at 4×10^8 PFU, two months apart as previously described[18]. It contains the full-length codon-optimized sequence of *gag* (encoding amino acids [aa] 1 to 512) fused with fragments from *pol* (encoding aa 172 to 219, 325 to 383, and 461 to 519) and *nef* (encoding aa 66 to 147 and 182 to 206) from the Bru/Lai isolate (Los Alamos database accession number K02013). Blood samples were collected longitudinally in EDTA, to count leukocytes, or Lithium-Heparin to measure soluble plasma factors and perform single-cell mass cytometry analyses.

For Figure S2, six macaques were injected subcutaneously with a buffer containing 10 mM Tris-HCl, saccharose 5% (w/v), 10 mM NaGlu, 50 mM NaCl, pH8.0 and one month later with the same dose and batch of MVA HIV B as the other five animals.

Quantification of plasma soluble factors. C-reactive protein (CRP) was quantified in plasma by Laboratoire Vébio (Arcueil, France) using an immunoturbidimetry assay (CRP Plus, Thermo Scientific). Cytokine, chemokine and growth factor levels were assessed with a multiplex immunoassay (MILLIPLEX MAP non-human primate cytokine magnetic bead panel, Millipore), except plasma IP-10 concentrations, which were assessed by ELISA (human CXCR10/IP-10, R&D systems). Post-prime (PP) and post-boost (PB) samples were assessed independently.

Staining, mass cytometry acquisition, and data processing. Blood processing, staining, and acquisition using a CyTOF (Fluidigm), as well as initial leukocyte gating, were performed as previously described[10]. Briefly, 1 mL of blood was incubated with a fixation mixture containing PFA and glycerol[10,90] for 10 min at 4 °C. After centrifugation, erythrocytes were lysed in 10 mL of milli-Q water at room temperature for 20 min. Cells were then washed in DPBS 1× and stored at −80 °C at a final concentration of $15 \cdot 10^6$ cells in the fixation mixture. Three millions of fixed leukocytes were thawed. After 2 washes with PBS/BSA at 0.5%, they were incubated with the surface antibodies at 4 °C for 30 min (Supplementary Table S3). They were washed twice in PBS 1× and fixed in PBS/PFA 1.6% for 20 min RT. After permeabilization in Perm/Wash Buffer 1× (BD Biosciences) for 10 min at RT, cells were incubated with intracellular antibodies at 4 °C for 30 min (Supplementary Table S3). Finally cells were washed in PBS and incubated overnight with 0.1 µM of iridium RNA/DNA intercalator in PBS/PFA at 1.6%. The next day, cells were washed three times with milli-Q water and filtered using a 35 µm nylon mesh cell stainer (BD Biosciences). EQ™ four elements calibration beads (Fluidigm, San Fransisco, USA) were added following manufacturer's protocol. Each sample was divided into two replicates and acquisition was performed using the autosampler device for CyTOF (both from DVS Fluidigm). 5 stainings/acquisitions were done (one per animal) using the same batch of antibodies each time. In addition, we followed an established strategy[91] to control the quality of each staining/acquisition and their reproducibility by including the same two control samples (Supplementary Figure S13).

Automatic identification of cell populations. Cell populations were identified using the Spanning-tree Progression Analysis of Density-normalized Events (SPADE) algorithm[19]. Briefly, a random pre-downsampling was used to select 60,000 cells from each sample (60,000 corresponded to the number of cells contained in the smallest sample -Table S5). Then the SPADE algorithm *per se* was applied to all samples (all macaques and all timepoints) to define the phenotype of each cluster as well as the topology of the tree. Full upsampling was eventually performed.

For our dataset, the optimal SPADE settings were determined with SPADEVizR package[20] as 20 clustering markers (CD66, HLA-DR, CD3, CD64, CD8, CD123, CD11a, CD11b, CD4, CD23, CD86, CD32, CXCR4, CCR5, CD16, CD11c, CD14, CD45, CD20 and CCR7), 600 clusters, a density-based downsampling of 10%, and an outlier density parameter of 0.01. The clustering quality was expressed as the percentage of clusters displaying a unimodal and narrow distribution of all clustering markers, as well as the percentage of small clusters (clusters with less than 50 cells in total). Markers distributions were assessed using the Hartigan's dip test (p-value < 0.05 to reject the uni-modality hypothesis). Markers distributions with an interquartile range (IQR) < 2 were considered to be narrow. These settings resulted in the highest percentage of uniform clusters and the absence of small clusters. Numbers and percentages of non-uniform clusters for each marker are displayed in Table S6.

Leukocyte counts, absolute number calculation, and abundance profiles. The leukocyte counts were quantified using an HmX instrument (Beckman Coulter). The absolute number of cells in a population was computed as: N = the absolute number of leukocytes expressed per µL of blood x number of cells in the population detected by the CyTOF/total number of leukocytes (defined as non $CD3^+CD66^+$ cells) detected by the CyTOF. The absolute number kinetics was called the abundance profile.

Heatmap representations of the cell cluster phenotypes. Heatmaps of the cell cluster phenotypes were generated using SPADEVizR[20]. The mean of the median of the mean signal intensity (MSI) for each marker among samples was displayed according to five phenotypic bins calculated by dividing the marker range of

expression between the 5th and the 95th percentile into five categories for all cell clusters. For each cluster, samples contributing less than 10 cells were excluded. Hierarchical clusterings of cell clusters and markers were performed using the Euclidean metric based on the ward.D linkage.

Phenotypic and kinetic families. Cell clusters sharing similar phenotypes were gathered into phenotypic families based on the cluster dendrogram. Phenotypic families sharing similar dynamics were gathered into kinetic families based on their abundance profiles. This determination was performed using SPADEVizR[20] with the hierarchical method based on the Pearson correlation and complete linkage.

Statistical tests. Soluble factor concentrations and cell abundances were compared between timepoints using the permutation test available in the "exactRankTests" R package. The area under the curve (AUC) corresponds to the sum over time of all plasma soluble factor concentrations (cumulated concentration) or cell abundances (cumulated abundance) between H3 and D14. PP AUC and PB AUC were compared using the permutation test. Correlation analyses were performed using the Pearson coefficient. The density distributions of markers were compared using the Kolmogorov-Smirnov distance using CytoCompare[92].

Modeling. The linear regression model was constructed using SPADEVizR[20]. The abundance profiles of kinetic families were used as the entry parameter and IP-10 concentration as the biological value to predict. The validity of the model was assessed by excluding either one sample or one individual and by comparing predicted and observed values.

Discrimination between post-prime and post-boost innate myeloid responses. The Least Absolute Shrinkage and Selection Operator (LASSO) approach was performed on R using the "lars" package. Centered and reduced abundance profiles of kinetic families were used as entry parameters. The validity of classification at each iteration was assessed by cross-validation. The best configuration was chosen as the lowest number of kinetic families used and the lowest error rate in cross-validation. Linear Discriminant Analysis (LDA) was performed on R with the "MASS" package based on the abundance profiles of kinetic families and classes (post-prime or post-boost) as entry parameters.

Data availability and interactivity. Mass cytometry data were deposited publicly. FCS files are available on the FlowRepository database through ID FR-FCM-ZYBG, and the Cytobank platform under accession numbers 68443 and 68590. The http://data.idmitcenter.fr/MVA-innate-myeloid/ website provides interactive SPADE quality control data, interactive SPADE trees, interactive heatmaps, and interactive histograms. The interactive heatmaps avoid to juggle between Fig. 4 (heatmaps), Supplementary Figures S8–9 (phenotypic families abundance profiles), Fig. 5a (kinetic families), Table 1 (correspondance between phenotypic and kinetic families), and Fig. 7c (kinetic families LDA selection). They directly connect clusters and phenotypic families to their annotation, kinetic families, and their relevance as signature of the response to a first or a second immunization.

References

1. Iwasaki, A. & Medzhitov, R. Regulation of adaptive immunity by the innate immune system. *Science* **327**, 291–295 (2010).
2. Schlitzer, A., McGovern, N. & Ginhoux, F. Dendritic cells and monocyte-derived cells: Two complementary and integrated functional systems. *Semin. Cell Dev. Biol.* **41**, 9–22 (2015).
3. Jaillon, S. *et al.* Neutrophils in innate and adaptive immunity. *Semin. Immunopathol.* **35**, 377–394 (2013).
4. Takeuchi, O. & Akira, S. Pattern recognition receptors and inflammation. *Cell* **140**, 805–820 (2010).
5. Arts, R. J. W. & Netea, M. G. Adaptive Characteristics of Innate Immune Responses in Macrophages. *Microbiol. Spectr.* **4**, (2016).
6. Wen, Y.-M., Mu, L. & Shi, Y. Immunoregulatory functions of immune complexes in vaccine and therapy. *EMBO Mol Med* **8**, 1120–1133 (2016).
7. Bournazos, S. & Ravetch, J. V. Fcgamma Receptor Function and the Design of Vaccination Strategies. *Immunity* **47**, 224–233 (2017).
8. Kardani, K., Bolhassani, A. & Shahbazi, S. Prime-boost vaccine strategy against viral infections: Mechanisms and benefits. *Vaccine* **34**, 413–423 (2016).
9. Hart, T. *et al.* C. H. The translational value of non-human primates in preclinical research on infection and immunopathology. *Eur. J. Pharmacol.* **759**, 69–83 (2015).
10. Elhmouzi-Younes, J. *et al.* In depth comparative phenotyping of blood innate myeloid leukocytes from healthy humans and macaques using mass cytometry. *Cytom. Part A J. Int. Soc. Anal. Cytol.* **91**, 969–982 (2017).
11. Earl, P. L. *et al.* Immunogenicity of a highly attenuated MVA smallpox vaccine and protection against monkeypox. *Nature* **428**, 182–185 (2004).
12. Frey, S. E. *et al.* Clinical and immunologic responses to multiple doses of IMVAMUNE (Modified Vaccinia Ankara) followed by Dryvax challenge. *Vaccine* **25**, 8562–8573 (2007).
13. Seaman, M. S. *et al.* Effect of vaccination with modified vaccinia Ankara (ACAM3000) on subsequent challenge with Dryvax. *J. Infect. Dis.* **201**, 1353–1360 (2010).
14. Hatch, G. J. *et al.* Assessment of the protective effect of Imvamune and Acam2000 vaccines against aerosolized monkeypox virus in cynomolgus macaques. *J. Virol.* **87**, 7805–7815 (2013).
15. Drexler, I., Staib, C. & Sutter, G. Modified vaccinia virus Ankara as antigen delivery system: how can we best use its potential? *Curr. Opin. Biotechnol.* **15**, 506–512 (2004).
16. Price, P. J. R., Torres-Domínguez, L. E., Brandmüller, C., Sutter, G. & Lehmann, M. H. Modified Vaccinia virus Ankara: innate immune activation and induction of cellular signalling. *Vaccine* **31**, 4231–4234 (2013).
17. Swadling, L. *et al.* A human vaccine strategy based on chimpanzee adenoviral and MVA vectors that primes, boosts, and sustains functional HCV-specific T cell memory. *Sci. Transl. Med.* **6**, 261ra153 (2014).
18. Pejoski, D. *et al.* Identification of Vaccine-Altered Circulating B Cell Phenotypes Using Mass Cytometry and a Two-Step Clustering Analysis. *J. Immunol. (Baltimore, Md. 1950)* **196**, 4814–4831 (2016).
19. Qiu, P. *et al.* Extracting a cellular hierarchy from high-dimensional cytometry data with SPADE. *Nat. Biotechnol.* **29**, 886–91 (2011).
20. Gautreau, G. *et al.* SPADEVizR: an R package for Visualization, Analysis and Integration of SPADE results. *Bioinformatics*. **33**, 779–781 (2016).

21. Saeys, Y., Gassen, S., Van & Lambrecht, B. N. Computational flow cytometry: helping to make sense of high-dimensional immunology data. *Nat. Rev. Immunol.* **16**, 449–462 (2016).
22. Dutertre, C.-A. *et al*. TLR3-Responsive, XCR1+, CD141(BDCA-3)+/CD8+-Equivalent Dendritic Cells Uncovered in Healthy and Simian Immunodeficiency Virus-Infected Rhesus Macaques. *J. Immunol.* **192**, 4697–4708 (2014).
23. Sugimoto, C. *et al*. Differentiation Kinetics of Blood Monocytes and Dendritic Cells in Macaques: Insights to Understanding Human Myeloid Cell Development. *J. Immunol.* **195**, 1774–1781 (2015).
24. Guilliams, M. *et al*. Unsupervised High-Dimensional Analysis Aligns Dendritic Cells across Tissues and Species. *Immunity* **45**, 669–684 (2016).
25. O'Hagan, D. T., Ott, G. S., De Gregorio, E. & Seubert, A. The mechanism of action of MF59 - an innately attractive adjuvant formulation. *Vaccine* **30**, 4341–4348 (2012).
26. Antal-Szalmas, P., Strijp, J. A., Weersink, A. J., Verhoef, J. & Van Kessel, K. P. Quantitation of surface CD14 on human monocytes and neutrophils. *J. Leukoc. Biol.* **61**, 721–728 (1997).
27. Biswas, P. *et al*. Expression of CD4 on human peripheral blood neutrophils. *Blood* **101**, 4452–4456 (2003).
28. Vella, A. *et al*. Expression of FCepsilonII/CD23 on human neutrophils isolated from rheumatoid arthritis patients. *Inflammation* **23**, 471–479 (1999).
29. Benoni, G. *et al*. CD23 and CD69 expression on human neutrophils of healthy subjects and patients with peripheral arterial occlusive disease. *Int. J. Immunopathol. Pharmacol.* **14**, 161–167 (2001).
30. Lewis, S. M. *et al*. Expression of CD11c and EMR2 on neutrophils: potential diagnostic biomarkers for sepsis and systemic inflammation. *Clin. Exp. Immunol.* **182**, 184–194 (2015).
31. Denny, M. F. *et al*. A distinct subset of proinflammatory neutrophils isolated from patients with systemic lupus erythematosus induces vascular damage and synthesizes type I IFNs. *J. Immunol. (Baltimore, Md. 1950)* **184**, 3284–3297 (2010).
32. Pillay, J. *et al*. A subset of neutrophils in human systemic inflammation inhibits T cell responses through Mac-1. *J. Clin. Invest.* **122**, 327–36 (2012).
33. Cid, J., Aguinaco, R., Sanchez, R., Garcia-Pardo, G. & Llorente, A. Neutrophil CD64 expression as marker of bacterial infection: a systematic review and meta-analysis. *J. Infect.* **60**, 313–319 (2010).
34. Li, S. *et al*. Neutrophil CD64 expression as a biomarker in the early diagnosis of bacterial infection: a meta-analysis. *Int. J. Infect. Dis. IJID Off. Publ. Int. Soc. Infect. Dis.* **17**, e12–23 (2013).
35. Rider, P. *et al*. IL-1α and IL-1β recruit different myeloid cells and promote different stages of sterile inflammation. *J. Immunol. (Baltimore, Md. 1950)* **187**, 4835–4843 (2011).
36. Barry, K. C., Fontana, M. F., Portman, J. L., Dugan, A. S. & Vance, R. E. IL-1α signaling initiates the inflammatory response to virulent Legionella pneumophila *in vivo*. *J. Immunol. (Baltimore, Md. 1950)* **190**, 6329–6339 (2013).
37. Beauvillain, C. *et al*. CCR7 is involved in the migration of neutrophils to lymph nodes. *Blood* **117**, 1196–1204 (2011).
38. Moreno, S. E. *et al*. IL-12, but not IL-18, is critical to neutrophil activation and resistance to polymicrobial sepsis induced by cecal ligation and puncture. *J. Immunol. (Baltimore, Md. 1950)* **177**, 3218–3224 (2006).
39. Langlet, C. *et al*. CD64 expression distinguishes monocyte-derived and conventional dendritic cells and reveals their distinct role during intramuscular immunization. *J. Immunol.* (*Baltimore*, *Md. 1950*) **188**, 1751–1760 (2012).
40. Landmann, R., Ludwig, C., Obrist, R. & Obrecht, J. P. Effect of cytokines and lipopolysaccharide on CD14 antigen expression in human monocytes and macrophages. *J. Cell. Biochem.* **47**, 317–329 (1991).
41. Tso, C., Rye, K.-A. & Barter, P. Phenotypic and functional changes in blood monocytes following adherence to endothelium. *PLoS One* **7**, e37091 (2012).
42. Kadowaki, N., Antonenko, S., Lau, J. Y. & Liu, Y. J. Natural interferon alpha/beta-producing cells link innate and adaptive immunity. *J. Exp. Med.* **192**, 219–226 (2000).
43. Van Raemdonck, K. *et al*. CXCR3 ligands in disease and therapy. *Cytokine Growth Factor Rev.* **26**, 311–327 (2015).
44. von Krempelhuber, A. *et al*. A randomized, double-blind, dose-finding Phase II study to evaluate immunogenicity and safety of the third generation smallpox vaccine candidate IMVAMUNE. *Vaccine* **28**, 1209–1216 (2010).
45. Wilck, M. B. *et al*. Safety and immunogenicity of modified vaccinia Ankara (ACAM3000): effect of dose and route of administration. *J. Infect. Dis.* **201**, 1361–1370 (2010).
46. Treanor, J., Wu, H., Liang, H. & Topham, D. J. Immune responses to vaccinia and influenza elicited during primary versus recent or distant secondary smallpox vaccination of adults. *Vaccine* **24**, 6913–6923 (2006).
47. Frey, S. E., Newman, F. K., Yan, L., Lottenbach, K. R. & Belshe, R. B. Response to smallpox vaccine in persons immunized in the distant past. *JAMA* **289**, 3295–3299 (2003).
48. Teigler, J. E. *et al*. The canarypox virus vector ALVAC induces distinct cytokine responses compared to the vaccinia virus-based vectors MVA and NYVAC in rhesus monkeys. *J. Virol.* **88**, 1809–1814 (2014).
49. Simon, W. L., Salk, H. M., Ovsyannikova, I. G., Kennedy, R. B. & Poland, G. A. Cytokine production associated with smallpox vaccine responses. *Immunotherapy* **6**, 1097–1112 (2014).
50. Lehmann, M. H. *et al*. Modified vaccinia virus ankara triggers chemotaxis of monocytes and early respiratory immigration of leukocytes by induction of CCL2 expression. *J. Virol.* **83**, 2540–2552 (2009).
51. Delaloye, J. *et al*. Innate immune sensing of modified vaccinia virus Ankara (MVA) is mediated by TLR2-TLR6, MDA-5 and the NALP3 inflammasome. *PLoS Pathog.* **5**, e1000480 (2009).
52. Dai, P. *et al*. Modified vaccinia virus Ankara triggers type I IFN production in murine conventional dendritic cells via a cGAS/STING-mediated cytosolic DNA-sensing pathway. *PLoS Pathog.* **10**, e1003989 (2014).
53. Pascutti, M. F. *et al*. Interplay between modified vaccinia virus Ankara and dendritic cells: phenotypic and functional maturation of bystander dendritic cells. *J. Virol.* **85**, 5532–5545 (2011).
54. Kwissa, M., Nakaya, H. I., Oluoch, H. & Pulendran, B. Distinct TLR adjuvants differentially stimulate systemic and local innate immune responses in nonhuman primates. *Blood* **119**, 2044–2055 (2012).
55. Epaulard, O. *et al*. Macrophage- and neutrophil-derived TNF-α instructs skin langerhans cells to prime antiviral immune responses. *J. Immunol. (Baltimore, Md. 1950)* **193**, 2416–2426 (2014).
56. Liang, F. *et al*. Vaccine priming is restricted to draining lymph nodes and controlled by adjuvant-mediated antigen uptake. *Sci. Transl. Med.* **9**, (2017).
57. Abadie, V. *et al*. Original encounter with antigen determines antigen-presenting cell imprinting of the quality of the immune response in mice. *PLoS One* **4**, e8159 (2009).
58. Calabro, S. *et al*. Vaccine adjuvants alum and MF59 induce rapid recruitment of neutrophils and monocytes that participate in antigen transport to draining lymph nodes. *Vaccine* **29**, 1812–1823 (2011).
59. Morel, S. *et al*. Adjuvant System AS03 containing α-tocopherol modulates innate immune response and leads to improved adaptive immunity. *Vaccine* **29**, 2461–2473 (2011).
60. Piccioli, D. *et al*. Functional specialization of human circulating CD16 and CD1c myeloid dendritic-cell subsets. *Blood* **109**, 5371–5379 (2007).
61. Macdonald, K. P. A. *et al*. Characterization of human blood dendritic cell subsets. *Cell* **100**, 4512–4520 (2002).
62. Autissier, P., Soulas, C., Burdo, T. H. & Williams, K. C. Immunophenotyping of lymphocyte, monocyte and dendritic cell subsets in normal rhesus macaques by 12-color flow cytometry: clarification on DC heterogeneity. *J. Immunol. Methods* **360**, 119–128 (2010).

63. Dutertre, C.-A. *et al*. Pivotal role of M-DC8^{+} monocytes from viremic HIV-infected patients in TNFα overproduction in response to microbial products. *Blood* **120**, 2259–2268 (2012).
64. Bronte, V. *et al*. Recommendations for myeloid-derived suppressor cell nomenclature and characterization standards. *Nat. Commun.* **7**, 12150 (2016).
65. Villani, A.-C. *et al*. Single-cell RNA-seq reveals new types of human blood dendritic cells, monocytes, and progenitors. *Science* **356**, (2017).
66. See, P. *et al*. Mapping the human DC lineage through the integration of high-dimensional techniques. *Science* **356**, (2017).
67. O'Gorman, W. E. *et al*. The Split Virus Influenza Vaccine rapidly activates immune cells through Fcγ receptors. *Vaccine* **32**, 5989–5997 (2014).
68. Narni-Mancinelli, E. *et al*. Inflammatory monocytes and neutrophils are licensed to kill during memory responses *in vivo*. *PLoS Pathog.* **7**, e1002457 (2011).
69. Soudja, S. M. *et al*. Memory-T-cell-derived interferon-γ instructs potent innate cell activation for protective immunity. *Immunity* **40**, 974–988 (2014).
70. Schenkel, J. M. *et al*. T cell memory. Resident memory CD8 T cells trigger protective innate and adaptive immune responses. *Science* **346**, 98–101 (2014).
71. Muschaweckh, A. *et al*. Antigen-dependent competition shapes the local repertoire of tissue-resident memory CD8+ T cells. *J. Exp. Med.* **213**, 3075–3086 (2016).
72. Jiang, X. *et al*. Skin infection generates non-migratory memory CD8+ T(RM) cells providing global skin immunity. *Nature* **483**, 227–231 (2012).
73. Khan, T. N., Mooster, J. L., Kilgore, A. M., Osborn, J. F. & Nolz, J. C. Local antigen in nonlymphoid tissue promotes resident memory CD8+ T cell formation during viral infection. *J. Exp. Med.* **213**, 951–966 (2016).
74. van Gisbergen, K. P. J. M., Ludwig, I. S., Geijtenbeek, T. B. H. & van Kooyk, Y. Interactions of DC-SIGN with Mac-1 and CEACAM1 regulate contact between dendritic cells and neutrophils. *FEBS Lett.* **579**, 6159–6168 (2005).
75. Mukaida, N. Interleukin-8: an expanding universe beyond neutrophil chemotaxis and activation. *Int. J. Hematol.* **72**, 391–398 (2000).
76. Kasten, K. R., Muenzer, J. T. & Caldwell, C. C. Neutrophils are significant producers of IL-10 during sepsis. *Biochem. Biophys. Res. Commun.* **393**, 28–31 (2010).
77. Ocuin, L. M. *et al*. Neutrophil IL-10 suppresses peritoneal inflammatory monocytes during polymicrobial sepsis. *J. Leukoc. Biol.* **89**, 423–432 (2011).
78. Lewkowicz, N. *et al*. Induction of human IL-10-producing neutrophils by LPS-stimulated Treg cells and IL-10. *Mucosal Immunol.* **9**, 364–378 (2016).
79. Kamenyeva, O. *et al*. Neutrophil recruitment to lymph nodes limits local humoral response to Staphylococcus aureus. *PLoS Pathog.* **11**, e1004827 (2015).
80. Trinchieri, G. Interleukin-12: a proinflammatory cytokine with immunoregulatory functions that bridge innate resistance and antigen-specific adaptive immunity. *Annu. Rev. Immunol.* **13**, 251–276 (1995).
81. Bruhns, P. & Jönsson, F. Mouse and human FcR effector functions. *Immunol. Rev.* **268**, 25–51 (2015).
82. Ley, K., Laudanna, C., Cybulsky, M. I. & Nourshargh, S. Getting to the site of inflammation: the leukocyte adhesion cascade updated. *Nat. Rev. Immunol.* **7**, 678–689 (2007).
83. Pugin, J. *et al*. CD14 is a pattern recognition receptor. *Immunity* **1**, 509–516 (1994).
84. Cravens, P. D. & Lipsky, P. E. Dendritic cells, chemokine receptors and autoimmune inflammatory diseases. *Immunol. Cell Biol.* **80**, 497–505 (2002).
85. Kabashima, K. *et al*. CXCL12-CXCR4 engagement is required for migration of cutaneous dendritic cells. *Am. J. Pathol.* **171**, 1249–1257 (2007).
86. Saunders, A. E. & Johnson, P. Modulation of immune cell signalling by the leukocyte common tyrosine phosphatase, CD45. *Cell. Signal.* **22**, 339–348 (2010).
87. DiSpirito, J. R. & Shen, H. Quick to remember, slow to forget: rapid recall responses of memory CD8+ T cells. *Cell Res.* **20**, 13–23 (2010).
88. Querec, T. D. *et al*. Systems biology approach predicts immunogenicity of the yellow fever vaccine in humans. *Nat. Immunol.* **10**, 116–125 (2009).
89. Nakaya, H. I. *et al*. Systems Analysis of Immunity to Influenza Vaccination across Multiple Years and in Diverse Populations Reveals Shared Molecular Signatures. *Immunity* **43**, 1186–1198 (2015).
90. Egger, G., Burda, A. & Glasner, A. A simple method for measuring the F-actin content of human polymorphonuclear leukocytes in whole blood. *Virchows Arch.* **438**, 394–7 (2001).
91. Kleinsteuber, K. *et al*. Standardization and quality control for high-dimensional mass cytometry studies of human samples. *Cytom. Part A J. Int. Soc. Anal. Cytol.* **89**, 903–913 (2016).
92. Platon, L. *et al*. A computational approach for phenotypic comparisons of cell populations in high-dimensional cytometry data. *Methods*. **132**, 66–75 (2018).
93. Lillacci, G. & Khammash, M. The signal within the noise: efficient inference of stochastic gene regulation models using fluorescence histograms and stochastic simulations. *Bioinformatics* **29**, 2311–2319 (2013).

Acknowledgements

This work was supported by the "Investissements d'Avenir" programs managed by the ANR under reference ANR-10-LABX-77-01 funding the Vaccine Research Institute (VRI), Créteil (ImMemory research program), ANR-11-INBS-0008 funding the Infectious Disease Models and Innovative Therapies (IDMIT, Fontenay-aux-Roses, France) infrastructure, and ANR-10-EQPX-02–01 funding the FlowCyTech facility (IDMIT, Fontenay-aux-Roses, France), and by the European Union, EVHA H2020 project (Grant N°681032). We would like to thank all members of the ASW and L2I groups from IDMIT as well as Malvina Schatz, Marie-Laurence Baron, and Philippe V. Alfonso.

Author Contributions

Y.L., R.L.G. and A.S.B. designed the study. N.D.B. supervised immunizations and samples collection. I.N., S.D. and A.S.B. developed the antibody panel. I.N. processed blood samples and performed the multiplex assays. S.D. stained and acquired samples. P.R. and F.M. compared buffer and M.V.A. injection. J.E.Y. and A.C. set the CyTOF instrument. J.L.P. and N.T. analyzed the data. J.L.P., N.T., R.L.G. and A.S.B. wrote the paper.

Additional Information

Supplementary information accompanies this paper at https://doi.org/10.1038/s41598-018-21222-2.

Competing Interests: The authors declare no competing interests.

Publisher's note: Springer Nature remains neutral with regard to jurisdictional claims in published maps and institutional affiliations.

Open Access This article is licensed under a Creative Commons Attribution 4.0 International License, which permits use, sharing, adaptation, distribution and reproduction in any medium or format, as long as you give appropriate credit to the original author(s) and the source, provide a link to the Creative Commons license, and indicate if changes were made. The images or other third party material in this article are included in the article's Creative Commons license, unless indicated otherwise in a credit line to the material. If material is not included in the article's Creative Commons license and your intended use is not permitted by statutory regulation or exceeds the permitted use, you will need to obtain permission directly from the copyright holder. To view a copy of this license, visit http://creativecommons.org/licenses/by/4.0/.

© The Author(s) 2018

Chapter 4. NK cell responses after a prime-boost vaccination following a classical schedule

Overview

Knowing that MVA prime and boost induced distinct innate myeloid cell responses (Palgen et al., 2018), we investigated in the very same animals whether this was also the case for the NK cell response.

Our first observations revealed that conversely to myeloid NK cells, NK cell number tended to decrease at early (< 3 days) timepoints after immunization, whereas it re-increases afterwards (around 1-2 weeks). At the scale of the full NK cell compartment, no difference could be observed between response to prime and to boost. But NK cell number correlated with the expression of several genes associated with NK cell cytotoxic activity among the full PBMC (peripheral blood mononuclear cell) compartment. Noteworthy, this NK-cell associated gene signature was associated with the IL-12 signaling pathway. Since IL-12 was part of the signature of monocytes and cDCs responding to the boost (Palgen et al., 2018), it suggested that NK cells could also differ between both immunizations.

We thus designed a mass cytometry antibody panel targeting NK cell biology and followed a similar analysis strategy as for Chapter 3. We also used extemporaneously fixed leukocyte samples, which revealed to be more troublesome for studying NK cells. Indeed, the low frequency of NK cells within whole blood (compared to PBMCs) reduced the number of NK cells retrieved per sample. In addition, most antibodies targeting NK receptors (*e.g.* NKp30, NKp46, NKp80, CD158a) lacked reactivity with macaque fixed cells, precluding their use in our analysis. Still, we were able to include many relevant markers involved in NK cell activation (*e.g.* CD2, CD7, CD16, CD69), NK cell cytotoxic activity (*e.g.* granzyme B, perforin, CD107a, CD11a), as well as chemokine receptor (CCR5, CCR7, CXCR4), and two NK receptors (NKG2A/C and NKG2D).

As for the innate myeloid cells, we were able to identify a high phenotypic diversity within the NK cell compartment. Namely, we identified three major groups of NK cells differing in maturation, migration capabilities and cytotoxic activity potential in term of phenotype: poorly cytotoxic NK cells being defined as CD11a^{mid} CD7^{low} CD107a^{mid} granzyme B^{mid}, whereas intermediately and highly cytotoxic NK cells were CD11a^{high} CD7^{high} CD107a^{high} granzyme B^{high}. Intermediately cytotoxic NK cells were NKG2D^{mid} CCR5^{mid} CXCR4^{mid} CD56^{mid}, whereas highly cytotoxic NK cells were NKG2D^{high} CCR5^{high} CXCR4^{high} CD56^{high}.

In term of dynamics, NK cells subphenotypes were also differently abundant between prime and boost, as confirmed by linear discriminant analysis. Conversely to innate myeloid cells, a first shift in NK cell subphenotype composition was observed at early timepoints (as early as 1 day) post-prime, and was maintained until 2 weeks post-prime; a second shift in phenotype occurred between two weeks and two months and was maintained until the boost.

The discrimination was not as sharp and precise as for innate myeloid cells though, since most subphenotypes were impacted by both immunizations (although with different kinetics). This may have been the result of the lack of NK cell markers in our panel, which impairs our ability to investigate the complete NK cell repertoire and thus the complete diversity of the NK cell compartment (Wilk & Blish, 2018). Also, note that a wide inter-individual variability was observed at baseline, both in term of NK cell subphenotype composition and NK cell number. Immunization significantly reduced this variability, although it did not abrogate it completely. This may also participate in this more blurred distinction between responses to prime and boost.

Still, despite these caveats, we revealed the major differences that discriminate between responses to each immunization. Strikingly activation/maturation markers, including CD11a, CD16, CD69, granzyme B, perforin and CD107a were upregulated on NK cells responding to boost compared to those responding to prime. Whether these more phenotypically mature/cytotoxic NK cells, which likely correspond to memory NK cells (Min-Oo et al., 2013; Geiger & Sun, 2016; Paust et al., 2017), were antigen-specific or not, and which exact enhanced functions they display, remains to be addressed.

Interestingly, the NK cells observed between one day and two weeks after prime were conversely characterized as poorly cytotoxic NK cells. This suggest that either cytotoxic NK cells were all recruited out of blood in the first two weeks after prime, or that poorly cytotoxic NK cells were newly generated or released in blood following immunization. Note that we did not observe a shift of NK cell phenotype between one day and three days after boost. Due to lack of samples, we were not able to investigate whether it could have occurred at latter timepoints, for example at day 8 or day 14 post-boost. Actually, at each timepoint, the maximum blood volume allowed by the ethical comity, which takes into account volemia, anemia, steady-state hematopoiesis, and animal welfare was collected. Unfortunately, at some timepoints, the quantity blood to prepare fixed leukocytes

to analyze innate responses was not sufficient to analyze both innate myeloid and NK cells, as well as T and C cells at late timepoints. The corresponding samples were used in priority for the characterization of innate myeloid cell immune response.

Overall this study showed that similarly to innate myeloid cells, prime vaccination induced phenotypic changes in the NK cell compartment. The dynamics was different though, suggesting that distinct mechanisms might be at play. Accordingly, generation mechanisms of memory NK cells are not fully characterized in literature, and they may not be shared with innate myeloid cell training, as mentioned in the Introduction.

"NK cell immune responses differ after prime and boost vaccination"

All these results were published in the *Journal of Leukocyte Biology* (Palgen et al., 2019). The corresponding publication is provided hereafter. The data are available in an interactive fashion on the IDMIT dissemination platform (http://data.idmitcenter.fr/).

DOI: 10.1002/JLB.4A1018-391RR

JLB JOURNAL OF LEUKOCYTE BIOLOGY

ARTICLE

NK cell immune responses differ after prime and boost vaccination

Jean-Louis Palgen[1,2] | Nicolas Tchitchek[1,2] | Nicolas Huot[2,3] | Jamila Elhmouzi-Younes[1,2] | Cécile Lefebvre[2,4] | Pierre Rosenbaum[1,2] | Nathalie Dereuddre-Bosquet[1,2] | Frédéric Martinon[1,2] | Hakim Hocini[2,4] | Antonio Cosma[1,2] | Michaela Müller-Trutwin[2,3] | Yves Lévy[2,4] | Roger Le Grand[1,2] | Anne-Sophie Beignon[1,2]

[1]CEA, Université Paris Sud 11, INSERM U1184, Immunology of Viral Infections and Autoimmune Diseases, IDMIT, IBFJ, CEA, Fontenay-aux-Roses, France

[2]Vaccine Research Institute, Henri Mondor Hospital, Créteil, France

[3]Institut Pasteur, Unit on HIV, Inflammation and Persistence, Paris, France

[4]Institut Mondor de Recherche Biomédicale, INSERM U955, Créteil, France

Correspondence
Anne-Sophie Beignon, CEA, Université Paris Sud 11, INSERM U1184, Immunology of Viral Infections and Autoimmune Diseases, IDMIT, IBFJ, CEA, 18, route du Panorama, 92265 Fontenay-aux-Roses, France.
Email: anne-sophie.beignon@cea.fr

Abstract

A better understanding of innate responses induced by vaccination is critical for designing optimal vaccines. Here, we studied the diversity and dynamics of the NK cell compartment after prime-boost immunization with the modified vaccinia virus Ankara using cynomolgus macaques as a model. Mass cytometry was used to deeply characterize blood NK cells. The NK cell subphenotype composition was modified by the prime. Certain phenotypic changes induced by the prime were maintained over time and, as a result, the NK cell composition prior to boost differed from that before prime. The key phenotypic signature that distinguished NK cells responding to the boost from those responding to the prime included stronger expression of several cytotoxic, homing, and adhesion molecules, suggesting that NK cells at recall were functionally distinct. Our data reveal potential priming or imprinting of NK cells after the first vaccine injection. This study provides novel insights into prime-boost vaccination protocols that could be used to optimize future vaccines.

KEYWORDS

innate lymphoid immunity, mass cytometry, MVA, NHP, NK cells, prime-boost, vaccination, transcriptomics

1 | INTRODUCTION

A better understanding of the early events following vaccination is critical for identifying key biomarkers and mechanisms involved in the subsequent establishment of immune memory to optimize future vaccines.[1] This requires extensive characterization of the vaccine-induced innate immune response.

NK cells are innate lymphoid cells that can constitutively kill cells carrying an abnormal MHC signature, via interactions of activating and inhibitory receptors between NK cells and their targets.[2–4] The wide diversity of the NK cell receptor repertoire implies a large range of potential NK cell subpopulations.[5] NK cells exhibit numerous functions other than cytotoxicity, including modulation of the behavior of other innate and adaptive immune cell populations, such as through cross-talk with dendritic cells (DCs) or cytokine production.[6–10] In particular, NK cells strongly interact with DCs, resulting in the activation of both cell types.[11,12] Also, NK cells were shown to orientate the B cell response and the underlying affinity maturation via the restriction of follicular helper T cells, a feature that is key in the generation of broadly neutralizing antibodies.[13] NK cell functions are influenced by vaccination and infection.[14,15] In addition, recent findings in mice, macaques, and humans indicate that NK cells show adaptive-like features.[16–19] However, it is not yet fully clear how these findings can be exploited to

Abbreviations: CBC, complete blood count; DC, dendritic cell; LASSO, least absolute shrinkage and selection operator; LDA, linear discriminant analysis; MCMV, mouse cytomegalovirus; MSI, mean signal intensity; MVA, modified vaccinia virus Ankara; NHP, nonhuman primates; SPADE, spanning-tree progression analyses of density-normalized events

Received: 15 October 2018 | Revised: 14 February 2019 | Accepted: 15 February 2019

 ©2019 Society for Leukocyte Biology

improve the immunogenicity and protective efficacy of vaccines.[20,21] More studies on vaccine-induced NK cell immunity are thus admittedly required for improving vaccine design.

Modified vaccinia virus Ankara (MVA) is an attenuated vaccine derived from vaccinia virus, first developed as a vaccine against smallpox, which now serves as the vector for many recombinant vaccine candidates because of its capacity to induce strong and long-lasting immunity.[22] MVA is known to activate NK cells in mouse bone marrow and spleen, where it induces NK cell proliferation,[23] as well as in lymph nodes, where NK cells accumulate via CXCR3 signaling after being sensed by macrophages. Such recruitment is crucial for the induction of Th1 responses.[24] Moreover, the vaccine we used (MVA HIV B) was reported to prime human NK cells via NK-DC cross-talk in vitro.[25] Other studies in mice reported that NK cells are recruited to tissues in response to MVA-induced CCL2 (MCP-1) expression by macrophages.[26] We previously reported a difference in the level of CCL2 in the blood of macaques after an MVA boost relative to prime.[27] These and other studies show that MVA modulates NK cell activity and trafficking. They moreover suggest an important contribution of NK cells to MVA-induced immunity.

Nonhuman primates (NHP) are an important animal model in vaccinology, given their close immune proximity with humans, including innate immunity.[28] Immune responses in macaques to human vaccine injection are highly predictive of vaccine immunogenicity in humans. This is particularly true for MVA.[29] Human NK cells are usually subdivided based on CD56 and CD16 expression, whereas most NK cells from macaques are CD8α^+ CD56$^-$.[30] In addition, both human and macaque NK cells express NKp46, but in macaques, NKp46 may not be expressed by all NK cell subpopulations.[28,31] Nevertheless, close phenotypic analogies have been found between macaque and human NK cell subpopulations, and functional studies have revealed similar behavior in both species.[32–35]

We previously uncovered the phenotypic complexity and diversity of innate myeloid cells in the blood and the impact of vaccinations on the dynamics of their subset composition by mass cytometry[27] in cynomolgus macaques immunized with a recombinant MVA HIV-B. We used the very same animals and a similar analytical workflow, but a 31-marker mass cytometry antibody panel dedicated to the analysis of NK cells, to determine the phenotype of blood NK cell subpopulations, as well as their diversity and evolution throughout the vaccination process.

We demonstrated a high phenotypic diversity within the blood NK cell compartment in macaques. Importantly, the study reveals the induction of changes within the NK cell subphenotype composition by the prime, some of which were maintained over time. Hence, the NK cells present at recall were different from those present at baseline. The key phenotypic signature discriminating NK cells responding to boost from those responding to prime was identified and included stronger expression of several cytotoxic, homing, and adhesion molecules.

This study has important implications for understanding the role of NK cells in vaccine-induced responses, as well as for the optimization of vaccine protocols.

2 | MATERIALS AND METHODS

2.1 | Ethics statement

The experimental protocols were approved by the ethics committee "Comité d'éthique en expérimentation animale n°44" under the reference 2015031314518254.02 (APAFIS#319) for the longitudinal analysis of the MVA-induced response, and 2015062215324227v1 (APAFIS#891) when comparing MVA and buffer injections, and the "Ministère de l'Education Nationale, de l'Enseignement Supérieur et de la Recherche" (France). Animals were handled by veterinary staff in accordance with national regulations (CEA Permit Number A 92-32-02) and the European Directive (2010/63, recommendation No. 9) and in compliance with the Standards for the Humane Care and Use of Laboratory Animals of the Office for Laboratory Animal Welfare (OLAW, USA) under OLAW Assurance number #A5826-01.

2.2 | Experimental design

Five male adult cynomolgus macaques, originating from Mauritius and identified as BB078, BB231, BC641, BD619, and BD620, were housed individually. Before inclusion in the study, they were tested to be negative for SIV, herpesvirus B, filovirus, STLV-1, SRV-1, SRV-2, measles virus, hepatitis B Ag, and antibodies. Regarding CMV, BB078, BB231, and BC641 were seropositive, whereas BD620 was seronegative. Animals were captive-born (first generation, F1), 7–8-year-old and weighed 8.2–10.7 kg at the beginning of the study.

Without prior selection, unbiased distribution of MHC haplotype was observed in our group of animals, with animals carrying 1 of the complete 7 common haplotypes (with H1, H2, and H3 being the most common), or recombinants, and none of them being homozygous, or matching with one another for an entire MHC haplotype.

Animals were inoculated subcutaneously with 4×10^8 PFU of the ANRS MVA HIV-B vaccine (MVATG17401; Transgene, Illkirch-Graffenstaden, France),[36] encoding HIV-Gag (amino acids 1–519), Pol (amino acids 172–219, 325–383, and 461–519), and Nef (amino acids 66–147 and 182–206) proteins, as previously described.[27,37] Animals were immunized 2 months apart following a homologous prime-boost strategy.

For comparison of buffer and MVA injection, 6 macaques received a subcutaneous injection with a buffer containing 10 mM Tris-HCl, saccharose 5% (w/v), 10 mM NaGlu, 50 mM NaCl, pH8.0. One month later, they were inoculated with 4×10^8 PFU of the ANRS MVA HIV-B vaccine. Animals were 2–5-year-old and weighed 4.9 to 6.7 kg. Without prior selection, unbiased distribution of MHC haplotype was observed in this control group of animals, with some animals carrying 1 of the complete 7 common haplotypes or recombinants, and none of them being homozygous or matching with one another for an entire MHC haplotype.

Blood was collected in EDTA tubes for complete blood count (CBC) and whole blood flow cytometry, lithium-heparin tubes for whole blood mass cytometry analysis, and heparin cell preparation tube (CPT) (Becton Dickinson, Franklin Lakes, USA) for PBMC isolation.

2.3 | Sample preparation

Fixed leukocytes were prepared for mass cytometry using a previously described cell fixation protocol,[27,38,39] which allows the recovery of all leukocytes, including granulocytes, from lithium-heparin whole blood. Briefly, 1 mL of blood was incubated with a fixation buffer containing formaldehyde and glycerol for 10 min at 4°C. After centrifugation, erythrocytes were lysed in 10 mL milli-Q water at room temperature for 20 min. Cells were then washed in 1× DPBS and stored at −80°C at a final concentration of 15×10^6 cells/mL in the fixation mixture. Note that cells were fixed extemporaneously without restimulation ex vivo.

PBMCs were prepared for transcriptome analysis. Blood was collected using CPT tubes. After centrifugation at 1200 × *g* for 30 min at room temperature, PBMCs were isolated, and remaining contaminating red blood cells, if any, were lysed with ACK lysis buffer (Thermo Fisher Scientific, Waltham, USA). PBMCs were then washed in complete culture medium composed of RPMI-1640 (Invitrogen, Carlsbad, USA) supplemented with 10% heat-inactivated FCS (Eurobio, Courtaboeuf, France) and 1% penicillin-streptomycin/neomycin (Thermo Fisher Scientific, Waltham, USA).

2.4 | Cell staining and acquisition

Fixed leukocyte staining and acquisition protocols were identical to those previously described.[27] The 31-marker antibody panel used in the present study is described in Table 1. A number of classic NK cell receptors and other markers of interest[6,40] could not be included at the time of the study due to lack of reactivity of the tested antibody clones with fixed macaque leukocytes (CD27: clones O323 and LG-7F9; NKp80: clones 4A4.D10 and 5D12; NKp30: clone AF29-4D12; CD117: clone 104D2; NKp46: clone BAB281; CX3CR1: clone 2A9-1; CXCR3: clone 1C6; CD122: clone Tu27; CD158a: clone HP-3E4; and CD161: clone DX12).

2.5 | Data processing and event selection

FCS files were normalized with the MATLAB normalizer from Rachel Finck *et al.*[41] Replicates were concatenated using the tool from Cytobank (Mountain View, USA). Leukocytes were gated based on event length, iridium content, and exclusion of nonspecifically stained $CD66^+CD3^+$ eosinophils.[27,39]

2.6 | CBC and cell population count

CBCs were performed using blood collected in EDTA with the HmX instrument (Beckman Coulter). The absolute number of cells in each sample for a given cell population was computed as follows: *N* = the absolute number of leukocytes (expressed per μL of blood) × the number of cells in the population detected by CyTOF/total number of leukocytes (excluding $CD3^+CD66^+$ cells) detected by CyTOF (given in Table 2).

2.7 | Identification of cell populations

The spanning-tree progression analyses of density-normalized events (SPADE)[42] algorithm was performed on the whole data set of samples from macaques BB078, BB231, BC641, and BD620 to automatically identify cell populations displaying similar expression levels for the given markers used for clustering: CD66abce, HLA-DR, CD3, CD107a, CD8, CD45, granzyme B, CD56, CD62L, CD4, CD11a, CD2, CD7, NKG2D, CD11c, CD69, CD25, CD16, CCR5, CXCR4, CD14, perforin, NKG2A/C, CD20, and CCR7. Prior to clustering, we performed random pre-downsampling of 50,000 cells (corresponding to the highest number of cells contained in all samples) to avoid bias in the analysis toward samples with more cells than others (Table 2). The quality of the SPADE clustering, defined as a narrow and unimodal distribution for each marker in all cell clusters and NK cell clusters, was assessed using the SPADEVizR R package we developed.[43]

Based on these quality control measurements, SPADE was parameterized to identify 900 clusters using a downsampling of 20%,

TABLE 1 Antibody panel

Metal	Marker	Clone	Surface	Intracellular
141Pr	CD66abce	TET2	●	
142Nd	HLA-DR	L243	●	
143Nd	CD3	SP34.2	●	
144Nd	CD107a	H4A3	●	
145Nd	CD8	RPAT8	●	
146Nd	CD45	D058-1283	●	
147Sm	IL-4	7A3-3		●
148Nd	Granzyme B	GB11		●
149Sm	CD56	NCAM16.2	●	
150Nd	CD62L	SK11	●	
152Sm	CD4	L200	●	
153Eu	CD11a	HI111	●	
154Sm	CD2	RPA2.10	●	
155Gd	CD7	M-T701	●	
156Gd	MIP-1β	D21-1351		●
159Tb	TNFα	MAb11		●
160Gd	Ki-67	B56		●
161Dy	NKG2D	1D11	●	
162Dy	CD11c	3.9	●	
164Dy	CD69	FN50	●	
165Ho	IFNγ	B27		●
166Er	CD25	4e 3	●	
167Er	CD16	3G8	●	
168Er	CCR5	3A9	●	
169Tm	CXCR4	12G5	●	
170Er	CD14	M5E2	●	
171Yb	Perforin	Pf-344		●
172Yb	NKG2A/C[a]	Z199	●	
174Yb	CD20	2H7	●	
175Lu	CCR7	G043H7	●	
176Lu	IL-10	JES3-9D7		●

Targeted markers, clones, and metals are shown. The right columns indicate whether the staining was extra- or intracellular.
[a]The antibody clone Z199 recognizes both NKG2A and NKG2C.

TABLE 2 Cells acquired with the CyTOF

	BB078	BB231	BC641	BD620
D-19PP	76,557	60,206	60,143	52,082
H0PP	74,607	93,135	na	67,358
H3PP	128,251	109,159	91,420	72,772
H6PP	124,104	161,898	128,497	66,482
D1PP	117,081	154,166	110,928	103,526
D3PP	79,789	81,863	76,958	na
D14PP	116,972	108,706	124,386	86,044
H0PB	135,810	140,496	na	92,991
H3PB	179,476	208,479	61,579	na
H6PB	177,204	222,968	196,870	118,859
D1PB	257,189	167,840	243,434	116,967
D3PB	72,879	130,925	na	95,656

For each sample, the number of leukocytes detected by the CyTOF (after exclusion of double-positive $CD3^+CD66^+$ eosinophils) is indicated. Not available samples are indicated na.

leading to 77.44% of all clusters with unimodal (Hartigan's dip test, $P \leq 0.05$) and narrow distribution (IQR ≤ 2) of all markers. Most of the nonunimodal distribution was attributable to perforin (154 clusters of 900 [17.11%]).

Among NK cell clusters identified on the SPADE tree, based on CD3 and CD8 expression, 66.67% (22 of 33) had a unimodal and narrow distribution for all markers. Nonunimodal or wide distribution was not associated with a particular marker; at worst, CD2 and CD16 expression was nonunimodal or wide for 4 of 33 clusters (12.12%) (Table 3).

Two sets of baseline samples were available: 19 days before the prime (BPD19) and just before the prime, coded 0 hour post-prime (H0PP) in our nomenclature. Only BPD19 samples (available for the 4 macaques) were used for SPADE analysis to avoid biasing the SPADE analysis toward baseline samples, because NK cells were more numerous before than early after immunization. H0PP samples (only available for 3 of 4 animals) were upsampled into the SPADE analysis, using the closest neighborhood method. Briefly, cells from H0PP samples were assigned to the cluster of its closest cell neighbor within the SPADE analysis. The neighborhood definition was based on the SPADE clustering markers. The closest neighbors were found using the FNN R package (available at https://CRAN.R-project.org/package=FNN) and the kd-tree approach.

Samples from macaque BD619 were not included in this SPADE analysis because only H3PP, H6PP, D1PP, and D1PB samples were available. Indeed, samples from this animal would have been underrepresented among the samples from the other animals, and they could have biased the clustering analysis toward early modification of the NK subphenotype composition. Nevertheless, BD619 samples were mapped afterward onto the SPADE tree for phenotypic characterization based on the same closest neighbor approach used to map H0PP baseline samples.

We directly identified blood NK cells on the SPADE tree based on CD3 and CD8 expression, rather than by manual gating followed by SPADE analysis of the NK cells to avoid a bias in the manual gating of $CD3^-$ $CD8^+$ events and contamination with $CD66^{low}$ neutrophils, which displayed a low background signal in all channels including CD8.

TABLE 3 Number and percentage of nonuniform NK cell clusters

Markers	Number of nonuniform NK cell clusters	Percentage of nonuniform NK cell clusters	ID of nonuniform NK cell clusters
CD2	4	12	582, 739, 788, 892
CD16	4	12	122, 380, 721, 788
Perforin	3	9	723, 757, 819
CD4	1	3	582
CD7	1	3	567
HLA-DR	1	3	567
NKG2A/C	1	3	892
CCR5	0	0	—
CCR7	0	0	—
CD3	0	0	—
CD8	0	0	—
CD11a	0	0	—
CD11c	0	0	—
CD14	0	0	—
CD20	0	0	—
CD25	0	0	—
CD45	0	0	—
CD66abce	0	0	—
CD62L	0	0	—
CD69	0	0	—
CD107a	0	0	—
CXCR4	0	0	—
Granzyme B	0	0	—
NKG2D	0	0	—

The number, percentage, and ID of NK cell clusters that do not reach the condition of uniformity are shown.

2.8 | Categorical heat map representation of NK cell clusters' phenotypes

The median expression among all samples was used to generate the categorical heat map using SPADEVizR.[43] The range of marker expression was divided into 5 categories between the 5th and the 95th percentiles to define the cell cluster phenotype. Samples containing fewer than 10 cells were removed from the median computation. Hierarchical clustering, represented by the cluster and marker dendrograms in the heat map, was performed using the Euclidean metric and the ward.D linkage method. The cluster dendrogram was used to define phenotypic families.

2.9 | LASSO-LDA model to classify post-prime and post-boost NK cell immune profiles

The classification of post-prime (PP) and post-boost (PB) NK cell immune profiles was performed using a combination of the least

absolute shrinkage and selection operator (LASSO) and linear discriminant analysis (LDA) methods. The LASSO method was based on the lars R package (available at https://CRAN.R-project.org/package=lars). Abundance profiles of phenotypic families were centered and reduced. Model validity was assessed through the leave-one-out cross-validation method. The best configuration was chosen using the elbow criterion. Essentially, the minimum number of phenotypic families was chosen such that adding more phenotypic families did not improve the model. Graphically, this corresponds to the number of phenotypic families for which a break in slope (an "elbow") is observed when plotting the mean square error of the model as a function of the number of phenotypic families used (Supplemental Fig. S5B). The LDA method was based on the MASS R package (available at https://CRAN.R-project.org/package=MASS). Marker expression density distributions were compared using the CytoCompare R package[44] based on the Kolmogorov-Smirnov distance.

2.10 | Validation of the LASSO-LDA model

The LASSO-LDA classifier generated using BB078, BB231, BC641, and BD620 samples was used to classify BD619 samples and validate the model. Cell cluster abundances from BD619 samples were centered and reduced with the abundance of the 4 other animals.

2.11 | RNA extraction and gene-expression profiling

PBMCs were cultured overnight at 2.5×10^6 PBMCs/well in U-bottom 96-well plates (BD Falcon) in duplicate. PBMCs were recovered and lysed in 350 μL of RLT Plus buffer (Qiagen, Hilden, Germany) with 1% of mercaptoethanol. RNA was then purified using the RNeasy Plus Micro Kit (Qiagen, Hilden, Germany). Purified RNA was quantified using an ND-8000 spectrophotometer (NanoDrop Technologies, Fisher Scientific, Illkirch, France) and the integrity was verified on a 2100 BioAnalyzer (Agilent Technologies, Massy, France). cDNA was synthesized and biotin labeled using Ambion Illumina TotalPrep RNA Amplification kits (Applied Biosystem/Ambion, Saint-Aubin, France). Labeled cRNA was hybridized to Illumina Human HT-12V4 BeadChips, previously successfully used to analyze cynomolgus macaque whole genome.[45,46] All steps were performed following the manufacturers' protocols.

2.12 | Transcriptomic analysis

Transcriptomic signals were background corrected and quantile normalized using the limma R package (available at https://bioconductor.org/packages/release/bioc/html/limma.html).

We identified genes associated with NK cell abundance (which is relatively low among PBMCs) by performing a two-step analysis approach. First, genes for which the expression correlated with total NK cell abundance (Pearson correlation, $|R| \geq 0.65$ and $P \leq 0.05$) were analyzed using the STRING database[47] to define interaction networks.

Transcriptomic data were expressed as fluorescence intensity (resulting from DNA probe hybridization) per 2.5×10^6 PBMCs. The percentage of NK cells among PBMCs was used for the correlation between transcript expressions and NK cell abundances. The number of PBMC in each leukocyte sample was estimated in our mass cytometry analysis by excluding $CD66^+$ cells. Thus, the percentage of NK cells among PBMCs was defined as the number of $CD3^-$ $CD8^+$ NK cells detected in the CyTOF analysis divided by the number of $CD66^-$ leukocytes identified in the CyTOF analysis multiplied by 100. The Pearson coefficient of correlation was used to quantify the association based on log-transformed data. The transcriptomic time point D57PP was associated with the mass cytometry time point H0PB (corresponding to D58PP). In addition, early transcriptomic time points (H3, H6, and D1) were missing for both immunizations. The transcriptomic time points used were D-19PP, D3PP, D57PP, and D3PB.

Second, genes having interactions with at least one other gene were selected, and a functional enrichment analysis was performed using Ingenuity Pathways Analysis software (Ingenuity Systems, Inc., IPA, Redwood City, USA) to further decipher the gene signature. IPA maps each gene identifier to its corresponding molecule in the Ingenuity Pathways Knowledge Base. For all analyses, P values generated by Fisher's exact test were adjusted by Benjamini-Hochberg Multiple Testing.

2.13 | Correlation between NK cell and innate myeloid cell dynamics

The Spearman correlation coefficient between the abundance (number of cells per mL) of blood NK cell phenotypic families and the abundance of blood innate myeloid cell kinetic families (groups of phenotypic families sharing similar dynamics as previously defined[27]) was computed. The correlation was considered significant when $|R| \geq 0.6$ and $P \leq 0.05$.

2.14 | Area under the curve

Areas under the curve (AUC) were calculated as the cumulative sum of concentrations of the population between H0 and D3 (either after prime or after boost). PP and PB AUC were compared using the permutation test from the exactRankTests R package (available at https://cran.r-project.org/web/packages/exactRankTests/index.html).

2.15 | Interindividual variability

The interindividual variability in terms of phenotypic composition was quantified as the percentage of NK cells that are not classified in the same phenotypic families between 2 animals.

2.16 | Flow cytometry

Flow cytometry staining was used to identify NK cells in a control group of 6 macaques used to assess whether the effect of immunizations on NK cell number was specific of MVA subcutaneous injection or could be induced by the sole buffer subcutaneous injection or no injection (only anesthetic). For each sample, 100 μL of blood was stained during 30 min with 90 μL of mix of antibodies diluted in BD Horizon stained buffer (BD Biosciences, Franklin Lakes, USA) containing CD123 (BD Biosciences, Franklin Lakes, USA, clone 7G3),

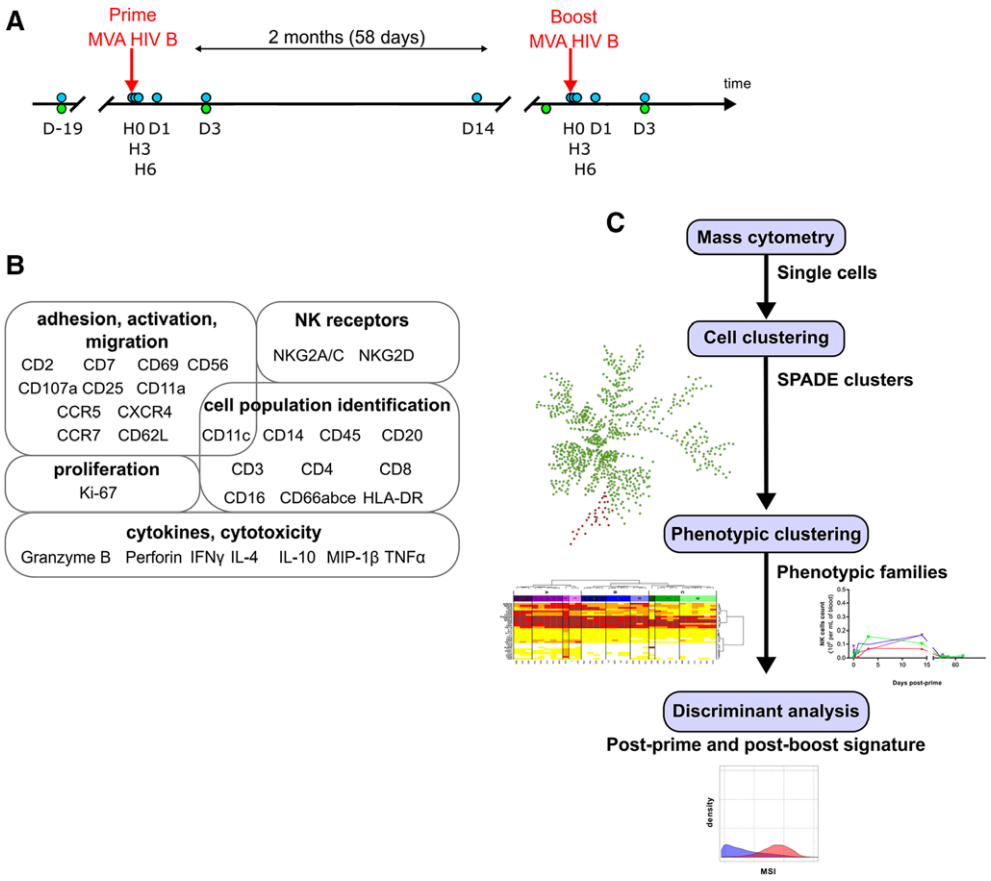

FIGURE 1 **Experimental design and analysis strategy**. The experimental approach, including (A) the vaccine schedule, (B) the 31-marker antibody panel, and (C) the analysis pipeline, is shown. Five cynomolgus macaques were subcutaneously immunized with MVA HIV B vaccine (4×10^8 PFU) twice, 2 months apart. Blood samples were collected at the indicated time points, hours (H) or days (D), PP, and PB, for mass cytometry (blue dots) or transcriptomic experiments (green dots). FCS files retrieved from mass cytometry were entered into the SPADE algorithm after exclusion of background events, dead cells, and nonspecifically stained putative eosinophils, to cluster leukocytes based on 25 clustering markers and identify NK cell clusters. NK cell clusters were further clustered into phenotypic families whose kinetics were analyzed. Prime vs. boost phenotypic signatures were eventually determined using the LASSO-LDA approach

HLA-DR (BD Biosciences, Franklin Lakes, USA, clone G46-6), CD163 (BD Biosciences, Franklin Lakes, USA, clone GHI/61), CD11c (BioLegend, San Diego, CA, USA clone 3.9), CD45 (BD Biosciences, Franklin Lakes, USA, clone DO58-1283), CD66 (Miltenyi Biotec, Bergisch Gladbach, Germany, clone TET2), CD3 (BD Biosciences, Franklin Lakes, USA, clone SP34-2), CD20 (BD Biosciences, Franklin Lakes, USA, clone 2H7), CD8 (BD Biosciences, Franklin Lakes, USA, clone RPA-T8), CD11b (Beckman Coulter, Brea, USA, clone Bear 1), CD14 (BD Biosciences, Franklin Lakes, USA, Clone M5E2), CD33 (Miltenyi Biotec, Bergisch Gladbach, Germany, clone AC104.3E3), CD16 (Beckman Coulter, Brea, USA, 3G8), and NKG2A (Beckman Coulter, Brea, USA, clone Z199), and then cells were fixed and red blood cells were removed with 1 mL of BD FACs Lysing (BD Biosciences, Franklin Lakes, USA) during 10 minutes at room temperature and washed twice using PBS. Samples were acquired with a BD LSRFortessa (BD Biosciences, Franklin Lakes, USA).

NK cells were gated as $CD66^-$ $CD3^-$ $CD20^-$ $CD14^-$ $CD8^+$ cells using FlowJo 9 software (FlowJo, Ashland, USA). The absolute count numbers were calculated as the percentage of NK cells among all cells × leukocyte count (CBC).

2.17 | Data availability

Gated cytometry profiles are available on the FlowRepository database[48] under accession number FR-FCM-ZYPY. Raw transcriptomic profiles are available on the EBI-ArrayExpress database[49] under accession number E-MTAB-7697. Main graphical representations and statistical results are available in an interactive format on the IDMIT data dissemination platform accessible at http://data.idmitcenter.fr/MVA-innate-NK/.

3 | RESULTS

3.1 | Total NK cell kinetics do not differ between prime and boost

We vaccinated 4 adult male cynomolgus macaques with a recombinant MVA-based vaccine following the homologous prime-boost strategy described in Fig. 1A.[27,37] Blood samples were taken before and at various time points during the vaccination time course and fixed extemporaneously without ex vivo restimulation with the vaccine. All samples

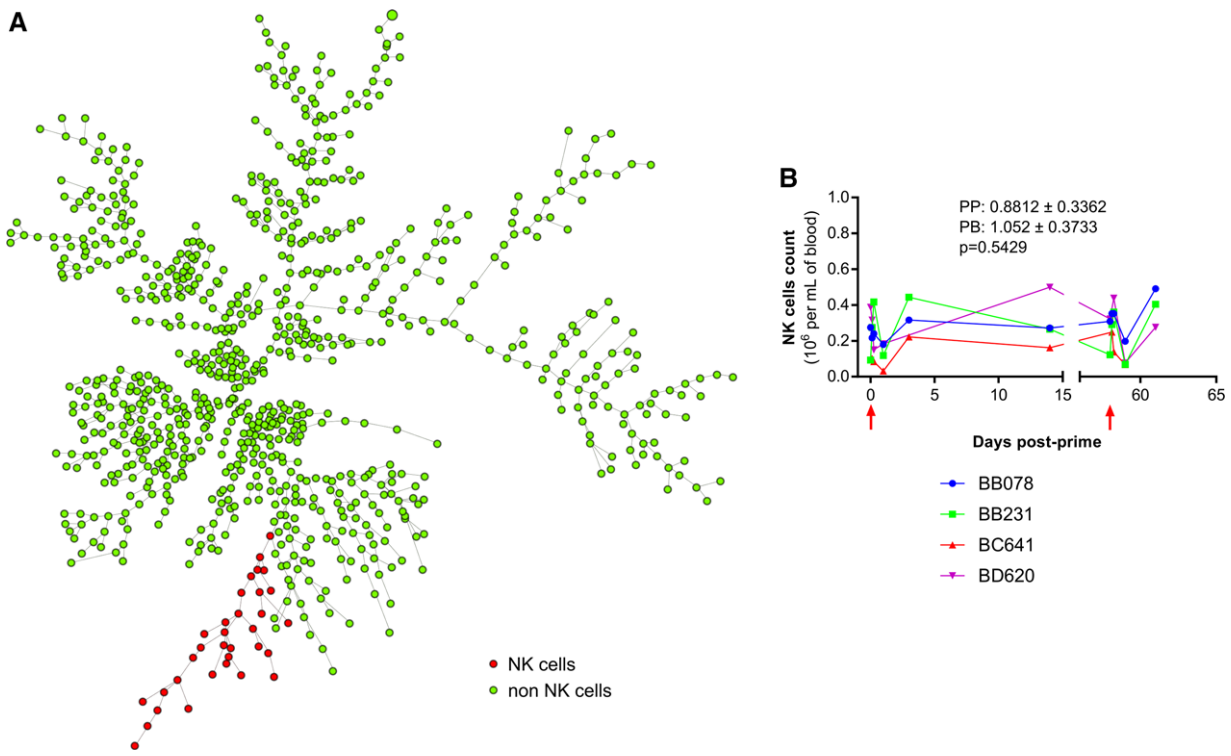

FIGURE 2 **Identification of blood NK cells.** (A) The generated SPADE tree is shown. This analysis was built using all samples from the data set, except H0PP samples, which were later mapped onto the analysis. NK cell clusters ($CD3^-$ $CD8^+$) are indicated in red. (B) The absolute number of total NK cells per individual animal at each time point is shown. Red arrows indicate MVA immunization. The mean AUC ± SD is indicated, as well as the *P* value, after comparison by the permutation test and considered statistically significant when $P \leq 0.05$

were stained with the antibody panel targeting markers of NK cell activation (e.g., CD25 and CD69), function (e.g., IFNγ, perforin, granzyme B, CD107a, and CD11a), and maturation (e.g., CD2, CD7, and CXCR4), described in Fig. 1B and detailed in Table 2. We then followed the analysis pipeline described in Fig. 1C. Preliminary analyses showed high interindividual variability in terms of NKG2A/C expression among NK cells, not associated with CMV serology (Supplemental Fig. S1).

First, we performed a SPADE analysis to identify cell populations based on the expression of the following markers: CD66abce, HLA-DR, CD3, CD107a, CD8, CD45, granzyme B, CD56, CD62L, CD4, CD11a, CD2, CD7, NKG2D, CD11c, CD69, CD25, CD16, CCR5, CXCR4, CD14, perforin, NKG2A/C, CD20, and CCR7. This strategy allowed the segregation of NK cells, defined classically for macaques as $CD3^-$ $CD8^+$ cells, from other leukocytes and into 33 cell clusters on a separate branch of the SPADE tree (Fig. 2A). Note that we notably excluded $CD66^+$ neutrophils, HLA-DR^+ $CD14^+$ monocytes, HLA-DR^+ $CD11c^+$ cDCs, $CD3^+$ T cells, and HLA-DR^+ $CD20^+$ B cells (Supplemental Fig. S2).

We analyzed the kinetics of all NK cell clusters in the blood throughout vaccination (Fig. 2B). As expected, the number of total NK cells in the blood was relatively low ($<0.5 \times 10^6$cells/mL for all time points). NK cell numbers were homogeneously affected by immunization in all animals. Indeed, NK cell numbers tended to decrease between 3 h (H3) and 6 h/1 day (H6-D1) post-immunization, both PP and PB. These changes in NK cell counts were likely to be MVA injection specific, as shown by 6 additional control animals (Supplemental Fig. S3). A high variability in terms of NK cell count was observed between baselines (untreated animals, before buffer injection, and before MVA injection) across the control animals (Supplemental Fig. S3A). Buffer injection did not induce a significant early decrease in total NK cell count ($P = 0.9839$) (Supplemental Fig. S3B), whereas MVA injection did ($P = 0.03697$) (Supplemental Fig. S3C).

This MVA-induced decrease in NK cell count likely corresponds to NK cell recruitment to either inflamed tissues or lymphoid organs, consistent with a previous study in mice describing the recruitment of NK cells to the draining lymph node within the first day after MVA injection.[24] There were no significant differences in the NK cell dynamics between the 2 immunizations based on the comparison of PP and PB AUCs.

To further complete the picture of the NK cell response at the whole compartment level, we analyzed the gene signature associated with NK cell number using microarrays on isolated PBMCs (Fig. 3A). There were numerous genes for which the expression correlated with NK cell abundance with a remarkably high number of gene interactions, among them, a cluster of NK cell-associated genes, such as activation/cytotoxic associated molecules (CD226, CD69, KLRK1 [NKG2D], granzyme B, and granzyme H),[50–53] as well as genes encoding proteins involved in these signaling pathways (notably ITGAL/CD11a and VAV3)[54] and the chemoattractant cytokine CCL27.[55]

Functional enrichment of this interacting network of genes confirmed a strong association with NK cells, which indicated that we were able to find an NK cell-associated signature within the PBMCs. More specifically, this gene signature was associated with NK cell/DC cross-talk, NK cell cytotoxic activity, and FcR-mediated phagocytosis.

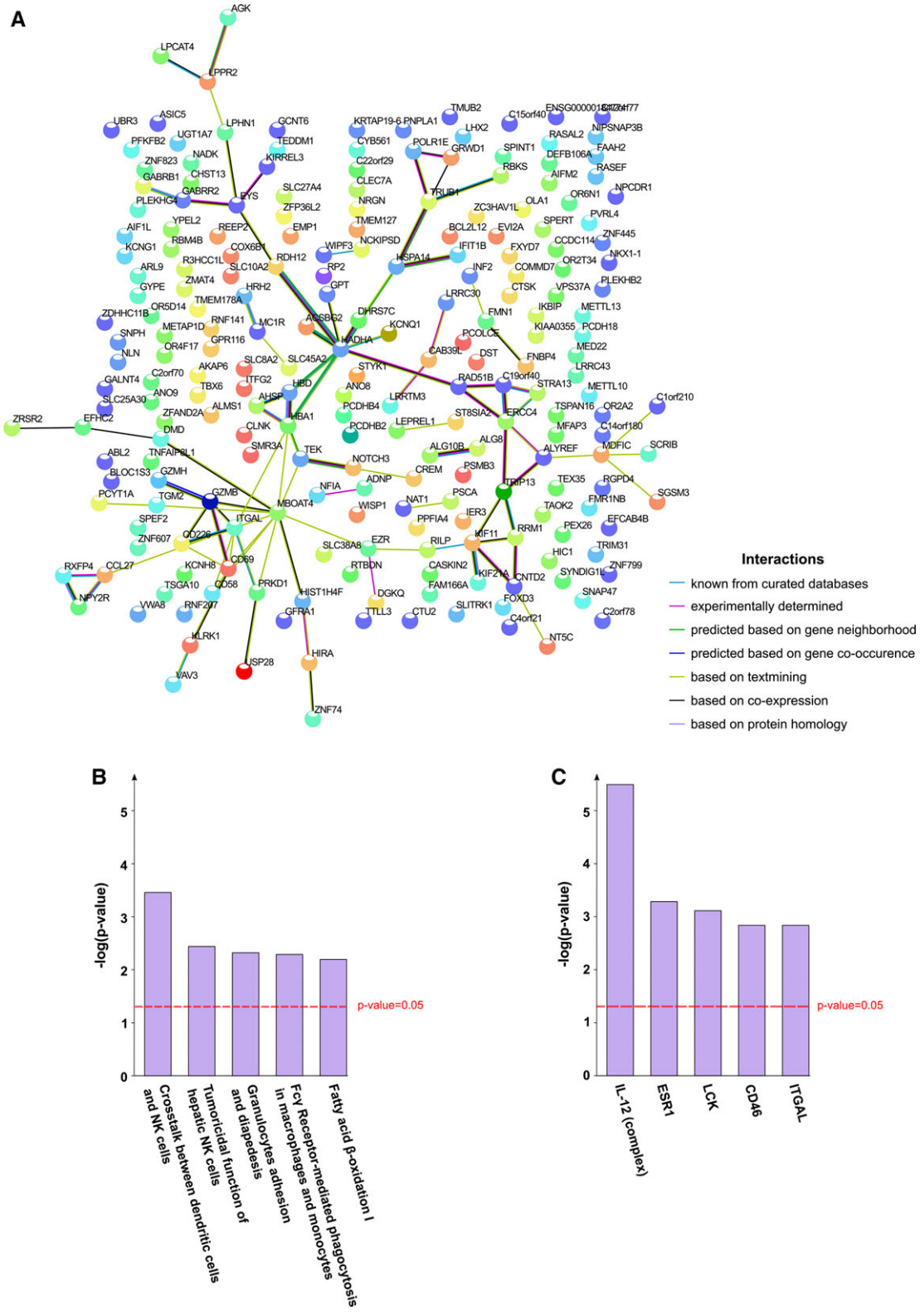

FIGURE 3 **NK cell-associated transcriptomic signature.** (A) Interactions among transcripts for which the expression correlated with NK cell abundance identified using the STRING database[47] ($|R| \geq 0.65, P \leq 0.05$). (B) Top 5 canonical pathways correlating with NK cell abundance identified using IPA (Ingenuity Systems, Inc.). (C) Top 5 upstream regulators correlating with NK cell abundance identified using IPA (Ingenuity Systems, Inc.)

To a lesser extent, this signature was associated with granulocyte diapedesis (a surprising signature, as only PBMC RNA was used) and fatty acid oxidation (Fig. 3B). Among regulators, the most statistically significant was the IL-12 complex (Fig. 3C), which is a well-known key cytokine in NK cell biology.[56] ESR1, LCK, CD46, and ITGAL/CD11a were also found to be engaged. ESR1, LCK, and ITGAL/CD11a are associated with NK cell cytotoxic activity,[54,57–59] whereas CD46 is associated with complement activity.[60]

We previously showed, with the very same animals, that IL-12 production was upregulated in blood neutrophils responding to the second MVA injection, as compared with those responding to the first MVA inoculation. IL-12 concentration in plasma did not differ between prime and boost though.[27] Thus, because no significant difference was found at the level of total NK cell number by contrast to IL-12 level in neutrophils, and because IL-12 signaling appeared correlated with NK cell number in blood, we further investigated whether differences could exist at a deeper phenotypic resolution of the NK cell compartment.

3.2 | The NK cell compartment displays numerous subphenotypes

We used high-dimensional analysis based on marker expression intensity to investigate potential changes in NK cell phenotype after immunization. The double clustering of markers and NK cell clusters resulted in a categorical heat map with a marker and cell cluster dendrogram. It facilitated the visualization of the phenotypes of all NK cell clusters at a glance (Fig. 4). On this heat map, marker expression was divided into 5 bins between the 5th and 95th percentiles of the distribution across the whole data set. This allowed us to qualify the expression of each marker for each cluster as very low, low, mid, high, or very high, according to the bin in which the cluster fell for the indicated marker.

The hierarchical clustering of markers represented in the marker dendrogram revealed 2 large groups of coexpressed markers, further subdivided into 4 subgroups (Fig. 4). One large group of coexpressed markers contained cytotoxic and maturation markers and comprised highly coexpressed markers among most NK cells (granzyme B, CD107a, NKG2A/C, CD8, CD7, CD45, and CD11a) in a first subgroup and highly/moderately coexpressed markers (perforin, NKG2D, CD16, CD2, CCR5, CD56, and CXCR4) in a second. The second large group contained, notably, several cytokine and chemokine receptors and consisted of moderately/weakly coexpressed markers (IL-10, Ki-67, MIP-1β, IL-4, TNFα, CD20, CD69, and CD11c) in a first subgroup and weakly/unexpressed markers (CD14, CD4, HLA-DR, CD25, CD62L, IFNγ, CCR7, CD66, and CD3) in a second.

The hierarchical clustering of NK cell clusters, represented in the cluster dendrogram, revealed 10 phenotypic NK cell families, arbitrarily numbered from 1 to 10, distributed within 3 superfamilies, named A to C (Fig. 4). Each phenotypic family contained NK cell clusters with similar phenotypes, and each superfamily was composed of proximal phenotypic families. Phenotypic families are likely to better correspond to biologically meaningful cell populations than cell clusters. Indeed, the number of leukocyte clusters chosen as an entry parameter in our SPADE analysis (900 cell clusters) was optimally defined to achieve a uniform and narrow expression of all clustering markers in a maximum number of leukocyte clusters. Admittedly, it could have resulted in a potentially artificially high number of NK cell clusters (33 NK cell clusters). The risk of overclustering was overcome by merging phenotypically similar NK cell clusters into phenotypic families.

Superfamily A (phenotypic families 5, 3, 8, and 1) consisted of NKG2D^{high} CD16^{high} CD107a^{high} CCR5^{high} NK cells. Superfamily B (phenotypic families 4, 2, and 6) consisted of NKG2D^{mid} CD16^{mid} CD107a^{high} CCR5^{mid} NK cells. Finally, superfamily C (phenotypic families 10, 7, and 9) contained NKG2D^{low} CD16^{low} CD107a^{mid} CCR5^{low} NK cells.

Beyond such wide phenotypic NK cell diversity, which underlined varying degrees of expression of cytotoxicity markers and likely past, ongoing, or future cytotoxicity, 2 phenotypic families (phenotypic families 1 and 4) in superfamilies A and B were CD2^{high}, suggesting higher activation ability toward antibody-coated pathogen/Ag binding. CD2 is a well-known NK cell activator,[61] which was shown to potentiate the CD16 signaling cascade in vivo in humans.[62] This action was later shown to be associated with CD58 engagement on infected cells by CD2^{+} NK cells in vitro.[63] Also, phenotypic family 9, within superfamily C, was the only one to be CD7^{mid} (all other NK clusters were CD7^{high}), likely related to a lower maturity. Indeed CD7 has been shown to be expressed on highly differentiated cytotoxic and cytokine-producing NK cells ex vivo in humans.[64] Moreover, 2 phenotypic families containing one single cluster displayed very peculiar phenotypes (Supplemental Fig. S4). Phenotypic family 8 was CD66^{high}, whereas other NK cell clusters were CD66$^{low/-}$, as expected. It may consist of activated NK cells that can be inhibited through CD66, as reported after homotypic CD66a interactions between melanoma and NK cells.[65] Phenotypic family 10 was HLA-DR^{high} granzyme B^{low} CD107a^{low} and may correspond to "NK DCs" observed in mouse tissues[66] and ex vivo in humans.[67]

3.3 | NK cell subphenotypes exhibit different kinetics

We then studied the dynamics of all identified NK cell phenotypic families (Fig. 5A), which, for some, contrasted with those of total NK cells (Fig. 2B). We identified distinct and complex patterns.

The phenotypic family 7 was more highly affected by the prime than the boost (AUC comparison, $P = 0.0286$).

By contrast, 2 phenotypic families (^{3} and ^{8}) were more highly affected by the boost than the prime (AUC comparison, $P = 0.057$ and 0.0286, respectively). In particular, family 3 showed a strong increase at H3PB compared with H3PP (P=0.0286).

The remaining 7 phenotypic families ($^{1,2,4-6,9}$, and ^{10}) displayed strong interindividual variability in their dynamics and various patterns. Phenotypic family 10 notably only showed a very low peak at D14PP. Still note that for phenotypic family 5, 3 animals of 4 showed a stronger increase in number PP than PB.

Although the number of total NK cells was low throughout vaccination and essentially transiently decreased (Fig. 2B), many NK cell subphenotypes (e.g., phenotypic families 7, 3, 5, 1, and 9) conversely showed an increase in absolute number for some time points (Fig. 5A).

We then determined the relative abundance of the phenotypic families within each animal for each time point (Fig. 5B). There was high interindividual diversity of the NK cell compartment relative to that of the innate myeloid cell compartment.[27] In addition, NK cell number and composition strongly differed between both baseline samples at D-19PP and H0PP, in the absence of any other experimental perturbation of the immune system (Supplemental Fig. S5). At baseline, prior to any immunization, there was high intraindividual variability in terms of cell number, with a difference of up to 0.8×10^{6} NK cells/mL

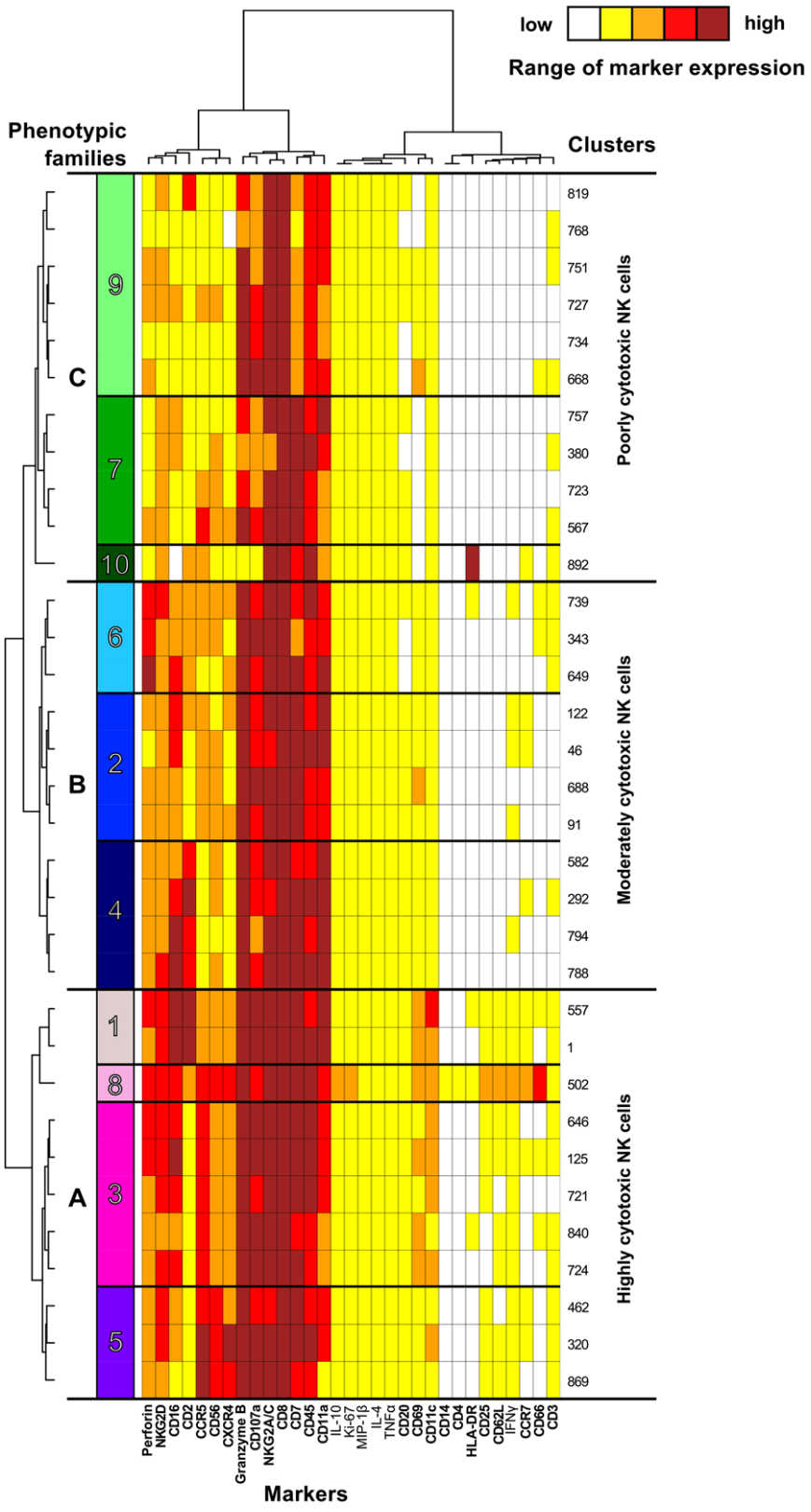

FIGURE 4 **Phenotypic heat map of NK cells.** Each line of the heat map corresponds to one cell cluster and each column to one marker. Marker expression is displayed according to phenotypical categorical bins, corresponding to the subdivision of marker range of expression in 5 categories between the 5th and 95th percentiles of expression (the color code is indicated). The marker and cluster dendrograms are shown on the top and left, respectively. The cluster dendrogram defined phenotypic families and superfamilies. Phenotypic families were randomly numbered and colored with different shades of the same color for each superfamily. Markers used as SPADE clustering makers are shown in bold

of blood between D19PP and H0PP (Supplemental Fig. S5). This is fully consistent with the results obtained on the 6 additional control animals (Supplemental Fig. S3A). To note, the phenotypic composition was remarkably stable within each animal between the 2 baselines (Supplemental Fig. S5).

Note that prior to any immunization, a high interindividual variability was observed in terms of the phenotypic composition of the NK cell compartment. Actually, on average 50 ± 6% of the NK cell compartment differs phenotypically between 2 animals (i.e.,50 ± 6% of NK cells were associated with distinct phenotypic families between

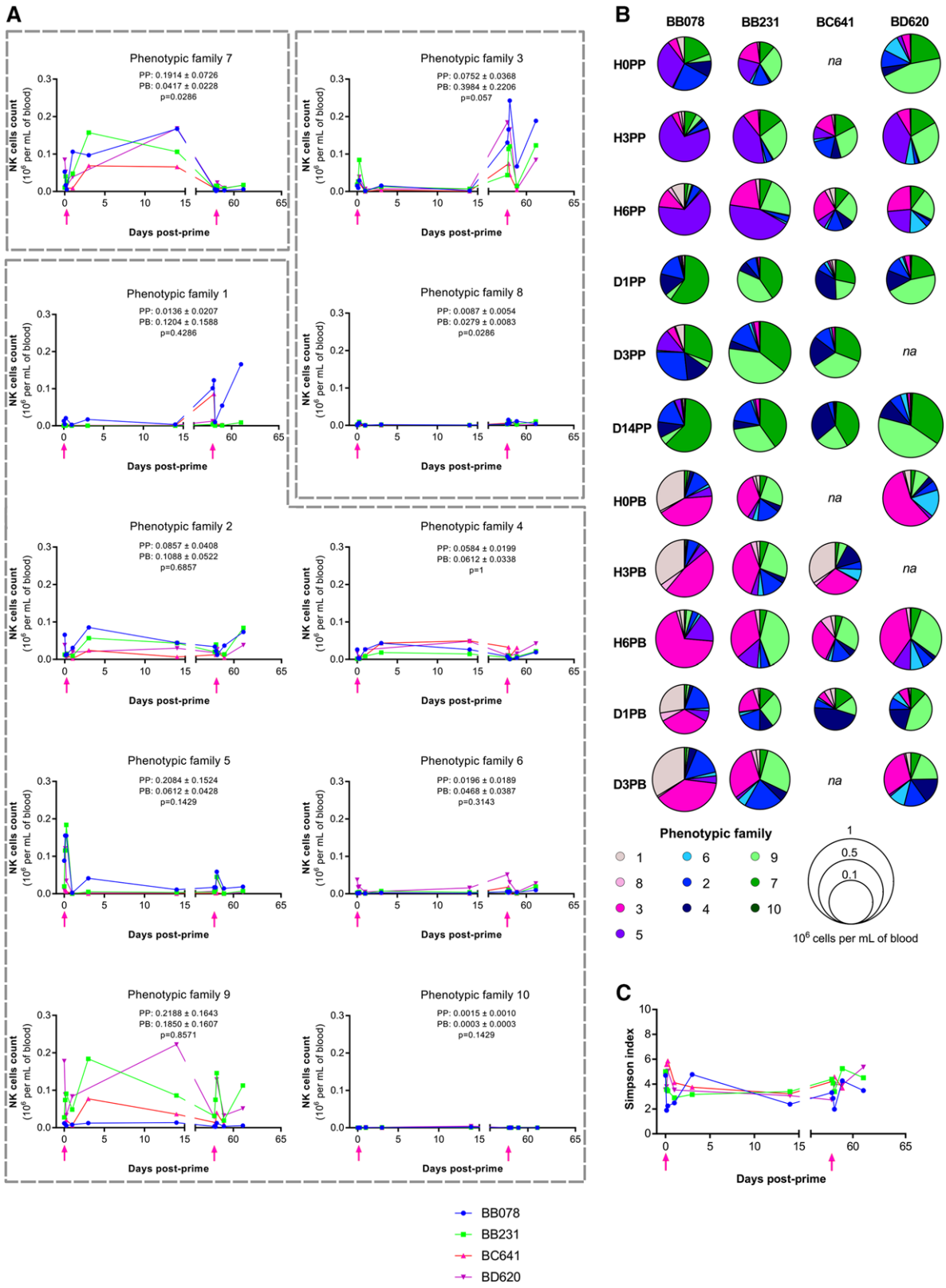

FIGURE 5 **Different enrichment of NK cells after each immunization.** (A) The individual abundance in the number of cells/μL of blood of each phenotypic family is shown over time. The mean AUC $\pm$ standard deviation and *P* value (permutation test) are shown, and the phenotypic families are grouped based on their profiles. (B) The composition of the phenotypic families is indicated over time for each time point and each animal. The size of the pie is proportional to the absolute count of total NK cells in the blood, as indicated. Pie slices correspond to phenotypic families and are color-coded as in Fig. 4. *na*, not available. (C) The inverse Simpson index, as a readout for diversity, is displayed for each animal over time. Each color represents a distinct animal

2 animals). Strikingly, the phenotypic composition of the NK cell compartment after immunization was far more similar between the different animals (32 ± 6% of difference between individuals at every other time point), indicating that immunization homogenizes the NK cell compartment composition.

The distribution of NK cell subphenotypes changed markedly throughout the prime, as early as H3PP, and dramatically between H6PP and D1PP. The major shift in the composition of the NK cell compartment remained relatively stable up to D14 (Fig. 5B). Further changes of the subphenotype composition occurred later, between D14PP and the boost (at D58PP = H0PB). This was not observed for innate myeloid cells, for which the shift occurred essentially between D14PP and the boost.[27] One explanation is that these subphenotypes correspond to newly generated immature NK cells arising from the bone marrow, whereas all NK cells expressing homing markers, such as CCR5, CCR7, CD62L, and CXCR4 (which is indeed the case for families 3, 5, and 8, which decreased in frequencies at these time points), were previously recruited to tissues. Consistent with this hypothesis, the major phenotypic families at these time points belonged to superfamily C of poorly cytotoxic NK cells (Fig. 4). In addition, this switch may also reflect the persistence of some poorly cytotoxic NK cells in the blood after vaccination, rather than a true increase in number or redistribution. For example, family 7 remained constant in number at D1PP but still became proportionally one of the most abundant families at this time point, because of the decrease in the numbers of the other NK cell populations (Fig. 5A and 5B).

Overall, this analysis demonstrated that the NK cell compartment was modified by the priming immunization, and the NK cell subphenotypes' composition was not similar at H0PB relative to that at baseline. Strikingly, NK cells were mainly phenotypically highly cytotoxic at H0PB (phenotypic families 3 and 8), compared with H0PP samples where most NK cells were poorly/moderately cytotoxic (Fig. 4 and Fig. 5B). Note that this phenotype modification occurred before the boosting immunization and is thus independent of the boost.

We finally analyzed the diversity and dynamics of the NK cell compartment using the Simpson index as a readout (Fig. 5C). The wide diversity of the NK cell receptor repertoire, for which each combination of NK cell receptors can virtually give rise to a new subset of NK cells, was recently uncovered.[5] However,the meaning of such NK cell diversity for vaccines is not yet understood. Admittedly, the lack of a larger set of inhibitory and activating NK receptors (which are difficult to analyze in NHP) in our antibody panel prevented us from directly addressing the issue of the NK cell repertoire, for which the diversity was previously shown to reflect immune experience.[68] Nonetheless, we were able to observe 2 distinct and complex kinetic patterns among our 4 animals (BB078 and BB231 vs. BC641 and BD620), but by no means did we detect a progressive increase in NK cell subphenotype diversity over time and after immunization.

Altogether, the mass cytometry analysis revealed that the prime induced the modification of the NK cell subphenotype composition in 2 main steps, at D1PP and between D14PP and the boost (D58PP). As a result of these phenotypic differences preexisting prior to the boost, the NK cell response differed between prime and boost.

3.4 | Key phenotypic signatures between the NK cell response to prime and boost

We then aimed to define the NK cell phenotypic families that discriminate the primary and secondary NK cell responses using an approach that combined LASSO and LDA methods.

We first used the LASSO method to determine the optimal number of phenotypic families that could account for PP and PB differences (Supplemental Fig. S6). Based on this analysis, we chose phenotypic families 3, 8, 7, 5, and 6 that were necessary and sufficiently informative to distinguish prime and boost samples through leave-one-out cross-validation (Supplemental Fig. S6). These 5 phenotypic families were then used to build the LDA classification (Fig. 6A and 6B). The classification of PP and PB samples was correct for 31 of 33 samples (94%) and showed that phenotypic families 5 and 7 were involved with the PP response, whereas phenotypic families 3, 6, and 8 were involved with the PB response.

We further determined the phenotypic differences that distinguished NK cells that responded to the prime from those responding to the boost. We examined the mean signal intensity (MSI) of prime-responding vs. boost-responding NK cells and identified 8 markers that differed in expression intensity between the 2 signatures (Fig. 6C and 6D): granzyme B, CD107a, perforin, CD69, CD66abce, CCR5, CD11c, and CD16. All were more highly expressed after the boost than the prime. To a lesser extent, CD11a was also more highly expressed after the boost than the prime (Fig. 6D). This suggests that NK cells involved with the PB immune response showed a more cytotoxic phenotype (including the ability for antibody-dependent cell cytotoxicity [ADCC] based on CD16 expression), associated with an increased ability to traffic to lymph nodes and inflamed tissues. Phenotypic family 5, which was involved in the PP response, also belonged to superfamily A of highly cytotoxic NK cells, together with phenotypic families 3 and 8 (Fig. 4). However, it displayed a higher CCR5 expression and lower levels of CD2, CD7, CD16, and CD11a than the PB highly cytotoxic NK cells from phenotypic families 3 and 8, suggesting a stronger ability to traffic to inflamed tissues, while simultaneously showing a less mature/activated phenotype. This observation is consistent with the fact that NK cells responding to the boost showed a more cytotoxic (and potentially more mature) phenotype in the blood than those responding to the prime.

3.5 | Validation of the phenotypic signature distinguishing NK responses to prime and boost

To validate the results and model obtained on samples from 4 animals, we used 4 samples from a fifth animal from the same cohort, macaque BD619, which was not included in the previous steps of the analysis. After associating each cell with the SPADE cluster it was the closest to, we were able to define the phenotypic composition of these samples with respect to our SPADE analysis (Fig. 7A). BD619 showed a phenotypic signature fairly consistent with the 4 animals used to build the model, with a high abundance of phenotypic families 7 and 9 at H3PP, H6PP, and D1PP, a high abundance of phenotypic families 2 and 4 at D1PP and D1PB, and high abundance of phenotypic family 3 at D1PB.

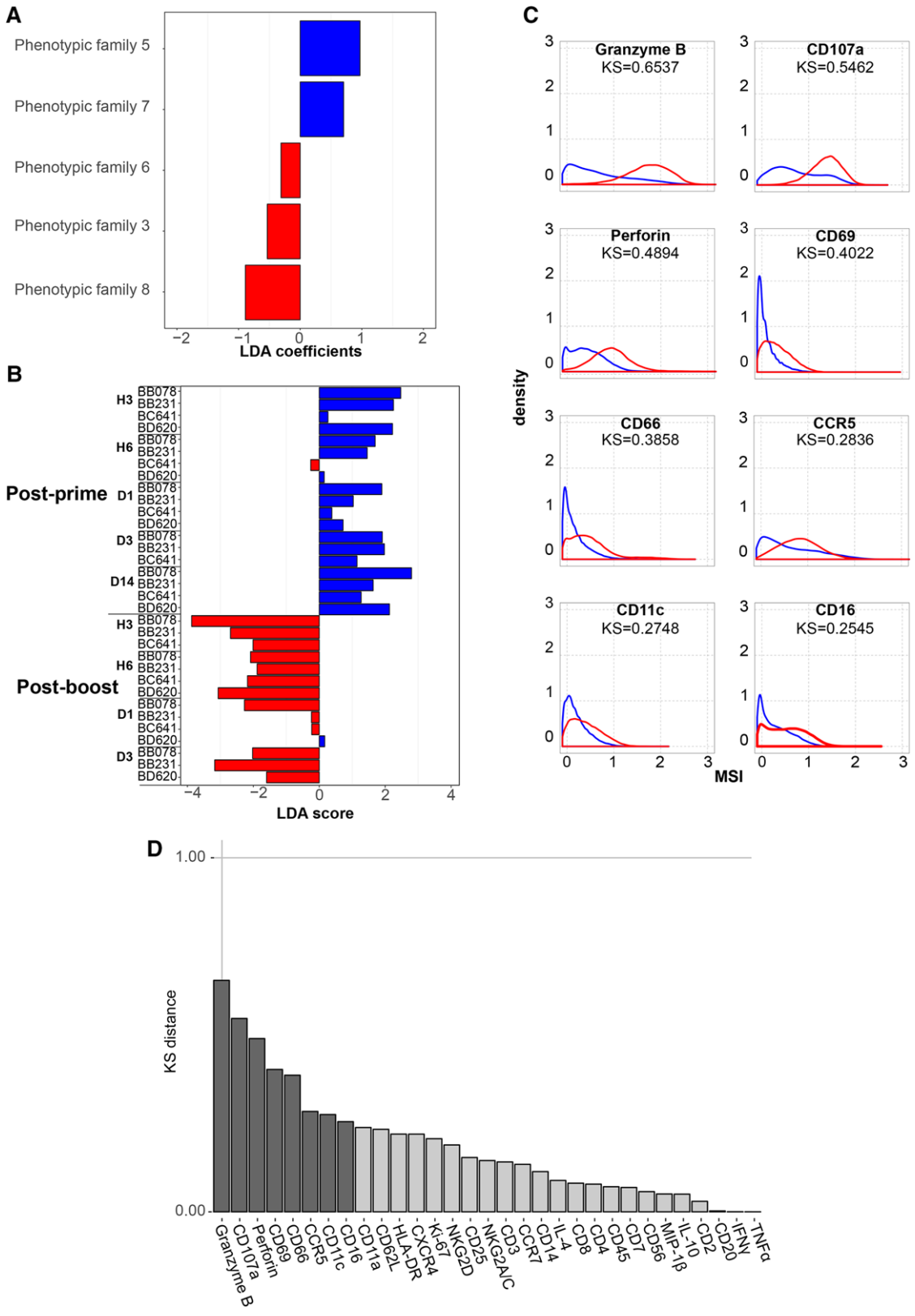

FIGURE 6 **Signature distinguishing the PP and PB NK cell response.** LDA was performed after LASSO regression to select the combination of phenotypic families that best discriminate between PP (blue, phenotypic families 5 and 7) and PB (red, phenotypic families 6, 3, and 8) samples. Note that the baseline samples (H0PP and H0PB) were not used for this analysis. (A) LDA coefficients and (B) LDA scores for each sample are shown. (C) MSI histograms for the 8 markers with the highest Kolmogorov-Smirnov distance between phenotypic families that best discriminate between the PP (blue) and the PB (red) responses as defined in A are displayed based on the merger of all samples and all time points. (D) The Kolmogorov-Smirnov distance of all markers, including the top 8 markers with the highest distance (bright gray vs. dark gray) between phenotypic families that best discriminate between the PP and the PB responses, is displayed

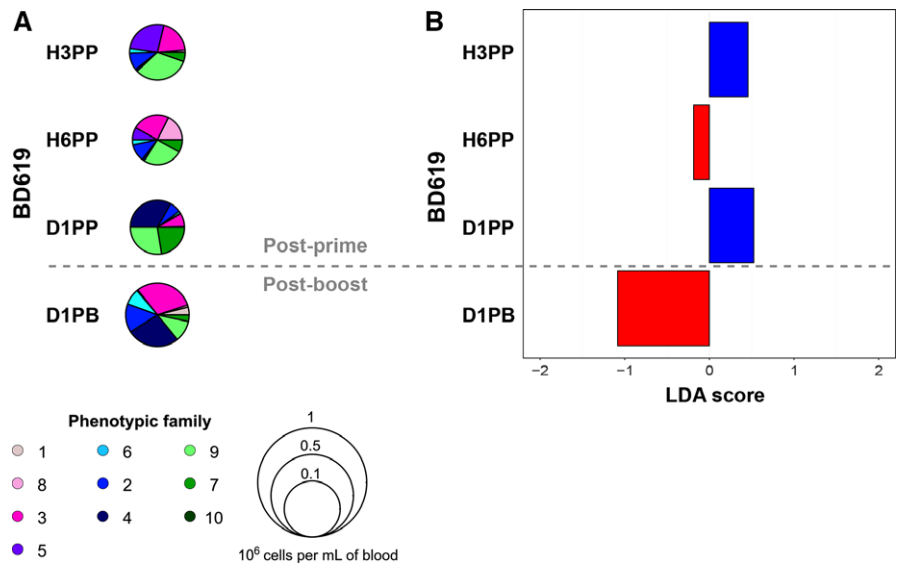

FIGURE 7 **Validation of the NK cell signature after immunization(s).** Samples from macaque BD619 were mapped into the existing SPADE tree to (A) define the phenotypic composition of the NK cells compartment of these samples, and (B) assess the quality of the LDA model using new samples in the model generation

We then applied the LDA classifier detailed in Fig. 6 on these new samples (Fig. 7B). Three samples (H3PP, D1PP, and D1PB) out of 4 were correctly classified. Interestingly, the sole error made was on H6PP (which obtained a low PB score), the time point for which the model already misclassified the BC641 sample. This misclassification is due to the relatively high abundance of family 8 at H6PP for these 2 animals, while family 8 is overall more enriched after the boost and was used as such in the LDA classifier.

In conclusion, applying our SPADE analysis and resulting LDA generated from "only" 4 animals (but 39 samples) on those previously unseen samples gave consistent results and strengthened the definition of our NK cell signature to prime and boost.

3.6 | The NK cell response correlates with the innate myeloid response

We further investigated how the NK cell response integrated with the innate myeloid response to MVA. We previously reported, in the same animals, that neutrophils, monocytes, and cDCs responded differently to the priming and boosting immunization. Some subphenotypes were enriched only after 1 of the 2 immunizations, with cells responding to the boost expressing higher levels of markers involved in phagocytosis, Ag presentation, costimulation, chemotaxis, and inflammation.[27] Here, we assessed the correlation between the dynamics of NK cell subphenotypes and those of these innate myeloid cell subphenotypes, based on cell abundance (Fig. 8).

The abundance of NK cells responding to the prime inversely correlated ($R < -0.6$) with that of the innate myeloid cells responding to the boost, but did not correlate ($|R| < 0.6$) with that of innate myeloid cells responding to the prime. In contrast, the abundance of NK cells responding to the boost positively correlated ($R > 0.6$) with that of innate myeloid cells responding to the boost, but there was no association ($|R| < 0.6$) with that of innate myeloid cells responding to the prime. One explanation may be that the kinetics of NK cells and innate myeloid cells are not synchronous. Indeed, NK cell expansion occurred mainly at H3-H6 for the PP-expanded subphenotypes, whereas innate myeloid cells that expanded PP were still numerous at D1. Conversely, innate myeloid cells that expanded PB expanded mainly around H6, simultaneously with NK cells. This also indicates that innate myeloid and NK cell responses are more synchronous during the response to the boost.

4 | DISCUSSION

We previously reported that vaccination elicits a distinct innate myeloid immunity between prime and after boost.[27] Using the very same animals, we show here that, NK cell immune responses also differ between each immunization. In contrast to the myeloid response, blood NK cell dynamics were driven mainly by decreases in cell number, and there was wider interindividual variability. We have previously documented a transient decrease of NK cell numbers in the blood after intradermal MVA injection in macaques.[46] In contrast to total NK cells, some NK cell subphenotypes increased in number after immunization, with some showing a differential enrichment after the prime and boost. More strikingly, our study revealed that some modifications of NK cell subphenotype composition toward a more mature and cytotoxic phenotype were induced by the prime. These changes occurred in 2 steps: a first early and quite long-lasting shift in phenotype (from D1PP and maintained up to D14PP), followed by a later one (between D14PP and D58PP). As a core result of these phenotypic changes, the NK cell composition before the prime and prior to the boost differed, and the NK cells responding to the boost were phenotypically more mature/cytotoxic.

There are numerous terminologies used in the literature to describe distinct NK cell subpopulations displaying memory-like

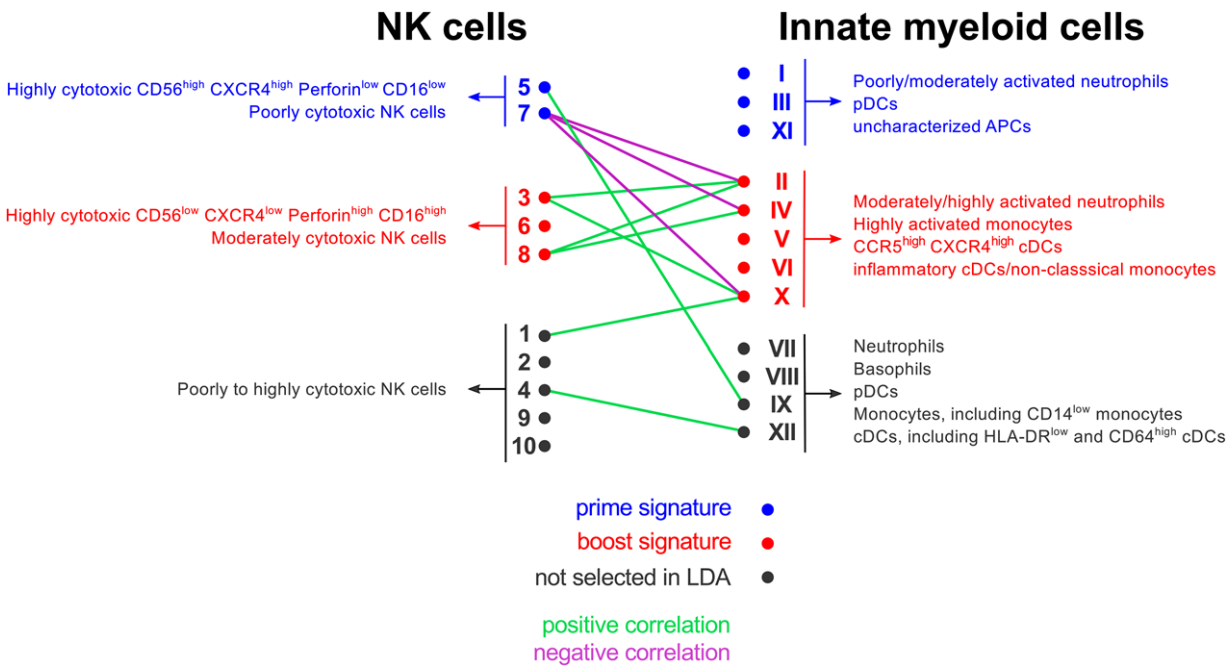

FIGURE 8 **Intercorrelation between NK cell and innate myeloid cell immune responses.** Correlations between the abundance of NK and innate myeloid cell subphenotypes[27] were computed using the Spearman method. Correlations with $|R| \geq 0.6$ and $P \leq 0.05$ are represented by green ($R \geq 0.6$) and purple ($R \leq 0.6$) lines joining the indicated subphenotypes. LASSO/LDA was used to discriminate PP (blue) and PB (red) NK cell (Fig. 6A) and innate myeloid cell subphenotypes.[27] Subphenotypes not necessary for the classification are shown in black

features including but not limited to Ag-specific NK cells,[17–19,69] cytokine-induced NK cells,[18,19] cytokine-activated NK cells,[69] liver-restricted NK cells,[19] memory-like NK cells,[18] or adaptive NK cells.[18] Many of these data were obtained in patients or animals infected by the cytomegalovirus. To our knowledge, there is not yet a clear consensus on the phenotype of these different subpopulations of NK cells, although some markers seem to be important, such as Ly49H and KLRG1 in mice or NKG2C and CD57 in humans.[19,69] Due to a lack of reactivity with fixed macaque cells of antibodies targeting many of NK receptors (such as NKp80, NKp46, NKp30, and CD158a), as well as CD57, those markers could not be included in our analyses, and available antibodies could not distinguish between NKG2A and NKG2C in macaques. In the present study, the main argument for induction of memory-like NK cells is the emergence or preponderance of some particular NK subphenotypes and overall their persistence long after MVA prime (2 months). Whether these MVA prime-induced NK cells correspond to memory-like NK cells, and which one (cytokine-induced or Ag-specific), remain to be fully tested with functional assays and transcriptional profiling approaches.

In addition, these missing markers may impair the capture of the whole NK cell diversity and explain why our LDA classifier was less efficient when dealing with NK cell subpopulation to distinguish PP and PB samples than the LDA generated on innate myeloid cell subpopulations,[27] despite strong correlations between NK cell and innate myeloid cell response at the boost.

Besides, we noticed a high interindividual variability in NK cell counts and phenotypes at steady state, prior to any immunization, while this interindividual variability was low after immunization, with all 4 animals behaving similarly. This indicated that changes induced by vaccination went beyond the sole interindividual variability. In other words, at baseline, without stimulation, the NK cell compartment activity is highly variable, whereas, upon stimulation (e.g., immunization, very likely infection), this variability decreases. The number of animals ($n = 4$) was not sufficient to address in detail the variation in the phenotypic composition of the NK cell compartment prior to immunization. This would be a valuable problematic to tackle with, because this may explain some of the interindividual differences in terms of immune responses observed in various contexts (such as infectious diseases and cancer).

Interestingly, the total NK cell dynamics were associated with the modulation of NK cell-related genes in PBMCs, in particular with the involvement of IL-12. However, the lack of available transcriptomic data at very early time points (such as H3, H6, and D1 post-immunization) prevented us from further assessing the kinetics of these transcripts during this period in which many dramatic changes in the abundance of NK cell phenotypic families occurred. In addition, transcript levels were assessed at the PBMC level, with NK cells potentially overwhelmed by B cells, T cells, and monocytes. Overall, this transcriptomic data set was rather a complementary piece of evidence to show that immunizations impacted NK cells as a cellular compartment. Future studies addressing vaccine-induced NK cell response should include early time points and use purified NK cells or even single cells, given the wide diversity of the NK cell repertoire. Still, interestingly, IL-12 has been described to be required in the efficient differentiation of both Ag-specific memory NK cells and cytokine-activated NK cells in a mice model after MCMV infection.[69] Because we previously showed that IL-12 was upregulated in neutrophils in our vaccine schedule, we may hypothesize that IL-12 could play a similar

role in the development of the phenotypically modified NK cells we observed here.

We used mass cytometry to identify key markers that clearly distinguish the NK cell immune response to the prime from that to the boost. Granzyme B, CD107a, perforin, CD69, CD66, CCR5, CD11c, CD16, and, to a lesser extent, CD11a were upregulated by NK cells responding to the boost. Several hypotheses can explain these prime-boost differences among NK cells, notably the presence of primary circulating antibodies that could activate NK cells via FcRs (such as CD16), as well as the local immune reaction involving primary memory T cells and/or imprinting resident macrophages. But actually, these differences were induced by the prime and preexisted to the boost.

CD107a, CD11a, CD11c, CD69, CD16, granzyme B, and perforin are associated with NK cell maturation and cytotoxic activity,[53,54,70–72] suggesting that NK cells would be more cytotoxic after the boost than after the prime. The increase in CCR5 expression suggests that NK cells are more prone to recruitment to inflamed tissues, including the injection site or draining lymphoid organs.[73,74] CD66 inhibits NKG2D signaling and subsequent cytotoxicity and may thus play a role in the downregulation of inflammation,[65,75] consistent with the overall milder inflammation observed in the macaques at the boost relative to the prime.[27] This suggests that prime-induced modifications of the NK cell compartment likely make it more effective in responding to subsequent infection/immunization, given its high activation potential. Whether direct ligand/receptor interactions between MVA and NK cells or cytokines play a role remains to be determined. Also, functional analyses are required to define the exact enhanced functions of the phenotypically distinct NK cells responding to the boost. Deep phenotyping analyses were performed on these animals on different cell compartments, not only in this paper but also elsewhere.[27,37] As a consequence, the number of blood samples left available was too limited to assess NK cell functions at relevant time points.

Our results are in contrast to those obtained in mice, showing that MVA immunization, as opposed to vaccinia virus immunization, failed to induce memory-like NK cells after a single intraperitoneal injection.[76] This strongly suggests that live, replication-competent microorganisms are likely to be more efficient at priming innate immune memory. Several hypotheses could explain the discrepancies between these results in mice and ours, apart from the simple difference between animal models. Indeed, different routes of injection may differentially influence systemic immunity. For example, previous studies on trained immunity showed that intravenous, but not subcutaneous, injection of BCG-induced stem cells gave rise to trained myeloid progeny.[77] The impact that the route of injection could have on NK cell responses is still largely unaddressed.[21] Another explanation is that the authors focused on the NK cell compartment 6 months after priming, without analyzing intermediate time points. It is possible that the primed NK cells we observed in our setting may be only short-lived and would vanish in the long term in the absence of boosting.

Another question is whether those primed NK cells were Ag-specific (and in this case MVA or HIV) or not. Indeed, one may wonder to which extent these phenotypically modified NK cells provided cross-protection to a wide range of pathogens, as for trained innate myeloid cells[78] or whether they would be restricted to some specific Ags.[18] Indeed, should they be Ag-specific, they would respond differently to the boost only if the correct Ag is present in the boosting immunization. Should they be non-Ag-specific (cytokine-induced memory NK cells), they would likely respond differently irrespective of the boost. Further functional studies will be required to firmly conclude on Ag specificity.

Strikingly, CD16, CCR5, and, to a lesser extent, CD11a were more highly upregulated on NK cells after the boost than the prime, similarly to monocytes, DCs, and neutrophils.[27] This indicates that (i) these features are shared by both lymphoid and myeloid innate cells and (ii) one consequence of a boost is more consistent CCR5 upregulation, which is likely linked to tissue recruitment. However, the innate myeloid and NK cell responses were clearly distinct, with innate myeloid cells being rapidly enriched after immunization, whereas NK cell numbers decreased. In addition, the kinetics of subphenotype composition modifications induced by the prime differed between NK and innate myeloid cells. This suggests that the mechanisms behind the training of innate lymphoid and myeloid immune cells differ.

We found strong correlations between NK cell and innate myeloid cell responses. Responses to the boost clearly correlated between the 2 compartments. Similarly, the innate myeloid response to the boost negatively correlated with that of the NK cells to the prime. In contrast, the innate myeloid response to the prime did not correlate with that of the NK cells to the prime, neither did it negatively correlate with the NK cell response to the boost. Overall, this suggests that the innate response to the boost is more coordinated between NK cells and innate myeloid cells than the response to the prime. Whether this is the result of a more efficient cross-talk between NK cells and myeloid cells after the boost than after the prime is yet to be addressed.

Finally, addressing whether some features of the NK cell response correlate with the adaptive immune response and how this could be used to better predict the establishment of immune memory is still a challenge. Also, further investigating NK cell responses in tissues other than blood is another challenge that will need to be met to obtain a fully comprehensive picture of the vaccine-induced NK cell response.

To our knowledge, this is the first study using CyTOF technology for the longitudinal analysis of NK cells after vaccination. It revealed key features of NK cell phenotype after immunization and without any ex vivo restimulation with the vaccine, in contrast to other studies analyzing the "recall" NK cell response.[8,79,80] This work aims to pave the way for future studies aiming to exploit this knowledge to optimize future vaccine.

AUTHORSHIP

Conceptualization: R.L.G. and A.-S.B.; immunization and blood sampling: N.D.-B.; cytometry: J.-L.P., N.T., N.H., J.E.-Y., A.C., M.M.-T., and A.-S.B.; flow cytometry for MVA-buffer comparison: P.R., F.M., J.-L.P., N.T., and A.-S.B.; transcriptomics: J.-L.P., N.T., C.L., H.H., and A.-S.B.; writing of the original draft: J.-L.P., N.T., A.-S.B.; review and editing: N.H., J.E.-Y., C.L., P.R., N.D.-B., F.M., H.H., A.C., M.M.-T., Y.L., and R.L.G.; acquisition of funding: Y.L., R.L.G., and A.-S.B.; supervision: R.L.G. and A.-S.B.

ACKNOWLEDGMENTS

This work was supported by the "Investissements d'Avenir" programs managed by the ANR under reference ANR-10-LABX-77-01

funding the Vaccine Research Institute (VRI), Créteil (ImMemory research program), ANR-11-INBS-0008 funding the Infectious Disease Models and Innovative Therapies (IDMIT, Fontenay-aux-Roses, France) infrastructure, and ANR-10-EQPX-02-01 funding the FlowCyTech facility (IDMIT, Fontenay-aux-Roses, France), and by Horizon 2020 European HIV Alliance (EHVA) project (Grant N°681032). We would like to thank all members of the ASW and L2I groups from IDMIT as well as Romain Marlin. Nicolas Tchitchek held fellowships from the ANRS (France Recherche Nord and Sud Sida-HIV Hépatites).

DISCLOSURES

The authors declare no conflict of interest.

REFERENCES

1. Iwasaki A, Medzhitov R. Regulation of adaptive immunity by the innate immune system. *Science*. 2010;327:291–295.
2. Artis D, Spits H. The biology of innate lymphoid cells. *Nature*. 2015;517:293–301.
3. Eberl G, Di Santo JP, Vivier E. The brave new world of innate lymphoid cells. *Nat Immunol*. 2015;16:1–5.
4. Boudreau JE, Hsu KC. Natural killer cell education and the response to infection and cancer therapy: stay tuned. *Trends Immunol*. 2018;39:222–239.
5. Wilk AJ, Blish CA. Diversification of human NK cells: lessons from deep profiling. *J Leukoc Biol*. 2018;103:629–641.
6. Vivier E, Tomasello E, Baratin M, Walzer T, Ugolini S. Functions of natural killer cells. *Nat Immunol*. 2008;9:503–510.
7. Pampena MB, Levy EM. Natural killer cells as helper cells in dendritic cell cancer vaccines. *Front Immunol*. 2015;6:13.
8. Horowitz A, Behrens RH, Okell L, Fooks AR, Riley EM. NK cells as effectors of acquired immune responses: effector CD4+ T cell-dependent activation of NK cells following vaccination. *J Immunol*. 2010;185:2808–2818.
9. Gao N, Jennings P, Yuan D. Requirements for the natural killer cell-mediated induction of IgG1 and IgG2a expression in B lymphocytes. *Int Immunol*. 2008;20:645–657.
10. Crouse J, Xu HC, Lang PA, Oxenius A. NK cells regulating T cell responses: mechanisms and outcome. *Trends Immunol*. 2015;36:49–58.
11. Cooper MA, Fehniger TA, Fuchs A, Colonna M, Caligiuri MA. NK cell and DC interactions. *Trends Immunol*. 2004;25:47–52.
12. Van Elssen CHMJ, Oth T, Germeraad WTV, Bos GMJ, Vanderlocht J. Natural killer cells: the secret weapon in dendritic cell vaccination strategies. *Clin Cancer Res*. 2014;20:1095–1103.
13. Rydyznski CE, Cranert SA, Zhou JQ, Xu H, Kleinstein SH, Singh H, Waggoner SN. Affinity maturation is impaired by natural killer cell suppression of germinal centers. *Cell Rep*. 2018;24:3367-3373.e4.
14. Vargas-Inchaustegui DA, Ying O, Demberg T, Robert-Guroff M. Evaluation of functional NK cell responses in vaccinated and SIV-infected rhesus macaques. *Front Immunol*. 2016;7:340.
15. Costanzo MC, Kim D, Creegan M, et al. Transcriptomic signatures of NK cells suggest impaired responsiveness in HIV-1 infection and increased activity post-vaccination. *Nat Commun*. 2018;9:1212.
16. Sun JC, Ugolini S, Vivier E. Immunological memory within the innate immune system. *EMBO J*. 2014;33:1295–1303.
17. Reeves RK, Li H, Jost S, et al. Antigen-specific NK cell memory in rhesus macaques. *Nat Immunol*. 2015;16:927–932.
18. Paust S, Blish CA, Reeves RK. Redefining memory: building the case for adaptive NK cells. *J Virol*. 2017;91. pii: e00169-17.
19. Min-Oo G, Kamimura Y, Hendricks DW, Nabekura T, Lanier LL. Natural killer cells: walking three paths down memory lane. *Trends Immunol*. 2013;34:251–258.
20. Jost S, Altfeld M. Control of human viral infections by natural killer cells. *Annu Rev Immunol*. 2013;31:163–194.
21. Rydyznski CE, Waggoner SN. Boosting vaccine efficacy the natural (killer) way. *Trends Immunol*. 2015;36:536–546.
22. Volz A, Sutter G. Modified vaccinia virus ankara: history, value in basic research, and current perspectives for vaccine development. *Adv Virus Res*. 2017;97:187–243.
23. Milo I, Blecher-Gonen R, Barnett-Itzhaki Z, et al. The bone marrow is patrolled by NK cells that are primed and expand in response to systemic viral activation. *Eur J Immunol*. 2018. https://doi.org/10.1002/eji.201747378
24. Garcia Z, Lemaître F, van Rooijen N, et al. Subcapsular sinus macrophages promote NK cell accumulation and activation in response to lymph-borne viral particles. *Blood*. 2012;120:4744–4750.
25. Moreno-Nieves UY, Didier C, Lévy Y, Barré-Sinoussi F, Scott-Algara D, ANRS HIV Vaccine Network (AHVN). NK cells are primed by ANRS MVA(HIV)-infected DCs, via a mechanism involving NKG2D and membrane-bound IL-15, to control HIV-1 infection in CD4+ T cells. *Eur J Immunol*. 2014;44:2370–2379.
26. Lehmann MH, Torres-Domínguez LE, Price PJR, Brandmüller C, Kirschning CJ, Sutter G. CCL2 expression is mediated by type I IFN receptor and recruits NK and T cells to the lung during MVA infection. *J Leukoc Biol*. 2016;99:1057–1064.
27. Palgen J-L, Tchitchek N, Elhmouzi-Younes J, et al. Prime and boost vaccination elicit a distinct innate myeloid cell immune response. *Sci Rep*. 2018;8:3087.
28. Hong HS, Rajakumar PA, Billingsley JM, Reeves RK, Johnson RP. No monkey business: why studying NK cells in non-human primates pays off. *Front Immunol*. 2013;4:32.
29. Davies DH, Wyatt LS, Newman FK, et al. Antibody profiling by proteome microarray reveals the immunogenicity of the attenuated smallpox vaccine modified vaccinia virus ankara is comparable to that of Dryvax. *J Virol*. 2008;82:652–663.
30. Carter DL, Shieh TM, Blosser RL, et al. CD56 identifies monocytes and not natural killer cells in rhesus macaques. *Cytometry*. 1999;37:41–50.
31. Sivori S, Vitale M, Morelli L, et al. p46, a novel natural killer cell-specific surface molecule that mediates cell activation. *J Exp Med*. 1997;186:1129–1136.
32. Huot N, Jacquelin B, Garcia-Tellez T, et al. Natural killer cells migrate into and control simian immunodeficiency virus replication in lymph node follicles in African green monkeys. *Nat Med*. 2017;23:1277–1286.
33. Vargas-Inchaustegui DA, Helmold Hait S, Chung HK, Narola J, Hoang T, Robert-Guroff M. Phenotypic and functional characterization of circulatory, splenic, and hepatic NK cells in simian immunodeficiency virus-controlling macaques. *J Immunol*. 2017;199:3202–3211.
34. Webster RL, Johnson RP. Delineation of multiple subpopulations of natural killer cells in rhesus macaques. *Immunology*. 2005;115:206–214.
35. Reeves RK, Evans TI, Gillis J, Johnson RP. Simian immunodeficiency virus infection induces expansion of alpha4beta7+ and cytotoxic CD56+ NK cells. *J Virol*. 2010;84:8959–8963.
36. Brandler S, Lepelley A, Desdouits M, et al. Preclinical studies of a modified vaccinia virus Ankara-based HIV candidate vaccine: antigen presentation and antiviral effect. *J Virol*. 2010;84:5314–5328.

37. Pejoski D, Tchitchek N, Rodriguez Pozo A, et al. Identification of vaccine-altered circulating B cell phenotypes using mass cytometry and a two-step clustering analysis. *J Immunol*. 2016;196:4814–4831.
38. Egger G, Burda A, Glasner A. A simple method for measuring the F-actin content of human polymorphonuclear leukocytes in whole blood. *Virchows Arch*. 2001;438:394–397.
39. Elhmouzi-Younes J, Palgen J-L, Tchitchek N, et al. In depth comparative phenotyping of blood innate myeloid leukocytes from healthy humans and macaques using mass cytometry. *Cytometry A*. 2017; https://doi.org/10.1002/cyto.a.23107
40. Montaldo E, Del Zotto G, Della Chiesa M, et al. Human NK cell receptors/markers: a tool to analyze NK cell development, subsets and function. *Cytometry A*. 2013;83:702–713.
41. Finck R, Simonds EF, Jager A, et al. Normalization of mass cytometry data with bead standards. *Cytometry A*. 2013;83:483–494.
42. Qiu P, Simonds EF, Bendall SC, et al. Extracting a cellular hierarchy from high-dimensional cytometry data with SPADE. *Nat Biotechnol*. 2011;29:886–891.
43. Gautreau G, Pejoski D, Le Grand R, Cosma A, Beignon A-S, Tchitchek N. SPADEVizR: an R package for visualization, analysis and integration of SPADE results. *Bioinformatics*. 2017;33:779–781.
44. Platon L, Pejoski D, Gautreau G, et al. A computational approach for phenotypic comparisons of cell populations in high-dimensional cytometry data. *Methods*. 2018;132:66–75.
45. Marlin R, Nugeyre M-T, Tchitchek N, et al. Modified vaccinia virus ankara vector induces specific cellular and humoral responses in the female reproductive tract, the main HIV portal of entry. *J Immunol*. 2017;199:1923–1932.
46. Rosenbaum P, Tchitchek N, Joly C, et al. Molecular and cellular dynamics in the skin, the lymph nodes, and the blood of the immune response to intradermal injection of modified vaccinia ankara vaccine. *Front Immunol*. 2018;9: https://doi.org/10.3389/fimmu.2018.00870
47. Szklarczyk D, Morris JH, Cook H, et al. The STRING database in 2017: quality-controlled protein-protein association networks, made broadly accessible. *Nucleic Acids Res*. 2017;45:D362–D368.
48. Spidlen J, Breuer K, Rosenberg C, Kotecha N, Brinkman RR. FlowRepository: a resource of annotated flow cytometry datasets associated with peer-reviewed publications. *Cytometry A*. 2012;81:727–731.
49. Kolesnikov N, Hastings E, Keays M, et al. ArrayExpress update–simplifying data submissions. *Nucleic Acids Res*. 2015;43:D1113–1116.
50. Martinet L, Ferrari De Andrade L, Guillerey C, et al. DNAM-1 expression marks an alternative program of NK cell maturation. *Cell Rep*. 2015;11:85–97.
51. Biassoni R, Fogli M, Cantoni C, et al. Molecular and functional characterization of NKG2D, NKp80, and NKG2C triggering NK cell receptors in rhesus and cynomolgus macaques: monitoring of NK cell function during simian HIV infection. *J Immunol*. 2005;174:5695–5705.
52. Borrego F, Robertson MJ, Ritz J, Peña J, Solana R. CD69 is a stimulatory receptor for natural killer cell and its cytotoxic effect is blocked by CD94 inhibitory receptor. *Immunology*. 1999;97:159–165.
53. Trapani JA, Smyth MJ. Functional significance of the perforin/granzyme cell death pathway. *Nat Rev Immunol*. 2002;2:735–747.
54. Urlaub D, Höfer K, Müller M-L, Watzl C. LFA-1 activation in NK cells and their subsets: influence of receptors, maturation, and cytokine stimulation. *J Immunol*. 2017;198:1944–1951.
55. Gao J-Q, Tsuda Y, Han M, et al. NK cells are migrated and indispensable in the anti-tumor activity induced by CCL27 gene therapy. *Cancer Immunol Immunother*. 2009;58:291–299.
56. Zwirner NW, Ziblat A. Regulation of NK cell activation and effector functions by the IL-12 family of cytokines: the case of IL-27. *Front Immunol*. 2017;8. https://doi.org/10.3389/fimmu.2017.00025
57. Barber DF, Faure M, Long EO. LFA-1 contributes an early signal for NK cell cytotoxicity. *J Immunol*. 2004;173:3653–3659.
58. Kovats S. Estrogen receptors regulate innate immune cells and signaling pathways. *Cell Immunol*. 2015;294:63–69.
59. Brumbaugh KM, Binstadt BA, Billadeau DD, et al. Functional role for Syk tyrosine kinase in natural killer cell–mediated natural cytotoxicity. *J Exp Med*. 1997;186:1965–1974.
60. Cardone J, Le Friec G, Kemper C. CD46 in innate and adaptive immunity: an update. *Clin Exp Immunol*. 2011;164:301–311.
61. McNerney ME, Kumar V. The CD2 family of natural killer cell receptors. *Curr Top Microbiol Immunol*. 2006;298:91–120.
62. Liu LL, Landskron J, Ask EH, et al. Critical role of CD2 co-stimulation in adaptive natural killer cell responses revealed in NKG2C-deficient humans. *Cell Rep*. 2016;15:1088–1099.
63. Rölle A, Halenius A, Ewen E-M, Cerwenka A, Hengel H, Momburg F. CD2-CD58 interactions are pivotal for the activation and function of adaptive natural killer cells in human cytomegalovirus infection. *Eur J Immunol*. 2016;46:2420–2425.
64. Milush JM, Long BR, Snyder-Cappione JE, et al. Functionally distinct subsets of human NK cells and monocyte/DC-like cells identified by coexpression of CD56, CD7, and CD4. *Blood*. 2009;114:4823–4831.
65. Markel G, Lieberman N, Katz G, et al. CD66a interactions between human melanoma and NK cells: a novel class I MHC-independent inhibitory mechanism of cytotoxicity. *J Immunol*. 2002;168:2803–2810.
66. Pillarisetty VG, Katz SC, Bleier JI, Shah AB, Dematteo RP. Natural killer dendritic cells have both antigen presenting and lytic function and in response to CpG produce IFN-gamma via autocrine IL-12. *J Immunol*. 2005;174:2612–2618.
67. Zingoni A, Sornasse T, Cocks BG, Tanaka Y, Santoni A, Lanier LL. Cross-talk between activated human NK cells and CD4+ T cells via OX40-OX40 ligand interactions. *J Immunol*. 2004;173:3716–3724.
68. Strauss-Albee DM, Fukuyama J, Liang EC, et al. Human NK cell repertoire diversity reflects immune experience and correlates with viral susceptibility. *Sci Transl Med*. 2015;7:297ra115.
69. Nabekura T, Lanier LL. Tracking the fate of antigen-specific versus cytokine-activated natural killer cells after cytomegalovirus infection. *J Exp Med*. 2016;213:2745–2758.
70. Bruhns P, Jönsson F. Mouse and human FcR effector functions. *Immunol Rev*. 2015;268:25–51.
71. Burt BM, Plitas G, Stableford JA, et al. CD11c identifies a subset of murine liver natural killer cells that responds to adenoviral hepatitis. *J Leukoc Biol*. 2008;84:1039–1046.
72. Aranami T, Miyake S, Yamamura T. Differential expression of CD11c by peripheral blood NK cells reflects temporal activity of multiple sclerosis. *J Immunol*. 2006;177:5659–5667.
73. Khan IA, Thomas SY, Moretto MM, et al. CCR5 is essential for NK cell trafficking and host survival following Toxoplasma gondii infection. *PLoS Pathog*. 2006;2:e49.
74. Weiss ID, Shoham H, Wald O, et al. Ccr5 deficiency regulates the proliferation and trafficking of natural killer cells under physiological conditions. *Cytokine*. 2011;54:249–257.
75. Mizrahi S 'ar, Yefenof E, Gross M, et al. A phenotypic and functional characterization of NK cells in adenoids. *J Leukoc Biol*. 2007;82:1095–1105.

76. Gillard GO, Bivas-Benita M, Hovav A-H, et al. Thy1+ NK [corrected] cells from vaccinia virus-primed mice confer protection against vaccinia virus challenge in the absence of adaptive lymphocytes. *PLoS Pathog*. 2011;7:e1002141.

77. Kaufmann E, Sanz J, Dunn JL, et al. BCG Educates hematopoietic stem cells to generate protective innate immunity against tuberculosis. *Cell*. 2018;172:176-190.e19.

78. Netea MG, van der Meer JWM. Trained immunity: an ancient way of remembering. *Cell Host Microbe*. 2017;21:297–300.

79. Long BR, Michaelsson J, Loo CP, et al. Elevated frequency of gamma interferon-producing NK cells in healthy adults vaccinated against influenza virus. *Clin Vaccine Immunol*. 2008;15:120–130.

80. Darboe A, Danso E, Clarke E, et al. Enhancement of cytokine-driven NK cell IFN-γ production after vaccination of HCMV infected Africans. *Eur J Immunol*. 2017;47:1040–1050.

SUPPORTING INFORMATION

Additional information may be found online in the Supporting Information section at the end of the article.

How to cite this article: Palgen J-L, Tchitchek N, Huot N, et al. NK cell immune responses differ after prime and boost vaccination. *J Leukoc Biol*. 2019;1-19. https://doi.org/10.1002/JLB.4A1018-391RR

Part III.
Impact of a shortened delay between prime and boost on vaccine-induced immune responses

Rationale

After having characterized the innate immune responses induced after a prime-boost vaccination at two months apart (classical vaccination schedule), and associated with a potent secondary antibody response, we investigated the impact of the delay between prime and boost immunization. Whether this classical schedule is the most optimal ones still remains to be addressed. Besides, a shortened vaccine schedule might be of high interest to cope with a health emergency to rapidly protect a population. In addition a shorter delay between both prime and boost MVA immunizations was shown detrimental in anti-smallpox antibody generation in human (Jackson et al., 2017), but the mechanisms at play, and in particular the role of innate cells has not been investigated. We thus chose to study a vaccine schedule with a shorter prime-boost delay.

Similarly to the classical boost group, five animals were immunized subcutaneously twice with MVA HIV B vaccine at 4.10^8 PFU for both prime and boost. But, for this cohort, boost was administered two weeks after the prime. Among other considerations, in animals primed and boosted 2 months later, two weeks correspond to a timeframe before the shift in subphenotype composition of the innate myeloid compartment occurred, and between the first and second shift in subphenotype composition of the NK cell compartment. This cohort will latter be referred as the early boost cohort.

Once again, given the complexity of the analysis, we split the immune response characterization in two parts: innate myeloid cell and NK cell responses.

Chapter 5. Innate myeloid cell responses during an early boost vaccination schedule and correlation with adaptive immune memory

Overview

We first investigated the impact of the reduction of the prime-boost delay on the induction of humoral responses, using different ELISA and neutralization assays to biophysically and functionally profile vaccine-induced antibodies. These assays were performed by André Rodriguez-Pozo, a former PhD student from the laboratory.

These analyses revealed that both vaccine schedules induced similar level of IgG (essentially IgG1) in short and long-term, with a faster decrease in antibody titer for the early boost schedule. Conversely, secondary IgA generation was strongly reduced in the early boost group compared to the classical boost group. Consistently, MVA neutralization titer and Fc binding affinity towards dimers of Fc receptors, chiefly CD16, was strongly reduced in the early boost compared to the classical boost cohort. This indicated that the early boost induced a qualitatively and quantitatively distinct humoral response than the classical boost. Since the neutralization titer and FcR binding affinity appeared reduced after the early boost, we may hypothesize that the early boost schedule is less protective than the classical boost. Note that in addition to the existing data, current experiments are ongoing to further address Fc functions of the antibody response, notably through the assessment of CD16 and CD32 dimer binding affinity using simian FcR rather human ones, which are currently used. Overall, these results suggest that the early boost did not provide fully the expected boosting effect, possibly through the impairment of primary B cell maturation.

I then characterized in depth the innate myeloid responses induced in the early boost schedule to address whether and how the innate myeloid responses differed between the early boost schedule and the classical boost. Noteworthily, cytokines induced by vaccination were similar in the early boost schedule compared to the classical one (*e.g.* IP-10 and IL-6), although no difference between prime and boost could be observed in the early boost cohort.

We refined our CyTOF antibody panel dedicated to innate myeloid cells notably by adding markers distinguishing cDC subpopulations (CADM1, CD172a and CD1c (Guilliams et al., 2016)). We also used heparin in our staining procedure to prevent the non-specific binding of metals by eosinophilic granules (Rahman et al., 2016), thus allowing to study this cell population behavior in response to vaccinations. Finally, these analyses were performed with the last generation of CyTOF device, the Helios, which allowed to recover more cells than the CyTOF I used in the previous Chapters.

We firstly followed a similar analysis pipeline to analyze these data. Interestingly, although we unveiled a high diversity in the granulocyte compartment, it was lower in the early boost cohort than in the classical boost cohort, illustrated by a lower number of phenotypic families determined. In particular, the $CD4^+$ neutrophil subphenotypes that were present in the classical boost schedule and strongly induced post-boost, were missing in the early boost cohort dataset. Still, we unveiled here the phenotypic diversity of circulating eosinophils. This notably included the detection of $CD123^+$ eosinophils, which were rarely described in literature (Valent, 1994), though IL-3 signaling via CD123 might strongly impact eosinophil functions (Rothenberg et al., 1988).

Within the monocyte-DC compartment, we identified a lower diversity among monocytes, but a higher diversity in cDCs, which is very likely linked to the addition of new markers in the early boost schedule study compared to the classical boost schedule study.

Strikingly, while CADM1 staining clearly allowed to identify cDC1, CD172a staining in cDCs (in contrast to neutrophils and eosinophils) was quite low and did not clearly allowed to identify cDC2. This may have been caused by epitope degradation on fixed cDCs. Accordingly, staining tests on fresh whole blood allowed for a staining profile consistent with the literature (Guilliams et al., 2016). It is however not clear why this epitope would be degraded in cDCs but not in granulocytes.

Also, the uncharacterized APCs ($CD3^-$ $CD8^-$ $CD14^-$ $CD20^-$ $CD11c^-$ $CD16^-$ $CD123^-$ $HLA\text{-}DR^+$ cells) that were identified in the classical boost schedule, were present in the early boost dataset. They could be further segregated between $CADM1^+$ $CD141^{+/-}$ "uncharacterized" APCs and $CADM1^-$ $CD141^+$ "uncharacterized" APCs.

When it came to characterize the kinetics of these subphenotypes, most of them were similarly impacted by both immunizations, and only few of them were impacted by only one immunization, in contrast to the classical boost schedule. As a result, linear discriminant analyses failed to accurately distinguish response to prime and response to boost.

We then wanted to more accurately address the similarities and discrepancies between innate myeloid cells characterized in the classical boost cohort and in the early boost cohort. This was quite challenging, since these data came from different cohorts, were obtained using different antibody panels and batches of antibodies, and were generated using different CyTOF devices, which is known to induce a high variability in term of staining profiles(Tricot et al., 2015; Leipold et al., 2018), precluding the direct MSI comparison. To meet this challenge, we thus adapted our analytical strategy to compare the categories of expression defined on the SPADEVizR package (Gautreau et al., 2017), which divides in five bins the range of expression of all markers between the 5^{th} and 95^{th} percentiles of the dataset, rather than directly MSI.

The resulting analysis indicated that, among the granulocytes compartment, all the highly activated neutrophils ($CD66^{high}$ $CD11b^{high}$ $CD32^{high}$ $CD45^{high}$), which were mainly expanded after the classical boost did not match a counterpart in the early boost dataset. This strongly supports that the early boost failed to mobilize these cells. Actually the early boost occurs at a time when no "likely trained" cells was present in blood, thus the absence of these cells in the early boost schedule may results from a too short timeperiod left to generated them.

On the monocyte-DC compartment, most cells from both datasets matched a counterpart in one another dataset. This suggest that phenotypically more active/mature monocytes-DCs were present in the early boost schedule too but were poorly enriched in number by immunization.

Given the strong differences we observed between both cohorts, both in innate myeloid and adaptive immunity, we eventually addressed the correlations existing between innate and adaptive immunity across the two cohorts. Some studies in literature reported the potential of innate responses to predict some parameters of adaptive immune responses (Nakaya et al., 2015; Thompson et al., 2018). Strikingly, we identified here strong correlations between the generation of "likely trained" innate myeloid cells and the quality and quantity of the short- and long-term humoral responses. This supports the hypothesis of a key role played by these "likely trained" innate cells induced by the prime in the restimulation and modulation of antibody response.

In addition, to address the functionality of immune cells, at least on available PBMC samples, at each immunization, we assessed the production of cytokines by PBMCs isolated at D3PP and D3PB, and left unstimulated *ex vivo*. Strikingly, the production of several cytokines (G-SCF, IL-12/23, IL-1β, IL-18, IL-1Ra, TGFα, IFNγ, IL-4, IL-8, IL-13, MIP-1α, MIP-1β, TNFα and sCD40L), including some produced mainly by innate cells (myeloid and NK cells), was increased three days post-boost in the classical boost cohort, but not (or with a significantly lower amplitude) in the early boost cohort. Admittedly, the use of PBMC precluded the analysis of granulocyte-derived cytokine production. Also, we cannot formally distinguish whether this distinct cytokine production was due to the phenotypic modifications of innate cells, and/or the differential stimuli provided by either

specific antibodies, or memory T and B cells, which also differ between both schedules. Both explanations are not mutually exclusive and are likely to occur simultaneously. To note, IL-12, which was one of most differentially expressed markers between innate cells responding to prime *vs.* responding to boost 2 months later, is also more produced by PBMC after a boost at 2 months, than after the prime or a boost at 2 weeks, connecting the phenotype identified with mass cytometry and the resulting cell functions.

Overall, this support a strong interconnection between the generation of "likely trained" innate myeloid cell and the adaptive response, mediated by both T and B cells. It suggests that induction of 'likely trained" innate myeloid cell is at least a surrogate of the quality and quantity of adaptive memory, and may be a kay player in the re-activation of primary memory and induction of secondary memory

"The timing of vaccine boosting regulates the induction of memory innate myeloid cells and the quality of the secondary antibody response"

All those results are part of a manuscript in preparation, formatted according to *Cell Host and Microbes* guidelines. The manuscript is provided hereafter.

The timing of vaccine boosting regulates the induction of memory innate myeloid cells and the quality of the secondary antibody response

Jean-Louis Palgen[1,2], Nicolas Tchitchek[1,2], André Rodriguez-Pozo[1,2], Quentin Jouhault[1,2], Hadjer Abdelhouahab[1,2], Bruce Wines[3], Mark Hogarth[3], Stephen J Kent[4], Nathalie Dereuddre-Bosquet[1,2], Vanessa Conteras[1,2], Antonio Cosma[1,2], Yves Lévy[2,5], Roger Le Grand[1,2], and Anne-Sophie Beignon[1,2*]

[1] CEA – Université Paris Sud 11 – INSERM U1184, Immunology of Viral Infections and Autoimmune Diseases, IDMIT department, IBFJ, 92265 Fontenay-aux-Roses, France

[2] Vaccine Research Institute, Henri Mondor Hospital, 94010 Créteil, France

[3] Centre for Biomedical Research, Burnet Institute, Melbourne, Victoria, Australia.

[4] Dept. of Microbiology and Immunology, Peter Doherty Institute, University of Melbourne, Australia

[5] Institut Mondor de Recherche Biomédicale – INSERM U955, Eq.16, 94010, Créteil, France

*Corresponding author: Anne-Sophie Beignon; 18, route du Panorama; 92265 Fontenay-aux-Roses, France; Phone: +33 1 46 54 80 27; Fax : +33 1 46 54 77 26; email: anne-sophie.beignon@cea.fr

Keywords: innate myeloid cells, granulocytes, neutrophils, monocytes, DCs, CyTOF, mass cytometry, vaccination, prime-boost

Abstract

Background: Understanding the impact of the delay between prime and boost immunizations is critical for improving the design of vaccines. Indeed, this time-lapse is mainly empirically defined in the current vaccination recommendations. Moreover, the early events occurring after each immunization must be better understood to optimize vaccination processes.

Methods: Five cynomolgus macaques were immunized twice with the modified vaccinia virus Ankara following a schedule including a very early boost at two weeks after the prime. Using a mass cytometry panel of 35-markers and systems immunology approaches, we deciphered in depth the phenotype of the blood innate myeloid cells induced by early boost vaccination.

Results: We show that this early boost did not induce a distinct innate myeloid response compared to the prime. These results are in contrast with a prime-boost schedule at 2 months-apart that we previously reported. Strong correlations were found between the antibody response and the abundances of cell subsets responding to each immunization. These results highlights a strong association between the modifications within the innate myeloid compartment by the prime and both the quality and durability of the antibody response.

Impacts: These results outline the importance of the early events that follow immunizations and the impact of the delay between the prime and boost on the development of long-term protection.

Introduction

Vaccination is one of the main progress ever made in the field of public health (Greenwood, 2014; Rappuoli et al., 2014). Still, many vaccine-induced mechanisms remain unknown, limiting the design of effective vaccines. In particular, while most vaccines use a first immunization (so-called prime) followed by one or more immunizations (so-called boosts), we are far to understand how the delay between the prime, and boost will impact the resulting immune response (Kardani et al., 2016; Ramshaw and Ramsay, 2000; Woodland, 2004). While antibodies are the primary correlate of protection for most licensed vaccines (Plotkin, 2010), it is critical to determine how the innate immunity is induced by each immunization. Indeed, innate immunity initially triggers the immune response. In addition, some studies reported the potential of the innate immunity to predict long-term adaptive response (Nakaya et al., 2015).

The modified vaccinia virus Ankara (MVA), a vaccinia-based vaccine against smallpox, is a relevant vaccine model since it induces both strong humoral and cellular immunity (Earl et al., 2004). Moreover, MVA is currently used as a vector to develop new vaccines against several pathogens and diseases, including HIV, and malaria (Volz and Sutter, 2017; Sebastian and Gilbert, 2016; Drexler et al., 2004). Besides, non-human primates are a well-recognized model in vaccine research, given their close phylogenetic proximity with humans and their similar immunogenicity with several vaccines (’t Hart et al., 2015; Rivera-Hernandez et al., 2014).

We previously showed that a homologous prime-boost immunization at two months apart induced a long-lasting immunity using cynomolgus macaques and MVA (Pejoski et al., 2016). Also, we observed changed in the phenotypes of both myeloid (including neutrophils, monocytes, and classical dendritic cells –cDCS) and lymphoid (including NK cells) (Palgen et al., 2018, 2019) cells between two weeks and two months after the prime. More precisely, these innate cells presented a more mature and activated phenotype two months – but not 2 weeks – after the prime. In addition to the potential role of memory T-cells and circulating antibodies, these changes resulted in an innate response deeply distinct between priming and boosting immunizations.

To assess how the delay between the prime and boost impacts the innate immunity, we used the same animal and vaccine models but with a prime-boost vaccination schedule of two weeks apart. We took advantage of mass cytometry technology to assess the phenotype of innate myeloid cells during the timecourse of the vaccination schedule. Mass cytometry is indeed a key technology to decipher induced immune response since it allows for the simultaneous measurement of more than 40 parameters at the single-cell level (Reeves et al., 2018; Simoni et al., 2018). To handle generated high-dimensional cytometry data and compare these data with a two months apart vaccination schedule, we used analysis bioinformatics pipeline including the SPADE algorithm (Qiu et al., 2011) and different algorithms that we developed (Gautreau et al., 2016; Platon et al., 2018).

Results

Classical and early boost induced distinct humoral responses

Two groups of five cynomolgus macaques were immunized subcutaneously with MVA, following a homologous prime-boost at either two weeks-apart (so called the early boost) or two months-apart (so called the classical boost) (**Figure 1**). The specific antibody response developed by each animal for the classical schedule was reported in a previous publication (Pejoski et al., 2016). The sample collection schedule during the priming phase was common to both groups. MVA-specific IgG, IgA antibodies were detected as early as 14 days after the first immunization in both groups (**Figure 2A and Figure 2B**). IgG responses were significantly higher than IgA ($p < 0.01$, at D8PB). Four out of ten macaques did not show an IgA antibodies response 14 days post-prime (D14PP). The peaks of MVA-specific IgG levels were reached after the second immunization (**Figure 2A and Figure 2B**) in both immunization regimens. Note that IgG produced were essentially IgG1 (**Figure S1**). Besides, the peak of MVA-specific IgA levels was reached only in classical boost schedule ($p<0.0001$, D57PP *vs.* D8PB) and observed in all animals. However, all animals produced some IgA at D8PB in early boost schedule. Note that IgM levels appeared low or inexistent at all timepoints (**Figure 2C**). The decay in MVA-specific levels (IgG and IgA) between days D28 and M6PB were not similar for both groups, with classical boost schedule showing a faster decrease than the early boost schedule (**Figure 2D, Figure 2E** and **Table S1**).

Neutralizing antibodies (nAb) responses against MVA were only detected in the classical boos schedule group (**Figure 2F)**. At D8PB, all animals developed nAb responses. We addressed the ability of MVA-specific antibodies to cross-link Fc-receptors in both groups. Lately, the role of HIV non-neutralizing antibodies in vaccine-mediated protection has gained importance as they can induce

significant Fc effector-mediated functions. In both groups, binding affinity of vaccine-induced MVA-specific antibodies were detected by dimeric FcγRIIIa after the second immunizations (**Figure 2G**). Peaks are reached at D14 post boost and were higher in classical boost schedule protocol ($p < 0.01$).

Overall, these results showed that although poorly impacting IgG levels, the delay between prime and boost has a strong impact on the generation of IgA and nAb as well as in the generation of antibody affine to FcR. Besides, the innate myeloid immune response induced by the classical boost schedule was previously published (Palgen et al., 2018). It was phenotypically highly distinct between prime and boost. We thus focused on the characterization of these cells in theearly boost schedule to assees whether it was also the case.

Early boost schedule induced similar cytokines and leukocyte count than the classical schedule

As a read-out of innate immunity, plasma samples collected longitudinally were analyzed with cytokine assay to address the release of systemic cytokines during the timecourse of vaccination (**Figure S2 and Table S2**).

As expected, only a few cytokines were impacted by vaccination (**Figure S2A and S2B**). IP-10 displayed peaks of concentration one day (D1) after each immunization. IL-1Ra displayed an increase at D1PP solely, although D1PP level is not significantly different from D1PB level. IL-6 showed a peak of concentration at 6 hours (H6) after each immunization. Surprisingly, MCP-1, which was previously shown to be impacted by a two month-apart vaccination schedule, displayed a high inter-individual variability. This inter-individual variability can explain why the increase at H6 post-immunization

observed for some individuals is not significant. Also, IL-8 tends to be at a higher concentration at D3PB and D8PB compared to D3PP and D8PP, although none of these timepoints displayed significant differences compared to baseline levels.

Overall, very small differences between responses to the prime and to the boost were observed at the cytokine level. These results are in contrast to with a classical vaccine schedule at two months-apart where significant differences in IP-10 concentrations were observed between the prime and the boost.

We also analyzed the number of circulating leukocytes throughout the timecourse of vaccination (**Figure S2C**). As expected, a strong increase in cell number was observed at H6 and D1 ($p < 0.01$ for H6PP, D1PP and H6PB and $p=0.0159$ for D1PB) post-immunizations, but without any difference in term of areas under the curve (AUC) between the prime and the boost. The peak of leukocytes increase was thinner (it waned more rapidly) after the boost compared to the prime, since the leukocyte number is slightly lower at D1PB compared to D1PP ($p=0.0317$). These results are similar to the leukocyte count assessed in the classical boost schedule.

Still, in the classical boost schedule, the innate myeloid responses were highly distinct between the prime and boost, as reported in a previous publication (Palgen et al., 2018). To assess whether this was the case also in the early boost schedule, we took advantage of mass cytometry to characterize in depth the phenotypes of all myeloid cells along the vaccination schedule.

Phenotypical diversity of identified cell populations within the early boost schedule

Whole blood was stained with a 35 antibody panel detailed in **Figure 3A** and **Table S3**. The analysis pipeline displayed in **Figure 3B** was then followed. The SPADE algorithm was applied to identify clusters of leukocytes sharing similar phenotypes based on all samples. The parametrization of the SPADE algorithm was optimized and we identified 800 clusters based on the following 28 clustering markers: CD66, HLA-DR, CD3, CD64, CD8, CD123, CD11a, CD11b, CD62L, CD4, FcεRI, CD86, CD125, CD172a, CD45, CD1c, CD32, CD39, CCR5, CD16, CD11c, CXCR4, CD14, CD23, CD141, CD20, CCR7, and CADM1.

On the resulting SPADE tree (**Figure 3C**), cell clusters were annotated based on the expression of CD66, CD3, HLA-DR, CD8, CD123, CD4, CD125, CD172a, CD1c, CD16, CD11c, CD14, CD141, CD20, and CADM1 (**Figure S3**). We identified 192 clusters of granulocytes that included $CD66^{high}$ $CD125^{-}$ neutrophils, $CD66^{-}$ $HLA\text{-}DR^{-}$ $CD123^{+}$ basophils, and $CD66^{mid}$ $CD125^{+}$ eosinophils. We identified 322 clusters of monocytes-cDCs that included $HLA\text{-}DR^{+}$ $CD14^{-}$ $CD11c^{+}$ $CD16^{+}$ $CD141^{+}$ cDCs (including $CADM1^{+}$ cDC1s and $CADM1^{-}$ cDC2s), $HLA\text{-}DR^{+}$ $CD14^{+}$ $CD141^{+}$ monocytes (including $HLA\text{-}DR^{+}$ $CD14^{+}$ $CD11c^{+}$ $CD16^{+}$ non-classical monocytes inflammatory cDCs), $HLA\text{-}DR^{+}$ $CD123^{+}$ pDCs, $HLA\text{-}DR^{+}$ $CD3^{-}$ $CD8^{-}$ $CD14^{-}$ $CD11c^{-}$ $CD16^{-}$ $CD20^{-}$ $CD141^{+}$ $CADM1^{-}$ APCs, and $HLA\text{-}DR^{+}$ $CD3^{-}$ $CD8^{-}CD14^{-}$ $CD11c^{-}$ $CD16^{-}$ $CD20^{-}$ $CD141^{+/-}$ $CADM1^{+}$ APCs. Furthermore, we identified 280 cell clusters of lymphocytes that included $CD3^{+}$ T cells, $HLA\text{-}DR^{+}$ $CD20^{+}$ B cells, and CD3- CD8+ NK cells. Six clusters were undefined as $CD66^{-}$ $CD125^{-}$ $CD3^{-}$ $CD4^{-}$ $CD8^{-}$ $HLA\text{-}DR^{-}$ $CD20^{-}$ $CD14^{-}$ $CD11c^{-}$ $CD123^{-}$ $CD16^{-}$ $CADM1^{-}$. Since our panel was solely dedicated to target innate myeloid cells, we focused the analysis on the granulocytes and monocytes-DCs compartments.

In-depth phenotypic characterization of the innate myeloid cells within the early boost schedule

To further decipher the phenotype of innate myeloid cells involved in vaccine response, we displayed these cell cluster phenotypes on two categorical heatmaps of marker expressions, one for the granulocytes compartment and one for the monocytes-DCs compartments (**Figure 4**). Based on a hierarchical clustering, we regrouped cell clusters sharing similar phenotypes into so-called phenotypic families.

In the granulocytes compartment (**Figure 4A**), 16 distinct phenotypic families (named from 1 to 16) were distinguished and grouped into 4 super phenotypic families.

Superfamily A contained solely eosinophils (families 4, 11, and 7), and clearly segregated apart from the rest of the granulocytes. Interestingly all eosinophils displayed high expression of CD39, CD45, CD62L, CD11b, CD125, CD23, IL-1α, CADM1, CCR7, CXCR4, CD86, IL-4, CD123, and FceRI, as well as a mid-expression of CD66, and CD32. The three families expressed IL-12, CD64, CD172a CD20 CD4 IP-10 CD11c, and CCR5 at different levels (high, low, and mid for families 4, 11, and 7 respectively). This surprising signature suggests a highly activated phenotype. Still, caution should be taken in the interpretation of these phenotypes, since eosinophils could potentially bind to lanthanides despite the use of heparin during the staining.

Two superfamilies B and D comprised neutrophils. Overall superfamily B (families 1, 6, 2, 13, and 15) contained $CD39^{high}$ $CD45^{high}$ $IL\text{-}8^{high}$ neutrophils whereas superfamily D (families 10, 14, 8, 3, and 9) was $CD39^{mid}$ $CD45^{mid}$ $IL\text{-}8^{mid}$ and may correspond to less active/mature neutrophils. Also note

that among superfamily B, family 13 showed a high expression of CD14, a feature previously reported in neutrophils subpopulation, without its function being clearly defined (Antal-Szalmas et al., 1997; Palgen et al., 2018). In addition, phenotypic families 1 and 6 display a strong expression of CD172a, the inhibitor of phagocytosis that recognize CD47, which likely act as a dampener of activity on these otherwise highly activated neutrophils. To mention family 15 showed various patterns of expression of CCR7, CXCR4, CD86, CD123, and FcεRI, which might be due to unspecific staining or might be related to incompletely differentiated progenitor.

Finally, superfamily C contained one family regrouping basophils (family 12) and one family (family 5) of $CD23^{low}$ $IL\text{-}1\alpha^{low}$ $CADM1^{low}$ $CCR7^{low}$ $CXCR4^{low}$ $CD86^{low}$ CD123high CD125high that were annotated as eosinophils based on their localization on the SPADE tree (**Figure 3**). Note that all basophils were all $CD32^{mid/high}$ $CD39^{high}$ $FcεRI^{high}$ $IL\text{-}4^{high}$, which is consistent with the basophil phenotype identified in the classical boost (Palgen et al., 2018).

Overall, several subphenotypes were detected in the dataset, but still, the diversity is far lower than what was observed with the classical schedule. Indeed, only twelve phenotypical families were identified here, compared to the 20 obtained in the classical schedule. In addition, CD66 and CD32 expression seemed pretty homogeneous across all neutrophils clusters, whereas a strong modulation of these markers was observed across the neutrophil compartment in the classical schedule.

To be mentioned, two phenotypic families (15 and 16) contained very few clusters (3 and 1) displaying a phenotype in patchwork, with various degrees of marker expression and may account for background events.

Among the monocytes-DC compartment (**Figure 4B**), 21 phenotypic families (17 to 37) were identified and can be grouped into 3 distinct superfamilies.

Superfamily E (families 20, 33, 26, 37, 27, 24, 25, 29, and 23) contained cDCs as well as inflammatory cDCs, non-classical monocytes (family 27). Families 20 and 33 were CADM1^{high} CD39$^{low/mid}$ CD86$^{low/mid}$ CD45$^{low/mid}$ HLA-DR$^{low/mid}$ CXCR4$^{low/mid}$ CCR5$^{low/mid}$ CD1c$^{low/mid}$ IP-10$^{low/mid}$ and may be labelled as cDC1s, whereas families 26, 24, 25, 29, and 23 were CADM1^{low} and displayed different levels of CD39 CD86 CD45 HLA-DR CXCR4 CCR5 CD1c, and IP-10 and may be labeled as cDC2s. Caution has to be taken though, since CD172a signal was low in cDCs compared to granulocytes compartment, which resulted in most cDCs appearing in very low (white) or low (yellow) categories, preventing us to firmly use it as a classical cDC2 marker. To mention, family 37 contained one only cluster and may correspond to background events.

Superfamily F (families 36, 34, 28, and 35) contained HLA-DR^{+} CD14^{-} CD11c^{-} CD16^{-} CD20^{-} CD141$^{+/-}$ CADM1^{+} APCs segregated into CD1c^{low} (family 36), and CD1c^{high} (family 34) APCs, pDCs family 12), and HLA-DR^{+} CD14^{-} CD11c^{-} CD16^{-} CD20^{-} CD141^{+} CADM1^{-} IL-12^{high} CD172a^{high} IP-10^{high} APCs (family 35).

Superfamily G (families 31, 18, 22, 21, 19, 32, 30, and 17 contained $CD39^{high}$ $CD86^{high}$ $CD45^{high}$ $CD11b^{high}$ $CD64^{high}$ monocytes that were positive –but with different level of expression– for HLA-DR CXCR4 CCR5 CD1cIP-10 CD141 CD32, and CD14.

Kinetic of cell subphenotype within the early boost schedule

We grouped together phenotypic families sharing the same kinetic into so-called kinetic families (I to XIII in roman numerals) to analyze the kinetics of innate immune responses (**Figure 5, Figure S4**, **Figure S5**, and **Table S4)**.

Interestingly out of these 13 kinetic families, 4 displayed a similar kinetic after prime and after the boost, in term of AUC with an increase (kinetic families I, and II) or decrease (kinetic families III, and XI) post immunization. Three kinetic families displayed heterogeneous kinetics (Kinetic families, V, VI, and IX) and 4 kinetic families an no/undetectable response (kinetic families VII, X, XII, and XIII). Note that the kinetic family VI showed a tendency to be more enriched after boost than prime (p=0.0794). Some of these families tend to show a thinner, and slightly higher increase/decrease post-boost than post-prime (**Table S5**). Overall, none of them showed significantly different AUC between prime, and boost.

Only two kinetic families displayed significant changes after each immunization ($p<0.05$). Kinetic family IV, comprising $CD123^{+}$ eosinophils and basophils phenotypic families, showed a decrease after both immunizations but it increased to a level higher than baseline after the boost, but not after prime, especially when comparing D8PP and D8PB (p=0.0286). By contrast, the kinetic family VII,

comprising monocytes (including HLA-DR^{low}) monocytes, pDCs, and inflammatory cDCs / non-classical monocytes, displayed an increase after each immunization, but the magnitude of the increase was far lower for the boost compared to the prime ($p<0.05$ for D1 and D3). Note that, in term of cell number, these kinetics concerns at most 3-4.10^6 cells at a given timepoint. This is in contrast to the classical boost at two months where the vast majority of cells, in term of cell number, belonged to kinetic families displaying distinct prime-boost kinetics (Palgen et al., 2018).

Interestingly, inflammatory cDCs / non-classical monocytes (phenotypic family 27) belonged to the kinetic family VII, showing a stronger expansion after prime compared to boost. Note that in the classical boost, these cells were present at the prime response, but expanded far more after the classical boost compared to the prime. This difference supports further that response to the early boost strongly differs from the response to a classical boost.

Strikingly, basophils displayed a different response to prime and early boost, whereas they showed a very similar response to prime and classical boost.

To further assess the evolution of the phenotypic composition of each compartment, we also represented those data with pie charts displaying the phenotypic composition of each compartment along the timecourse of vaccination (**Figure S6**). Consistently with the kinetic pattern, prime and boost responses appear quite similar. Note that the baseline composition was remarkably stable among one given individual, which is in deep contrast to what was observed on NK cells compartment (Palgen et al., 2019).

Non-discrimination of post-prime versus post-boost samples within the early boost schedule

We eventually used MDS representation to more firmly take into account cell number variation in each kinetic family and visualize the overall response at each timepoint (**Figure S7A**). As for the boost at two months, most timepoints were overlapping together with the exceptions of H6PP, D1PP, and H6PB. Since, D1PB was overlapping, with the other samples, this suggests a tendency for post-boost response to be shorter. Still, using a two months-apart boost, PP samples and PB samples clearly segregated apart, whereas they were very close to each other for the early boost schedule. This strengthens the finding, that conversely to the classical schedule, innate myeloid responses to prime and boost are similar in the early boost schedule.

Post-prime and post-boost responses seemed hardly distinguishable based on these data. Still to more deeply addressed this question since some kinetic families displayed a distinct pattern, we use a multi-variate LASSO approach to extract features (kinetic families) allowing to distinguish PP samples from PB samples. As expectedly given the previous statement, the cross-validation could only build a model with a very high error rate on class prediction (the minimal mean square error (MSE) is 0.79, indicating an error of 0.89 for a targeted value around 1), which is around 4 times less accurate than the model built for the classical vaccine schedule (**Figure S7B**). This results indicates a poor accuracy of the model and supports our results conclusion that post-prime and post-boost responses are very similar to each other in the early boost schedule.

Association of phenotypes from the classical and the early boost schedule

We then wanted to associate the phenotypes that we identified in the early schedule study with the phenotypes we previously identified in the classical schedule study. We used in this comparison different animals a different CyTOF and a partially different antibody panels. Thus, the direct comparison of cell population phenotypes was challenging. To meet this challenge, we used the categorical heatmaps created in both studies. We performed a side-by-side phenotypic comparison of each dataset, using the Manhattan distance as the read-out of cell cluster phenotypes similarity (**Figure 6**).

Within the granulocytes compartment, all neutrophils phenotypic families impacted by early boost were associated with both intermediately and poorly activated neutrophils impacted by the classical boost. Some rare associations were found with the highly activated neutrophils and none were found with $CD4^+$ $CD23^+$ $CD11c^+$ neutrophils.

In the classical boost schedule, poorly activated neutrophils were more enriched at prime than at boost, intermediately activated neutrophils were impacted at both immunizations and highly activated neutrophils and $CD4^+$ $CD23^+$ $CD11c^+$ neutrophils were more enriched at boost than at prime. In addition, note that CD14+ neutrophils are associated with intermediately activated neutrophils whereas they were among poorly activated neutrophils in classical boost.

Basophils clusters were expectedly associated with each other in both studies By contrast and also expectedly, eosinophils did not match any phenotypic family in the classical boost, where eosinophils were removed from the analysis due to unspecific staining (Rahman et al., 2016) .

One discrepancy can be found in this compartment since phenotypic family 13 ($CD14^+$ neutrophils) was not associated with a counterpart in the classical boost (family 13), which is likely due to the expression of CD66 and CD11b being higher in the present study.

Overall, consistently with our results on kinetics, populations that were specifically enriched after the classical boost at two months were not found when the boost was done at two weeks.

Within the monocytes-DCs compartment, all the DCs subcompartment was associated with its counterpart in the classical boost and the same was mostly true for monocytes, suggesting that some phenotypically modified monocytes-DCs were generated in the early boost schedule, although they were not enriched much after the boost. Interestingly and expectedly inflammatory cDCs / non-classical monocytes were associated with their counterpart in the classical vaccine schedule both subcompartments.

Note also that the non-monocytes non-pDCs, non-cDCs APCs (uncharacterized APCs) from the classical boost were nicely associated with the three families of other APCs (28, 18, and 19) from the present study.

One discrepancy can still be observed, since phenotypic families 19, and 32 from the present study, which are respectively HLA-DR^{low}, and CCR5^{mid} CXCR4^{mid}, were not associated with families 22, 36 (HLA-DR^{low}), and 25 (CCR5^{mid} CXCR4^{mid}). This may be due to family 19 being CD32^{high} CD11b^{high} CD11a^{low}, whereas families 22 and 36 (classical boost) were CD32^{mid}, CD11b^{mid} CD11a^{mid}. Besides, family 32 is CD11alow CD14mid whereas family 25 (classical boost) was CD11a^{mid} CD14^{high}.

Interconnection between innate myeloid and adaptive in both schedule

Given the tremendous differences observed in both schedules in term of both antibody and innate myeloid responses, we sought to find a correlation between innate myeloid subphenotypes and antibody responses. We assessed the correlation between the peak of antibody response at D8PB, the long-term persistence of antibody response, for IgG, IgA, nAb, and FcγR affinity, and the overall response to prime (or boost) of poorly activated neutrophils, intermediately activated neutrophils, and highly activated monocytes (**Figure 7A and 7B**). Note that highly activated neutrophils, and poorly activated monocytes could not be used in this analysis, due to a low association between the two schedules.

Overall, an overall assocication was found between monocyte subpopulations, cDC subpopulations, nAb and FcγR affinity in the long-term on one side (**Figure 7A**). On the other side, an overall association was found between neutrophil subpopulations, IgG and IgA titers, and peak of FcγR affinity (**Figure 7A**).

It clearly showed that poorly activated neutrophil response was nicely anti-correlated with IgA peak, FcγR affinity peak, and nAb peak.Highly activated monocytes were positively correlated with FcγR affinity peak, and nAb peak. Eventually, highly activated cDCs were positively correlated with nAb peak, and long-term persistence. To note, intermediately activated neutrophils were not correlated with any variable, which may be caused by this population containing heterogeneously both cell responding to the prime or to the boost. Also, note that PP response only adds low correlation $0.5 < |R| < 0.7$ that were thus not taken into account.

Strikingly, while IgA peak was correlated with IgA long-term and nAb peak with nAb long-term persistence, FcγR affinity peak and long-term level were not correlated, neither was IgG peak and IgG long-term persistence. Still, interestingly, IgA in long-term was correlated with IgG long-term suggesting a similar mechanism behind their maintenance. Also nAb long-term and FcγR affinity long-term correlated, suggesting the same idea.

In addition, we investigated the functionality of the immune response to the boost compare to the prime, by assessing cytokine production. PBMCs were isolated at D3PP and D3PB and cytokine production was assessed without *ex vivo* re-stimulation. Interestingly, in the classical boost schedule, the production of many cytokines (G-SCF, IL-12/23, IL-1β, IL-18, IL-1Ra, TGFα, IFNγ, IL-4, IL-8, IL-13, MIP-1α, MIP-1β, TNFα and sCD40L) was enhanced after the boost compared to after the prime (ratio > 1). This was not the case for the early boost schedule (with the notable exception of IL-1β, whose production was also enhanced, although the amplitude was lower than in the classical boost schedule). Some of these cytokines were reported to be produced by adaptive cells (sCD40L) (Elgueta et al., 2009), or both innate and adaptive cells (IFNγ, IL-4, IL-8, IL-13, MIP-1α, MIP-1β and TNFα) (Akdis et al., 2016;

Menten et al., 2002), but some of them were associated with innate cell production, including myeloid and NK cells (G-SCF, IL-12/23, IL-1β, IL-18, IL-1Ra and TGFα).

Since PBMCs were used, granulocytes were missing in this cytokine production assessment. Besides, since T cells and B cells were present, we cannot differentiate here whether the enhanced production of innate cytokines observed in the classical boost schedule is due to the phenotype modification of innate cells, or by a differential stimulation by memory cells. Still, it worth to note, that IL-12, whose expression was enhanced in monocytes and cDCs pre-existing and responding to the classical boost, belong to the cytokines whose production was enhanced after the boost by unstimulated PBMCs. This connects the phenotype of the cell observed and the resulting functions of the immune system. Overall, this indicate that the immune response to the early boost and the classical (integrating both innate and adaptive compartment) differ in cytokine production capabilities.

Taken together, these results unveiled a deep interaction between innate myeloid responses, essentially to the boost and the adaptive responses.

Discussion

We first revealed a tremendous impact of the delay between the prime and boost on the IgA, nAb titer induced, as well as on the FcγR affinity of these antibodies. This is consistent with studies in humans showing that a delay between prime and boost below three weeks, impaired the ability of individuals to develop anti-smallpox protective immunity (Jackson et al., 2017).

Using mass cytometry technology, we were able to dissect in details the phenotype of the innate myeloid cells in blood during the classical boost and early boost schedule. Refining an existing panel of mass cytometry dedicated to this compartment, we were able to shed light on new populations among the monocytes-DCs compartment, such as CADM1^{+} APCs and FcεRI^{+} CD141^{+} APCs, previously undescribed to our knowledge. Note that the expression of CD172a on cDCs was remarkably low in our settings compared to literature (Guilliams et al., 2016), which may be casued by the fixation that was done prior to the staining. Besides, we also unveiled some more features of neutrophils subpopulations, such as the wide expression of CD39.

Surprisingly, we also found a population of CD123^{+} eosinophils. Interestingly, IL-3 was found to regulated eosinophil functions, which likely goes through CD123 binding (Rothenberg et al., 1988; Valent, 1994). Strikingly, these CD123^{+} eosinophils belong to the few populations that were more abundant after boost than after prime, suggesting that were sufficient to imprint those cells. Unfortunately, eosinophils were not analyzed in the classical boost schedule, since the protocol of staining with heparin was not available then (Palgen et al., 2018; Rahman et al., 2016).

Overall, we show that conversely to a classical schedule with a boost at two months, an early boost at weeks did not induce tremendous distinct innate myeloid response between prime and boost. Actually, no model was able to fully discriminate responses to the prime and boost in this schedule. This is consistent with the changes in innate myeloid cells phenotype occurring between 2 weeks, and 2 months as we previously reported (Palgen et al., 2018). It strongly indicates that restimulation with vaccine during the time period where the shift is occurring alters the ability of the innate immune cells to be trained. Since it also strongly impaired the ability to generate protective antibodies, one open question remains to know if both phenomena are solely correlated and causative of one another.

Interestingly, recent studies in mice indicated that the sole MVA stimulation of monocytes failed to induce innate training (Blok et al., 2019). This suggests either that monocyte training requires the actions of other cell types to occur, for example CD8 T cells, as for alveolar macrophages(Yao et al., 2018), or that training is performed not at the differentiated cell level, but rather at the progenitor levels. Indeed, training of hematopoietic stem cells was observed in mice (Kaufmann et al., 2018; Mitroulis et al., 2018). This would be consistent with the early boost at two weeks impairing the hematopoietic training, which is likely to be occurring during the first month post-prime. This might be extended to neutrophil training in addition to monocyte-DC compartment.

Although the same subpopulations were responding to prime and boost in the early boost schedule, there was a trend to have a more intense and rapid cell response to boost. Thus, it might be that this early boost would serve as a second prime and that a latter boost months after the early one could involve trained innate immunity and overall protective immune memory.

Interestingly when we associated the cells induced during this early boost schedule with the one induced in the classical boost we saw different patterns in granulocytes vs. monocytes-DCs. In the granulocytes compartment, the cells that were responding to the sole classical boost were not found at all when the boost occurred at two weeks. This is fully consistent with the early boost schedule failing to induce trained innate myeloid immunity. In the monocytes-DCs compartment, almost all cells could be associated with a counterpart in both schedules. This is consistent with monocytes-DCs subpopulations responding more to one of the two immunizations in the classical schedule but being present at every timepoints. This suggests here more an inability to recruit or expand an existing population of monocytes-DCs.

Also from an analytical point of view, our comparison analysis was performed on the dataset obtained on different animals, using different panels and using different mass cytometry devices and it allowed us to find the biologically relevant associations of cells in both datasets. This opens new perspectives with the possibility to combine dataset coming from very different settings (including potential data obtained from different labs with different devices), which has always been a tricky issue when it came to mass cytometry data (Leipold et al., 2018).

We were also able to unveil a strong relationship between innate myeloid responses and antibody responses. Interestingly, there was a strong association with the peak of the antibody response (in term of IgA, nAb, and FcγR affinity), suggesting that the peak of the response strongly correlate on the innate immunity induced. On the contrary, only the long-term persistence of nAb (and not of IgG and IgA) was highly correlated with innate myeloid responses (for IgG, $0.6 < |R| < 0.7$ and for IgA $0.5 < |R| < 0.6$), strongly suggesting that long-term persistence of IgG and IgA likely involve

other mechanisms. This is consistent with literature aiming at predicting antibody response based on innate responses (Nakaya et al., 2015). Still, not that for IgA and nAb the peak of the response and long-term persistence were highly correlated and the same tendency existed for IgG (R=0.65) suggesting that there is actually a direct link between peak and long-term persistence.

Interestingly a study in rhesus macaques vaccinated with malaria antigen Pfs25 with different adjuvants, showed a strong correlation between innate immune parameters, including MCP-1, IL-1Ra and IFNα production, as well as DC associated transcripts on one side, and antibody half-life on the other side (Thompson et al., 2018). This consistently supports our finding regarding the close interaction between innate myeloid cells and humoral response.

Eventually, the subphenotype composition of the innate myeloid compartment was associated with distinct cytokine production capability of the immune system, both innate and adaptive. Within our settings, it was unfortunately not possible to deconvoluate the cytokine production due to the phenotypically distinct innate myeloid and cytokine produced either by memory T ot B cells directly or innate cells stimulated by memory T or B cells. Still, it indicated that the overall immune response to the boost (integrating innate myeloid subphenotypes as well as T and B cells), differ functionally (in term of cytokine production) from the overall response to the prime in the classical boost schedule but poorly in the early boost schedule.

To our knowledge, this the first time that a study assesses the impact of the time-lapse between prime and boost on the development of innate immune response and immune memory. This shed light on the importance of this delay for the development of a strong innate immunity and a qualitatively distinct adaptive response. This is a first valuable step to understand the mechanisms at play in prime-boost vaccination, involving the interplay of both innate and adaptive immunity and better refine the development of future vaccines.

Methods

Ethics statement

This experiment was approved by the «Ministère de l'Éducation Nationale, de l'Enseignement Supérieur et de la Recherche» (France) and the ethical committee «Comité d'éthique en expérimentation animale n°44» (France) under the reference 2015031314518254.02 (APAFIS#319) for the classical boost and 2015031314518254 (APAFIS#319).02 for the early boost schedule. Animals were handled by veterinarians in accordance with national regulations (CEA Permit Number A 92-32-02) and the European Directive (2010/63, recommendation Nº9) and in compliance with Standards for Human Care and Use of Laboratory of the Office for Laboratory Animal Welfare (OLAW, USA) under OLAW Assurance number #A5826-01.

Vaccine schedule, and blood sampling

Five cynomolgus macaques , identified as BC554D BT145, CBL004, CC840, and CCB116, were immunized subcutaneously two weeks apart with the ANRS recombinant MVA HIV B vaccine (MVATG17401; Transgene, Illkirch-Graffenstaden, France) at $4x10^8$ plaque forming units (**Figure 1**). As previously described (Palgen et al., 2018, 2019; Pejoski et al., 2016), this vaccine encodes for the full-length *gag* sequence (amino acids 1 to 512), fragments of the *pol* sequence (amino acids 172 to 219, 325 to 383, and 461 to 519), and fragments of the *nef* sequence (amino acids 66 to 147, and 182 to 206) from the Bru/Lai isolate (Los Alamos database accession number K02013). Blood samples were longitudinally collected in Lithium-Heparin for soluble plasma proteins quantification and single-cell mass cytometry profiling, and in EDTA for complete blood count.

Serology

In brief, wild-type MVA (obtained from B. Verrier, Biologie tissulaire et ingenierie therapeutique, Institute of Biology and Chemistry of Proteins, Lyon, France) was used to coat 96-well MaxiSorp microplates (Nunc; Thermo Fisher) at 10^5 PFU/well in coating buffer (200 mM $NaHCO_3$, 80 mM Na_2CO_3, pH 9.5) overnight at 4˚C. Wells were washed five times with wash buffer (PBS, 0.1% Tween 20, 10 mM EDTA) and blocked for 1 h at RT with 3% w/v BSA (Sigma). Plates were washed five times and incubated with 2-fold serial dilutions of macaque serum diluted in 1% w/v BSA in PBS for 2 h at RT, starting at 1:50 for IgG and IgA or 1:20 for IgM. Plates were then washed five times and 1:20000, 1:5000 or 1:1000, peroxidase-conjugated goat anti-monkey H+L chain IgG (Bio-Rad, Marne-la-Coquette, France), IgA (Alpha Diagnostic, San Antonio, TX) or IgM (AbD Serotec), respectively, in 1% BSA (w/v) PBS was added and incubated for 1 h at RT. In the case of IgG1, IgG2, and IgG3 (NHP Bioresources), antibodies were biotinylated (Thermo Scientific) according to manufacturer's instruction. The biotinylated Ab diluted at 1:500, 1:100 or 1:100, respectively, were used and incubated for 1hr at RT. Plates were washed five times and incubated with 1:1000 streptavidin-biotin (Thermo Scientific) with PBSE + 1% BSA for 1 h at RT. All plates were washed five times and 100 µL 3,39,5,59-tetramethylbenzidine (Thermo Scientific) was added and incubated for 20 min at RT in the dark. The reaction was stopped by adding 100 µL 2N H_2SO_4. Absorbance was measured at 492 nm using a spectrophotometer and data were analyzed using Magellan software (both from Tecan, Lyon, France). Ab titers were calculated by extrapolation from the OD as a function of a serum dilution curve (five-parameter logistic curve) and were defined as the dilution of the test serum reaching 2 x OD of the corresponding pre-immune serum tested at 1:50.

Antibody neutralization assay

Neutralizing antibody (nAb) titer was determined using a modified version of a standard plaque inhibition assay. In brief, wild-type MVA (1 PFU/cell) was mixed with an equal volume of 2-fold serial dilutions of serum in assay medium (DMEM, 2% FCS), starting at 1:20. After 60 min of incubation at 37˚C, 0.1 ml of the serum-virus mixture was transferred, in duplicate, to a 96-well plate containing subconfluent HeLa cells. After 48 h of incubation at 37˚C, cell viability was quantified using an MTS/PMS assay (CellTiter 96 AQueous Non-Radioactive Cell Proliferation Assay; Promega). Absorbance was measured at 492 nm using a spectrophotometer (Multiskan FC; Thermo Scientific) and data were analyzed using SoftMax Pro software (version 4.6; Molecular Devices). The sample dilution versus the percentage viability was plotted (four-parameter logistic curve) to calculate a neutralizing concentration, corresponding to the sample dilution resulting in 50% neutralization of virus-mediated cell mortality. Cell viability in uninfected control cells and in infected cells incubated with undiluted vaccinia immune globulin i.v. (human polyclonal anti-vaccinia virus IgG; BEI Resources) was equivalent as expected.

ELISA-based FcγRIIIa dimer-binding assay

The Fc-regions binding to FcgR was used as in (Chung and Kent, 2017). Briefly, recombinant soluble biotin-tagged homodimers of FcgRIIIa was used in this study to quantify the IgG specific to MVA viral particles binding FcgRIIIa dimers in close proximity. MVA Ags at **50** ng per well diluted in PBS as well as no Ag control for each sample was coated on 96-well flat-bottom MaxiSorp plates (Nalgene Nunc, Rochester, NY). VIGIV (#3957; National Institutes of Health AIDS Reagent) at 5 mg/ml was coated on the plate at the same time to normalize FcgR activity across different plates. Following overnight incubation at 4˚C, the ELISA plates were washed with PBS containing 0.05% Tween20 (Sigma-Aldrich)

and blocked for 1 h at 37˚C with 140 ml PBS containing 1 mM EDTA (Sigma-Aldrich) and 1% BSA (Sigma-Aldrich) (PBSE + 1% BSA). Following plate washing, heat-inactivated macaque (56˚C for 45 min) serum was added at 1:10 dilution in PBSE + 1% BSA. After incubation and washing, 0.1 mg/ml purified FcgIIIa-V158 dimer-biotin diluted in PBSE + 1% BSA was added to every well of the plate. Following incubation and wash, HRP-conjugated streptavidin (Thermo Scientific) was added in 1:1000 dilution with PBSE + 1% BSA. After incubation and washing, the color was developed using 3,395,59-tetramethylbenzidine (Sigma-Aldrich) followed by 1 M HCl stop solution. Absorbance at 450 nm wavelength was recorded as OD. A positive signal was defined as an OD higher than mean + 2 x OD obtained using sera from MVA negative donors against each Ag tested.

Quantification of circulating proteins

Circulating protein (cytokines, chemokines and growth factors, except IP-10) levels were quantified with a multiplex immunoassay (MILLIPLEX MAP non-human primate cytokine magnetic bead panel, Millipore). Note that blood samples at D-27PP were not available for this assay. IP-10 concentration was assessed by ELISA (human CXCR10/IP-10, R&D systems).

Whole blood fixation

Whole blood processing was done as previously described (Elhmouzi-Younes et al., 2017; Palgen et al., 2018, 2019) to preserve all leukocytes including granulocytes. Briefly, 1mL of blood was incubated with a fixation mixture containing PFA and glycerol (Elhmouzi-Younes et al., 2017; Egger et al., 2001) for 10min at 4°C. After centrifugation, erythrocytes were lysed in 10mL of milli-Q water at

room temperature for 20min. Cells were then washed in DPBS 1X and stored at -80°C at a final concentration of 15.10^6 cells in the fixation mixture.

Cell staining and mass cytometry acquisitions

Cell staining was done similarly as previously described (Elhmouzi-Younes et al., 2017; Palgen et al., 2018, 2019). Briefly, three millions of fixed leukocytes were thawed per sample. After 2 washes with PBS/BSA at 0.5%, cells were incubated with the surface antibodies at 4°C for 30min (**Table S3**). Note that the staining mixture contained 300U of heparin to prevent unspecific binding of metal by eosinophils as suggested in the literature (Rahman et al., 2016). Samples were washed twice in PBS 1X and fixed in PBS/PFA 1.6% for 20min RT. After permeabilization in Perm/Wash Buffer 1X (BD Biosciences) for 10min at RT, cells were incubated with intracellular antibodies at 4°C for 30min. Cells were barcoded with the Cell-ID 20-Plex Pd barcoding kit (Fluidigm, San Fransisco, USA). In details, after 2 washes in the Barcode perm Buffer, cells were incubated with one of the indicated combinations of Pd for 30min RT. Finally, cells were washed in PBS and incubated overnight with 0.1µM of iridium RNA/DNA intercalator in PBS/PFA at 1.6%. The next day, cells were washed three times with milli-Q water and filtered using a 35µm nylon mesh cell strainer (BD Biosciences). EQ™ four elements calibration beads (Fluidigm, San Fransisco, USA) were added following manufacturer's protocol. Sample acquisitions were performed using a Helios CyTOF (Fluidigm).

In details, 5 staining acquisitions were performed (one per animal) using the same batch of antibodies. In addition, we followed an established strategy (Kleinsteuber et al., 2016) to control the quality of each staining/acquisition and their reproducibility by including two identical control samples.

Note that samples from D21PB were not available for mass cytometry analysis.

Data preprocessing and leukocyte gating

To avoid bias in density estimation by the Spanning-tree Progression Analysis of Density-normalized Events (SPADE) algorithm (Qiu et al., 2011), null values of mean signal intensities (MSI) were randomized between -1 and 0. Data were then normalized using the MATLAB normalizer from Rachel Finck *et al.* (Finck et al., 2013).

Initial gating was done as previously described (Elhmouzi-Younes et al., 2017; Palgen et al., 2018). Note that although the use of heparin strongly reduced the unspecific staining of eosinophils, some $CD3^{+}CD66^{+}$ cells were still excluded at that step (around 0.2% of all the acquired events).

Automatic identification of cell populations

The SPADE algorithm was used to automatically identify cell populations as previously described to (Palgen et al., 2018, 2019). Briefly, a uniform pre-downsampling was used to select 95,000 cells from each sample (which corresponded to the number of cells contained in the smallest sample –**Table S6**). Cell clusters (groups of cells having similar phenotypic patterns) were identified using SPADE, applied on all samples (all macaques and all timepoints). Upsampling was eventually performed.

The optimal SPADE settings were determined using the SPADEVizR package (Gautreau et al., 2016). These parameters were 28 clustering markers (CD66, HLA-DR, CD3, CD64, CD8, CD123, CD11a, CD11b, CD62L, CD4, FcεRI, CD86, CD125, CD172a, CD45, CD1c, CD32, CD39, CCR5, CD16, CD11c, CXCR4, CD14, CD23, CD141, CD20, CCR7, and CADM1), 800 clusters, a density-based downsampling of 10% and an outlier density parameter of 0.01. The clustering quality was quantified as the percentage of clusters displaying a unimodal and narrow distribution for all clustering markers. Markers distributions were assessed using the Hartigan's dip test (p-value<0.05 to reject the uni-modality hypothesis). Markers distributions with an interquartile range (IQR) < 2 were considered to be narrow. These settings resulted in a clustering quality of 80.12% of uniform clusters. For each marker, the numbers and percentages of non-uniform clusters are displayed in **Table S7**.

Leukocyte counts, absolute number calculation, and abundance profiles

The leukocyte counts were quantified using an HMX instrument (Beckman Coulter). The absolute number of cells in a population was computed as N=the absolute number of leukocytes expressed per µL of blood x number of cells in the population detected by the CyTOF/total number of leukocytes (defined as non-$CD3^{+}CD66^{+}$ cells) detected by the CyTOF. The absolute number kinetics was called the abundance profile.

Note that complete blood count was not available for samples at D28PB.

Heatmap representations of the cell cluster phenotypes

Categorical heatmaps showing the phenotype of cell cluster phenotypes were generated using SPADEVizR (Gautreau et al., 2016). The marker range of expression was divided between the 5^{th}, and the 95^{th} percentile into five categories for all cell clusters. The mean of the median MSI for each marker among samples was mapped onto those five categories to infer cell cluster phenotype. For each cluster, samples contributing less than 10 cells were excluded for cell cluster phenotype inference. Hierarchical clusterings of cell clusters and markers, represented in the heatmaps, were performed using the Euclidean metric based on the ward.D linkage.

Phenotypic and kinetic families

For each compartment, cell clusters sharing similar phenotypes were gathered into phenotypic families based on the cluster dendrogram resulting from the hierarchical clustering computed on phenotypic categories of expression. Phenotypic families sharing similar dynamics were gathered into kinetic families based on their abundance profiles. This determination was performed with the hierarchical method based on the Pearson correlation and complete linkage.

Statistical tests

Blood protein concentrations and cell abundances were compared between timepoints using the permutation test available in the "exactRankTests" R package (available at https://cran.r-project.org/web/packages/exactRankTests/index.html). The area under the curve (AUC) corresponds to the sum over time of all plasma soluble factor concentrations (cumulated concentration) or cell abundances (cumulated abundance) between H6 and D14. PP AUC and PB AUC were compared using a permutation test.

Discrimination between post-prime and post-boost innate myeloid responses

The Least Absolute Shrinkage,and Selection Operator (LASSO) approach was performed on R using the "lars" package. Centered and reduced abundance profiles of kinetic families were used as entry parameters. The validity of classification at each iteration was assessed by cross-validation.

Phenotypic comparison of cell clusters from the two vaccine schedules

Cell cluster phenotypes from this study and the classical 2 months apart schedule (Palgen et al., 2018) were compared using the Manhattan distance and visualized using CytoCompare R-package (Platon et al., 2018). Distances were computed based on the heatmap expression categories of the 27 markers shared in both panels (CCR5, CCR7, CD3, CD4, CD8, CD11a, CD11b, CD11c, CD14, CD16, CD20, CD23, CD32, CD45, CD64, CD66, CD86, CD123, CXCR4, HLA-DR, IFNα, IL-1α, IL-4, IL-6, IL-8, IL-12, and IP-10). Basically, distances consisted of the sum of the absolute value of the difference between the values of each cluster for each marker. This distance was penalized when any of the terms was above 2. Distances equal or below 9 were considered as significant.

Two clusters were considered as associated when their distance calculated for the 27 markers was equal or below 9 and their distance calculated for each of the 27 markers was equal or below 2.

Pairs of clusters, having a distance equal or below 9, without were considered as similar when the distance between them was without the clusters having a distance above to 2 for any marker.

Correlations between antibody response and innate myeloid responses

Innate myeloid cell populations were associated in the two schedules based on the Manhattan distance. Two populations were associated only if they were the closest neighbor of each other, based on the ratio between the actual number of associations (clusters linked together) and the number of potential associations between them. The area under the curve was used to assess the magnitude of the response PP (H0PP, H6PP, D1PP, D3PPa, and D8PP) and the boost (H0PB, H6PB, D1PB, D3PB, and D8PB). To avoid technical bias in this calculation, the area was normalized based on the mean abundance of each cell population within each schedule during the response to prime. In other words, for a given animal and a given cell population: AUC = sum(abundances during the prime (respectively the boost))/mean(abundances during the prime for all animals from the same vaccine schedule). Pearson correlation was computed between the area under the curve of each innate myeloid cell population abundance and the antibody response at the peak (either D8PB or D14PB according to the response) and the long-term (at M6PB).

Cytokines production by immune cells assessment

PBMCs were isolated and left overnight at 37°C without re-stimulation. Supernatant were harvessed the next day and cytokines released in the medium were assessed with a multiplex immunoassay (MILLIPLEX MAP non-human primate cytokine magnetic bead panel, Millipore).

Acknowledgments

This work was supported by the “Investissements d’Avenir” programs managed by the ANR under reference ANR-10-LABX-77-01 funding the Vaccine Research Institute (VRI), Créteil (ImMemory research program), ANR-11-INBS-0008 funding the Infectious Disease Models and Innovative Therapies (IDMIT, Fontenay-aux-Roses, France) infrastructure, and ANR-10-EQPX-02-01 funding the FlowCyTech facility (IDMIT, Fontenay-aux-Roses, France) and by the European Union, EVHA H2020 project (Grant N°681032). We would like to thank all members of the ASW and L2I groups from IDMIT.

Author’s contributions

RLG, and ASB designed the study. NDB supervised immunizations, and samples collection. ARP and ASB performed serology analyses.BW, MH and SJK provided the FcR binding affinity measurement technology. JLP and ASB developed the innate myeloid antibody panel. HA processed blood samples. JLP stained and acquired samples. QJ and AC set the CyTOF instrument. JLP and NT analyzed the data. JLP, NT, RLG, and ASB wrote the paper. ARP, QJ, HA, BW, MH, SJK, NDB, VC, AC, and YL reviewed the manuscript.

Competing financial interests

The authors declare no conflict of interest.

References

Akdis, M., Aab, A., Altunbulakli, C., Azkur, K., Costa, R.A., Crameri, R., Duan, S., Eiwegger, T., Eljaszewicz, A., Ferstl, R., et al. (2016). Interleukins (from IL-1 to IL-38), interferons, transforming growth factor β, and TNF-α: Receptors, functions, and roles in diseases. J. Allergy Clin. Immunol. *138*, 984–1010.

Antal-Szalmas, P., Strijp, J.A., Weersink, A.J., Verhoef, J., and Van Kessel, K.P. (1997). Quantitation of surface CD14 on human monocytes and neutrophils. J. Leukoc. Biol. *61*, 721–728.

Blok, B.A., Jensen, K.J., Aaby, P., Fomsgaard, A., van Crevel, R., Benn, C.S., and Netea, M.G. (2019). Opposite effects of Vaccinia and modified Vaccinia Ankara on trained immunity. Eur. J. Clin. Microbiol. Infect. Dis.

Chung, A.W., and Kent, S.J. (2017). Dimeric Fc g Receptor Enzyme-Linked Immunosorbent Assay To Study HIV-Specific Antibodies: A New Look into Breadth of Fc g Receptor Antibodies Induced by the RV144 Vaccine Trial.

Drexler, I., Staib, C., and Sutter, G. (2004). Modified vaccinia virus Ankara as antigen delivery system: how can we best use its potential? Curr. Opin. Biotechnol. *15*, 506–512.

Earl, P.L., Americo, J.L., Wyatt, L.S., Eller, L.A., Whitbeck, J.C., Cohen, G.H., Eisenberg, R.J., Hartmann, C.J., Jackson, D.L., Kulesh, D.A., et al. (2004). Immunogenicity of a highly attenuated MVA smallpox vaccine and protection against monkeypox. Nature *428*, 182–185.

Egger, G., Burda, A., and Glasner, A. (2001). A simple method for measuring the F-actin content of human polymorphonuclear leukocytes in whole blood. Virchows Archiv : An International Journal of Pathology *438*, 394–397.

Elgueta, R., Benson, M.J., de Vries, V.C., Wasiuk, A., Guo, Y., and Noelle, R.J. (2009). Molecular mechanism and function of CD40/CD40L engagement in the immune system. Immunol. Rev. *229*, 152–172.

Elhmouzi-Younes, J., Palgen, J.-L., Tchitchek, N., Delandre, S., Namet, I., Bodinham, C.L., Pizzoferro, K., Lewis, D.J.M., Le Grand, R., Cosma, A., et al. (2017). In depth comparative phenotyping of blood innate myeloid leukocytes from healthy humans and macaques using mass cytometry. Cytometry. Part A: The Journal of the International Society for Analytical Cytology.

Finck, R., Simonds, E.F., Jager, A., Krishnaswamy, S., Sachs, K., Fantl, W., Pe'er, D., Nolan, G.P., and Bendall, S.C. (2013). Normalization of mass cytometry data with bead standards. Cytometry A *83*, 483–494.

Gautreau, G., Pejoski, D., Le Grand, R., Cosma, A., Beignon, A.-S., and Tchitchek, N. (2016). SPADEVizR: an R package for Visualization, Analysis and Integration of SPADE results. Bioinformatics (Oxford, England).

Greenwood, B. (2014). The contribution of vaccination to global health: past, present and future. Philos. Trans. R. Soc. Lond., B, Biol. Sci. *369*, 20130433.

Guilliams, M., Dutertre, C.-A., Scott, C.L., McGovern, N., Sichien, D., Chakarov, S., Van Gassen, S., Chen, J., Poidinger, M., De Prijck, S., et al. (2016). Unsupervised High-Dimensional Analysis Aligns Dendritic Cells across Tissues and Species. Immunity *45*, 669–684.

't Hart, B.A., Bogers, W.M., Haanstra, K.G., Verreck, F.A., and Kocken, C.H. (2015). The translational value of non-human primates in preclinical research on infection and immunopathology. Eur. J. Pharmacol. *759*, 69–83.

Jackson, L.A., Frey, S.E., El Sahly, H.M., Mulligan, M.J., Winokur, P.L., Kotloff, K.L., Campbell, J.D., Atmar, R.L., Graham, I., Anderson, E.J., et al. (2017). Safety and immunogenicity of a modified vaccinia Ankara vaccine using three immunization schedules and two modes of delivery: A randomized clinical non-inferiority trial. Vaccine *35*, 1675–1682.

Kardani, K., Bolhassani, A., and Shahbazi, S. (2016). Prime-boost vaccine strategy against viral infections: Mechanisms and benefits. Vaccine *34*, 413–423.

Kaufmann, E., Sanz, J., Dunn, J.L., Khan, N., Mendonça, L.E., Pacis, A., Tzelepis, F., Pernet, E., Dumaine, A., Grenier, J.-C., et al. (2018). BCG Educates Hematopoietic Stem Cells to Generate Protective Innate Immunity against Tuberculosis. Cell *172*, 176-190.e19.

Kleinsteuber, K., Corleis, B., Rashidi, N., Nchinda, N., Lisanti, A., Cho, J.L., Medoff, B.D., Kwon, D., and Walker, B.D. (2016). Standardization and quality control for high-dimensional mass cytometry studies of human samples. Cytometry. Part A: The Journal of the International Society for Analytical Cytology *89*, 903–913.

Leipold, M.D., Obermoser, G., Fenwick, C., Kleinstuber, K., Rashidi, N., McNevin, J.P., Nau, A.N., Wagar, L.E., Rozot, V., Davis, M.M., et al. (2018). Comparison of CyTOF assays across sites: Results of a six-center pilot study. J. Immunol. Methods *453*, 37–43.

Menten, P., Wuyts, A., and Van Damme, J. (2002). Macrophage inflammatory protein-1. Cytokine Growth Factor Rev. *13*, 455–481.

Mitroulis, I., Ruppova, K., Wang, B., Chen, L.-S., Grzybek, M., Grinenko, T., Eugster, A., Troullinaki, M., Palladini, A., Kourtzelis, I., et al. (2018). Modulation of Myelopoiesis Progenitors Is an Integral Component of Trained Immunity. Cell *172*, 147-161.e12.

Nakaya, H.I., Hagan, T., Duraisingham, S.S., Lee, E.K., Kwissa, M., Rouphael, N., Frasca, D., Gersten, M., Mehta, A.K., Gaujoux, R., et al. (2015). Systems Analysis of Immunity to Influenza Vaccination across Multiple Years and in Diverse Populations Reveals Shared Molecular Signatures. Immunity *43*, 1186–1198.

Palgen, J.-L., Tchitchek, N., Elhmouzi-Younes, J., Delandre, S., Namet, I., Rosenbaum, P., Dereuddre-Bosquet, N., Martinon, F., Cosma, A., Lévy, Y., et al. (2018). Prime and Boost Vaccination Elicit a Distinct Innate Myeloid Cell Immune Response. Sci Rep *8*, 3087.

Palgen, J.-L., Tchitchek, N., Huot, N., Elhmouzi-Younes, J., Lefebvre, C., Rosenbaum, P., Dereuddre-Bosquet, N., Martinon, F., Hocini, H., Cosma, A., et al. (2019). NK cell immune responses differ after prime and boost vaccination. J. Leukoc. Biol.

Pejoski, D., Tchitchek, N., Rodriguez Pozo, A., Elhmouzi-Younes, J., Yousfi-Bogniaho, R., Rogez-Kreuz, C., Clayette, P., Dereuddre-Bosquet, N., Lévy, Y., Cosma, A., et al. (2016). Identification of Vaccine-Altered Circulating B Cell Phenotypes Using Mass Cytometry and a Two-Step Clustering Analysis. J. Immunol. *196*, 4814–4831.

Platon, L., Pejoski, D., Gautreau, G., Targat, B., Le Grand, R., Beignon, A.-S., and Tchitchek, N. (2018). A computational approach for phenotypic comparisons of cell populations in high-dimensional cytometry data. Methods *132*, 66–75.

Plotkin, S.A. (2010). Correlates of protection induced by vaccination. Clin. Vaccine Immunol. *17*, 1055–1065.

Qiu, P., Simonds, E.F., Bendall, S.C., Gibbs, K.D., Bruggner, R. V, Linderman, M.D., Sachs, K., Nolan, G.P., and Plevritis, S.K. (2011). Extracting a cellular hierarchy from high-dimensional cytometry data with SPADE. Nature Biotechnology *29*, 886–891.

Rahman, A.H., Tordesillas, L., and Berin, M.C. (2016). Heparin reduces nonspecific eosinophil staining artifacts in mass cytometry experiments. Cytometry A *89*, 601–607.

Ramshaw, I.A., and Ramsay, A.J. (2000). The prime-boost strategy: exciting prospects for improved vaccination. Immunol. Today *21*, 163–165.

Rappuoli, R., Pizza, M., Del Giudice, G., and De Gregorio, E. (2014). Vaccines, new opportunities for a new society. Proc. Natl. Acad. Sci. U.S.A. *111*, 12288–12293.

Reeves, P.M., Sluder, A.E., Paul, S.R., Scholzen, A., Kashiwagi, S., and Poznansky, M.C. (2018). Application and utility of mass cytometry in vaccine development. FASEB J. *32*, 5–15.

Rivera-Hernandez, T., Carnathan, D.G., Moyle, P.M., Toth, I., West, N.P., Young, P.L., Silvestri, G., and Walker, M.J. (2014). The Contribution of Non-human Primate Models to the Development of Human Vaccines. Discov Med *18*, 313–322.

Rothenberg, M.E., Owen, W.F., Silberstein, D.S., Woods, J., Soberman, R.J., Austen, K.F., and Stevens, R.L. (1988). Human eosinophils have prolonged survival, enhanced functional properties, and become hypodense when exposed to human interleukin 3. J. Clin. Invest. *81*, 1986–1992.

Sebastian, S., and Gilbert, S.C. (2016). Recombinant modified vaccinia virus Ankara-based malaria vaccines. Expert Rev Vaccines *15*, 91–103.

Simoni, Y., Chng, M.H.Y., Li, S., Fehlings, M., and Newell, E.W. (2018). Mass cytometry: a powerful tool for dissecting the immune landscape. Curr. Opin. Immunol. *51*, 187–196.

Thompson, E.A., Ols, S., Miura, K., Rausch, K., Narum, D.L., Spångberg, M., Juraska, M., Wille-Reece, U., Weiner, A., Howard, R.F., et al. (2018). TLR-adjuvanted nanoparticle vaccines differentially influence the quality and longevity of responses to malaria antigen Pfs25. JCI Insight *3*.

Valent, P. (1994). The phenotype of human eosinophils, basophils, and mast cells. J. Allergy Clin. Immunol. *94*, 1177–1183.

Volz, A., and Sutter, G. (2017). Modified Vaccinia Virus Ankara: History, Value in Basic Research, and Current Perspectives for Vaccine Development. Adv. Virus Res. *97*, 187–243.

Woodland, D.L. (2004). Jump-starting the immune system: prime-boosting comes of age. Trends Immunol. *25*, 98–104.

Yao, Y., Jeyanathan, M., Haddadi, S., Barra, N.G., Vaseghi-Shanjani, M., Damjanovic, D., Lai, R., Afkhami, S., Chen, Y., Dvorkin-Gheva, A., et al. (2018). Induction of Autonomous Memory Alveolar Macrophages Requires T Cell Help and Is Critical to Trained Immunity. Cell *175*, 1634-1650.e17.

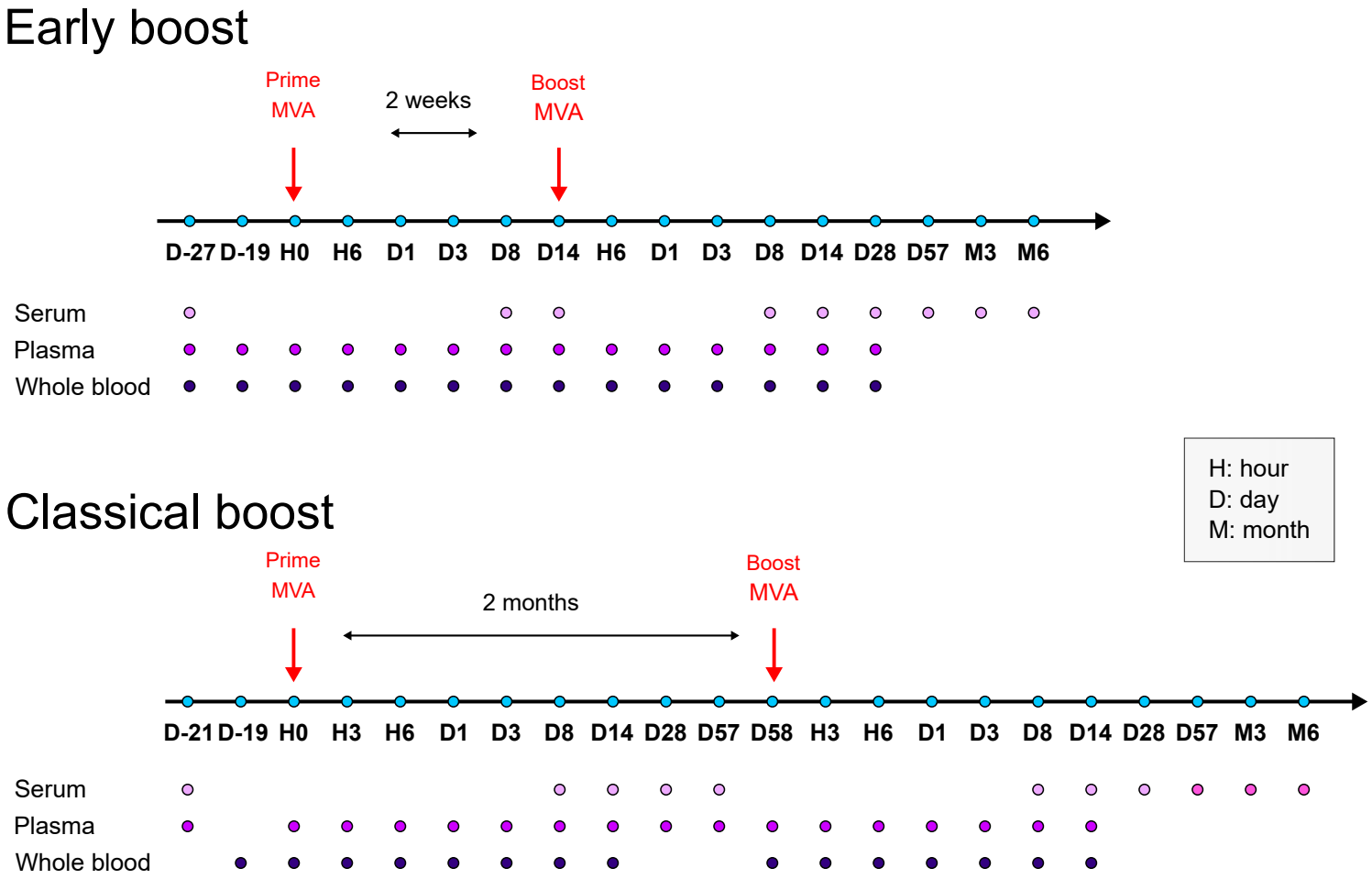

Figure 1 – Overview of the experimental design. Blood samples from five adult cynomolgus macaques were collected longitudinally at the indicated timepoints – hours (H), days (D), and months (M) post-prime (PP), and post-boost (PB). Macaques were immunized twice subcutaneously with MVA HIV-B at a dose of $4x10^8$ PFU, two weeks apart (early boost schedule) or two months apart (classical schedule).

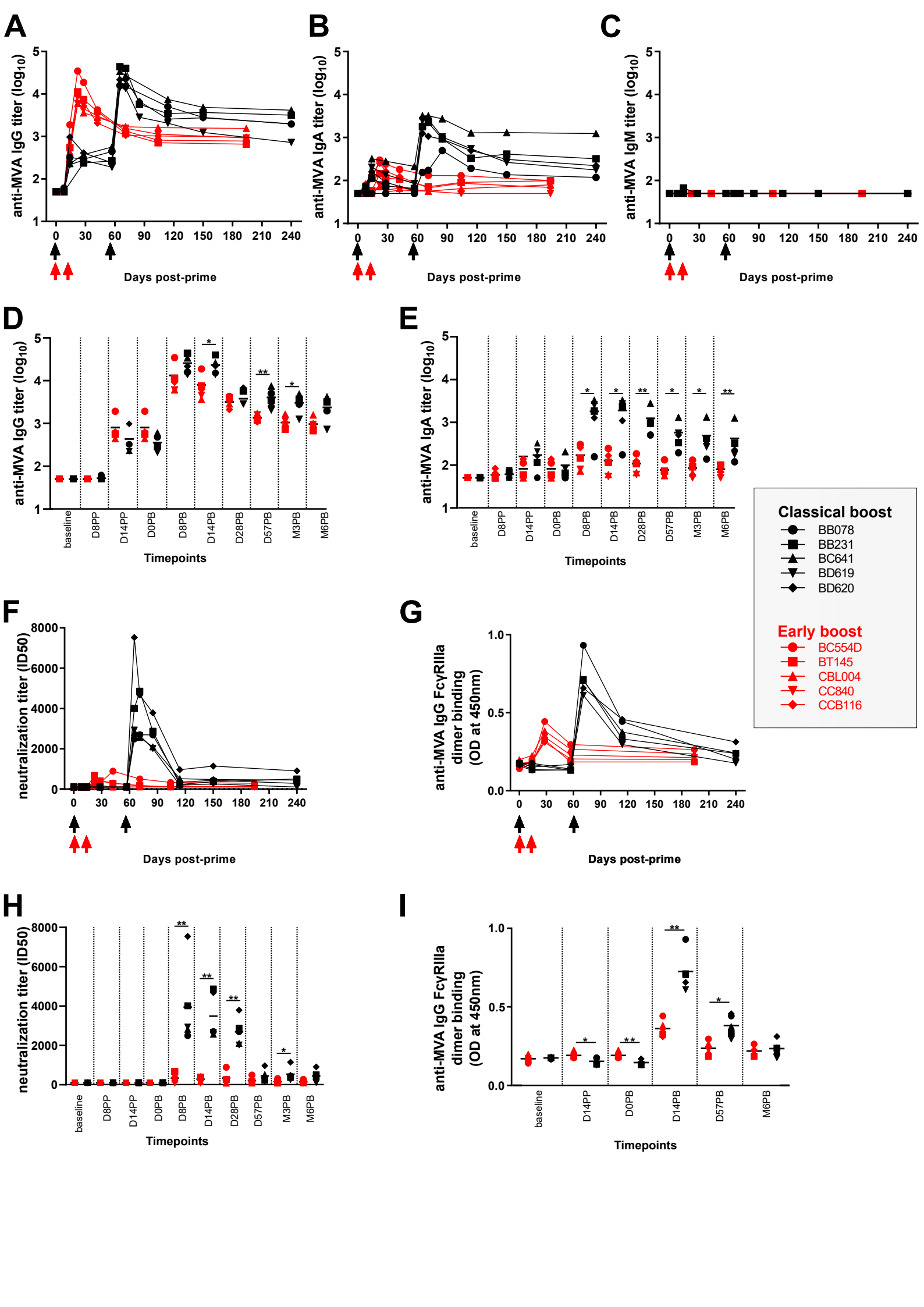
A
anti-MVA IgG titer (log10)
Days post-prime
B
anti-MVA IgA titer (log10)
Days post-prime
C
anti-MVA IgM titer (log10)
Days post-prime
D
anti-MVA IgG titer (log10)
baseline
D8PP
D14PP
D0PB
D8PB
D14PB
D28PB
D57PB
M3PB
M6PB
Timepoints
E
anti-MVA IgA titer (log10)
Timepoints
Classical boost
BB078
BB231
BC641
BD619
BD620
Early boost
BC554D
BT145
CBL004
CC840
CCB116
F
neutralization titer (ID50)
Days post-prime
G
anti-MVA IgG FcγRIIIa dimer binding (OD at 450nm)
Days post-prime
H
neutralization titer (ID50)
Timepoints
I
anti-MVA IgG FcγRIIIa dimer binding (OD at 450nm)
Timepoints

Figure 2. MVA-specific serum antibody isotypes induced by vaccine regimens. MVA-specific Ab binding (**A**) IgG, (**B**) IgA, and (**C**) IgM titers were measured by direct ELISA in macaque serum, and expressed in individual concentrations over time. Comparison of MVA specific antibody binding (**D**) IgG, and (**E**) IgA were performed at the indicated timepoints between early boost, and classical boost strategies. (**F**) MVA-nAb titers were detected by a HeLa cell assay at the indicated time points. (**G**) Fc_{γ} receptor binding induced by prime-boost strategies was measured. Comparisons were performed using permutation tests (*$p<0.05$, **$p<0.01$). Colors indicate immunization strategy: EB (red), and CB (black). Immunizations are indicated by arrows.

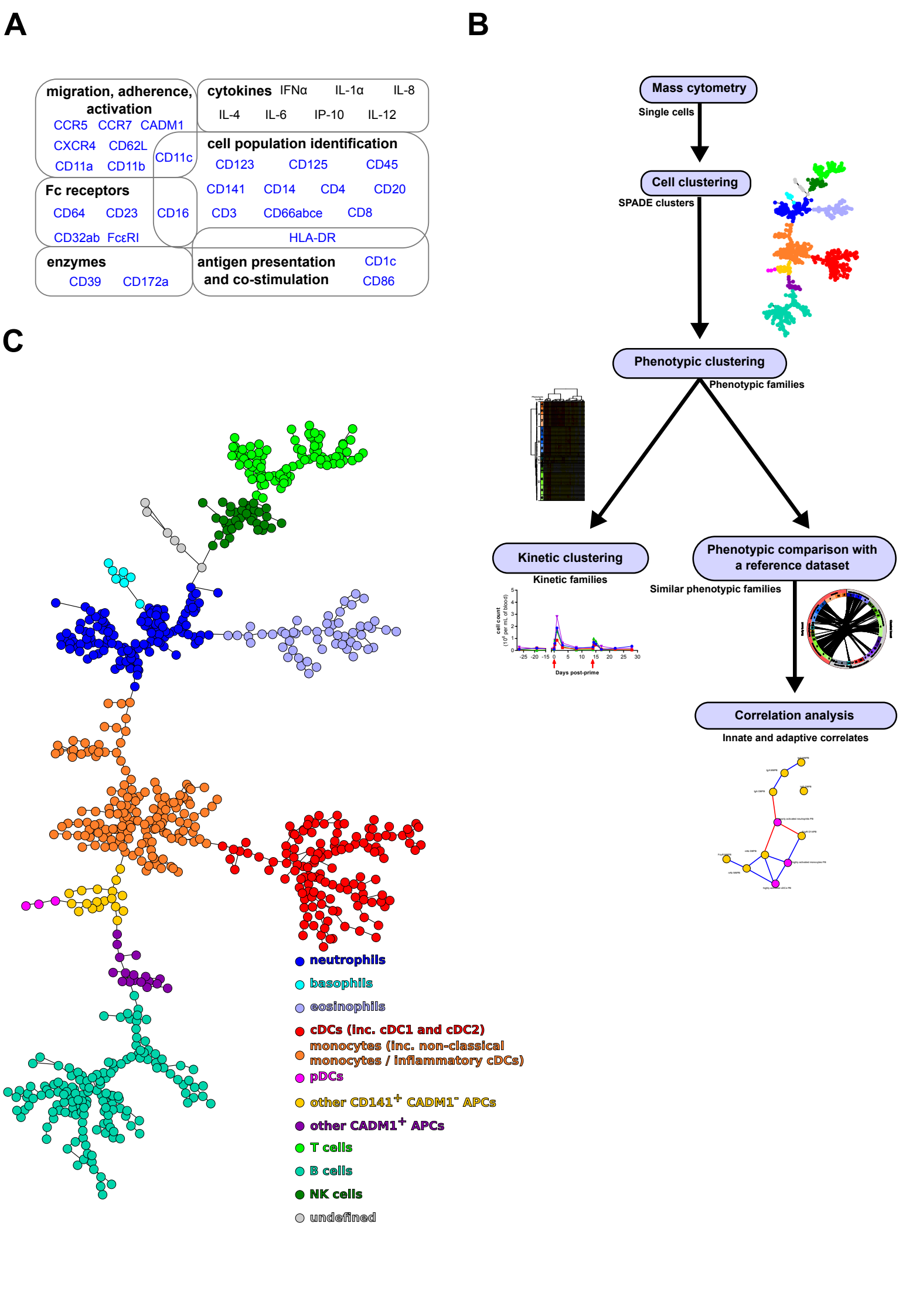
A
migration, adherence, activation
CCR5 CCR7 CADM1
CXCR4 CD62L
CD11a CD11b
CD11c
cytokines IFNα IL-1α IL-8
IL-4 IL-6 IP-10 IL-12
cell population identification
CD123 CD125 CD45
CD141 CD14 CD4 CD20
CD3 CD66abce CD8
Fc receptors
CD64 CD23
CD32ab FcεRI
CD16
HLA-DR
enzymes
CD39 CD172a
antigen presentation and co-stimulation
CD1c
CD86
B
Mass cytometry
Single cells
Cell clustering
SPADE clusters
Phenotypic clustering
Phenotypic families
Kinetic clustering
Kinetic families
cell count
Days post-prime
Phenotypic comparison with a reference dataset
Similar phenotypic families
Correlation analysis
Innate and adaptive correlates
C
neutrophils
basophils
eosinophils
cDCs (inc. cDC1 and cDC2)
monocytes (inc. non-classical monocytes / inflammatory cDCs)
pDCs
other CD141+ CADM1- APCs
other CADM1+ APCs
T cells
B cells
NK cells
undefined

Figure 3 – Bioinformatics pipeline used for the analysis of high-dimensional cytometry profiles. (**A**) A mass cytometry panel of 35 markers dedicated to the characterization of innate myeloid cells was used to stain fixed leukocytes obtained from macaque blood samples. Markers used for the SPADE clustering are indicated in blue. (**B**) The SPADE algorithm was used to identify groups of cells sharing similar phenotype in the whole dataset. Phenotypic families, corresponding to groups of cell clusters having similar phenotypes, were defined for both the granulocyte and monocyte-DC compartments. Kinetic families, corresponding to phenotypic families sharing the same abundance profiles, were derivated from these phenotypic families. Finally, phenotypical comparisons with a vaccine schedule study at 2 months apart, previously published (Palgen et al., 2018), were performed. (**C**) The resulting SPADE tree, generated using all samples of the dataset, was annotated based on the expression of 15 markers (**Figure S3**). Granulocytes clusters were defined as neutrophils ($CD66^+$ $CD125^-$), eosinophils ($CD66^+$ $CD125^+$), and basophils ($CD66^-$ $CD123^+$ $HLA\text{-}DR^-$). Monocytes-DCs clusters were defined as monocytes ($CD14^+$ $HLA\text{-}DR^+$), cDCs ($CD14^-$ $HLA\text{-}DR^+$ $CD11c^+$ $CD16^+$), inflammatory cDCs/non-classical monocytes ($CD14^+$ $HLA\text{-}DR^+$ $CD11c^+$ $CD16^+$), pDCs ($CD123^+$ $HLA\text{-}DR^+$), other $CADM1^+$ APCs ($HLA\text{-}DR^+$ $CD3^-$ $CD8^-$ $CD14^-$ $CD11c^-$ $CD16^-$ $CD20^-$ $CADM1^+$), and other $CD141^+$ $CADM1^-$ APCs ($HLA\text{-}DR^+$ $CD3^-$ $CD8^-$ $CD14^-$ $CD11c^-$ $CD16^-$ $CD20^-$ $CD141^+$ $CADM1^-$). Lymphocytes clusters were defined as B cells ($CD20^+$ $HLA\text{-}DR^+$), T cells ($CD3^+$), and NK cells ($CD3^-$ $CD8^+$). The undefined category corresponds to cell clusters that did not fit with any of these phenotypes. Neutrophils, eosinophils, and basophils were assigned to the granulocyte compartment. Monocytes, cDCs, pDCs, inflammatory cDCs/non-classical monocytes, and APCs were assigned to the monocyte-DC compartment.

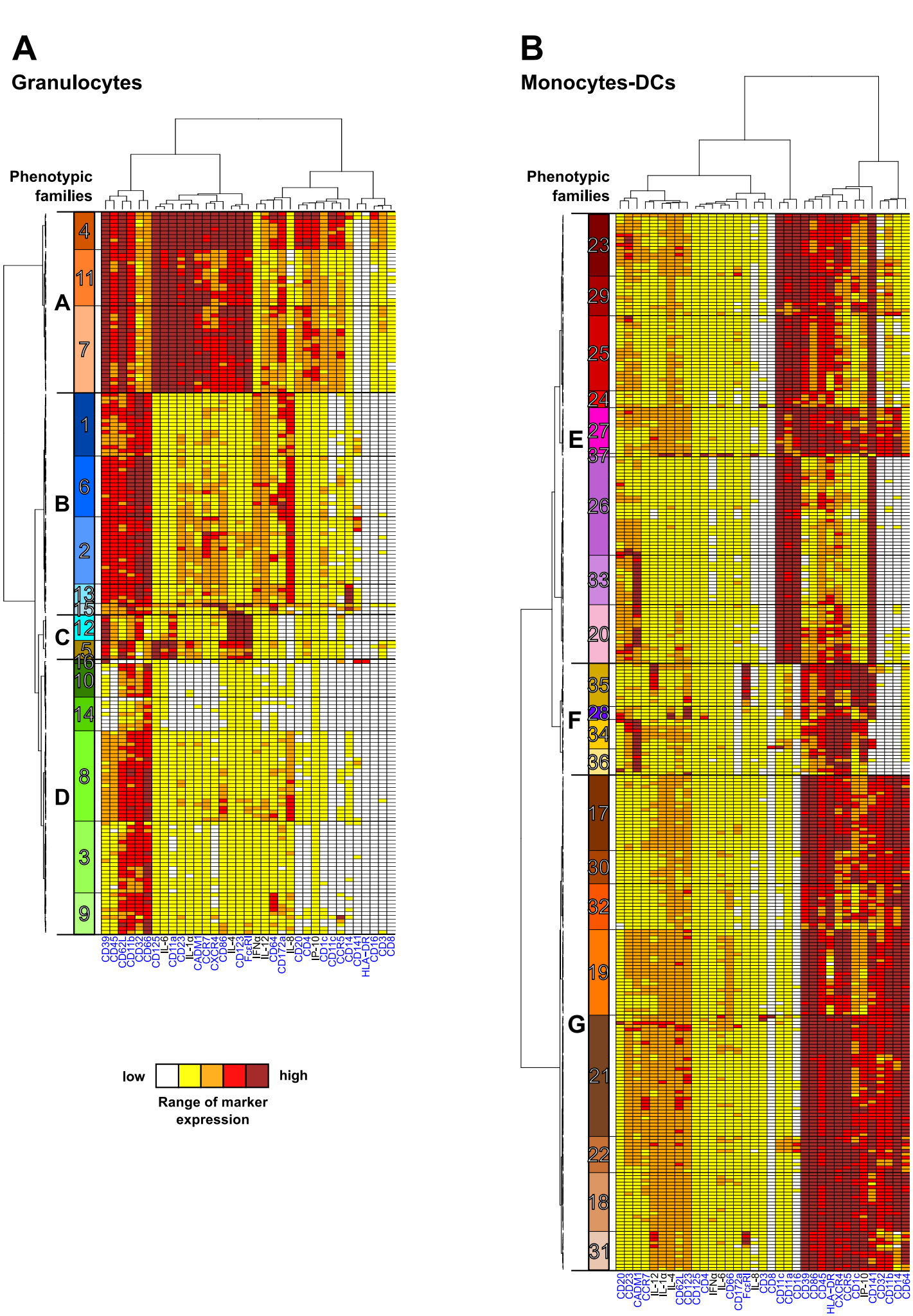
A
Granulocytes
Phenotypic families
A
B
C
D
4
11
7
1
6
2
13
15
12
5
16
10
14
8
3
9
CD39
CD45
CD62L
CD15
CD35
CD66
CD125
IL-6
CD11a
CD23
IL-1α
CADM1
CCR7
CXCR4
CD86
IL-4
CD123
FcεRI
IL-10
IL-1β
CD64
CD172a
IL-8
CD20
CD4
IP-10
CD11c
CCR5
CD14
CD141
HLA-DR
CD16
CD3
CD8
low
high
Range of marker expression
B
Monocytes-DCs
Phenotypic families
E
F
G
23
29
25
24
27
37
26
33
20
35
28
34
36
17
30
32
19
21
22
18
31
CD20
CD23
CADM1
CCR7
IL-12
IL-1α
IL-4
CD27
CD123
CD125
CD4
IFNα
IL-6
CD66
CD172a
FcεRI
IL-8
CD3
CD8
CD11c
CD11a
CD16
CD86
CD45
HLA-DR
CXCR4
CCR5
CD1c
IP-10
CD141
CD32
CD11b
CD14
CD64

Figure 4 – Moderate phenotypic diversity in granulocytes and high phenotypic diversity in monocytes-DCs. Categorical heatmaps showing marker relative expressions for (**A**) granulocyte or (**B**) monocyte-DC clusters. Each row corresponds to a cell cluster, and each column corresponds to a cell marker. Phenotypic families,corresponding to groups of cell clusters, were delineated based one the cluster dendrogram. The 16 granulocyte phenotypic families, and the 21 monocytes-DCs phenotypic families are indicated in different colors, and Arabic numbers displayed on the left of each heatmap. Black frames labeled with capital letters indicate superfamilies of phenotypic families. Clustering markers are indicated in blue.

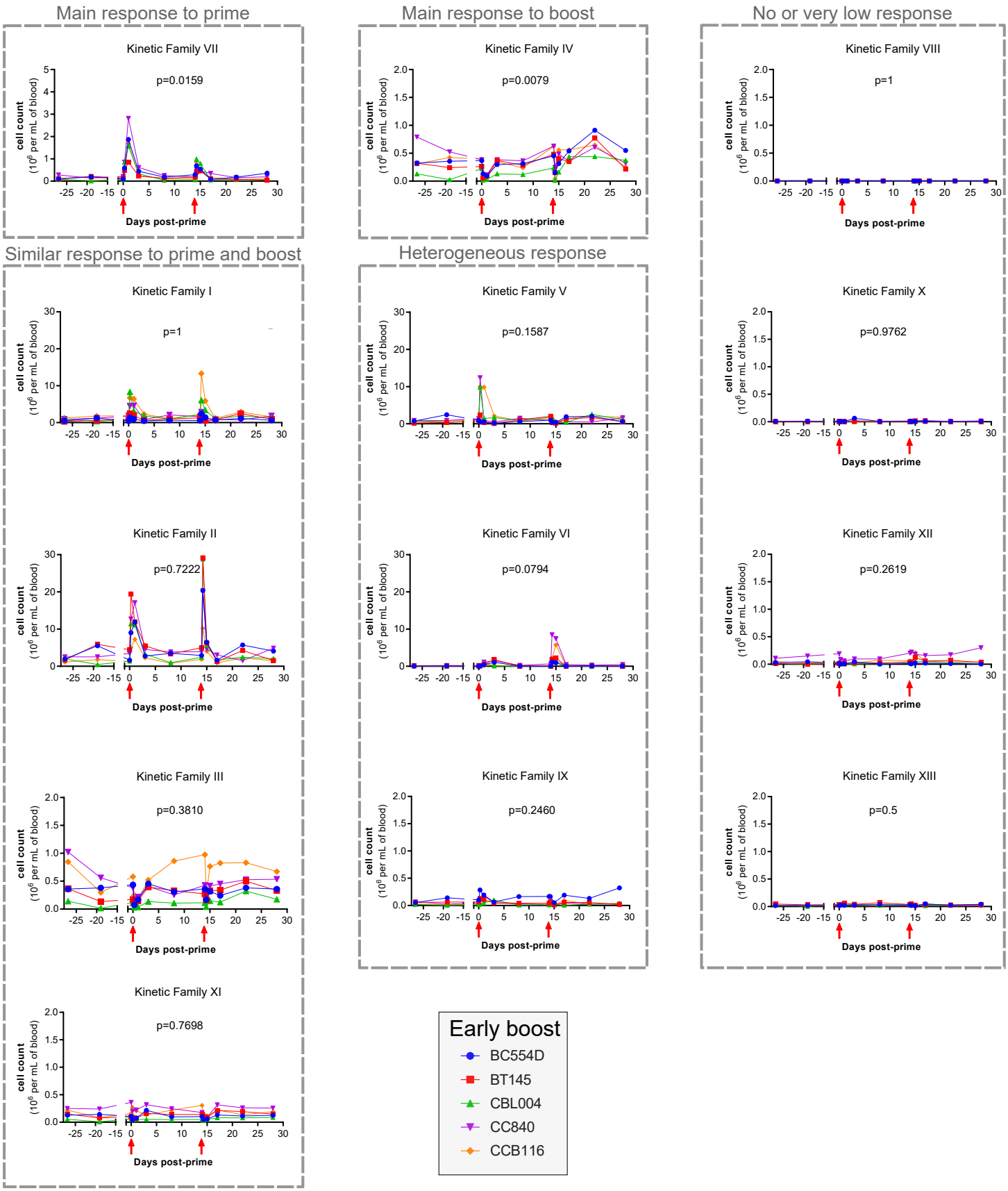

Figure 5 – Similar kinetic profiles of innate myeloid cells after first, and second immunizations. The kinetic patterns of the thirteen kinetic families (numbered I to XIII) are displayed. Kinetic families were further regrouped based on their kinetic pattern indicated in gray. Represented p-values asserted the statistical comparison between the individual AUC after prime (H6-D14PP) and boost (H6-D14PB) using a permutation test. P-values lower than 0.05 were considered as significant. The scale of the Y-axis is specific to each kinetic family. The immunizations are indicated with red arrows.

A

Granulocytes

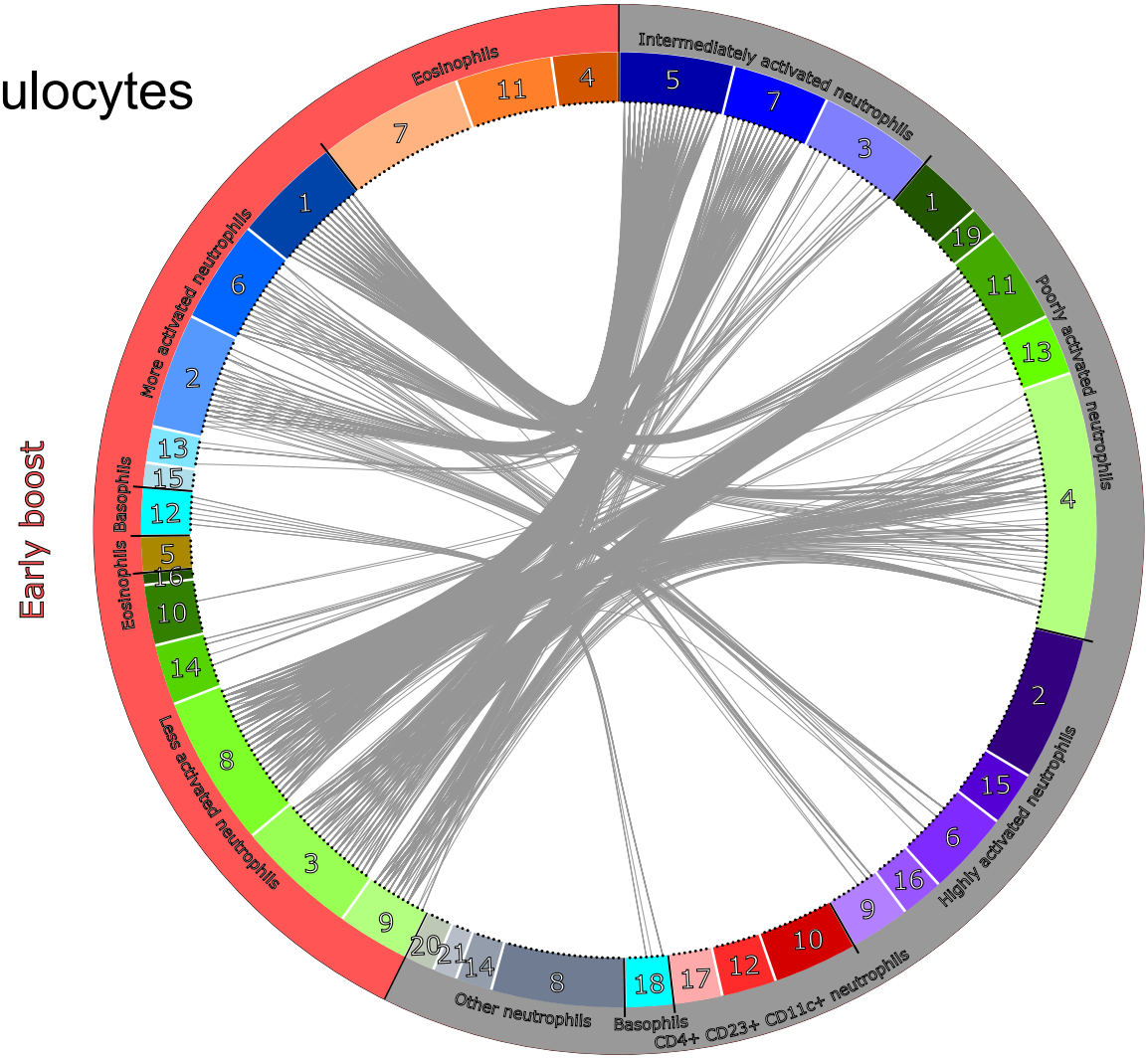

B

Monocytes-DCs

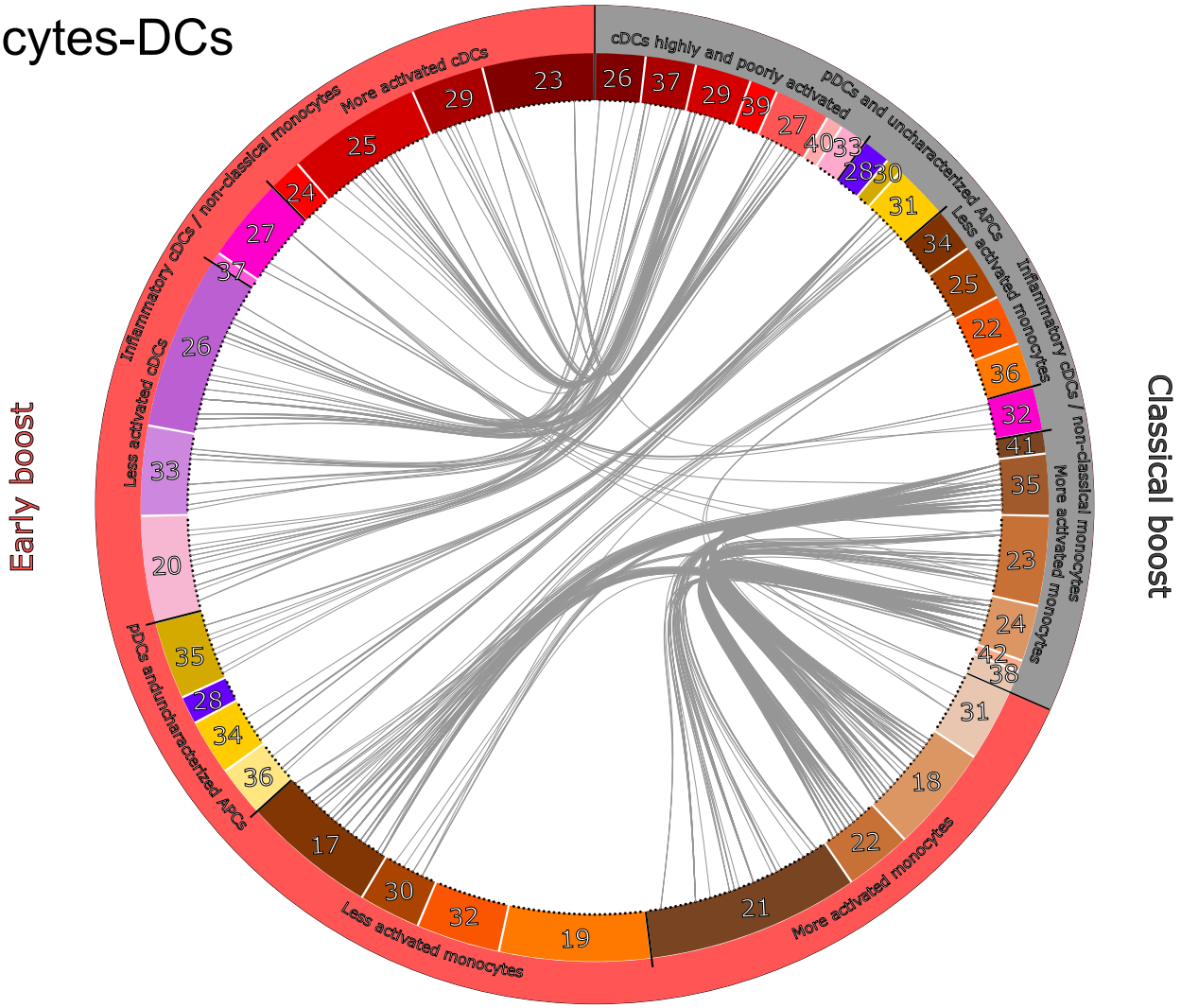

Figure 6 – Comparisons of cell cluster phenotypes identified in the two vaccine schedules. The phenotype of each cluster of (**A**) granulocytes, and (**B**) monocytes-DCs compartments, was compared to this of the clusters identified in the 2 months apart vaccine schedule. The similarity between clusters was computed as the Manhattan distance, calculated on all the categories of expression of the 27 markers shared in both experiments.

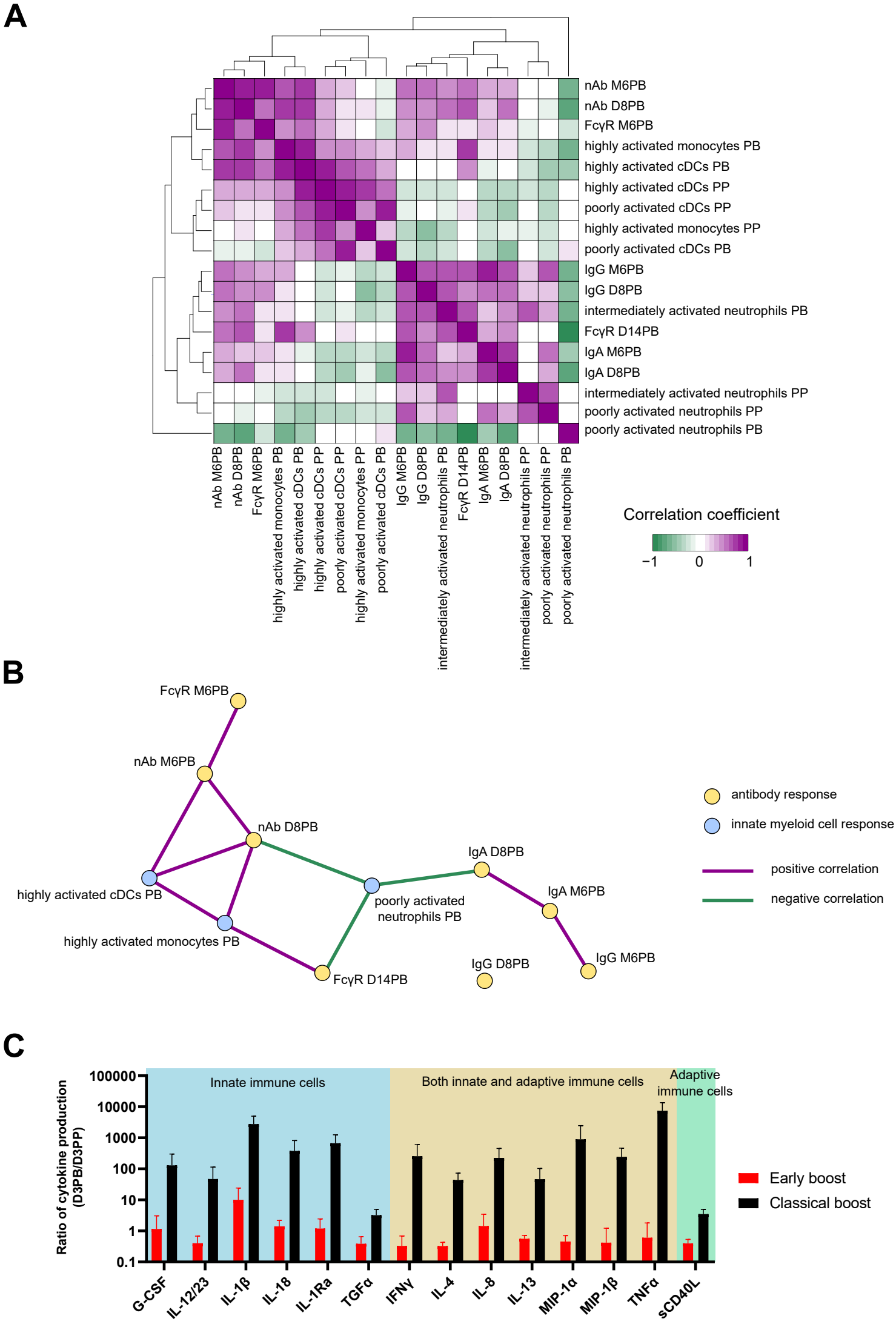
A
nAb M6PB
nAb D8PB
FcγR M6PB
highly activated monocytes PB
highly activated cDCs PB
highly activated cDCs PP
poorly activated cDCs PP
highly activated monocytes PP
poorly activated cDCs PB
IgG M6PB
IgG D8PB
intermediately activated neutrophils PB
FcγR D14PB
IgA M6PB
IgA D8PB
intermediately activated neutrophils PP
poorly activated neutrophils PP
poorly activated neutrophils PB
Correlation coefficient
−1
0
1
B
FcγR M6PB
nAb M6PB
nAb D8PB
highly activated cDCs PB
highly activated monocytes PB
poorly activated neutrophils PB
IgA D8PB
IgA M6PB
IgG D8PB
IgG M6PB
FcγR D14PB
antibody response
innate myeloid cell response
positive correlation
negative correlation
C
Ratio of cytokine production (D3PB/D3PP)
100000
10000
1000
100
10
1
0.1
Innate immune cells
Both innate and adaptive immune cells
Adaptive immune cells
G-CSF
IL-12/23
IL-1β
IL-18
IL-1Ra
TGFα
IFNγ
IL-4
IL-8
IL-13
MIP-1α
MIP-1β
TNFα
sCD40L
Early boost
Classical boost

Figure 7 – Strong interconnection between innate myeloid subphenotypes and adaptive response. (**A-B**) The correlation between the peak and long-term persistence of antibody response (obtained at the indicated timepoint) and the innate myeloid cell response, given by the normalized area under the curve for each cell population were assessed. All correlations are displayed in (**A**), after hierarchical clustering of the correlation coefficients with complete linkage. All antibody responses were represented, and all the innate myeloid responses that correlated ($|R| \geq 0.7$) with at least one antibody response were considered to generate the correlation graph in (**B**). (**C**) The *ex vivo* cytokine production of unstimulated PBMC was assessed at D3PP and D3PB. For each of the indicated cytokines, the ratio of cytokine level at D3PB over the level at D3PP is represented, as the mean +/- standard deviation across the five animals. The main immune cell producers (innate, adaptive or both) are also indicated. Note that only cytokines that displayed significantly different ratio between the two schedules are represented. Significance was assessed by $p < 0.01$ with a Mann-Whitney-Wilcoxon test.

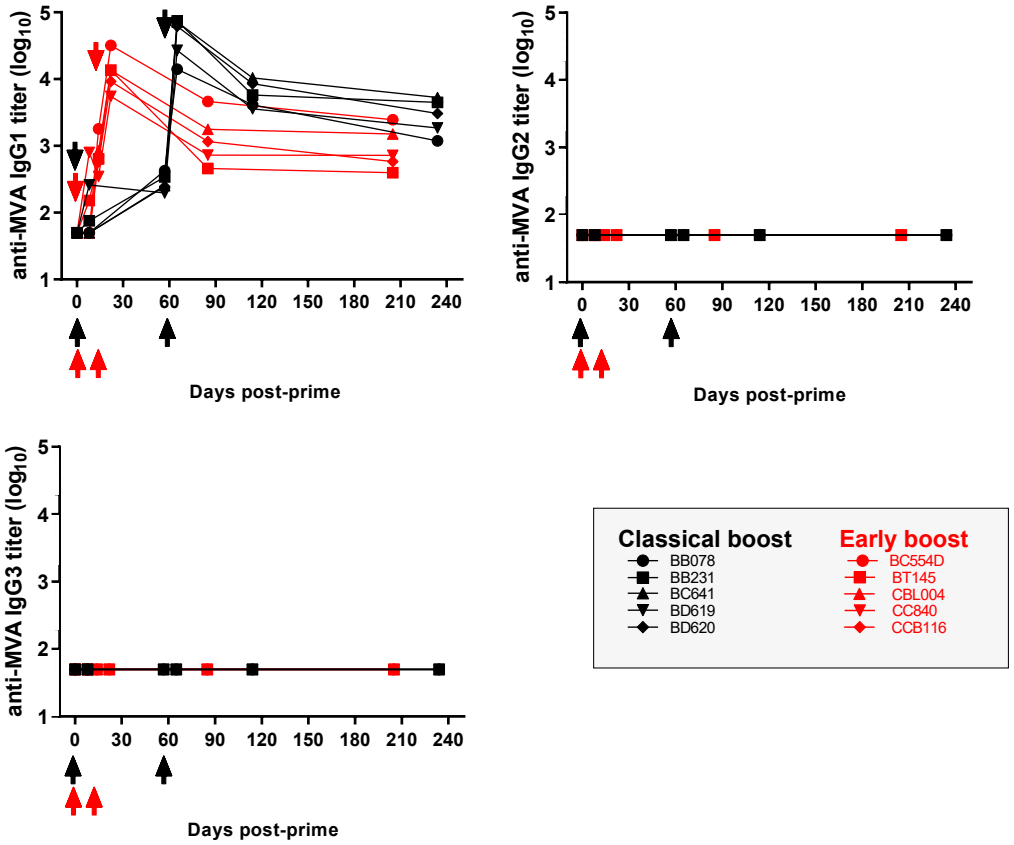

Figure S1 – MVA-specific IgG subclasses in serum over time. MVA-specific IgG1 (**A**), IgG2 (**B**), and IgG3 (**C**) titers were measured by direct ELISA during the early (red) or classical (black) vaccination schedule. Individual titers are shown. Immunizations are indicated by arrows.

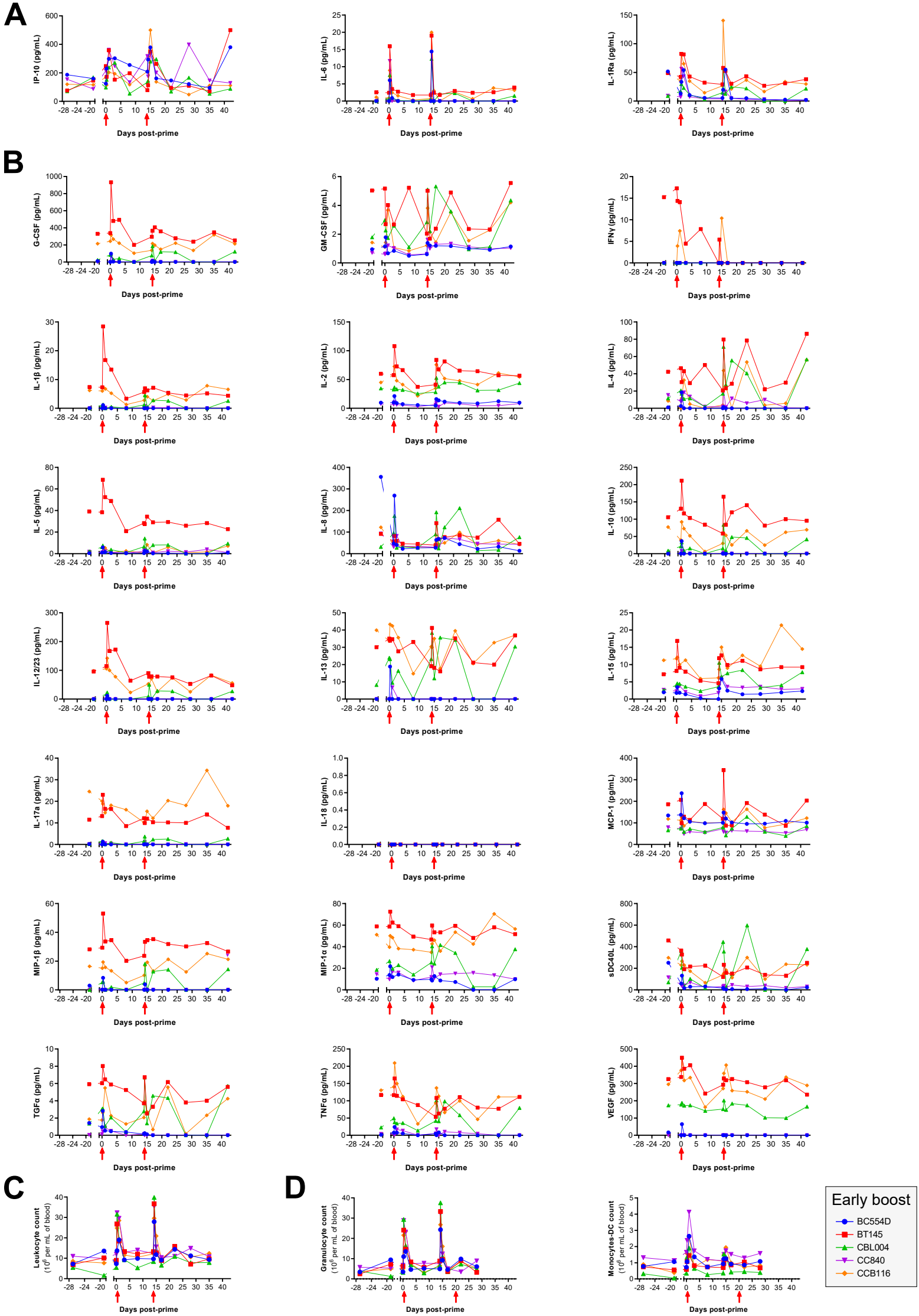
A
IP-10 (pg/mL)
IL-6 (pg/mL)
IL-1Ra (pg/mL)
B
G-CSF (pg/mL)
GM-CSF (pg/mL)
IFNγ (pg/mL)
IL-1β (pg/mL)
IL-2 (pg/mL)
IL-4 (pg/mL)
IL-5 (pg/mL)
IL-8 (pg/mL)
IL-10 (pg/mL)
IL-12/23 (pg/mL)
IL-13 (pg/mL)
IL-15 (pg/mL)
IL-17a (pg/mL)
IL-18 (pg/mL)
MCP-1 (pg/mL)
MIP-1β (pg/mL)
MIP-1α (pg/mL)
sDC40L (pg/mL)
TGFα (pg/mL)
TNFα (pg/mL)
VEGF (pg/mL)
Days post-prime
C
Leukocyte count (10^6 per mL of blood)
D
Granulocyte count (10^6 per mL of blood)
Monocytes-DC count (10^6 per mL of blood)
Early boost
BC554D
BT145
CBL004
CC840
CCB116

Figure S2 – Cytokines and leukocyte count following vaccination. (**A**) Cytokines significantly impacted by vaccination. (**B**) Cytokines not significantly impacted by vaccination. (**C**) Leukocytes count after vaccination. (**A-C**) The individual curves are displayed. Immunizations are indicated by red arrows.

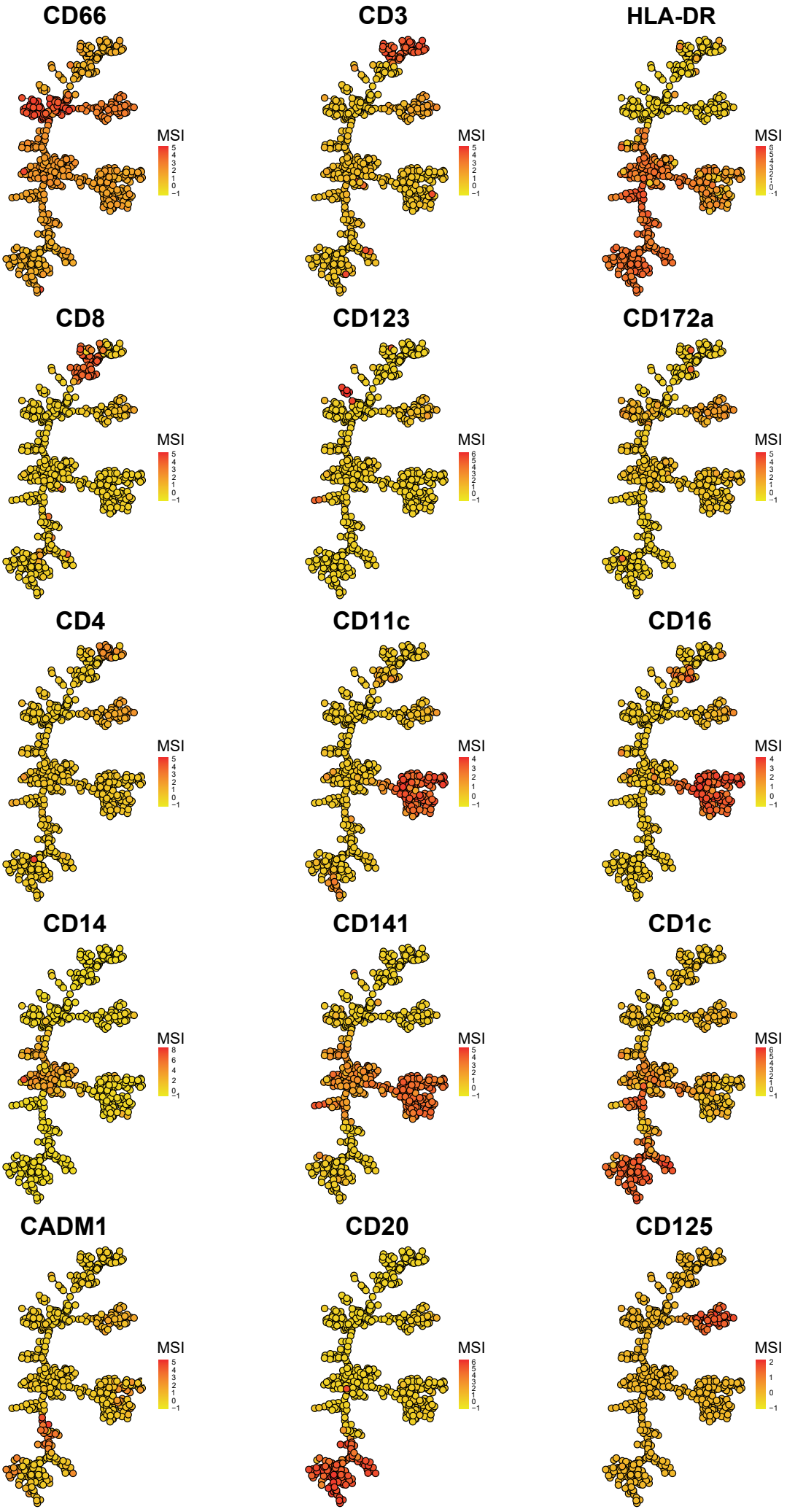
CD66
MSI
CD3
MSI
HLA-DR
MSI
CD8
MSI
CD123
MSI
CD172a
MSI
CD4
MSI
CD11c
MSI
CD16
MSI
CD14
MSI
CD141
MSI
CD1c
MSI
CADM1
MSI
CD20
MSI
CD125
MSI

Figure S3 – SPADE tree annotation. The topology of the SPADE tree is displayed, with each node colored by the expression of the 15 markers used to annotate cell clusters.

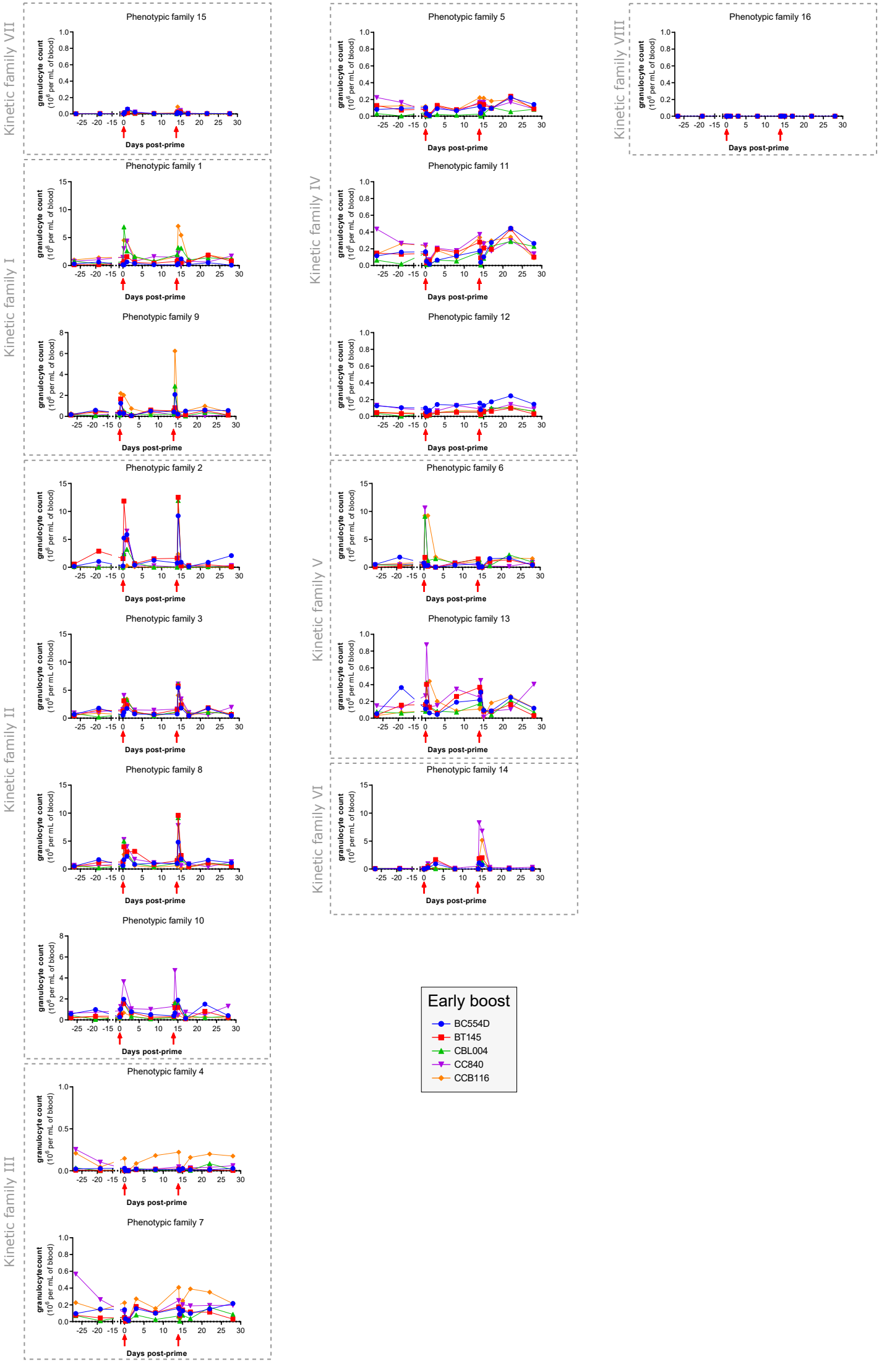
Kinetic family VII
Phenotypic family 15
Kinetic family I
Phenotypic family 1
Phenotypic family 9
Kinetic family II
Phenotypic family 2
Phenotypic family 3
Phenotypic family 8
Phenotypic family 10
Kinetic family III
Phenotypic family 4
Phenotypic family 7
Kinetic family IV
Phenotypic family 5
Phenotypic family 11
Phenotypic family 12
Kinetic family V
Phenotypic family 6
Phenotypic family 13
Kinetic family VI
Phenotypic family 14
Kinetic family VIII
Phenotypic family 16
granulocyte count (10^6 per mL of blood)
Days post-prime
Early boost
BC554D
BT145
CBL004
CC840
CCB116

Figure S4 – Abundance of granulocyte phenotypic families. The absolute count of each of the 16 granulocytes phenotypic families are displayed. Grey frames regroup phenotypic families into their associated kinetic families. Kinetic families are ordered with respect to **Figure 5**.

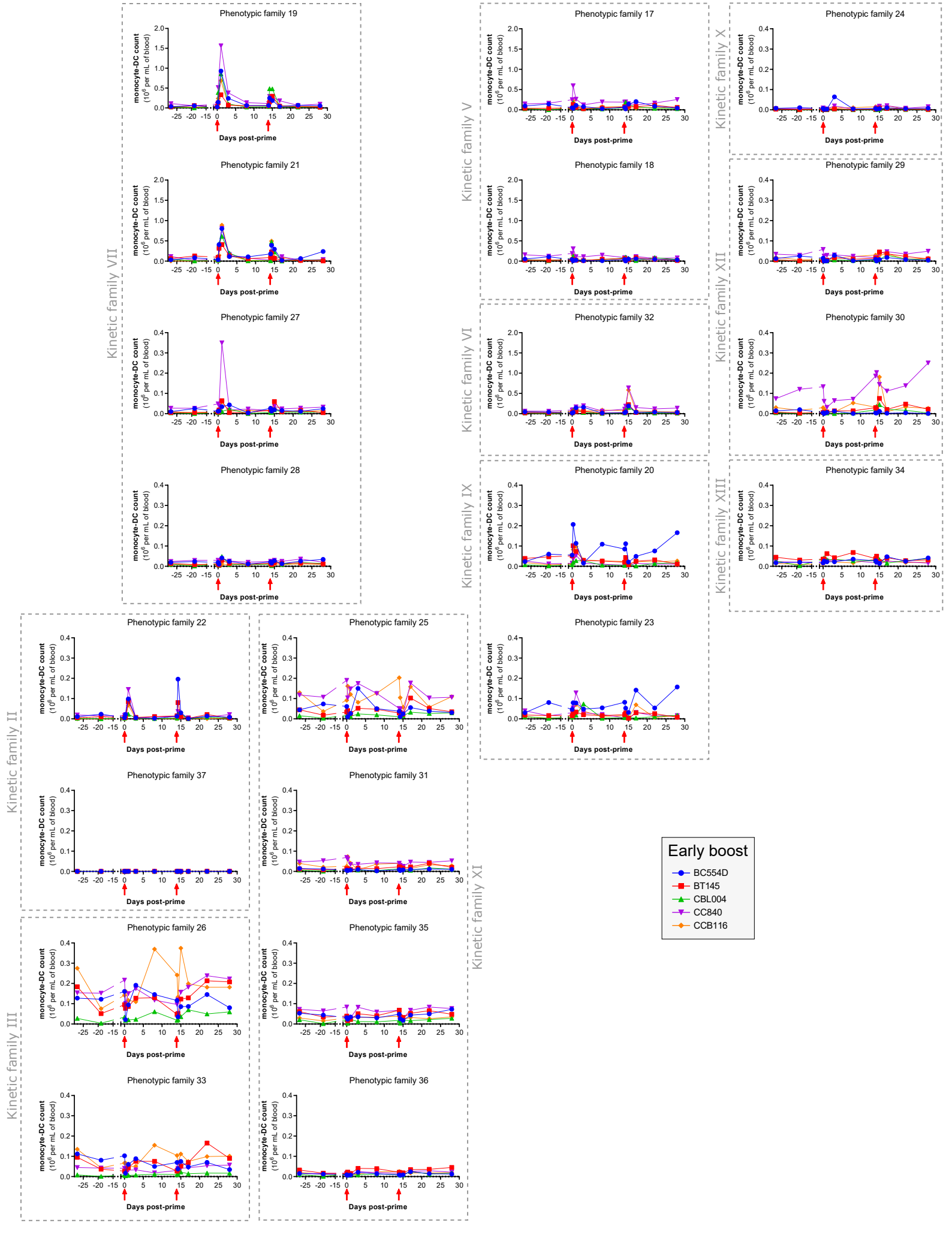
Kinetic family VII
Phenotypic family 19
Phenotypic family 21
Phenotypic family 27
Phenotypic family 28
Kinetic family V
Phenotypic family 17
Phenotypic family 18
Kinetic family VI
Phenotypic family 32
Kinetic family IX
Phenotypic family 20
Phenotypic family 23
Kinetic family X
Phenotypic family 24
Kinetic family XII
Phenotypic family 29
Phenotypic family 30
Kinetic family XIII
Phenotypic family 34
Kinetic family II
Phenotypic family 22
Phenotypic family 37
Kinetic family III
Phenotypic family 26
Phenotypic family 33
Kinetic family XI
Phenotypic family 25
Phenotypic family 31
Phenotypic family 35
Phenotypic family 36
monocyte-DC count (10^6 per mL of blood)
Days post-prime
Early boost
BC554D
BT145
CBL004
CC840
CCB116

Figure S5 – Abundance of monocytes-DCs phenotypic families. The absolute counts of each of the 21 monocytes-DCs phenotypic families are displayed. Grey frames regroup phenotypic families into their associated kinetic families. Kinetic families are ordered with respect to **Figure 5**.

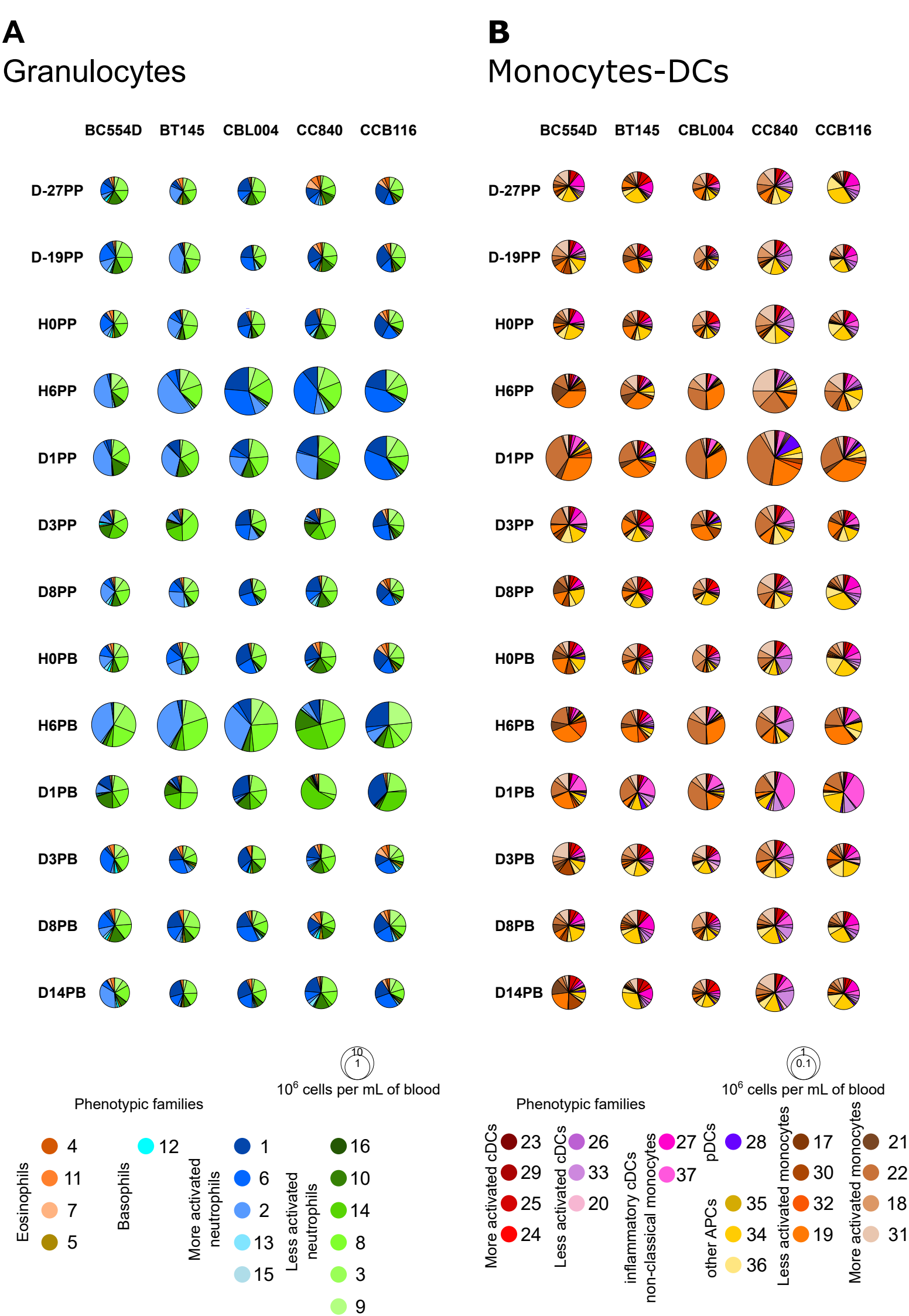
A
Granulocytes
BC554D
BT145
CBL004
CC840
CCB116
D-27PP
D-19PP
H0PP
H6PP
D1PP
D3PP
D8PP
H0PB
H6PB
D1PB
D3PB
D8PB
D14PB
10
1
10^6 cells per mL of blood
Phenotypic families
Eosinophils
4
11
7
5
Basophils
12
More activated neutrophils
1
6
2
13
15
Less activated neutrophils
16
10
14
8
3
9
B
Monocytes-DCs
BC554D
BT145
CBL004
CC840
CCB116
D-27PP
D-19PP
H0PP
H6PP
D1PP
D3PP
D8PP
H0PB
H6PB
D1PB
D3PB
D8PB
D14PB
1
0.1
10^6 cells per mL of blood
Phenotypic families
More activated cDCs
23
29
25
24
Less activated cDCs
26
33
20
inflammatory cDCs non-classical monocytes
27
37
pDCs
28
other APCs
35
34
36
Less activated monocytes
17
30
32
19
More activated monocytes
21
22
18
31

Figure S6 – Similar phenotypic composition of innate myeloid cell compartments after first and second immunizations. The composition in phenotypic families of the **(A)** granulocytes, and **(B)** monocytes-DCs compartments along the timecourse of vaccination. Cell abundance is given by the size of the pie chart. The color-code for each phenotypic families is conserved for the pie-charts, and the heatmaps from **Figure 4**.

A

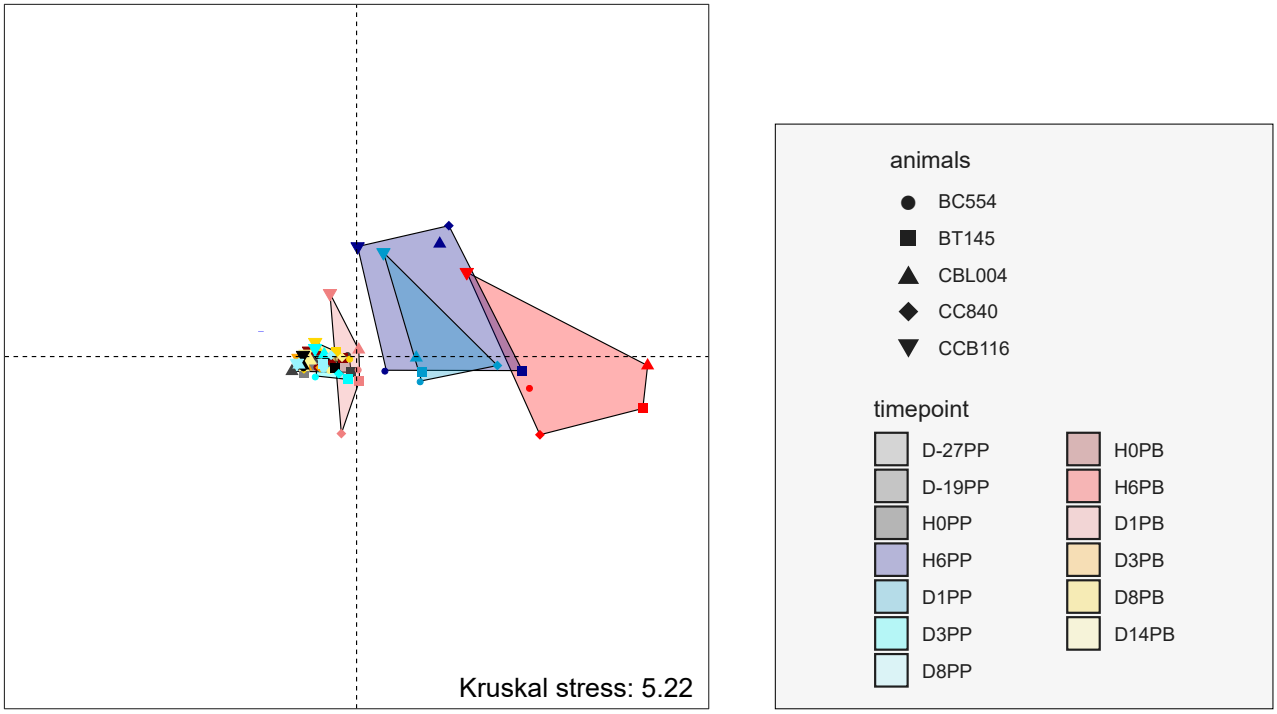
Kruskal stress: 5.22
animals
BC554
BT145
CBL004
CC840
CCB116
timepoint
D-27PP
D-19PP
H0PP
H6PP
D1PP
D3PP
D8PP
H0PB
H6PB
D1PB
D3PB
D8PB
D14PB

B

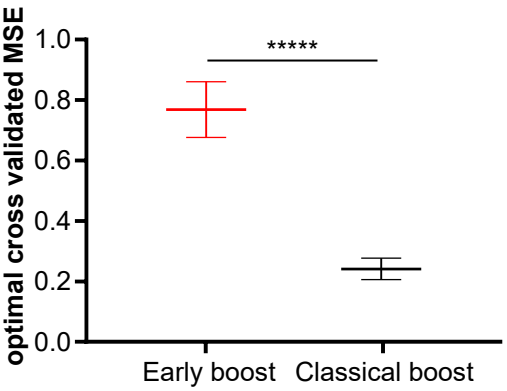
optimal cross validated MSE
1.0
0.8
0.6
0.4
0.2
0.0
*****
Early boost
Classical boost

Figure S7 – Visualization of similarity between post-prime, and post-boost innate myeloid cell responses. (**A**) Multidimensional Scaling (MDS) representation was calculated based on the cell abundances of the kinetic family. The proportion of information lost during the dimensionality reduction process is indicated with the Kruskal Stress. Samples belonging to the same timepoint, were delineated using convex hulls, and different colors. (**B**) The Least Absolute Shrinkage and Selection Operator (LASSO) approach was applied to discriminate samples from post-prime and post-boost responses. The mean square error (MSE) of the model at each step of the LASSO is indicated. (**C**) Comparison of mean square error (MSE) of the optimal LDA obtained on the early boost dataset compared to the optimal LDA obtained on the classical boost dataset. *****, p-value <0.00001 using a t-test.

		IgG	IgA	nAb	FcγRIIIa dimer binding
Early boost	baseline vs D8PP	1,0000	0,4444	1,0000	\
	baseline vs D14PP	0,0079	0,1667	1,0000	0,2063
	baseline vs D8PB	0,0079	0,0079	0,0476	\
	baseline vs D14PB	0,0079	0,1667	0,0476	0,0079
	baseline vs D28PB	0,0079	0,0079	0,0476	\
	baseline vs D57PB	0,0079	0,0079	0,0476	0,0238
	baseline vs M3PB	0,0079	0,0476	0,1667	\
	baseline vs M6PB	0,0079	0,0476	0,1667	0,0238
	D8PP vs D14PP	0,0079	0,3651	1,0000	\
	D8PP vs D8PB	0,0079	0,0238	0,0476	\
	D8PP vs D14PB	0,0079	0,2063	0,0476	\
	D8PP vs D28PB	0,0079	0,0714	0,0476	\
	D8PP vs D57PB	0,0079	0,2937	0,0476	\
	D8PP vs M3PB	0,0079	0,1032	0,1667	\
	D8PP vs M6PB	0,0079	0,1270	0,1667	\
	D14PP vs D8PB	0,0079	0,1111	0,0476	\
	D14PP vs D14PB	0,0079	0,4048	0,0476	0,0079
	D14PP vs D28PB	0,0159	0,5317	0,0476	\
	D14PP vs D57PB	0,1349	0,9762	0,0476	0,1111
	D14PP vs M3PB	0,4603	0,9444	0,1667	\
	D14PP vs M6PB	0,5714	1,0000	0,1667	\
	D8PB vs D14PB	0,4921	0,5238	0,7063	\
	D8PB vs D28PB	0,0476	0,2619	1,0000	\
	D8PB vs D57PB	0,0079	0,0714	0,3651	\
	D8PB vs M3PB	0,0079	0,1667	0,1270	\
	D8PB vs M6PB	0,0079	0,1349	0,1032	0,1667
	D14PB vs D28PB	0,0794	0,7937	0,8571	\
	D14PBvs D57PB	0,0079	0,2937	0,4683	0,0079
	D14PB vs M3PB	0,0079	0,4444	0,1270	\
	D14PB vs M6PB	0,0079	0,4524	0,1032	0,0079
	D28PB vs D57PB	0,0079	0,3810	0,5556	\
	D28PB vs M3PB	0,0079	0,4286	0,3810	\
	D28PB vs M6PB	0,0079	0,3333	0,3333	\
	D57PB vs M3PB	0,1349	0,7460	0,5397	\
	D57PB vs M6PB	0,1032	1,0000	0,5714	0,5556
	M3PB vs M6PB	0,6190	0,8016	0,8571	\
Classical boost	baseline vs D8PP	0,4444	0,0476	1,0000	\
	baseline vs D14PP	0,0079	0,0476	1,0000	0,0952
	baseline vs D8PB	0,0079	0,0476	0,0079	\
	baseline vs D14PB	0,0079	0,0476	0,0079	0,0079
	baseline vs D28PB	0,0476	0,0079	0,0079	\
	baseline vs D57PB	0,0079	0,0079	0,0079	0,0079
	baseline vs M3PB	0,0079	0,0079	0,0079	\
	baseline vs M6PB	0,0079	0,0079	0,0079	0,0397
	D8PP vs D14PP	0,0079	0,0556	1,0000	\
	D8PP vs D8PB	0,0079	0,0476	0,0079	\
	D8PP vs D14PB	0,0079	0,0476	0,0079	\
	D8PP vs D28PB	0,0476	0,0079	0,0079	\
	D8PP vs D57PB	0,0079	0,0079	0,0079	\
	D8PP vs M3PB	0,0079	0,0079	0,0079	\
	D8PP vs M6PB	0,0079	0,0079	0,0079	\
	D14PP vs D8PB	0,0079	0,0476	0,0079	\
	D14PP vs D14PB	0,0079	0,0476	0,0079	0,0079
	D14PP vs D28PB	0,1429	0,0079	0,0079	\
	D14PP vs D57PB	0,0159	0,0714	0,0079	0,0079
	D14PP vs M3PB	0,0159	0,1032	0,0079	\
	D14PP vs M6PB	0,0397	0,0079	0,0079	\
	D8PB vs D14PB	0,7460	1,0000	0,7619	\
	D8PB vs D28PB	0,0238	0,4048	0,2222	\
	D8PB vs D57PB	0,0079	0,1111	0,0079	\
	D8PB vs M3PB	0,0079	0,1032	0,0079	\
	D8PB vs M6PB	0,0079	0,4921	0,0079	0,0159
	D14PB vs D28PB	0,0238	0,4127	0,2302	\
	D14PBvs D57PB	0,0079	0,0873	0,0079	0,0079
	D14PB vs M3PB	0,0079	0,0873	0,0079	\
	D14PB vs M6PB	0,0079	0,5873	0,0079	0,0079
	D28PB vs D57PB	0,9206	0,1587	0,0079	\
	D28PB vs M3PB	0,6587	0,2222	0,0079	\
	D28PB vs M6PB	0,3968	0,1190	0,0079	\
	D57PB vs M3PB	0,5079	0,6349	0,6032	\
	D57PB vs M6PB	0,2460	0,0317	0,9841	0,0159
	M3PB vs M6PB	0,4921	0,0238	0,6587	\

Table S1 – Statistics for antibody titers. P-values of the permutation tests are given for the indicated comparisons.
Red indicate significant differences, $p < 0.05$.

Cytokine	H6PP vs H0PP	D1PP vs H0PP	D3PP vs H0PP	D8PP vs H0PP	H0PB vs H0PP	H6PB vs H0PP	D1PB vs H0PP	D3PB vs H0PP	D8PB vs H0PP	D14PB vs H0PP	D28PB vs H0PP	H6PP vs H6PB	D1PP vs D1PB	D3PP vs D3PB	D8PP vs D8PB	D14PP vs D14PB
IP-10	0,8810	0,0476	0,1508	0,7302	0,9365	0,4286	0,0079	0,4603	0,0556	1,0000	0,0714	0,9365	0,6190	0,1508	0,7381	0,2937
G-CSF	0,5952	0,8889	1,0000	0,4841	0,8413	0,9206	1,0000	1,0000	1,0000	0,6032	0,9524	0,8413	0,6349	0,7619	0,8413	0,4444
GM-CSF	0,8730	1,0000	0,8016	0,7937	0,5635	0,3095	0,7222	1,0000	0,5476	0,6429	0,4127	0,5635	0,1667	0,4524	0,6905	0,3730
IFNγ	1,0000	1,0000	1,0000	1,0000	1,0000	1,0000	1,0000	1,0000	1,0000	1,0000	1,0000	1,0000	0,7222	0,7222	1,0000	1,0000
IL10	0,5159	1,0000	0,9206	0,5635	0,6429	0,5714	0,8095	1,0000	0,7778	0,6429	1,0000	0,6429	0,8333	0,8413	0,9048	0,4048
IL-12/23	0,5952	1,0000	1,0000	0,3651	0,6349	0,7143	0,6032	0,5238	0,6825	0,3651	0,4921	0,6349	0,5159	0,5635	0,7222	0,3651
IL-13	0,7619	1,0000	0,8571	0,3651	0,6667	0,7143	0,6190	0,7143	0,8095	0,2857	0,7619	0,6667	1,0000	0,6667	1,0000	0,2857
IL-15	0,4762	1,0000	0,9206	0,3095	0,3889	0,4286	0,2857	0,7540	0,5556	0,9048	0,6032	0,3889	0,9206	0,2540	0,7381	0,1349
IL-17a	0,7619	0,8413	1,0000	0,7619	0,6825	0,7619	0,7619	0,6825	1,0000	0,7619	0,8413	0,6825	0,4365	0,8413	0,6825	0,7619
IL-18	1,0000	1,0000	1,0000	1,0000	1,0000	1,0000	1,0000	1,0000	1,0000	1,0000	1,0000	1,0000	1,0000	1,0000	1,0000	1,0000
IL-1β	0,7222	0,8810	0,9206	0,3651	0,8095	0,8730	0,8413	1,0000	1,0000	0,5238	1,0000	0,8095	0,7222	0,7222	0,8016	0,2857
IL-1Ra	0,0635	0,0476	0,8016	0,2063	0,5476	0,2381	0,2460	0,5476	0,9444	0,1905	0,7381	0,5476	0,8651	0,4286	0,6746	0,3254
IL-2	0,5476	1,0000	0,9524	0,2857	0,5635	0,5635	0,8413	0,7381	1,0000	0,9365	1,0000	0,5635	1,0000	0,8333	0,6825	0,2460
IL-4	0,8492	0,7698	0,7937	0,6032	0,5714	0,1984	1,0000	0,7937	0,3095	0,5397	0,2778	0,5714	0,2222	0,5397	0,6667	0,2063
IL-5	0,7222	0,8810	0,8810	0,7222	0,8810	0,7619	1,0000	1,0000	1,0000	0,7222	1,0000	0,8810	0,8016	0,8810	0,8810	0,5159
IL-6	0,0079	0,3810	0,9206	0,5635	0,7143	0,0159	0,9206	1,0000	0,4286	0,8413	0,3968	0,7143	0,3968	0,6190	0,9206	0,1667
IL-8	0,2698	0,9206	0,1111	0,0794	0,4683	0,3571	0,7143	0,1984	0,1984	0,4841	0,7540	0,4683	0,7540	0,7143	0,0079	0,0159
MCP-1	0,7222	0,3095	0,3889	0,6429	0,4206	0,6270	0,4365	0,3254	0,8730	0,2857	1,0000	0,4206	0,5397	1,0000	0,6825	0,4048
MIP-1α	0,8571	1,0000	1,0000	0,6905	0,7778	0,7937	1,0000	1,0000	0,8810	0,5317	0,8333	0,7778	1,0000	0,9286	1,0000	0,4921
MIP-1β	0,6190	1,0000	1,0000	0,6429	0,8254	0,7540	1,0000	0,7619	0,7937	0,8413	0,8730	0,8254	0,7937	1,0000	1,0000	0,3254
sCD40L	0,8730	0,2222	0,2540	0,0952	0,5635	0,6190	0,1508	0,2302	1,0000	0,1111	0,7381	0,5635	0,6825	0,6190	0,6508	0,3254
TGFα	0,6429	0,8730	1,0000	0,5794	0,6667	0,5714	0,4762	0,6667	0,7143	0,2460	0,7381	0,6667	1,0000	0,3413	0,7302	0,5000
TNFα	0,6429	1,0000	0,8333	0,2857	0,6667	0,9206	0,7381	0,7857	0,9444	0,3095	1,0000	0,6667	0,8810	0,7302	1,0000	0,3492
VEGF	0,7381	0,9048	1,0000	0,4921	0,7619	1,0000	1,0000	0,9048	0,8095	0,6032	0,6825	0,7619	0,7302	1,0000	0,9048	0,6667

Table S2 – Statistics for cytokines concentrations. P-values of the permutation tests are given for the indicated comparisons. Red indicate significant differences, p <0.05.

Metal	Marker	Clone	Surface	Intra-cellular
141Pr	CD66abce	TET2	●	
142Nd	HLA-DR	L243	●	
143Nd	CD3	SP34.2	●	
144Nd	CD64	10.1	●	
145Nd	CD8	RPAT8	●	
146Nd	IL-6	MQ2.13A5		●
147Sm	CD123	7G3	●	
148Nd	IL-4	8D48		●
149Sm	CD11a	HI111	●	
150Nd	CD11b	ICRF144	●	
151Eu	CD62L	SK11	●	
152Sm	CD4	L200	●	
153Eu	FcεRI	AER37	●	
154Sm	CD86	IT2.2	●	
155Gd	CD125	A14	●	
156Gd	CD172a	15-414	●	
158Gd	IP-10	6D4		●
159Tb	CD45	D058-1283	●	
160Gd	IL-1α	364/3B3		●
161Dy	CD1c	AF5910	●	
162Dy	IL-12	C8.6		●
163Dy	CD32	FLI8.26	●	
164Dy	IFNα	LT27/295		●
165Ho	CD39	eBioA1	●	
166Er	CCR5	3A9	●	
167Er	CD16	3G8	●	
168Er	CD11c	3.9	●	
169Tm	CXCR4	12G5	●	
170Er	CD14	M5E2	●	
171Yb	IL-8	G265.8		●
172Yb	CD23	9P25	●	
173Yb	CD141	1A4	●	
174Yb	CD20	2H7	●	
175Lu	CCR7	G043H7	●	
176Yb	CADM1	3 E1	●	

Table S3 – Antibody panel for mass cytometry. Antibody target, clone, and associated metal is indicated as well as whether the antibody was used intra- or extra-cellularly.

Kinetic family	Phenotypic family	Cell population	Kinetic Pattern
VII	Granulocytes 15 Monocytes-DCs 19, 21, 27 and 28	Neutrophils Highly activated and HLA-DRlow monocytes, pDCs and inflammatory cDCs / non-classical monocytes	Main response to the prime
IV	Granulocytes 5, 11 and 12	Eosinophils and basophils	Main response to the boost
I	Granulocytes 1 and 9	Diversely activated neutrophils, eosinophils Highly activated monocytes, diversely activated cDCs, FceRI+ CD141+ APCs, CADM1+ APCs	Similar response to prime and boost
II	Granulocytes 2, 3, 8 and 10 Monocytes-DCs 22 and 37		
III	Granulocytes 4 and 7 Monocytes-DCs 26 and 33		
XI	Monocytes-DC 25, 31, 35 and 36		
V	Granulocytes 6 and 13 Monocytes-DC 17 and 18	Diversely activated neutrophils including CD14+ neutrophils Diversely activated monocytes and cDCS	Heterogeneous response
VI	Granulocytes 14 Monocytes-DC 32		
IX	Monocytes-DC 20 and 23		
VIII	Granulocytes 16	peculiar neutrophil cluster Highly activated cDCs, highly activated monocytes and CADM1+ APCs	No or very low response
X	Monocytes-DC 24		
XII	Monocytes-DC 29 and 30		
XIII	Monocytes-DC 34		

Table S4 – Correspondence between kinetic and phenotypic families. For each kinetic family, its composition in terms of phenotypic families are indicated. Moreover, its main cell populations, phenotypes, and kinetic pattern are provided (as classified in **Figure 5**).

Kinetic Family	H6PP vs H0PP	D1PP vs H0PP	D3PP vs H0PP	D8PP vs H0PP	H0PB vs H0PP	H6PB vs H0PP	D1PB vs H0PP	D3PB vs H0PP	D8PB vs H0PP	D14PB vs H0PP	H6PP vs H6PB	D1PP vs D1PB	D3PP vs D3PB	D8PP vs D8PB	D14PP vs D14PB
I	0,0476	0,0952	0,9048	1,0000	0,2698	0,0238	0,3889	0,5556	0,2460	0,7857	0,9048	0,4762	0,4603	0,2778	0,5079
II	0,0159	0,0079	0,2698	1,0000	0,4603	0,0079	0,0159	0,4206	0,4444	0,6270	0,1032	0,0238	0,0476	0,5317	0,6667
III	0,0556	0,1349	0,8651	0,8571	0,6825	0,1905	0,7778	0,8571	0,2540	0,6111	0,2540	0,0397	1,0000	0,4048	1,0000
IV	0,0079	0,0079	0,7619	0,3095	0,1032	0,0159	0,6032	0,1032	0,0079	0,9048	0,4206	0,0159	0,1190	0,0079	0,2143
V	0,0556	0,8333	0,9444	1,0000	0,1746	0,8413	0,0079	0,7937	0,0714	0,7381	0,0556	0,1667	0,8095	0,1032	0,4841
VI	0,5635	0,0159	0,0873	1,0000	0,8016	0,0079	0,0079	0,6270	0,5873	0,7222	0,0079	0,0238	0,0873	0,5556	0,7222
VII	0,0079	0,0079	0,0238	0,5952	0,4683	0,0079	0,0079	0,6429	1,0000	0,6429	0,6825	0,0079	0,0476	0,6270	0,9365
VIII	0,0397	0,4286	0,0873	0,0952	0,1270	0,1270	0,0397	0,1508	0,2937	0,0238	0,3968	0,7698	0,9048	0,7698	0,5952
IX	0,0714	0,0556	0,5397	0,8492	1,0000	0,5397	0,2460	0,5397	1,0000	0,8968	0,2460	0,0159	0,7698	0,8810	0,7222
X	0,4444	0,2698	0,3175	0,9286	0,8968	0,6825	0,1349	0,0556	0,9365	0,6825	0,1984	0,0635	0,7857	1,0000	0,7619
XI	0,7143	0,7460	0,9127	0,9206	1,0000	0,3175	0,1508	0,6349	1,0000	1,0000	0,5000	0,4206	0,8810	0,9206	1,0000
XII	0,6270	0,6429	0,8889	0,8571	0,6587	0,8333	0,2540	0,7778	0,8810	0,7222	0,5476	0,0635	0,4603	0,5317	1,0000
XIII	0,6111	0,3651	0,4444	0,3810	0,4921	0,5714	0,6111	0,4365	1,0000	0,5635	0,7857	0,0873	0,9365	0,3571	1,0000

Table S5 – Statistics for kinetic family cell abundance. P-values of the permutation tests are given for the indicated comparisons. Red indicate significant differences, $p < 0.05$.

	BD554D	BT145	CBL004	CC840	CCB116	ALL
D-27PP	379 216	542 145	426 000	835 039	453 826	2 636 226
D-19PP	572 958	514 273	649 982	516 674	240 091	2 493 978
H0PP	485 631	549 104	387 036	830 053	620 959	2 872 783
H6PP	470 642	670 857	568 345	772 846	621 498	3 104 188
D1PP	632 618	653 277	469 087	838 483	752 279	3 345 744
D3PP	796 397	363 416	762 792	677 265	587 500	3 187 370
D8PP	822 189	659 918	495 605	759 876	459 273	3 196 861
H0PB	860 727	778 709	642 882	657 108	545 693	3 485 119
H6PB	697 280	759 853	821 341	676 713	767 993	3 723 180
D1PB	667 939	598 244	861 405	670 555	452 805	3 250 948
D3PB	447 317	736 728	96 283	674 066	718 784	2 673 178
D8PB	242 058	327 046	593 431	291 948	519 604	1 974 087
D14PB	536 453	172 437	321 208	499 992	474 893	2 004 983
D28PB	564 540	396 758	554 592	1 035 383	623 748	3 175 021
TOTAL	8 175 965	7 722 765	7 649 989	9 736 001	7 838 946	41 123 666

Table S6 – Numbers of cells per sample. The number of events acquired with the CyTOF is indicated for each sample.

Markers	Number of non-uniform clusters	Percentage of non-uniform clusters
CD32	24	3,00
CD4	18	2,25
CD125	14	1,75
CADM1	14	1,75
CD16	12	1,50
CD123	11	1,38
CD11a	10	1,25
HLA-DR	9	1,13
CD3	9	1,13
FcεRI	8	1,00
CD86	8	1,00
CD11c	8	1,00
CD8	7	0,88
CD14	7	0,88
CD45	6	0,75
CCR5	6	0,75
CD23	6	0,75
CD141	6	0,75
CD11b	5	0,63
CD39	5	0,63
CCR7	5	0,63
CD172a	4	0,50
CD66	3	0,38
CD62L	3	0,38
CD1c	3	0,38
CXCR4	3	0,38
CD64	2	0,25
CD20	2	0,25

Table S7 – Uniformity of markers across clusters. For each marker, the numbers, and percentages of non-uniform clusters is indicated.

Chapter 6. NK cell responses during an early boost vaccination schedule and correlation with adaptive immune memory

Overview

Knowing the tremendous differences that existed in both adaptive and innate myeloid immunity in the early boost *vs.* classical boost schedule, as reported in Chapter 5, we next investigated the NK cell response induced in the early boost cohort to assess whether it differed from the classical boost study.

To do so, we used the same strategy as for the innate myeloid cells analysis. We refined our NK cell antibody panel, notably by adding the chemokine receptor CXCR3, as well as more FcRs (CD32 and CD64). Note that similarly to innate myeloid cells, this analysis was performed using the Helios mass cytometer, in contrast to the CyTOF I mass cytometer used in the study of the classical boost cohort.

A wide diversity of NK cells was observed in the early boost dataset, actually larger than the one found in the classical boost dataset (Palgen et al., 2019). In particular, although the frontier between poorly and intermediately cytotoxic NK cells was more blurred in the early boost cohort than in the classical boost cohort, there was a far wider diversity among highly cytotoxic NK cells, notably with a clear subdivision of these NK cells into $CD2^{mid}$ and $CD2^{high}$ NK cells.

This difference in phenotypic diversity may be due on one side to the new markers we added in the early boost dataset panel. On the other side, it may rely on the fact that, in the early boost dataset, samples at late timepoint (up to 28 days post-boost) were included in the SPADE analysis, whereas the latest sample used in the classical boost cohort was 3 days post-boost. In addition, a key timepoint, day 8 post-prime, was present

in the early boost schedule but missing in the early boost schedule analysis. On this day, a subpopulation of HLA-DR$^+$ NK cells expanded and then waned and was almost missing at the next timepoint (day 14 post-prime), which was analyzed in both cohorts.

Still, in term of kinetics, and as the innate myeloid cells, NK cell subphenotypes were mostly impacted by both immunizations, and in a similar manner. As a result, linear discriminant analyses failed to distinguish NK cell response to the prime and the boost, in the early boost cohort. Note that compared to the classical boost cohort, the switch of NK cells toward a less cytotoxic phenotype between day 1 and day 14 post-prime seems less pronounced. Though, after the boost there is a tendency to have even less cytotoxic NK cells than after the prime.

When comparing the phenotypes that were present in the early boost cohort compared to those identified in the classical boost cohort, most subphenotypes from both datasets found their counterparts in one another dataset. A first potential explanation is that, similarly to what happened for monocytes-DCs, more active/mature “memory” NK cells were generated in the early boost schedule but with a dramatically altered kinetics and magnitude compared to the classical schedule. A second non exclusive explanation is that, since most NK receptors were missing in our NK cell panel, due to the lack of cross-reactivity on macaque fixed cells, as described before, we may not have captured the full NK cell diversity and we may not be able to characterize perfectly the NK cell populations induced by each schedule.

In spite of these issues, we used the phenotypic associations between schedules to assess the correlations between the humoral response previously described in Chapter 5 and the NK cell response. Interestingly, we found associations between the abundances of NK cell subsets and the quality and quantity of the humoral response, though correlations were weaker than for innate myeloid cells. This apparent weakness may be explained by the missing samples from the NK cell dataset. Indeed, similarly to Chapter 4, for some timepoints for which only few blood could be collected for ethical reasons, analyses were prioritized towards innate myeloid immunity analysis.

Overall, this analysis showed that NK cell response is also strongly affected by the vaccine schedule and that early boost cohort failed to induce phenotypically more cytotoxic “memory” NK cells, in contrast to classical boost schedules. This "likely memory" NK cell response was strongly associated with the quality of the adaptive humoral response.

"Boost vaccination timing impacts the quality of NK cell response, which correlates with a differential humoral response"

Those results are part of a manuscript in preparation, provided hereafter.

Boost vaccination timing impacts the quality of NK cell response, which correlates with a differential humoral response

Jean-Louis Palgen[1,2], Nicolas Tchitchek[1,2], Quentin Jouhault[1,2], Hadjer Abdelhouahab[1,2], Nathalie Dereuddre-Bosquet[1,2], Antonio Cosma[1,2], Yves Lévy[2,3], Roger Le Grand[1,2], and Anne-Sophie Beignon[1,2*]

[1] CEA – Université Paris Sud 11 – INSERM U1184, Immunology of Viral Infections and Autoimmune Diseases, IDMIT department, IBFJ, 92265 Fontenay-aux-Roses, France

[2] Vaccine Research Institute, Henri Mondor Hospital, 94010 Créteil, France

[3] Institut Mondor de Recherche Biomédicale – INSERM U955, Eq.16, 94010, Créteil, France

*Corresponding author: Anne-Sophie Beignon; 18, route du Panorama; 92265 Fontenay-aux-Roses, France; Phone: +33 1 46 54 80 27; Fax : +33 1 46 54 77 26 ;email: anne-sophie.beignon@cea.fr

Short title: NK cell response after immunizations

Abstract

Understanding the early immune response that follows vaccination is critical for an optimized vaccine design. In particular the impact of the delay between prime and boost on the resulting immunity is not well characterized. We previously showed that an early boost, by contrast to a classical boost, failed to induce a distinct innate myeloid immune response, which was correlated with a qualitatively and quantitatively distinct antibody response.

Here we show that, similarly to the innate myeloid cells the early boost induced NK cell response comparable to the prime, which is in deep contrast to the classical boost schedule. These features correlated with the resulting antibody response, strongly strengthening the interplay between early innate immune responses and late adaptive responses.

Keywords: innate lymphoid immunity, NK cells, prime-boost, vaccination, MVA, NHP, mass cytometry.

Introduction

The early events that follows immunization are key to understand the resulting immune response and establishment of long-term immune memory (Iwasaki and Medzhitov, 2010). A better understanding of the innate response induced at each immunization is thus require to better understand vaccine-induced immune response and optimize vaccine design, all the more since it was shown to be an efficient predictor of the resulting adaptive responses (Nakaya et al., 2015). Besides, while most vaccines require several immunizations (a first one called prime and the other called boost(s)) to be efficient (Kardani et al., 2016; Ramshaw and Ramsay, 2000; Woodland, 2004), little is known about the impact of the delay between prime and boost on the resulting immune response.

To tackle with this issue, we used a non-human primate model, the cynomolgus macaques, which is known to be close to human in term of immune system and is thus a highly valuable model for vaccine design (’t Hart et al., 2015; Rivera-Hernandez et al., 2014). As vaccine model, we used the modified vaccinia virus Ankara (MVA), a smallpox vaccine that is currently tested as a viral platform for vaccines against complex diseases such as malaria, tuberculosis of HIV (Drexler et al., 2004; Sebastian and Gilbert, 2016; Volz and Sutter, 2017). We also take advantage of the mass cytometry technology that allows for the simultaneous measurement of up to 40 parameters at a single-cell level, to decipher in depth the phenotype of cells responding to each immunization (Bendall et al., 2012; Reeves et al., 2018).

With these tools we previously showed that a classical prime-boost strategy with a delay of 2 months between both immunizations induced a robust and strong innate response of myeloid cells –neutrophils, monocytes and dendritic cells (DC) – (Palgen et al., 2018) and NK cells (Palgen et al., 2019). Interestingly both innate myeloid cells and NK cells responded differently to prime and boost, with cells responding to the boost and pre-existing to it being more mature/active/cytotoxic than those responding to the prime. Interestingly, when the delay between prime and boost was reduced to two weeks, the innate myeloid cell response was similar between prime and boost, suggesting that two weeks is not a time-lapse sufficient to establish the modification of the innate myeloid compartment. On the very same animals that we assessed the innate myeloid response, we addressed here the NK cell response induced by a boost two weeks after the prime. We reveal that similarly to innate myeloid response, the NK cells response is very similar to the prime response with only few slight differences that did not allow to fully discriminate each response. In addition, NK cell response correlated with the quality and quantity of antibody response.

Material and Methods

Ethics statement

The experimental protocols were approved by the ethics committee «Comité d'éthique en expérimentation animale n°44 » under the reference 2015031314518254 (APAFIS#319).02 for the longitudinal analysis of the MVA-induced response, and the «Ministère de l'Education Nationale, de l'Enseignement Supérieur et de la Recherche» (France). Animals were handled by veterinary staff in accordance with national regulations (CEA Permit Number A 92-32-02) and the European Directive (2010/63, recommendation Nº9) and in compliance with the Standards for the Humane Care and Use of Laboratory Animals of the Office for Laboratory Animal Welfare (OLAW, USA) under OLAW Assurance number #A5826-01.

Experimental design

Five cynomolgus macaques originating from Mauritius and identified as BC554D BT145, CBL004, CC840 and CCB116, were immunized two weeks apart with the ANRS recombinant MVA HIV B vaccine (MVATG17401; Transgene, Illkirch-Graffenstaden, France) at $4x10^8$ plaque forming units (**Figure 1**). As previously described (Palgen et al., 2018, 2019; Pejoski et al., 2016), this vaccine encodes for the full-length *gag* (amino acids 1 to 512), and parts of *pol* (amino acids 172 to 219, 325 to 383, and 461 to 519) and *nef* (amino acids 66 to 147 and 182 to 206) from the Bru/Lai isolate (Los Alamos database accession number K02013). Blood samples were longitudinally collected either in Lithium-Heparin for single-cell mass cytometry analysis or in EDTA for complete blood count.

Sample preparation

Fixed leukocytes were prepared for mass cytometry using a previously described cell fixation protocol that recover all leukocytes, including neutrophils (Egger et al., 2001; Elhmouzi-Younes et al., 2017; Palgen et al., 2018, 2019). Briefly, 1 mL of blood was incubated with a fixation buffer containing formaldehyde and glycerol for 10 min at 4°C. Erythrocytes were then lysed in 10 mL milli-Q water at room temperature for 20 min. Cells were eventually washed in 1X DPBS and stored at -80°C at a final concentration of $15x10^6$ cells/mL in the fixation mixture. Cells were fixed extemporaneously without re-stimulation *ex vivo*.

Cell staining and acquisition

Fixed leukocytes staining and acquisition protocols were identical to those previously described (Palgen et al., 2018, 2019). The 34-marker antibody panel used here is described in **Table 1**.

Data processing and event selection

As previously described (Palgen et al., 2018) (NK paper IMA VAC1516), FCS files were normalized with the MATLAB normalizer from Rachel Finck *et al.* (Finck et al., 2013). Replicates were concatenated using the tool from Cytobank (Mountain View, USA). Leukocytes were gated based on event length, iridium content, and exclusion of non-specifically stained $CD66^+CD3^+$ eosinophils (Elhmouzi-Younes et al., 2017; Palgen et al., 2018).

Complete blood count and cell population count

Complete blood counts (CBCs) were performed using blood collected in EDTA with the HmX instrument (Beckman Coulter). The absolute number of cells in each sample for a given cell population was computed as follows: N = the absolute number of leukocytes (expressed per µL of blood) x the number of cells in the population detected by CyTOF/total number of leukocytes (excluding $CD3^+CD66^+$ cells) detected by CyTOF (given in **Table S1**).

Identification of cell populations

The Spanning-tree Progression Analyses of Density-normalized Events (SPADE) (Qiu et al., 2011) algorithm was performed on the whole dataset (samples from every animals and every timepoints) to automatically identify cell populations displaying similar expression levels for the given markers used for clustering: CD66abce, HLA-DR, CD3, CD64, CD8, CD226, granzyme B, CD11a, CD11b, CD62L, CD4, CD56, CD2, CD7, NKG2D, CD45, CD1c, CD25, CD32, CD69, CD39, CCR5, CD16, CD11c, CXCR4, CD14, perforin, NKG2A/C, CD107a, CD20, CCR7 and CXCR3. Prior to clustering, we performed random pre-downsampling of 190,000 cells (corresponding to the highest number of cells contained in all samples) to avoid bias in the analysis towards samples with more cells than others (**Table S1**). The quality of the SPADE clustering, defined as a narrow and unimodal distribution for each marker in all cell clusters and NK cell clusters was assessed using the SPADEVizR R package we developed (Gautreau et al., 2016).

Based on these quality control measurements, SPADE was parameterized to identify 900 clusters using a downsampling of 30%, leading to 58.33% of all clusters with unimodal (Hartigan's dip test, p-value ≤ 0.05) and narrow distribution (IQR ≤ 2) of all markers. This relatively low percentage of uniform clusters is mainly caused by CD66 staining, which is non-uniform for xxx clusters. Actually the negative population is represented by two peaks within a low range of expression (both around 0), which explains why they fail to pass the test (**Figure S1**). Excluding CD66, 77.77% of clusters are uniform.

Among NK cell clusters identified on the SPADE tree, based on CD3 and CD8 expression 69.23% (90 out of 130) had a unimodal and narrow distribution for all markers, excluding CD66, which accounted for the most non-uniform clusters (46 out of 130) (**Table S2**).

We directly identified blood NK cells on the SPADE tree based on CD3 and CD8 expression, rather than by manual gating followed by SPADE analysis of the NK cells to avoid a bias in the manual gating of $CD3^-$ $CD8^+$ events and contamination with $CD66^{low}$ neutrophils, which displayed a low background signal in all channels including CD8.

Categorical heatmap representation of NK cell clusters phenotypes

The categorical heatmap were generated using the median expression among all samples and SPADEVizR R-package (Gautreau et al., 2016). All samples containing less than 10 cells were removed from the median computation. Marker expression range was divided into five categories (5^{th} - 95^{th} percentiles) to define the cell cluster phenotype. Hierarchical

clustering, represented by the cluster and marker dendrograms in the heatmap, was performed using the Euclidean metric and the ward.D linkage method. Phenotypic family were defined based on the cluster dendrogram.

LASSO-LDA model to classify post-prime and post-boost NK cell immune profiles

The classification of post-prime and post-boost NK cell immune profiles was performed using a combination of the Least Absolute Shrinkage and Selection Operator (LASSO) and Linear Discriminant Analysis (LDA) methods. The LASSO method was based on the lars R package (available at https://CRAN.R-project.org/package=lars). Abundance profiles of phenotypic families were centered and reduced. Model validity was assessed through the leave-one-out cross-validation method. The best configuration was chosen using the elbow criterion.

Kinetic homogeneity

Kinetics of kinetic families were considered as homogeneous when cell abundance for at least one timepoint differed either from baseline, or from the corresponding timepoint with the other immunization (*e.g.* D8PP *vs.* D8PB). Cell abundances were compared using the permutation test from the exactRankTests R package (available at https://cran.r-project.org/web/packages/exactRankTests/index.html).

Correlations between antibody response and NK cell responses

Similarly to previous analyses on innate myeloid cells, NK cell populations were associated in the two schedules (early boost, this study, and classical boost, previously published (NK paper) based on the Manhattan distance. Two populations were associated only if they were the closest neighbor of each other, based on the ratio between the actual number of associations (clusters linked together) and the number of potential associations between them. The area under the curve was used to assess the magnitude of the response PP (H6PP, D1PP, D3PP) and the boost (H6PB, D1PB, D3PB). To avoid technical bias in this calculation, the area was normalized based on the mean abundance of each cell population within each schedule during the response to prime. In other words, for a given animal and a given cell population:

AUC = sum(abundances during the prime (respectively the boost))/mean(abundances during the prime for all animals from the same vaccine schedule)

Pearson correlation was computed between the area under the curve of each NK cell population abundance and the antibody response at the peak (either D8PB or D14PB according to the response) and the long-term (at M6PB).

Results

NK cell kinetics do not differ between prime and boost

As previously described, five cynomolgus macaques were immunized with the MVA HIV B vaccine following a prime-boost strategy with a delay of two weeks between each immunization. Blood samples collected longitudinally (**Figure 1**) were stained with a CyTOF antibody panel dedicated to NK cell biology (**Figure 2A**) and followed an established analysis pipeline (**Figure 2B**) (Palgen et al., 2018, 2019).

We first perform Spanning-tree Progression Analyses of Density-normalized Events (SPADE) to cluster together cells that share a similar phenotype in a wide set of markers: CD66abce, HLA-DR, CD3, CD64, CD8, CD226, granzyme B, CD11a, CD11b, CD62L, CD4, CD56, CD2, CD7, NKG2D, CD45, CD1c, CD25, CD32, CD69, CD39, CCR5, CD16, CD11c, CXCR4, CD14, perforin, NKG2A/C, CD107a, CD20, CCR7 and CXCR3. Based on the resulting SPADE tree (**Figure 2C**), NK cell cluster were annotated as $CD3^-$ $CD8^-$. Note that in this process, the other blood cell type (T cells, B cells, monocytes, dendritic cells, neutrophils…) were excluded.

Looking at the dynamics of the gated NK cells (**Figure 2D**), we observed a slight tendency for a decrease at H6PP-D1PP followed by an increase at D8PP then a new decrease at D14PP. The same pattern was observed after the boost. This kinetics is consistent with our previous analysis with the classical schedule, in which we also observed a decrease in NK cell count (the D8PP, D8PB, D14PB and D28PB timepoints were missing in this previous study). Note that we also observed here a high inter-individual variability in term of NK cell count prior to any immunization. This variability is reduced after immunization.

That similar NK response to prime and boost is consistent with the innate myeloid response observed in this schedule. To assess whether this still stands true after a deep phenotypic characterization of the phenotype we used the several markers measured by mass cytometry.

High phenotypic variability amongst NK cells

To visualize at a glance the phenotype of all NK cell clusters, we used heatmap representation. On this heatmap (**Figure 3**), and based on the hierarchical clustering of the clusters, clusters that were phenotypically close to each other were grouped into so-called phenotypic families, that mitigate the stringency of our SPADE clustering, which resulted in a high number of clusters.

17 phenotypic families were obtained. This is a higher diversity than what was observed with the classical schedule, which may be explained by the missing timepoints (D8PP, D8PB, D14PB and D28PB) in the classical schedule analysis.

Three superfamilies (groups of phenotypic families) could be identified. A first superfamily A (phenotypic families 1, 11, 2, 4, 15 and 7) that consisted in highly activated CD107a^{high} IL-6^{high} CD69^{high} CD16^{high} CD2^{high}, with differential levels of CXCR4 CD56 CCR5 CD11c CD11a and CD7. A second superfamily B (phenotypic families 10, 16, 13 and 5) also consisted in highly activated NK cells, similar to family A except that these cells awee CD2^{low}, which may

suggest a different step in differentiation process. Note that among them, the phenotypic family 16 was $CD3^{high}$, and might thus correspond to NKT cells. The last superfamily C (phenotypic families 9, 17, 8, 12, 3, 6 and 14) consisted of poorly-intermediately activated NK cells that were $CD107a^{mid}$ $IL\text{-}6^{mid}$ $CD69^{mid}$ $CD16^{mid/low}$. Note that among them, families 9 and 6 were $CD2^{high}$ whereas the other were $CD2^{low}$. In addition families 14 and 6, which displayed the lowest cytotoxic phenotype, were $CXCR4^{low}$ $CD56^{low}$ $CCR5^{low}$ $CD11c^{low}$ $CXCR3^{low}$ $CD11a^{low}$ $CD7^{low}$.

Slight different kinetics between prime and boost

To assess the dynamics of these distinct subphenotypes (**Figure S2**), we cluster together the phenotypic families that share similar kinetics into so-called kinetic families. 6 kinetic families were obtained so (numbered I to VI), their kinetics and composition is displayed on **Figure 4** and **Table 2**.

Kinetic families 1, 2 and 3 showed heterogeneous kinetics. Still, kinetic family I showed a tendency kinetic similar to all NK cells (decrease at H6-D1 post-immunization, increase afterwards), with CCB116 being an outlier in term of amplitude.

Kinetic family 4, containing poorly activated NK cells, remained low in number until an increase at D8PP, then it re-decreased in number at H6PB, and re-increased after the boost and remained slightly higher after the boost compared to the prime. Kinetic family 5, containing poorly activated NK cells increased in number at late time post-immunization, but

only significantly at D3PB. Kinetic family 6, containing two HLA-DR^{+} NK cell cluster (phenotypic family 17) interestingly show an only peak at D8PP and was completely missing after the boost.

Overall, slight differences between prime and boost could be observed, with some poorly activated CXCR4^{low} CD56^{low} CCR5^{low} CD11c^{low} CXCR3^{low} CD11a^{low} CD7^{low} NK cells (phenotypic families 6 and 14) were induced lately after the prime (D8PP and D14PP), similarly to what was observed in the classical schedule (Palgen et al., 2019). These cells remained higher in number after boost compared to prime, which is in deep contrast to the classical schedule, in which these cells were missing after the boost. Also, similarly to the classical schedule (Palgen et al., 2019) the HLA-DR^{+} that were induced at D8PP and decreased at H0PB, were lost after the boost.

To take a look from another point of view, we then further assessed the longitudinal evolution the phenotype composition of the NK cell compartment (**Figure 5**).

Interestingly, the composition in NK cell subphenotypes remains quite stable early after prime, a feature we previously observed in the classical boost schedule (Palgen et al., 2019). Still, while we observed a tremendous shift from D1PP to D14PP in the classical boost schedule, the same tendency was observed here, with an increase in proportion of CXCR4^{low} CD56^{low} CCR5^{low} CD11c^{low} populations (phenotypic families 1, 11 , 2, 10, 16 and 13),but with a lower amplitude. This may be due to a reduced resolution of the capture of NK cell diversity in the classical boost schedule. Strikingly, after boost, while highly activated NK cells were

induced after the classical boost (Palgen et al., 2019), a high proportion of poorly activated NK cells was induced by the early boost (**Figure 5**), which would suggest either the emptiness of the mature NK cells compartment or the exhaustion of the existing compartment.

Non-discrimination between prime and boost response based on NK cell count

Given the slight differences we observed in NK cell response to the prime and the boost, we wanted to address whether this was sufficient to distinguish prime response and boost response. To do so, we used LASSO-LDA approach to define a model discriminating each response (**Figure 6**). The best model we could build doing show a tremendous error around 1 (for a targeted value of one), which is far bigger than the model we built in the classical schedule analysis . This indicated that the NK cell response to the prime and the boost are not sufficiently different to allow to discriminate between them, in the early boost schedule.

Association between NK cells from both schedules

To assess whether the NK cell subphenotypes we found in the classical boost were also found with the early, we performed a phenotypic comparison of both dataset. Associations were found for almost all subsets (**Figure 7**). Interestingly, note that the $CD2^+$ highly activated NK cells from the early boost were closer to the intermediately activated NK cells from the classical boost schedule, whereas the $CD2^-$ highly activated NK cells were closer to the highly activated NK cells from the classical boost schedule.

Still note that some discrepancies were found. In particular, phenotypic family 10, among $CD2^-$ highly activated NK cells, did not match a counterpart within the classical boost dataset, although this family was present at baseline and after prime. This may be due to distinct CD7 pattern between the two datasets: family 10 is $CD7^{low}$, whereas all highly activated NK cells were $CD7^{high}$ in the classical boost dataset.

Overall these results suggests that most NK cell subphenotypes impacted by vaccination, were present at baseline and after prime, but that their expansion/shrinking in number differ according to prime-boost delay.

Correlation between NK cell response and antibody response

To go further, given the variability we observed in the classical boost schedule and the early boost schedule, both in term of NK cell response and antibody response (Palgen et al., 2019), we assessed whether we could find early correlates between NK cell response and the later humoral response (**Figure 8,** and **Figure S3**).

Strikingly, looking at the overall associations, antibody response and NK cell response clustered apart (**Figure 8A**). In addition, highly activated segregated apart from poorly and intermediately activated NK cells. It suggest that in addition to phenotypic proximity, poorly and intermediately activated NK cells share similar kinetics.

Still, some associations were found (0.6 ≤ R < 0 .7) between NK cell and antibody responses (**Figure 8B**), weaker than the ones found in the analysis of the innate myeloid responses. This may be due to the fact that we could not include D8 measurements in the area undert the curve calculation since two many observations were lacking.

Still, the abundance of the post-boost highly activated NK cell response correlated with the peak of FcγR binding affinity at D14PB (note that the highly activated monocytes also correlated with this antibody feature). Also, strikingly, the post-boost poorly activated $CXCR4^{low}$ $CD56^{low}$ $CCR5^{low}$ $CD11c^{low}$ $CXCR3^{low}$ $CD11a^{low}$ $CD7^{low}$ NK cell response correlated negatively with both the peak of FcγR binding affinity and also the long-term persistence of IgG, a feature that was not well correlated with innate myeloid cell response.

This supports a strong interconnection between NK cell response and the humoral response.

Discussion

Using mass cytometry technology and a panel dedicated to NK cells, we were able to unveil the phenotypic diversity and complexity of this compartment during a prime boost vaccination at two weeks apart.

A high phenotypic diversity was observed within the NK cell compartment, notably with wide ranges of expression of FcR (CD16), adhesion molecules (CD2, CD7), and various chemokines receptors (CCR5, CXCR4), suggesting various functionalities (Berahovich et al., 2006; Bruhns and Jönsson, 2015; Khan et al., 2006; McNerney and Kumar, 2006; Rabinowich et al., 1994; Sempowski et al., 1999). Interestingly, the expression of CD2 was observed both amongst intermediately and highly activated NK cells, with a clear cut between positive and negative population, suggesting a distinct ability to be activated within these populations, since CD2 is involved in NK cell functions, including cytotoxicity and cytokine production (McNerney and Kumar, 2006). Also, CD7 was clearly segregating positive and negative populations in all categories, likely linked to distinct activation capabilities (Rabinowich et al., 1994; Sempowski et al., 1999).

In both analyses we could unfortunately not include NK receptors such as NKp80, NKP46… due to a lack of reactivity of the corresponding antibodies, either with fixed cells or macaque cells (Palgen et al., 2019). As a consequence, we could not investigate the impact of vaccination on NK cell repertoire, which was shown to be impacted by individual infection history (Wilk and Blish, 2018). Further studies using single-cell transcriptomics or mass cytometry-based RNA detection (Frei et al., 2016) could help by-passing the issue in the future. Still these existing data brought valuable information for NK cell dynamics and overall response following vaccination.

Similarly to the classical schedule (with two months delay between prime and boost), NK cells dynamics is marked by a decrease at early timepoints post-immunization, followed by an increase at the late timepoints. Note that this expansion peaked around D8 post-immunization, since at D14PP, NK cell number is almost back to baseline. In term of NK cell count, no difference was observed between the prime and boost of the two schedule.

Though, compared to the classical boost schedule, we reveal here that the NK cell response if far more similar between prime and early boost. As a consequence, discriminant analyses could not distinguish between prime and early boost responses. Still slight some differences could be observed. For example, poorly activated NK cells responded to the early boost, whereas they were not in the classical schedule. This has to be linked with the induction of poorly activated NK cells between D1 and D14PP, observed in both schedules (Palgen et al., 2019). The high abundance of poorly cytotoxic NK cells in the post-boost response might correspond to exhausted NK cells reported in cancer (Mamessier et al., 2011; Platonova et al., 2011) and chronic infections (Jost and Altfeld, 2012). Interestingly, this exhaustion was shown reversible in a mice model (Ardolino et al., 2014), consistently with disappearance of these potentially exhausted NK cells in the classical boost (Palgen et al., 2019).

The poor differences between prime and early boost responses was previously observed in the innate myeloid compartment, by contrast to a distinct response observed after the classical boost (Palgen et al., 2018). This strongly suggest, that the modification of the innate arm of the immune system (myeloid and lymphoid), which is induced by the prime and will result in a differential immune response, takes more than two weeks to occur.

It is still unclear which exact modifications of NK cells are induced by the prime, and which type of memory-like NK cells were generated in the classical boost (Palgen et al., 2019). Indeed, several terminologies co-exist in littérature, such as adaptive NK cells, cytokine activated NK cells, cytokine induced NK cells or antigen-specific NK cells, and the exact phenotype and function of each is not currently well-established (Min-Oo et al., 2013; Nabekura and Lanier, 2016; O'Leary et al., 2006; Paust et al., 2017). Still, our results indicate that the generation of these memory-like NK cells following vaccination, is impaired by an early boost. As a result these cells are not recruited after the early boost.

Both in our previous analyses of innate myeloid response and here of NK cell response, we found correlations with the antibdoy responses, both at the peak of the response and in the long term. This indicates that innate responses to the early boost are good predictors of the resulting humoral response, even in the long term. Studies in literature previously highlighted the role of NK cell in B cell / antibody response, for example In IgG subclass switching (Gao et al., 2001, 2008), Tfh and germinal center modulation (Cook et al., 2015; Rydyznski et al., 2018). Our results consistently support that NK cell may strongly participate to humoral immunity generation. This reinforces the importance of NK cell functions targeting in optimizing vaccines (Rydyznski and Waggoner, 2015; Wagstaffe et al., 2018).

Authorship

Conceptualization: RLG and ASB; immunization and blood sampling: NDB; sample processing and storage: HA; mass cytometry staining: JLP; mass cytometry acquisitions: JLP, QJ and AC; mass cytometry analysis: JLP, NT and ASB; writing of the original draft: JLP, NT and ASB; review and editing: QJ, HA, NDB, AC and RLG; acquisition of funding: YL, RLG, and ASB; supervision: RLG and ASB.

Acknowledgments

This work was supported by the “Investissements d’Avenir” programs managed by the ANR under reference ANR-10-LABX-77-01, funding the Vaccine Research Institute (VRI), Créteil (ImMemory research program), ANR-11-INBS-0008, funding the Infectious Disease Models and Innovative Therapies (IDMIT, Fontenay-aux-Roses, France) infrastructure, and ANR-10-EQPX-02-01, funding the FlowCyTech facility (IDMIT, Fontenay-aux-Roses, France), and by the European Union EVHA H2020 project (Grant N°681032). We would like to thank all members of the ASW and L2I groups from IDMIT as well as Romain Marlin. Nicolas Tchitchek held a fellowships from the ANRS (France Recherche Nord&Sud Sida-HIV Hépatites).

Conflict of interest disclosure

The authors declare no conflict of interest.

References

Ardolino, M., Azimi, C.S., Iannello, A., Trevino, T.N., Horan, L., Zhang, L., Deng, W., Ring, A.M., Fischer, S., Garcia, K.C., et al. (2014). Cytokine therapy reverses NK cell anergy in MHC-deficient tumors. J. Clin. Invest. *124*, 4781–4794.

Bendall, S.C., Nolan, G.P., Roederer, M., and Chattopadhyay, P.K. (2012). A deep profiler's guide to cytometry. Trends Immunol. *33*, 323–332.

Berahovich, R.D., Lai, N.L., Wei, Z., Lanier, L.L., and Schall, T.J. (2006). Evidence for NK cell subsets based on chemokine receptor expression. J. Immunol. *177*, 7833–7840.

Bruhns, P., and Jönsson, F. (2015). Mouse and human FcR effector functions. Immunol. Rev. *268*, 25–51.

Cook, K.D., Kline, H.C., and Whitmire, J.K. (2015). NK cells inhibit humoral immunity by reducing the abundance of CD4+ T follicular helper cells during a chronic virus infection. J. Leukoc. Biol. *98*, 153–162.

Drexler, I., Staib, C., and Sutter, G. (2004). Modified vaccinia virus Ankara as antigen delivery system: how can we best use its potential? Curr. Opin. Biotechnol. *15*, 506–512.

Egger, G., Burda, A., and Glasner, A. (2001). A simple method for measuring the F-actin content of human polymorphonuclear leukocytes in whole blood. Virchows Arch. *438*, 394–397.

Elhmouzi-Younes, J., Palgen, J.-L., Tchitchek, N., Delandre, S., Namet, I., Bodinham, C.L., Pizzoferro, K., Lewis, D.J.M., Le Grand, R., Cosma, A., et al. (2017). In depth comparative phenotyping of blood innate myeloid leukocytes from healthy humans and macaques using mass cytometry. Cytometry A.

Finck, R., Simonds, E.F., Jager, A., Krishnaswamy, S., Sachs, K., Fantl, W., Pe'er, D., Nolan, G.P., and Bendall, S.C. (2013). Normalization of mass cytometry data with bead standards. Cytometry A *83*, 483–494.

Frei, A.P., Bava, F.-A., Zunder, E.R., Hsieh, E.W.Y., Chen, S.-Y., Nolan, G.P., and Gherardini, P.F. (2016). Highly multiplexed simultaneous detection of RNAs and proteins in single cells. Nat. Methods *13*, 269–275.

Gao, N., Dang, T., and Yuan, D. (2001). IFN-gamma-dependent and -independent initiation of switch recombination by NK cells. J. Immunol. *167*, 2011–2018.

Gao, N., Jennings, P., and Yuan, D. (2008). Requirements for the natural killer cell-mediated induction of IgG1 and IgG2a expression in B lymphocytes. Int. Immunol. *20*, 645–657.

Gautreau, G., Pejoski, D., Le Grand, R., Cosma, A., Beignon, A.-S., and Tchitchek, N. (2016). SPADEVizR: an R package for Visualization, Analysis and Integration of SPADE results. Bioinformatics.

't Hart, B.A., Bogers, W.M., Haanstra, K.G., Verreck, F.A., and Kocken, C.H. (2015). The translational value of non-human primates in preclinical research on infection and immunopathology. Eur. J. Pharmacol. *759*, 69–83.

Iwasaki, A., and Medzhitov, R. (2010). Regulation of adaptive immunity by the innate immune system. Science *327*, 291–295.

Jost, S., and Altfeld, M. (2012). Evasion from NK cell-mediated immune responses by HIV-1. Microbes Infect. *14*, 904–915.

Kardani, K., Bolhassani, A., and Shahbazi, S. (2016). Prime-boost vaccine strategy against viral infections: Mechanisms and benefits. Vaccine *34*, 413–423.

Khan, I.A., Thomas, S.Y., Moretto, M.M., Lee, F.S., Islam, S.A., Combe, C., Schwartzman, J.D., and Luster, A.D. (2006). CCR5 is essential for NK cell trafficking and host survival following Toxoplasma gondii infection. PLoS Pathog. *2*, e49.

Mamessier, E., Sylvain, A., Thibult, M.-L., Houvenaeghel, G., Jacquemier, J., Castellano, R., Gonçalves, A., André, P., Romagné, F., Thibault, G., et al. (2011). Human breast cancer cells enhance self tolerance by promoting evasion from NK cell antitumor immunity. J. Clin. Invest. *121*, 3609–3622.

McNerney, M.E., and Kumar, V. (2006). The CD2 family of natural killer cell receptors. Curr. Top. Microbiol. Immunol. *298*, 91–120.

Min-Oo, G., Kamimura, Y., Hendricks, D.W., Nabekura, T., and Lanier, L.L. (2013). Natural killer cells: walking three paths down memory lane. Trends Immunol. *34*, 251–258.

Nabekura, T., and Lanier, L.L. (2016). Tracking the fate of antigen-specific versus cytokine-activated natural killer cells after cytomegalovirus infection. J. Exp. Med. *213*, 2745–2758.

Nakaya, H.I., Hagan, T., Duraisingham, S.S., Lee, E.K., Kwissa, M., Rouphael, N., Frasca, D., Gersten, M., Mehta, A.K., Gaujoux, R., et al. (2015). Systems Analysis of Immunity to Influenza Vaccination across Multiple Years and in Diverse Populations Reveals Shared Molecular Signatures. Immunity *43*, 1186–1198.

O'Leary, J.G., Goodarzi, M., Drayton, D.L., and von Andrian, U.H. (2006). T cell- and B cell-independent adaptive immunity mediated by natural killer cells. Nat. Immunol. *7*, 507–516.

Palgen, J.-L., Tchitchek, N., Elhmouzi-Younes, J., Delandre, S., Namet, I., Rosenbaum, P., Dereuddre-Bosquet, N., Martinon, F., Cosma, A., Lévy, Y., et al. (2018). Prime and Boost Vaccination Elicit a Distinct Innate Myeloid Cell Immune Response. Sci Rep *8*, 3087.

Palgen, J.-L., Tchitchek, N., Huot, N., Elhmouzi-Younes, J., Lefebvre, C., Rosenbaum, P., Dereuddre-Bosquet, N., Martinon, F., Hocini, H., Cosma, A., et al. (2019). NK cell immune responses differ after prime and boost vaccination. J. Leukoc. Biol.

Paust, S., Blish, C.A., and Reeves, R.K. (2017). Redefining Memory: Building the Case for Adaptive NK Cells. J. Virol. *91*.

Pejoski, D., Tchitchek, N., Rodriguez Pozo, A., Elhmouzi-Younes, J., Yousfi-Bogniaho, R., Rogez-Kreuz, C., Clayette, P., Dereuddre-Bosquet, N., Lévy, Y., Cosma, A., et al. (2016). Identification of Vaccine-Altered Circulating B Cell Phenotypes Using Mass Cytometry and a Two-Step Clustering Analysis. J. Immunol. *196*, 4814–4831.

Platonova, S., Cherfils-Vicini, J., Damotte, D., Crozet, L., Vieillard, V., Validire, P., André, P., Dieu-Nosjean, M.-C., Alifano, M., Régnard, J.-F., et al. (2011). Profound coordinated alterations of intratumoral NK cell phenotype and function in lung carcinoma. Cancer Res. *71*, 5412–5422.

Qiu, P., Simonds, E.F., Bendall, S.C., Gibbs, K.D., Bruggner, R.V., Linderman, M.D., Sachs, K., Nolan, G.P., and Plevritis, S.K. (2011). Extracting a cellular hierarchy from high-dimensional cytometry data with SPADE. Nat. Biotechnol. *29*, 886–891.

Rabinowich, H., Pricop, L., Herberman, R.B., and Whiteside, T.L. (1994). Expression and function of CD7 molecule on human natural killer cells. J. Immunol. *152*, 517–526.

Ramshaw, I.A., and Ramsay, A.J. (2000). The prime-boost strategy: exciting prospects for improved vaccination. Immunol. Today *21*, 163–165.

Reeves, P.M., Sluder, A.E., Paul, S.R., Scholzen, A., Kashiwagi, S., and Poznansky, M.C. (2018). Application and utility of mass cytometry in vaccine development. FASEB J. *32*, 5–15.

Rivera-Hernandez, T., Carnathan, D.G., Moyle, P.M., Toth, I., West, N.P., Young, P.L., Silvestri, G., and Walker, M.J. (2014). The Contribution of Non-human Primate Models to the Development of Human Vaccines. Discov Med *18*, 313–322.

Rydyznski, C.E., and Waggoner, S.N. (2015). Boosting vaccine efficacy the natural (killer) way. Trends Immunol. *36*, 536–546.

Rydyznski, C.E., Cranert, S.A., Zhou, J.Q., Xu, H., Kleinstein, S.H., Singh, H., and Waggoner, S.N. (2018). Affinity Maturation Is Impaired by Natural Killer Cell Suppression of Germinal Centers. Cell Rep *24*, 3367-3373.e4.

Sebastian, S., and Gilbert, S.C. (2016). Recombinant modified vaccinia virus Ankara-based malaria vaccines. Expert Rev Vaccines *15*, 91–103.

Sempowski, G.D., Lee, D.M., Kaufman, R.E., and Haynes, B.F. (1999). Structure and function of the CD7 molecule. Crit. Rev. Immunol. *19*, 331–348.

Volz, A., and Sutter, G. (2017). Modified Vaccinia Virus Ankara: History, Value in Basic Research, and Current Perspectives for Vaccine Development. Adv. Virus Res. *97*, 187–243.

Wagstaffe, H.R., Mooney, J.P., Riley, E.M., and Goodier, M.R. (2018). Vaccinating for natural killer cell effector functions. Clin Transl Immunology *7*, e1010.

Wilk, A.J., and Blish, C.A. (2018). Diversification of human NK cells: Lessons from deep profiling. J. Leukoc. Biol. *103*, 629–641.

Woodland, D.L. (2004). Jump-starting the immune system: prime-boosting comes of age. Trends Immunol. *25*, 98–104.

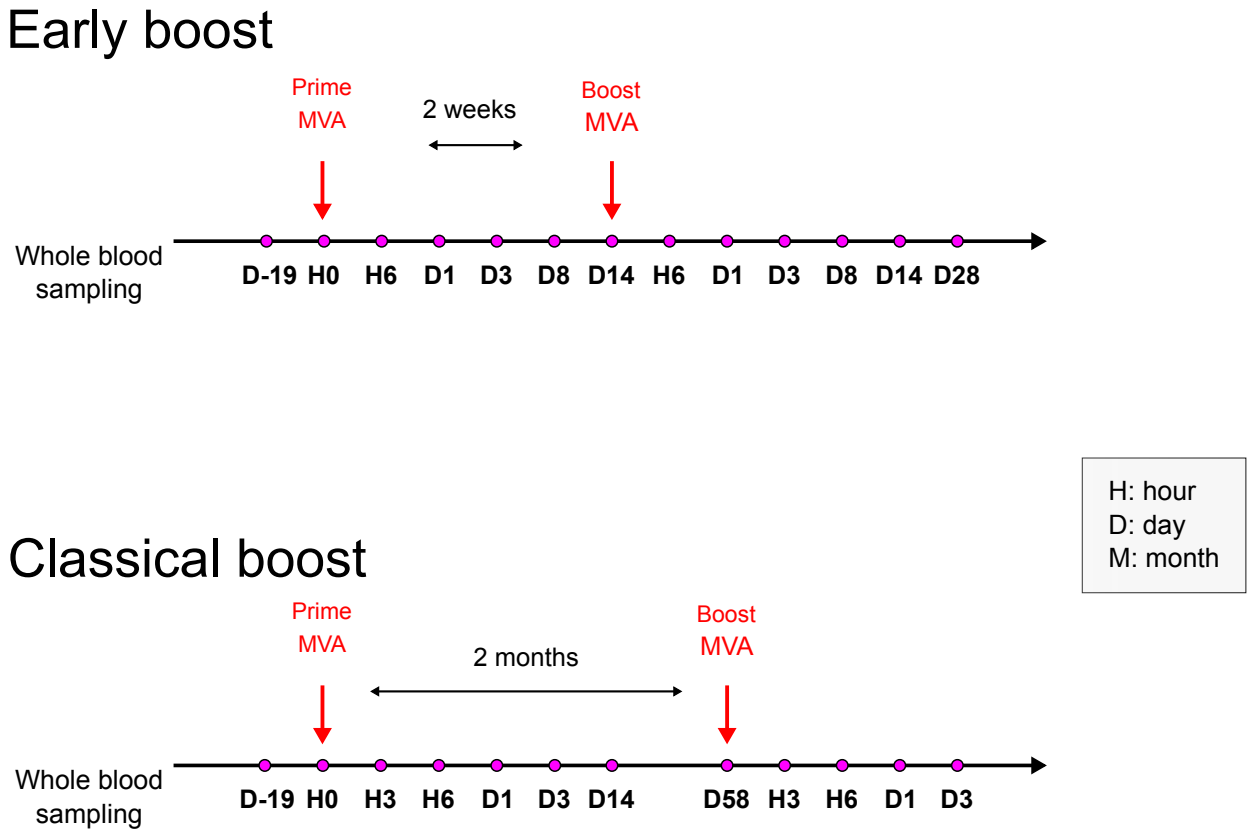

Figure 1. Experimental design and analysis strategy . Blood samples from five adult cynomolgus macaques were collected longitudinally at the indicated timepoints – hours (H) and days (D) post-prime (PP) and post-boost (PB). Macaques were immunized twice subcutaneously with MVA HIV-B at a dose of $4x10^8$ PFU, two weeks apart (early boost schedule) or two months apart (classical schedule)

A

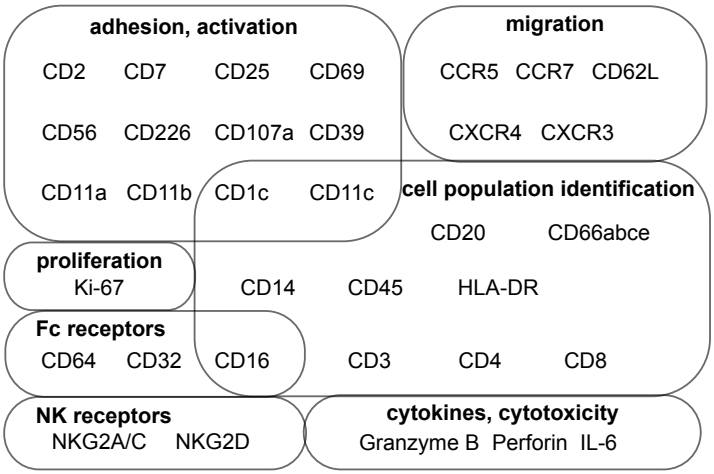
adhesion, activation
CD2 CD7 CD25 CD69
CD56 CD226 CD107a CD39
CD11a CD11b CD1c CD11c
migration
CCR5 CCR7 CD62L
CXCR4 CXCR3
cell population identification
CD20 CD66abce
CD14 CD45 HLA-DR
CD3 CD4 CD8
proliferation
Ki-67
Fc receptors
CD64 CD32 CD16
NK receptors
NKG2A/C NKG2D
cytokines, cytotoxicity
Granzyme B Perforin IL-6

B

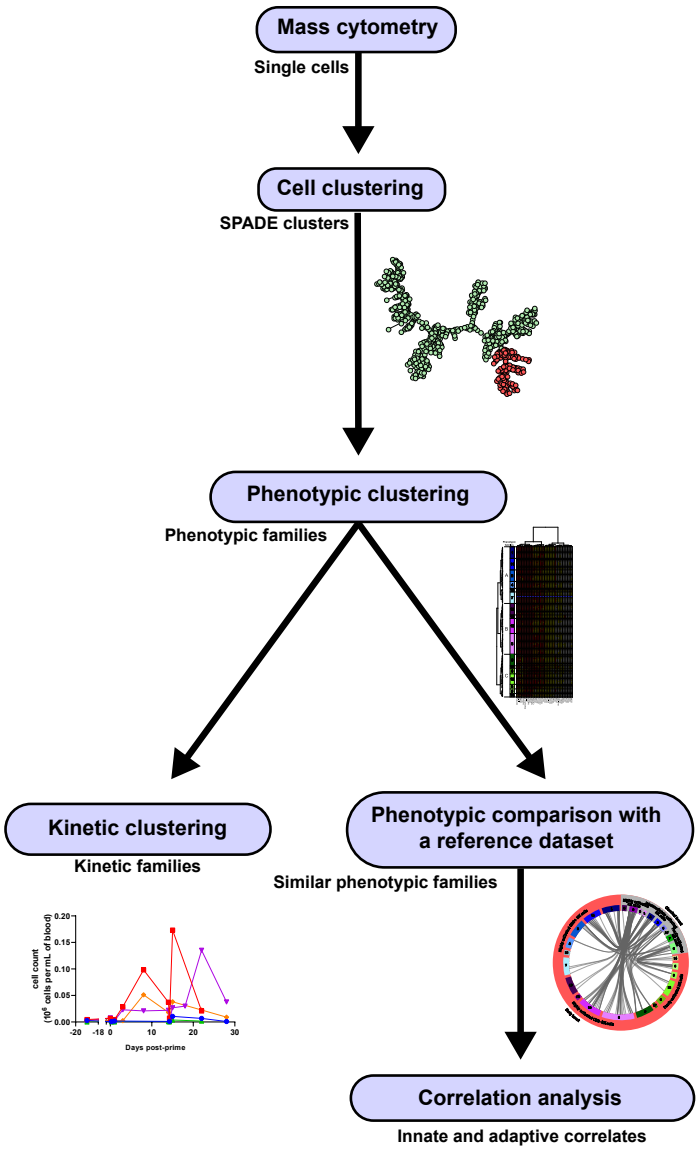
Mass cytometry
Single cells
Cell clustering
SPADE clusters
Phenotypic clustering
Phenotypic families
Kinetic clustering
Kinetic families
Phenotypic comparison with a reference dataset
Similar phenotypic families
Correlation analysis
Innate and adaptive correlates

C

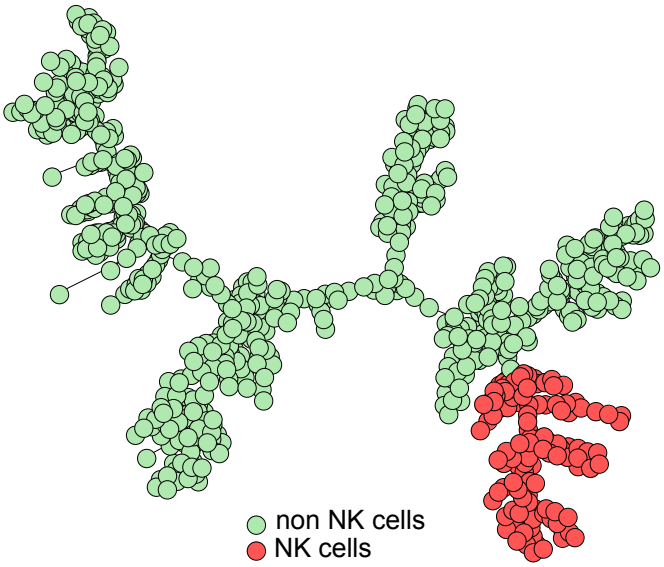
non NK cells
NK cells

D

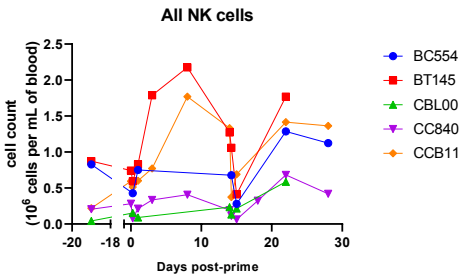
All NK cells
cell count
(10^6 cells per mL of blood)
Days post-prime
BC554
BT145
CBL00
CC840
CCB11

Figure 2. Analytical strategy to study NK cells. (**A**) The panel of 34 antibodies is displayed. (**B**) The SPADE algorithm was used to identify groups of cells sharing similar phenotype in the dataset. Phenotypic families (groups of cell clusters having similar phenotype) were generated. Kinetic families, were constructed as groups of phenotypic families sharing the same abundance profiles. A phenotypical comparison with the previous vaccine schedule study at 2 months apart was done. (**C**) generated SPADE tree is shown. This analysis was built using all samples from the dataset NK cell clusters ($CD3^-$ $CD8^+$) are indicated in red. (**D**) The absolute number of total NK cells per individual animal at each timepoint is shown. Red arrows indicate MVA immunization.

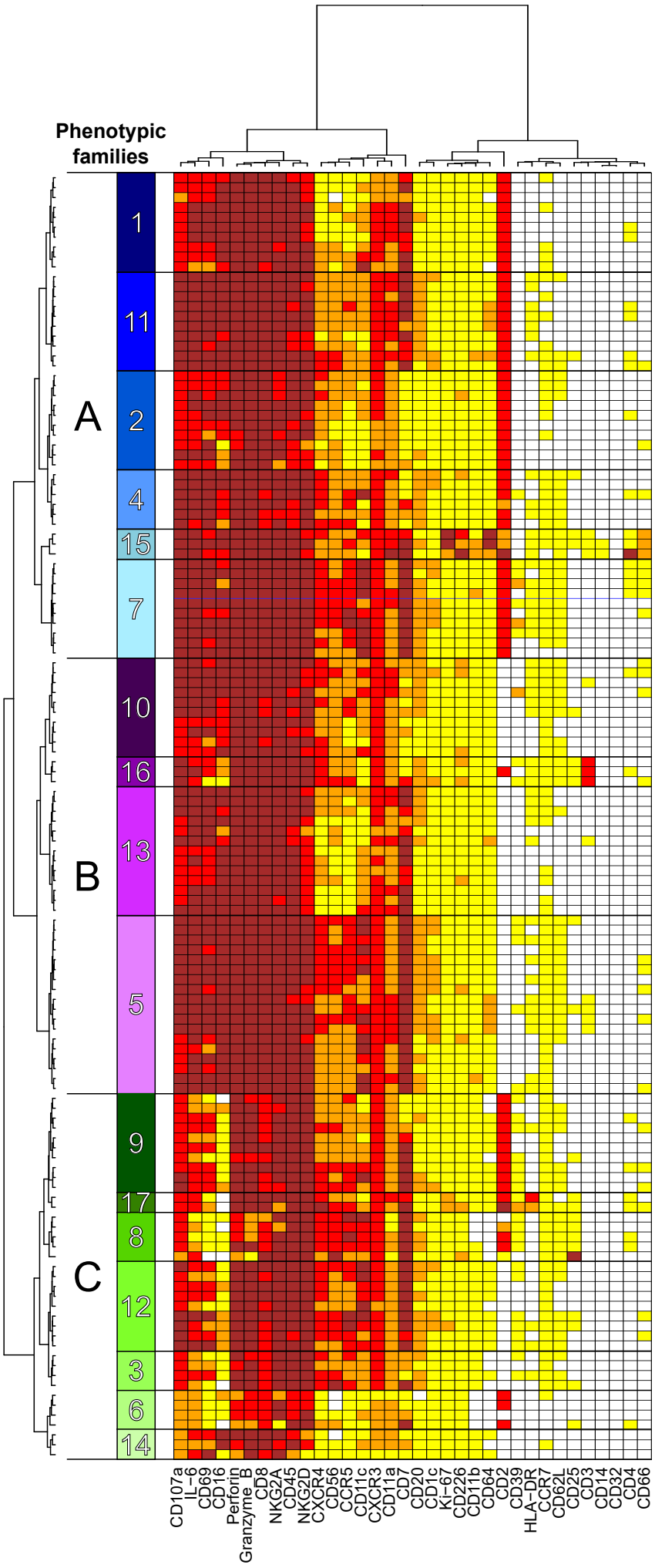
Phenotypic families
A
B
C
1
11
2
4
15
7
10
16
13
5
9
17
8
12
3
6
14
CD107a
IL−6
CD69
CD16
Perforin
Granzyme B
CD8
NKG2A
CD45
NKG2D
CXCR4
CD56
CCR5
CD11c
CXCR3
CD11a
CD7
CD20
CD1c
Ki−67
CD226
CD11b
CD64
CD2
CD39
HLA−DR
CCR7
CD62L
CD25
CD3
CD14
CD32
CD4
CD66

Figure 3. Phenotypic heatmap of NK cells. Each line of the heatmap corresponds to one cell cluster and each column to one marker. Marker expression is displayed according to phenotypical categorical bins, corresponding to the subdivision of marker range of expression in five categories between the 5^{th} and 95^{th} percentile of expression (the color code is indicated). The marker and cluster dendrograms are shown on the top and left, respectively. The cluster dendrogram defined phenotypic families and superfamilies. Phenotypic families were randomly numbered and colored with different shades of the same color for each superfamily.

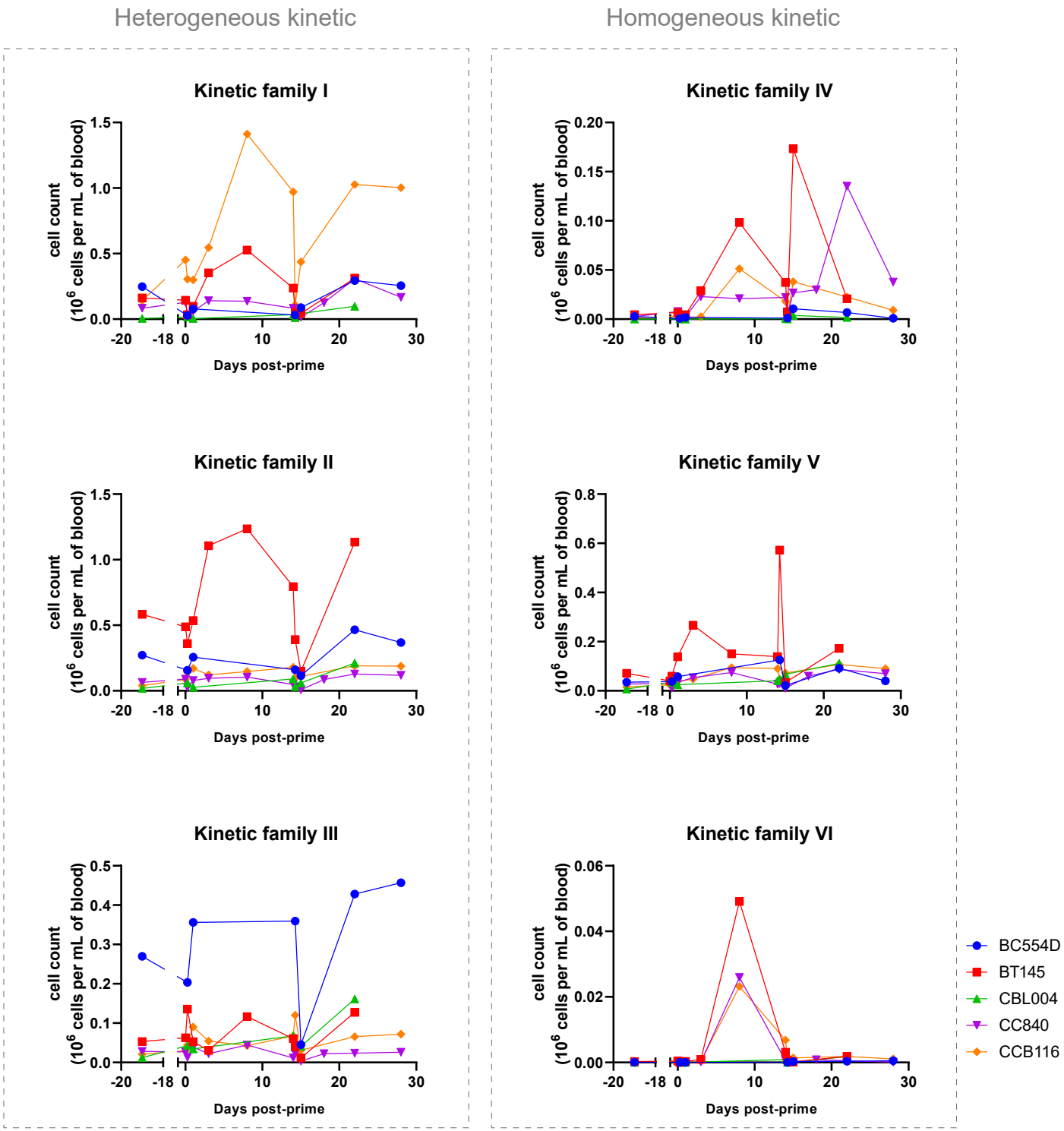

Figure 4. Different enrichment of NK cells after each immunization. For each kinetic family, the individual abundance in the number of cells/µL of blood is displayed over time.

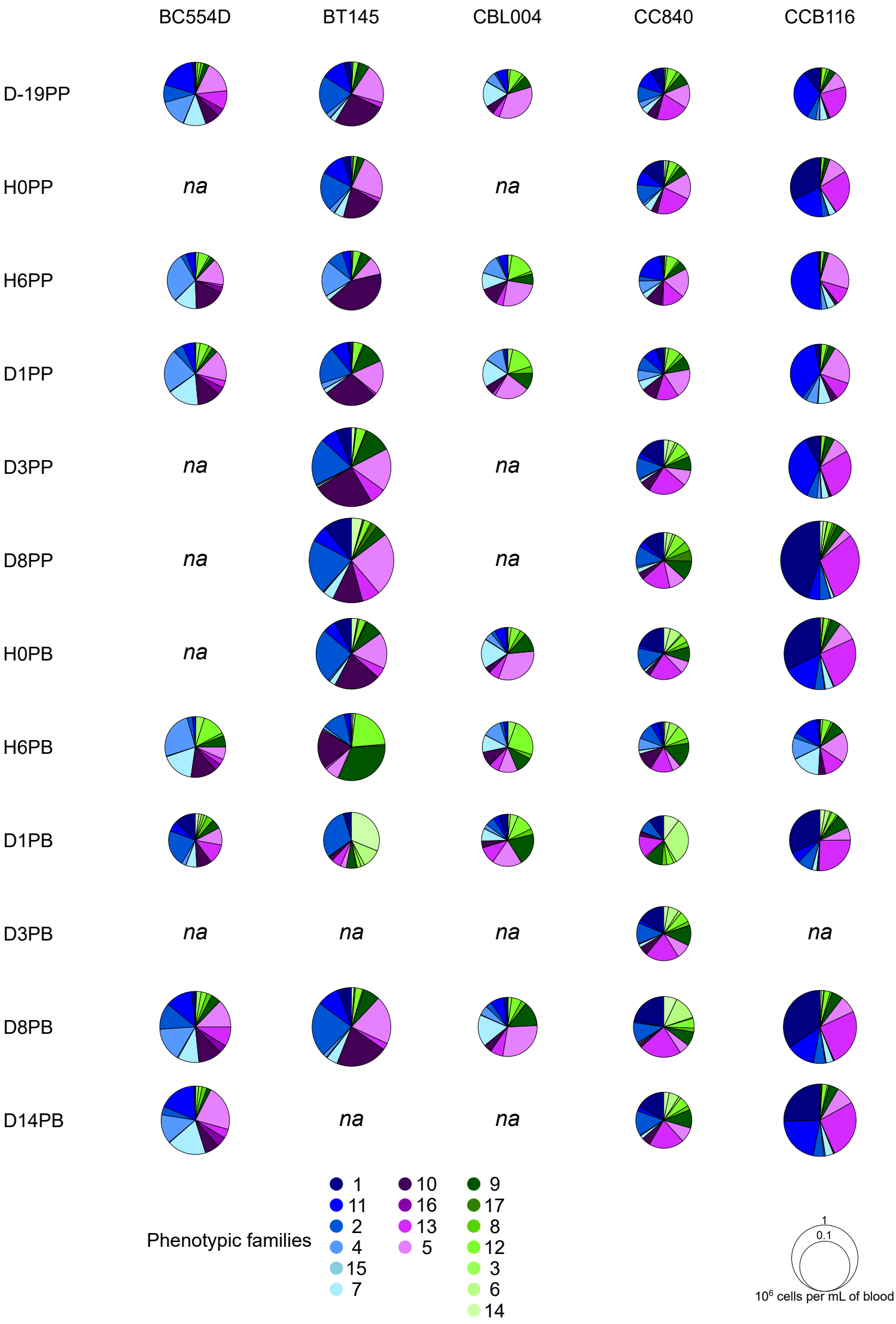
BC554D
BT145
CBL004
CC840
CCB116
D-19PP
H0PP
H6PP
D1PP
D3PP
D8PP
H0PB
H6PB
D1PB
D3PB
D8PB
D14PB
na
Phenotypic families
1
11
2
4
15
7
10
16
13
5
9
17
8
12
3
6
14
1
0.1
10^6 cells per mL of blood

Figure 5. Phenotypic composition of NK cells compartment. The composition in phenotypic families of the NK cell compartment is indicated over time for each timepoint and each animal. Pie size is proportional to the absolute count of blood NK cells. Slices correspond to phenotypic families. *na*: not available. (**C**) The inverse Simpson index, as a readout for diversity, is displayed for each animal over time. Each color represents a distinct animal.

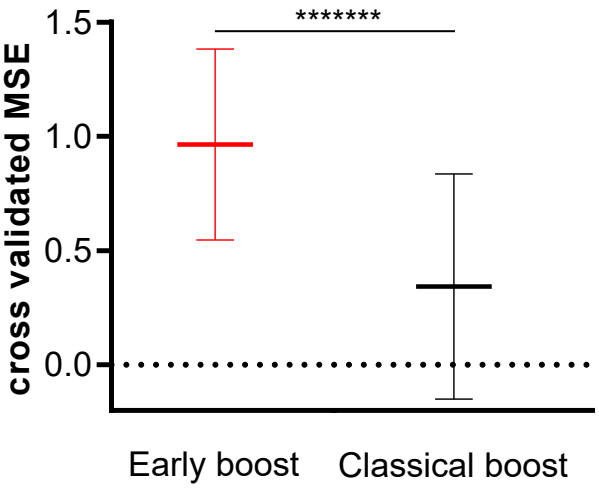

Figure 6. Prime and boost response segregation in early and classical boost schedules. In each vaccine schedule LASSO-LDA was used to optimize a model distinguishing prime and boost responses, to identify the specific signature of each. The mean square error (MSE) is displayed for the optimal model in the early boost and classical boost schedule.

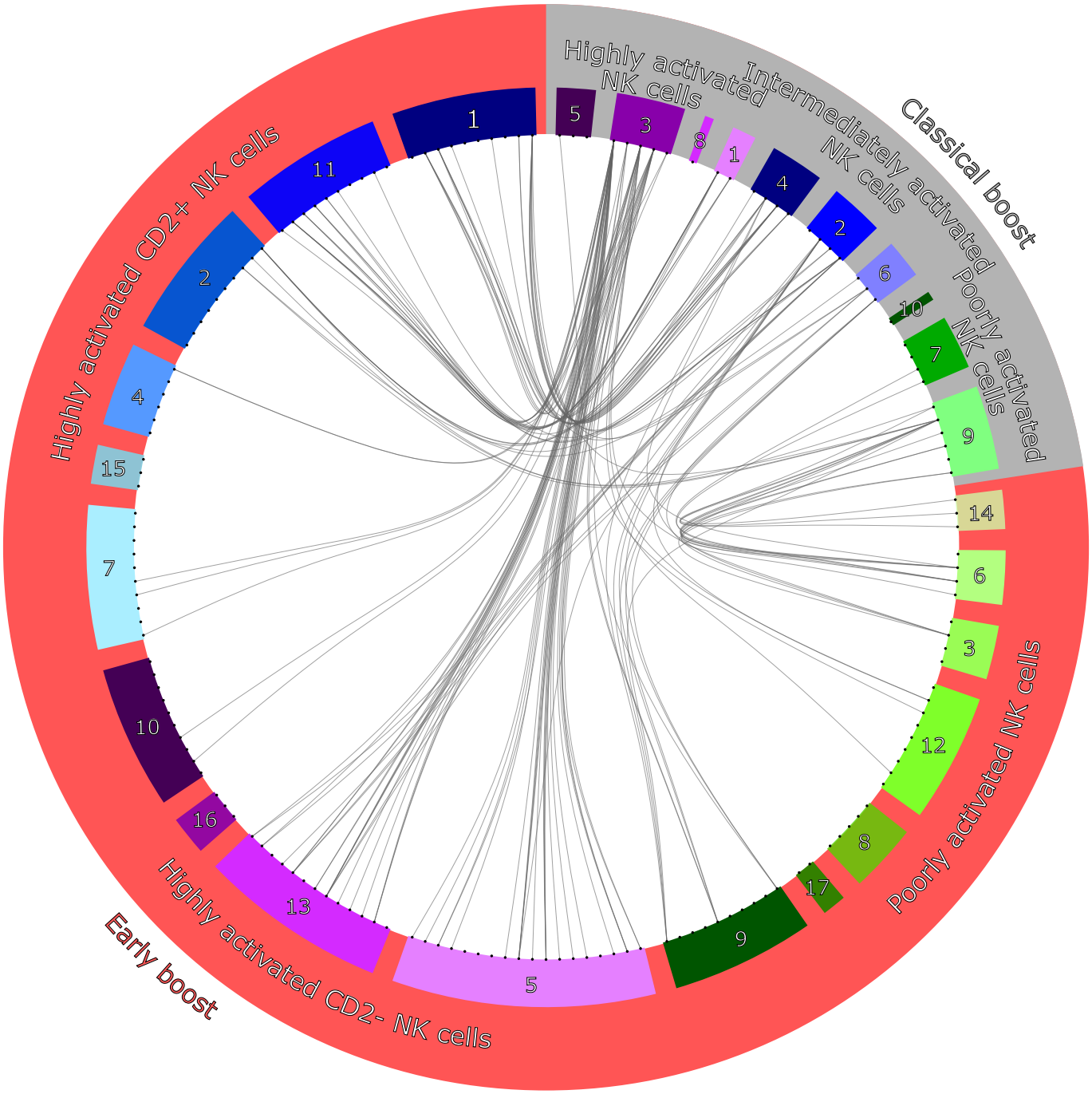

Figure 7. Comparisons of cell cluster phenotypes identified in the two vaccine schedules. The phenotype of each NK cell cluster was compared to the NK cell clusters identified in classical schedule The similarity between clusters was computed as the Manhattan distance, calculated on the expression of the 26 markers shared in both experiments.

A

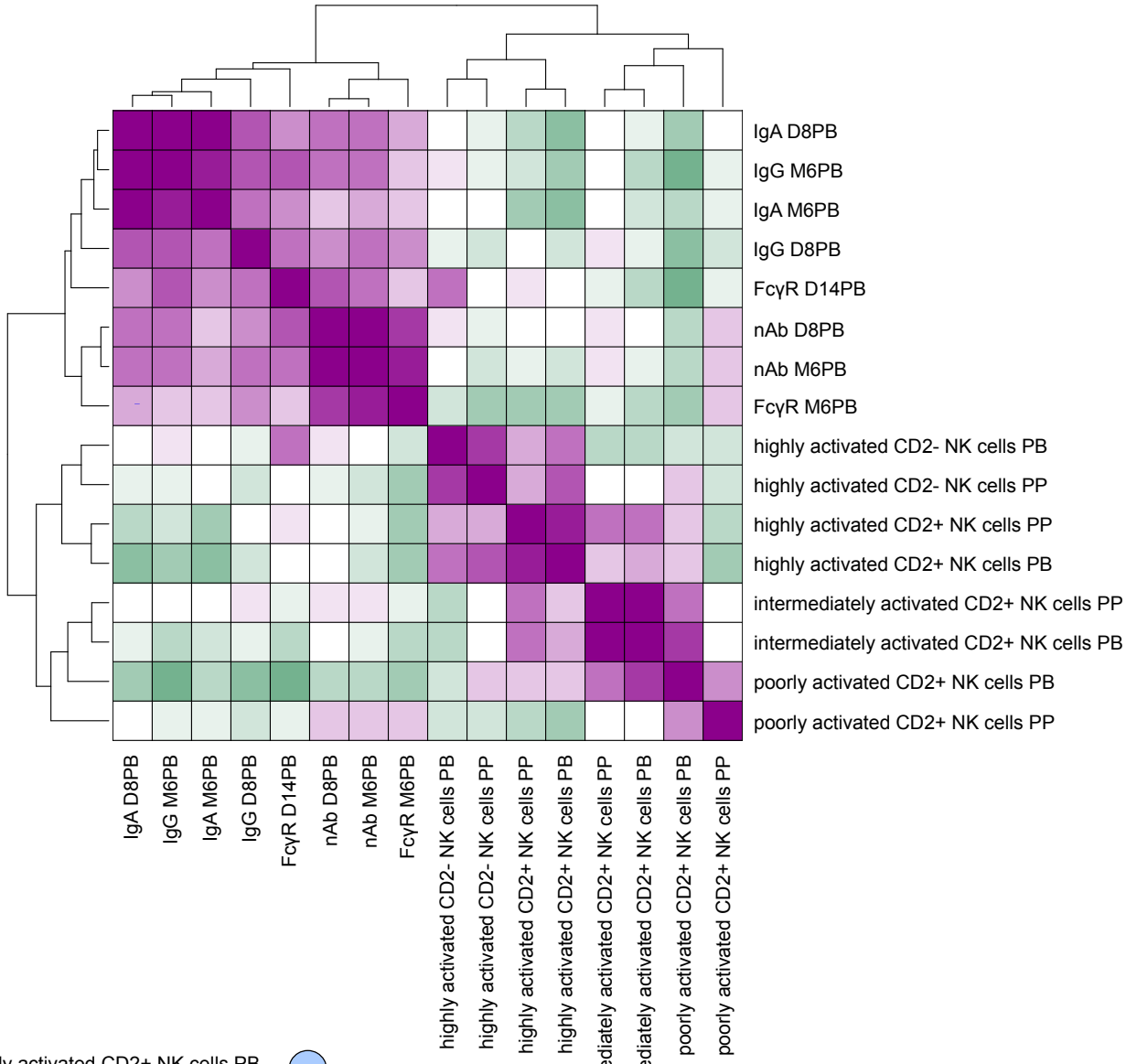
IgA D8PB
IgG M6PB
IgA M6PB
IgG D8PB
FcγR D14PB
nAb D8PB
nAb M6PB
FcγR M6PB
highly activated CD2- NK cells PB
highly activated CD2- NK cells PP
highly activated CD2+ NK cells PP
highly activated CD2+ NK cells PB
intermediately activated CD2+ NK cells PP
intermediately activated CD2+ NK cells PB
poorly activated CD2+ NK cells PB
poorly activated CD2+ NK cells PP

B

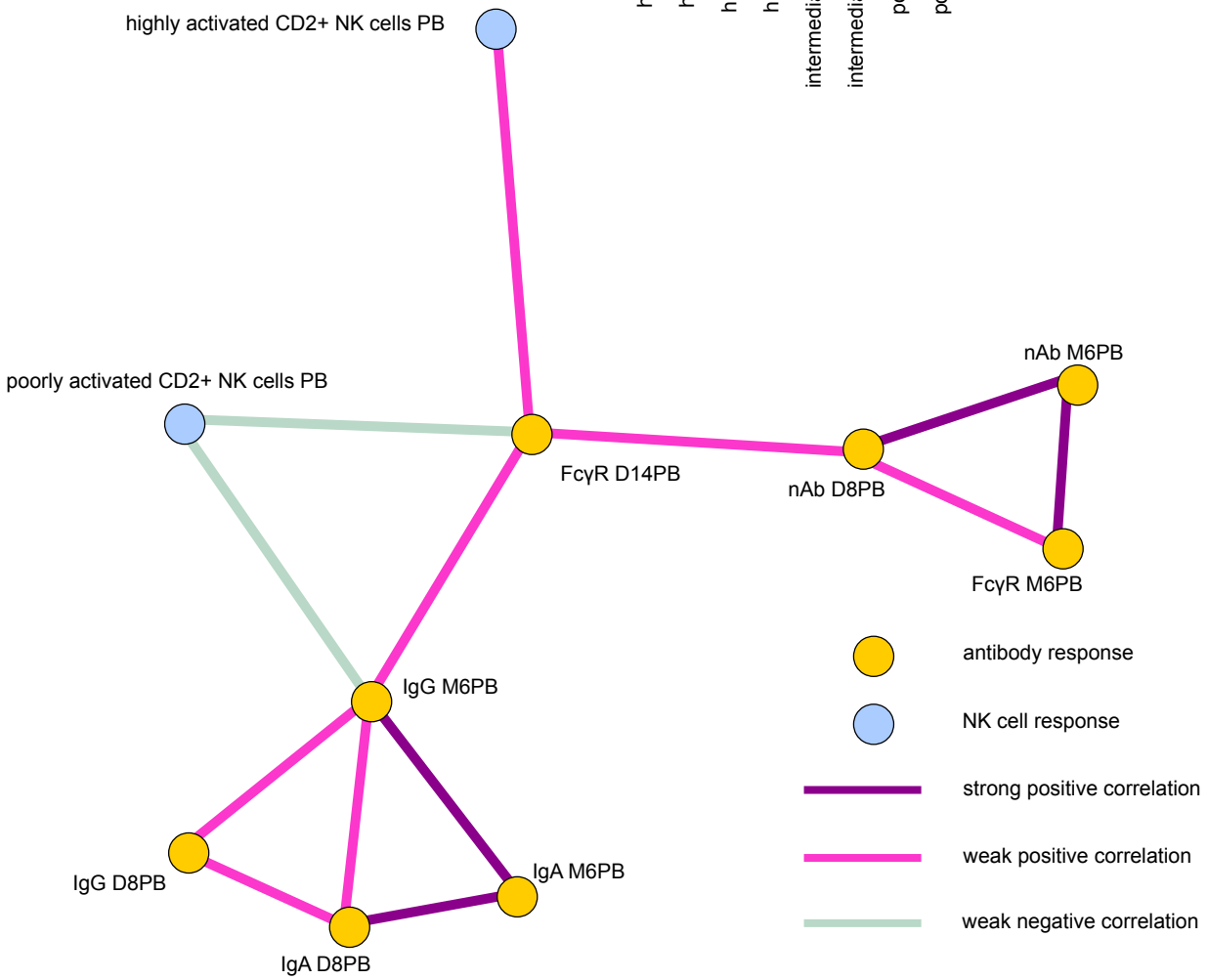
highly activated CD2+ NK cells PB
poorly activated CD2+ NK cells PB
FcγR D14PB
nAb M6PB
nAb D8PB
FcγR M6PB
IgG M6PB
IgG D8PB
IgA M6PB
IgA D8PB
antibody response
NK cell response
strong positive correlation
weak positive correlation
weak negative correlation

Figure 8 – Correlation between antibody response and NK cell response. (**A-B**) The correlation between NK cell response (normalized area under the curve for each population) and the peak and long-term persistence of antibody response were assessed. All correlations were represented in (**A**) after hierarchical clustering with the complete method. In addition, in (**B**) All antibody response and all the NK cell responses that correlated ($|R| > 0.6$) with at least one antibody response were considered to build the correlation graph. Correlations with $0.6 \leq |R| \leq 0.7$ were considered as weak; correlations with $|R| > 0.7$ were considered as strong.

Metal	Marker	Clone	Surface	Intra-cellular
141Pr	CD66	TET2	●	
142Nd	HLA-DR	L243	●	
143Nd	CD3	SP34.2	●	
144Nd	CD64	10.1	●	
145Nd	CD8	RPAT8	●	
146Nd	IL-6	MQ2.13A5		●
147Sm	CD226	DX11	●	
148Nd	Granzyme B	GB11		●
149Sm	CD11a	HI111	●	
150Nd	CD11b	ICRF144	●	
151Eu	CD62L	SK11	●	
152Sm	CD4	L200	●	
153Eu	CD56	NCAM16.2	●	
154Sm	CD2	RPA2.10	●	
155Gd	CD7	M-T701	●	
156Gd	NKG2D	1D11	●	
159Tb	CD45	D058-1283	●	
160Gd	KI-67	B56		●
161Dy	CD1c	AF5910	●	
162Dy	CD25	4E 3	●	
163Dy	CD32	FLI8.26	●	
164Dy	CD69	FN50	●	
165Ho	CD39	eBioA1	●	
166Er	CCR5	3A9	●	
167Er	CD16	3G8	●	
168Er	CD11c	3.9	●	
169Tm	CXCR4	12G5	●	
170Er	CD14	M5E2	●	
171Yb	Perforin	Pf-344		●
172Yb	NKG2A	Z199	●	
173Yb	CD107a	H4A3	●	
174Yb	CD20	2H7	●	
175Lu	CCR7	G043H7	●	
176Yb	CXCR3	G025H7	●	

Table 1. Antibody panel targeting NK cells for mass cytometry. Marker targeted, antibody clone, and conjugated metal are indicated. Whether the staining was intra- or extra-cellular is also stated.

Kinetic family	Phenotypic family	Cell population	Kinetic Pattern
I	1, 11, 13	Highly activated NK cells (CD2- and CD2+)	Homogeneous response
IV	6, 14	Poorly activated NK cells (CD2- and CD2+)	
VI	17	HLA-DR+ CD2+ poorly activated NK cells	
III	3, 4, 7, 8, 16	CD2+ NK cells (poorly and highly activated) and CD3+ potential NKT cells	Heterogeneous response
II	2, 5, 10, 15	Highly activated NK cells (CD2- and CD2+)	
V	9, 12	Poorly activated NK cells (CD2- and CD2+)	

Table 2. Composition of kinetic families. The composition in of phenotypic families is in displayed for each kinetic family. The main cell populations, phenotypes, and kinetic pattern associated are also provided (as classified in **Figure 4**).

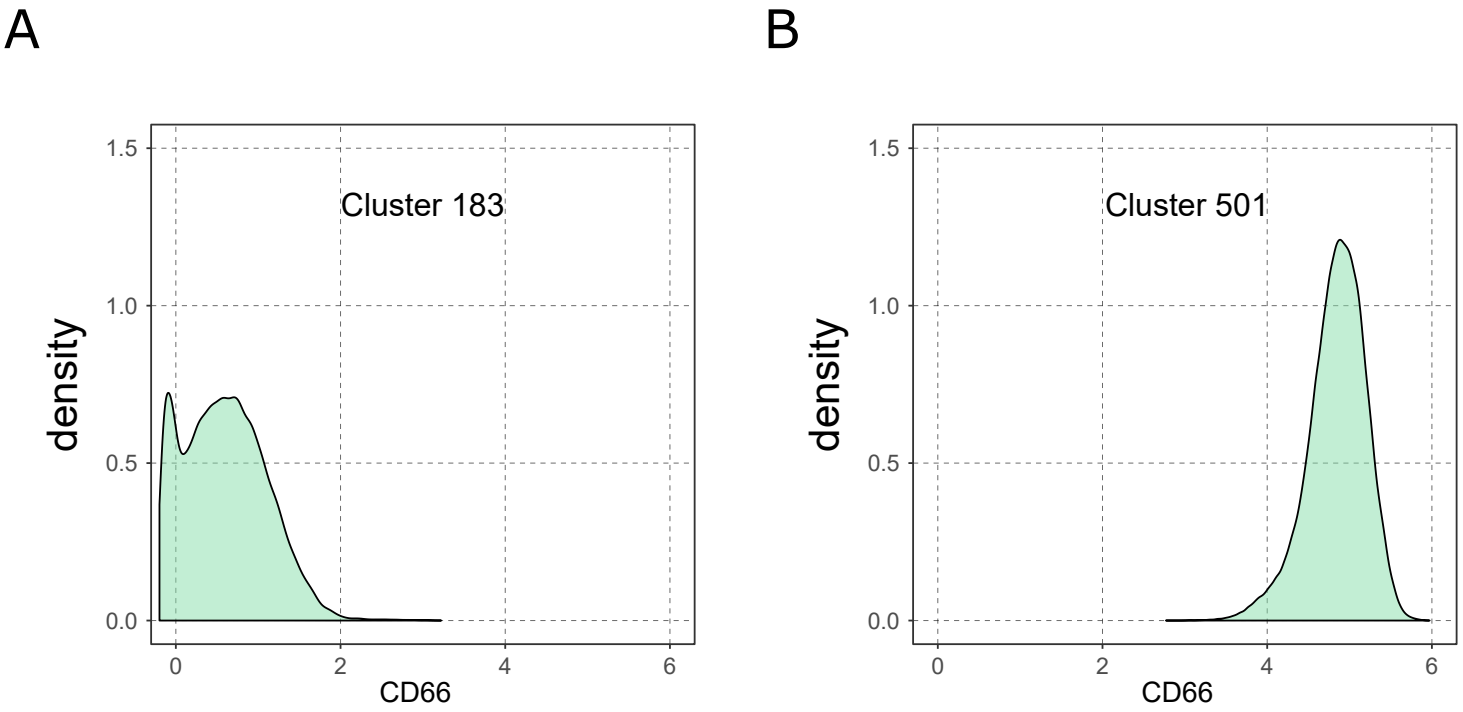

Figure S1. Staining profile of CD66. A representative non-uniform CD66$^{low/-}$ cluster (A) and a representative CD66$^{high/+}$ cluster (B) are displayed.

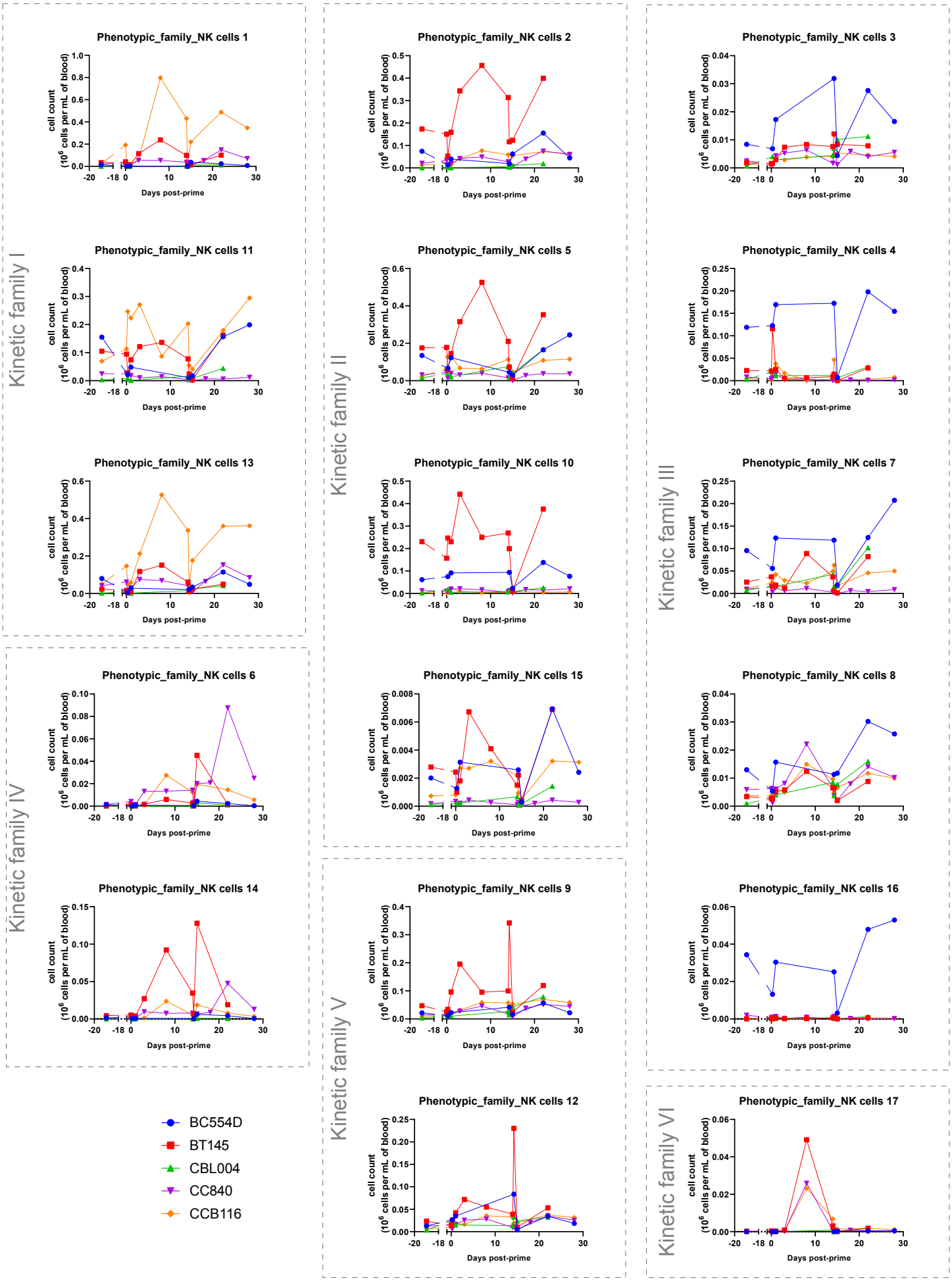

Figure S2. Kinetics of the 17 NK cell phenotypic families. Individual curves are displayed. Dotted frames indicate the kinetic families.

	IgG M6PB	IgA M6PB	nAb M6PB	FcγR M6PB	IgG D8PB	IgA D8PB	nAb D8PB	FcγR D14PB
highly activated CD2+ NK cells PP	−0.12	−0.03	−0.23	−0.49	−0.26	−0.1	−0.13	0.01
highly activated CD2+ NK cells PB	0.11	−0.03	0.05	−0.26	−0.12	−0.08	0.18	0.6
highly activated CD2- NK cells PP	−0.28	−0.43	−0.19	−0.49	0.1	−0.35	−0.09	0.12
highly activated CD2- NK cells PP	−0.45	−0.59	−0.22	−0.43	−0.25	−0.56	−0.1	0.04
poorly activated CD2+ NK cells PP	−0.17	−0.19	0.23	0.23	−0.22	−0.08	0.26	−0.14
poorly activated CD2+ NK cells PB	−0.61	−0.4	−0.38	−0.49	−0.53	−0.44	−0.31	−0.63
Intermediately activated NK cells PP	−0.04	−0.04	0.1	−0.19	0.18	0.09	0.15	−0.17
Intermediately activated NK cells PB	−0.32	−0.2	−0.11	−0.31	−0.11	−0.16	−0.07	−0.4

Figure S3. Correlation between NK cell and antibody responses. The Spearman coefficient of correlation is given. blue: significant positive correlation; red: significant negative correlation.

	BC554D	BT145	CBL004	CC840	CCB116	ALL
BPD019H00	527 489	482 666	561 095	478 147	231 762	2 281 159
PPD000H00		492 152		699 936	504 700	1 696 788
PPD000H06	452 724	666 844	449 514	734 437	433 356	2 736 875
PPD001H00	545 064	701 931	344 099	819 306	598 751	3 009 151
PPD003H00		373 720		566 820	378 002	1 318 542
PPD008H00		573 394		588 903	366 662	1 528 959
PBD000H00		688 897	427 351	544 143	426 364	2 086 755
PBD000H06	495 294	727 372	542 156	702 312	689 619	3 156 753
PBD001H00	401 139	467 860	475 397	681 465	392 377	2 418 238
PBD003H00				636 262		636 262
PBD008H00	191 006	447 243	473 213	280 084	445 144	1 836 690
PBD014H00	634 835			640 607	371 437	1 646 879
PBD028H00	529 883	671 975	570 475		473 697	2 246 030
TOTAL	3 777 434	6 294 054	3 843 300	7 372 422	5 311 871	26 599 081

Table S1. Cell number across samples. The number of events acquired by mass cytometry is indicated for each sample.

Markers	Number of non-uniform clusters	Percentage of non-uniform clusters
CD66	46	35,38
CD7	15	11,54
CD16	9	6,92
CD2	7	5,38
CD39	6	4,62
CD25	2	1,54
CD11c	2	1,54
NKG2A	2	1,54
HLA-DR	1	0,77
CD3	1	0,77
Granzyme B	1	0,77
CD64	0	0,00
CD8	0	0,00
CD226	0	0,00
CD11a	0	0,00
CD11b	0	0,00
CD62L	0	0,00
CD4	0	0,00
CD56	0	0,00
NKG2D	0	0,00
CD45	0	0,00
CD1c	0	0,00
CD32	0	0,00
CD69	0	0,00
CCR5	0	0,00
CXCR4	0	0,00
CD14	0	0,00
Perforin	0	0,00
CD107a	0	0,00
CD20	0	0,00
CCR7	0	0,00
CXCR3	0	0,00

Table S2. Uniformity of markers across clusters. The number and corresponding percentages of non-uniform clusters is given for each marker.

Conclusions and perspectives

Conclusions and perspectives

Results summary

The aim of my PhD project was to characterize the innate immunity induced by prime-boost vaccination, its interactions with adaptive immunity and especially with immunological memory, depending on the vaccine schedule. As an experimental strategy, I used cynomolgus macaque as animal model, MVA HIV B vaccine as vaccine model, and mass cytometry as the main technological approach.

Employing this strategy, I was able to unveil the wide phenotypic diversity of blood innate immune cells within both innate myeloid cell and NK cell compartments. Each immunization similarly induced major, early and transient changes in cell number, even at the scale of granulocytes, monocytes-DCs and NK cell compartment. These kinetics differed between innate myeloid cells and NK cells though. Indeed, innate myeloid increased in number after the first immunization, before going back to their initial number at later timepoints. By contrast, NK cells first decrease in number, a decrease that coincides with a shift toward a less active phenotype (likely linked to the recruitment of immature NK cells in blood), before re-increasing in number (**Figure 29**).

Strikingly, in a classical (two months apart) prime-boost vaccination schedule known to induce robust antigen-specific antibodies and memory B cell responses, prime vaccination induced tremendous and long-lasting changes in innate immune cell phenotypes. More precisely, in innate myeloid cells (not only monocytes, as usually reported for innate training, but also cDCs and neutrophils) and NK cells, prime led to a late upregulation of several markers involved in cell maturation/activation (*e.g.* FcR, chemokine receptor, cytotoxic molecules), between two weeks and two months. This phenotype suggested a stronger ability for these innate cells to respond to subsequent pathogen encounters. These phenotypic changes likely correspond to innate trained immunity. These results are thus likely the first report of the extensive phenotypic characterization of trained innate cells induced by vaccination (**Figure 29**A).

Interestingly, reducing the delay between prime and boost to two weeks, a time-lapse strongly suggested detrimental to humoral response generation in humans in literature, strongly impacted both adaptive and innate responses in NHPs in our settings. Notably, prime vaccination did not induce changes in innate cell phenotype in two weeks, as previously observed. Still, for NK cells, a tendency for a less cytotoxic phenotype was found after the boost, suggesting a sub-optimal response, associated with potentially exhausted NK cells. Strikingly, no upregulation of activation/maturation markers was found, even at late timepoints post-early boost, which would correspond to late timepoints post-prime in the classical schedule -at which the "likely trained" appear in blood. This strongly suggests that the prime-induced maturation of innate cells, giving rise to "likely trained" cells between two weeks and two months post-prime, was perturbed and impaired by the early boost immunization (**Figure 29**B).

Regarding the humoral response, secondary IgA levels were far lower in the early boost schedule. In addition, while secondary IgG levels remained quite similar in both schedules, the neutralization titer and the ability of antigen-specific antibody to aggregate CD16 dimers (as a surrogate of CD16 binding affinity and resulting ADCC) were reduced in the early boost schedule. This confirmed that this schedule was sub-optimal (**Figure 30**).

Consistently, the presence of phenotypically “likely trained” innate cells correlated with IgA titer, neutralization titer and Fc-FcR binding affinity. Also, their presence was associated with an overall increased cytokine production by PBMCs in the post-boost response. This increased cytokine production in the response to the boost likely arise from the deep interaction between memory B and T cells induced by the prime and innate immune cells, as well as the intrinsic phenotype change of innate cell phenotype induced by the prime. Altogether, this strongly support a key role of these “likely trained” cells in the re-stimulation of primary immune memory and generation of a long-lasting secondary immune memory (**Figure 30**).

Overall, in my PhD project I characterized in depth the innate immunity induced by prime and boost vaccination. I highlight the early effector phase and late “memory-like” innate immunity induced by prime and responding to the boost, according to the schedule used. I also unveiled the association between “likely trained” innate immunity, humoral responses and cytokine production by innate and adaptive PBMCs. In addition, from a computational point of view, the analytical strategy that was developed in the project to explore the mass cytometry datasets and identify cell/marker signatures distinguishing different immune conditions (*e.g.* prime and boost) can be applied to high-dimensional data in numerous contexts. This makes it valuable to answer other key questions in the field of immunology and beyond.

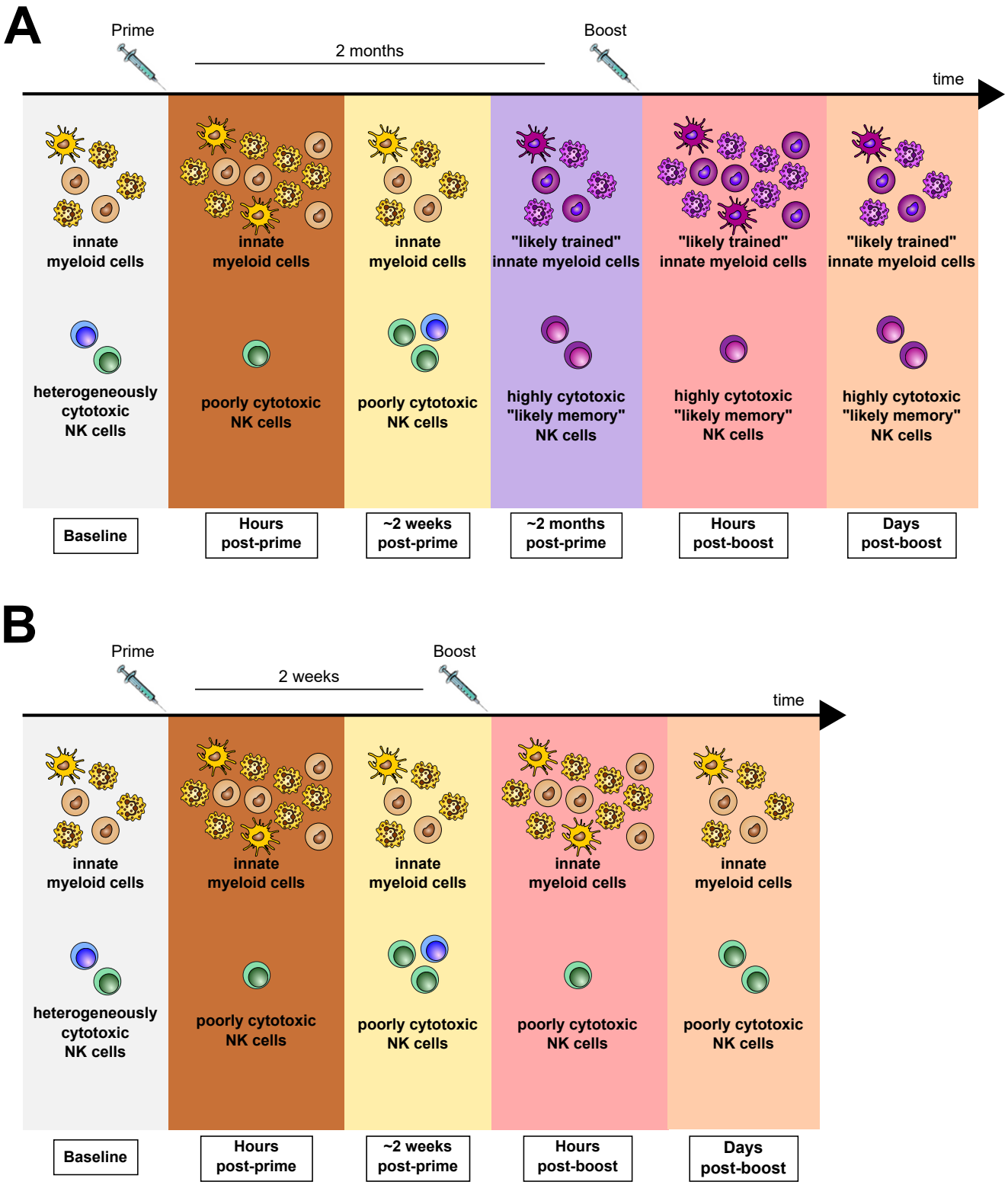

Figure 29. Characterization of innate responses after prime and boost with respect to vaccine schedule. The kinetics and overall phenotype of innate cells (both myeloid and NK cells) are displayed for the classical boost schedule **(A)** and the early boost schedule **(B)**.

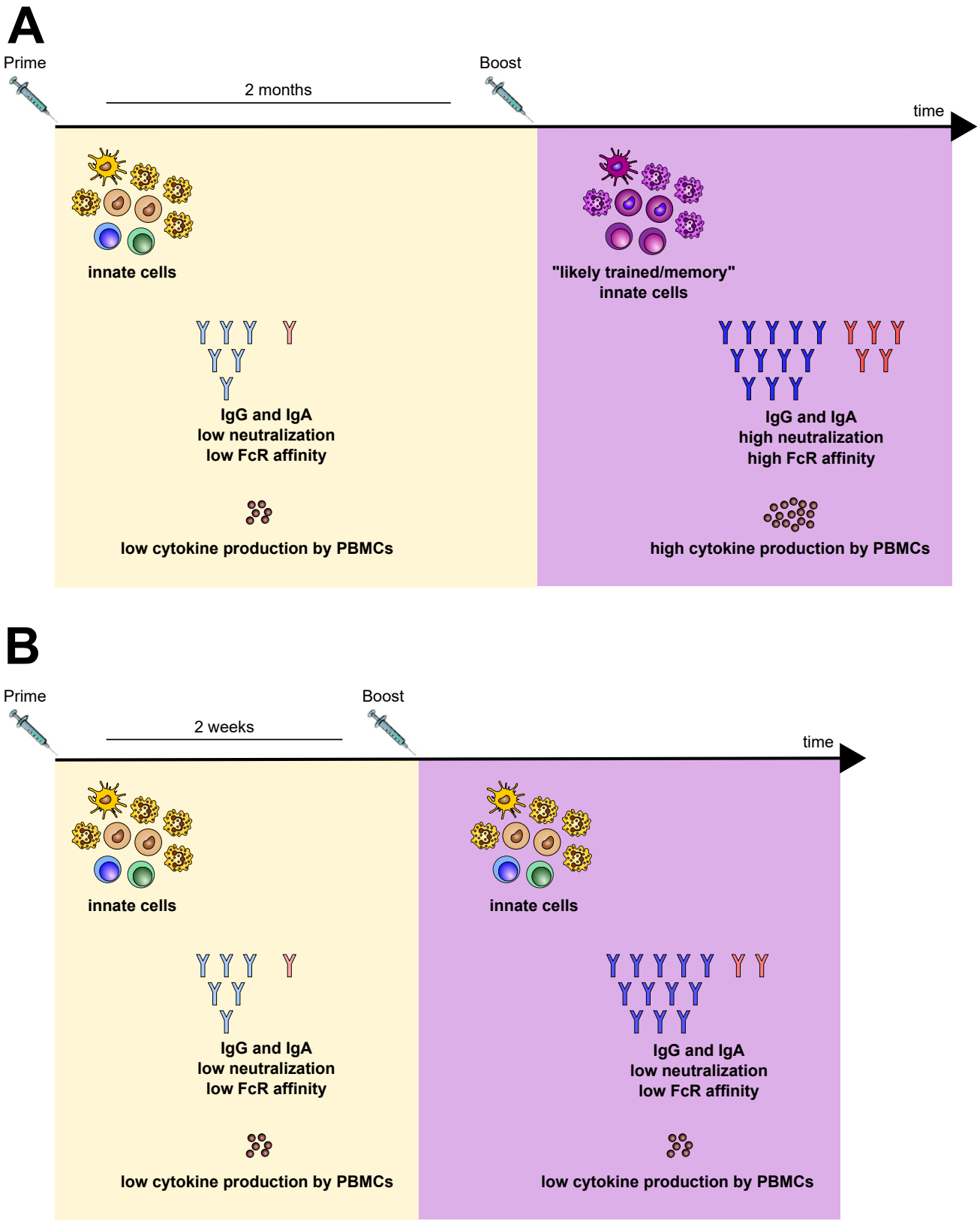

Figure 30. Associations between innate responses and adaptive responses. The presence of the "likely trained" innate cells is associated with increased IgA and neutralizing antibody titers, as well as increased affinity towards FcR (namely CD16), and increased cytokine production by PBMCs in the classical boost schedule. In the early boost schedule, in which no modification ("training") of innate cells was induced, the aforementioned antibody parameters and cytokine production were lower.

Opened questions

Several questions arose from the obtained results of this project, and I will give here an overview of the main ones to my view.

Innate and cellular adaptive immunity interactions

Our association analysis between innate cells and adaptive responses was limited to the humoral response and the cytokine production by innate and adaptive PMBCs. The cellular adaptive B and T cell immune responses have not been included so far.

Actually, the in depth characterization of B and T cell responses with mass cytometry is ongoing within the laboratory, with part of the B cell response characterization on selected timepoints previously published (Pejoski et al., 2016) and other analyses not completed. The data were generated in the very same animals used for the characterization of innate immune cells, using dedicated panels designed and applied to PBMCs samples. They notably include the assessment of antigen-specific B cell immunity (with the follow-up of B cells with specific BCR) and T cell effector functions (notably after *ex vivo* MVA re-stimulation).

NK cell phenotyping

In term of immune cell phenotyping, we must acknowledge that NK cell characterization was imperfect. Our results strongly support the development of memory-like NK cells with likely enhanced functions (functional tests would be required to firmly conclude though), based on the expression of several maturation markers. Still, since we needed to use fixed samples in our settings, we were not able to include most NK cell receptors in our NK cell dedicated antibody panel. As a result, the diversity of NK cell repertoire, which was shown to be highly diverse and impacted by immune experience (Strauss-Albee et al., 2015; Strauss-Albee & Blish, 2016; Wilk & Blish, 2018), could not be assessed.

One solution would be to use either fresh blood or frozen PBMCs to include more of these receptors in our antibody panel. The availability of antibodies cross-reacting with macaque cells may be a strong limitations, though it is possible to combine RNA probes labelled with an heavy metal to overcome this issue, the so-called proximity ligation assay for RNA (Frei et al., 2016). This approach was successfully used to discriminate NKG2A and NKG2C (two molecules with a high homology impairing their distinguishment via antibodies) in rhesus macaques (Ram et al., 2018).

Still, the high number of NK cell receptor may outnumber the channels available in a single mass cytometry antibody panel. To by-pass these issues, switching to single-cell RNAseq analysis and focusing on the sole NK cell population may be highly valuable (**Table 3**). As mentioned in Chapter 1, this technology allows to sequence potentially all cell transcripts (with respect to sensitivity issue), though currently on a limited number (around 10,000) of cells ; this number may increase in the oncoming years (Svensson et al., 2018). On the purified population of NK cells, this may be sufficient to assess NK cell phenotype and it would allow for the full characterization of the NK cell repertoire. Additionally, antibodies barcoded with oligonucleotides could be added, according to the cellular indexing of transcriptomes and epitopes by sequencing (CITE-seq) or the RNA expression and protein sequencing assay (REAP-seq) approached that allow to quantify more than 80 proteins and thousands of genes simultaneously (Stoeckius et al., 2017; Peterson et al., 2017).

Table 3. High-dimensional technologies to study NK cell compartment.

Technology	Advantages	Challenges
single-cell RNAseq	Analysis of all NK receptors transcripts, the whole repertoire covered	Low number of NK cells analyzed, a representative part of the compartment not analyzed
mass cytometry	High number of NK cells analyzed, a representative part of the compartment likely analyzed	Reduced number of NK receptor expression assessed, the whole repertoire not analyzed

Advantages and drawbacks of mass cytometry and single-cell RNAseq with respect to NK cell compartment characterization are displayed.

Innate immune memory duration

We showed that reducing the delay between prime and boost induced significantly distinct immune responses, compared to the classical schedule. The early boost likely perturbed the development of the primary effector and memory B cell response, resulting in an altered secondary antibody response. Strikingly, the early boost simultaneously failed to mobilize "likely trained" innate cells and induced innate responses similar to the prime. However, what would happen if the delay between prime and boost is increased, especially regarding innate training, remains unaddressed (**Figure 31**).

Indeed, the training of innate cells was observed at two months, but it is not clear neither whether this training was complete or had already started to wane, nor for how long it will persist. As a consequence, a slightly sooner or later boost may better harness immune training by targeting more completely trained innate cells. By contrast, a far later boost could act on innate cells that lost their training and would be potentially not more efficient than at the prime (with the exception of the distinct signals provided by memory T and B cells, as well as circulating antibodies). This may be also correlated with a less efficient secondary adaptive immune response (**Figure 31**).

As mentioned in the introduction, the duration of innate immune training is not clear. For NK cells, a duration of more than a year was proposed based on BCG vaccination results and evolution of NK cell repertoire along lifespan (Strauss-Albee et al., 2015; Suliman et al., 2016). By contrast published data on trained myeloid cell and modified progenitor bone marrow cell lifespan are more scarce since functional tests rarely went beyond one month post-training induction in mice or humans (Arts et al., 2018b; Mitroulis et al., 2018; Yao et al., 2018). There are some exceptions though. In mice, training of hematopoietic progenitors still occurred after five months (Kaufmann et al., 2018). BCG vaccination of healthy volunteers resulted in the maintenance of trained monocytes up to one year post-vaccination, although it had started to wane (Kleinnijenhuis et al., 2014a). Taken together, epidemiological studies suggest that immune training elicited by vaccination could be at play for years (Benn et al., 2013). Discussions in the community suggest that this training could start to wane after a year though. Thus should a boost be given after this period, it would likely be less efficient in harnessing innate training (**Figure 31**).

Also, we may wonder whether the boost will also induce a secondary training of innate immune cells. Indeed, at two weeks post-classical boost, a tendency for changes of the innate myeloid compartment was observed (Palgen et al., 2018). The NK cell compartment composition could not be investigated at these late post-boost timepoints (Palgen et al., 2019). Thus we may suspect that the boost could induce secondary trained innate cells that would have an even more active/mature phenotype, inducing a distinct response at a second boost.

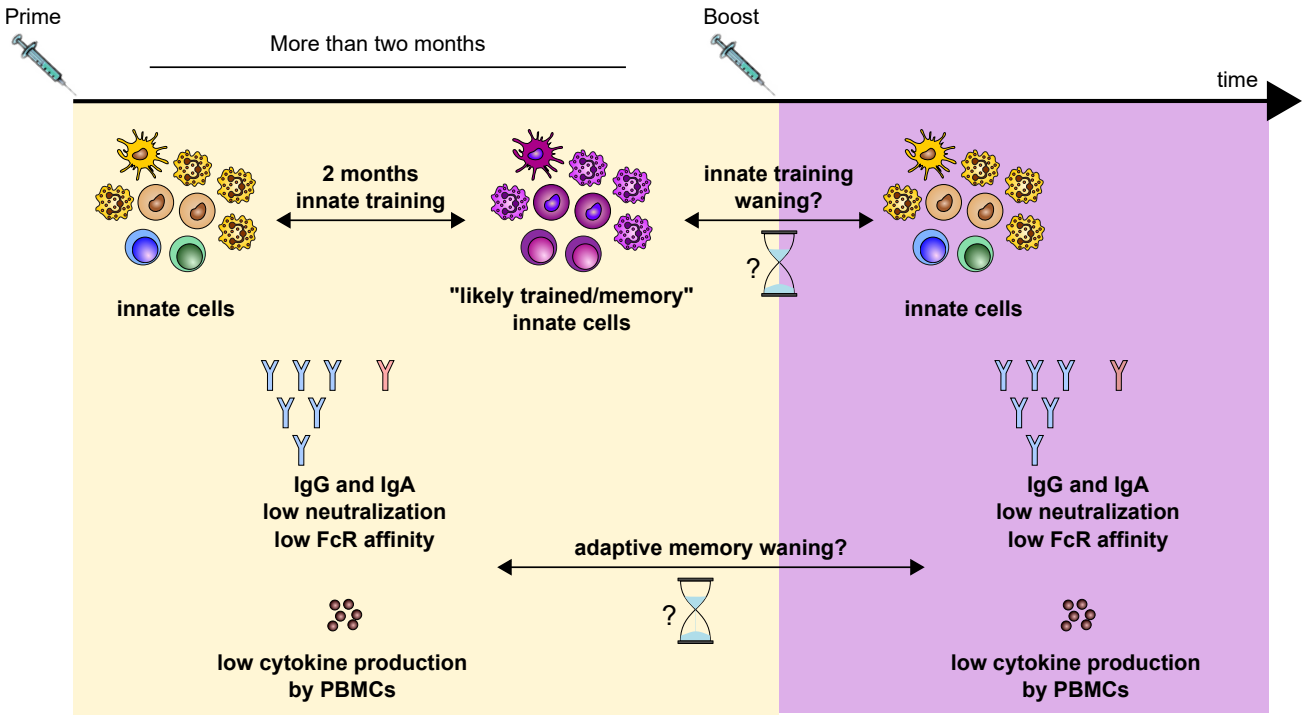

Figure 31. Potential impact of a late boost on the resulting immune response. Depending of the training waning of innate cells, as well as memory waning of adaptive cells, responses to a late boost may differ from the classical boost, potentially going back to a prime response.

Enhanced functions of "likely trained" cells and adaptive immunity activation

We showed that there was a strong correlation between "likely trained" innate cells, antibody responses and cytokine production by PBMCs. Correlation does not mean causality though. Indeed, prime could induce independently adaptive memory cells and trained immune cells. In such a scenario, the quality of the secondary antibody response would be associated with but not directly shaped by "likely trained" innate immune cells.

Still, adaptive immunity was shown important in macrophage training (Yao et al., 2018), and trained innate monocytes were able to potentiate CD8 T cell response (Walk et al., 2019). There is a deep interconnection of innate and adaptive immunity, as described in the Introduction, and consistently with modification of cytokine production of both innate and adaptive cells in the classical boost schedule (Chapter 5). Thus it is very likely that both responses (trained innate cells and adaptive memory cells) are connected. We may then hypothesize that the boost improved immune memory (*e.g.* better neutralizing antibody titer) not only because it targets primary adaptive memory cells induced by the prime, but also because the innate immunity to the boost displays intrinsically enhanced functions (*e.g.* signals 1, 2 and 3 provided during T cell activation).

Functional analyses remain to be conducted to better understand the role of each innate compartment. Indeed, most results obtained in this project focused on the phenotype of the cells, which was partially linked to functions with the cytokine production assay. Still, assessment of the ability of "likely trained" cells to better phagocyte pathogen or better present antigen are currently missing.

Actually, phenotyping allows to define subphenotypes, as identified in this project, but may be not be fully sufficient to characterize a "true" cell subpopulation. Indeed, a cell within a given subpopulation may change the expression of its marker, without necessarily changing of subpopulation. For instance, an NK cell that degranulated granzyme shows an increase expression CD107a at the cell surface and a reduced intra-cellular expression of granzyme but remains in the same NK cell subpopulation. Definition of cell subpopulation may require ontogeny analysis and/or functional characterization, as proposed in literature for DC, neutrophils or NK cells for example (Vu Manh et al., 2015; Rosales, 2018; Wilk & Blish, 2018). The exact distinction between subphenotypes and subpopulations may be blurred though, given the plasticity of cells to deeply alter both their phenotype and functions (Liu et al., 2001; Galli et al., 2011; Cichocki et al., 2014).

Functional analysis of the subphenotypes identified in these project, notably with respect to their ability to activated adaptive immunity, are planned in the future projects of the laboratory.

"Likely trained" innate immune cell ontogeny

It is as well important to better understand at which step of cell differentiation the phenotypic modifications, likely corresponding to innate training, occur. On one hand training of fully differentiated cells was shown for example after β glucan or BCG simulation of monocytes *ex vivo* (Quintin et al., 2012; Bekkering et al., 2016; Garcia-Valtanen et al., 2017), and trained resident cells were shown to self-maintain in tissues (Yao et al., 2018). On the other hand training of hematopoietic stem cells was also shown *in vivo* (Kaufmann et al., 2018; Mitroulis et al., 2018), suggesting that training could happen during immune cell generation in the bone marrow. Whether a distinct training origin results in phenotypically and functionally distinct trained cells remains to be addressed.

It is not clear whether the mature trained cells observed *in vivo* after vaccination (Kleinnijenhuis et al., 2012; Arts et al., 2018b) arise from trained differentiated cells and/or trained progenitor cells. Indeed, the progeny may not be expected to survive for a long timeperiod. Actually, we observed a "likely training" effect of vaccination on neutrophils, a population well described as short-lived (Pillay et al., 2010), supporting that training would occur during the maturation process of innate cells, either stem cells or early progenitors that are not yet fully characterized (*e.g.* pre-neutrophils).

In addition, the training of non-immune cells was also shown (Hamada et al., 2018) suggesting that stromal could also participate in the training. For instance, one may imagine that a stromal cell that would have captured vaccine antigen could deliver it to newly generated cells, inducing phenotypic changes in these cells.

The persistence of the vaccine or its antigens may also be at play in the process. The inability of MVA to replicate in mammalian cells makes it unlikely in our settings, though one may hypothesize for example that infected cells could survive in a niche via unknown protection mechanisms. Besides, BCG training of hematopoietic stem cells was proved independent of BCG persistence in mice, since the transfer of trained hematopoietic stem cells into a naive host still gave rise to a trained progeny, without the stem cells being infected themselves (Kaufmann et al., 2018).

In our settings, the three non mutually exclusive scenarios (modifications of progenitors, of by-stander stromal cells, or of differentiated cells) could lead to the "likely trained" innate immune cells we observed (**Figure 32**).

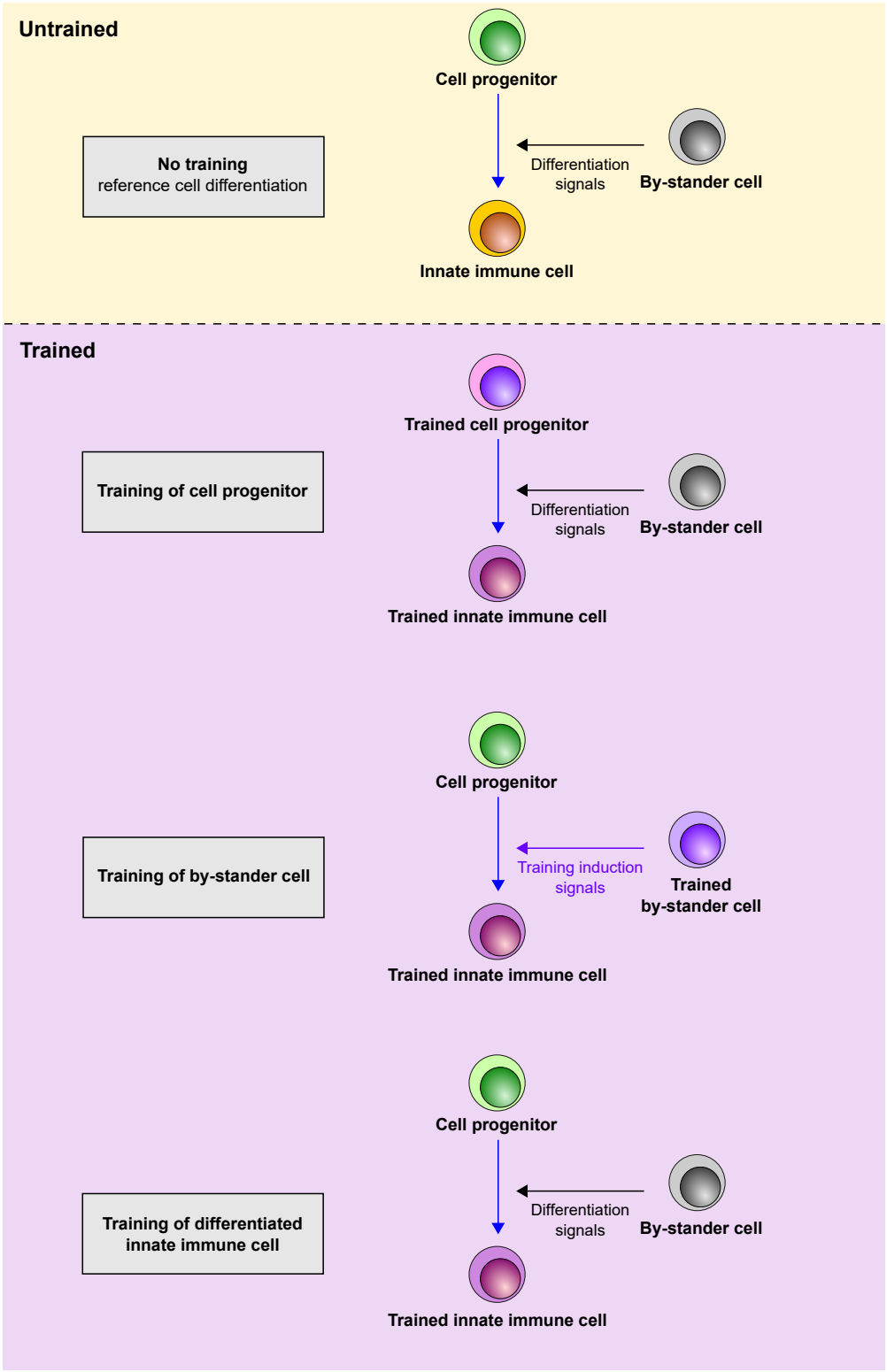

Figure 32. Generation of trained innate immune cells. The reference, untrained, generation of mature innate cells is presented on top. The three different steps at which training could occur are represented: training of cell progenitor, training of a by-stander cell providing differentiation signal, or training of fully differentiated cell. Each model ends up with the generation of a trained terminally differentiated innate immune cell. The three proposed models are not mutually exclusive. Note that the trained innate immune cells can potentially self-renew. Blue arrows indicate differentiation.

The same issue of innate memory origin stands true for memory-like NK cells. In mice the self maintenance of fully differentiated homeostatic proliferation-induced memory NK cells was proved (Sun et al., 2011), as well as expansion of cytokine-induced memory NK cells in recipient animals (Cooper et al., 2009). By contrast, the clonal expansion of cytomegalovirus antigen-specific memory NK cells relied on KLRG1^{-} NK cell progenitors in mice (Kamimura & Lanier, 2015). In addition, a CD34^{+} CD226^{+} CXCR4^{+} NK cell progenitor giving rise to NK cell with enhanced functions was identified in humans during chronic inflammation (Bozzano et al., 2015). Further insights into the generation and development of memory NK cell would also be highly valuable to target and harvest them in vaccine design optimization.

Current projects from the laboratory aim to address the identity of the cell that is modified or trained, as well as the nature of the modification (phenotypic, transcriptomic and/or epigenetic). To do so, bioinformatic methods dedicated to the assessment of cell differentiation trajectories, based on single-cell measurements, can be exploited, such as k-nearest neighbor graphs (Bendall et al., 2014), or diffusion maps (Haghverdi et al., 2015; 2016). Rather than the repartition in subpopulations, these methods focus on phenotype evolution within a wider cell population.

A k-nearest neighbor graph algorithm, called *Wanderlust* was successfully applied to mass cytometry data to decipher B cell differentiation (Bendall et al., 2014). It relies on the construction of the shortest path to transit from a user-defined initial cell (usually a stem cell) to the most differentiated cell in the dataset. Though powerful, it is limited by the strong assumptions of non-branching differentiation, impeding the study of several cell types simultaneously, as well as the required presence of all cell types in all samples, impeding the study of initially absent trained cells.

Diffusion map approaches rely on Markovian transition probability to assess the likelihood of connection between every cells in the datasets. This approach was particularly adapted to single-cell RNA sequencing with a development of a dedicated R-package (Angerer et al., 2016), and successful applications in literature in several contexts (*e.g.* Fan et al. (2018); Fergusson et al. (2018); Massaia et al. (2018). It was also successfully applied to mass cytometry data to follow the reconstitution of the immune of stem cell after transplantation in human patients (Chen et al., 2018).

Such approaches can serve to further investigate the differentiation processes resulting in the generation of "likely trained" innate cells, especially in bone marrow. Overall, given the complexity of the hematopoietic compartment, we may need to switch to single-cell RNAseq, CITE-seq or REAP-seq to capture the full diversity of all transitional cell types.

Innate immune training related pathways

Another remaining question in the field of innate training is the determination of the stimuli and associated pathways resulting in training (Song & Colonna, 2018). Strikingly, in vaccination, only live-attenuated vaccines were reported or suspected to induce training so far (BCG, smallpox, measles, poliomyelitis, yellow fever and live-attenuated pertussis vaccines) (Benn et al., 2013; Saadatian-Elahi et al., 2016; Cauchi & Locht, 2018). This suggests that adjuvanted recombinant vaccines, or even dead vaccines, would lack a crucial stimulus to induce immune training.

Which exact feature of live-attenuated vaccines is involved (*e.g.* peak of viremia or bacteremia, potential persistence of vaccine in some cells)is unknown. The determination of the exact nature of this stimulus remains to be determined, though mevalonate, IL-1 and IFNγ were proved important (Bekkering et al., 2018; Moorlag et al., 2018; Domínguez-Andrés et al., 2018). A better characterization of the pathways involved may enable the development of recombinant vaccines inducing trained immunity.

Besides, regarding MVA, recent finding indicated that *in vitro* stimulation of monocytes with MVA did not induce training, and rather tolerance, whereas vaccinia virus trained monocytes (Blok et al., 2019b). This is in contrast to our findings *in vivo* (Palgen et al., 2018). Still, in that study (Blok et al., 2019b), MVA and VAVC simulation were not compared at the same doses, making the side-by-side comparison tricky. In addition, it might well be that training of monocytes by MVA require the action of other cells, for example specific CD8 T cell IFNγ, as for lung macrophages training following adenovirus vaccination (Yao et al., 2018). Then the lack of these cells in the aforementioned *in vitro* experiment could have precluded monocyte training.

Also, other results in mice suggested that MVA, in contrast to VACV, did not induce memory NK cells (Gillard et al., 2011). Still, the authors focused on the detection of such NK cells 6 months after prime, without intermediate timepoints. Thus, it is possible that the NK cells we observed in our settings were also induced in mice but waned before 6 months. Interestingly, MVA is known to strongly activate NALP3/NLRP3 inflammasome (Delaloye et al., 2009), a PRR linked to trained immunity following western-diet in mice (Christ et al., 2018), suggesting that this pathway might be involved in the development of "likely trained" innate cells we observed in our settings. This is further supported by the reported involvement of NALP3/NLRP3 inflammasome in NK cell memory induction in mice (van den Boorn et al., 2016).

Whether the memory-like NK cells we observed were antigen-specific or not is also a remaining question. Memory NK cells induced by VACV vaccination were likely not antigen-specific, since they were more responsive to an unrelated adenovirus re-stimulation (Gillard et al., 2011), suggesting that it might also not be the case in our settings.

Eventually, the MVA vaccine construct we used contained an HIV insert which may participate in the innate memory induction we observed. A comparison of wild-type MVA *vs.* MVA HIV B vaccine could contribute to further address this concern.

Overtraining and innate immune exhaustion

Also, whether an overstimulation or overtraining can lead to "exhausted-like" innate cells needs to be further elucidated. Indeed, in the early boost schedule, we found NK cells that display low cytotoxic ability at the boost, and may correspond to exhausted NK cells previously described in chronic inflammation contexts, such as cancer (Platonova et al., 2011; Mamessier et al., 2011), or HIV infection (Jost & Altfeld, 2012). Similarly, patients recovering from sepsis showed impaired responsiveness of their monocytes (Bomans et al., 2018; Bouras et al., 2018).

This suggests that continuous stimulation may result in long-lasting impairment of innate immune cells. This phenomenon might be at play in the reduced efficacy of the immune system of elderly people, since low but constitutive inflammation was observed in elderlies, which came by alteration of several functions of the immune system, especially in the innate arm (Pinti et al., 2016). For instance, chemotaxis responsiveness of neutrophils, cytokine production of innate cells in response to PRR engagement, and ROS production in phagocytes were reduced in aged people, and NK cell dysfunctions were reported in elderlies too (Pinti et al., 2016).

Impact of the immunization route

Also, we essentially focused in this project on the characterization of the impact of the delay between prime and boost on the resulting immune response. Other parameters are important to understand vaccine-induced immune response. For example, the route of immunization highly matters. Indeed, with respect to trained innate immunity, route of immunization was proved crucial in BCG vaccination in mice, in which intravenous but not subcutaneous injection induced changes in hematopoietic stem cells (Kaufmann et al., 2018). The authors linked it with a distinct ability for the vaccine to reach the bone marrow and hematopoietic stem cells according to the route of immunization (Kaufmann et al., 2018).

Actually, the project of another research group within the team was to characterize the similarities and discrepancies of the immune response induced with the same vaccine and the same animal model, but comparing also intradermal, intramuscular and subcutaneous routes (unpublished yet). It includes the characterization of both the early molecular and cellular events at the site of injection and the later MVA specific antibody, B and T cell effector and memory responses in blood, draining lymph node and site of immunization. A part of the first characterization of the immune response induced by intradermal injection using flow cytometry, confocal microscopy and luminex was published (Rosenbaum et al., 2018), the rest of the analyses is still ongoing. In addition, within our research group, the mass cytometry characterization of early and late innate myeloid response induced after intradermal immunization of cynomolgus macaques with the MVA HIV B vaccine is currently ongoing.

Note also that comparing the results we obtained on MVA vaccination with other vaccines (*e.g.* dead vaccines, recombinant vaccines, different types of adjuvants, heterologous prime boosts) will also be important. Indeed, such knowledges would be rewarding to better understand vaccine-induced immune response in a more general context.

Vaccine efficacy assessment

A limitation in the use of our vaccine model, MVA, is that it is not possible to challenge the animal with the cognate pathogen, variola virus. Indeed, since the eradication of smallpox in 1980, stocks of frozen smallpox virus are securely stored in the centers for disease control and prevention in the United States, and the state research centre of virology and biotechnology in Russia, and are not available for research for obvious public health safety concern. Challenges with the related monkeypox virus could potentially be done but would require the use of biosafety level 4 facilities. Eventually, VACV challenge could also be done, though the access to the virus is restricted.

It was thus not possible to assess firmly whether each schedule was protective. Still, the high level of neutralizing antibodies induced in the classical boost schedule suggests that it was protective, since the titer was similar to an immunoglobulin pool of plasma from human volunteers boosted with Dryvax smallpox vaccine (vaccinia immune globulin intravenous (human), VIGIV), which was shown protective after passive transfer into rhesus macaques (Edghill-Smith et al., 2005).

We could also use a challenge with an unrelated pathogen to assess cross-protection induced by vaccination, for example with yellow fever vaccine or plasmodium, as previously done in literature (Arts et al., 2018b; Walk et al., 2019). This could also help refining the functions of the "likely trained" innate immune cells, as mentioned in the previous sections. In this project, this was not feasible, since organs were harvested at euthanasia one year post-boost to assess the tissue distribution of adaptive cells, especially B cells. This currently ongoing analysis prevented the use of animal challenge that has to be postpone for future dedicated studies.

Harnessing innate immune training to improve vaccine design

Eventually, inducing a potent trained innate immune system is a promising strategy to improve vaccine in a longer-term perspective (Sánchez-Ramón et al., 2018).

Caution should be taken obviously. Indeed one should consider the potential adverse effects of overall immune system activation regarding auto-immune and inflammatory disorders (Bekkering et al., 2013; Leentjens et al., 2018; Arts et al., 2018a; Braza et al., 2018). Still, innate immune training in vaccination could be used to induce cross-protection against heterologous diseases, which could be especially valuable in young children highly exposed to numerous pathogens in their first years of life (**Figure 33A**).

In addition, assuming that these trained innate cells have an increased ability to clear pathogen and present antigens, we may use this to enhance an heterologous prime. For instance, for a given vaccine when one prime and several boost(s) are required to induce a potent and long-lasting immunity, if the initial prime is made in the presence of already unspecifically trained innate cells, induction of memory cells could be improved, resulting in the requirement of a lower number of boost(s). Further researches are indeed require to address and explore this possibility and orientate the choice of the vector used in homologous or heterologous prime-boost (**Figure 33B**).

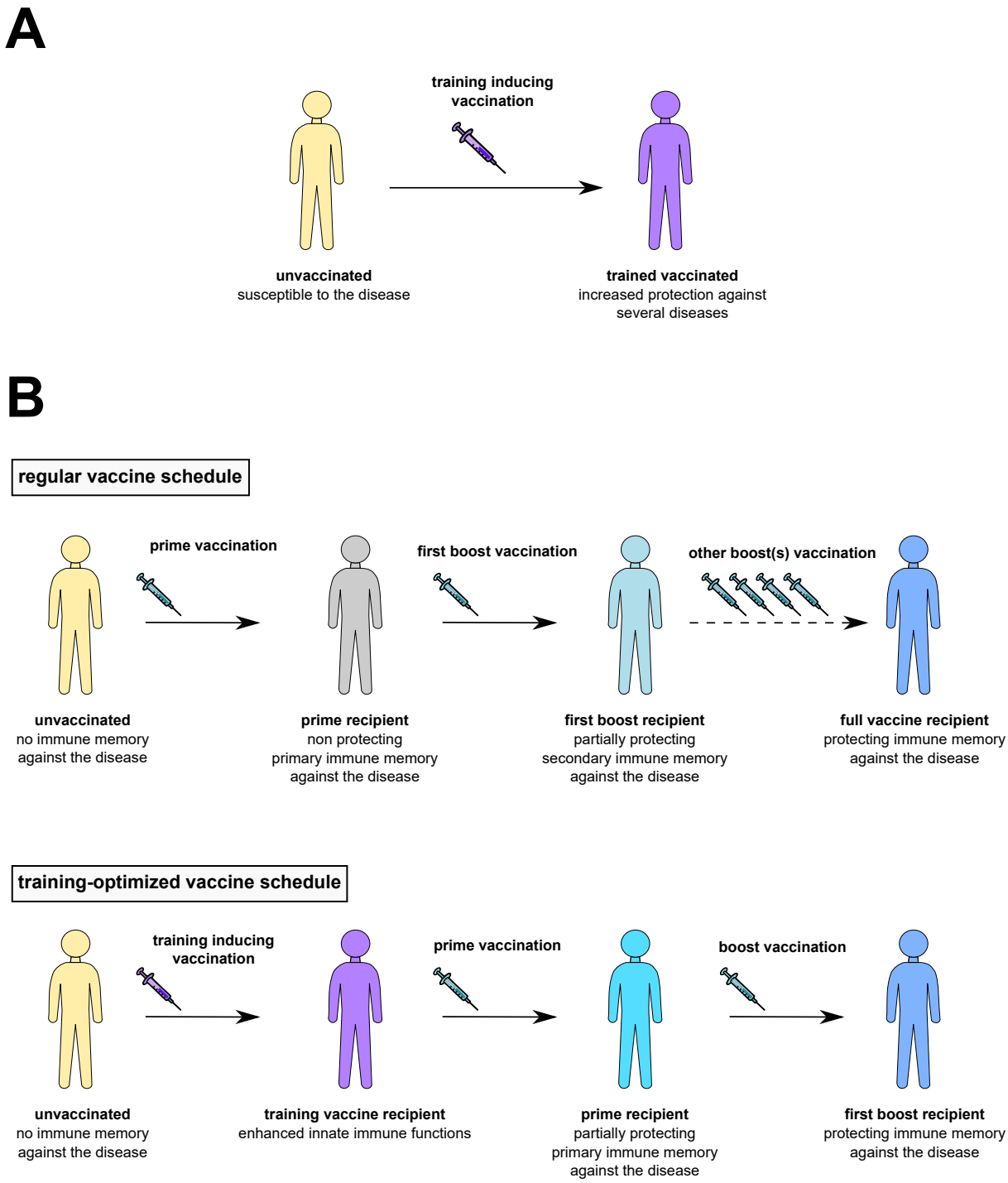

Figure 33. Harnessing vaccine-induced training to optimize vaccines. Innate training could be used on one side **(A)** to mediate heterologous protection, a feature valuable in public health. On the other side **(B)**, it could be used to enhance a new prime to improve the initial response of a heterologous vaccine, resulting in a reduced number of boost compared to a reference schedule.

Concluding remarks

Vaccination is a tremendous progress made in public health, and the main prevention measure that exists today against infectious diseases. The rationale optimization of current and future vaccines is crucial to counteract complex or emerging diseases. This necessarily goes through a better understanding of vaccine-induced immune response to better target and improve the vaccine-induced memory establishment. In this process, the innate immunity, as the initial trigger required for naive B and T cells activation, memory B and T cells restimulation, and polarization of humoral and cellular responses, plays a central role.

The results obtained in my project aim to contribute to fulfill this goal, with the in depth description of innate responses induced following different vaccine schedules, with a vaccine approved against smallpox in case of bioterrorism and currently tested as a vector against multiple diseases. My work particularly highlights the striking role of trained innate immunity in vaccination, consistently with the recent literature prompting to a new interest towards the targeting and harnessing of innate immunity in vaccination. Though many questions remain opened, I think these results are a valuable step towards the improved rational optimization of vaccines.

References

Bibliography

Aaby, P., Benn, C., Nielsen, J., Lisse, I. M., Rodrigues, A., & Ravn, H. 2012 Testing the hypothesis that diphtheria-tetanus-pertussis vaccine has negative non-specific and sex-differential effects on child survival in high-mortality countries. *BMJ open* **2**.

Abi Abdallah, D. S., Egan, C. E., Butcher, B. A., & Denkers, E. Y. 2011 Mouse neutrophils are professional antigen-presenting cells programmed to instruct Th1 and Th17 T-cell differentiation. *International Immunology* **23**, 317–326.

Adam, C., King, S., Allgeier, T., Braumüller, H., Lüking, C., Mysliwietz, J., Kriegeskorte, A., Busch, D. H., Röcken, M., & Mocikat, R. 2005 DC-NK cell cross talk as a novel CD4+ T-cell-independent pathway for antitumor CTL induction. *Blood* **106**, 338–344.

Adib-Conquy, M., Scott-Algara, D., Cavaillon, J.-M., & Souza-Fonseca-Guimaraes, F. 2014 TLR-mediated activation of NK cells and their role in bacterial/viral immune responses in mammals. *Immunology and Cell Biology* **92**, 256–262.

Adrover, J. M., Nicolás-Ávila, J. A., & Hidalgo, A. 2016 Aging: A Temporal Dimension for Neutrophils. *Trends in Immunology* **37**, 334–345.

Akdis, M., Aab, A., Altunbulakli, C., Azkur, K., Costa, R. A., Crameri, R., Duan, S., Eiwegger, T., Eljaszewicz, A., Ferstl, R., Frei, R., Garbani, M., Globinska, A., Hess, L., Huitema, C., Kubo, T., Komlosi, Z., Konieczna, P., Kovacs, N., Kucuksezer, U. C., Meyer, N., Morita, H., Olzhausen, J., O'Mahony, L., Pezer, M., Prati, M., Rebane, A., Rhyner, C., Rinaldi, A., Sokolowska, M., Stanic, B., Sugita, K., Treis, A., van de Veen, W., Wanke, K., Wawrzyniak, M., Wawrzyniak, P., Wirz, O. F., Zakzuk, J. S., & Akdis, C. A. 2016 Interleukins (from IL-1 to IL-38), interferons, transforming growth factor β, and TNF-α: Receptors, functions, and roles in diseases. *The Journal of Allergy and Clinical Immunology* **138**, 984–1010.

Akira, S., Uematsu, S., & Takeuchi, O. 2006 Pathogen recognition and innate immunity. *Cell* **124**, 783–801.

Akkina, R., Allam, A., Balazs, A. B., Blankson, J. N., Burnett, J. C., Casares, S., Garcia, J. V., Hasenkrug, K. J., Kashanchi, F., Kitchen, S. G., Klein, F., Kumar, P., Luster, A. D., Poluektova, L. Y., Rao, M., Sanders-Beer, B. E., Shultz, L. D., & Zack, J. A. 2016 Improvements and Limitations of Humanized Mouse Models for HIV Research: NIH/NIAID "Meet the Experts" 2015 Workshop Summary. *AIDS research and human retroviruses* **32**, 109–119.

Alcántara-Hernández, M., Leylek, R., Wagar, L. E., Engleman, E. G., Keler, T., Marinkovich, M. P., Davis, M. M., Nolan, G. P., & Idoyaga, J. 2017 High-Dimensional Phenotypic Mapping of Human Dendritic Cells Reveals Interindividual Variation and Tissue Specialization. *Immunity* **47**, 1037–1050.e6.

Altenburg, A. F., Kreijtz, J. H. C. M., de Vries, R. D., Song, F., Fux, R., Rimmelzwaan, G. F., Sutter, G., & Volz, A. 2014 Modified vaccinia virus ankara (MVA) as production platform for vaccines against influenza and other viral respiratory diseases. *Viruses* **6**, 2735–2761.

Alter, G. & Altfeld, M. 2011 Mutiny or scrutiny: NK cell modulation of DC function in HIV-1 infection. *Trends in Immunology* **32**, 219–224.

Amanna, I. J., Carlson, N. E., & Slifka, M. K. 2007 Duration of humoral immunity to common viral and vaccine antigens. *The New England Journal of Medicine* **357**, 1903–1915.

Amanna, I. J., Slifka, M. K., & Crotty, S. 2006 Immunity and immunological memory following smallpox vaccination. *Immunological Reviews* **211**, 320–337.

Amano, K., Hirayama, M., Azuma, E., Iwamoto, S., Keida, Y., & Komada, Y. 2015 Neutrophils induced licensing of natural killer cells. *Mediators of Inflammation* **2015**, 747680.

Amir, E.-a. D., Davis, K. L., Tadmor, M. D., Simonds, E. F., Levine, J. H., Bendall, S. C., Shenfeld, D. K., Krishnaswamy, S., Nolan, G. P., & Pe'er, D. 2013 viSNE enables visualization of high dimensional single-cell data and reveals phenotypic heterogeneity of leukemia. *Nature Biotechnology* **31**, 545–552.

Andersen, P. & Doherty, T. M. 2005 The success and failure of BCG - implications for a novel tuberculosis vaccine. *Nature Reviews. Microbiology* **3**, 656–662.

Andrews, D. M., Estcourt, M. J., Andoniou, C. E., Wikstrom, M. E., Khong, A., Voigt, V., Fleming, P., Tabarias, H., Hill, G. R., van der Most, R. G., Scalzo, A. A., Smyth, M. J., & Degli-Esposti, M. A. 2010 Innate immunity defines the capacity of antiviral T cells to limit persistent infection. *The Journal of Experimental Medicine* **207**, 1333–1343.

Angerer, P., Haghverdi, L., Büttner, M., Theis, F. J., Marr, C., & Buettner, F. 2016 destiny: diffusion maps for large-scale single-cell data in R. *Bioinformatics (Oxford, England)* **32**, 1241–1243.

Antony, J. M. & MacDonald, K. S. 2015 A critical analysis of the cynomolgus macaque, Macaca fascicularis, as a model to test HIV-1/SIV vaccine efficacy. *Vaccine* **33**, 3073–3083.

Arase, H., Mocarski, E. S., Campbell, A. E., Hill, A. B., & Lanier, L. L. 2002 Direct recognition of cytomegalovirus by activating and inhibitory NK cell receptors. *Science (New York, N.Y.)* **296**, 1323–1326.

Ariotti, S., Hogenbirk, M. A., Dijkgraaf, F. E., Visser, L. L., Hoekstra, M. E., Song, J.-Y., Jacobs, H., Haanen, J. B., & Schumacher, T. N. 2014 T cell memory. Skin-resident memory $CD8^+$ T cells trigger a state of tissue-wide pathogen alert. *Science (New York, N.Y.)* **346**, 101–105.

Arts, R. J. W., Joosten, L. A. B., & Netea, M. G. 2018a The Potential Role of Trained Immunity in Autoimmune and Autoinflammatory Disorders. *Frontiers in Immunology* **9**, 298.

Arts, R. J. W., Moorlag, S. J. C. F. M., Novakovic, B., Li, Y., Wang, S.-Y., Oosting, M., Kumar, V., Xavier, R. J., Wijmenga, C., Joosten, L. A. B., Reusken, C. B. E. M., Benn, C. S., Aaby, P., Koopmans, M. P., Stunnenberg, H. G., van Crevel, R., & Netea, M. G. 2018b BCG Vaccination Protects against Experimental Viral Infection in Humans through the Induction of Cytokines Associated with Trained Immunity. *Cell Host & Microbe* **23**, 89–100.e5.

Atkuri, K. R., Stevens, J. C., & Neubert, H. 2015 Mass cytometry: a highly multiplexed single-cell technology for advancing drug development. *Drug Metabolism and Disposition: The Biological Fate of Chemicals* **43**, 227–233.

Autissier, P., Soulas, C., Burdo, T. H., & Williams, K. C. 2010 Immunophenotyping of lymphocyte, monocyte and dendritic cell subsets in normal rhesus macaques by 12-color flow cytometry: clarification on DC heterogeneity. *Journal of Immunological Methods* **360**, 119–128.

Balka, K. R. & De Nardo, D. 2018 Understanding early TLR signaling through the Myddosome. *Journal of Leukocyte Biology*.

Bandura, D. R., Baranov, V. I., Ornatsky, O. I., Antonov, A., Kinach, R., Lou, X., Pavlov, S., Vorobiev, S., Dick, J. E., & Tanner, S. D. 2009 Mass cytometry: technique for real time single cell multitarget immunoassay based on inductively coupled plasma time-of-flight mass spectrometry. *Analytical Chemistry* **81**, 6813–6822.

Barban, V., Munoz-Jordan, J. L., Santiago, G. A., Mantel, N., Girerd, Y., Gulia, S., Claude, J.-B., & Lang, J. 2012 Broad neutralization of wild-type dengue virus isolates following immunization in monkeys with a tetravalent dengue vaccine based on chimeric yellow fever 17d/dengue viruses. *Virology* **429**, 91–98.

Barouch, D. H. 2008 Challenges in the development of an HIV-1 vaccine. *Nature* **455**, 613–619.

Barton, E. S., White, D. W., Cathelyn, J. S., Brett-McClellan, K. A., Engle, M., Diamond, M. S., Miller, V. L., & Virgin, H. W. 2007 Herpesvirus latency confers symbiotic protection from bacterial infection. *Nature* **447**, 326–329.

Batista, F. D. & Harwood, N. E. 2009 The who, how and where of antigen presentation to B cells. *Nature Reviews. Immunology* **9**, 15–27.

Bedoui, S., Whitney, P. G., Waithman, J., Eidsmo, L., Wakim, L., Caminschi, I., Allan, R. S., Wojtasiak, M., Shortman, K., Carbone, F. R., Brooks, A. G., & Heath, W. R. 2009 Cross-presentation of viral and self antigens by skin-derived CD103+ dendritic cells. *Nature Immunology* **10**, 488–495.

Bekkering, S., Arts, R. J. W., Novakovic, B., Kourtzelis, I., van der Heijden, C. D. C. C., Li, Y., Popa, C. D., Ter Horst, R., van Tuijl, J., Netea-Maier, R. T., van de Veerdonk, F. L., Chavakis, T., Joosten, L. A. B., van der Meer, J. W. M., Stunnenberg, H., Riksen, N. P., & Netea, M. G. 2018 Metabolic Induction of Trained Immunity through the Mevalonate Pathway. *Cell* **172**, 135–146.e9.

Bekkering, S., Blok, B. A., Joosten, L. A. B., Riksen, N. P., van Crevel, R., & Netea, M. G. 2016 In Vitro Experimental Model of Trained Innate Immunity in Human Primary Monocytes. *Clinical and vaccine immunology: CVI* **23**, 926–933.

Bekkering, S., Joosten, L. A. B., van der Meer, J. W. M., Netea, M. G., & Riksen, N. P. 2013 Trained innate immunity and atherosclerosis. *Current Opinion in Lipidology* **24**, 487–492.

Belongia, E. A. & Naleway, A. L. 2003 Smallpox vaccine: the good, the bad, and the ugly. *Clinical Medicine & Research* **1**, 87–92.

Bendall, S. C., Davis, K. L., Amir, E.-A. D., Tadmor, M. D., Simonds, E. F., Chen, T. J., Shenfeld, D. K., Nolan, G. P., & Pe'er, D. 2014 Single-cell trajectory detection uncovers progression and regulatory coordination in human B cell development. *Cell* **157**, 714–725.

Bendall, S. C., Nolan, G. P., Roederer, M., & Chattopadhyay, P. K. 2012 A deep profiler's guide to cytometry. *Trends in Immunology* **33**, 323–332.

Benn, C. S., Netea, M. G., Selin, L. K., & Aaby, P. 2013 A small jab - a big effect: nonspecific immunomodulation by vaccines. *Trends in Immunology* **34**, 431–439.

Benoni, G., Adami, A., Vella, A., Ariosto, E., Ortolani, R., & Cuzzolin, L. 2001 CD23 and CD69 expression on human neutrophils of healthy subjects and patients with peripheral arterial occlusive disease. *International Journal of Immunopathology and Pharmacology* **14**, 161–167.

Beyrend, G., Stam, K., Höllt, T., Ossendorp, F., & Arens, R. 2018 Cytofast: A workflow for visual and quantitative analysis of flow and mass cytometry data to discover immune signatures and correlations. *Computational and Structural Biotechnology Journal* **16**, 435–442.

Bistoni, F., Verducci, G., Perito, S., Vecchiarelli, A., Puccetti, P., Marconi, P., & Cassone, A. 1988 Immunomodulation by a low-virulence, agerminative variant of Candida albicans. Further evidence for macrophage activation as one of the effector mechanisms of nonspecific anti-infectious protection. *Journal of Medical and Veterinary Mycology: Bi-Monthly Publication of the International Society for Human and Animal Mycology* **26**, 285–299.

Biswas, P., Mantelli, B., Sica, A., Malnati, M., Panzeri, C., Saccani, A., Hasson, H., Vecchi, A., Saniabadi, A., Lusso, P., Lazzarin, A., & Beretta, A. 2003 Expression of CD4 on human peripheral blood neutrophils. *Blood* **101**, 4452–4456.

Bjornson-Hooper, Z. B., Fragiadakis, G. K., Spitzer, M. H., Madhireddy, D., McIlwain, D., & Nolan, G. P. 2019 A comprehensive atlas of immunological differences between humans, mice and non-human primates. *bioRxiv*.

Blanchard, T. J., Alcami, A., Andrea, P., & Smith, G. L. 1998 Modified vaccinia virus Ankara undergoes limited replication in human cells and lacks several immunomodulatory proteins: implications for use as a human vaccine. *The Journal of General Virology* **79 (Pt 5)**, 1159–1167.

Blanchard-Rohner, G., Pulickal, A. S., Jol-van der Zijde, C. M., Snape, M. D., & Pollard, A. J. 2009 Appearance of peripheral blood plasma cells and memory B cells in a primary and secondary immune response in humans. *Blood* **114**, 4998–5002.

Blazkova, J., Gupta, S., Liu, Y., Gaudilliere, B., Ganio, E. A., Bolen, C. R., Saar-Dover, R., Fragiadakis, G. K., Angst, M. S., Hasni, S., Aghaeepour, N., Stevenson, D., Baldwin, N., Anguiano, E., Chaussabel, D., Altman, M. C., Kaplan, M. J., Davis, M. M., & Furman, D. 2017 Multicenter Systems Analysis of Human Blood Reveals Immature Neutrophils in Males and During Pregnancy. *Journal of Immunology (Baltimore, Md.: 1950)* **198**, 2479–2488.

Blok, B. A., de Bree, L. C. J., Diavatopoulos, D. A., Langereis, J. D., Joosten, L. A. B., Aaby, P., Crevel, R. v., Benn, C. S., & Netea, M. G. 2019a Interacting non-specific immunological effects of BCG and Tdapf vaccinations: an explorative randomized trial. *Clinical Infectious Diseases: An Official Publication of the Infectious Diseases Society of America*.

Blok, B. A., Jensen, K. J., Aaby, P., Fomsgaard, A., van Crevel, R., Benn, C. S., & Netea, M. G. 2019b Opposite effects of Vaccinia and modified Vaccinia Ankara on trained immunity. *European Journal of Clinical Microbiology & Infectious Diseases: Official Publication of the European Society of Clinical Microbiology*.

Boeltz, S., Amini, P., Anders, H.-J., Andrade, F., Bilyy, R., Chatfield, S., Cichon, I., Clancy, D. M., Desai, J., Dumych, T., Dwivedi, N., Gordon, R. A., Hahn, J., Hidalgo, A., Hoffmann, M. H., Kaplan, M. J., Knight, J. S., Kolaczkowska, E., Kubes, P., Leppkes, M., Manfredi, A. A., Martin, S. J., Maueröder, C., Maugeri, N., Mitroulis, I., Munoz, L. E., Nakazawa, D., Neeli, I., Nizet, V., Pieterse, E., Radic, M. Z., Reinwald, C., Ritis, K., Rovere-Querini, P., Santocki, M., Schauer, C., Schett, G., Shlomchik, M. J., Simon, H.-U., Skendros, P., Stojkov, D., Vandenabeele, P., Berghe, T. V., van der Vlag, J., Vitkov, L., von Köckritz-Blickwede, M., Yousefi, S., Zarbock, A., & Herrmann, M. 2019 To NET or not to NET:current opinions and state of the science regarding the formation of neutrophil extracellular traps. *Cell Death and Differentiation* **26**, 395–408.

Bogdan, C. 2001 Nitric oxide and the immune response. *Nature Immunology* **2**, 907–916.

Bohana-Kashtan, O., Ziporen, L., Donin, N., Kraus, S., & Fishelson, Z. 2004 Cell signals transduced by complement. *Molecular Immunology* **41**, 583–597.

Bomans, K., Schenz, J., Sztwiertnia, I., Schaack, D., Weigand, M. A., & Uhle, F. 2018 Sepsis Induces a Long-Lasting State of Trained Immunity in Bone Marrow Monocytes. *Frontiers in Immunology* **9**, 2685.

Boraschi, D. & Italiani, P. 2018 Innate Immune Memory: Time for Adopting a Correct Terminology. *Frontiers in Immunology* **9**, 799.

Borducchi, E. N., Cabral, C., Stephenson, K. E., Liu, J., Abbink, P., Ng'ang'a, D., Nkolola, J. P., Brinkman, A. L., Peter, L., Lee, B. C., Jimenez, J., Jetton, D., Mondesir, J., Mojta, S., Chandrashekar, A., Molloy, K., Alter, G., Gerold, J. M., Hill, A. L., Lewis, M. G., Pau, M. G., Schuitemaker, H., Hesselgesser, J., Geleziunas, R., Kim, J. H., Robb, M. L., Michael, N. L., & Barouch, D. H. 2016 Ad26/MVA therapeutic vaccination with TLR7 stimulation in SIV-infected rhesus monkeys. *Nature* **540**, 284–287.

Bos, S., Gadea, G., & Despres, P. 2018 Dengue: a growing threat requiring vaccine development for disease prevention. *Pathogens and Global Health* **112**, 294–305.

Bouabe, H. & Okkenhaug, K. 2013 Gene targeting in mice: a review. *Methods in Molecular Biology (Clifton, N.J.)* **1064**, 315–336.

Bouras, M., Asehnoune, K., & Roquilly, A. 2018 Contribution of Dendritic Cell Responses to Sepsis-Induced Immunosuppression and to Susceptibility to Secondary Pneumonia. *Frontiers in Immunology* **9**, 2590.

Bozzano, F., Marras, F., Ascierto, M. L., Cantoni, C., Cenderello, G., Dentone, C., Di Biagio, A., Orofino, G., Mantia, E., Boni, S., De Leo, P., Picciotto, A., Braido, F., Antonini, F., Wang, E., Marincola, F., Moretta, L., & De Maria, A. 2015 'Emergency exit' of bone-marrow-resident CD34(+)DNAM-1(bright)CXCR4(+)-committed lymphoid precursors during chronic infection and inflammation. *Nature Communications* **6**, 8109.

Brandler, S., Lepelley, A., Desdouits, M., Guivel-Benhassine, F., Ceccaldi, P.-E., Lévy, Y., Schwartz, O., & Moris, A. 2010 Preclinical studies of a modified vaccinia virus Ankara-based HIV candidate vaccine: antigen presentation and antiviral effect. *Journal of Virology* **84**, 5314–5328.

Braza, M. S., van Leent, M. M. T., Lameijer, M., Sanchez-Gaytan, B. L., Arts, R. J. W., Pérez-Medina, C., Conde, P., Garcia, M. R., Gonzalez-Perez, M., Brahmachary, M., Fay, F., Kluza, E., Kossatz, S., Dress, R. J., Salem, F., Rialdi, A., Reiner, T., Boros, P., Strijkers, G. J., Calcagno, C. C., Ginhoux, F., Marazzi, I., Lutgens, E., Nicolaes, G. A. F., Weber, C., Swirski, F. K., Nahrendorf, M., Fisher, E. A., Duivenvoorden, R., Fayad, Z. A., Netea, M. G., Mulder, W. J. M., & Ochando, J. 2018 Inhibiting Inflammation with Myeloid Cell-Specific Nanobiologics Promotes Organ Transplant Acceptance. *Immunity* **49**, 819–828.e6.

Brehm, M. A., Shultz, L. D., Luban, J., & Greiner, D. L. 2013 Overcoming current limitations in humanized mouse research. *The Journal of Infectious Diseases* **208 Suppl 2**, S125–130.

Brezar, V., Godot, V., Cheng, L., Su, L., Lévy, Y., & Seddiki, N. 2016 T-Regulatory Cells and Vaccination "Pay Attention and Do Not Neglect Them": Lessons from HIV and Cancer Vaccine Trials. *Vaccines* **4**.

Brodin, P., Jojic, V., Gao, T., Bhattacharya, S., Angel, C. J. L., Furman, D., Shen-Orr, S., Dekker, C. L., Swan, G. E., Butte, A. J., Maecker, H. T., & Davis, M. M. 2015 Variation in the human immune system is largely driven by non-heritable influences. *Cell* **160**, 37–47.

Brok, H. P., Bauer, J., Jonker, M., Blezer, E., Amor, S., Bontrop, R. E., Laman, J. D., & 't Hart, B. A. 2001 Non-human primate models of multiple sclerosis. *Immunological Reviews* **183**, 173–185.

Brown, K. N. & Barratt-Boyes, S. M. 2009 Surface phenotype and rapid quantification of blood dendritic cell subsets in the rhesus macaque. *Journal of Medical Primatology* **38**, 272–278.

Bruhns, P. & Jönsson, F. 2015 Mouse and human FcR effector functions. *Immunological Reviews* **268**, 25–51.

Brynjolfsson, S. F., Persson Berg, L., Olsen Ekerhult, T., Rimkute, I., Wick, M.-J., Mårtensson, I.-L., & Grimsholm, O. 2018 Long-Lived Plasma Cells in Mice and Men. *Frontiers in Immunology* **9**, 2673.

Buchbinder, S. P., Mehrotra, D. V., Duerr, A., Fitzgerald, D. W., Mogg, R., Li, D., Gilbert, P. B., Lama, J. R., Marmor, M., Del Rio, C., McElrath, M. J., Casimiro, D. R., Gottesdiener, K. M., Chodakewitz, J. A., Corey, L., Robertson, M. N., & Step Study Protocol Team 2008 Efficacy assessment of a cell-mediated immunity HIV-1 vaccine (the Step Study): a double-blind, randomised, placebo-controlled, test-of-concept trial. *Lancet (London, England)* **372**, 1881–1893.

Budhwar, S., Verma, P., Verma, R., Rai, S., & Singh, K. 2018 The Yin and Yang of Myeloid Derived Suppressor Cells. *Frontiers in Immunology* **9**, 2776.

Budnik, B., Levy, E., Harmange, G., & Slavov, N. 2018 SCoPE-MS: mass spectrometry of single mammalian cells quantifies proteome heterogeneity during cell differentiation. *Genome Biology* **19**, 161.

Butterfield, L. H., Zhao, F., Lee, S., Tarhini, A. A., Margolin, K. A., White, R. L., Atkins, M. B., Cohen, G. I., Whiteside, T. L., Kirkwood, J. M., & Lawson, D. H. 2017 Immune Correlates of GM-CSF and Melanoma Peptide Vaccination in a Randomized Trial for the Adjuvant Therapy of Resected High-Risk Melanoma (E4697). *Clinical Cancer Research: An Official Journal of the American Association for Cancer Research* **23**, 5034–5043.

Cabo Beltran, O. R. & Rosales Ledezma, R. 2019 MVA E2 therapeutic vaccine for marked reduction in likelihood of recurrence of respiratory papillomatosis. *Head & Neck* **41**, 657–665.

Cai, X., Chiu, Y.-H., & Chen, Z. J. 2014 The cGAS-cGAMP-STING pathway of cytosolic DNA sensing and signaling. *Molecular Cell* **54**, 289–296.

Caligiuri, M. A. 2008 Human natural killer cells. *Blood* **112**, 461–469.

Campbell, K. S. & Hasegawa, J. 2013 Natural killer cell biology: an update and future directions. *The Journal of Allergy and Clinical Immunology* **132**, 536–544.

Carlsson, H.-E., Schapiro, S. J., Farah, I., & Hau, J. 2004 Use of primates in research: a global overview. *American Journal of Primatology* **63**, 225–237.

Casimiro, D. R., Wang, F., Schleif, W. A., Liang, X., Zhang, Z.-Q., Tobery, T. W., Davies, M.-E., McDermott, A. B., O'Connor, D. H., Fridman, A., Bagchi, A., Tussey, L. G., Bett, A. J., Finnefrock, A. C., Fu, T.-m., Tang, A., Wilson, K. A., Chen, M., Perry, H. C., Heidecker, G. J., Freed, D. C., Carella, A., Punt, K. S., Sykes, K. J., Huang, L., Ausensi, V. I., Bachinsky, M., Sadasivan-Nair, U., Watkins, D. I., Emini, E. A., & Shiver, J. W. 2005 Attenuation of simian immunodeficiency virus SIVmac239 infection by prophylactic immunization with dna and recombinant adenoviral vaccine vectors expressing Gag. *Journal of Virology* **79**, 15547–15555.

Cassone, A. 2018 The Case for an Expanded Concept of Trained Immunity. *mBio* **9**.

Cauchi, S. & Locht, C. 2018 Non-specific Effects of Live Attenuated Pertussis Vaccine Against Heterologous Infectious and Inflammatory Diseases. *Frontiers in Immunology* **9**, 2872.

Chan, C. J., Smyth, M. J., & Martinet, L. 2014 Molecular mechanisms of natural killer cell activation in response to cellular stress. *Cell Death and Differentiation* **21**, 5–14.

Chattopadhyay, P. K. & Roederer, M. 2015 A mine is a terrible thing to waste: high content, single cell technologies for comprehensive immune analysis. *American Journal of Transplantation: Official Journal of the American Society of Transplantation and the American Society of Transplant Surgeons* **15**, 1155–1161.

Chen, Y., Lakshmikanth, T., Olin, A., Mikes, J., Remberger, M., & Brodin, P. 2018 Continuous Immune Cell Differentiation Inferred From Single-Cell Measurements Following Allogeneic Stem Cell Transplantation. *Frontiers in Molecular Biosciences* **5**, 81.

Cheng, Y., Zhu, Y. O., Becht, E., Aw, P., Chen, J., Poidinger, M., de Sessions, P. F., Hibberd, M. L., Bertoletti, A., Lim, S. G., & Newell, E. W. 2019 Multifactorial heterogeneity of virus-specific T cells and association with the progression of human chronic hepatitis B infection. *Science Immunology* **4**.

Chevrier, S., Crowell, H. L., Zanotelli, V. R. T., Engler, S., Robinson, M. D., & Bodenmiller, B. 2018 Compensation of Signal Spillover in Suspension and Imaging Mass Cytometry. *Cell Systems* **6**, 612–620.e5.

Cho, Y., Usui, K., Honda, S.-I., Tahara-Hanaoka, S., Shibuya, K., & Shibuya, A. 2006 Molecular characteristics of IgA and IgM Fc binding to the Fcalpha/muR. *Biochemical and Biophysical Research Communications* **345**, 474–478.

Choi, Y. & Chang, J. 2013 Viral vectors for vaccine applications. *Clinical and Experimental Vaccine Research* **2**, 97–105.

Christ, A., Günther, P., Lauterbach, M. A. R., Duewell, P., Biswas, D., Pelka, K., Scholz, C. J., Oosting, M., Haendler, K., Bassler, K., Klee, K., Schulte-Schrepping, J., Ulas, T., Moorlag, S. J. C. F. M., Kumar, V., Park, M. H., Joosten, L. A. B., Groh, L. A., Riksen, N. P., Espevik, T., Schlitzer, A., Li, Y., Fitzgerald, M. L., Netea, M. G., Schultze, J. L., & Latz, E. 2018 Western Diet Triggers NLRP3-Dependent Innate Immune Reprogramming. *Cell* **172**, 162–175.e14.

Ciabattini, A., Pettini, E., Fiorino, F., Pastore, G., Andersen, P., Pozzi, G., & Medaglini, D. 2016 Modulation of Primary Immune Response by Different Vaccine Adjuvants. *Frontiers in Immunology* **7**, 427.

Cichocki, F., Sitnicka, E., & Bryceson, Y. T. 2014 NK cell development and function–plasticity and redundancy unleashed. *Seminars in Immunology* **26**, 114–126.

Cocita, C., Guiton, R., Bessou, G., Chasson, L., Boyron, M., Crozat, K., & Dalod, M. 2015 Natural Killer Cell Sensing of Infected Cells Compensates for MyD88 Deficiency but Not IFN-I Activity in Resistance to Mouse Cytomegalovirus. *PLoS pathogens* **11**, e1004897.

Coffman, R. L., Sher, A., & Seder, R. A. 2010 Vaccine adjuvants: putting innate immunity to work. *Immunity* **33**, 492–503.

Collin, M. & Bigley, V. 2018 Human dendritic cell subsets: an update. *Immunology* **154**, 3–20.

Colucci, F., Di Santo, J. P., & Leibson, P. J. 2002 Natural killer cell activation in mice and men: different triggers for similar weapons? *Nature Immunology* **3**, 807–813.

Condit, R. C., Moussatche, N., & Traktman, P. 2006 In a nutshell: structure and assembly of the vaccinia virion. *Advances in Virus Research* **66**, 31–124.

Cook, K. D., Kline, H. C., & Whitmire, J. K. 2015 NK cells inhibit humoral immunity by reducing the abundance of CD4+ T follicular helper cells during a chronic virus infection. *Journal of Leukocyte Biology* **98**, 153–162.

Cooper, M. A., Elliott, J. M., Keyel, P. A., Yang, L., Carrero, J. A., & Yokoyama, W. M. 2009 Cytokine-induced memory-like natural killer cells. *Proceedings of the National Academy of Sciences of the United States of America* **106**, 1915–1919.

Cooper, M. A., Fehniger, T. A., & Caligiuri, M. A. 2001 The biology of human natural killer-cell subsets. *Trends in Immunology* **22**, 633–640.

Corneau, A., Cosma, A., Even, S., Katlama, C., Le Grand, R., Frachet, V., Blanc, C., & Autran, B. 2017 Comprehensive Mass Cytometry Analysis of Cell Cycle, Activation, and Coinhibitory Receptors Expression in CD4 T Cells from Healthy and HIV-Infected Individuals. *Cytometry. Part B, Clinical Cytometry* **92**, 21–32.

Corthay, A. 2009 How do regulatory T cells work? *Scandinavian Journal of Immunology* **70**, 326–336.

Costa, S., Bevilacqua, D., Cassatella, M. A., & Scapini, P. 2019 Recent advances on the crosstalk between neutrophils and B or T lymphocytes. *Immunology* **156**, 23–32.

Costantini, C. & Cassatella, M. A. 2011 The defensive alliance between neutrophils and NK cells as a novel arm of innate immunity. *Journal of Leukocyte Biology* **89**, 221–233.

Cottingham, M. G. & Carroll, M. W. 2013 Recombinant MVA vaccines: dispelling the myths. *Vaccine* **31**, 4247–4251.

Crotty, S. 2015 A brief history of T cell help to B cells. *Nature Reviews. Immunology* **15**, 185–189.

Dai, P., Wang, W., Cao, H., Avogadri, F., Dai, L., Drexler, I., Joyce, J. A., Li, X.-D., Chen, Z., Merghoub, T., Shuman, S., & Deng, L. 2014 Modified vaccinia virus Ankara triggers type I IFN production in murine conventional dendritic cells via a cGAS/STING-mediated cytosolic DNA-sensing pathway. *PLoS pathogens* **10**, e1003989.

Dambuza, I. M. & Brown, G. D. 2015 C-type lectins in immunity: recent developments. *Current Opinion in Immunology* **32**, 21–27.

Damon, I. K., Davidson, W. B., Hughes, C. M., Olson, V. A., Smith, S. K., Holman, R. C., Frey, S. E., Newman, F., Belshe, R. B., Yan, L., & Karem, K. 2009 Evaluation of smallpox vaccines using variola neutralization. *The Journal of General Virology* **90**, 1962–1966.

de Groot, N. G., Otting, N., Robinson, J., Blancher, A., Lafont, B. A. P., Marsh, S. G. E., O'Connor, D. H., Shiina, T., Walter, L., Watkins, D. I., & Bontrop, R. E. 2012 Nomenclature report on the major histocompatibility complex genes and alleles of Great Ape, Old and New World monkey species. *Immunogenetics* **64**, 615–631.

de Jong, M. & Maina, T. 2010 Of mice and humans: are they the same?–Implications in cancer translational research. *Journal of Nuclear Medicine: Official Publication, Society of Nuclear Medicine* **51**, 501–504.

Delaloye, J., Roger, T., Steiner-Tardivel, Q.-G., Le Roy, D., Knaup Reymond, M., Akira, S., Petrilli, V., Gomez, C. E., Perdiguero, B., Tschopp, J., Pantaleo, G., Esteban, M., & Calandra, T. 2009 Innate immune sensing of modified vaccinia virus Ankara (MVA) is mediated by TLR2-TLR6, MDA-5 and the NALP3 inflammasome. *PLoS pathogens* **5**, e1000480.

Delgado-Rizo, V., Martínez-Guzmán, M. A., Iñiguez-Gutierrez, L., García-Orozco, A., Alvarado-Navarro, A., & Fafutis-Morris, M. 2017 Neutrophil Extracellular Traps and Its Implications in Inflammation: An Overview. *Frontiers in Immunology* **8**, 81.

Dharmadhikari, A. S. & Nardell, E. A. 2008 What animal models teach humans about tuberculosis. *American Journal of Respiratory Cell and Molecular Biology* **39**, 503–508.

Di Pilato, M., Mejías-Pérez, E., Zonca, M., Perdiguero, B., Gómez, C. E., Trakala, M., Nieto, J., Nájera, J. L., Sorzano, C. O. S., Combadière, C., Pantaleo, G., Planelles, L., & Esteban, M. 2015 NFκB activation by modified vaccinia virus as a novel strategy to enhance neutrophil migration and HIV-specific T-cell responses. *Proceedings of the National Academy of Sciences of the United States of America* **112**, E1333–1342.

Domínguez-Andrés, J., Joosten, L. A., & Netea, M. G. 2018 Induction of innate immune memory: the role of cellular metabolism. *Current Opinion in Immunology* **56**, 10–16.

Dowson, C., Simpson, N., Duffy, L., & O'Reilly, S. 2017 Innate Immunity in Systemic Sclerosis. *Current Rheumatology Reports* **19**, 2.

Drechsler, S., Lynch, M. A., Novella, S., González-Navarro, H., Hecimovic, S., Barini, E., Tucci, V., Castro, R. E., Vandenbroucke, R. E., Osuchowski, M., & Potter, P. K. 2016 With mouse age comes wisdom: A review and suggestions of relevant mouse models for age-related conditions. *Mechanisms of Ageing and Development* **160**, 54–68.

Drexler, I., Heller, K., Wahren, B., Erfle, V., & Sutter, G. 1998 Highly attenuated modified vaccinia virus Ankara replicates in baby hamster kidney cells, a potential host for virus propagation, but not in various human transformed and primary cells. *The Journal of General Virology* **79 (Pt 2)**, 347–352.

Dörner, T. & Radbruch, A. 2005 Selecting B cells and plasma cells to memory. *The Journal of Experimental Medicine* **201**, 497–499.

Dubsky, P., Ueno, H., Piqueras, B., Connolly, J., Banchereau, J., & Palucka, A. K. 2005 Human dendritic cell subsets for vaccination. *Journal of Clinical Immunology* **25**, 551–572.

Dudziak, D., Kamphorst, A. O., Heidkamp, G. F., Buchholz, V. R., Trumpfheller, C., Yamazaki, S., Cheong, C., Liu, K., Lee, H.-W., Park, C. G., Steinman, R. M., & Nussenzweig, M. C. 2007 Differential antigen processing by dendritic cell subsets in vivo. *Science (New York, N.Y.)* **315**, 107–111.

Duffy, D., Perrin, H., Abadie, V., Benhabiles, N., Boissonnas, A., Liard, C., Descours, B., Reboulleau, D., Bonduelle, O., Verrier, B., Van Rooijen, N., Combadière, C., & Combadière, B. 2012 Neutrophils transport antigen from the dermis to the bone marrow, initiating a source of memory CD8+ T cells. *Immunity* **37**, 917–929.

DuPage, M. & Bluestone, J. A. 2016 Harnessing the plasticity of CD4(+) T cells to treat immune-mediated disease. *Nature Reviews. Immunology* **16**, 149–163.

Dustin, M. L. 2016 Complement Receptors in Myeloid Cell Adhesion and Phagocytosis. *Microbiology Spectrum* **4**.

Dutertre, C.-A., Amraoui, S., DeRosa, A., Jourdain, J.-P., Vimeux, L., Goguet, M., Degrelle, S., Feuillet, V., Liovat, A.-S., Müller-Trutwin, M., Decroix, N., Deveau, C., Meyer, L., Goujard, C., Loulergue, P., Launay, O., Richard, Y., & Hosmalin, A. 2012 Pivotal role of M-DC8$^+$ monocytes from viremic HIV-infected patients in TNFα overproduction in response to microbial products. *Blood* **120**, 2259–2268.

Earl, P. L., Americo, J. L., Wyatt, L. S., Eller, L. A., Whitbeck, J. C., Cohen, G. H., Eisenberg, R. J., Hartmann, C. J., Jackson, D. L., Kulesh, D. A., Martinez, M. J., Miller, D. M., Mucker, E. M., Shamblin, J. D., Zwiers, S. H., Huggins, J. W., Jahrling, P. B., & Moss, B. 2004 Immunogenicity of a highly attenuated MVA smallpox vaccine and protection against monkeypox. *Nature* **428**, 182–185.

Ebeling, M., Küng, E., See, A., Broger, C., Steiner, G., Berrera, M., Heckel, T., Iniguez, L., Albert, T., Schmucki, R., Biller, H., Singer, T., & Certa, U. 2011 Genome-based analysis of the nonhuman primate Macaca fascicularis as a model for drug safety assessment. *Genome Research* **21**, 1746–1756.

Edghill-Smith, Y., Golding, H., Manischewitz, J., King, L. R., Scott, D., Bray, M., Nalca, A., Hooper, J. W., Whitehouse, C. A., Schmitz, J. E., Reimann, K. A., & Franchini, G. 2005 Smallpox vaccine-induced antibodies are necessary and sufficient for protection against monkeypox virus. *Nature Medicine* **11**, 740–747.

Egger, G., Burda, A., & Glasner, A. 2001 A simple method for measuring the F-actin content of human polymorphonuclear leukocytes in whole blood. *Virchows Archiv: An International Journal of Pathology* **438**, 394–397.

Eickhoff, S., Brewitz, A., Gerner, M. Y., Klauschen, F., Komander, K., Hemmi, H., Garbi, N., Kaisho, T., Germain, R. N., & Kastenmüller, W. 2015 Robust Anti-viral Immunity Requires Multiple Distinct T Cell-Dendritic Cell Interactions. *Cell* **162**, 1322–1337.

El Kebir, D. & Filep, J. G. 2010 Role of neutrophil apoptosis in the resolution of inflammation. *TheScientificWorldJournal* **10**, 1731–1748.

El Mubarak, H. S., Yüksel, S., van Amerongen, G., Mulder, P. G. H., Mukhtar, M. M., Osterhaus, A. D. M. E., & de Swart, R. L. 2007 Infection of cynomolgus macaques (Macaca fascicularis) and rhesus macaques (Macaca mulatta) with different wild-type measles viruses. *The Journal of General Virology* **88**, 2028–2034.

Elahi, S., Holmstrom, J., & Gerdts, V. 2007 The benefits of using diverse animal models for studying pertussis. *Trends in Microbiology* **15**, 462–468.

Elhmouzi-Younes, J., Palgen, J.-L., Tchitchek, N., Delandre, S., Namet, I., Bodinham, C. L., Pizzoferro, K., Lewis, D. J. M., Le Grand, R., Cosma, A., & Beignon, A.-S. 2017 In depth comparative phenotyping of blood innate myeloid leukocytes from healthy humans and macaques using mass cytometry. *Cytometry. Part A: The Journal of the International Society for Analytical Cytology* **91**, 969–982.

Ellenbroek, B. & Youn, J. 2016 Rodent models in neuroscience research: is it a rat race? *Disease Models & Mechanisms* **9**, 1079–1087.

Estes, J. D., Wong, S. W., & Brenchley, J. M. 2018 Nonhuman primate models of human viral infections. *Nature Reviews. Immunology* **18**, 390–404.

Evering, T. H. & Tsuji, M. 2018 Human Immune System Mice for the Study of Human Immunodeficiency Virus-Type 1 Infection of the Central Nervous System. *Frontiers in Immunology* **9**, 649.

Evrard, M., Kwok, I. W. H., Chong, S. Z., Teng, K. W. W., Becht, E., Chen, J., Sieow, J. L., Penny, H. L., Ching, G. C., Devi, S., Adrover, J. M., Li, J. L. Y., Liong, K. H., Tan, L., Poon, Z., Foo, S., Chua, J. W., Su, I.-H., Balabanian, K., Bachelerie, F., Biswas, S. K., Larbi, A., Hwang, W. Y. K., Madan, V., Koeffler, H. P., Wong, S. C., Newell, E. W., Hidalgo, A., Ginhoux, F., & Ng, L. G. 2018 Developmental Analysis of Bone Marrow Neutrophils Reveals Populations Specialized in Expansion, Trafficking, and Effector Functions. *Immunity* **48**, 364–379.e8.

Fan, X., Moltedo, B., Mendoza, A., Davydov, A. N., Faire, M. B., Mazutis, L., Sharma, R., Pe'er, D., Chudakov, D. M., & Rudensky, A. Y. 2018 CD49b defines functionally mature Treg cells that survey skin and vascular tissues. *The Journal of Experimental Medicine* **215**, 2796–2814.

Farber, D. L., Yudanin, N. A., & Restifo, N. P. 2014 Human memory T cells: generation, compartmentalization and homeostasis. *Nature Reviews. Immunology* **14**, 24–35.

Fennessey, C. M. & Keele, B. F. 2013 Using nonhuman primates to model HIV transmission. *Current opinion in HIV and AIDS* **8**, 280–287.

Fergusson, J. R., Morgan, M. D., Bruchard, M., Huitema, L., Heesters, B. A., van Unen, V., van Hamburg, J. P., van der Wel, N. N., Picavet, D., Koning, F., Tas, S. W., Anderson, M. S., Marioni, J. C., Holländer, G. A., & Spits, H. 2018 Maturing Human CD127+ CCR7+ PDL1+ Dendritic Cells Express AIRE in the Absence of Tissue Restricted Antigens. *Frontiers in Immunology* **9**, 2902.

Feuerer, M., Beckhove, P., Garbi, N., Mahnke, Y., Limmer, A., Hommel, M., Hämmerling, G. J., Kyewski, B., Hamann, A., Umansky, V., & Schirrmacher, V. 2003 Bone marrow as a priming site for T-cell responses to blood-borne antigen. *Nature Medicine* **9**, 1151–1157.

Finck, R., Simonds, E. F., Jager, A., Krishnaswamy, S., Sachs, K., Fantl, W., Pe'er, D., Nolan, G. P., & Bendall, S. C. 2013 Normalization of mass cytometry data with bead standards. *Cytometry. Part A: The Journal of the International Society for Analytical Cytology* **83**, 483–494.

Flower, D. R., Macdonald, I. K., Ramakrishnan, K., Davies, M. N., & Doytchinova, I. A. 2010 Computer aided selection of candidate vaccine antigens. *Immunome Research* **6 Suppl 2**, S1.

Foley, B., Cooley, S., Verneris, M. R., Pitt, M., Curtsinger, J., Luo, X., Lopez-Vergès, S., Lanier, L. L., Weisdorf, D., & Miller, J. S. 2012 Cytomegalovirus reactivation after allogeneic transplantation promotes a lasting increase in educated NKG2c+ natural killer cells with potent function. *Blood* **119**, 2665–2674.

Foster, S. L., Hargreaves, D. C., & Medzhitov, R. 2007 Gene-specific control of inflammation by TLR-induced chromatin modifications. *Nature* **447**, 972–978.

Fox, S., Leitch, A. E., Duffin, R., Haslett, C., & Rossi, A. G. 2010 Neutrophil apoptosis: relevance to the innate immune response and inflammatory disease. *Journal of Innate Immunity* **2**, 216–227.

Franchi, L., Warner, N., Viani, K., & Nuñez, G. 2009 Function of Nod-like receptors in microbial recognition and host defense. *Immunological Reviews* **227**, 106–128.

Frei, A. P., Bava, F.-A., Zunder, E. R., Hsieh, E. W. Y., Chen, S.-Y., Nolan, G. P., & Gherardini, P. F. 2016 Highly multiplexed simultaneous detection of RNAs and proteins in single cells. *Nature Methods* **13**, 269–275.

Freire, M. O. & Van Dyke, T. E. 2013 Natural resolution of inflammation. *Periodontology 2000* **63**, 149–164.

Freud, A. G., Mundy-Bosse, B. L., Yu, J., & Caligiuri, M. A. 2017 The Broad Spectrum of Human Natural Killer Cell Diversity. *Immunity* **47**, 820–833.

Fridlender, Z. G., Sun, J., Mishalian, I., Singhal, S., Cheng, G., Kapoor, V., Horng, W., Fridlender, G., Bayuh, R., Worthen, G. S., & Albelda, S. M. 2012 Transcriptomic analysis comparing tumor-associated neutrophils with granulocytic myeloid-derived suppressor cells and normal neutrophils. *PloS One* **7**, e31524.

Frimpong, A., Kusi, K. A., Ofori, M. F., & Ndifon, W. 2018 Novel Strategies for Malaria Vaccine Design. *Frontiers in Immunology* **9**, 2769.

Fulginiti, V. A., Papier, A., Lane, J. M., Neff, J. M., & Henderson, D. A. 2003a Smallpox vaccination: a review, part I. Background, vaccination technique, normal vaccination and revaccination, and expected normal reactions. *Clinical Infectious Diseases: An Official Publication of the Infectious Diseases Society of America* **37**, 241–250.

Fulginiti, V. A., Papier, A., Lane, J. M., Neff, J. M., & Henderson, D. A. 2003b Smallpox vaccination: a review, part II. Adverse events. *Clinical Infectious Diseases: An Official Publication of the Infectious Diseases Society of America* **37**, 251–271.

Furman, D. & Davis, M. M. 2015 New approaches to understanding the immune response to vaccination and infection. *Vaccine* **33**, 5271–5281.

Gabrilovich, D. I. & Nagaraj, S. 2009 Myeloid-derived suppressor cells as regulators of the immune system. *Nature Reviews. Immunology* **9**, 162–174.

Gabryšová, L., Howes, A., Saraiva, M., & O'Garra, A. 2014 The regulation of IL-10 expression. *Current Topics in Microbiology and Immunology* **380**, 157–190.

Galli, S. J., Borregaard, N., & Wynn, T. A. 2011 Phenotypic and functional plasticity of cells of innate immunity: macrophages, mast cells and neutrophils. *Nature Immunology* **12**, 1035–1044.

Gamliel, M., Goldman-Wohl, D., Isaacson, B., Gur, C., Stein, N., Yamin, R., Berger, M., Grunewald, M., Keshet, E., Rais, Y., Bornstein, C., David, E., Jelinski, A., Eisenberg, I., Greenfield, C., Ben-David, A., Imbar, T., Gilad, R., Haimov-Kochman, R., Mankuta, D., Elami-Suzin, M., Amit, I., Hanna, J. H., Yagel, S., & Mandelboim, O. 2018 Trained Memory of Human Uterine NK Cells Enhances Their Function in Subsequent Pregnancies. *Immunity* **48**, 951–962.e5.

Gao, N., Dang, T., & Yuan, D. 2001 IFN-gamma-dependent and -independent initiation of switch recombination by NK cells. *Journal of Immunology (Baltimore, Md.: 1950)* **167**, 2011–2018.

Gao, N., Jennings, P., & Yuan, D. 2008 Requirements for the natural killer cell-mediated induction of IgG1 and IgG2a expression in B lymphocytes. *International Immunology* **20**, 645–657.

Garcia-Valtanen, P., Guzman-Genuino, R. M., Williams, D. L., Hayball, J. D., & Diener, K. R. 2017 Evaluation of trained immunity by β-1, 3 (d)-glucan on murine monocytes in vitro and duration of response in vivo. *Immunology and Cell Biology* **95**, 601–610.

Gardner, M. B. & Luciw, P. A. 2008 Macaque models of human infectious disease. *ILAR journal* **49**, 220–255.

Gasteiger, G., Hemmers, S., Bos, P. D., Sun, J. C., & Rudensky, A. Y. 2013a IL-2-dependent adaptive control of NK cell homeostasis. *The Journal of Experimental Medicine* **210**, 1179–1187.

Gasteiger, G., Hemmers, S., Firth, M. A., Le Floc'h, A., Huse, M., Sun, J. C., & Rudensky, A. Y. 2013b IL-2-dependent tuning of NK cell sensitivity for target cells is controlled by regulatory T cells. *The Journal of Experimental Medicine* **210**, 1167–1178.

Gautreau, G., Pejoski, D., Le Grand, R., Cosma, A., Beignon, A.-S., & Tchitchek, N. 2017 SPADEVizR: an R package for visualization, analysis and integration of SPADE results. *Bioinformatics (Oxford, England)* **33**, 779–781.

Ge, M. Q., Ho, A. W. S., Tang, Y., Wong, K. H. S., Chua, B. Y. L., Gasser, S., & Kemeny, D. M. 2012 NK cells regulate CD8+ T cell priming and dendritic cell migration during influenza A infection by IFN-γ and perforin-dependent mechanisms. *Journal of Immunology (Baltimore, Md.: 1950)* **189**, 2099–2109.

Geginat, J., Paroni, M., Maglie, S., Alfen, J. S., Kastirr, I., Gruarin, P., De Simone, M., Pagani, M., & Abrignani, S. 2014 Plasticity of human CD4 T cell subsets. *Frontiers in Immunology* **5**, 630.

Geiger, T. L. & Sun, J. C. 2016 Development and maturation of natural killer cells. *Current Opinion in Immunology* **39**, 82–89.

Geretti, A. M. 1999 Simian immunodeficiency virus as a model of human HIV disease. *Reviews in Medical Virology* **9**, 57–67.

Gervassi, A., Lejarcegui, N., Dross, S., Jacobson, A., Itaya, G., Kidzeru, E., Gantt, S., Jaspan, H., & Horton, H. 2014 Myeloid derived suppressor cells are present at high frequency in neonates and suppress in vitro T cell responses. *PloS One* **9**, e107816.

Getahun, A. & Cambier, J. C. 2015 Of ITIMs, ITAMs, and ITAMis: revisiting immunoglobulin Fc receptor signaling. *Immunological Reviews* **268**, 66–73.

Gillard, G. O., Bivas-Benita, M., Hovav, A.-H., Grandpre, L. E., Panas, M. W., Seaman, M. S., Haynes, B. F., & Letvin, N. L. 2011 Thy1+ NK [corrected] cells from vaccinia virus-primed mice confer protection against vaccinia virus challenge in the absence of adaptive lymphocytes. *PLoS pathogens* **7**, e1002141.

Ginhoux, F. & Guilliams, M. 2016 Tissue-Resident Macrophage Ontogeny and Homeostasis. *Immunity* **44**, 439–449.

Glish, G. L. & Vachet, R. W. 2003 The basics of mass spectrometry in the twenty-first century. *Nature Reviews. Drug Discovery* **2**, 140–150.

Gonzalez-Mejia, M. E. & Doseff, A. I. 2009 Regulation of monocytes and macrophages cell fate. *Frontiers in Bioscience (Landmark Edition)* **14**, 2413–2431.

Good, Z., Sarno, J., Jager, A., Samusik, N., Aghaeepour, N., Simonds, E. F., White, L., Lacayo, N. J., Fantl, W. J., Fazio, G., Gaipa, G., Biondi, A., Tibshirani, R., Bendall, S. C., Nolan, G. P., & Davis, K. L. 2018 Single-cell developmental classification of B cell precursor acute lymphoblastic leukemia at diagnosis reveals predictors of relapse. *Nature Medicine* **24**, 474–483.

Goodridge, H. S., Ahmed, S. S., Curtis, N., Kollmann, T. R., Levy, O., Netea, M. G., Pollard, A. J., van Crevel, R., & Wilson, C. B. 2016 Harnessing the beneficial heterologous effects of vaccination. *Nature Reviews. Immunology* **16**, 392–400.

Goodyear, C. S. & Silverman, G. J. 2005 B cell superantigens: a microbe's answer to innate-like B cells and natural antibodies. *Springer Seminars in Immunopathology* **26**, 463–484.

Gordon, S. 2016 Phagocytosis: An Immunobiologic Process. *Immunity* **44**, 463–475.

Gordon, S. & Plüddemann, A. 2017 Tissue macrophages: heterogeneity and functions. *BMC biology* **15**, 53.

Gourbal, B., Pinaud, S., Beckers, G. J. M., Van Der Meer, J. W. M., Conrath, U., & Netea, M. G. 2018 Innate immune memory: An evolutionary perspective. *Immunological Reviews* **283**, 21–40.

Grandpre, L. E., Duke-Cohan, J. S., Ewald, B. A., Devoy, C., Barouch, D. H., Letvin, N. L., Reinherz, E. L., Baden, L. R., Dolin, R., & Seaman, M. S. 2009 Immunogenicity of recombinant Modified Vaccinia Ankara following a single or multi-dose vaccine regimen in rhesus monkeys. *Vaccine* **27**, 1549–1556.

Greenwood, B. 2014 The contribution of vaccination to global health: past, present and future. *Philosophical Transactions of the Royal Society of London. Series B, Biological Sciences* **369**, 20130433.

Guilliams, M., Dutertre, C.-A., Scott, C. L., McGovern, N., Sichien, D., Chakarov, S., Van Gassen, S., Chen, J., Poidinger, M., De Prijck, S., Tavernier, S. J., Low, I., Irac, S. E., Mattar, C. N., Sumatoh, H. R., Low, G. H. L., Chung, T. J. K., Chan, D. K. H., Tan, K. K., Hon, T. L. K., Fossum, E., Bogen, B., Choolani, M., Chan, J. K. Y., Larbi, A., Luche, H., Henri, S., Saeys, Y., Newell, E. W., Lambrecht, B. N., Malissen, B., & Ginhoux, F. 2016 Unsupervised High-Dimensional Analysis Aligns Dendritic Cells across Tissues and Species. *Immunity* **45**, 669–684.

Guirakhoo, F., Pugachev, K., Zhang, Z., Myers, G., Levenbook, I., Draper, K., Lang, J., Ocran, S., Mitchell, F., Parsons, M., Brown, N., Brandler, S., Fournier, C., Barrere, B., Rizvi, F., Travassos, A., Nichols, R., Trent, D., & Monath, T. 2004 Safety and efficacy of chimeric yellow Fever-dengue virus tetravalent vaccine formulations in nonhuman primates. *Journal of Virology* **78**, 4761–4775.

Guirakhoo, F., Weltzin, R., Chambers, T. J., Zhang, Z. X., Soike, K., Ratterree, M., Arroyo, J., Georgakopoulos, K., Catalan, J., & Monath, T. P. 2000 Recombinant chimeric yellow fever-dengue type 2 virus is immunogenic and protective in nonhuman primates. *Journal of Virology* **74**, 5477–5485.

Guy, B., Barban, V., Mantel, N., Aguirre, M., Gulia, S., Pontvianne, J., Jourdier, T.-M., Ramirez, L., Gregoire, V., Charnay, C., Burdin, N., Dumas, R., & Lang, J. 2009 Evaluation of interferences between dengue vaccine serotypes in a monkey model. *The American Journal of Tropical Medicine and Hygiene* **80**, 302–311.

Haghverdi, L., Büttner, M., Wolf, F. A., Buettner, F., & Theis, F. J. 2016 Diffusion pseudotime robustly reconstructs lineage branching. *Nature Methods* **13**, 845–848.

Haghverdi, L., Buettner, F., & Theis, F. J. 2015 Diffusion maps for high-dimensional single-cell analysis of differentiation data. *Bioinformatics (Oxford, England)* **31**, 2989–2998.

Halle, S., Halle, O., & Förster, R. 2017 Mechanisms and Dynamics of T Cell-Mediated Cytotoxicity In Vivo. *Trends in Immunology* **38**, 432–443.

Halstead, S. B. 2013 Identifying protective dengue vaccines: guide to mastering an empirical process. *Vaccine* **31**, 4501–4507.

Hamada, A., Torre, C., Drancourt, M., & Ghigo, E. 2018 Trained Immunity Carried by Non-immune Cells. *Frontiers in Microbiology* **9**, 3225.

Hammer, Q., Rückert, T., Borst, E. M., Dunst, J., Haubner, A., Durek, P., Heinrich, F., Gasparoni, G., Babic, M., Tomic, A., Pietra, G., Nienen, M., Blau, I. W., Hofmann, J., Na, I.-K., Prinz, I., Koenecke, C., Hemmati, P., Babel, N., Arnold, R., Walter, J., Thurley, K., Mashreghi, M.-F., Messerle, M., & Romagnani, C. 2018 Peptide-specific recognition of human cytomegalovirus strains controls adaptive natural killer cells. *Nature Immunology* **19**, 453–463.

Hansmann, L., Blum, L., Ju, C.-H., Liedtke, M., Robinson, W. H., & Davis, M. M. 2015 Mass cytometry analysis shows that a novel memory phenotype B cell is expanded in multiple myeloma. *Cancer Immunology Research* **3**, 650–660.

Hatziioannou, T. & Evans, D. T. 2012 Animal models for HIV/AIDS research. *Nature Reviews. Microbiology* **10**, 852–867.

Hayakawa, Y., Andrews, D. M., & Smyth, M. J. 2010 Subset analysis of human and mouse mature NK cells. *Methods in Molecular Biology (Clifton, N.J.)* **612**, 27–38.

He, X.-S., Draghi, M., Mahmood, K., Holmes, T. H., Kemble, G. W., Dekker, C. L., Arvin, A. M., Parham, P., & Greenberg, H. B. 2004 T cell-dependent production of IFN-gamma by NK cells in response to influenza A virus. *The Journal of Clinical Investigation* **114**, 1812–1819.

Headland, S. E. & Norling, L. V. 2015 The resolution of inflammation: Principles and challenges. *Seminars in Immunology* **27**, 149–160.

Heesters, B. A., van der Poel, C. E., Das, A., & Carroll, M. C. 2016 Antigen Presentation to B Cells. *Trends in Immunology* **37**, 844–854.

Heremans, H., Dillen, C., Groenen, M., Martens, E., & Billiau, A. 1996 Chronic relapsing experimental autoimmune encephalomyelitis (CREAE) in mice: enhancement by monoclonal antibodies against interferon-gamma. *European Journal of Immunology* **26**, 2393–2398.

Hisaeda, H., Yasutomo, K., & Himeno, K. 2005 Malaria: immune evasion by parasites. *The International Journal of Biochemistry & Cell Biology* **37**, 700–706.

Höllt, T., Pezzotti, N., Unen, V. v., Koning, F., Eisemann, E., Lelieveldt, B., & Vilanova, A. 2016 Cytosplore: Interactive Immune Cell Phenotyping for Large Single-Cell Datasets. *Computer Graphics Forum* **35**, 171–180.

HogenEsch, H. 2002 Mechanisms of stimulation of the immune response by aluminum adjuvants. *Vaccine* **20 Suppl 3**, S34–39.

Hong, H. S., Rajakumar, P. A., Billingsley, J. M., Reeves, R. K., & Johnson, R. P. 2013 No monkey business: why studying NK cells in non-human primates pays off. *Frontiers in Immunology* **4**, 32.

Horowitz, A., Behrens, R. H., Okell, L., Fooks, A. R., & Riley, E. M. 2010 NK cells as effectors of acquired immune responses: effector CD4+ T cell-dependent activation of NK cells following vaccination. *Journal of Immunology (Baltimore, Md.: 1950)* **185**, 2808–2818.

Horowitz, A., Strauss-Albee, D. M., Leipold, M., Kubo, J., Nemat-Gorgani, N., Dogan, O. C., Dekker, C. L., Mackey, S., Maecker, H., Swan, G. E., Davis, M. M., Norman, P. J., Guethlein, L. A., Desai, M., Parham, P., & Blish, C. A. 2013 Genetic and environmental determinants of human NK cell diversity revealed by mass cytometry. *Science Translational Medicine* **5**, 208ra145.

Hoving, J. C., Wilson, G. J., & Brown, G. D. 2014 Signalling C-type lectin receptors, microbial recognition and immunity. *Cellular Microbiology* **16**, 185–194.

Huang, B., Pan, P.-Y., Li, Q., Sato, A. I., Levy, D. E., Bromberg, J., Divino, C. M., & Chen, S.-H. 2006 Gr-1+CD115+ immature myeloid suppressor cells mediate the development of tumor-induced T regulatory cells and T-cell anergy in tumor-bearing host. *Cancer Research* **66**, 1123–1131.

Hur, S. 2019 Double-Stranded RNA Sensors and Modulators in Innate Immunity. *Annual Review of Immunology* **37**, 349–375.

Ifrim, D. C., Quintin, J., Joosten, L. A. B., Jacobs, C., Jansen, T., Jacobs, L., Gow, N. A. R., Williams, D. L., van der Meer, J. W. M., & Netea, M. G. 2014 Trained immunity or tolerance: opposing functional programs induced in human monocytes after engagement of various pattern recognition receptors. *Clinical and vaccine immunology: CVI* **21**, 534–545.

Iwasaki, A. & Pillai, P. S. 2014 Innate immunity to influenza virus infection. *Nature Reviews. Immunology* **14**, 315–328.

Iyer, S. S. & Amara, R. R. 2014 DNA/MVA Vaccines for HIV/AIDS. *Vaccines* **2**, 160–178.

Jackson, L. A., Frey, S. E., El Sahly, H. M., Mulligan, M. J., Winokur, P. L., Kotloff, K. L., Campbell, J. D., Atmar, R. L., Graham, I., Anderson, E. J., Anderson, E. L., Patel, S. M., Fields, C., Keitel, W., Rouphael, N., Hill, H., & Goll, J. B. 2017 Safety and immunogenicity of a modified vaccinia Ankara vaccine using three immunization schedules and two modes of delivery: A randomized clinical non-inferiority trial. *Vaccine* **35**, 1675–1682.

Jacobs, B. L., Langland, J. O., Kibler, K. V., Denzler, K. L., White, S. D., Holechek, S. A., Wong, S., Huynh, T., & Baskin, C. R. 2009 Vaccinia virus vaccines: past, present and future. *Antiviral Research* **84**, 1–13.

Jensen, K., Dela Pena-Ponce, M. G., Piatak, M., Shoemaker, R., Oswald, K., Jacobs, W. R., Fennelly, G., Lucero, C., Mollan, K. R., Hudgens, M. G., Amedee, A., Kozlowski, P. A., Estes, J. D., Lifson, J. D., Van Rompay, K. K. A., Larsen, M., & De Paris, K. 2017 Balancing Trained Immunity with Persistent Immune Activation and the Risk of Simian Immunodeficiency Virus Infection in Infant Macaques Vaccinated with Attenuated Mycobacterium tuberculosis or Mycobacterium bovis BCG Vaccine. *Clinical and vaccine immunology: CVI* **24**.

Johnson, K. E. & Wilgus, T. A. 2014 Vascular Endothelial Growth Factor and Angiogenesis in the Regulation of Cutaneous Wound Repair. *Advances in Wound Care* **3**, 647–661.

Johnston, C. J. C., Smyth, D. J., Dresser, D. W., & Maizels, R. M. 2016 TGF-β in tolerance, development and regulation of immunity. *Cellular Immunology* **299**, 14–22.

Jones, D. I., McGee, C. E., Sample, C. J., Sempowski, G. D., Pickup, D. J., & Staats, H. F. 2016 Modified Vaccinia Ankara Virus Vaccination Provides Long-Term Protection against Nasal Rabbitpox Virus Challenge. *Clinical and vaccine immunology: CVI* **23**, 648–651.

Josefowicz, S. Z., Lu, L.-F., & Rudensky, A. Y. 2012 Regulatory T cells: mechanisms of differentiation and function. *Annual Review of Immunology* **30**, 531–564.

Jost, S. & Altfeld, M. 2012 Evasion from NK cell-mediated immune responses by HIV-1. *Microbes and Infection* **14**, 904–915.

Jost, S., Tomezsko, P. J., Rands, K., Toth, I., Lichterfeld, M., Gandhi, R. T., & Altfeld, M. 2014 CD4+ T-cell help enhances NK cell function following therapeutic HIV-1 vaccination. *Journal of Virology* **88**, 8349–8354.

Julander, J. G., Testori, M., Cheminay, C., & Volkmann, A. 2018 Immunogenicity and Protection After Vaccination With a Modified Vaccinia Virus Ankara-Vectored Yellow Fever Vaccine in the Hamster Model. *Frontiers in Immunology* **9**, 1756.

Kabelitz, D., Wesch, D., & Oberg, H.-H. 2006 Regulation of regulatory T cells: role of dendritic cells and toll-like receptors. *Critical Reviews in Immunology* **26**, 291–306.

Kadoki, M., Patil, A., Thaiss, C. C., Brooks, D. J., Pandey, S., Deep, D., Alvarez, D., von Andrian, U. H., Wagers, A. J., Nakai, K., Mikkelsen, T. S., Soumillon, M., & Chevrier, N. 2017 Organism-Level Analysis of Vaccination Reveals Networks of Protection across Tissues. *Cell* **171**, 398–413.e21.

Kamimura, Y. & Lanier, L. L. 2015 Homeostatic control of memory cell progenitors in the natural killer cell lineage. *Cell Reports* **10**, 280–291.

Kanneganti, T.-D., Lamkanfi, M., & Núñez, G. 2007 Intracellular NOD-like receptors in host defense and disease. *Immunity* **27**, 549–559.

Kaplan, M. J. & Radic, M. 2012 Neutrophil extracellular traps: double-edged swords of innate immunity. *Journal of Immunology (Baltimore, Md.: 1950)* **189**, 2689–2695.

Kaufmann, E., Sanz, J., Dunn, J. L., Khan, N., Mendonça, L. E., Pacis, A., Tzelepis, F., Pernet, E., Dumaine, A., Grenier, J.-C., Mailhot-Léonard, F., Ahmed, E., Belle, J., Besla, R., Mazer, B., King, I. L., Nijnik, A., Robbins, C. S., Barreiro, L. B., & Divangahi, M. 2018 BCG Educates Hematopoietic Stem Cells to Generate Protective Innate Immunity against Tuberculosis. *Cell* **172**, 176–190.e19.

Kawamoto, Y., Kawamoto, S., Matsubayashi, K., Nozawa, K., Watanabe, T., Stanley, M.-A., & Perwitasari-Farajallah, D. 2008 Genetic diversity of longtail macaques (Macaca fascicularis) on the island of Mauritius: an assessment of nuclear and mitochondrial DNA polymorphisms. *Journal of Medical Primatology* **37**, 45–54.

Kelley, J., Walter, L., & Trowsdale, J. 2005 Comparative genomics of natural killer cell receptor gene clusters. *PLoS genetics* **1**, 129–139.

Kelly, J. M., Darcy, P. K., Markby, J. L., Godfrey, D. I., Takeda, K., Yagita, H., & Smyth, M. J. 2002 Induction of tumor-specific T cell memory by NK cell-mediated tumor rejection. *Nature Immunology* **3**, 83–90.

Kennedy, R. B., Ovsyannikova, I. G., Haralambieva, I. H., O'Byrne, M. M., Jacobson, R. M., Pankratz, V. S., & Poland, G. A. 2012 Multigenic control of measles vaccine immunity mediated by polymorphisms in measles receptor, innate pathway, and cytokine genes. *Vaccine* **30**, 2159–2167.

Kennedy, R. B., Ovsyannikova, I. G., Jacobson, R. M., & Poland, G. A. 2009 The immunology of smallpox vaccines. *Current Opinion in Immunology* **21**, 314–320.

Kimura, T., McKolanis, J. R., Dzubinski, L. A., Islam, K., Potter, D. M., Salazar, A. M., Schoen, R. E., & Finn, O. J. 2013 MUC1 vaccine for individuals with advanced adenoma of the colon: a cancer immunoprevention feasibility study. *Cancer Prevention Research (Philadelphia, Pa.)* **6**, 18–26.

Kipp, M., Nyamoya, S., Hochstrasser, T., & Amor, S. 2017 Multiple sclerosis animal models: a clinical and histopathological perspective. *Brain Pathology (Zurich, Switzerland)* **27**, 123–137.

Kiripolsky, J., McCabe, L. G., & Kramer, J. M. 2017 Innate immunity in Sjögren's syndrome. *Clinical Immunology (Orlando, Fla.)* **182**, 4–13.

Klechevsky, E., Morita, R., Liu, M., Cao, Y., Coquery, S., Thompson-Snipes, L., Briere, F., Chaussabel, D., Zurawski, G., Palucka, A. K., Reiter, Y., Banchereau, J., & Ueno, H. 2008 Functional specializations of human epidermal Langerhans cells and CD14+ dermal dendritic cells. *Immunity* **29**, 497–510.

Kleinnijenhuis, J., Quintin, J., Preijers, F., Benn, C. S., Joosten, L. A. B., Jacobs, C., van Loenhout, J., Xavier, R. J., Aaby, P., van der Meer, J. W. M., van Crevel, R., & Netea, M. G. 2014a Long-lasting effects of BCG vaccination on both heterologous Th1/Th17 responses and innate trained immunity. *Journal of Innate Immunity* **6**, 152–158.

Kleinnijenhuis, J., Quintin, J., Preijers, F., Joosten, L. A. B., Ifrim, D. C., Saeed, S., Jacobs, C., van Loenhout, J., de Jong, D., Stunnenberg, H. G., Xavier, R. J., van der Meer, J. W. M., van Crevel, R., & Netea, M. G. 2012 Bacille Calmette-Guerin induces NOD2-dependent nonspecific protection from reinfection via epigenetic reprogramming of monocytes. *Proceedings of the National Academy of Sciences of the United States of America* **109**, 17537–17542.

Kleinnijenhuis, J., Quintin, J., Preijers, F., Joosten, L. A. B., Jacobs, C., Xavier, R. J., van der Meer, J. W. M., van Crevel, R., & Netea, M. G. 2014b BCG-induced trained immunity in NK cells: Role for non-specific protection to infection. *Clinical Immunology (Orlando, Fla.)* **155**, 213–219.

Kleinsteuber, K., Corleis, B., Rashidi, N., Nchinda, N., Lisanti, A., Cho, J. L., Medoff, B. D., Kwon, D., & Walker, B. D. 2016 Standardization and quality control for high-dimensional mass cytometry studies of human samples. *Cytometry. Part A: The Journal of the International Society for Analytical Cytology* **89**, 903–913.

Klos, A., Tenner, A. J., Johswich, K.-O., Ager, R. R., Reis, E. S., & Köhl, J. 2009 The role of the anaphylatoxins in health and disease. *Molecular Immunology* **46**, 2753–2766.

Knapp, D. J. H. F., Kannan, N., Pellacani, D., & Eaves, C. J. 2017 Mass Cytometric Analysis Reveals Viable Activated Caspase-3+ Luminal Progenitors in the Normal Adult Human Mammary Gland. *Cell Reports* **21**, 1116–1126.

Knitlova, J., Hajkova, V., Voska, L., Elsterova, J., Obrova, B., & Melkova, Z. 2014 Development of eczema vaccinatum in atopic mouse models and efficacy of MVA vaccination against lethal poxviral infection. *PloS One* **9**, e114374.

Koch, U. & Radtke, F. 2011 Mechanisms of T cell development and transformation. *Annual Review of Cell and Developmental Biology* **27**, 539–562.

Kohl, K., Schnautz, S., Pesch, M., Klein, E., Aumailley, M., Bieber, T., & Koch, S. 2007 Subpopulations of human dendritic cells display a distinct phenotype and bind differentially to proteins of the extracellular matrix. *European Journal of Cell Biology* **86**, 719–730.

Kolodziejczyk, A. A., Kim, J. K., Svensson, V., Marioni, J. C., & Teichmann, S. A. 2015 The technology and biology of single-cell RNA sequencing. *Molecular Cell* **58**, 610–620.

Kondělková, K., Vokurková, D., Krejsek, J., Borská, L., Fiala, Z., & Ctirad, A. 2010 Regulatory T cells (TREG) and their roles in immune system with respect to immunopathological disorders. *Acta Medica (Hradec Kralove)* **53**, 73–77.

Korsholm, K. S., Petersen, R. V., Agger, E. M., & Andersen, P. 2010 T-helper 1 and T-helper 2 adjuvants induce distinct differences in the magnitude, quality and kinetics of the early inflammatory response at the site of injection. *Immunology* **129**, 75–86.

Krebs, P., Barnes, M. J., Lampe, K., Whitley, K., Bahjat, K. S., Beutler, B., Janssen, E., & Hoebe, K. 2009 NK-cell-mediated killing of target cells triggers robust antigen-specific T-cell-mediated and humoral responses. *Blood* **113**, 6593–6602.

Kumar, N., Chahroudi, A., & Silvestri, G. 2016 Animal models to achieve an HIV cure. *Current opinion in HIV and AIDS* **11**, 432–441.

Kunicki, M. A., Amaya Hernandez, L. C., Davis, K. L., Bacchetta, R., & Roncarolo, M.-G. 2018 Identity and Diversity of Human Peripheral Th and T Regulatory Cells Defined by Single-Cell Mass Cytometry. *Journal of Immunology (Baltimore, Md.: 1950)* **200**, 336–346.

Kwissa, M., Nakaya, H. I., Oluoch, H., & Pulendran, B. 2012 Distinct TLR adjuvants differentially stimulate systemic and local innate immune responses in nonhuman primates. *Blood* **119**, 2044–2055.

Lahaye, X., Gentili, M., Silvin, A., Conrad, C., Picard, L., Jouve, M., Zueva, E., Maurin, M., Nadalin, F., Knott, G. J., Zhao, B., Du, F., Rio, M., Amiel, J., Fox, A. H., Li, P., Etienne, L., Bond, C. S., Colleaux, L., & Manel, N. 2018 NONO Detects the Nuclear HIV Capsid to Promote cGAS-Mediated Innate Immune Activation. *Cell* **175**, 488–501.e22.

Lanier, L. L. 1998 NK cell receptors. *Annual Review of Immunology* **16**, 359–393.

Laudanski, K., Stentz, M., DiMeglio, M., Furey, W., Steinberg, T., & Patel, A. 2018 Potential Pitfalls of the Humanized Mice in Modeling Sepsis. *International Journal of Inflammation* **2018**, 6563454.

Laurenti, E. & Göttgens, B. 2018 From haematopoietic stem cells to complex differentiation landscapes. *Nature* **553**, 418–426.

Lee, S.-H., Kim, K.-S., Fodil-Cornu, N., Vidal, S. M., & Biron, C. A. 2009 Activating receptors promote NK cell expansion for maintenance, IL-10 production, and CD8 T cell regulation during viral infection. *The Journal of Experimental Medicine* **206**, 2235–2251.

Leentjens, J., Bekkering, S., Joosten, L. A. B., Netea, M. G., Burgner, D. P., & Riksen, N. P. 2018 Trained Innate Immunity as a Novel Mechanism Linking Infection and the Development of Atherosclerosis. *Circulation Research* **122**, 664–669.

Lehmann, M. H., Kastenmuller, W., Kandemir, J. D., Brandt, F., Suezer, Y., & Sutter, G. 2009 Modified vaccinia virus ankara triggers chemotaxis of monocytes and early respiratory immigration of leukocytes by induction of CCL2 expression. *Journal of Virology* **83**, 2540–2552.

Leipold, M. D., Obermoser, G., Fenwick, C., Kleinstuber, K., Rashidi, N., McNevin, J. P., Nau, A. N., Wagar, L. E., Rozot, V., Davis, M. M., DeRosa, S., Pantaleo, G., Scriba, T. J., Walker, B. D., Olsen, L. R., & Maecker, H. T. 2018 Comparison of CyTOF assays across sites: Results of a six-center pilot study. *Journal of Immunological Methods* **453**, 37–43.

Leung-Theung-Long, S., Coupet, C.-A., Gouanvic, M., Schmitt, D., Ray, A., Hoffmann, C., Schultz, H., Tyagi, S., Soni, H., Converse, P. J., Arias, L., Kleinpeter, P., Sansas, B., Mdluli, K., Vilaplana, C., Cardona, P.-J., Nuermberger, E., Marchand, J.-B., Silvestre, N., & Inchauspé, G. 2018 A multi-antigenic MVA vaccine increases efficacy of combination chemotherapy against Mycobacterium tuberculosis. *PloS One* **13**, e0196815.

Levinson, A. I., Kozlowski, L., Zheng, Y., & Wheatley, L. 1995 B-cell superantigens: definition and potential impact on the immune response. *Journal of Clinical Immunology* **15**, 26S–36S.

Lewis, S. M., Treacher, D. F., Edgeworth, J., Mahalingam, G., Brown, C. S., Mare, T. A., Stacey, M., Beale, R., & Brown, K. A. 2015 Expression of CD11c and EMR2 on neutrophils: potential diagnostic biomarkers for sepsis and systemic inflammation. *Clinical and Experimental Immunology* **182**, 184–194.

Li, X., Shu, C., Yi, G., Chaton, C. T., Shelton, C. L., Diao, J., Zuo, X., Kao, C. C., Herr, A. B., & Li, P. 2013 Cyclic GMP-AMP synthase is activated by double-stranded DNA-induced oligomerization. *Immunity* **39**, 1019–1031.

Li, Z., Jackson, R. J., & Ranasinghe, C. 2018 Vaccination route can significantly alter the innate lymphoid cell subsets: a feedback between IL-13 and IFN-γ. *NPJ vaccines* **3**, 10.

Lillacci, G. & Khammash, M. 2013 The signal within the noise: efficient inference of stochastic gene regulation models using fluorescence histograms and stochastic simulations. *Bioinformatics (Oxford, England)* **29**, 2311–2319.

Lin, A., Liang, F., Thompson, E. A., Vono, M., Ols, S., Lindgren, G., Hassett, K., Salter, H., Ciaramella, G., & Loré, K. 2018 Rhesus Macaque Myeloid-Derived Suppressor Cells Demonstrate T Cell Inhibitory Functions and Are Transiently Increased after Vaccination. *Journal of Immunology (Baltimore, Md.: 1950)* **200**, 286–294.

Lin, A. & Loré, K. 2017 Granulocytes: New Members of the Antigen-Presenting Cell Family. *Frontiers in Immunology* **8**, 1781.

Lin, P. L., Rodgers, M., Smith, L., Bigbee, M., Myers, A., Bigbee, C., Chiosea, I., Capuano, S. V., Fuhrman, C., Klein, E., & Flynn, J. L. 2009 Quantitative comparison of active and latent tuberculosis in the cynomolgus macaque model. *Infection and Immunity* **77**, 4631–4642.

Lingblom, C. M. D., Kowli, S., Swaminathan, N., Maecker, H. T., & Lambert, S. L. 2018 Baseline immune profile by CyTOF can predict response to an investigational adjuvanted vaccine in elderly adults. *Journal of Translational Medicine* **16**, 153.

Liu, Y. J., Kanzler, H., Soumelis, V., & Gilliet, M. 2001 Dendritic cell lineage, plasticity and cross-regulation. *Nature Immunology* **2**, 585–589.

Loo, Y.-M. & Gale, M. 2011 Immune signaling by RIG-I-like receptors. *Immunity* **34**, 680–692.

Lopez-Vergès, S., Milush, J. M., Schwartz, B. S., Pando, M. J., Jarjoura, J., York, V. A., Houchins, J. P., Miller, S., Kang, S.-M., Norris, P. J., Nixon, D. F., & Lanier, L. L. 2011 Expansion of a unique CD57^{+}NKG2chi natural killer cell subset during acute human cytomegalovirus infection. *Proceedings of the National Academy of Sciences of the United States of America* **108**, 14725–14732.

Lu, X., Nagata, M., & Yamasaki, S. 2018 Mincle: 20 years of a versatile sensor of insults. *International Immunology* **30**, 233–239.

Lublin, F. D., Knobler, R. L., Kalman, B., Goldhaber, M., Marini, J., Perrault, M., D'Imperio, C., Joseph, J., Alkan, S. S., & Korngold, R. 1993 Monoclonal anti-gamma interferon antibodies enhance experimental allergic encephalomyelitis. *Autoimmunity* **16**, 267–274.

Lund, F. E. 2008 Cytokine-producing B lymphocytes-key regulators of immunity. *Current Opinion in Immunology* **20**, 332–338.

Lynch, R. M., Yamamoto, T., & McDermott, A. B. 2013 HIV vaccine research and discovery in the nonhuman primates model: a unified theory in acquisition prevention and control of SIV infection. *Current opinion in HIV and AIDS* **8**, 288–294.

Maaten, L. v. d. & Hinton, G. 2008 Visualizing Data using t-SNE. *Journal of Machine Learning Research* **9**, 2579–2605.

MacLeod, M. K. L., Kappler, J. W., & Marrack, P. 2010 Memory CD4 T cells: generation, reactivation and re-assignment. *Immunology* **130**, 10–15.

Maiello, P., DiFazio, R. M., Cadena, A. M., Rodgers, M. A., Lin, P. L., Scanga, C. A., & Flynn, J. L. 2018 Rhesus Macaques Are More Susceptible to Progressive Tuberculosis than Cynomolgus Macaques: a Quantitative Comparison. *Infection and Immunity* **86**.

Mamessier, E., Sylvain, A., Thibult, M.-L., Houvenaeghel, G., Jacquemier, J., Castellano, R., Gonçalves, A., André, P., Romagné, F., Thibault, G., Viens, P., Birnbaum, D., Bertucci, F., Moretta, A., & Olive, D. 2011 Human breast cancer cells enhance self tolerance by promoting evasion from NK cell antitumor immunity. *The Journal of Clinical Investigation* **121**, 3609–3622.

Manz, M. G., Traver, D., Miyamoto, T., Weissman, I. L., & Akashi, K. 2001 Dendritic cell potentials of early lymphoid and myeloid progenitors. *Blood* **97**, 3333–3341.

Marini, O., Costa, S., Bevilacqua, D., Calzetti, F., Tamassia, N., Spina, C., De Sabata, D., Tinazzi, E., Lunardi, C., Scupoli, M. T., Cavallini, C., Zoratti, E., Tinazzi, I., Marchetta, A., Vassanelli, A., Cantini, M., Gandini, G., Ruzzenente, A., Guglielmi, A., Missale, F., Vermi, W., Tecchio, C., Cassatella, M. A., & Scapini, P. 2017 Mature CD10+ and immature CD10- neutrophils present in G-CSF-treated donors display opposite effects on T cells. *Blood* **129**, 1343–1356.

Marrack, P., Scott-Browne, J., & MacLeod, M. K. L. 2010 Terminating the immune response. *Immunological Reviews* **236**, 5–10.

Martin, C., Burdon, P. C. E., Bridger, G., Gutierrez-Ramos, J. C., Williams, T. J., & Rankin, S. M. 2003 Chemokines acting via CXCR2 and CXCR4 control the release of neutrophils from the bone marrow and their return following senescence. *Immunity* **19**, 583–593.

Martinez, F. O. & Gordon, S. 2014 The M1 and M2 paradigm of macrophage activation: time for reassessment. *F1000prime Reports* **6**, 13.

Martinez, J., Huang, X., & Yang, Y. 2010 Direct TLR2 signaling is critical for NK cell activation and function in response to vaccinia viral infection. *PLoS pathogens* **6**, e1000811.

Martinon, F., Brochard, P., Ripaux, M., Delache, B., Aurégan, G., Vaslin, B., & Le Grand, R. 2008 Improved protection against simian immunodeficiency virus mucosal challenge in macaques primed with a DNA vaccine and boosted with the recombinant modified vaccinia virus Ankara and recombinant Semliki Forest virus. *Vaccine* **26**, 532–545.

Martins, K. A. O., Steffens, J. T., van Tongeren, S. A., Wells, J. B., Bergeron, A. A., Dickson, S. P., Dye, J. M., Salazar, A. M., & Bavari, S. 2014 Toll-like receptor agonist augments virus-like particle-mediated protection from Ebola virus with transient immune activation. *PloS One* **9**, e89735.

Martín-Fontecha, A., Thomsen, L. L., Brett, S., Gerard, C., Lipp, M., Lanzavecchia, A., & Sallusto, F. 2004 Induced recruitment of NK cells to lymph nodes provides IFN-gamma for T(H)1 priming. *Nature Immunology* **5**, 1260–1265.

Mason, G. M., Lowe, K., Melchiotti, R., Ellis, R., de Rinaldis, E., Peakman, M., Heck, S., Lombardi, G., & Tree, T. I. M. 2015 Phenotypic Complexity of the Human Regulatory T Cell Compartment Revealed by Mass Cytometry. *Journal of Immunology (Baltimore, Md.: 1950)* **195**, 2030–2037.

Masopust, D., Ha, S.-J., Vezys, V., & Ahmed, R. 2006 Stimulation history dictates memory CD8 T cell phenotype: implications for prime-boost vaccination. *Journal of Immunology (Baltimore, Md.: 1950)* **177**, 831–839.

Massaia, A., Chaves, P., Samari, S., Miragaia, R. J., Meyer, K., Teichmann, S. A., & Noseda, M. 2018 Single Cell Gene Expression to Understand the Dynamic Architecture of the Heart. *Frontiers in Cardiovascular Medicine* **5**, 167.

Mauri, C. & Menon, M. 2015 The expanding family of regulatory B cells. *International Immunology* **27**, 479–486.

McAleer, J. P. & Vella, A. T. 2010 Educating CD4 T cells with vaccine adjuvants: lessons from lipopolysaccharide. *Trends in Immunology* **31**, 429–435.

McArthur, M. A., Sztein, M. B., & Edelman, R. 2013 Dengue vaccines: recent developments, ongoing challenges and current candidates. *Expert Review of Vaccines* **12**, 933–953.

McEwan, W. A., Tam, J. C. H., Watkinson, R. E., Bidgood, S. R., Mallery, D. L., & James, L. C. 2013 Intracellular antibody-bound pathogens stimulate immune signaling via the Fc receptor TRIM21. *Nature Immunology* **14**, 327–336.

McFadden, G. 2005 Poxvirus tropism. *Nature Reviews. Microbiology* **3**, 201–213.

McNab, F., Mayer-Barber, K., Sher, A., Wack, A., & O'Garra, A. 2015 Type I interferons in infectious disease. *Nature Reviews. Immunology* **15**, 87–103.

Medzhitov, R. 2001 Toll-like receptors and innate immunity. *Nature Reviews. Immunology* **1**, 135–145.

Merle, N. S., Church, S. E., Fremeaux-Bacchi, V., & Roumenina, L. T. 2015a Complement System Part I - Molecular Mechanisms of Activation and Regulation. *Frontiers in Immunology* **6**, 262.

Merle, N. S., Noe, R., Halbwachs-Mecarelli, L., Fremeaux-Bacchi, V., & Roumenina, L. T. 2015b Complement System Part II: Role in Immunity. *Frontiers in Immunology* **6**, 257.

Messaoudi, I., Estep, R., Robinson, B., & Wong, S. W. 2011 Nonhuman primate models of human immunology. *Antioxidants & Redox Signaling* **14**, 261–273.

Mestas, J. & Hughes, C. C. W. 2004 Of mice and not men: differences between mouse and human immunology. *Journal of Immunology (Baltimore, Md.: 1950)* **172**, 2731–2738.

Metzger, R. N., Krug, A. B., & Eisenächer, K. 2018 Enteric Virome Sensing-Its Role in Intestinal Homeostasis and Immunity. *Viruses* **10**.

Meyer, H., Sutter, G., & Mayr, A. 1991 Mapping of deletions in the genome of the highly attenuated vaccinia virus MVA and their influence on virulence. *The Journal of General Virology* **72 (Pt 5)**, 1031–1038.

Michel, T., Hentges, F., & Zimmer, J. 2012 Consequences of the crosstalk between monocytes/macrophages and natural killer cells. *Frontiers in Immunology* **3**, 403.

Min-Oo, G., Kamimura, Y., Hendricks, D. W., Nabekura, T., & Lanier, L. L. 2013 Natural killer cells: walking three paths down memory lane. *Trends in Immunology* **34**, 251–258.

Misra, A., Thippeshappa, R., & Kimata, J. T. 2013 Macaques as model hosts for studies of HIV-1 infection. *Frontiers in Microbiology* **4**, 176.

Mitroulis, I., Ruppova, K., Wang, B., Chen, L.-S., Grzybek, M., Grinenko, T., Eugster, A., Troullinaki, M., Palladini, A., Kourtzelis, I., Chatzigeorgiou, A., Schlitzer, A., Beyer, M., Joosten, L. A. B., Isermann, B., Lesche, M., Petzold, A., Simons, K., Henry, I., Dahl, A., Schultze, J. L., Wielockx, B., Zamboni, N., Mirtschink, P., Coskun, n., Hajishengallis, G., Netea, M. G., & Chavakis, T. 2018 Modulation of Myelopoiesis Progenitors Is an Integral Component of Trained Immunity. *Cell* **172**, 147–161.e12.

Mocikat, R., Braumüller, H., Gumy, A., Egeter, O., Ziegler, H., Reusch, U., Bubeck, A., Louis, J., Mailhammer, R., Riethmüller, G., Koszinowski, U., & Röcken, M. 2003 Natural killer cells activated by MHC class I(low) targets prime dendritic cells to induce protective CD8 T cell responses. *Immunity* **19**, 561–569.

Moorlag, S. J. C. F. M., Röring, R. J., Joosten, L. A. B., & Netea, M. G. 2018 The role of the interleukin-1 family in trained immunity. *Immunological Reviews* **281**, 28–39.

Moss, B. 2006 Poxvirus entry and membrane fusion. *Virology* **344**, 48–54.

Moss, B. 2011 Smallpox vaccines: targets of protective immunity. *Immunological Reviews* **239**, 8–26.

Mourits, V. P., Wijkmans, J. C., Joosten, L. A., & Netea, M. G. 2018 Trained immunity as a novel therapeutic strategy. *Current Opinion in Pharmacology* **41**, 52–58.

Mrdjen, D., Pavlovic, A., Hartmann, F. J., Schreiner, B., Utz, S. G., Leung, B. P., Lelios, I., Heppner, F. L., Kipnis, J., Merkler, D., Greter, M., & Becher, B. 2018 High-Dimensional Single-Cell Mapping of Central Nervous System Immune Cells Reveals Distinct Myeloid Subsets in Health, Aging, and Disease. *Immunity* **48**, 380–395.e6.

Musich, T., Rahman, M. A., Mohanram, V., Miller-Novak, L., Demberg, T., Venzon, D. J., Felber, B. K., Franchini, G., Pavlakis, G. N., & Robert-Guroff, M. 2018 Neutrophil Vaccination Dynamics and Their Capacity To Mediate B Cell Help in Rhesus Macaques. *Journal of Immunology (Baltimore, Md.: 1950)* **201**, 2287–2302.

Nabekura, T. & Lanier, L. L. 2016 Tracking the fate of antigen-specific versus cytokine-activated natural killer cells after cytomegalovirus infection. *The Journal of Experimental Medicine* **213**, 2745–2758.

Nair, N., Newell, E. W., Vollmers, C., Quake, S. R., Morton, J. M., Davis, M. M., He, X. S., & Greenberg, H. B. 2016 High-dimensional immune profiling of total and rotavirus VP6-specific intestinal and circulating B cells by mass cytometry. *Mucosal Immunology* **9**, 68–82.

Nakaya, H. I., Hagan, T., Duraisingham, S. S., Lee, E. K., Kwissa, M., Rouphael, N., Frasca, D., Gersten, M., Mehta, A. K., Gaujoux, R., Li, G.-M., Gupta, S., Ahmed, R., Mulligan, M. J., Shen-Orr, S., Blomberg, B. B., Subramaniam, S., & Pulendran, B. 2015 Systems Analysis of Immunity to Influenza Vaccination across Multiple Years and in Diverse Populations Reveals Shared Molecular Signatures. *Immunity* **43**, 1186–1198.

Narni-Mancinelli, E., Campisi, L., Bassand, D., Cazareth, J., Gounon, P., Glaichenhaus, N., & Lauvau, G. 2007 Memory CD8+ T cells mediate antibacterial immunity via CCL3 activation of TNF/ROI+ phagocytes. *The Journal of Experimental Medicine* **204**, 2075–2087.

Neefjes, J., Jongsma, M. L. M., Paul, P., & Bakke, O. 2011 Towards a systems understanding of MHC class I and MHC class II antigen presentation. *Nature Reviews. Immunology* **11**, 823–836.

Netea, M. G. & van der Meer, J. W. M. 2017 Trained Immunity: An Ancient Way of Remembering. *Cell Host & Microbe* **21**, 297–300.

Newell, E. W., Sigal, N., Bendall, S. C., Nolan, G. P., & Davis, M. M. 2012 Cytometry by time-of-flight shows combinatorial cytokine expression and virus-specific cell niches within a continuum of CD8+ T cell phenotypes. *Immunity* **36**, 142–152.

Ng, L. G., Ostuni, R., & Hidalgo, A. 2019 Heterogeneity of neutrophils. *Nature Reviews. Immunology*.

Nikolaev, S., Montoya-Burgos, J. I., Margulies, E. H., NISC Comparative Sequencing Program, Rougemont, J., Nyffeler, B., & Antonarakis, S. E. 2007 Early history of mammals is elucidated with the ENCODE multiple species sequencing data. *PLoS genetics* **3**, e2.

Nolan, J. P. & Condello, D. 2013 Spectral flow cytometry. *Current Protocols in Cytometry* **Chapter 1**, Unit1.27.

Norton, S. E., Ward-Hartstonge, K. A., McCall, J. L., Leman, J. K. H., Taylor, E. S., Munro, F., Black, M. A., Fazekas de St Groth, B., McGuire, H. M., & Kemp, R. A. 2019 High-Dimensional Mass Cytometric Analysis Reveals an Increase in Effector Regulatory T Cells as a Distinguishing Feature of Colorectal Tumors. *Journal of Immunology (Baltimore, Md.: 1950)*.

Novakovic, B., Habibi, E., Wang, S.-Y., Arts, R. J. W., Davar, R., Megchelenbrink, W., Kim, B., Kuznetsova, T., Kox, M., Zwaag, J., Matarese, F., van Heeringen, S. J., Janssen-Megens, E. M., Sharifi, N., Wang, C., Keramati, F., Schoonenberg, V., Flicek, P., Clarke, L., Pickkers, P., Heath, S., Gut, I., Netea, M. G., Martens, J. H. A., Logie, C., & Stunnenberg, H. G. 2016 β-Glucan Reverses the Epigenetic State of LPS-Induced Immunological Tolerance. *Cell* **167**, 1354–1368.e14.

Ochoa, M. T., Loncaric, A., Krutzik, S. R., Becker, T. C., & Modlin, R. L. 2008 "Dermal dendritic cells" comprise two distinct populations: CD1+ dendritic cells and CD209+ macrophages. *The Journal of Investigative Dermatology* **128**, 2225–2231.

O'Donnell, E. A., Ernst, D. N., & Hingorani, R. 2013 Multiparameter flow cytometry: advances in high resolution analysis. *Immune Network* **13**, 43–54.

O'Garra, A. 2000 Commitment factors for T helper cells. *Current biology: CB* **10**, R492–494.

Ogawa, L. M. & Vallender, E. J. 2014 Genetic substructure in cynomolgus macaques (Macaca fascicularis) on the island of Mauritius. *BMC genomics* **15**, 748.

O'Gorman, W. E., Huang, H., Wei, Y.-L., Davis, K. L., Leipold, M. D., Bendall, S. C., Kidd, B. A., Dekker, C. L., Maecker, H. T., Chien, Y.-H., & Davis, M. M. 2014 The Split Virus Influenza Vaccine rapidly activates immune cells through Fcγ receptors. *Vaccine* **32**, 5989–5997.

Ohto, U., Ishida, H., Shibata, T., Sato, R., Miyake, K., & Shimizu, T. 2018 Toll-like Receptor 9 Contains Two DNA Binding Sites that Function Cooperatively to Promote Receptor Dimerization and Activation. *Immunity* **48**, 649–658.e4.

O'Leary, J. G., Goodarzi, M., Drayton, D. L., & von Andrian, U. H. 2006 T cell- and B cell-independent adaptive immunity mediated by natural killer cells. *Nature Immunology* **7**, 507–516.

Olingy, C. E., Dinh, H. Q., & Hedrick, C. C. 2019 Monocyte heterogeneity and functions in cancer. *Journal of Leukocyte Biology*.

Omilusik, K. D. & Goldrath, A. W. 2017 The origins of memory T cells. *Nature* **552**, 337–339.

O'Neill, L. A. J., Golenbock, D., & Bowie, A. G. 2013 The history of Toll-like receptors - redefining innate immunity. *Nature Reviews. Immunology* **13**, 453–460.

Orkin, S. H. & Zon, L. I. 2008 Hematopoiesis: an evolving paradigm for stem cell biology. *Cell* **132**, 631–644.

Ornatsky, O., Bandura, D., Baranov, V., Nitz, M., Winnik, M. A., & Tanner, S. 2010 Highly multiparametric analysis by mass cytometry. *Journal of Immunological Methods* **361**, 1–20.

Ortega-Gómez, A., Perretti, M., & Soehnlein, O. 2013 Resolution of inflammation: an integrated view. *EMBO molecular medicine* **5**, 661–674.

Osińska, I., Popko, K., & Demkow, U. 2014 Perforin: an important player in immune response. *Central-European Journal of Immunology* **39**, 109–115.

Palgen, J.-L., Tchitchek, N., Elhmouzi-Younes, J., Delandre, S., Namet, I., Rosenbaum, P., Dereuddre-Bosquet, N., Martinon, F., Cosma, A., Lévy, Y., Le Grand, R., & Beignon, A.-S. 2018 Prime and Boost Vaccination Elicit a Distinct Innate Myeloid Cell Immune Response. *Scientific Reports* **8**, 3087.

Palgen, J.-L., Tchitchek, N., Huot, N., Elhmouzi-Younes, J., Lefebvre, C., Rosenbaum, P., Dereuddre-Bosquet, N., Martinon, F., Hocini, H., Cosma, A., Müller-Trutwin, M., Lévy, Y., Le Grand, R., & Beignon, A.-S. 2019 NK cell immune responses differ after prime and boost vaccination. *Journal of Leukocyte Biology*.

Palis, J. & Yoder, M. C. 2001 Yolk-sac hematopoiesis: the first blood cells of mouse and man. *Experimental Hematology* **29**, 927–936.

Palucka, K. & Banchereau, J. 2013 Human dendritic cell subsets in vaccination. *Current Opinion in Immunology* **25**, 396–402.

Panchanathan, V., Chaudhri, G., & Karupiah, G. 2008 Correlates of protective immunity in poxvirus infection: where does antibody stand? *Immunology and Cell Biology* **86**, 80–86.

Panitch, H. S., Hirsch, R. L., Haley, A. S., & Johnson, K. P. 1987 Exacerbations of multiple sclerosis in patients treated with gamma interferon. *Lancet (London, England)* **1**, 893–895.

Paust, S., Blish, C. A., & Reeves, R. K. 2017 Redefining Memory: Building the Case for Adaptive NK Cells. *Journal of Virology* **91**.

Paust, S., Gill, H. S., Wang, B.-Z., Flynn, M. P., Moseman, E. A., Senman, B., Szczepanik, M., Telenti, A., Askenase, P. W., Compans, R. W., & von Andrian, U. H. 2010 Critical role for the chemokine receptor CXCR6 in NK cell-mediated antigen-specific memory of haptens and viruses. *Nature Immunology* **11**, 1127–1135.

Peña, J. C. & Ho, W.-Z. 2015 Monkey models of tuberculosis: lessons learned. *Infection and Immunity* **83**, 852–862.

Pedroza-Pacheco, I., Madrigal, A., & Saudemont, A. 2013 Interaction between natural killer cells and regulatory T cells: perspectives for immunotherapy. *Cellular & Molecular Immunology* **10**, 222–229.

Peixoto, A., Evaristo, C., Munitic, I., Monteiro, M., Charbit, A., Rocha, B., & Veiga-Fernandes, H. 2007 CD8 single-cell gene coexpression reveals three different effector types present at distinct phases of the immune response. *The Journal of Experimental Medicine* **204**, 1193–1205.

Pejoski, D., Tchitchek, N., Rodriguez Pozo, A., Elhmouzi-Younes, J., Yousfi-Bogniaho, R., Rogez-Kreuz, C., Clayette, P., Dereuddre-Bosquet, N., Lévy, Y., Cosma, A., Le Grand, R., & Beignon, A.-S. 2016 Identification of Vaccine-Altered Circulating B Cell Phenotypes Using Mass Cytometry and a Two-Step Clustering Analysis. *Journal of Immunology (Baltimore, Md.: 1950)* **196**, 4814–4831.

Pelissier Vatter, F. A., Schapiro, D., Chang, H., Borowsky, A. D., Lee, J. K., Parvin, B., Stampfer, M. R., LaBarge, M. A., Bodenmiller, B., & Lorens, J. B. 2018 High-Dimensional Phenotyping Identifies Age-Emergent Cells in Human Mammary Epithelia. *Cell Reports* **23**, 1205–1219.

Perdiguero, E. G. & Geissmann, F. 2016 The development and maintenance of resident macrophages. *Nature Immunology* **17**, 2–8.

Perelman, P., Johnson, W. E., Roos, C., Seuánez, H. N., Horvath, J. E., Moreira, M. A. M., Kessing, B., Pontius, J., Roelke, M., Rumpler, Y., Schneider, M. P. C., Silva, A., O'Brien, S. J., & Pecon-Slattery, J. 2011 A molecular phylogeny of living primates. *PLoS genetics* **7**, e1001342.

Perié, L. & Duffy, K. R. 2016 Retracing the in vivo haematopoietic tree using single-cell methods. *FEBS letters* **590**, 4068–4083.

Perona-Wright, G., Mohrs, K., Szaba, F. M., Kummer, L. W., Madan, R., Karp, C. L., Johnson, L. L., Smiley, S. T., & Mohrs, M. 2009 Systemic but not local infections elicit immunosuppressive IL-10 production by natural killer cells. *Cell Host & Microbe* **6**, 503–512.

Peterson, V. M., Zhang, K. X., Kumar, N., Wong, J., Li, L., Wilson, D. C., Moore, R., McClanahan, T. K., Sadekova, S., & Klappenbach, J. A. 2017 Multiplexed quantification of proteins and transcripts in single cells. *Nature Biotechnology* **35**, 936–939.

Pettie, S. & Ramachandran, V. 2002 An Optimal Minimum Spanning Tree Algorithm. *J. ACM* **49**, 16–34.

Pezzotti, N., Höllt, T., Lelieveldt, B., Eisemann, E., & Vilanova, A. 2016 Hierarchical Stochastic Neighbor Embedding. *Computer Graphics Forum* **35**, 21–30.

Phan, T. G. & Tangye, S. G. 2017 Memory B cells: total recall. *Current Opinion in Immunology* **45**, 132–140.

Phillips, K. A., Bales, K. L., Capitanio, J. P., Conley, A., Czoty, P. W., 't Hart, B. A., Hopkins, W. D., Hu, S.-L., Miller, L. A., Nader, M. A., Nathanielsz, P. W., Rogers, J., Shively, C. A., & Voytko, M. L. 2014 Why primate models matter. *American Journal of Primatology* **76**, 801–827.

Pieper, K., Grimbacher, B., & Eibel, H. 2013 B-cell biology and development. *The Journal of Allergy and Clinical Immunology* **131**, 959–971.

Pietras, E. M. 2017 Inflammation: a key regulator of hematopoietic stem cell fate in health and disease. *Blood* **130**, 1693–1698.

Pillay, J., den Braber, I., Vrisekoop, N., Kwast, L. M., de Boer, R. J., Borghans, J. A. M., Tesselaar, K., & Koenderman, L. 2010 In vivo labeling with 2h2o reveals a human neutrophil lifespan of 5.4 days. *Blood* **116**, 625–627.

Pinti, M., Appay, V., Campisi, J., Frasca, D., Fülöp, T., Sauce, D., Larbi, A., Weinberger, B., & Cossarizza, A. 2016 Aging of the immune system: Focus on inflammation and vaccination. *European Journal of Immunology* **46**, 2286–2301.

Platon, L., Pejoski, D., Gautreau, G., Targat, B., Le Grand, R., Beignon, A.-S., & Tchitchek, N. 2018 A computational approach for phenotypic comparisons of cell populations in high-dimensional cytometry data. *Methods (San Diego, Calif.)* **132**, 66–75.

Platonova, S., Cherfils-Vicini, J., Damotte, D., Crozet, L., Vieillard, V., Validire, P., André, P., Dieu-Nosjean, M.-C., Alifano, M., Régnard, J.-F., Fridman, W.-H., Sautès-Fridman, C., & Cremer, I. 2011 Profound coordinated alterations of intratumoral NK cell phenotype and function in lung carcinoma. *Cancer Research* **71**, 5412–5422.

Plotkin, S. 2014 History of vaccination. *Proceedings of the National Academy of Sciences of the United States of America* **111**, 12283–12287.

Plotkin, S. A. 2008 Vaccines: correlates of vaccine-induced immunity. *Clinical Infectious Diseases: An Official Publication of the Infectious Diseases Society of America* **47**, 401–409.

Poli, A., Michel, T., Thérésine, M., Andrès, E., Hentges, F., & Zimmer, J. 2009 CD56bright natural killer (NK) cells: an important NK cell subset. *Immunology* **126**, 458–465.

Porpiglia, E., Samusik, N., Ho, A. T. V., Cosgrove, B. D., Mai, T., Davis, K. L., Jager, A., Nolan, G. P., Bendall, S. C., Fantl, W. J., & Blau, H. M. 2017 High-resolution myogenic lineage mapping by single-cell mass cytometry. *Nature Cell Biology* **19**, 558–567.

Powell, D., Tauzin, S., Hind, L. E., Deng, Q., Beebe, D. J., & Huttenlocher, A. 2017 Chemokine Signaling and the Regulation of Bidirectional Leukocyte Migration in Interstitial Tissues. *Cell Reports* **19**, 1572–1585.

Prame Kumar, K., Nicholls, A. J., & Wong, C. H. Y. 2018 Partners in crime: neutrophils and monocytes/macrophages in inflammation and disease. *Cell and Tissue Research* **371**, 551–565.

Price, P. J. R., Torres-Domínguez, L. E., Brandmüller, C., Sutter, G., & Lehmann, M. H. 2013 Modified Vaccinia virus Ankara: innate immune activation and induction of cellular signalling. *Vaccine* **31**, 4231–4234.

Qiu, P., Simonds, E. F., Bendall, S. C., Gibbs, K. D., Bruggner, R. V., Linderman, M. D., Sachs, K., Nolan, G. P., & Plevritis, S. K. 2011 Extracting a cellular hierarchy from high-dimensional cytometry data with SPADE. *Nature Biotechnology* **29**, 886–891.

Querec, T., Bennouna, S., Alkan, S., Laouar, Y., Gorden, K., Flavell, R., Akira, S., Ahmed, R., & Pulendran, B. 2006 Yellow fever vaccine YF-17d activates multiple dendritic cell subsets via TLR2, 7, 8, and 9 to stimulate polyvalent immunity. *The Journal of Experimental Medicine* **203**, 413–424.

Quintin, J., Saeed, S., Martens, J. H. A., Giamarellos-Bourboulis, E. J., Ifrim, D. C., Logie, C., Jacobs, L., Jansen, T., Kullberg, B.-J., Wijmenga, C., Joosten, L. A. B., Xavier, R. J., van der Meer, J. W. M., Stunnenberg, H. G., & Netea, M. G. 2012 Candida albicans infection affords protection against reinfection via functional reprogramming of monocytes. *Cell Host & Microbe* **12**, 223–232.

Rahman, A. H., Tordesillas, L., & Berin, M. C. 2016 Heparin reduces nonspecific eosinophil staining artifacts in mass cytometry experiments. *Cytometry. Part A: The Journal of the International Society for Analytical Cytology* **89**, 601–607.

Ram, D. R., Manickam, C., Hueber, B., Itell, H. L., Permar, S. R., Varner, V., & Reeves, R. K. 2018 Tracking KLRC2 (NKG2c)+ memory-like NK cells in SIV+ and rhCMV+ rhesus macaques. *PLoS pathogens* **14**, e1007104.

Ramezanpour, B., Haan, I., Osterhaus, A., & Claassen, E. 2016 Vector-based genetically modified vaccines: Exploiting Jenner's legacy. *Vaccine* **34**, 6436–6448.

Ramshaw, I. A. & Ramsay, A. J. 2000 The prime-boost strategy: exciting prospects for improved vaccination. *Immunology Today* **21**, 163–165.

Raphael, I., Nalawade, S., Eagar, T. N., & Forsthuber, T. G. 2015 T cell subsets and their signature cytokines in autoimmune and inflammatory diseases. *Cytokine* **74**, 5–17.

Rappuoli, R., Pizza, M., Del Giudice, G., & De Gregorio, E. 2014 Vaccines, new opportunities for a new society. *Proceedings of the National Academy of Sciences of the United States of America* **111**, 12288–12293.

Reeves, P. M., Sluder, A. E., Paul, S. R., Scholzen, A., Kashiwagi, S., & Poznansky, M. C. 2018 Application and utility of mass cytometry in vaccine development. *FASEB journal: official publication of the Federation of American Societies for Experimental Biology* **32**, 5–15.

Reeves, R. K., Li, H., Jost, S., Blass, E., Li, H., Schafer, J. L., Varner, V., Manickam, C., Eslamizar, L., Altfeld, M., von Andrian, U. H., & Barouch, D. H. 2015 Antigen-specific NK cell memory in rhesus macaques. *Nature Immunology* **16**, 927–932.

Reikine, S., Nguyen, J. B., & Modis, Y. 2014 Pattern Recognition and Signaling Mechanisms of RIG-I and MDA5. *Frontiers in Immunology* **5**, 342.

Rivera-Hernandez, T., Carnathan, D. G., Moyle, P. M., Toth, I., West, N. P., Young, P. L., Silvestri, G., & Walker, M. J. 2014 The Contribution of Non-human Primate Models to the Development of Human Vaccines. *Discovery medicine* **18**, 313–322.

Rizzetto, L., Ifrim, D. C., Moretti, S., Tocci, N., Cheng, S.-C., Quintin, J., Renga, G., Oikonomou, V., De Filippo, C., Weil, T., Blok, B. A., Lenucci, M. S., Santos, M. A. S., Romani, L., Netea, M. G., & Cavalieri, D. 2016 Fungal Chitin Induces Trained Immunity in Human Monocytes during Cross-talk of the Host with Saccharomyces cerevisiae. *The Journal of Biological Chemistry* **291**, 7961–7972.

Robb, M. 2011 HIV vaccine development: a new beginning. *Expert Review of Vaccines* **10**, 925–927.

Robertson, A. L., Holmes, G. R., Bojarczuk, A. N., Burgon, J., Loynes, C. A., Chimen, M., Sawtell, A. K., Hamza, B., Willson, J., Walmsley, S. R., Anderson, S. R., Coles, M. C., Farrow, S. N., Solari, R., Jones, S., Prince, L. R., Irimia, D., Rainger, G. E., Kadirkamanathan, V., Whyte, M. K. B., & Renshaw, S. A. 2014 A zebrafish compound screen reveals modulation of neutrophil reverse migration as an anti-inflammatory mechanism. *Science Translational Medicine* **6**, 225ra29.

Rock, K. L., Reits, E., & Neefjes, J. 2016 Present Yourself! By MHC Class I and MHC Class II Molecules. *Trends in Immunology* **37**, 724–737.

Romano, M., Fanelli, G., Tan, N., Nova-Lamperti, E., McGregor, R., Lechler, R. I., Lombardi, G., & Scottà, C. 2018 Expanded Regulatory T Cells Induce Alternatively Activated Monocytes With a Reduced Capacity to Expand T Helper-17 Cells. *Frontiers in Immunology* **9**, 1625.

Romee, R., Rosario, M., Berrien-Elliott, M. M., Wagner, J. A., Jewell, B. A., Schappe, T., Leong, J. W., Abdel-Latif, S., Schneider, S. E., Willey, S., Neal, C. C., Yu, L., Oh, S. T., Lee, Y.-S., Mulder, A., Claas, F., Cooper, M. A., & Fehniger, T. A. 2016 Cytokine-induced memory-like natural killer cells exhibit enhanced responses against myeloid leukemia. *Science Translational Medicine* **8**, 357ra123.

Romee, R., Schneider, S. E., Leong, J. W., Chase, J. M., Keppel, C. R., Sullivan, R. P., Cooper, M. A., & Fehniger, T. A. 2012 Cytokine activation induces human memory-like NK cells. *Blood* **120**, 4751–4760.

Roquilly, A., McWilliam, H. E. G., Jacqueline, C., Tian, Z., Cinotti, R., Rimbert, M., Wakim, L., Caminschi, I., Lahoud, M. H., Belz, G. T., Kallies, A., Mintern, J. D., Asehnoune, K., & Villadangos, J. A. 2017 Local Modulation of Antigen-Presenting Cell Development after Resolution of Pneumonia Induces Long-Term Susceptibility to Secondary Infections. *Immunity* **47**, 135–147.e5.

Rosales, C. 2017 Fcγ Receptor Heterogeneity in Leukocyte Functional Responses. *Frontiers in Immunology* **8**, 280.

Rosales, C. 2018 Neutrophil: A Cell with Many Roles in Inflammation or Several Cell Types? *Frontiers in Physiology* **9**.

Rosales, C. & Uribe-Querol, E. 2017 Phagocytosis: A Fundamental Process in Immunity. *BioMed Research International* **2017**, 9042851.

Rosenbaum, P., Tchitchek, N., Joly, C., Stimmer, L., Hocini, H., Dereuddre-Bosquet, N., Beignon, A.-S., Chapon, C., Levy, Y., Le Grand, R., & Martinon, F. 2018 Molecular and Cellular Dynamics in the Skin, the Lymph Nodes, and the Blood of the Immune Response to Intradermal Injection of Modified Vaccinia Ankara Vaccine. *Frontiers in Immunology* **9**, 870.

Rosenkrands, I., Agger, E. M., Olsen, A. W., Korsholm, K. S., Andersen, C. S., Jensen, K. T., & Andersen, P. 2005 Cationic liposomes containing mycobacterial lipids: a new powerful Th1 adjuvant system. *Infection and Immunity* **73**, 5817–5826.

Rosser, E. C. & Mauri, C. 2015 Regulatory B cells: origin, phenotype, and function. *Immunity* **42**, 607–612.

Rothenberg, M. E., Owen, W. F., Silberstein, D. S., Woods, J., Soberman, R. J., Austen, K. F., & Stevens, R. L. 1988 Human eosinophils have prolonged survival, enhanced functional properties, and become hypodense when exposed to human interleukin 3. *The Journal of Clinical Investigation* **81**, 1986–1992.

Roussel, M., Ferrell, P. B., Greenplate, A. R., Lhomme, F., Le Gallou, S., Diggins, K. E., Johnson, D. B., & Irish, J. M. 2017 Mass cytometry deep phenotyping of human mononuclear phagocytes and myeloid-derived suppressor cells from human blood and bone marrow. *Journal of Leukocyte Biology* **102**, 437–447.

Roy Chowdhury, R., Vallania, F., Yang, Q., Lopez Angel, C. J., Darboe, F., Penn-Nicholson, A., Rozot, V., Nemes, E., Malherbe, S. T., Ronacher, K., Walzl, G., Hanekom, W., Davis, M. M., Winter, J., Chen, X., Scriba, T. J., Khatri, P., & Chien, Y.-H. 2018 A multi-cohort study of the immune factors associated with M. tuberculosis infection outcomes. *Nature* **560**, 644–648.

Rudolph, M. E., McArthur, M. A., Magder, L. S., Barnes, R. S., Chen, W. H., & Sztein, M. B. 2019 Diversity of Salmonella Typhi-responsive CD4 and CD8 T cells before and after Ty21a typhoid vaccination in children and adults. *International Immunology*.

Rueckert, C. & Guzmán, C. A. 2012 Vaccines: from empirical development to rational design. *PLoS pathogens* **8**, e1003001.

Rydyznski, C. E., Cranert, S. A., Zhou, J. Q., Xu, H., Kleinstein, S. H., Singh, H., & Waggoner, S. N. 2018 Affinity Maturation Is Impaired by Natural Killer Cell Suppression of Germinal Centers. *Cell Reports* **24**, 3367–3373.e4.

Rydyznski, C. E. & Waggoner, S. N. 2015 Boosting vaccine efficacy the natural (killer) way. *Trends in Immunology* **36**, 536–546.

Saadatian-Elahi, M., Aaby, P., Shann, F., Netea, M. G., Levy, O., Louis, J., Picot, V., Greenberg, M., & Warren, W. 2016 Heterologous vaccine effects. *Vaccine* **34**, 3923–3930.

Saijo, S. & Iwakura, Y. 2011 Dectin-1 and Dectin-2 in innate immunity against fungi. *International Immunology* **23**, 467–472.

Sallusto, F., Lanzavecchia, A., Araki, K., & Ahmed, R. 2010 From vaccines to memory and back. *Immunity* **33**, 451–463.

Sammicheli, S., Kuka, M., Di Lucia, P., de Oya, N. J., De Giovanni, M., Fioravanti, J., Cristofani, C., Maganuco, C. G., Fallet, B., Ganzer, L., Sironi, L., Mainetti, M., Ostuni, R., Larimore, K., Greenberg, P. D., de la Torre, J. C., Guidotti, L. G., & Iannacone, M. 2016 Inflammatory monocytes hinder antiviral B cell responses. *Science Immunology* **1**.

Sandmann, L. & Ploss, A. 2013 Barriers of hepatitis C virus interspecies transmission. *Virology* **435**, 70–80.

Saraiva, M. & O'Garra, A. 2010 The regulation of IL-10 production by immune cells. *Nature Reviews. Immunology* **10**, 170–181.

Sarkar, J. K., Mitra, A. C., & Mukherjee, M. K. 1975 The minimum protective level of antibodies in smallpox. *Bulletin of the World Health Organization* **52**, 307–311.

Sautto, G. A., Kirchenbaum, G. A., & Ross, T. M. 2018 Towards a universal influenza vaccine: different approaches for one goal. *Virology Journal* **15**, 17.

Saxena, M. & Yeretssian, G. 2014 NOD-Like Receptors: Master Regulators of Inflammation and Cancer. *Frontiers in Immunology* **5**, 327.

Schenkel, J. M., Fraser, K. A., Beura, L. K., Pauken, K. E., Vezys, V., & Masopust, D. 2014 T cell memory. Resident memory CD8 T cells trigger protective innate and adaptive immune responses. *Science (New York, N.Y.)* **346**, 98–101.

Schirrmacher, V., Feuerer, M., Fournier, P., Ahlert, T., Umansky, V., & Beckhove, P. 2003 T-cell priming in bone marrow: the potential for long-lasting protective anti-tumor immunity. *Trends in Molecular Medicine* **9**, 526–534.

Schlitzer, A., Sivakamasundari, V., Chen, J., Sumatoh, H. R. B., Schreuder, J., Lum, J., Malleret, B., Zhang, S., Larbi, A., Zolezzi, F., Renia, L., Poidinger, M., Naik, S., Newell, E. W., Robson, P., & Ginhoux, F. 2015 Identification of cDC1- and cDC2-committed DC progenitors reveals early lineage priming at the common DC progenitor stage in the bone marrow. *Nature Immunology* **16**, 718–728.

Schlums, H., Cichocki, F., Tesi, B., Theorell, J., Beziat, V., Holmes, T. D., Han, H., Chiang, S. C. C., Foley, B., Mattsson, K., Larsson, S., Schaffer, M., Malmberg, K.-J., Ljunggren, H.-G., Miller, J. S., & Bryceson, Y. T. 2015 Cytomegalovirus infection drives adaptive epigenetic diversification of NK cells with altered signaling and effector function. *Immunity* **42**, 443–456.

Schmidt, F. I., Bleck, C. K. E., & Mercer, J. 2012 Poxvirus host cell entry. *Current Opinion in Virology* **2**, 20–27.

Schmutz, S., Valente, M., Cumano, A., & Novault, S. 2016 Spectral Cytometry Has Unique Properties Allowing Multicolor Analysis of Cell Suspensions Isolated from Solid Tissues. *PloS One* **11**, e0159961.

Schneemann, M. & Schoedon, G. 2002 Species differences in macrophage NO production are important. *Nature Immunology* **3**, 102.

Schneider, W. M., Chevillotte, M. D., & Rice, C. M. 2014 Interferon-stimulated genes: a complex web of host defenses. *Annual Review of Immunology* **32**, 513–545.

Schweneker, M., Laimbacher, A. S., Zimmer, G., Wagner, S., Schraner, E. M., Wolferstätter, M., Klingenberg, M., Dirmeier, U., Steigerwald, R., Lauterbach, H., Hochrein, H., Chaplin, P., Suter, M., & Hausmann, J. 2017 Recombinant Modified Vaccinia Virus Ankara Generating Ebola Virus-Like Particles. *Journal of Virology* **91**.

Scurrah, C. R., Simmons, A. J., & Lau, K. S. 2019 Single-Cell Mass Cytometry of Archived Human Epithelial Tissue for Decoding Cancer Signaling Pathways. *Methods in Molecular Biology (Clifton, N.J.)* **1884**, 215–229.

Sebastian, S. & Gilbert, S. C. 2016 Recombinant modified vaccinia virus Ankara-based malaria vaccines. *Expert Review of Vaccines* **15**, 91–103.

See, P., Dutertre, C.-A., Chen, J., Günther, P., McGovern, N., Irac, S. E., Gunawan, M., Beyer, M., Händler, K., Duan, K., Sumatoh, H. R. B., Ruffin, N., Jouve, M., Gea-Mallorquí, E., Hennekam, R. C. M., Lim, T., Yip, C. C., Wen, M., Malleret, B., Low, I., Shadan, N. B., Fen, C. F. S., Tay, A., Lum, J., Zolezzi, F., Larbi, A., Poidinger, M., Chan, J. K. Y., Chen, Q., Rénia, L., Haniffa, M., Benaroch, P., Schlitzer, A., Schultze, J. L., Newell, E. W., & Ginhoux, F. 2017 Mapping the human DC lineage through the integration of high-dimensional techniques. *Science (New York, N.Y.)* **356**.

Segura, E., Durand, M., & Amigorena, S. 2013 Similar antigen cross-presentation capacity and phagocytic functions in all freshly isolated human lymphoid organ-resident dendritic cells. *The Journal of Experimental Medicine* **210**, 1035–1047.

Sellge, G. & Kufer, T. A. 2015 PRR-signaling pathways: Learning from microbial tactics. *Seminars in Immunology* **27**, 75–84.

Sen, N., Mukherjee, G., & Arvin, A. M. 2015 Single cell mass cytometry reveals remodeling of human T cell phenotypes by varicella zoster virus. *Methods (San Diego, Calif.)* **90**, 85–94.

Serafini, P., Mgebroff, S., Noonan, K., & Borrello, I. 2008 Myeloid-derived suppressor cells promote cross-tolerance in B-cell lymphoma by expanding regulatory T cells. *Cancer Research* **68**, 5439–5449.

Serhan, C. N. & Savill, J. 2005 Resolution of inflammation: the beginning programs the end. *Nature Immunology* **6**, 1191–1197.

Shaul, M. E. & Fridlender, Z. G. 2017 Neutrophils as active regulators of the immune system in the tumor microenvironment. *Journal of Leukocyte Biology* **102**, 343–349.

Shaw, P. J., Lamkanfi, M., & Kanneganti, T.-D. 2010 NOD-like receptor (NLR) signaling beyond the inflammasome. *European Journal of Immunology* **40**, 624–627.

Shedlock, D. J., Silvestri, G., & Weiner, D. B. 2009 Monkeying around with HIV vaccines: using rhesus macaques to define 'gatekeepers' for clinical trials. *Nature Reviews. Immunology* **9**, 717–728.

Shen, Y., Zhou, D., Chalifoux, L., Shen, L., Simon, M., Zeng, X., Lai, X., Li, Y., Sehgal, P., Letvin, N. L., & Chen, Z. W. 2002 Induction of an AIDS virus-related tuberculosis-like disease in macaques: a model of simian immunodeficiency virus- mycobacterium coinfection. *Infection and Immunity* **70**, 869–877.

Sheng, J., Chen, Q., Soncin, I., Ng, S. L., Karjalainen, K., & Ruedl, C. 2017 A Discrete Subset of Monocyte-Derived Cells among Typical Conventional Type 2 Dendritic Cells Can Efficiently Cross-Present. *Cell Reports* **21**, 1203–1214.

Shiver, J. W., Fu, T.-M., Chen, L., Casimiro, D. R., Davies, M.-E., Evans, R. K., Zhang, Z.-Q., Simon, A. J., Trigona, W. L., Dubey, S. A., Huang, L., Harris, V. A., Long, R. S., Liang, X., Handt, L., Schleif, W. A., Zhu, L., Freed, D. C., Persaud, N. V., Guan, L., Punt, K. S., Tang, A., Chen, M., Wilson, K. A., Collins, K. B., Heidecker, G. J., Fernandez, V. R., Perry, H. C., Joyce, J. G., Grimm, K. M., Cook, J. C., Keller, P. M., Kresock, D. S., Mach, H., Troutman, R. D., Isopi, L. A., Williams, D. M., Xu, Z., Bohannon, K. E., Volkin, D. B., Montefiori, D. C., Miura, A., Krivulka, G. R., Lifton, M. A., Kuroda, M. J., Schmitz, J. E., Letvin, N. L., Caulfield, M. J., Bett, A. J., Youil, R., Kaslow, D. C., & Emini, E. A. 2002 Replication-incompetent adenoviral vaccine vector elicits effective anti-immunodeficiency-virus immunity. *Nature* **415**, 331–335.

Shrimpton, R. E., Butler, M., Morel, A.-S., Eren, E., Hue, S. S., & Ritter, M. A. 2009 CD205 (DEC-205): a recognition receptor for apoptotic and necrotic self. *Molecular Immunology* **46**, 1229–1239.

Shultz, L. D., Brehm, M. A., Garcia-Martinez, J. V., & Greiner, D. L. 2012 Humanized mice for immune system investigation: progress, promise and challenges. *Nature Reviews. Immunology* **12**, 786–798.

Simoni, Y., Chng, M. H. Y., Li, S., Fehlings, M., & Newell, E. W. 2018 Mass cytometry: a powerful tool for dissecting the immune landscape. *Current Opinion in Immunology* **51**, 187–196.

Sitrin, J., Ring, A., Garcia, K. C., Benoist, C., & Mathis, D. 2013 Regulatory T cells control NK cells in an insulitic lesion by depriving them of IL-2. *The Journal of Experimental Medicine* **210**, 1153–1165.

Skinner, J. M., Caro-Aguilar, I. C., Payne, A. M., Indrawati, L., Fontenot, J., & Heinrichs, J. H. 2011 Comparison of rhesus and cynomolgus macaques in a Streptococcus pyogenes infection model for vaccine evaluation. *Microbial Pathogenesis* **50**, 39–47.

Smith, H. R. C., Heusel, J. W., Mehta, I. K., Kim, S., Dorner, B. G., Naidenko, O. V., Iizuka, K., Furukawa, H., Beckman, D. L., Pingel, J. T., Scalzo, A. A., Fremont, D. H., & Yokoyama, W. M. 2002 Recognition of a virus-encoded ligand by a natural killer cell activation receptor. *Proceedings of the National Academy of Sciences of the United States of America* **99**, 8826–8831.

Sánchez-Mejorada, G. & Rosales, C. 1998 Signal transduction by immunoglobulin Fc receptors. *Journal of Leukocyte Biology* **63**, 521–533.

Sánchez-Ramón, S., Conejero, L., Netea, M. G., Sancho, D., Palomares, s., & Subiza, J. L. 2018 Trained Immunity-Based Vaccines: A New Paradigm for the Development of Broad-Spectrum Anti-infectious Formulations. *Frontiers in Immunology* **9**, 2936.

Snounou, G., Grüner, A. C., Müller-Graf, C. D. M., Mazier, D., & Rénia, L. 2005 The Plasmodium sporozoite survives RTS,S vaccination. *Trends in Parasitology* **21**, 456–461.

Soares, H., Waechter, H., Glaichenhaus, N., Mougneau, E., Yagita, H., Mizenina, O., Dudziak, D., Nussenzweig, M. C., & Steinman, R. M. 2007 A subset of dendritic cells induces CD4+ T cells to produce IFN-gamma by an IL-12-independent but CD70-dependent mechanism in vivo. *The Journal of Experimental Medicine* **204**, 1095–1106.

Song, W. M. & Colonna, M. 2018 Immune Training Unlocks Innate Potential. *Cell* **172**, 3–5.

Soudja, S. M., Chandrabos, C., Yakob, E., Veenstra, M., Palliser, D., & Lauvau, G. 2014 Memory-T-cell-derived interferon-γ instructs potent innate cell activation for protective immunity. *Immunity* **40**, 974–988.

Soulas, C., Autissier, P. J., Burdo, T. H., Piatak, M., Lifson, J. D., & Williams, K. C. 2015 Distinct phenotype, longitudinal changes of numbers and cell-associated virus in blood dendritic cells in SIV-infected CD8-lymphocyte depleted macaques. *PloS One* **10**, e0119764.

Souza-Fonseca-Guimaraes, F., Adib-Conquy, M., & Cavaillon, J.-M. 2012 Natural killer (NK) cells in antibacterial innate immunity: angels or devils? *Molecular Medicine (Cambridge, Mass.)* **18**, 270–285.

Spitzer, M. H. & Nolan, G. P. 2016 Mass Cytometry: Single Cells, Many Features. *Cell* **165**, 780–791.

Stittelaar, K. J., van Amerongen, G., Kondova, I., Kuiken, T., van Lavieren, R. F., Pistoor, F. H. M., Niesters, H. G. M., van Doornum, G., van der Zeijst, B. A. M., Mateo, L., Chaplin, P. J., & Osterhaus, A. D. M. E. 2005 Modified vaccinia virus Ankara protects macaques against respiratory challenge with monkeypox virus. *Journal of Virology* **79**, 7845–7851.

Stoeckius, M., Hafemeister, C., Stephenson, W., Houck-Loomis, B., Chattopadhyay, P. K., Swerdlow, H., Satija, R., & Smibert, P. 2017 Simultaneous epitope and transcriptome measurement in single cells. *Nature Methods* **14**, 865–868.

Strauss-Albee, D. M. & Blish, C. A. 2016 Human NK Cell Diversity in Viral Infection: Ramifications of Ramification. *Frontiers in Immunology* **7**, 66.

Strauss-Albee, D. M., Fukuyama, J., Liang, E. C., Yao, Y., Jarrell, J. A., Drake, A. L., Kinuthia, J., Montgomery, R. R., John-Stewart, G., Holmes, S., & Blish, C. A. 2015 Human NK cell repertoire diversity reflects immune experience and correlates with viral susceptibility. *Science Translational Medicine* **7**, 297ra115.

Strauss-Albee, D. M., Horowitz, A., Parham, P., & Blish, C. A. 2014 Coordinated regulation of NK receptor expression in the maturing human immune system. *Journal of Immunology (Baltimore, Md.: 1950)* **193**, 4871–4879.

Strutt, T. M., McKinstry, K. K., Dibble, J. P., Winchell, C., Kuang, Y., Curtis, J. D., Huston, G., Dutton, R. W., & Swain, S. L. 2010 Memory CD4+ T cells induce innate responses independently of pathogen. *Nature Medicine* **16**, 558–564, 1p following 564.

Strutt, T. M., McKinstry, K. K., & Swain, S. L. 2011 Control of innate immunity by memory CD4 T cells. *Advances in Experimental Medicine and Biology* **780**, 57–68.

Suan, D., Sundling, C., & Brink, R. 2017 Plasma cell and memory B cell differentiation from the germinal center. *Current Opinion in Immunology* **45**, 97–102.

Sugimoto, C., Hasegawa, A., Saito, Y., Fukuyo, Y., Chiu, K. B., Cai, Y., Breed, M. W., Mori, K., Roy, C. J., Lackner, A. A., Kim, W.-K., Didier, E. S., & Kuroda, M. J. 2015 Differentiation Kinetics of Blood Monocytes and Dendritic Cells in Macaques: Insights to Understanding Human Myeloid Cell Development. *Journal of Immunology (Baltimore, Md.: 1950)* **195**, 1774–1781.

Sugimoto, M. A., Sousa, L. P., Pinho, V., Perretti, M., & Teixeira, M. M. 2016 Resolution of Inflammation: What Controls Its Onset? *Frontiers in Immunology* **7**, 160.

Suliman, S., Geldenhuys, H., Johnson, J. L., Hughes, J. E., Smit, E., Murphy, M., Toefy, A., Lerumo, L., Hopley, C., Pienaar, B., Chheng, P., Nemes, E., Hoft, D. F., Hanekom, W. A., Boom, W. H., Hatherill, M., & Scriba, T. J. 2016 Bacillus Calmette-Guérin (BCG) Revaccination of Adults with Latent Mycobacterium tuberculosis Infection Induces Long-Lived BCG-Reactive NK Cell Responses. *Journal of Immunology (Baltimore, Md.: 1950)* **197**, 1100–1110.

Sun, J. C., Beilke, J. N., Bezman, N. A., & Lanier, L. L. 2011 Homeostatic proliferation generates long-lived natural killer cells that respond against viral infection. *The Journal of Experimental Medicine* **208**, 357–368.

Sun, J. C., Beilke, J. N., & Lanier, L. L. 2009 Adaptive immune features of natural killer cells. *Nature* **457**, 557–561.

Sun, J. C., Beilke, J. N., & Lanier, L. L. 2010 Immune memory redefined: characterizing the longevity of natural killer cells. *Immunological Reviews* **236**, 83–94.

Sun, L., Wu, J., Du, F., Chen, X., & Chen, Z. J. 2013 Cyclic GMP-AMP synthase is a cytosolic DNA sensor that activates the type I interferon pathway. *Science (New York, N.Y.)* **339**, 786–791.

Sundling, C., Rönnberg, C., Yman, V., Asghar, M., Jahnmatz, P., Lakshmikanth, T., Chen, Y., Mikes, J., Forsell, M. N., Sondén, K., Achour, A., Brodin, P., Persson, K. E., & Färnert, A. 2019 B cell profiling in malaria reveals expansion and remodelling of CD11c+ B cell subsets. *JCI insight* **5**.

Svensson, V., Vento-Tormo, R., & Teichmann, S. A. 2018 Exponential scaling of single-cell RNA-seq in the past decade. *Nature Protocols* **13**, 599–604.

Swadling, L., Capone, S., Antrobus, R. D., Brown, A., Richardson, R., Newell, E. W., Halliday, J., Kelly, C., Bowen, D., Fergusson, J., Kurioka, A., Ammendola, V., Del Sorbo, M., Grazioli, F., Esposito, M. L., Siani, L., Traboni, C., Hill, A., Colloca, S., Davis, M., Nicosia, A., Cortese, R., Folgori, A., Klenerman, P., & Barnes, E. 2014 A human vaccine strategy based on chimpanzee adenoviral and MVA vectors that primes, boosts, and sustains functional HCV-specific T cell memory. *Science Translational Medicine* **6**, 261ra153.

Taams, L. S., van Amelsfort, J. M. R., Tiemessen, M. M., Jacobs, K. M. G., de Jong, E. C., Akbar, A. N., Bijlsma, J. W. J., & Lafeber, F. P. J. G. 2005 Modulation of monocyte/macrophage function by human CD4+CD25+ regulatory T cells. *Human Immunology* **66**, 222–230.

Takeuchi, O. & Akira, S. 2010 Pattern recognition receptors and inflammation. *Cell* **140**, 805–820.

Tangye, S. G., Ma, C. S., Brink, R., & Deenick, E. K. 2013 The good, the bad and the ugly - TFH cells in human health and disease. *Nature Reviews. Immunology* **13**, 412–426.

Taniguchi, H., Toyoshima, T., Fukao, K., & Nakauchi, H. 1996 Presence of hematopoietic stem cells in the adult liver. *Nature Medicine* **2**, 198–203.

Tanji, H., Ohto, U., Shibata, T., Taoka, M., Yamauchi, Y., Isobe, T., Miyake, K., & Shimizu, T. 2015 Toll-like receptor 8 senses degradation products of single-stranded RNA. *Nature Structural & Molecular Biology* **22**, 109–115.

Taylor, P. R. & Gordon, S. 2003 Monocyte heterogeneity and innate immunity. *Immunity* **19**, 2–4.

Teigler, J. E., Phogat, S., Franchini, G., Hirsch, V. M., Michael, N. L., & Barouch, D. H. 2014 The canarypox virus vector ALVAC induces distinct cytokine responses compared to the vaccinia virus-based vectors MVA and NYVAC in rhesus monkeys. *Journal of Virology* **88**, 1809–1814.

Thompson, E. A., Ols, S., Miura, K., Rausch, K., Narum, D. L., Spångberg, M., Juraska, M., Wille-Reece, U., Weiner, A., Howard, R. F., Long, C. A., Duffy, P. E., Johnston, L., O'Neil, C. P., & Loré, K. 2018 TLR-adjuvanted nanoparticle vaccines differentially influence the quality and longevity of responses to malaria antigen Pfs25. *JCI insight* **3**.

Tognotti, E. 2010 The eradication of smallpox, a success story for modern medicine and public health: what lessons for the future? *Journal of Infection in Developing Countries* **4**, 264–266.

Tordesillas, L., Rahman, A. H., Hartmann, B. M., Sampson, H. A., & Berin, M. C. 2016 Mass cytometry profiling the response of basophils and the complete peripheral blood compartment to peanut. *The Journal of Allergy and Clinical Immunology* **138**, 1741–1744.e9.

Töpfer, E., Boraschi, D., & Italiani, P. 2015 Innate Immune Memory: The Latest Frontier of Adjuvanticity. *Journal of Immunology Research* **2015**, 478408.

Trapani, J. A. 2001 Granzymes: a family of lymphocyte granule serine proteases. *Genome Biology* **2**, REVIEWS3014.

Trapani, J. A. & Smyth, M. J. 2002 Functional significance of the perforin/granzyme cell death pathway. *Nature Reviews. Immunology* **2**, 735–747.

Trentini, M. M., de Oliveira, F. M., Kipnis, A., & Junqueira-Kipnis, A. P. 2016 The Role of Neutrophils in the Induction of Specific Th1 and Th17 during Vaccination against Tuberculosis. *Frontiers in Microbiology* **7**, 898.

Tricot, S., Meyrand, M., Sammicheli, C., Elhmouzi-Younes, J., Corneau, A., Bertholet, S., Malissen, M., Le Grand, R., Nuti, S., Luche, H., & Cosma, A. 2015 Evaluating the efficiency of isotope transmission for improved panel design and a comparison of the detection sensitivities of mass cytometer instruments. *Cytometry. Part A: The Journal of the International Society for Analytical Cytology* **87**, 357–368.

Uhl, B., Vadlau, Y., Zuchtriegel, G., Nekolla, K., Sharaf, K., Gaertner, F., Massberg, S., Krombach, F., & Reichel, C. A. 2016 Aged neutrophils contribute to the first line of defense in the acute inflammatory response. *Blood* **128**, 2327–2337.

Ura, T., Okuda, K., & Shimada, M. 2014 Developments in Viral Vector-Based Vaccines. *Vaccines* **2**, 624–641.

Valent, P. 1994 The phenotype of human eosinophils, basophils, and mast cells. *The Journal of Allergy and Clinical Immunology* **94**, 1177–1183.

van de Sandt, C. E., Kreijtz, J. H. C. M., & Rimmelzwaan, G. F. 2012 Evasion of influenza A viruses from innate and adaptive immune responses. *Viruses* **4**, 1438–1476.

Van den Bergh, J. M. J., Guerti, K., Willemen, Y., Lion, E., Cools, N., Goossens, H., Vorsters, A., Van Tendeloo, V. F. I., Anguille, S., Van Damme, P., & Smits, E. L. J. M. 2014 HPV vaccine stimulates cytotoxic activity of killer dendritic cells and natural killer cells against HPV-positive tumour cells. *Journal of Cellular and Molecular Medicine* **18**, 1372–1380.

van den Boorn, J. G., Jakobs, C., Hagen, C., Renn, M., Luiten, R. M., Melief, C. J. M., Tüting, T., Garbi, N., Hartmann, G., & Hornung, V. 2016 Inflammasome-Dependent Induction of Adaptive NK Cell Memory. *Immunity* **44**, 1406–1421.

Van Dis, E., Sogi, K. M., Rae, C. S., Sivick, K. E., Surh, N. H., Leong, M. L., Kanne, D. B., Metchette, K., Leong, J. J., Bruml, J. R., Chen, V., Heydari, K., Cadieux, N., Evans, T., McWhirter, S. M., Dubensky, T. W., Portnoy, D. A., & Stanley, S. A. 2018 STING-Activating Adjuvants Elicit a Th17 Immune Response and Protect against Mycobacterium tuberculosis Infection. *Cell Reports* **23**, 1435–1447.

van Gisbergen, K. P. J. M., Sanchez-Hernandez, M., Geijtenbeek, T. B. H., & van Kooyk, Y. 2005 Neutrophils mediate immune modulation of dendritic cells through glycosylation-dependent interactions between Mac-1 and DC-SIGN. *The Journal of Experimental Medicine* **201**, 1281–1292.

van Helden, M. J. G., de Graaf, N., Boog, C. J. P., Topham, D. J., Zaiss, D. M. W., & Sijts, A. J. A. M. 2012 The bone marrow functions as the central site of proliferation for long-lived NK cells. *Journal of Immunology (Baltimore, Md.: 1950)* **189**, 2333–2337.

van Unen, V., Höllt, T., Pezzotti, N., Li, N., Reinders, M. J. T., Eisemann, E., Koning, F., Vilanova, A., & Lelieveldt, B. P. F. 2017 Visual analysis of mass cytometry data by hierarchical stochastic neighbour embedding reveals rare cell types. *Nature Communications* **8**, 1740.

Vandamme, T. F. 2015 Rodent models for human diseases. *European Journal of Pharmacology* **759**, 84–89.

van't Wout, J. W., Poell, R., & van Furth, R. 1992 The role of BCG/PPD-activated macrophages in resistance against systemic candidiasis in mice. *Scandinavian Journal of Immunology* **36**, 713–719.

Vasou, A., Sultanoglu, N., Goodbourn, S., Randall, R. E., & Kostrikis, L. G. 2017 Targeting Pattern Recognition Receptors (PRR) for Vaccine Adjuvantation: From Synthetic PRR Agonists to the Potential of Defective Interfering Particles of Viruses. *Viruses* **9**.

Vazquez, M. I., Catalan-Dibene, J., & Zlotnik, A. 2015 B cells responses and cytokine production are regulated by their immune microenvironment. *Cytokine* **74**, 318–326.

Veglia, F., Perego, M., & Gabrilovich, D. 2018 Myeloid-derived suppressor cells coming of age. *Nature Immunology* **19**, 108–119.

Vella, A., Bellavite, P., Adami, A., Ortolani, R., Benoni, G., Carletto, A., Biasi, D., Caramaschi, P., & Tridente, G. 1999 Expression of FCepsilonII/CD23 on human neutrophils isolated from rheumatoid arthritis patients. *Inflammation* **23**, 471–479.

Villani, A.-C., Satija, R., Reynolds, G., Sarkizova, S., Shekhar, K., Fletcher, J., Griesbeck, M., Butler, A., Zheng, S., Lazo, S., Jardine, L., Dixon, D., Stephenson, E., Nilsson, E., Grundberg, I., McDonald, D., Filby, A., Li, W., De Jager, P. L., Rozenblatt-Rosen, O., Lane, A. A., Haniffa, M., Regev, A., & Hacohen, N. 2017 Single-cell RNA-seq reveals new types of human blood dendritic cells, monocytes, and progenitors. *Science (New York, N.Y.)* **356**.

Vivier, E., Artis, D., Colonna, M., Diefenbach, A., Di Santo, J. P., Eberl, G., Koyasu, S., Locksley, R. M., McKenzie, A. N. J., Mebius, R. E., Powrie, F., & Spits, H. 2018 Innate Lymphoid Cells: 10 Years On. *Cell* **174**, 1054–1066.

Vivier, E., Tomasello, E., Baratin, M., Walzer, T., & Ugolini, S. 2008 Functions of natural killer cells. *Nature Immunology* **9**, 503–510.

Vollmar, J., Arndtz, N., Eckl, K. M., Thomsen, T., Petzold, B., Mateo, L., Schlereth, B., Handley, A., King, L., Hülsemann, V., Tzatzaris, M., Merkl, K., Wulff, N., & Chaplin, P. 2006 Safety and immunogenicity of IMVAMUNE, a promising candidate as a third generation smallpox vaccine. *Vaccine* **24**, 2065–2070.

Volz, A. & Sutter, G. 2017 Modified Vaccinia Virus Ankara: History, Value in Basic Research, and Current Perspectives for Vaccine Development. *Advances in Virus Research* **97**, 187–243.

Vono, M., Lin, A., Norrby-Teglund, A., Koup, R. A., Liang, F., & Loré, K. 2017 Neutrophils acquire the capacity for antigen presentation to memory CD4+ T cells in vitro and ex vivo. *Blood* **129**, 1991–2001.

Voss, G., Casimiro, D., Neyrolles, O., Williams, A., Kaufmann, S. H. E., McShane, H., Hatherill, M., & Fletcher, H. A. 2018 Progress and challenges in TB vaccine development. *F1000Research* **7**, 199.

Vu Manh, T.-P., Bertho, N., Hosmalin, A., Schwartz-Cornil, I., & Dalod, M. 2015 Investigating Evolutionary Conservation of Dendritic Cell Subset Identity and Functions. *Frontiers in Immunology* **6**, 260.

Wagstaffe, H. R., Mooney, J. P., Riley, E. M., & Goodier, M. R. 2018 Vaccinating for natural killer cell effector functions. *Clinical & Translational Immunology* **7**, e1010.

Waibler, Z., Anzaghe, M., Frenz, T., Schwantes, A., Pöhlmann, C., Ludwig, H., Palomo-Otero, M., Alcamí, A., Sutter, G., & Kalinke, U. 2009 Vaccinia virus-mediated inhibition of type I interferon responses is a multifactorial process involving the soluble type I interferon receptor B18 and intracellular components. *Journal of Virology* **83**, 1563–1571.

Waibler, Z., Anzaghe, M., Ludwig, H., Akira, S., Weiss, S., Sutter, G., & Kalinke, U. 2007 Modified vaccinia virus Ankara induces Toll-like receptor-independent type I interferon responses. *Journal of Virology* **81**, 12102–12110.

Walk, J., de Bree, L. C. J., Graumans, W., Stoter, R., van Gemert, G.-J., van de Vegte-Bolmer, M., Teelen, K., Hermsen, C. C., Arts, R. J. W., Behet, M. C., Keramati, F., Moorlag, S. J. C. F. M., Yang, A. S. P., van Crevel, R., Aaby, P., de Mast, Q., van der Ven, A. J. A. M., Stabell Benn, C., Netea, M. G., & Sauerwein, R. W. 2019 Outcomes of controlled human malaria infection after BCG vaccination. *Nature Communications* **10**, 874.

Walsh, N. C., Kenney, L. L., Jangalwe, S., Aryee, K.-E., Greiner, D. L., Brehm, M. A., & Shultz, L. D. 2017 Humanized Mouse Models of Clinical Disease. *Annual Review of Pathology* **12**, 187–215.

Wang, J. 2018 Neutrophils in tissue injury and repair. *Cell and Tissue Research* **371**, 531–539.

Wang, J., Hossain, M., Thanabalasuriar, A., Gunzer, M., Meininger, C., & Kubes, P. 2017 Visualizing the function and fate of neutrophils in sterile injury and repair. *Science (New York, N.Y.)* **358**, 111–116.

Wang, Y. J., Golson, M. L., Schug, J., Traum, D., Liu, C., Vivek, K., Dorrell, C., Naji, A., Powers, A. C., Chang, K.-M., Grompe, M., & Kaestner, K. H. 2016 Single-Cell Mass Cytometry Analysis of the Human Endocrine Pancreas. *Cell Metabolism* **24**, 616–626.

Wanke-Jellinek, L., Keegan, J. W., Dolan, J. W., & Lederer, J. A. 2016 Characterization of lung infection-induced TCR$\gamma\delta$ T cell phenotypes by CyTOF mass cytometry. *Journal of Leukocyte Biology* **99**, 483–493.

Warfel, J. M., Beren, J., Kelly, V. K., Lee, G., & Merkel, T. J. 2012 Nonhuman primate model of pertussis. *Infection and Immunity* **80**, 1530–1536.

Warfel, J. M., Zimmerman, L. I., & Merkel, T. J. 2014 Acellular pertussis vaccines protect against disease but fail to prevent infection and transmission in a nonhuman primate model. *Proceedings of the National Academy of Sciences of the United States of America* **111**, 787–792.

Wattenberg, M., Viégas, F., & Johnson, I. 2016 How to Use t-SNE Effectively. *Distill* **1**, e2.

Webster, R. L. & Johnson, R. P. 2005 Delineation of multiple subpopulations of natural killer cells in rhesus macaques. *Immunology* **115**, 206–214.

Weidenbusch, M., Kulkarni, O. P., & Anders, H.-J. 2017 The innate immune system in human systemic lupus erythematosus. *Clinical Science (London, England: 1979)* **131**, 625–634.

Weinberg, J. B. 1998 Nitric oxide production and nitric oxide synthase type 2 expression by human mononuclear phagocytes: a review. *Molecular Medicine (Cambridge, Mass.)* **4**, 557–591.

Welsh, R. M. & Waggoner, S. N. 2013 NK cells controlling virus-specific T cells: Rheostats for acute vs. persistent infections. *Virology* **435**, 37–45.

Wen, H., Miao, E. A., & Ting, J. P.-Y. 2013 Mechanisms of NOD-like receptor-associated inflammasome activation. *Immunity* **39**, 432–441.

Wilk, A. J. & Blish, C. A. 2018 Diversification of human NK cells: Lessons from deep profiling. *Journal of Leukocyte Biology* **103**, 629–641.

Wilson, N. S., Behrens, G. M. N., Lundie, R. J., Smith, C. M., Waithman, J., Young, L., Forehan, S. P., Mount, A., Steptoe, R. J., Shortman, K. D., de Koning-Ward, T. F., Belz, G. T., Carbone, F. R., Crabb, B. S., Heath, W. R., & Villadangos, J. A. 2006 Systemic activation of dendritic cells by Toll-like receptor ligands or malaria infection impairs cross-presentation and antiviral immunity. *Nature Immunology* **7**, 165–172.

Wirth, T. C., Xue, H.-H., Rai, D., Sabel, J. T., Bair, T., Harty, J. T., & Badovinac, V. P. 2010 Repetitive antigen stimulation induces stepwise transcriptome diversification but preserves a core signature of memory CD8(+) T cell differentiation. *Immunity* **33**, 128–140.

Withers, D. R. 2016 Innate lymphoid cell regulation of adaptive immunity. *Immunology* **149**, 123–130.

Wong, M. T., Chen, J., Narayanan, S., Lin, W., Anicete, R., Kiaang, H. T. K., De Lafaille, M. A. C., Poidinger, M., & Newell, E. W. 2015 Mapping the Diversity of Follicular Helper T Cells in Human Blood and Tonsils Using High-Dimensional Mass Cytometry Analysis. *Cell Reports* **11**, 1822–1833.

Wong, M. T., Ong, D. E. H., Lim, F. S. H., Teng, K. W. W., McGovern, N., Narayanan, S., Ho, W. Q., Cerny, D., Tan, H. K. K., Anicete, R., Tan, B. K., Lim, T. K. H., Chan, C. Y., Cheow, P. C., Lee, S. Y., Takano, A., Tan, E.-H., Tam, J. K. C., Tan, E. Y., Chan, J. K. Y., Fink, K., Bertoletti, A., Ginhoux, F., Curotto de Lafaille, M. A., & Newell, E. W. 2016 A High-Dimensional Atlas of Human T Cell Diversity Reveals Tissue-Specific Trafficking and Cytokine Signatures. *Immunity* **45**, 442–456.

Wong, P. C., Cai, H., Borchelt, D. R., & Price, D. L. 2002 Genetically engineered mouse models of neurodegenerative diseases. *Nature Neuroscience* **5**, 633–639.

Wong, S.-S. & Webby, R. J. 2013 Traditional and new influenza vaccines. *Clinical Microbiology Reviews* **26**, 476–492.

Woodland, D. L. 2004 Jump-starting the immune system: prime-boosting comes of age. *Trends in Immunology* **25**, 98–104.

Wrammert, J., Miller, J., Akondy, R., & Ahmed, R. 2009 Human immune memory to yellow fever and smallpox vaccination. *Journal of Clinical Immunology* **29**, 151–157.

Wu, J., Sun, L., Chen, X., Du, F., Shi, H., Chen, C., & Chen, Z. J. 2013 Cyclic GMP-AMP is an endogenous second messenger in innate immune signaling by cytosolic DNA. *Science (New York, N.Y.)* **339**, 826–830.

Wu, W.-K., Llewellyn, O. P. C., Bates, D. O., Nicholson, L. B., & Dick, A. D. 2010 IL-10 regulation of macrophage VEGF production is dependent on macrophage polarisation and hypoxia. *Immunobiology* **215**, 796–803.

Wyatt, L. S., Earl, P. L., Eller, L. A., & Moss, B. 2004 Highly attenuated smallpox vaccine protects mice with and without immune deficiencies against pathogenic vaccinia virus challenge. *Proceedings of the National Academy of Sciences of the United States of America* **101**, 4590–4595.

Yamamoto, K., Miwa, Y., Abe-Suzuki, S., Abe, S., Kirimura, S., Onishi, I., Kitagawa, M., & Kurata, M. 2016 Extramedullary hematopoiesis: Elucidating the function of the hematopoietic stem cell niche (Review). *Molecular Medicine Reports* **13**, 587–591.

Yan, N. & Chen, Z. J. 2012 Intrinsic antiviral immunity. *Nature Immunology* **13**, 214–222.

Yang, H., Biermann, M. H., Brauner, J. M., Liu, Y., Zhao, Y., & Herrmann, M. 2016 New Insights into Neutrophil Extracellular Traps: Mechanisms of Formation and Role in Inflammation. *Frontiers in Immunology* **7**, 302.

Yao, Y., Jeyanathan, M., Haddadi, S., Barra, N. G., Vaseghi-Shanjani, M., Damjanovic, D., Lai, R., Afkhami, S., Chen, Y., Dvorkin-Gheva, A., Robbins, C. S., Schertzer, J. D., & Xing, Z. 2018 Induction of Autonomous Memory Alveolar Macrophages Requires T Cell Help and Is Critical to Trained Immunity. *Cell* **175**, 1634–1650.e17.

Yoneyama, M., Onomoto, K., Jogi, M., Akaboshi, T., & Fujita, T. 2015 Viral RNA detection by RIG-I-like receptors. *Current Opinion in Immunology* **32**, 48–53.

Yoshida, T., Mei, H., Dörner, T., Hiepe, F., Radbruch, A., Fillatreau, S., & Hoyer, B. F. 2010 Memory B and memory plasma cells. *Immunological Reviews* **237**, 117–139.

Zabel, F., Mohanan, D., Bessa, J., Link, A., Fettelschoss, A., Saudan, P., Kündig, T. M., & Bachmann, M. F. 2014 Viral particles drive rapid differentiation of memory B cells into secondary plasma cells producing increased levels of antibodies. *Journal of Immunology (Baltimore, Md.: 1950)* **192**, 5499–5508.

Zhang, N. & Bevan, M. J. 2011 CD8(+) T cells: foot soldiers of the immune system. *Immunity* **35**, 161–168.

Zhang, Y., Wallace, D. L., de Lara, C. M., Ghattas, H., Asquith, B., Worth, A., Griffin, G. E., Taylor, G. P., Tough, D. F., Beverley, P. C. L., & Macallan, D. C. 2007 In vivo kinetics of human natural killer cells: the effects of ageing and acute and chronic viral infection. *Immunology* **121**, 258–265.

Zhang, Z., Ohto, U., Shibata, T., Krayukhina, E., Taoka, M., Yamauchi, Y., Tanji, H., Isobe, T., Uchiyama, S., Miyake, K., & Shimizu, T. 2016 Structural Analysis Reveals that Toll-like Receptor 7 Is a Dual Receptor for Guanosine and Single-Stranded RNA. *Immunity* **45**, 737–748.

Zhu, J. & Paul, W. E. 2008 CD4 T cells: fates, functions, and faults. *Blood* **112**, 1557–1569.

Zhu, J., Yamane, H., & Paul, W. E. 2010 Differentiation of effector CD4 T cell populations (*). *Annual Review of Immunology* **28**, 445–489.

Zúñiga-Pflücker, J. C. 2004 T-cell development made simple. *Nature Reviews. Immunology* **4**, 67–72.

Zitvogel, L., Pitt, J. M., Daillère, R., Smyth, M. J., & Kroemer, G. 2016 Mouse models in oncoimmunology. *Nature Reviews. Cancer* **16**, 759–773.

Zunder, E. R., Finck, R., Behbehani, G. K., Amir, E.-A. D., Krishnaswamy, S., Gonzalez, V. D., Lorang, C. G., Bjornson, Z., Spitzer, M. H., Bodenmiller, B., Fantl, W. J., Pe'er, D., & Nolan, G. P. 2015 Palladium-based mass tag cell barcoding with a doublet-filtering scheme and single-cell deconvolution algorithm. *Nature Protocols* **10**, 316–333.

Appendix

French resume/Résumé en français

Contexte. La vaccination est, après l'approvisionnement en eau potable, le plus grand progrès jamais réalisé en santé publique. Basée sur le principe de la mémoire immunitaire, la capacité du système immunitaire d'un individu à se souvenir des rencontres passées avec un pathogène afin de répondre plus efficacement aux rencontres suivantes, la vaccination consiste en l'injection ou l'administration de produits dérivés d'un pathogène (pathogène entier atténué, pathogène tué, protéines du pathogène, toxines inactivées du pathogène), afin d'induire une réponse immunitaire, sans la pathogénicité de l'agent infectieux, afin de protéger contre l'agent infectieux. La protection conférée par la vaccination opère à deux niveaux, à l'échelle individuelle, elle permet de se protéger soi, en empêchant l'infection par un pathogène donné ; à l'échelle de la population, si une proportion suffisante de la population est vaccinée contre un pathogène donné, cela empêche la propagation de la maladie, protégeant ainsi les personnes non vaccinées, et les personnes au système immunitaire affaibli (tels que jeunes enfants, personnes âgées, patients immuno-déprimés), et permettant potentiellement d'éradiquer le pathogène, s'il n'a pas d'autre réservoir que l'être humain.

Plusieurs grands succès ont été rencontrés grâce à l'approche vaccinale, succès parmi lesquels on peut compter l'éradication de la variole en 1980, après près de 40 ans de campagnes de vaccination dans le monde, ou la quasi-éradication de la poliomyélite, dont moins de 30 cas d'infection à travers le monde ont été rapportés par l'organisation mondiale de la santé (OMS) en 2018. A l'heure actuelle 26 vaccins contre de nombreuses maladies sont approuvés et référencés par l'OMS. Malgré tout, les recherches pour développer des vaccins contre de nombreuses maladies (SIDA, malaria, dengue...) rencontrent de nombreuses difficultés et n'ont pas pour l'instant abouti à des vaccins optimaux. L'une des raisons principales de cet état de fait est que malgré plusieurs décennies de recherches et de découvertes en immunologie, et les connaissances accumulées sur le système immunitaire, nous ne parvenons pas encore à l'heure actuelle à avoir une vision d'ensemble claire et intégrée de tous les acteurs cellulaires et moléculaires impliqués dans la réponse vaccinale. En conséquence, il reste difficile aujourd'hui de définir objectivement quels paramètres (nature du vaccin, antigène, voie d'injection...) utiliser dans le développement

de tel ou tel vaccin, et leur définition se fait souvent de manière empirique. En particulier, la plupart des vaccins utilisés aujourd'hui suivent une stratégie de primo-vaccination suivie de rappels, afin de restimuler la mémoire immunitaire et maintenir l'immunité sur le long terme ainsi qu'augmenter la fréquence des répondeurs. Néanmoins le délai entre primo-vaccination et le(s) rappel(s) est défini de manière purement empirique.

Afin d'optimiser les vaccins actuels et le développement de nouveaux vaccins une meilleure compréhension de la réponse immunitaire induite par la vaccination est requise. En particulier la réponse innée, la première ligne de défense du système immunitaire, est, de par ses fonctions antimicrobiennes et immunomodulatrices, un acteur clé ciblé par les vaccins, qui imitent autant que possible un pathogène (sans la pathogénicité associée bien entendu), afin de déclencher une réponse adaptative à l'origine de la mémoire immunitaire.

L'immunité innée repose sur de multiples et diverses cellules (neutrophiles, basophiles, éosinophiles, monocytes, cellules dendritiques, cellules tueuses naturelles...), principalement issues de l'hématopoïèse de la moelle osseuse. Elles expriment de nombreux récepteurs permettant la reconnaissance de patrons de pathogénicité (*e.g.* les lipopolysaccharides des parois bactériennes) ou de dommages cellulaires (*e.g.* de l'ADN extranucléaire), qui leur permet de détecter la plupart des pathogènes (ces récepteurs sont appelés PRR, pour Pattern Recognition Receptor ou récepteur de reconnaissance de patron). Cette reconnaissance peut également être facilitée par la liaison au pathogène de protéines du système du complément, ou par des anticorps spécifiques du pathogène (dans le cas où le pathogène avait déjà été rencontré par le système immunitaire précédemment). Par ailleurs, les cellules infectées vont également présenter des peptides dérivés du pathogène, ou du stress cellulaire induit par le pathogène, sur ses molécules du complexe majeur d'histocompatibilité de classe I (CMH I). Ce signal peut notamment être reconnu par les cellules tueuses naturelles, à l'aide de récepteurs spécifiques.

La reconnaissance d'une infection va donner lieu à l'activation de nombreuses voies signalétiques à la base du processus d'inflammation. Celui-ci correspond d'une part à l'activité antimicrobienne directe de l'immunité innée, ainsi qu'à la sécrétion de facteurs solubles, les cytokines, qui vont d'une part moduler et activer une réponse antimicrobienne des cellules réceptrices, et également permettre le recrutement de nouvelles cellules effectrices visant à combattre plus efficacement l'agent infectieux. L'un des défis de la conception de vaccins est notamment d'induire cette inflammation, mais sans garder la pathogénicité du micro-organisme et les effets secondaires associés. Pour ce faire, beaucoup de vaccins (notamment les vaccins recombinants), non-suffisamment immunogènes par eux-mêmes, contrairement aux vaccins vivant atténués, requièrent l'emploi d'adjuvants, des molécules spécifiquement conçues pour activer les PRR sur les cellules immunitaires innées.

En parallèle de cette fonction effectrice, une seconde fonction de l'immunité innée est l'activation de l'immunité adaptative, ou immunité acquise, composée des lymphocytes T et B. En effet, les cellules dendritiques migrent depuis le site d'inflammation jusqu'au tissus lymphoïde (notamment les ganglions lymphatiques), via les vaisseaux lymphatiques, et vont présenter aux lymphocytes T les antigènes du pathogène ou vaccins qu'elles auront phagocytés, via les molécules du CMH de classe I (lymphocytes T CD8) et de classe II (lymphocytes T CD4). Les interactions entre les molécules co-activatrices présentes à la surface des lymphocytes T et des cellules présentatrice d'antigène vont également contribuer à activer les lymphocytes T. Enfin, cette activation est également régulée par le contexte cytokinique, lui-même défini par la sécrétion cytokinique de multiples cellules. En parallèle, les cellules B vont être activées d'une part par leur reconnaissance directe des antigènes natifs des pathogènes, et d'autre part par les cytokines produites par d'autres types cellulaires, notamment les Tfh, une sous-population des lymphocytes T CD4. Chacune de ces cellules, T et B, est spécifique d'un antigène donné. De manière générale la modulation de l'activation des cellules immunitaires adaptatives est hautement régulée par l'immunité innée, qui est une cible privilégiée dans la conception de nouveaux vaccins.

L'activation des lymphocytes T et B spécifiques, qui vont s'expandre, va permettre à la phase effectrice de l'immunité adaptative d'entrer en jeu. Les lymphocytes T CD4 vont principalement moduler le comportement cellulaire des cellules de l'immunité via la production de cytokines, permettant ainsi une meilleure réponse. Les lymphocytes T CD8 vont éliminer les cellules infectées qu'elles reconnaissent aux antigènes présentés sur les molécules de CMH I. Enfin, les cellules B vont suivre un processus complexe de maturation qui va aboutir à la génération de cellules sécrétrices d'anticorps. Ces anticorps peuvent d'une part neutraliser le pathogène, réduisant ainsi son potentiel infectieux, et d'autre part, comme mentionné précédemment, signaler le pathogène aux cellules innées qui reconnaissent la fraction constante des anticorps liés aux pathogènes via des récepteurs spécifiques (appelés FcR), permettant notamment une amélioration de la phagocytose (un phénomène appelé opsonisation).

L'ensemble des cellules innées et adaptives va établir une véritable discussion médiée par des contacts cellulaires et la sécrétion de cytokines, modulant mutuellement leurs fonctions, ce qui aboutit à l'élimination du pathogène ou du vaccin. Cette phase est suivie par la résolution de l'inflammation, médiée par de nombreux acteurs cellulaires et moléculaires, qui va notamment aboutir à un retour à la normale des marqueurs d'inflammation et par la mort de la plupart des cellules immunitaires recrutées, pour revenir à un niveau basal.

Parmi les lymphocytes T et B activés lors de cette rencontre avec un pathogène, certains vont donner naissance à des populations dites mémoire (mémoire primaire dans le cas de la première rencontre avec un pathogène ou un vaccin), ayant une durée de vie supérieures aux autres, qui ne vont pas mourir à l'issue de la phase de résolution de l'inflammation et vont persister dans les tissus et de manière systémique. En particulier, des populations de cellules sécrétrices d'anticorps vont maintenir un titre d'anticorps anti-pathogène constitutif après la première rencontre avec un pathogène ou une primo-vaccination. Des populations de cellules naturelles tueuses spécifiques d'antigène ont aussi été rapportées en contexte post-infectieux ou post-vaccinatoire, plaçant de fait ces cellules à la frontière entre innée et acquis.

Aux rencontres suivantes avec le même pathogène ou au rappel vaccinal, ces cellules mémoires vont rapidement réagir à la présence du micro-organismes et instaurer plus rapidement une réponse immunitaire plus efficiente. De même, les anticorps circulant vont neutraliser et/ou opsoniser le pathogène/vaccin. En conséquence de quoi la réponse adaptative à la seconde rencontre avec un pathogène ou au rappel vaccinal varie de la première rencontre avec un pathogène ou une primo-vaccination. L'impact de cette mémoire immunitaire sur l'immunité innée induite au rappel reste cependant flou, de même que les interactions impliquées dans la ré-activation des lymphocytes mémoire primaire (plus facilement activables que les lymphocytes naïfs) par les cellules innées.

A l'instar de la première rencontre avec un pathogène/vaccin, cette seconde rencontre va générer une mémoire dite secondaire généralement à plus longue durée de vie que la mémoire primaire dont elle est issue. Dans la mesure où la génération de cette mémoire adaptative (primaire comme secondaire) est un processus dynamique (son établissement prend du temps, et elle peut disparaître sur le long terme), le délai qui sépare la primo-vaccination du rappel (ou deux rappels successifs) importe au sens où le vaccin ne rencontrera et n'activera pas les mêmes cellules. Le résultat en terme d'immunogénicité (qualité des réponses mémoire induites) et d'efficacité vaccinale (qualité et durée de la protection induite) reste encore une question ouverte.

La mémoire immunitaire est donc classiquement associée à l'immunité adaptive, utilisée en lecture de l'efficacité vaccinale (*e.g.* titre d'anticorps circulants). Néanmoins, de nombreuses études indiquent que l'immunité innée n'est pas non plus dépourvue de capacité de mémorisation, un phénomène nommé entraînement inné. Historiquement, des études épidémiologiques ont montré que la vaccination par des vaccins vivants atténués induisaient une protection croisée contre des pathologies infectieuses distinctes. Cet effet ne pouvait être médié par des cellules adaptatives spécifiques des antigènes exprimés par le pathogène, et le rôle de cellules innées, notamment les monocytes/macrophages dans ce phénomène a par la suite été mis au jour. Des études mécanistiques ont également montré l'implication de modifications épigénétiques (changement de méthylation de l'ADN et de modifications post-traductionnelles des histones) dans cet entraînement inné.

Cet entraînement inné a principalement été décrit sur les monocytes/macrophages, mais aussi sur les précurseurs hématopoïètiques de la moelle osseuse. Toutefois les mécanismes à l'origine de cette mémoire innée (stimuli, voies signalétiques impliquées...) reste méconnus, de même que les liens entre réponse effectrice et entraînement inné. Si la durée de vie cet entraînement est vraisemblablement moins longue que celle de la mémoire adaptative (vraisemblablement plusieurs mois/années contre potentiellement toute la vie), ces cellules entraînées n'en participent pas à moins à la génération d'une réponse immunitaire plus efficace dans le cas d'une rencontre avec un nouveau pathogène. Dans le cadre de la vaccination, cet entraînement inné pourrait donc impacter la réponse au rappel.

Objectifs et hypothèses. Etant donné le rôle central de l'immunité innée dans l'induction de la réponse immunitaire, en particulier vaccinale, en terme d'activation et de modulation de la maturation de l'immunité adaptative, et sachant le potentiel d'interaction avec les cellules mémoire adaptative et le potentiel d'entraînement inné, mieux comprendre les acteurs cellulaires et moléculaires innés impliqué dans la réponse à chaque immunisation est une étape-clé pour optimiser la conception de future vaccins, ce d'autant plus que les dernières technologies d'analyses cellulaires révèlent une complexité de sous-populations, au-delà de ce qui était historiquement connu. De fait, au sein d'un groupe de recherche disséquant les acteurs cellulaires et moléculaires impliqués dans la réponse vaccinale, ce projet de thèse visait à répondre aux questions suivantes :
- quelles sont les populations cellulaires innées impliquées dans la réponse immunitaire innée au vaccin et quelle est leur dynamique ?
- la réponse innée diffère-t-elle à la primo-vaccination et au rappel ?
- quel est l'impact du délai entre primo-vaccination et rappel sur la réponse immunitaire innée ?
- quels sont les liens entre les sous-populations innées induites par chaque immunisation et l'établissement de la mémoire immunitaire ?

Approche expérimentale. Pour mener à bien ce projet, j'ai utilisé comme modèle animal le macaque cynomolgus, un primate non-humain connu pour sa proximité immunologique avec l'homme et qui est largement utilisé dans les recherches biomédicales, en particulier vaccinales. En modèle vaccinal, j'ai employé le virus de la vaccine modifiée Ankara (MVA), un vaccin initialement développé et mis en circulation comme vaccin contre la variole, et qui, du fait de sa grande immunogénicité alliée à une grande tolérabilité, ainsi que de la possibilité d'inserts d'ADN dans son génome, sert aujourd'hui de vecteur pour des candidats vaccins contre de nombreuses maladies (*e.g.* VIH/SIDA, tuberculose).

Concrètement, deux cohortes de cinq animaux chacune ont été utilisées pour cette thèse. Pour les deux cohortes, le même vaccin, la même dose et la même voie d'injection sous-cutanée ont été utilisés, seul le calendrier vaccinal différait. La première cohorte, dite de calendrier classique, suit les recommandations vaccinales du MVA, avec un délai de 2 mois entre primo-vaccination et rappel. La seconde cohorte, dite de rappel précoce, a reçu la seconde injection 2 semaines après la primo-vaccination. Des échantillons de sang total ont été prélevés après chaque immunisation, à des temps précoces (quelques heures après

l'injection) et tardifs (quelques semaines après l'injection), pour caractériser la réponse innée induite par chaque immunisation dans chaque calendrier vaccinal. Afin de pouvoir étudier non seulement les monocytes, cellules dendritiques et cellules tueuses naturelles, mais aussi les granulocytes, une population relativement fragile, une solution de fixation du sang total, préservant toutes les populations cellulaires, a été utilisée sur chacun de ces échantillons.

En terme de technologie, l'approche principale a été la cytométrie de masse, une technologie développée récemment, qui mêle cytométrie de flux et spectrométrie de masse. Les cellules provenant des échantillons sont marqués à l'aide d'anticorps couplés à des métaux lourds (essentiellement des lanthanides), naturellement absents des cellules ; chaque cellule est ensuite isolée par brumisation, ionisée et son contenu en métaux lourds est analysé par spectrométrie de masse, ce qui permet de déduire l'expression des marqueurs ciblés par les anticorps. En définitive, une quarantaine de marqueurs extra- et intra-cellulaires peuvent ainsi être analysés à l'échelle de la cellule unique, permettant la caractérisation en profondeur des populations cellulaires, notamment des co-expressions de marqueurs epu étudiées jusqu'alors.

Du fait de la complexité et de la haute dimensionnalité des données générées par cytométrie de masse sur des suivis longitudinaux, nous avons développé des approches bioinformatiques et computationnelles afin d'explorer et exploiter de tels jeux de données. En particulier, notre stratégie analytique a reposé sur une version modifiée de l'algorithme SPADE (Spanning-tree progression analysis of density normalized events, analyse progressive en arbre couvrant d'évènement normalisés par densité), qui permet de regrouper ensemble les cellules qui partagent une forte proximité phénotypique, afin d'étudier ces groupes plutôt que les cellules directement, ce qui permet une représentation humainement visualisable de ces jeux de données. Plusieurs outils bio-informatiques (analyses de corrélation multivariée, analyses discrimantes...) ont également été développés et raffinés afin d'exploiter les résultats de l'algorithme SPADE, et ainsi valoriser nos jeux de données.

Résultats. Une première étude a consisté à la comparaison des échantillons prévaccinaux de macaques et de volontaires sains humains, grâce à la cytométire de masse, afin de valider notre approche expérimentale et nos outils d'analyse. Les résultats obtenus à haute résolution, et à l'échelle de la cellule unique confirme l'étroite proximité immunologique entre les deux espèces. En effet, malgré des patrons d'expression différant pour certains marqueurs (*e.g.* les différents FcR ne sont pas exprimés sur la même proportion des granulocytes dans les deux espèces), les proportions de chaque population cellulaire et leur phénotype général sont largement comparables entre macaques et humains.

Une seconde étude a consisté à caractériser la réponse innée myéloïde induite après primo-vaccination et rappel de la cohorte de calendrier classique. Des travaux antérieurs du laboratoire ont confirmé que ce calendrier vaccinal induisait une réponse humorale conséquente, compatible avec l'induction d'une mémoire immunitaire protectrice chez ces animaux.

A l'aide des stratégies analytiques susmentionnées, nous avons pu mettre en évidence une large diversité phénotypique dans le compartiment sanguin myéloïde de ces singes vaccinés, avec des patrons d'expression de marqueurs non décrits auparavant (*e.g.* le différentiel d'activation des neutrophiles basé sur l'expression de CD66, CD32, CD11b, CCR7 et CD45).

De manière intéressante, alors qu'à l'échelle des compartiments immunitaires innés (granulocytes et monocytes-cellules dendritiques), la réponse est similaire entre chaque immunisation, avec une augmentation drastique et transitoire du nombre de cellules circulantes dans les premières heures post-immunisations, à l'échelle des sous-populations composant ces compartiments, les sous-phénotypes répondant à chaque immunisation diffèrent grandement.

Plus précisément, à l'aide d'analyses discriminantes nous avons pu mettre en évidence que les cellules innées myéloïdes répondant au rappel sont plus actives/matures que les cellules répondant à la primo-vaccination. La surexpression de plusieurs marqueurs, notamment des molécules de CMH II et de FcR, suggère fortement des fonctions augmentées pour ces cellules. Dans la mesure où ces différences phénotypiques préexistent au rappel –elles apparaissent en effet entre deux semaines et deux mois post-primo-vaccination–, cela indique que la primo-vaccination a induit une modification tardive et durable du compartiment inné myéloïde, qui est cohérente avec le concept d'entraînement inné. Dans la mesure où certaines des cellules étudiées (notamment les neutrophiles) ont une durée de vie courte (moins d'une semaine), cette modification durable de leur compartiment suggère fortement une modification des progéniteurs cellulaires.

Une troisième étude a ciblé la réponse des cellules naturelles tueuses sur cette même cohorte de calendrier vaccinal classique. Contrairement aux cellules myéloïdes, les cellules tueuses naturelles sont caractérisées par une diminution de leur nombre dans les heures qui suivent les immunisations. Une cinétique similaire est suivie après la primo-vaccination et le rappel. Néanmoins, comme pour les cellules myéloïdes, les sous-populations composant le compartiment des cellules tueuses naturelles à chaque immunisation diffère.

Le compartiment des cellules tueuses naturelles a principalement été séparé en trois catégories : les cellules peu, moyennement et fortement cytotoxiques. Tandis qu'une forte diversité de ces cellules est trouvée avant vaccination, dans les heures qui suivent la primo-vaccination, la plupart des cellules tueuses naturelles circulant dans le sang sont peu cytotoxiques, et ces cellules restent majoritaires jusqu'à deux semaines après la primo-vaccination. En revanche, à deux mois post-primo-vaccination, le compartiment des cellules tueuses naturelles est caractérisé par l'abondance de cellules hautement cytotoxiques qui se maintiennent après le rappel.

Si les cinétiques diffèrent entre le compartiment des cellules tueuses naturelles et les cellules innées myéloïdes, avec notamment deux changements de phénotype observés pour les premières, contre un pour les secondes, dans les deux cas, une modification tardive des cellules innées a été induite par la primo-vaccination entre deux semaines et deux mois post-immunisation. Cela indique la capacité du système immunitaire inné à faire preuve de mémoire immunitaire.

Une quatrième étude a visé la caractérisation du compartiment inné myéloïde dans la cohorte au rappel précoce, et de la comparer à la cohorte de calendrier vaccinal classique, ainsi que de tester les liens entre immunité innée et adaptative dans ces deux cohortes. Nous avons mis en évidence de grandes différences en terme de qualité et de quantité de la réponse humorale induite dans ces deux calendriers vaccinaux. En particulier, le titre d'anticorps IgA, spécifiques du MVA, induits lors du rappel précoce est beaucoup plus faible que pour le rappel classique. De même, le titre d'IgG neutralisants ainsi que l'affinité des IgG pour leur FcR étaient également plus réduits dans le calendrier précoce. Ces résultats suggèrent que le calendrier au rappel précoce est sous-optimal par rapport au calendrier classique.

En terme d'immunité innée myéloïde lors de calendrier précoce, la réponse à la primo-vaccination et au rappel étaient complètement similaires, sans aucune surexpression des marqueurs d'activation/maturation précédemment mentionnés après le rappel. Ces résultats étaient cohérents avec le fait que le rappel intervienne avant la modification par la primo-vaccination du phénotype des cellules myéloïdes, modification qui intervient entre deux semaines et deux mois après la première injection. En conséquence, une analyse phénotypique comparative a confirmé l'absence des phénotypes de type entraîné lors du calendrier de rappel précoce.

Une analyse de corrélation inné-adaptatif croisant les données de ces deux cohortes a confirmé l'étroite association entre la présence des phénotypes plus matures/activés des cellules innées myéloïdes et les paramètres de la réponse humorale (titre d'IgA, titre d'IgG neutralisants). De même une analyse fonctionnelle des cellules mono-morpho nucléaire circulant dans le sang périphérique, révèle des fonctions accrues en terme de production cytokinique, à la fois des cytokines innées et adaptatives, lors du rappel à deux mois mais pas dans le cas d'un rappel précoce à deux semaines. Ces résultats mettent en évidence d'une part une forte intrication des réponses innées et adaptatives, avec des phénotypes innés corrélant avec l'état de mémoire du système immunitaire, ainsi que l'impact majeur du délai entre primo-vaccination et rappel sur l'établissement de la mémoire immunitaire.

Enfin, une cinquième étude ciblant la réponse des cellules naturelles tueuses dans le calendrier de rappel précoce a été réalisée. Similairement à la réponse innée myéloïde, la réponse de ces cellules tueuses naturelles lors du calendrier au rappel précoce était similaire à chaque immunisation. Toutefois une tendance des cellules répondant au rappel à être moins cytotoxiques que les cellules répondant à la primo-vaccination a été observée. Cela est cohérent avec le fait qu'au moment du rappel à deux semaines, les cellules tueuses naturelles sont globalement moins cytotoxiques qu'avant la vaccination.

En terme d'intégration avec l'immunité adaptative, l'abondance des différents sous-phénotypes des cellules tueuses naturelles corrèle avec les paramètres de la réponse humorale. En complément des résultats obtenus sur les cellules innées myéloïdes, cela traduit un association étroite entre réponse innée précoce et réponse adaptative, mais aussi entre une réponse innée vraisemblablement entraînée par la primo-vaccination, et l'immunité adaptative.

Conclusion et perspectives. En définitive, lors de ce projet de thèse, j'ai pu caractériser les réponses innées induites par chaque immunisation ainsi que leur dynamique. J'ai pu mettre en évidence que ces réponses diffèrent entre primo-vaccination et rappel à deux mois, au sens où la primo-vaccination induit une modification de type entraînement des cellules innées, qui vont présenter un phénotype plus mature/activé et donc répondre différemment lors du rappel.

Cette modification du compartiment innée requiert du temps, et j'ai pu montrer qu'une réduction à deux semaines du laps de temps entre primo-vaccination et rappel abroge l'induction de ces cellules vraisemblablement entraînées. De manière intéressante, la présence de ces cellules entraînées au moment du rappel est fortement associée à une qualité augmentée de la réponse humorale, ainsi qu'à une production accrue de cytokines par le système immunitaire.

De nombreuses questions sont soulevées par ces résultats. Par exemple la caractérisation fonctionnelle détaillée des cellules vraisemblablement entraînées reste à accomplir, non seulement en terme d'activité anti-microbienne mais également d'activité immunomodulatrice de la réponse adaptative. De plus, la durée de persistance de ces cellules vraisemblablement entrainées est à déterminer, et va vraisemblablement fortement impacter la réponse immunitaire développée lors d'un calendrier vaccinal avec un rappel plus tardif que le calendrier de référence. De plus, la nature exacte des cellules qui reçoivent l'entraînement est également floue au sens où les cellules différenciées vraisemblablement entraînées que nous observons peuvent découler de cellules précurseuses entraînées, ou de cellules ayant reçu un entraînement post-différenciation.

Une autre question ouverte est la possibilité d'investiguer l'impact de la vaccination sur le répertoire de récepteurs exprimés par les cellules tueuses naturelles, un aspect que nous n'avons pas pu aborder dans ce projet pour des questions de limitations techniques de l'approche utilisée (échantillons fixes et cytométrie de masse). Par ailleurs, il reste également à décortiquer plus en détails les intrications entre réponse innée et réponse adaptative, notamment en incluant les données caractérisant les réponses adaptatives des lymphocytes T et B dans les deux cohortes susmentionnées, analyses actuellement en cours dans le laboratoire.

Enfin, une meilleure caractérisation des voies signalétiques impliquées dans la mise en place de l'entraînement immunitaire inné est aussi un vaste champs de recherche du domaine. En vaccination en particulier, mieux pouvoir induire un entrainement immunitaire inné, jusqu'à présent seulement décrit ou suspecté pour des vaccins vivants atténués, pourrait permettre de grands progrès en santé publique, d'une part par la protection croisée que confère cet entrainement inné, et d'autre part par la possibilité d'optimiser les différentes injections vaccinales en capitalisant sur les fonctions améliorées de ces cellules entraînées.

En conclusion, ce projet a permis de mettre en lumière des caractéristiques majeures de l'immunité innée post-vaccinale et ses interactions avec l'immunité adaptative et l'établissement de la mémoire immunitaire. Il a permis de confirmer plus en détails l'impact du délai entre primo-vaccination et rappel sur la réponse immunitaire innée et humorale, et mettre en évidence l'étroite intrication entre les modifications phénotypiques de l'immunité innée (cohérentes avec le principe d'entrainement inné) et la mémoire immunitaire adaptative. Ces connaissances contribuent à la meilleure compréhension de la réponse immunitaire induite par la vaccination et pourront servir à l'optimisation rationnelle des vaccins de demain.

université PARIS-SACLAY

ÉCOLE DOCTORALE
Innovation thérapeutique : du fondamental à l'appliqué

Titre : Caractérisation de l'immunité innée induite par la vaccination et ses interactions avec l'immunité adaptative, en fonction du délai entre primo-vaccination et rappel

Mots clés : immunité innée, vaccination, immunologie des systèmes, immunité entraînée, cytométrie de masse (CyTOF), primates non humains

Résumé : La vaccination est l'un des plus grand progrès réalisé en santé publique. Toutefois, malgré de nombreuses connaissances sur le système immunitaire, de nombreux pans d'ombre empêchent la conception de vaccins contre des pathogènes complexes. Pour pallier ce problème, une meilleure compréhension des modes d'action des vaccins est requise. En particulier, la plupart des vaccins nécessitent plusieurs immunisations pour induire une mémoire immunitaire adaptative au long terme, mais l'impact du délai entre primo-vaccination, induisant une mémoire primaire, et rappel(s) la restimulant pour générer une mémoire secondaire, est peu défini. De plus, la réponse immunitaire innée, induite à chaque immunisation et façonnant l'immunité adaptative, reste peu caractérisée dans ce contexte vaccinal.
En vaccinant des macaques cynomolgus avec le virus de la vaccine modifiée Ankara, selon un schéma de primo-vaccination suivie d'un rappel homologue à deux mois, et en utilisant la cytométrie de masse couplée à des analyses bio-informatiques, nous avons caractérisé la réponse innée induite par chaque immunisation. Les réponses innées diffèrent entre primo-vaccination et rappel, avec induction par la primo-vaccination d'une modification phénotypique tardive des cellules innées, suggérant une meilleure capacité à répondre au rappel. De surcroît, la réduction à deux semaines du délai entre primo-vaccination et rappel abroge la mobilisation de ces cellules innées phénotypiquement modifiées et altère la qualité de la réponse humorale.
En définitive, en plus de la réponse innée précoce, ce projet a mis en évidence l'induction par la primo-vaccination d'un vraisemblable entraînement inné tardif, un concept émergent traduisant la capacité de mémorisation des cellules innées via des modifications épigénétiques. Ce vraisemblable entraînement, non seulement des monocytes et cellules tueuses naturelles, mais aussi des cellules dendritiques et surprenamment des neutrophiles, est corrélé à la qualité de la mémoire immunitaire adaptative, de manière hautement dépendante du délai entre primo-vaccination et rappel. Ces résultats contribuent à ouvrir la voie vers l'optimisation rationnelle des futurs vaccins, via l'optimisation des calendriers vaccinaux et la valorisation de l'entraînement inné.

Title : Characterization of the innate immunity elicited by vaccination and its interactions with adaptive immunity, depending on the delay between prime and boost

Keywords : innate immunity, vaccination, systems immunology, trained immunity, mass cytometry (CyTOF), non human primates

Abstract : Vaccination is one of the best achievements made in public health. However, designing vaccines against complex pathogens is currently challenging. The immune system is indeed uncompletely characterized, despite large amount of accumulated knowledges. A better understanding of vaccine-induced immunity is then required to optimize vaccine design. In particular, while most vaccines require several immunizations to induce a long-lasting adaptive immune memory, little is known on the impact of the delay beween the prime inducing a primary memory and the boost restimulating it to induce a secondary memory. Also, the innate immunity induced by each immunization and shaping the adaptative immunity is poorly characterized in this vaccine context.
We studied the innate immune responses in cynomolgus macaques immunized with the modified vaccinia virus Ankara, following an homologous prime-boost vaccination at two months apart. We applied mass cytometry and bioinformatic analyses to characterize the innate response induced by each immunization. We showed that prime and boost vaccination triggered distinct innate responses. Actually, prime induced late phenotypic modifications of innate cells. These phenotypic changes suggest a stronger ability to react to the boost. Moreover, reducing the delay between prime and boost to two weeks impeded the mobilization of these phenotypically modified innate cells, and qualitatively altered humoral response.
In conclusion, beyond the early innate responses, these results highlight the late induction by the prime of "likely trained" innate cells. This emerging concept corresponds to the ability of innate cells to display memory features based on epigenetic modifications. This "likely training" occured not only on monocytes and natural killer cells, but also on dendritic cells and strikingly on neutrophils. It was deeply connected with adaptive immune memory establishment, in a prime-boost delay dependant fashion. These findings contribute to pave the way towards to the rationale design of future vaccines, via vaccine schedule optimization and harnessment of innate training.

Université Paris-Saclay
CEA, département IDMIT
18, route du Panorama / 92265 Fontenay-aux-Roses, France